Nonlinear Regression Analysis and Its Applications

Douglas M. Bates

Department of Statistics
University of Wisconsin
Madison, Wisconsin

Donald G. Watts

Department of Mathematics
and Statistics
Queen's University
Kingston, Ontario, Canada

WILEY

JOHN WILEY & SONS

New York Chichester Brisbane Toronto Singapore

Copyright © 1988 by John Wiley & Sons, Inc.

All rights reserved. Published simultaneously in Canada.

Reproduction or translation of any part of this work
beyond that permitted by Section 107 or 108 of the
1976 United States Copyright Act without the permission
of the copyright owner is unlawful. Requests for
permission or further information should be addressed to
the Permissions Department, John Wiley & Sons, Inc.

Library of Congress Cataloging in Publication Data:

Bates, Douglas M.
Nonlinear regression analysis and its applications / Douglas M. Bates, Donald G. Watts.

p. cm.—(Wiley series in probability and mathematical statistics. Applied probability and statistics)
Bibliography: p.
Includes index.

ISBN 0-471-81643-4
1. Regression analysis. 2. Linear models (Statistics) 3. Parameter estimation. I. Watts, Donald G. II. Title. III. Series.
QA278.2.B375 1988 88-6065
519.5'36--dc19 CIP

Printed in the United States of America

10 9 8 7 6 5 4 3 2 1

To

Mary Ellen	Valery
Barbara	Lloyd
Michael	Megan

PREFACE

"Reading maketh a full man, conference; a ready man, and writing; an exact man."

– Francis Bacon

In this book we have tried to give a balanced presentation of the theory and practice of nonlinear regression.

We expect readers to have a working knowledge of linear regression at about the level of Draper and Smith (1981) or Montgomery and Peck (1982). Nevertheless, to provide background material and to establish notation, we give a summary review of linear least squares in Chapter 1, together with a geometrical development which is helpful in understanding both linear and nonlinear least squares. On the practical side, we discuss linear least squares in the context of modern computing methods and present useful material for checking the assumptions which are involved in regression and for modifying and improving fitted models. In Chapter 2 we discuss how nonlinear models can arise, and show how linear regression methods can be used iteratively to estimate the parameters. We also show how linear methods can be used to make approximate inferences about parameters and nonlinear model functions: again, the geometry is emphasized. The practical aspects of nonlinear estimation are discussed fully in Chapter 3, including such topics as getting starting values, transforming parameters, derivative-free methods, dealing with correlated residuals and with accumulated data, and comparing models.

In Chapter 4 we cover special methods for dealing with multiresponse data, and in Chapter 5, special techniques for compartment models in which the response function is specified as the solution to a set of linear differential equations.

In Chapter 6 we discuss improved methods for presenting the inferential results of a nonlinear analysis, using likelihood profile traces and profile t plots. Finally, in Chapter 7 we present material concerned with measuring how badly nonlinear a particular model–data set situation is. This chapter is helpful in understanding and appreciating the geometry of nonlinear least squares — and indeed, of linear least squares.

Extensive displays of geometrical constructs have been used to facilitate understanding. We have also used continuing examples so that readers can follow the development of ideas in manageable steps within familiar contexts.

All of the data sets used in this book are *real*, that is, the data were obtained from genuine physical, chemical, and biological experiments. We are grateful to the many authors, researchers, and publishers who gave permission to quote their data. In particular we would like to thank Don deBethizy, Rick Elliott, Steve Havriliak, Nico Linssen, Dave Pierson, Rob Stiratelli, Marg Treloar, and Eric Ziegel. We also acknowledge helpful comments made by participants in courses at Dalhousie University, Queen's University, and the University of Wisconsin, where the book was tested in class.

We are grateful to David Hamilton for stimulating discussions and collaborations, to Gunseog Kang for exemplary service in proofreading, and to Steve Czarniak, Mary Lindstrom and Dennis Wolf who also helped in proofreading.

The book was composed electronically using the *troff* text formatting language on the Statistics research computer at the University of Wisconsin–Madison. The figures were produced using the S language for statistics and graphics and both text and graphics were typeset on a Linotronic L300 using the PostScript language. We are appreciative of the good work done by Bea Shube and her colleagues at Wiley and by Bill Kasdorf of Impressions.

Considerable research was involved in developing the material in this book, and we thank the Natural Sciences and Engineering Research Council of Canada and the United States National Science Foundation for support.

Finally, we thank our wives for their continued love and encouragement.

June, 1988

Douglas M. Bates
Donald G. Watts

CONTENTS

1. Review of Linear Regression **1**

1.1 The Linear Regression Model / 1
1.1.1 The Least Squares Estimates / 4
1.1.2 Sampling Theory Inference Results / 5
1.1.3 Likelihood Inference Results / 6
1.1.4 Bayesian Inference Results / 7
1.1.5 Comments / 7
1.2 The Geometry of Linear Least Squares / 9
1.2.1 The Expectation Surface / 9
1.2.2 Determining the Least Squares Estimates / 12
1.2.3 Parameter Inference Regions / 15
1.2.3.1 The Geometry of Sampling Theory Results / 15
1.2.3.2 Marginal Confidence Intervals / 19
1.2.3.3 The Geometry of Likelihood Results / 23
1.3 Assumptions and Model Assessment / 23
1.3.1 Assumptions and Their Implications / 24
1.3.2 Model Assessment / 26
1.3.2.1 Plotting Residuals / 27
1.3.2.2 Stabilizing Variance / 28
1.3.2.3 Lack of Fit / 29

2. Nonlinear Regression: Iterative Estimation and Linear Approximations **32**

2.1 The Nonlinear Regression Model / 32
2.1.1 Transformably Linear Models / 34
2.1.2 Conditionally Linear Parameters / 36
2.1.3 The Geometry of the Expectation Surface / 36
2.2 Determining the Least Squares Estimates / 39

2.2.1 The Gauss–Newton Method / 40
2.2.1.1 Step Factor / 42
2.2.2 The Geometry of Nonlinear Least Squares / 43
2.2.3 Convergence / 47
2.3 Nonlinear Regression Inference Using the Linear Approximation / 52
2.3.1 Approximate Inference Regions for Parameters / 52
2.3.2 Approximate Inference Bands for the Expected Response / 58
2.4 Nonlinear Least Squares via Sums of Squares / 60
2.4.1 The Linear Approximation / 61
2.4.2 Overshoot / 64
2.5 Use of the Linear Approximation / 64

3. Practical Considerations in Nonlinear Regression 67

3.1 Model Specification / 67
3.1.1 The Expectation Function / 67
3.1.2 The Disturbance Term / 69
3.2 Preliminary Analysis / 70
3.3 Starting Values / 72
3.3.1 Interpreting the Expectation Function Behavior / 72
3.3.2 Interpreting Derivatives of the Expectation Function / 73
3.3.3 Transforming the Expectation Function / 73
3.3.4 Reducing Dimensions / 76
3.3.5 Conditional Linearity / 76
3.4 Parameter Transformations / 77
3.4.1 Constrained Parameters / 77
3.4.2 Facilitating Convergence / 78
3.5 Other Iterative Techniques / 79
3.5.1 A Newton–Raphson Method / 79
3.5.2 The Levenberg–Marquardt Compromise / 80
3.5.3 Numerical Derivatives / 82
3.5.4 Derivative-free Methods / 82
3.5.5 Removing Conditionally Linear Parameters / 85
3.6 Obtaining Convergence / 86
3.7 Assessing the Fit and Modifying the Model / 90
3.8 Correlated Residuals / 92
3.9 Accumulated Data / 96
3.9.1 Estimating the Parameters by Direct Integration / 98
3.10 Comparing Models / 103
3.10.1 Nested Models / 103
3.10.2 Incremental Parameters and Indicator Variables / 104
3.10.3 Non-nested Models / 107

3.11 Parameters as Functions of Other Variables / 108
3.12 Presenting the Results / 109
3.13 Nitrite Utilization: A Case Study / 110
3.13.1 Preliminary Analysis / 110
3.13.2 Model Selection / 113
3.13.3 Starting Values / 113
3.13.4 Assessing the Fit / 113
3.13.5 Modifying the Model / 114
3.13.6 Assessing the Fit / 116
3.13.7 Reducing the Model / 116
3.13.8 Assessing the Fit / 116
3.13.9 Comparing the Models / 120
3.13.10 Reporting the Results / 121
3.14 Experimental Design / 121
3.14.1 General Considerations / 122
3.14.2 The Determinant Criterion / 124
3.14.3 Starting Designs / 125
3.14.4 Sequential designs / 127
3.14.5 Subset designs / 129
3.14.6 Conditionally Linear Models / 129
3.14.7 Other design criteria / 131

4. Multiresponse Parameter Estimation 134

4.1 The Multiresponse Model / 134
4.1.1 The Determinant Criterion / 138
4.1.2 Inferences for Multiresponse Estimation / 139
4.1.3 Dimensional Considerations in Multiresponse Estimation / 140
4.2 A Generalized Gauss-Newton Method / 141
4.2.1 The Gradient and Hessian of the Determinant / 142
4.2.2 An Approximate Hessian / 143
4.2.3 Calculations for Each Iteration / 144
4.2.4 A Multiresponse Convergence Criterion / 145
4.3 Practical Considerations / 146
4.3.1 Obtaining Starting Values / 146
4.3.1.1 Starting Estimates for Multiresponse Models Described by Systems of Differential Equations / 147
4.3.2 Assessing the Fit / 149
4.3.3 Dependencies Among Responses / 154
4.3.4 Linear Combinations of Responses / 158
4.3.5 Comparing Models / 162
4.4 Missing Data / 164

5. Models Defined by Systems of Differential Equations 168

5.1 Compartment Models and System Diagrams / 168
5.2 Estimating Parameters in Compartment Models / 172
5.2.1 Solving Systems of Linear Differential Equations / 173
5.2.1.1 Dead Time / 175
5.2.1.2 Cessation of Infusion / 177
5.2.2 Derivatives of the Expectation Function / 178
5.3 Practical Considerations / 179
5.3.1 Parameter Transformations / 179
5.3.2 Identifiability / 180
5.3.3 Starting Values / 182
5.4 Lipoproteins: A Case Study / 182
5.4.1 Preliminary Analysis / 182
5.4.2 One Compartment / 182
5.4.3 Two Compartments / 183
5.4.4 Three Compartments / 184
5.4.5 Three Compartments, Common Parameters / 187
5.4.6 Conclusions / 187
5.5 Oil shale: A Case Study / 188
5.5.1 Preliminary Analysis / 188
5.5.2 Starting Values for the 673 K Data / 190
5.5.3 Fitting the Individual Temperature Data / 191
5.5.4 Starting Estimates for the Process Parameters / 193
5.5.5 Fitting the Complete Data Set / 194
5.5.6 Conclusions / 198

6. Graphical Summaries of Nonlinear Inference Regions 200

6.1 Likelihood Regions / 200
6.1.1 Joint Parameter Likelihood Regions / 200
6.1.2 Profile t Plots, Profile Traces, and Profile Pair Sketches / 205
6.1.2.1 Profile Traces / 207
6.1.2.2 Profile Pair Sketches / 209
6.1.3 Comments / 214
6.2 Bayes Regions / 216
6.2.1 Choice of Bayes Prior on the Parameters / 216
6.2.2 Joint HPD Regions / 219
6.3 Exact Sampling Theory Confidence Regions / 223
6.4 Comparison of the Likelihood, Bayes, and Sampling Theory Approaches / 229

7. Curvature Measures of Nonlinearity **232**

7.1 Velocity and Acceleration Vectors / 233
7.1.1 Tangential and Normal Accelerations / 234
7.1.2 The Acceleration in an Arbitrary Direction / 239
7.2 Relative Curvatures / 241
7.2.1 Interpreting Terms in the Curvature Arrays / 245
7.2.1.1 Intrinsic Curvature / 245
7.2.1.2 Parameter Effects Curvatures / 246
7.2.2 Reparametrization / 248
7.3 RMS Curvatures / 253
7.3.1 Calculating RMS Curvatures / 254
7.3.2 RMS Curvatures in Practice / 256
7.4 Direct Assessment of the Effects of Intrinsic Nonlinearity / 256

Appendix 1. Data Sets Used in Examples **267**

1.1 PCB / 267
1.2 Rumford / 268
1.3 Puromycin / 269
1.4 BOD / 270
1.5 Isomerization / 271
1.6 α-Pinene / 272
1.7 Sulfisoxazole / 273
1.8 Lubricant / 274
1.9 Chloride / 274
1.10 Ethyl Acrylate / 274
1.11 Saccharin / 277
1.12 Nitrite Utilization / 278
1.13 s-PMMA / 280
1.14 Tetracycline / 281
1.15 Oil Shale / 282
1.16 Lipoproteins / 282

Appendix 2. QR Decompositions Using Householder Transformations **286**

Appendix 3. Pseudocode for Computing Algorithms **290**

3.1 Nonlinear Least Squares / 290
3.1.1 Implementation in S / 291
3.1.2 Implementation in GAUSS / 293

3.1.3 Implementation in SAS/IML / 296
3.2 Linear Summaries and Studentized Residuals / 298
3.3 Multiresponse Estimation / 299
3.4 Linear Systems of Differential Equations / 300
3.5 Profile Calculations / 302
3.5.1 Generation of τ and the Profile Traces / 302
3.5.2 Profile Pair Plots / 303

Appendix 4. Data Sets Used in Problems **305**

4.1 BOD Data Set 2 / 305
4.2 Nitrendipene / 306
4.3 Saccharin Data Set 2 / 306
4.4 Steady State Adsorption / 306
4.5 Leaves / 310
4.6 α-Pinene Data Set 2 / 310
4.7 Coal Liquefaction / 311
4.8 Haloperidol / 315

Appendix 5. Evaluating Matrix Exponentials and Convolutions **316**

5.1 Diagonalizable A / 317
5.2 Nondiagonalizable A / 319
5.3 Complex Eigenvalues / 320

Appendix 6. Interpolating Profile Pair Contours **323**

Appendix 7. Key to Data Sets **329**

References **335**

Bibliography **343**

Author Index **355**

Subject Index **359**

Nonlinear Regression Analysis and Its Applications

CHAPTER 1.

Review of Linear Regression

"Non sunt multiplicanda entia praeter necessitatem."
(Entities are not to be multiplied beyond necessity.)

– William of Ockham

We begin with a brief review of linear regression, because a thorough grounding in linear regression is fundamental to understanding nonlinear regression. For a more complete presentation of linear regression see, for example, Draper and Smith (1981), Montgomery and Peck (1982), or Seber (1977). Detailed discussion of regression diagnostics is given in Belsley, Kuh, and Welsch (1980) and Cook and Weisberg (1982), and the Bayesian approach is discussed in Box and Tiao (1973).

Two topics which we emphasize are modern numerical methods and the geometry of linear least squares. As will be seen, attention to efficient computing methods increases understanding of linear regression, while the geometric approach provides insight into the methods of linear least squares and the analysis of variance, and subsequently into nonlinear regression.

1.1 The Linear Regression Model

Linear regression provides estimates and other inferential results for the *parameters* $\boldsymbol{\beta} = (\beta_1, \beta_2, \ldots, \beta_P)^{\mathrm{T}}$ in the model

$$\begin{aligned} Y_n &= \beta_1 x_{n1} + \beta_2 x_{n2} + \cdots + \beta_P x_{nP} + Z_n \\ &= (x_{n1}, \ldots, x_{nP})\boldsymbol{\beta} + Z_n \end{aligned} \tag{1.1}$$

In this model, the random variable Y_n, which represents the *response* for *case* n, $n = 1, 2, \ldots, N$, has a *deterministic* part and a *stochastic* part. The deterministic part, $(x_{n1}, \ldots, x_{nP})\boldsymbol{\beta}$, depends upon the parameters $\boldsymbol{\beta}$ and upon the *predictor*

or *regressor variables* x_{np}, $p = 1, 2, \ldots, P$. The stochastic part, represented by the random variable Z_n, is a *disturbance* which perturbs the response for that case. The superscript ^{T} denotes the transpose of a matrix.

The model for N cases can be written

$$\boldsymbol{Y} = \mathbf{X}\boldsymbol{\beta} + \boldsymbol{Z} \tag{1.2}$$

where $\boldsymbol{Y}$ is the vector of random variables representing the data we may get, $\mathbf{X}$ is the $N \times P$ matrix of regressor variables,

$$\mathbf{X} = \begin{bmatrix} x_{11} & x_{12} & x_{13} & \cdots & x_{1P} \\ x_{21} & x_{22} & x_{23} & \cdots & x_{2P} \\ \cdot & \cdot & \cdot & & \cdot \\ \cdot & \cdot & \cdot & & \cdot \\ \cdot & \cdot & \cdot & & \cdot \\ x_{N1} & x_{N2} & x_{N3} & \cdots & x_{NP} \end{bmatrix}$$

and $\boldsymbol{Z}$ is the vector of random variables representing the disturbances. (We will use bold face italic letters for vectors of random variables.)

The deterministic part, $\mathbf{X}\boldsymbol{\beta}$, a function of the parameters and the regressor variables, gives the mathematical model or the model function for the responses. Since a nonzero mean for Z_n can be incorporated into the model function, we assume that

$$\mathrm{E}[\boldsymbol{Z}] = \mathbf{0} \tag{1.3}$$

or, equivalently,

$$\mathrm{E}[\boldsymbol{Y}] = \mathbf{X}\boldsymbol{\beta}$$

We therefore call $\mathbf{X}\boldsymbol{\beta}$ the *expectation function* for the regression model. The matrix $\mathbf{X}$ is called the *derivative matrix*, since the (n,p)th term is the derivative of the nth row of the expectation function with respect to the pth parameter.

Note that for linear models, *derivatives with respect to any of the parameters are independent of all the parameters.*

If we further assume that $\boldsymbol{Z}$ is normally distributed with

$$\mathrm{Var}[\boldsymbol{Z}] = \mathrm{E}[\boldsymbol{Z}\boldsymbol{Z}^{\mathrm{T}}] = \sigma^2\mathbf{I} \tag{1.4}$$

where $\mathbf{I}$ is an $N \times N$ identity matrix, then the joint probability density function for $\boldsymbol{Y}$, given $\boldsymbol{\beta}$ and the *variance* σ^2, is

$$\begin{aligned} p(\mathbf{y} \mid \boldsymbol{\beta}, \sigma^2) &= (2\pi\sigma^2)^{-N/2} \exp\left[\frac{-(\mathbf{y}-\mathbf{X}\boldsymbol{\beta})^{\mathrm{T}}(\mathbf{y}-\mathbf{X}\boldsymbol{\beta})}{2\sigma^2}\right] \\ &= (2\pi\sigma^2)^{-N/2} \exp\left[\frac{-\|\mathbf{y}-\mathbf{X}\boldsymbol{\beta}\|^2}{2\sigma^2}\right] \end{aligned} \tag{1.5}$$

where the double vertical bars denote the length of a vector. When provided

with a derivative matrix **X** and a vector of observed data **y**, we wish to make inferences about σ^2 and the P parameters $\boldsymbol{\beta}$.

Example: PCB 1

As a simple example of a linear regression model, we consider the concentration of polychlorinated biphenyls (PCBs) in Lake Cayuga trout as a function of age (Bache et al., 1972). The data set is described in Appendix 1, Section A1.1. A plot of the PCB concentration versus age, Figure 1.1, reveals a curved relationship between PCB concentration and age. Furthermore, there is increasing variance in the PCB concentration as the concentration increases. Since the assumption (1.4) requires that the variance of the disturbances be constant, we seek a transformation of the PCB concentration which will stabilize the variance (see Section 1.3.2). Plotting the PCB concentration on a logarithmic scale, as in Figure 1.2*a*, nicely stabilizes the variance and produces a more nearly linear relationship. Thus, a linear expectation function of the form

$$\ln(\text{PCB}) = \beta_1 + \beta_2 \text{ age}$$

could be considered appropriate, where ln denotes the natural logarithm (logarithm to the base e). Transforming the regressor variable (Box and Tidwell, 1962) can produce an even straighter plot, as shown in Figure 1.2*b*, where we use the cube root of age. Thus a simple expectation function to be fitted is

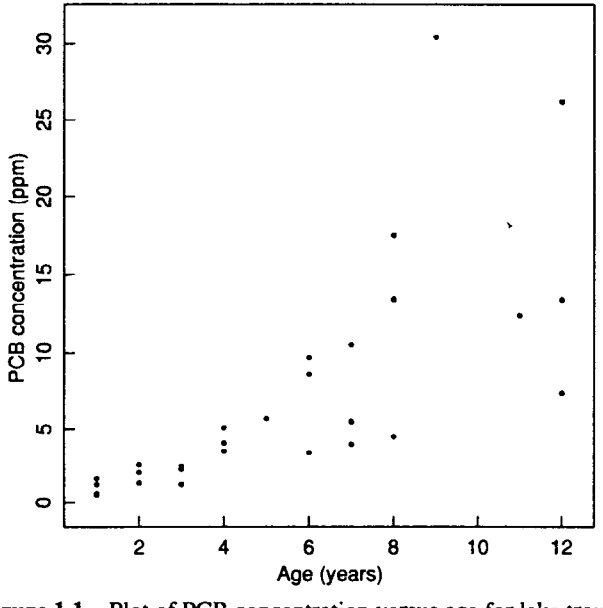

Figure 1.1 Plot of PCB concentration versus age for lake trout.

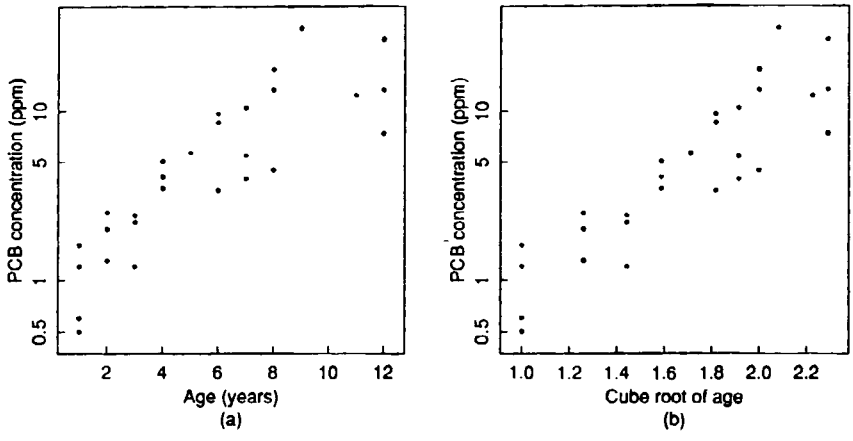

Figure 1.2 Plot of PCB concentration versus age for lake trout. The concentration, on a logarithmic scale, is plotted versus age in part *a* and versus $\sqrt[3]{\text{age}}$ in part *b*.

$$\ln(\text{PCB}) = \beta_1 + \beta_2\sqrt[3]{\text{age}}$$

(Note that the methods of Chapter 2 can be used to fit models of the form

$$f(\mathbf{x},\boldsymbol{\beta},\boldsymbol{\alpha}) = \beta_0 + \beta_1 x_1^{\alpha_1} + \beta_2 x_2^{\alpha_2} + \cdots + \beta_P x_P^{\alpha_P}$$

by simultaneously estimating the conditionally linear parameters $\boldsymbol{\beta}$ and the transformation parameters $\boldsymbol{\alpha}$. The powers $\alpha_1, \ldots, \alpha_P$ are used to transform the factors so that a simple linear model in $x_1^{\alpha_1}, \ldots, x_P^{\alpha_P}$ is appropriate. In this book we use the power $\alpha = 0.33$ for the age variable even though, for the PCB data, the optimal value is 0.20.) ■

1.1.1 The Least Squares Estimates

The *likelihood function*, or more simply, the *likelihood*, $l(\boldsymbol{\beta},\sigma \mid \mathbf{y})$, for $\boldsymbol{\beta}$ and σ is identical in form to the joint probability density (1.5) except that $l(\boldsymbol{\beta},\sigma \mid \mathbf{y})$ is regarded as a function of the parameters conditional on the observed data, rather than as a function of the responses conditional on the values of the parameters. Suppressing the constant $(2\pi)^{-N/2}$, we write

$$l(\boldsymbol{\beta},\sigma \mid \mathbf{y}) \propto \sigma^{-N} \exp\left[\frac{-\|\mathbf{y}-\mathbf{X}\boldsymbol{\beta}\|^2}{2\sigma^2}\right] \tag{1.6}$$

The likelihood is maximized with respect to $\boldsymbol{\beta}$ when the *residual sum of squares*

$$\begin{aligned} S(\boldsymbol{\beta}) &= \|\mathbf{y}-\mathbf{X}\boldsymbol{\beta}\|^2 \\ &= \sum_{n=1}^{N}\left[y_n - \left(\sum_{p=1}^{P} x_{np}\beta_p\right)\right]^2 \end{aligned} \tag{1.7}$$

is a minimum. Thus the *maximum likelihood estimate* $\hat{\boldsymbol{\beta}}$ is the value of $\boldsymbol{\beta}$ which minimizes $S(\boldsymbol{\beta})$. This $\hat{\boldsymbol{\beta}}$ is called the *least squares* estimate and can be written

$$\hat{\boldsymbol{\beta}} = (\mathbf{X}^T\mathbf{X})^{-1}\mathbf{X}^T\mathbf{y} \tag{1.8}$$

Least squares estimates can also be derived by using sampling theory, since the least squares estimator is the minimum variance unbiased estimator for $\boldsymbol{\beta}$, or by using a Bayesian approach with a noninformative prior density on $\boldsymbol{\beta}$ and σ. In the Bayesian approach, $\hat{\boldsymbol{\beta}}$ is the mode of the marginal posterior density function for $\boldsymbol{\beta}$.

All three of these methods of inference, the likelihood approach, the sampling theory approach, and the Bayesian approach, produce the same point estimates for $\boldsymbol{\beta}$. As we will see shortly, they also produce similar regions of "reasonable" parameter values. First, however, it is important to realize that the least squares estimates are only appropriate when the model (1.2) and the assumptions on the disturbance term, (1.3) and (1.4), are valid. Expressed in another way, in using the least squares estimates we assume:

(1) The expectation function is correct.
(2) The response is expectation function plus disturbance.
(3) The disturbance is independent of the expectation function.
(4) Each disturbance has a normal distribution.
(5) Each disturbance has zero mean.
(6) The disturbances have equal variances.
(7) The disturbances are independently distributed.

When these assumptions appear reasonable and have been checked using diagnostic plots such as those described in Section 1.3.2, we can go on to make further inferences about the regression model.

Looking in detail at each of the three methods of statistical inference, we can characterize some of the properties of the least squares estimates.

1.1.2 Sampling Theory Inference Results

The least squares estimator has a number of desirable properties as shown, for example, in Seber (1977):

(1) The least squares estimator $\hat{\boldsymbol{\beta}}$ is normally distributed. This follows because the estimator is a linear function of Y, which in turn is a linear function of Z. Since Z is assumed to be normally distributed, $\hat{\boldsymbol{\beta}}$ is normally distributed.

(2) $E[\hat{\boldsymbol{\beta}}] = \boldsymbol{\beta}$: the least squares estimator is unbiased.

(3) $\mathrm{Var}[\hat{\boldsymbol{\beta}}] = \sigma^2(\mathbf{X}^T\mathbf{X})^{-1}$: the covariance matrix of the least squares estimator depends on the variance of the disturbances and on the derivative matrix $\mathbf{X}$.

(4) A $1-\alpha$ *joint confidence region* for $\boldsymbol{\beta}$ is the ellipsoid

$$(\boldsymbol{\beta}-\hat{\boldsymbol{\beta}})^{\mathrm{T}}\,\mathbf{X}^{\mathrm{T}}\mathbf{X}(\boldsymbol{\beta}-\hat{\boldsymbol{\beta}}) \le Ps^2F(P, N-P;\alpha) \tag{1.9}$$

where

$$s^2 = \frac{S(\hat{\boldsymbol{\beta}})}{N-P}$$

is the *residual mean square* or *variance estimate* based on $N-P$ *degrees of freedom*, and $F(P, N-P;\alpha)$ is the upper α quantile for Fisher's F distribution with P and $N-P$ degrees of freedom.

(5) A $1-\alpha$ *marginal confidence interval* for the parameter β_p is

$$\hat{\beta}_p \pm \mathrm{se}(\hat{\beta}_p)\, t(N-P;\alpha/2) \tag{1.10}$$

where $t(N-P;\alpha/2)$ is the upper $\alpha/2$ quantile for Student's T distribution with $N-P$ degrees of freedom and the standard error of the parameter estimator is

$$\mathrm{se}(\hat{\beta}_p) = s\sqrt{\{(\mathbf{X}^{\mathrm{T}}\mathbf{X})^{-1}\}_{pp}} \tag{1.11}$$

with $\{(\mathbf{X}^{\mathrm{T}}\mathbf{X})^{-1}\}_{pp}$ equal to the pth diagonal term of the matrix $(\mathbf{X}^{\mathrm{T}}\mathbf{X})^{-1}$.

(6) A $1-\alpha$ confidence interval for the expected response at $\mathbf{x}_0$ is

$$\mathbf{x}_0^{\mathrm{T}}\hat{\boldsymbol{\beta}} \pm s\sqrt{\mathbf{x}_0^{\mathrm{T}}(\mathbf{X}^{\mathrm{T}}\mathbf{X})^{-1}\mathbf{x}_0}\;\; t(N-P;\alpha/2) \tag{1.12}$$

(7) A $1-\alpha$ confidence band for the response function at any $\mathbf{x}$ is given by

$$\mathbf{x}^{\mathrm{T}}\hat{\boldsymbol{\beta}} \pm s\sqrt{\mathbf{x}^{\mathrm{T}}(\mathbf{X}^{\mathrm{T}}\mathbf{X})^{-1}\mathbf{x}}\;\; \sqrt{P\,F(P, N-P;\alpha)} \tag{1.13}$$

The expressions (1.12) and (1.13) differ because (1.12) concerns an interval at a single specific point, whereas (1.13) concerns the band produced by the intervals at all the values of $\mathbf{x}$ considered simultaneously.

1.1.3 Likelihood Inference Results

The likelihood $l(\boldsymbol{\beta},\sigma\,|\,\mathbf{y})$, equation (1.6), depends on $\boldsymbol{\beta}$ only through $\|\mathbf{y}-\mathbf{X}\boldsymbol{\beta}\|$, so likelihood contours are of the form

$$\|\mathbf{y}-\mathbf{X}\boldsymbol{\beta}\|^2 = c \tag{1.14}$$

where c is a constant. A likelihood region bounded by the contour for which

$$c = S(\hat{\boldsymbol{\beta}})\left[1+\frac{P}{N-P}F(P, N-P;\alpha)\right]$$

is identical to a $1-\alpha$ joint confidence region from the sampling theory approach. The interpretation of a likelihood region is quite different from that of a

confidence region, however.

1.1.4 Bayesian Inference Results

As shown in Box and Tiao (1973), the Bayesian marginal posterior density for $\boldsymbol{\beta}$, assuming a noninformative prior density for $\boldsymbol{\beta}$ and σ of the form

$$p(\boldsymbol{\beta}, \sigma) \propto \sigma^{-1} \tag{1.15}$$

is

$$p(\boldsymbol{\beta} \mid \mathbf{y}) \propto \left\{ 1 + \frac{(\boldsymbol{\beta} - \hat{\boldsymbol{\beta}})^{\mathrm{T}} \mathbf{X}^{\mathrm{T}} \mathbf{X} (\boldsymbol{\beta} - \hat{\boldsymbol{\beta}})}{\nu s^2} \right\}^{-(\nu+P)/2} \tag{1.16}$$

which is in the form of a P-variate Student's T density with *location parameter* $\hat{\boldsymbol{\beta}}$, *scaling matrix* $s^2(\mathbf{X}^{\mathrm{T}}\mathbf{X})^{-1}$, and $\nu = N - P$ degrees of freedom. Furthermore, the marginal posterior density for a single parameter β_p, say, is a univariate Student's T density with location parameter $\hat{\beta}_p$, scale parameter $s^2\{(\mathbf{X}^{\mathrm{T}}\mathbf{X})^{-1}\}_{pp}$, and degrees of freedom $N-P$. The marginal posterior density for the mean of y at $\mathbf{x}_0$ is a univariate Student's T density with location parameter $\mathbf{x}_0^{\mathrm{T}}\hat{\boldsymbol{\beta}}$, scale parameter $s^2\mathbf{x}_0^{\mathrm{T}}(\mathbf{X}^{\mathrm{T}}\mathbf{X})^{-1}\mathbf{x}_0$, and degrees of freedom $N-P$.

A *highest posterior density* (HPD) region of content $1-\alpha$ is defined (Box and Tiao, 1973) as a region R in the parameter space such that $\Pr\{\boldsymbol{\beta} \in \mathrm{R}\} = 1-\alpha$ and, for $\boldsymbol{\beta}_1 \in \mathrm{R}$ and $\boldsymbol{\beta}_2 \notin \mathrm{R}$, $p(\boldsymbol{\beta}_1 \mid \mathbf{y}) \geq p(\boldsymbol{\beta}_2 \mid \mathbf{y})$. For linear models with a noninformative prior, an HPD region is therefore given by the ellipsoid defined in (1.9). Similarly, the marginal HPD regions for β_p and $\mathbf{x}_0^{\mathrm{T}}\boldsymbol{\beta}$ are numerically identical to the sampling theory regions (1.10, 1.12, and 1.13).

1.1.5 Comments

Although the three approaches to statistical inference differ considerably, they lead to essentially identical inferences. In particular, since the joint confidence, likelihood, and Bayesian HPD regions are identical, we refer to them all as *inference regions*.

In addition, when referring to standard errors or correlations, we will use the Bayesian term "the standard error of β_p" when, for the sampling theory or likelihood methods, we should more properly say "the standard error of the estimate of β_p."

For linear least squares, any of the approaches can be used. For nonlinear least squares, however, the likelihood approach has the simplest and most direct geometrical interpretation, and so we emphasize it.

Example: PCB 2

The PCB data can be used to determine parameter estimates and joint and marginal inference regions. In this linear situation, the regions can be summarized using $\hat{\boldsymbol{\beta}}$, s^2, $\mathbf{X}^T\mathbf{X}$, and $\nu = N - P$. For the ln(PCB) data with $\sqrt[3]{\text{age}}$ as the regressor, we have $\hat{\boldsymbol{\beta}} = (-2.391, 2.300)^T$, $s^2 = 0.246$ on $\nu = 26$ degrees of freedom, and

$$\mathbf{X}^T\mathbf{X} = \begin{bmatrix} 28.000 & 46.941 \\ 46.941 & 83.367 \end{bmatrix}$$

$$(\mathbf{X}^T\mathbf{X})^{-1} = \begin{bmatrix} 0.6374 & -0.3589 \\ -0.3589 & 0.2141 \end{bmatrix}$$

The joint 95% inference region is then

$$28.00\,(\beta_1 + 2.391)^2 + 93.88\,(\beta_1 + 2.391)\,(\beta_2 - 2.300) + 83.37\,(\beta_2 - 2.300)^2 = 2\,(0.246)\,3.37 = 1.66$$

the marginal 95% inference interval for the parameter β_1 is

$$-2.391 \pm (0.496)\sqrt{0.6374}\;(2.056)$$

or

$$-3.21 \le \beta_1 \le -1.58$$

and the marginal 95% inference interval for the parameter β_2 is

$$2.300 \pm (0.496)\sqrt{0.2141}\;(2.056)$$

or

$$1.83 \le \beta_2 \le 2.77$$

The 95% inference band for the ln(PCB) value at any $\sqrt[3]{\text{age}} = x$, is

$$-2.391 + 2.300x \pm (0.496)\sqrt{0.637 - 0.718x + 0.214x^2}\;\sqrt{2\,(3.37)}$$

These regions are plotted in Figure 1.3. ■

While it is possible to give formal expressions for the least squares estimators and the regression summary quantities in terms of the matrices $\mathbf{X}^T\mathbf{X}$ and $(\mathbf{X}^T\mathbf{X})^{-1}$, the use of these matrices for computing the estimates is not recommended. Superior computing methods are presented in Section 1.2.2.

Finally, the assumptions which lead to the use of the least squares estimates should always be examined when using a regression model. Further discussion on assumptions and their implications is given in Section 1.3.

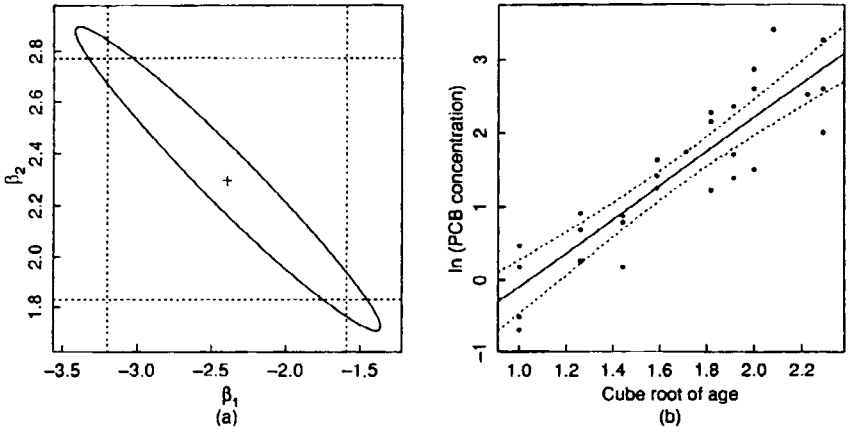

Figure 1.3 Inference regions for the model $\ln(\text{PCB}) = \beta_1 + \beta_2\sqrt[3]{\text{age}}$. Part *a* shows the least squares estimates (+), the parameter joint 95% inference region (solid line), and the marginal 95% inference intervals (dotted lines). Part *b* shows the fitted response (solid line) and the 95% inference band (dotted lines).

1.2 The Geometry of Linear Least Squares

The model (1.2) and assumptions (1.3) and (1.4) lead to the use of the least squares estimate (1.8) which minimizes the residual sum of squares (1.7). As implied by (1.7), $S(\boldsymbol{\beta})$ can be regarded as the square of the distance from the data vector $\mathbf{y}$ to the expected response vector $\mathbf{X}\boldsymbol{\beta}$. This links the subject of linear regression to Euclidean geometry and linear algebra. The assumption of a normally distributed disturbance term satisfying (1.3) and (1.4) indicates that the appropriate scale for measuring the distance between $\mathbf{y}$ and $\mathbf{X}\boldsymbol{\beta}$ is the usual Euclidean distance between vectors. In this way the Euclidean geometry of the N-dimensional response space becomes statistically meaningful. This connection between geometry and statistics is exemplified by the use of the term *spherical normal* for the normal distribution with the assumptions (1.3) and (1.4), because then contours of constant probability are spheres.

Note that when we speak of the linear form of the expectation function $\mathbf{X}\boldsymbol{\beta}$, we are regarding it as a function of the parameters $\boldsymbol{\beta}$, and that when determining parameter estimates we are only concerned with how the expected response depends on the *parameters*, not with how it depends on the *variables*. In the PCB example we fit the response to $\sqrt[3]{\text{age}}$ using linear least squares because the parameters $\boldsymbol{\beta}$ enter the model linearly.

1.2.1 The Expectation Surface

The process of calculating $S(\boldsymbol{\beta})$ involves two steps:

(1) Using the P-dimensional parameter vector $\boldsymbol{\beta}$ and the $N \times P$ derivative matrix $\mathbf{X}$ to obtain the N-dimensional *expected response vector* $\boldsymbol{\eta}(\boldsymbol{\beta}) = \mathbf{X}\boldsymbol{\beta}$ and

(2) Calculating the squared distance from $\boldsymbol{\eta}(\boldsymbol{\beta})$ to the observed response $\mathbf{y}$, $\| \mathbf{y} - \boldsymbol{\eta}(\boldsymbol{\beta}) \|^2$.

The possible expected response vectors $\boldsymbol{\eta}(\boldsymbol{\beta})$ form a P-dimensional *expectation surface* in the N-dimensional response space. This surface is a linear subspace of the response space, so we call it the *expectation plane* when dealing with a linear model.

Example: PCB 3

To illustrate the geometry of the expectation surface, consider just three cases from the ln(PCB) versus $\sqrt[3]{\text{age}}$ data.

$\sqrt[3]{\text{age}}$	ln(PCB)
1.26	0.92
1.82	2.15
2.22	2.52

The matrix $\mathbf{X}$ is then

$$\mathbf{X} = \begin{bmatrix} 1 & 1.26 \\ 1 & 1.82 \\ 1 & 2.22 \end{bmatrix}$$

which consists of two column vectors $\mathbf{x}_1 = (1, 1, 1)^T$ and $\mathbf{x}_2 = (1.26, 1.82, 2.22)^T$. These two vectors in the 3-dimensional response space are shown in Figure 1.4*b*, and correspond to the points $\boldsymbol{\beta} = (1, 0)^T$ and $\boldsymbol{\beta} = (0, 1)^T$ in the parameter plane, shown in Figure 1.4*a*. The expectation function $\boldsymbol{\eta}(\boldsymbol{\beta}) = \mathbf{X}\boldsymbol{\beta}$ defines a 2-dimensional expectation plane in the 3-dimensional response space. This is shown in Figure 1.4*c*, where the parameter lines corresponding to the lines $\beta_1 = -3, \ldots, 5$ and $\beta_2 = -2, \ldots, 2$, shown in Figure 1.4*a*, are given. A parameter line is associated with the parameter which is varying so the lines corresponding to $\beta_1 = -3, \ldots, 5$ (dot–dashed lines) are called β_2 lines.

Note that the parameter lines in the parameter plane are straight, parallel, and equispaced, and that their images on the expectation plane are also straight, parallel, and equispaced. Because the vector $\mathbf{x}_1$ is shorter than $\mathbf{x}_2$ ($\| \mathbf{x}_1 \| = \sqrt{3}$ while $\| \mathbf{x}_2 \| = \sqrt{9.83}$), the spacing between the lines of constant β_1 on the expectation plane is less than that between the lines of constant β_2. Also, the vectors $\mathbf{x}_1$ and $\mathbf{x}_2$ are not orthogonal. The angle ω between them can be calculated from

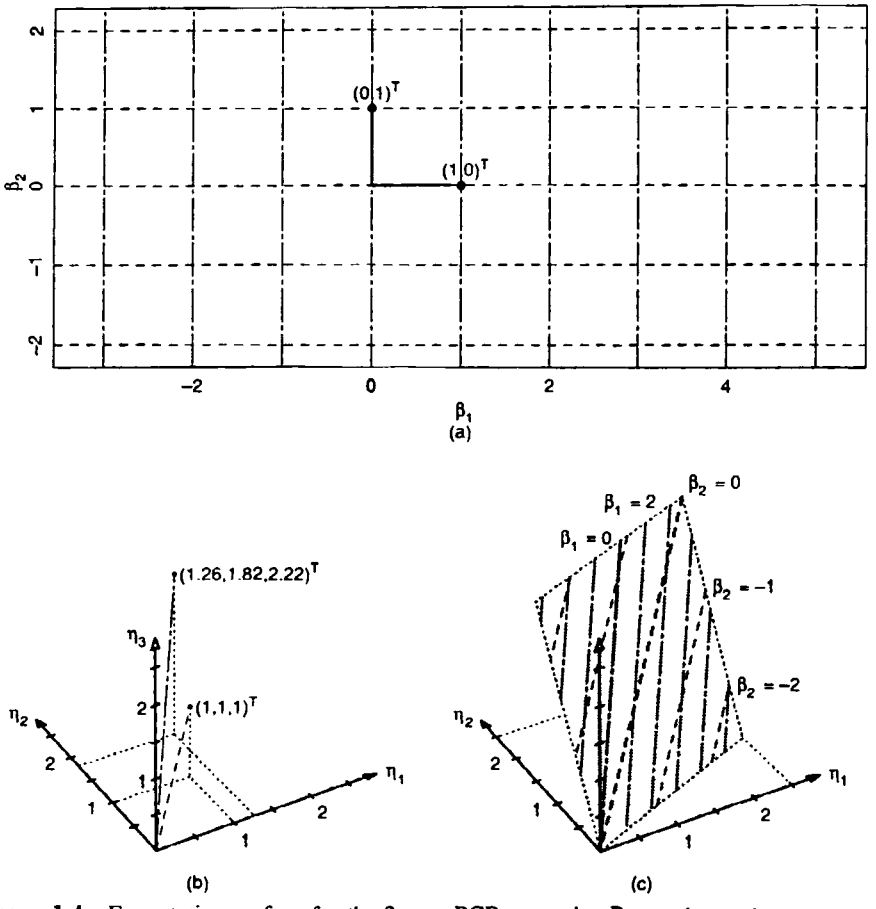

Figure 1.4 Expectation surface for the 3-case PCB example. Part *a* shows the parameter plane with β_1 parameter lines (dashed) and β_2 parameter lines (dot–dashed). Part *b* shows the vectors $\mathbf{x}_1$ (dashed line) and $\mathbf{x}_2$ (dot–dashed line) in the response space. The end points of the vectors correspond to $\boldsymbol{\beta}=(1,0)^T$ and $\boldsymbol{\beta}=(0,1)^T$ respectively. Part *c* shows a portion of the expectation plane (shaded) in the response space, with β_1 parameter lines (dashed) and β_2 parameter lines (dot–dashed).

$$\cos\omega = \frac{\mathbf{x}_1^T\mathbf{x}_2}{\|\mathbf{x}_1\|\ \|\mathbf{x}_2\|}$$

$$= \frac{5.30}{\sqrt{(3)(9.83)}}$$

$$= 0.98$$

to be about 11°, so the parameter lines on the expectation plane are not at

right angles as they are on the parameter plane.

As a consequence of the unequal length and nonorthogonality of the vectors, unit squares on the parameter plane map to parallelograms on the expectation plane. The area of the parallelogram is

$$\begin{aligned} \|\mathbf{x}_1\| \, \|\mathbf{x}_2\| \sin\omega &= \|\mathbf{x}_1\| \, \|\mathbf{x}_2\| \sqrt{1-\cos^2\omega} \\ &= \sqrt{(\mathbf{x}_1^T\mathbf{x}_1)(\mathbf{x}_2^T\mathbf{x}_2)-(\mathbf{x}_1^T\mathbf{x}_2)^2} \\ &= \sqrt{|\mathbf{X}^T\mathbf{X}|} \end{aligned} \tag{1.17}$$

That is, the *Jacobian determinant* of the transformation from the parameter plane to the expectation plane is a constant equal to $|\mathbf{X}^T\mathbf{X}|^{1/2}$. Conversely, the ratio of areas in the parameter plane to those on the expectation plane is $|\mathbf{X}^T\mathbf{X}|^{-1/2}$. ■

The simple linear mapping seen in the above example is true for all linear regression models. That is, for linear models, straight parallel equispaced lines in the parameter space map to straight parallel equispaced lines on the expectation plane in the response space. Consequently, rectangles in one plane map to parallelepipeds in the other plane, and circles or spheres in one plane map to ellipses or ellipsoids in the other plane. Furthermore, the Jacobian determinant, $|\mathbf{X}^T\mathbf{X}|^{1/2}$, is a constant for linear models, and so regions of fixed size in one plane map to regions of fixed size in the other, no matter where they are on the plane. These properties, which make linear least squares especially simple, are discussed further in Section 1.2.3.

1.2.2 Determining the Least Squares Estimates

The geometric representation of linear least squares allows us to formulate a very simple scheme for determining the parameters estimates $\hat{\boldsymbol{\beta}}$. Since the expectation surface is linear, all we must do to determine the point on the surface which is closest to the point $\mathbf{y}$, is to project $\mathbf{y}$ onto the expectation plane. This gives us $\hat{\boldsymbol{\eta}}$, and $\hat{\boldsymbol{\beta}}$ is then simply the value of $\boldsymbol{\beta}$ corresponding to $\hat{\boldsymbol{\eta}}$.

One approach to defining this projection is to observe that, after the projection, the residual vector $\mathbf{y}-\hat{\boldsymbol{\eta}}$ will be *orthogonal*, or *normal*, to the expectation plane. Equivalently, the residual vector must be orthogonal to all the columns of the $\mathbf{X}$ matrix, so

$$\mathbf{X}^T(\mathbf{y}-\mathbf{X}\hat{\boldsymbol{\beta}}) = \mathbf{0}$$

which is to say that the least squares estimate $\hat{\boldsymbol{\beta}}$ satisfies the *normal equations*

$$\mathbf{X}^T\mathbf{X}\hat{\boldsymbol{\beta}} = \mathbf{X}^T\mathbf{y} \tag{1.18}$$

Because of (1.18) the least squares estimates are often written $\hat{\boldsymbol{\beta}} = (\mathbf{X}^T\mathbf{X})^{-1}\mathbf{X}^T\mathbf{y}$ as in (1.8). However, another way of expressing the estimate, and a more stable way of computing it, involves decomposing $\mathbf{X}$ into the pro-

duct of an orthogonal matrix and an easily inverted matrix. Two such decompositions are the *QR* decomposition and the singular value decomposition (Dongarra et al., 1979, Chapters 9 and 11). We use the *QR* decomposition, where

$$\mathbf{X} = \mathbf{QR}$$

with the $N \times N$ matrix $\mathbf{Q}$ and the $N \times P$ matrix $\mathbf{R}$ constructed so that $\mathbf{Q}$ is orthogonal (that is, $\mathbf{Q}^T\mathbf{Q} = \mathbf{QQ}^T = \mathbf{I}$) and $\mathbf{R}$ is zero below the main diagonal. Writing

$$\mathbf{R} = \begin{bmatrix} \mathbf{R}_1 \\ \mathbf{0} \end{bmatrix}$$

where $\mathbf{R}_1$ is $P \times P$ and upper triangular, and

$$\mathbf{Q} = [\mathbf{Q}_1 \mid \mathbf{Q}_2]$$

with $\mathbf{Q}_1$ the first P columns and $\mathbf{Q}_2$ the last $N-P$ columns of $\mathbf{Q}$, we have

$$\mathbf{X} = \mathbf{QR} = \mathbf{Q}_1\mathbf{R}_1 \tag{1.19}$$

Performing a *QR* decomposition is straightforward, as is shown in Appendix 2.

Geometrically, the columns of $\mathbf{Q}$ define an *orthonormal*, or *orthogonal*, basis for the response space with the property that the first P columns span the expectation plane. Projection onto the expectation plane is then very easy if we work in the coordinate system given by $\mathbf{Q}$. For example we transform the response vector to

$$\mathbf{w} = \mathbf{Q}^T\mathbf{y} \tag{1.20}$$

with components

$$\mathbf{w}_1 = \mathbf{Q}_1^T\mathbf{y} \tag{1.21}$$

and

$$\mathbf{w}_2 = \mathbf{Q}_2^T\mathbf{y} \tag{1.22}$$

The projection of $\mathbf{w}$ onto the expectation plane is then simply

$$\begin{bmatrix} \mathbf{w}_1 \\ \mathbf{0} \end{bmatrix}$$

in the $\mathbf{Q}$ coordinates and

$$\hat{\boldsymbol{\eta}} = \mathbf{Q}\begin{bmatrix} \mathbf{w}_1 \\ \mathbf{0} \end{bmatrix} = \mathbf{Q}_1\mathbf{w}_1 \tag{1.23}$$

in the original coordinates.

Example: PCB 4

As shown in Appendix 2, the QR decomposition (1.19) of the matrix

$$\mathbf{X} = \begin{bmatrix} 1 & 1.26 \\ 1 & 1.82 \\ 1 & 2.22 \end{bmatrix}$$

for the 3-case PCB example is

$$\begin{bmatrix} 0.5774 & -0.7409 & 0.3432 \\ 0.5774 & 0.0732 & -0.8132 \\ 0.5774 & 0.6677 & 0.4700 \end{bmatrix} \begin{bmatrix} 1.7321 & 3.0600 \\ 0 & 0.6820 \\ 0 & 0 \end{bmatrix}$$

which gives [equation (1.20)]

$$\mathbf{w} = \begin{bmatrix} 3.23 \\ 1.16 \\ -0.24 \end{bmatrix}$$

In Figure 1.5a we show the expectation plane and observation vector in the original coordinate system. We also show the vectors $\mathbf{q}_1, \mathbf{q}_2, \mathbf{q}_3$, which are the columns of $\mathbf{Q}$. It can be seen that $\mathbf{q}_1$ and $\mathbf{q}_2$ lie in the expectation plane and $\mathbf{q}_3$ is orthogonal to it. In Figure 1.5b we show, in the transformed

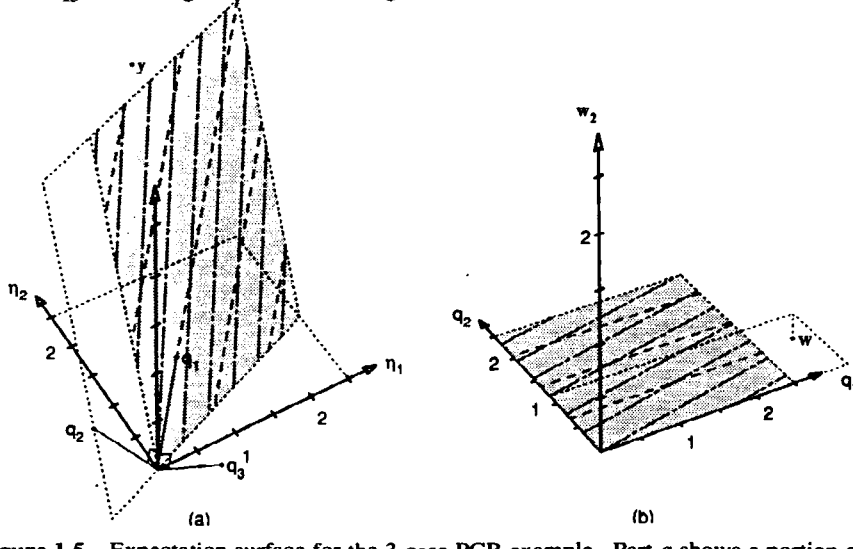

Figure 1.5 Expectation surface for the 3-case PCB example. Part a shows a portion of the expectation plane (shaded) in the response space with β_1 parameter lines (dashed) and β_2 parameter lines (dot–dashed) together with the response vector $\mathbf{y}$. Also shown are the orthogonal unit vectors $\mathbf{q}_1$ and $\mathbf{q}_2$ in the expectation plane, and $\mathbf{q}_3$ orthogonal to the plane. Part b shows the response vector $\mathbf{w}$, and a portion of the expectation plane (shaded) in the rotated coordinates given by $\mathbf{Q}$.

coordinates, the observation vector and the expectation plane, which is now horizontal. Note that projecting $\mathbf{w}$ onto the expectation plane is especially simple, since it merely requires replacing the last element in $\mathbf{w}$ by zero. ■

To determine the least squares estimate we must find the value $\hat{\boldsymbol{\beta}}$ corresponding to $\hat{\boldsymbol{\eta}}$. Since

$$\hat{\boldsymbol{\eta}} = \mathbf{X}\hat{\boldsymbol{\beta}}$$

using (1.23) and (1.19)

$$\mathbf{R}_1\hat{\boldsymbol{\beta}} = \mathbf{w}_1 \tag{1.24}$$

and we solve for $\hat{\boldsymbol{\beta}}$ by back-substitution (Stewart, 1973).

Example: PCB 5

For the complete ln(PCB), $\sqrt[3]{\text{age}}$ data set,

$$\mathbf{R}_1 = \begin{bmatrix} 5.29150 & 8.87105 \\ 0 & 2.16134 \end{bmatrix}$$

and $\mathbf{w}_1 = (7.7570, 4.9721)^{\mathrm{T}}$, so $\hat{\boldsymbol{\beta}} = (-2.391, 2.300)^{\mathrm{T}}$. ■

1.2.3 Parameter Inference Regions

Just as the least squares estimates have informative geometric interpretations, so do the parameter inference regions (1.9), (1.10), (1.14) and those derived from (1.16). Such interpretations are helpful for understanding linear regression, and are essential for understanding nonlinear regression. (The geometric interpretation is less helpful in the Bayesian approach, so we discuss only the sampling theory and likelihood approaches.)

The main difference between the likelihood and sampling theory geometric interpretations is that the likelihood approach centers on the point $\mathbf{y}$ and the length of the residual vector at $\boldsymbol{\eta}(\boldsymbol{\beta})$ compared to the shortest residual vector, while the sampling theory approach focuses on possible values of $\boldsymbol{\eta}(\boldsymbol{\beta})$ and the angle that the resulting residual vectors could make with the expectation plane.

1.2.3.1 The Geometry of Sampling Theory Results

To develop the geometric basis of linear regression results from the sampling theory approach, we transform to the $\mathbf{Q}$ coordinate system. The model for the random variable $\boldsymbol{W} = \mathbf{Q}^{\mathrm{T}}\boldsymbol{Y}$ is

$$\boldsymbol{W} = \mathbf{R}\boldsymbol{\beta} + \mathbf{Q}^{\mathrm{T}}\boldsymbol{Z}$$

or

$$\boldsymbol{U} = \boldsymbol{W} - \mathbf{R}\boldsymbol{\beta} \tag{1.25}$$

where $U = \mathbf{Q}^{\mathrm{T}}\mathbf{Z}$.

The spherical normal distribution of Z is not affected by the orthogonal transformation, so U also has a spherical normal distribution. This can be established on the basis of the geometry, since the spherical probability contours will not be changed by a rigid rotation or reflection, which is what an orthogonal transformation must be. Alternatively, this can be established analytically because $\mathbf{Q}^{\mathrm{T}}\mathbf{Q} = \mathbf{I}$, so the determinant of $\mathbf{Q}$ is ± 1 and $\|\mathbf{Qx}\| = \|\mathbf{x}\|$ for any N-vector $\mathbf{x}$. Now the joint density for the random variables $\mathbf{Z} = (Z_1, \ldots, Z_n)^{\mathrm{T}}$ is

$$p_{\mathbf{Z}}(\mathbf{z}) = (2\pi\sigma^2)^{-N/2}\exp\left[\frac{-\mathbf{z}^{\mathrm{T}}\mathbf{z}}{2\sigma^2}\right]$$

and, after transformation, the joint density for $U = \mathbf{Q}^{\mathrm{T}}\mathbf{Z}$ is

$$p_U(\mathbf{u}) = (2\pi\sigma^2)^{-N/2}\,|\mathbf{Q}|\exp\left[\frac{-\mathbf{u}^{\mathrm{T}}\mathbf{Q}^{\mathrm{T}}\mathbf{Q}\mathbf{u}}{2\sigma^2}\right]$$

$$= (2\pi\sigma^2)^{-N/2}\exp\left[\frac{-\mathbf{u}^{\mathrm{T}}\mathbf{u}}{2\sigma^2}\right]$$

From (1.25), the form of $\mathbf{R}$ leads us to partition U into two components:

$$U = \begin{bmatrix} U_1 \\ U_2 \end{bmatrix}$$

where U_1 consists of the first P elements of U, and U_2 the remaining $N-P$ elements. Each of these components has a spherical normal distribution of the appropriate dimension. Furthermore, independence of elements in the original disturbance vector Z leads to independence of the elements of U, so the components U_1 and U_2 are independent.

The dimensions ν_i of the components U_i, called the *degrees of freedom*, are $\nu_1 = P$ and $\nu_2 = N-P$. The sum of squares of the coordinates of a ν-dimensional spherical normal vector has a $\sigma^2\chi^2$ distribution on ν degrees of freedom, so

$$\|U_1\|^2 \sim \sigma^2\chi^2_P$$

$$\|U_2\|^2 \sim \sigma^2\chi^2_{N-P}$$

where the symbol $\sim$ is read "is distributed as." Using the independence of U_1 and U_2, we have

$$\frac{\|U_1\|^2/P}{\|U_2\|^2/(N-P)} \sim F(P, N-P; \alpha) \tag{1.26}$$

since the scaled ratio of two independent χ^2 random variables is distributed as Fisher's F distribution.

The distribution (1.26) gives a reference distribution for the ratio of the squared component lengths or, equivalently, for the angle that the disturbance

vector makes with the horizontal plane. We may therefore use (1.25) and (1.26) to test the hypothesis that $\boldsymbol{\beta}$ equals some specific value, say $\boldsymbol{\beta}^0$, by calculating the residual vector $\mathbf{u}^0 = \mathbf{Q}^T\mathbf{y} - \mathbf{R}\boldsymbol{\beta}^0$ and comparing the lengths of the components $\mathbf{u}_1^0$ and $\mathbf{u}_2^0$ as in (1.26). The reasoning here is that a large $\|\mathbf{u}_1^0\|$ compared to $\|\mathbf{u}_2^0\|$ suggests that the vector $\mathbf{y}$ is not very likely to have been generated by the model (1.2) with $\boldsymbol{\beta} = \boldsymbol{\beta}^0$, since $\mathbf{u}^0$ has a suspiciously large component in the $\mathbf{Q}_1$ plane.

Note that

$$\frac{\|\mathbf{u}_2^0\|^2}{N-P} = \frac{S(\hat{\boldsymbol{\beta}})}{N-P} = s^2$$

and

$$\|\mathbf{u}_1^0\|^2 = \|\mathbf{R}_1\boldsymbol{\beta}^0 - \mathbf{w}_1\|^2 \tag{1.27}$$

and so the ratio (1.26) becomes

$$\frac{\|\mathbf{R}_1\boldsymbol{\beta}^0 - \mathbf{w}_1\|^2}{Ps^2} \tag{1.28}$$

Example: PCB 6

We illustrate the decomposition of the residual $\mathbf{u}$ for testing the null hypothesis

$$H_0 : \boldsymbol{\beta} = (-2.0, 2.0)^T$$

versus the alternative

$$H_A : \boldsymbol{\beta} \neq (-2.0, 2.0)^T$$

for the full PCB data set in Figure 1.6. Even though the rotated data vector $\mathbf{w}$ and the expectation surface for this example are in a 28-dimensional space, the relevant distances can be pictured in the 3-dimensional space spanned by the expectation surface (vectors $\mathbf{q}_1$ and $\mathbf{q}_2$) and the residual vector. The scaled lengths of the components $\mathbf{u}_1$ and $\mathbf{u}_2$ are compared to determine if the point $\boldsymbol{\beta}^0 = (-2.0, 2.0)^T$ is reasonable.

The numerator in (1.28) is

$$\left\| \begin{bmatrix} 5.29150 & 8.87105 \\ 0 & 2.16134 \end{bmatrix} \begin{bmatrix} -2.0 \\ 2.0 \end{bmatrix} - \begin{bmatrix} 7.7570 \\ 4.9721 \end{bmatrix} \right\|^2 = 0.882$$

The ratio is then $0.882/(2 \times 0.246) = 1.79$, which corresponds to a tail probability (or p value) of 0.19 for an F distribution with 2 and 26 degrees of freedom. Since the probability of obtaining a ratio at least as large as 1.79 is 19%, we do not reject the null hypothesis. ■

A $1-\alpha$ joint confidence region for the parameters $\boldsymbol{\beta}$ consists of all those values for which the above hypothesis test is not rejected at level α. Thus, a

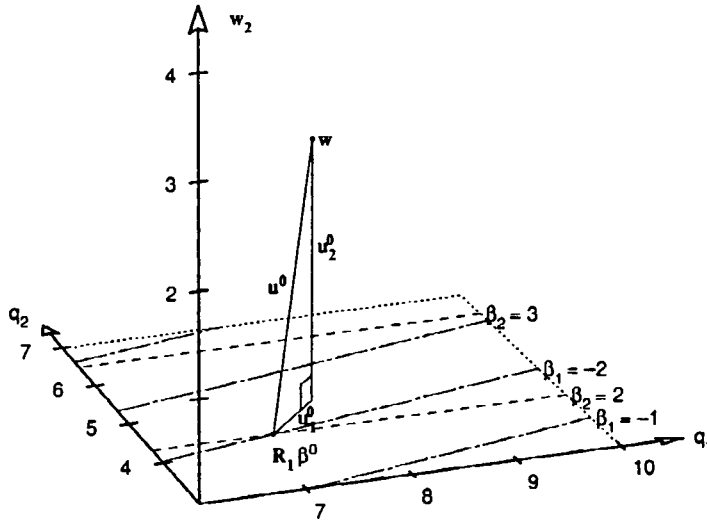

Figure 1.6 A geometric interpretation of the test $H_0 : \boldsymbol{\beta} = (-2.0, 2.0)^T$ for the full PCB data set. We show the projections of the response vector $\mathbf{w}$ and a portion of the expectation plane projected into the 3-dimensional space given by the tangent vectors $\mathbf{q}_1$ and $\mathbf{q}_2$, and the orthogonal component of the response vector, $\mathbf{w}_2$. For the test point $\boldsymbol{\beta}^0$, the residual vector $\mathbf{u}^0$ is decomposed into a tangential component $\mathbf{u}_1^0$ and an orthogonal component $\mathbf{u}_2^0$.

value $\boldsymbol{\beta}^0$ is within a $1-\alpha$ confidence region if

$$\frac{\| \mathbf{u}_1^0 \|^2 / P}{\| \mathbf{u}_2^0 \|^2 / (N-P)} \leq F(P, N-P; \alpha)$$

Since s^2 does not depend on $\boldsymbol{\beta}^0$, the points inside the confidence region form a disk on the expectation plane defined by

$$\| \mathbf{u}_1 \|^2 \leq P s^2 F(P, N-P; \alpha)$$

Furthermore, from (1.24) and (1.27) we have

$$\| \mathbf{u}_1 \|^2 = \| \mathbf{R}_1 (\boldsymbol{\beta} - \hat{\boldsymbol{\beta}}) \|^2$$

so a point on the boundary of the confidence region in the parameter space satisfies

$$\mathbf{R}_1 (\boldsymbol{\beta} - \hat{\boldsymbol{\beta}}) = \sqrt{P s^2 F(P, N-P; \alpha)}\ \mathbf{d}$$

where $\| \mathbf{d} \| = 1$. That is, the confidence region is given by

$$\{ \boldsymbol{\beta} = \hat{\boldsymbol{\beta}} + \sqrt{P s^2 F(P, N-P; \alpha)}\ \mathbf{R}_1^{-1} \mathbf{d} \mid \| \mathbf{d} \| = 1 \} \tag{1.29}$$

Thus the region of "reasonable" parameter values is a disk centered at $\mathbf{R}_1 \hat{\boldsymbol{\beta}}$ on the expectation plane and is an ellipse centered at $\hat{\boldsymbol{\beta}}$ in the parameter space.

Example: PCB 7

For the ln(PCB) versus $\sqrt[3]{\text{age}}$ data, $\hat{\boldsymbol{\beta}} = (-2.391, 2.300)^T$ and $s^2 = 0.246$ based on 26 degrees of freedom, so the 95% confidence disk on the transformed expectation surface is

$$\mathbf{R}_1\boldsymbol{\beta} = \begin{bmatrix} 7.7570 \\ 4.9721 \end{bmatrix} + 1.288 \begin{bmatrix} \cos\omega \\ \sin\omega \end{bmatrix}$$

where $0 \le \omega < 2\pi$. The disk is shown in the expectation plane in Figure 1.7*a*, and the corresponding ellipse

$$\boldsymbol{\beta} = \begin{bmatrix} -2.391 \\ 2.300 \end{bmatrix} + 1.288 \begin{bmatrix} 0.18898 & -0.77566 \\ 0 & 0.46268 \end{bmatrix} \begin{bmatrix} \cos\omega \\ \sin\omega \end{bmatrix}$$

is shown in the parameter plane in Figure 1.7*b*. ■

1.2.3.2 Marginal Confidence Intervals

We can create a marginal confidence interval for a single parameter, say β_1, by "inverting" a hypothesis test of the form

$$H_0: \beta_1 = \beta_1^0$$

versus

$$H_A: \beta_1 \neq \beta_1^0$$

Any β_1^0 for which H_0 is not rejected at level α is included in the $1-\alpha$

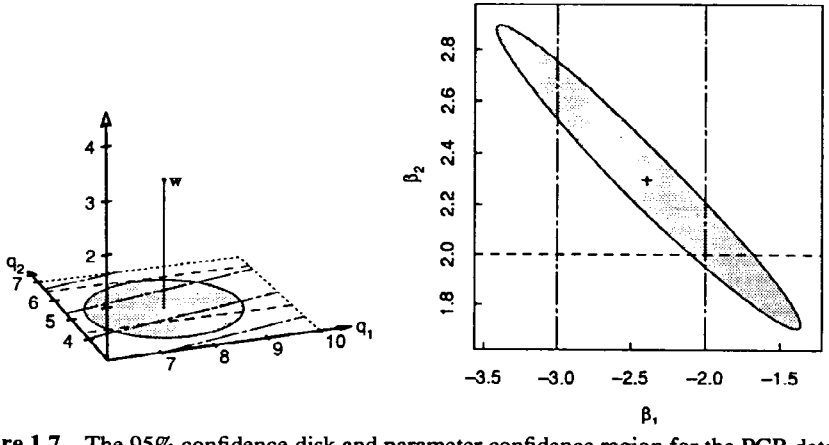

Figure 1.7 The 95% confidence disk and parameter confidence region for the PCB data. Part *a* shows the response vector **w** and a portion of the expectation plane projected into the 3-dimensional space given by the tangent vectors $\mathbf{q}_1$ and $\mathbf{q}_2$, and the orthogonal component of the response vector, $\mathbf{w}_2$. The 95% confidence disk (shaded) in the expectation plane (part *a*) maps to the elliptical confidence region (shaded) in the parameter plane (part *b*).

confidence interval. To perform the hypothesis test, we choose any parameter vector with $\beta_1 = \beta_1^0$, say $(\beta_1^0, \mathbf{0}^T)^T$, calculate the transformed residual vector $\mathbf{u}^0$, and divide it into three components: the first component $\mathbf{u}_1^0$ of dimension $P-1$ and parallel to the hyperplane defined by $\beta_1 = \beta_1^0$; the second component u_2^0 of dimension 1 and in the expectation plane but orthogonal to the β_1^0 hyperplane; and the third component $\mathbf{u}_3^0$ of length $(N-P)s^2$ and orthogonal to the expectation plane. The component u_2^0 is the same for any parameter $\boldsymbol{\beta}$ with $\beta_1 = \beta_1^0$, and, assuming that the true β_1 is β_1^0, the scaled ratio of the corresponding random variables U_2 and U_3 has the distribution

$$\frac{U_2^2/1}{\| U_3 \|^2/(N-P)} \sim F(1, N-P)$$

Thus we reject H_0 at level α if

$$(u_2^0)^2 > s^2 F(1, N-P; \alpha)$$

Example: PCB 8

To test the null hypothesis

$$H_0: \beta_1 = -2.0$$

versus the alternative

$$H_A: \beta_1 \neq -2.0$$

for the complete PCB data set, we decompose the transformed residual vector at $\boldsymbol{\beta}^0 = (-2.0, 2.2)^T$ into three components as shown in Figure 1.8 and calculate the ratio

$$\frac{(u_2^0)^2}{s^2} = \frac{0.240}{0.246}$$

$$= 0.97$$

This corresponds to a p value of 0.33, and so we do not reject the null hypothesis. ■

We can create a $1-\alpha$ marginal confidence interval for β_1 as all values for which

$$(u_2^0)^2 \leq s^2 F(1, N-P; \alpha)$$

or, equivalently,

$$|u_2^0| \leq s\, t(N-P; \alpha/2) \tag{1.30}$$

Since $|u_2^0|$ is the distance from the point $\mathbf{R}_1\hat{\boldsymbol{\beta}}$ to the line corresponding to $\beta_1 = \beta_1^0$ on the transformed parameter plane, the confidence interval will include all values β_1^0 for which the corresponding parameter line intersects the disk

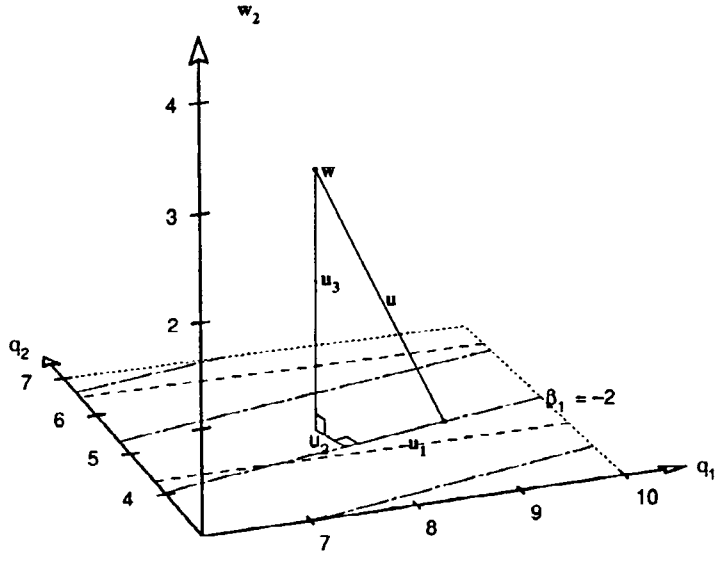

Figure 1.8 A geometric interpretation of the test $H_0 : \beta_1 = -2.0$ for the full PCB data set. We show the response vector $\mathbf{w}$, and a portion of the expectation plane projected into the 3-dimensional space given by the tangent vectors $\mathbf{q}_1$ and $\mathbf{q}_2$, and the orthogonal component of the response vector, $\mathbf{w}_2$. For a representative point on the line $\beta_1 = -2$ the residual vector $\mathbf{u}$ is decomposed into a tangential component $\mathbf{u}_1^0$ along the line, a tangential component u_2^0 perpendicular to the line, and an orthogonal component $\mathbf{u}_3^0$.

$$\{\mathbf{R}_1\hat{\boldsymbol{\beta}} + s\,t(N-P;\alpha/2)\,\mathbf{d} \mid \|\mathbf{d}\| = 1\} \tag{1.31}$$

Instead of determining the value of $|u_2^0|$ for each β_1^0, we take the disk (1.31) and determine the minimum and maximum values of β_1 for points on the disk. Writing $\mathbf{r}^1$ for the first row of $\mathbf{R}_1^{-1}$, the values of β_1 corresponding to points on the expectation plane disk are

$$\mathbf{r}^1(\mathbf{R}_1\hat{\boldsymbol{\beta}} + s\,t(N-P;\alpha/2)\,\mathbf{d}) = \hat{\beta}_1 + s\,t(N-P;\alpha/2)\,\mathbf{r}^1\mathbf{d}$$

and the minimum and maximum occur for the unit vectors in the direction of $\mathbf{r}^1$; that is, $\mathbf{d} = \pm\mathbf{r}^{1T}/\|\mathbf{r}^1\|$. This gives the confidence interval

$$\hat{\beta}_1 \pm s\,\|\mathbf{r}^1\|\,t(N-P;\alpha/2)$$

In general, a marginal confidence interval for parameter β_p is

$$\hat{\beta}_p \pm s\,\|\mathbf{r}^p\|\,t(N-P;\alpha/2) \tag{1.32}$$

where $\mathbf{r}^p$ is the pth row of $\mathbf{R}_1^{-1}$. The quantity

$$\mathrm{se}(\hat{\beta}_p) = s\,\|\mathbf{r}^p\| \tag{1.33}$$

is called the *standard error* for the pth parameter. Since

$$(\mathbf{X}^T\mathbf{X})^{-1} = (\mathbf{R}_1^T\mathbf{R}_1)^{-1}$$
$$= \mathbf{R}_1^{-1}\mathbf{R}_1^{-T}$$

$\| \mathbf{r}^p \|^2 = \{(\mathbf{X}^T\mathbf{X})^{-1}\}_{pp}$, so the standard error can be written as in equation (1.11).

A convenient summary of the variability of the parameter estimates can be obtained by factoring $\mathbf{R}_1^{-1}$ as

$$\mathbf{R}_1^{-1} = \text{diag}(\| \mathbf{r}^1 \|, \| \mathbf{r}^2 \|, \ldots, \| \mathbf{r}^p \|)\mathbf{L} \tag{1.34}$$

where $\mathbf{L}$ has unit length rows. The diagonal matrix provides the parameter standard errors, while the *correlation matrix*

$$\mathbf{C} = \mathbf{L}\mathbf{L}^T \tag{1.35}$$

gives the correlations between the parameter estimates.

Example: PCB 9

For the ln(PCB) data, $\hat{\boldsymbol{\beta}} = (-2.391, 2.300)^T$, $s^2 = 0.246$ with 26 degrees of freedom, and

$$\mathbf{R}_1^{-1} = \begin{bmatrix} 5.29150 & 8.87105 \\ 0 & 2.16134 \end{bmatrix}^{-1}$$
$$= \begin{bmatrix} 0.18898 & -0.77566 \\ 0 & 0.46268 \end{bmatrix}$$
$$= \begin{bmatrix} 0.798 & 0 \\ 0 & 0.463 \end{bmatrix} \begin{bmatrix} 0.237 & -0.972 \\ 0 & 1 \end{bmatrix}$$

which gives standard errors of $0.798\sqrt{0.246} = 0.396$ for β_1 and $0.463\sqrt{0.246} = 0.230$ for β_2. Also

$$\mathbf{C} = \begin{bmatrix} 1 & -0.972 \\ -0.972 & 1 \end{bmatrix}$$

so the correlation between β_1 and β_2 is -0.97. The 95% confidence intervals for the parameters are given by $-2.391 \pm 2.056(0.396)$ and $2.300 \pm 2.056(0.230)$, which are plotted in Figure 1.3*a*. ■

Marginal confidence intervals for the expected response at a design point $\mathbf{x}_0$ can be created by determining which hyperplanes formed by constant $\mathbf{x}_0^T\boldsymbol{\beta}$ intersect the disk (1.31). Using the same argument as was used to derive (1.32), we obtain a standard error for the expected response at $\mathbf{x}_0$ as $s \| \mathbf{x}_0^T\mathbf{R}_1^{-1} \|$, so the confidence interval is

$$\mathbf{x}_0^T\hat{\boldsymbol{\beta}} \pm s \| \mathbf{x}_0^T\mathbf{R}_1^{-1} \| \, t(N-P; \alpha/2) \tag{1.36}$$

Similarly, a confidence band for the response function is

$$\mathbf{x}^T\hat{\boldsymbol{\beta}} \pm s \, \| \mathbf{x}^T \mathbf{R}_1^{-1} \| \sqrt{P\,F(P, N-P; \alpha)} \tag{1.37}$$

Example: PCB 10

A plot of the fitted expectation function and the 95% confidence bands for the PCB example was given in Figure 1.3*b*. ■

Ansley (1985) gives derivations of other sampling theory results in linear regression using the *QR* decomposition, which, as we have seen, is closely related to the geometric approach to regression.

1.2.3.3 The Geometry of Likelihood Results

The likelihood function indicates the plausibility of values of $\boldsymbol{\eta}$ relative to $\mathbf{y}$, and consequently has a simple geometrical interpretation. If we allow $\boldsymbol{\eta}$ to take on any value in the N-dimensional response space, the likelihood contours are spheres centered on $\mathbf{y}$. Values of $\boldsymbol{\eta}$ of the form $\boldsymbol{\eta} = \mathbf{X}\boldsymbol{\beta}$ generate a P-dimensional expectation plane, and so the intersection of the plane with the likelihood spheres produces disks.

Analytically, the likelihood function (1.6) depends on $\boldsymbol{\eta}$ through

$$\begin{aligned} \| \boldsymbol{\eta} - \mathbf{y} \|^2 &= \| \mathbf{Q}^T(\boldsymbol{\eta} - \mathbf{y}) \|^2 \\ &= \| \mathbf{Q}_1^T(\boldsymbol{\eta} - \mathbf{y}) \|^2 + \| \mathbf{Q}_2^T(\boldsymbol{\eta} - \mathbf{y}) \|^2 \\ &= \| \mathbf{w}(\boldsymbol{\beta}) - \mathbf{w}_1 \|^2 + \| \mathbf{w}_2 \|^2 \end{aligned} \tag{1.38}$$

where $\mathbf{w}(\boldsymbol{\beta}) = \mathbf{Q}_1^T\boldsymbol{\eta}$ and $\mathbf{Q}_2^T\boldsymbol{\eta} = \mathbf{0}$. A constant value of the total sum of squares specifies a disk of the form

$$\| \mathbf{w}(\boldsymbol{\beta}) - \mathbf{w}_1 \|^2 = c$$

on the expectation plane. Choosing

$$c = Ps^2 F(P, N-P; \alpha)$$

produces the disk corresponding to a $1-\alpha$ confidence region. In terms of the total sum of squares, the contour is

$$S(\boldsymbol{\beta}) = S(\hat{\boldsymbol{\beta}}) \left\{ 1 + \frac{P}{N-P} F(P, N-P; \alpha) \right\} \tag{1.39}$$

As shown previously, and illustrated in Figure 1.7, this disk transforms to an ellipsoid in the parameter space.

1.3 Assumptions and Model Assessment

The statistical assumptions which lead to the use of the least squares estimates encompass several different aspects of the regression model. As with any sta-

tistical analysis, if the assumptions on the model and data are not appropriate, the results of the analysis will not be valid.

Since we cannot guarantee *a priori* that the different assumptions are all valid, we must proceed in an iterative fashion as described, for example, in Box, Hunter, and Hunter (1978). We entertain a plausible statistical model for the data, analyze the data using that model, then go back and use *diagnostics* such as plots of the residuals to assess the assumptions. If the diagnostics indicate failure of assumptions in either the deterministic or stochastic components of the model, we must modify the model or the analysis and repeat the cycle.

It is important to recognize that the design of the experiment and the method of data collection can affect the chances of assumptions being valid in a particular experiment. In particular *randomization* can be of great help in ensuring the appropriateness of all the assumptions, and *replication* allows greater ability to check the appropriateness of specific assumptions.

1.3.1 Assumptions and Their Implications

The assumptions, as listed in Section 1.1.1, are:

(1) *The expectation function is correct.* Ensuring the validity of this assumption is, to some extent, the goal of all science. We wish to build a model with which we can predict natural phenomena. It is in building the mathematical model for the expectation function that we frequently find ourselves in an iterative loop. We proceed as though the expectation function were correct, but we should be prepared to modify it as the data and the analyses dictate. In almost all linear, and in many nonlinear, regression situations we do not know the "true" model, but we choose a plausible one by examining the situation, looking at data plots and cross-correlations, and so on. As the analysis proceeds we can modify the expectation function and the assumptions about the disturbance term to obtain a more sensible and useful answer. Models should be treated as just models, and it must be recognized that some will be more appropriate or adequate than others. Nevertheless, assumption (1) is a strong one, since it implies that the expectation function includes all the important predictor variables in precisely the correct form, and that it does *not* include any unimportant predictor variables. A useful technique to enable checking the adequacy of a model function is to include replications in the experiment. It is also important to actually manipulate the predictor variables and randomize the order in which the experiments are done, to ensure that *causation*, not *correlation*, is being determined (Box, 1960).

(2) *The response is expectation function plus disturbance.* This assumption is important theoretically, since it allows the probability density function for the random variable Y describing the responses to be simply calculated from the probability density function for the random variable Z describing the disturbances. Thus,

$$p_Y(\mathbf{y} \mid \boldsymbol{\beta}, \sigma^2) = p_Z(\mathbf{y} - \mathbf{X}\boldsymbol{\beta} \mid \sigma^2)$$

In practice, this assumption is closely tied to the assumption of constant variance of the disturbances. It may be the case that the disturbances can be considered as having constant variance, but as entering the model multiplicatively, since in many phenomena, as the level of the "signal" increases, the level of the "noise" increases. This lack of additivity of the disturbance will manifest itself as a nonconstant variance in the diagnostic plots. In both cases, the corrective action is the same—either use weighted least squares or take a transformation of the response as was done in Example PCB 1.

(3) *The disturbance is independent of the expectation function.* This assumption is closely related to assumption (2), since they both relate to appropriateness of the additive model. One of the implications of this assumption is that the control or predictor variables are measured perfectly. Also, as a converse to the implication in assumption (1) that all important variables are included in the model, this assumption implies that *any important variables which are not included are not systematically related* to the response. An important technique to improve the chances that this is true is to randomize the order in which the experiments are done, as suggested by Fisher (1935). In this way, if an important variable has been omitted, its effect may be manifested as a disturbance (and hence simply inflate the variability of the observations) rather than being confounded with one of the predictor effects (and hence bias the parameter estimates). And, of course, it is important to actually manipulate the predictor variables not merely record their values.

(4) *Each disturbance has a normal distribution.* The assumption of normality of the disturbances is important, since this dictates the form of the sampling distribution of the random variables describing the responses, and through this, the likelihood function for the parameters. This leads to the criterion of least squares, which is enormously powerful because of its mathematical tractability. For example, given a linear model, it is possible to write down the analytic solution for the parameter estimators and to show [Gauss's theorem (Seber, 1977)] that the least squares estimates are the best *both individually and in any linear combination*, in the sense that they have the smallest mean square error of any linear estimators. The normality assumption can be justified by appealing to the central limit theorem, which states that the resultant of many disturbances, no one of which is dominant, will tend to be normally distributed. Since most experiments involve many operations to set up and measure the results, it is reasonable to assume, at least tentatively, that the disturbances will be normally distributed. Again, the assumption of normality will be more likely to be appropriate if the order of the experiments is randomized. The assumption of normality may be checked by examining the residuals.

(5) *Each disturbance has zero mean.* This assumption is primarily a simplifying one, which reduces the number of unknown parameters to a manageable level. Any nonzero mean common to all observations can be accommodated by introducing a constant term in the expectation function, so this assumption

is unimportant in linear regression. It can be important in nonlinear regression, however, where many expectation functions occur which do not include a constant. The main implication of this assumption is that there is no systematic bias in the disturbances such as could be caused by an unsuspected influential variable. Hence, we see again the value of randomization.

(6) *The disturbances have equal variances.* This assumption is more important practically than theoretically, since a solution exists for the least squares estimation problem for the case of unequal variances [see, e.g., Draper and Smith (1981) concerning weighted least squares]. Practically, however, one must describe how the variances vary, which can only be done by making further assumptions, or by using information from replications and incorporating this into the analysis through generalized least squares, or by transforming the data. When the variance is constant, the likelihood function is especially simple, since the parameters can be estimated independently of the nuisance parameter σ^2. The main implication of this assumption is that all data values are *equally unreliable*, and so the simple least squares criterion can be used. The appropriateness of this assumption can sometimes be checked after a model has been fitted by plotting the residuals versus the fitted values, but it is much better to have replications. With replications, we can check the assumption before even fitting a model, and can in fact use the replication averages and variances to determine a suitable *variance-stabilizing* transformation; see Section 1.3.2. Transforming to constant variance often has the additional effect of making the disturbances behave more normally. This is because a constant variance is necessarily independent of the mean (and anything else, for that matter), and this independence property is fundamental to the normal density.

(7) *The disturbances are distributed independently.* The final assumption is that the disturbances in different experiments are independent of one another. This is an enormously simplifying assumption, because then the joint probability density function for the vector $\boldsymbol{Y}$ is just the product of the probability densities for the individual random variables Y_n, $n = 1,2,\ldots,N$. The implication of this assumption is that the disturbances on separate runs are not systematically related, an assumption which can usually be made to be more appropriate by randomization. Nonindependent disturbances can be treated by generalized least squares, but, as in the case where there is nonconstant variance, modifications to the model must be made either through information gained from the data, or by additional assumptions as to the nature of the interdependence.

1.3.2 Model Assessment

In this subsection we present some simple methods for verifying the appropriateness of assumptions, especially through plots of residuals. Further discussion on regression diagnostics for linear models is given in Hocking (1983), and in the books by Belsley, Kuh, and Welsch (1980), Cook and Weisberg (1982), and Draper and Smith (1981). In Chapter 3 we discuss model assessment for non-

linear models.

1.3.2.1 Plotting Residuals

A simple, effective method for checking the adequacy of a model is to plot the *studentized residuals*, $\hat{z}_n / s\sqrt{1-h_{nn}}$, versus the predictor variables and any other possibly important "lurking" variables (Box, 1960; Joiner, 1981). The term h_{nn} is the nth diagonal term of the "hat" matrix $\mathbf{H} = \mathbf{X}(\mathbf{X}^T\mathbf{X})^{-1}\mathbf{X}^T = \mathbf{Q}_1\mathbf{Q}_1^T$, and $\hat{z}_n$ is the residual for the nth case,

$$\hat{z}_n = y_n - \hat{y}_n$$

A relationship between the residuals and any variable then suggests that there is an effect due to that variable which has not been accounted for. Features to look for include systematic linear or curvilinear behavior of the residuals with respect to a variable. Important common "lurking" variables include time or the order number of the experiment; if a plot of residuals versus time shows suspicious behavior, such as runs of residuals of the same sign, then the assumption of independence of the disturbances may be inappropriate.

Plotting residuals versus the fitted values $\hat{y}_n$ is also useful, since such plots can reveal outliers or general inadequacy in the form of the expectation function. It is also a very effective plot for revealing whether the assumption of constant variance is appropriate. The most common form of nonconstant variance is an increase in the variability in the responses when the level of the response changes. This behavior was noticed in the original PCB data. If a regression model is fitted to such data, the plot of the studentized residuals versus the fitted values tends to have a wedge-shaped pattern.

When residual plots or the data themselves give an indication of nonconstant variance, the estimation procedure should be modified. Possible changes include transforming the data as was done with the PCB data or using weighted least squares.

A quantile–quantile plot (Chambers et al., 1983) of the studentized residuals versus a normal distribution gives a direct check on the assumption of normality. If the expectation function is correct and the assumption of normality is appropriate, such a *normal probability plot* of the residuals should be a fairly straight line. Departures from a straight line therefore suggest inappropriateness of the normality assumption, although, as demonstrated in Daniel and Wood (1980), considerable variability can be expected in normal plots. Normal probability plots are also good for revealing outliers.

Example: PCB 11

Plots of residuals are given in Figure 1.9 for the fit of ln(PCB) to $\sqrt[3]{\text{age}}$. Since the fitted values are a linear function of the regressor variable $\sqrt[3]{\text{age}}$, the form of the plot of the studentized residuals versus $\hat{y}$ will be the same as that versus $\sqrt[3]{\text{age}}$, so we only display the former. The plot versus $\hat{y}$ and the quantile–quantile plot are well behaved. Neither plot reveals outliers. ■

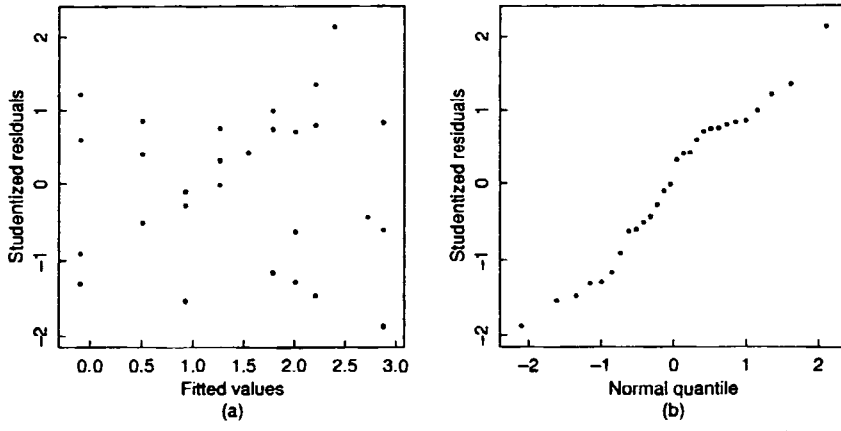

Figure 1.9 Studentized residuals for the PCB data plotted versus fitted values in part *a* and versus normal quantiles in part *b*.

1.3.2.2 Stabilizing Variance

An experiment which includes replications allows further tests to be made on the appropriateness of assumptions. For example, even before an expectation function has been proposed, it is possible to check the assumption of constant variance by using an analysis of variance to get averages and variances for each set of replications and plotting the variances and standard deviations versus the averages. If the plots show systematic relationships, then one can use a variance-stabilizing procedure to transform to constant variance.

One procedure is to try a range of power transformations in the form (Box and Cox, 1964)

$$y^{(\lambda)} = \begin{cases} \dfrac{y^{\lambda}-1}{\lambda} & \lambda \neq 0 \\ \ln y & \lambda = 0 \end{cases}$$

We calculate and plot variances versus averages for $y^{(\lambda)}$, $\lambda = 0, \pm 0.5, \pm 1, \ldots$ and select that value of λ for which the variance appears to be most stable. Alternatively, for a random variable Y, if there is a power relationship between the standard deviation σ and the mean μ such that $\sigma \propto \mu^{\alpha}$, it can be shown (Box, Hunter, and Hunter, 1978; Draper and Smith, 1981; Montgomery and Peck, 1982) that the variance of the transformed random variable $Y^{1-\alpha}$ will be approximately constant.

Variance-stabilizing transformations usually have the additional benefit of making the distribution of the disturbances appear more nearly normal, as discussed in Section 1.3.1. Alternatively, one can use the replication information to assist in choosing a form of weighting for weighted least squares.

Example: PCB 12

A plot of the standard deviations versus the averages for the original PCB data is given in Figure 1.10*a*. It can be seen that there is a good straight line relationship between s and $\bar{y}$, and so the variance-stabilizing technique leads to the logarithmic transformation. In Figure 1.10*b* we plot the standard deviations versus the averages for the ln(PCB) data. This plot shows no systematic relationship, and hence substantiates the effectiveness of the logarithmic transformation in stabilizing the variance. ■

1.3.2.3 Lack of Fit

When the data set includes replications, it is also possible to perform tests for *lack of fit* of the expectation function. Such analyses are based on an analysis of variance in which the residual sum of squares $S(\hat{\boldsymbol{\beta}})$ with $N-P$ degrees of freedom is decomposed into the *replication* sum of squares S_r (equal to the total sum of squares of deviations of the replication values about their averages) with, say, ν_r degrees of freedom, and the *lack of fit* sum of squares $S_l = S(\hat{\boldsymbol{\beta}}) - S_r$, with $\nu_l = N - P - \nu_r$ degrees of freedom. We then compare the ratio of the lack of fit mean square over the replication mean square with the appropriate value in the F table. That is, we compare

$$\frac{S_l/\nu_l}{S_r/\nu_r} \quad \text{with} \quad F(\nu_l, \nu_r; \alpha)$$

to determine whether there is significant lack of fit at level α. The geometric justification for this analysis is that the replication subspace is always orthogonal to the subspace containing the averages and the expectation function.

If no lack of fit is found, then the lack of fit analysis of variance has served its purpose, and the estimate of σ^2 should be based on the residual mean

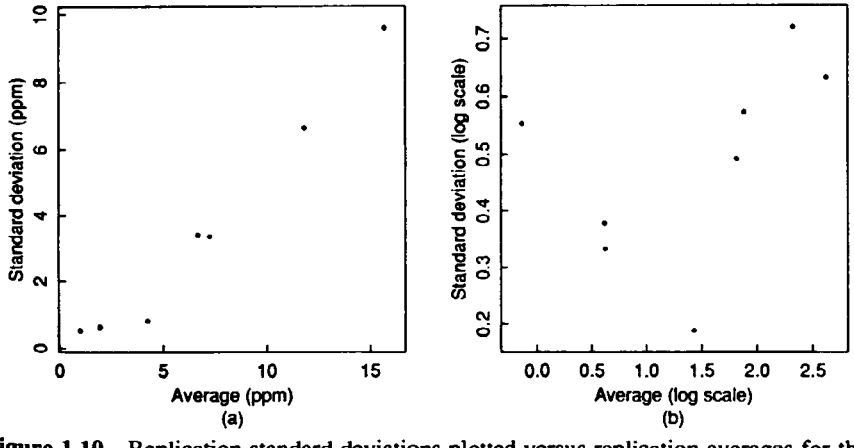

Figure 1.10 Replication standard deviations plotted versus replication averages for the PCB data in part *a* and for the ln(PCB) data in part *b*.

square. That is, the replication and lack of fit sums of squares and degrees of freedom should be recombined to give an estimate with the largest number of degrees of freedom, so as to provide the most reliable parameter and expected value confidence regions. If lack of fit is found, the analyst should attempt to discover why, and modify the expectation function accordingly. Further discussion on assessing the fit of a model and on modifying and comparing models is given in Sections 3.7 and 3.10.

Example: PCB 13

For the ln(PCB) versus $\sqrt[3]{\text{age}}$ data, the lack of fit analysis is presented in Table 1.1. Because the p value suggests no lack of fit, we combine the lack of fit and replication sums of squares and degrees of freedom and take as our estimate of σ^2, the residual mean square of 0.246 based on 26 degrees of freedom. If there had been lack of fit, we would have had to modify the model: in either situation, we do not simply use the replication mean square as an estimate of the variance. ■

Table 1.1 Lack of fit analysis of the model fitted to the PCB data

Source	Degrees of Freedom	Sum of Squares	Mean Square	F Ratio	p Value
Lack of fit	9	1.923	0.214	0.812	0.61
Replication	17	4.475	0.263		
Residuals	26	6.398	0.246		

Exercises

1.1 Write a computer routine in a language of your choice to perform a QR decomposition of a matrix using Householder transformations.

1.2 Draw a picture to show the Householder transformation of a vector $\mathbf{y}=(y_1, y_2)^T$ to the x axis. Use both forms of the vector $\mathbf{u}$ corresponding to equations (A2.1) and (A2.2). Hint: Draw a circle of radius $\|\mathbf{y}\|$.

1.3 Perform a QR decomposition of the matrix $\mathbf{X}$ from Example PCB 3,

$$\mathbf{X}=\begin{bmatrix} 1 & 1.26 \\ 1 & 1.82 \\ 1 & 2.22 \end{bmatrix}$$

using $\mathbf{u}$ as in equation (A2.2). Compare the result with that in Appendix 2.

1.4 (a) Perform a QR decomposition of the matrix

$$\mathbf{D} = \begin{bmatrix} 0 & 1 \\ 0 & 1 \\ 0 & 1 \\ 1 & 1 \\ 0 & 1 \end{bmatrix}$$

and obtain the matrix $\mathbf{Q}_1$. This matrix is used in Example α-pinene 6, Section 4.3.4.

(b) Calculate $\mathbf{Q}_2^T\mathbf{y}$, where $\mathbf{y} = (50.4, 32.9, 6.0, 1.5, 9.3)^T$, without explicitly solving for $\mathbf{Q}_2$.

1.5 (a) Fit the model $\ln(\text{PCB}) = \beta_1 + \beta_2\,\text{age}$ to the PCB data and perform a lack of fit analysis of the model. What do you conclude about the adequacy of this model?

(b) Plot the residuals versus age, and assess the adequacy of the model. Now what do you conclude about the adequacy of the model?

(c) Fit the model $\ln(\text{PCB}) = \beta_1 + \beta_2\,\text{age} + \beta_3\,\text{age}^2$ to the PCB data and perform a lack of fit analysis of the model. What do you conclude about the adequacy of this model?

(d) Perform an extra sum of squares analysis to determine whether the quadratic term is a useful addition.

(e) Explain the difference between your answers in (a), (b), and (d).

CHAPTER 2.

Nonlinear Regression: Iterative Estimation and Linear Approximations

"Although this may seem a paradox, all exact science is dominated by the idea of approximation."

– Bertrand Russell

Linear regression is a powerful method for analyzing data described by models which are linear in the parameters. Often, however, a researcher has a mathematical expression which relates the response to the predictor variables, and these models are usually nonlinear in the parameters. In such cases, linear regression techniques must be extended, which introduces considerable complexity.

2.1 The Nonlinear Regression Model

A nonlinear regression model can be written

$$Y_n = f(\mathbf{x}_n, \boldsymbol{\theta}) + Z_n \tag{2.1}$$

where f is the expectation function and $\mathbf{x}_n$ is a vector of associated regressor variables or independent variables for the nth case. This model is of exactly the same form as (1.1) except that the expected responses are nonlinear functions of the parameters. That is, for nonlinear models, *at least one of the derivatives of the expectation function with respect to the parameters depends on at least one of the parameters.*

To emphasize the distinction between linear and nonlinear models, we use $\boldsymbol{\theta}$ for the parameters in a nonlinear model. As before, we use P for the number

of parameters.

When analyzing a particular set of data we consider the vectors $\mathbf{x}_n$, $n = 1, 2, \ldots, N$, as fixed and concentrate on the dependence of the expected responses on $\boldsymbol{\theta}$. We create the N-vector $\boldsymbol{\eta}(\boldsymbol{\theta})$ with nth element

$$\eta_n(\boldsymbol{\theta}) = f(\mathbf{x}_n, \boldsymbol{\theta}) \qquad n = 1, \ldots, N$$

and write the nonlinear regression model as

$$\boldsymbol{Y} = \boldsymbol{\eta}(\boldsymbol{\theta}) + \boldsymbol{Z} \tag{2.2}$$

with $\boldsymbol{Z}$ assumed to have a spherical normal distribution. That is,

$$\mathrm{E}[\boldsymbol{Z}] = \mathbf{0}$$

$$\mathrm{Var}(\boldsymbol{Z}) = \mathrm{E}[\boldsymbol{Z}\boldsymbol{Z}^{\mathrm{T}}] = \sigma^2\mathbf{I}$$

as in the linear model.

Example: Rumford 1

Count Rumford of Bavaria was one of the early experimenters on the physics of heat. In 1798 he performed an experiment in which a cannon barrel was heated by grinding it with a blunt bore. When the cannon had reached a steady temperature of 130°F, it was allowed to cool and temperature readings were taken at various times. The ambient temperature during the experiment was 60°F, so [under Newton's law of cooling, which states that $df/dt = -\theta(f - T_0)$, where T_0 is the ambient temperature] the temperature at time t should be

$$f(t, \theta) = 60 + 70e^{-\theta t}$$

Since $\partial f/\partial\theta = -70te^{-\theta t}$ depends on the parameter θ, this model is nonlinear. Rumford's data are presented in Appendix 1, Section A1.2. ■

Example: Puromycin 1

The Michaelis–Menten model for enzyme kinetics relates the initial "velocity" of an enzymatic reaction to the substrate concentration x through the equation

$$f(x, \boldsymbol{\theta}) = \frac{\theta_1 x}{\theta_2 + x} \tag{2.3}$$

In Appendix 1, Section A1.3 we present data from Treloar (1974) on the initial rate of a reaction for which the Michaelis–Menten model is believed to be appropriate. The data, for an enzyme treated with Puromycin, are plotted in Figure 2.1.

Differentiating f with respect to θ_1 and θ_2 gives

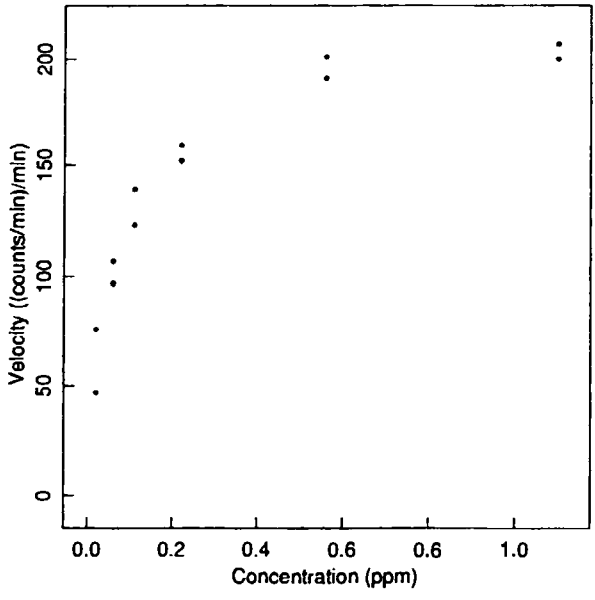

Figure 2.1 Plot of reaction velocity versus substrate concentration for the Puromycin data.

$$\frac{\partial f}{\partial \theta_1} = \frac{x}{\theta_2 + x}$$
$$\frac{\partial f}{\partial \theta_2} = \frac{-\theta_1 x}{(\theta_2 + x)^2} \tag{2.4}$$

and since both these derivatives involve at least one of the parameters, the model is recognized as nonlinear. ■

2.1.1 Transformably Linear Models

The Michaelis–Menten model (2.3) can be transformed to a linear model by expressing the reciprocal of the velocity as a function of the reciprocal substrate concentration,

$$\frac{1}{f} = \frac{1}{\theta_1} + \frac{\theta_2}{\theta_1}\frac{1}{x}$$
$$= \beta_1 + \beta_2 u \tag{2.5}$$

We call such models *transformably linear*. Some authors use the term "intrinsically linear," but we reserve the term "intrinsic" for a special geometric property

of nonlinear models, as discussed in Chapter 7. As will be seen in Chapter 3, transformably linear models have some advantages in nonlinear regression because it is easy to get starting values for some of the parameters.

It is important to understand, however, that a transformation of the data involves a transformation of the disturbance term too, which affects the assumptions on it. Thus, if we assume the model function (2.2) with an additive, spherical normal disturbance term is an appropriate representation of the experimental situation, then these same assumptions will not be appropriate for the transformed data. Hence we should use nonlinear regression on the original data, or else weighted least squares on the transformed data. Sometimes, of course, transforming a data set to induce constant variance also produces a linear expectation function in which case linear regression can be used on the transformed data.

Example: Puromycin 2

Because there are replications in the Puromycin data set, it is easy to see from Figure 2.1 that the variance of the original data is constant, and hence that nonlinear regression should be used to estimate the parameters. However, the reciprocal data, plotted in Figure 2.2*a*, while showing a simple straight line relationship, also show decidely nonconstant variance.

If we use linear regression to fit the model (2.5) to these data, we obtain the estimates

$$\hat{\boldsymbol{\beta}} = (0.005107, 0.0002472)^{\mathrm{T}}$$

corresponding to

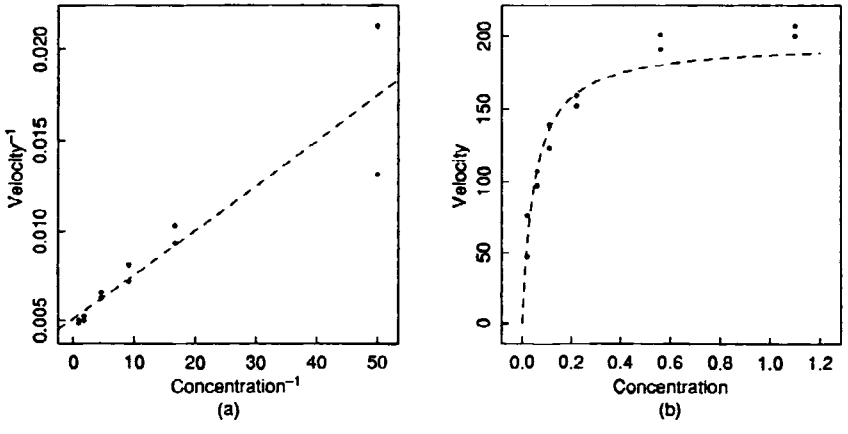

Figure 2.2 Plot of inverse velocity versus inverse substrate concentration for the Puromycin experiment with the linear regression line (dashed) in part *a*, and the corresponding fitted curve (dashed) in the original scale in part *b*.

$$\hat{\boldsymbol{\theta}} = (195.8, 0.04841)^{\mathrm{T}}$$

The fitted curve is overlaid with the data in the original scale in Figure 2.2*b*, where we see that the predicted asymptote is too small. Because the variance of the replicates has been distorted by the transformation, the cases with low concentration (high reciprocal concentration) dominate the determination of the parameters and the curve does not fit the data well at high concentrations. ■

This example demonstrates two important features. First, it emphasizes the value of replications, because without replications it may not be possible to detect either the constant variance in the original data or the nonconstant variance in the transformed data; and second, it shows that while transforming can produce simple linear behavior, it also affects the disturbances.

2.1.2 Conditionally Linear Parameters

The Michaelis–Menten model is also an example of a model in which there is a conditionally linear parameter, θ_1. It is *conditionally linear* because the derivative of the expectation function with respect to θ_1 does not involve θ_1. We can therefore estimate θ_1, conditional on θ_2, by a linear regression of velocity on $x/(\theta_2 + x)$. Models with conditionally linear parameters enjoy some advantageous properties, which can be exploited in nonlinear regression.

2.1.3 The Geometry of the Expectation Surface

The assumption of a spherical normal distribution for the disturbance term Z leads us to consider the Euclidean geometry of the N-dimensional response space, because again we will be interested in the least squares estimates $\hat{\boldsymbol{\theta}}$ of the parameters. The N-vectors $\boldsymbol{\eta}(\boldsymbol{\theta})$ define a P-dimensional surface called the *expectation surface* in the response space, and the least squares estimates correspond to the point on the expectation surface,

$$\hat{\boldsymbol{\eta}} = \boldsymbol{\eta}(\hat{\boldsymbol{\theta}})$$

which is closest to $\mathbf{y}$. That is, $\hat{\boldsymbol{\theta}}$ minimizes the residual sum of squares

$$S(\boldsymbol{\theta}) = \| \mathbf{y} - \boldsymbol{\eta}(\boldsymbol{\theta}) \|^2$$

Example: Rumford 2

To illustrate the geometry of nonlinear models, consider the two cases $t = 4$ and $t = 41$ for the Rumford data. Under the assumption that Newton's law of cooling holds for these data, the expected responses are

$$\eta(\theta) = \begin{bmatrix} 60+70e^{-4\theta} \\ 60+70e^{-41\theta} \end{bmatrix} \qquad \theta \geq 0$$

Substituting values for θ in these equations and plotting the points in a 2-dimensional response space gives the 1-dimensional expectation surface (curve) shown in Figure 2.3.

Note that the expectation surface is *curved* and of *finite extent*, which is in contrast to the linear model in which the expectation surface is a plane of infinite extent. Note, too, that points with equal spacing on the parameter line (θ) map to points with unequal spacing on the expectation surface. ■

Example: Puromycin 3

As another example, consider the three cases from Example Puromycin 1: $x = 1.10$, $x = 0.56$, and $x = 0.22$. Under the assumption that the expectation function (2.3) is the correct one, the expected responses for these substrate values are

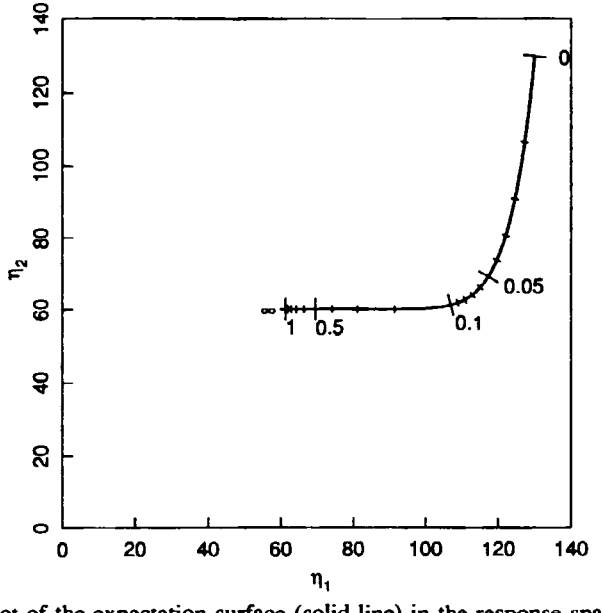

Figure 2.3 Plot of the expectation surface (solid line) in the response space for the 2-case Rumford data. The points corresponding to $\theta = 0, 0.01, 0.02, \ldots, 0.1, 0.2, \ldots, 1, \infty$ are marked.

$$\boldsymbol{\eta}(\boldsymbol{\theta}) = \begin{bmatrix} \dfrac{\theta_1(1.10)}{\theta_2+1.10} \\ \dfrac{\theta_1(0.56)}{\theta_2+0.56} \\ \dfrac{\theta_1(0.22)}{\theta_2+0.22} \end{bmatrix} \qquad \theta_1, \theta_2 \geq 0$$

and so we can plot the expectation surface by substituting values for $\boldsymbol{\theta}$ in these equations. A portion of the 2-dimensional expectation surface for these x values is shown in Figure 2.4. Again, in contrast to the linear model, this expectation surface is not an infinite plane, and in general, straight lines in the parameter plane do not map to straight lines on the expectation surface. It is also seen that unit squares in the parameter plane map to irregularly shaped areas on the expectation surface and that the sizes of these areas vary. Thus, the Jacobian determinant is not constant, which can be seen analytically, of course, because the derivatives (2.4) depend on $\boldsymbol{\theta}$.

For this model, there are straight lines on the expectation surface in Figure 2.4 corresponding to the θ_1 parameter lines (lines with θ_2 held con-

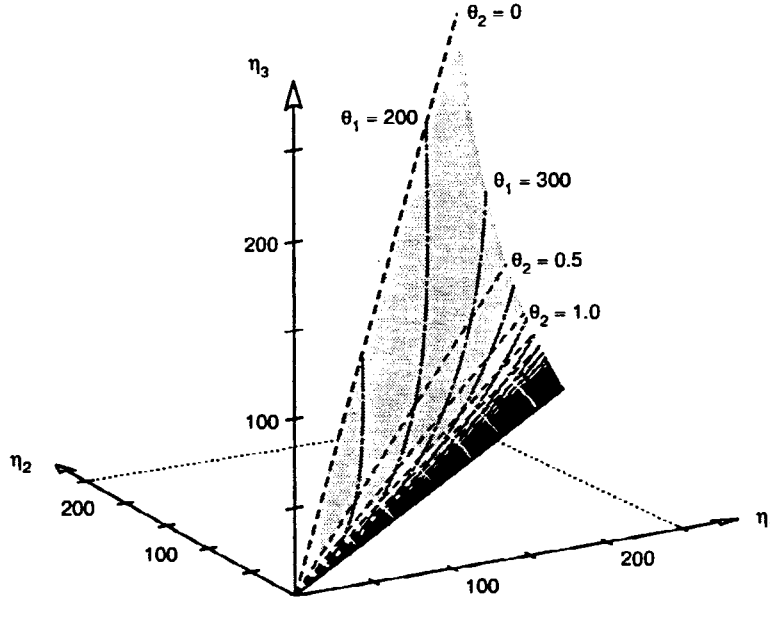

Figure 2.4 Expectation surface for the 3-case Puromycin example. We show a portion of the expectation surface (shaded) in the expectation space with θ_1 parameter lines (dashed) and θ_2 parameter lines (dot–dashed).

stant), reflecting the fact that θ_1 is conditionally linear. However, the θ_1 parameter lines are neither parallel nor equispaced. The θ_2 lines are not straight, parallel, or equispaced. ■

As can be seen from these examples, for nonlinear models with P parameters, it is generally true that:

(1) the expectation surface, $\boldsymbol{\eta}(\boldsymbol{\theta})$, is a P-dimensional *curved surface* in the N-dimensional response space;
(2) parameter *lines* in the parameter space map to *curves* on the curved expectation surface;
(3) the *Jacobian determinant*, which measures how large unit areas in $\boldsymbol{\theta}$ become in $\boldsymbol{\eta}(\boldsymbol{\theta})$, is *not constant.*

We explore these interesting and important aspects of the expectation surface later, but first we discuss how to obtain the least squares estimates $\hat{\boldsymbol{\theta}}$ for the parameters $\boldsymbol{\theta}$. Nonlinear least squares estimation from the point of view of sum of squares contours is given in Section 2.4.

2.2 Determining the Least Squares Estimates

The problem of finding the least squares estimates can be stated very simply geometrically—given a data vector $\mathbf{y}$, an expectation function $f(\mathbf{x}_n, \boldsymbol{\theta})$, and a set of design vectors $\mathbf{x}_n$, $n = 1, \ldots, N$

(1) find the point $\hat{\boldsymbol{\eta}}$ on the expectation surface which is closest to $\mathbf{y}$, and then
(2) determine the parameter vector $\hat{\boldsymbol{\theta}}$ which corresponds to the point $\hat{\boldsymbol{\eta}}$.

For a linear model, step (1) is straightforward because the expectation surface is a plane of infinite extent, and we may write down an explicit expression for the point on that plane which is closest to $\mathbf{y}$,

$$\hat{\boldsymbol{\eta}} = \mathbf{Q}_1\mathbf{Q}_1^T\mathbf{y}$$

For a linear model, step (2) is also straightforward because the P-dimensional parameter plane maps linearly and invertibly to the expectation plane, so once we know where we are on one plane we can easily find the corresponding point on the other. Thus

$$\hat{\boldsymbol{\beta}} = \mathbf{R}_1^{-1}\mathbf{Q}_1^T\hat{\boldsymbol{\eta}}$$

In the nonlinear case, however, the two steps are very difficult: the first because the expectation surface is curved and often of finite extent (or, at least, has edges) so that it is difficult even to find $\hat{\boldsymbol{\eta}}$, and the second because we can map points easily only in one direction—from the parameter plane to the expec-

tation surface. That is, even if we know $\hat{\boldsymbol{\eta}}$, it is extremely difficult to determine the parameter plane coordinates $\hat{\boldsymbol{\theta}}$ corresponding to that point. To overcome these difficulties, we use iterative methods to determine the least squares estimates.

2.2.1 The Gauss–Newton Method

An approach suggested by Gauss is to use a linear approximation to the expectation function to iteratively improve an initial guess $\boldsymbol{\theta}^0$ for $\boldsymbol{\theta}$ and keep improving the estimates until there is no change. That is, we expand the expectation function $f(\mathbf{x}_n, \boldsymbol{\theta})$ in a first order Taylor series about $\boldsymbol{\theta}^0$ as

$$f(\mathbf{x}_n, \boldsymbol{\theta}) = f(\mathbf{x}_n, \boldsymbol{\theta}^0) + v_{n1}(\theta_1 - \theta_1^0) + v_{n2}(\theta_2 - \theta_2^0) + \cdots + v_{nP}(\theta_P - \theta_P^0)$$

where

$$v_{np} = \left.\frac{\partial f(\mathbf{x}_n, \boldsymbol{\theta})}{\partial \theta_p}\right|_{\boldsymbol{\theta}^0} \qquad p = 1, 2, \ldots, P$$

Incorporating all N cases, we write

$$\boldsymbol{\eta}(\boldsymbol{\theta}) \simeq \boldsymbol{\eta}(\boldsymbol{\theta}^0) + \mathbf{V}^0(\boldsymbol{\theta} - \boldsymbol{\theta}^0) \tag{2.6}$$

where $\mathbf{V}^0$ is the $N \times P$ derivative matrix with elements $\{v_{np}\}$. This is equivalent to approximating the residuals, $\mathbf{z}(\boldsymbol{\theta}) = \mathbf{y} - \boldsymbol{\eta}(\boldsymbol{\theta})$, by

$$\mathbf{z}(\boldsymbol{\theta}) \simeq \mathbf{y} - [\boldsymbol{\eta}(\boldsymbol{\theta}^0) + \mathbf{V}^0\boldsymbol{\delta}] = \mathbf{z}^0 - \mathbf{V}^0\boldsymbol{\delta} \tag{2.7}$$

where $\mathbf{z}^0 = \mathbf{y} - \boldsymbol{\eta}(\boldsymbol{\theta}^0)$ and $\boldsymbol{\delta} = \boldsymbol{\theta} - \boldsymbol{\theta}^0$.

We then calculate the *Gauss increment* $\boldsymbol{\delta}^0$ to minimize the approximate residual sum of squares $\|\mathbf{z}^0 - \mathbf{V}^0\boldsymbol{\delta}\|^2$, using

$$\mathbf{V}^0 = \mathbf{QR} = \mathbf{Q}_1\mathbf{R}_1 \qquad \text{[cf. (1.19)]}$$

$$\mathbf{w}_1 = \mathbf{Q}_1^{\mathrm{T}}\mathbf{z}^0 \qquad \text{[cf. (1.21)]}$$

$$\hat{\boldsymbol{\eta}}^1 = \mathbf{Q}_1\mathbf{w}_1 \qquad \text{[cf. (1.23)]}$$

and so

$$\mathbf{R}_1\boldsymbol{\delta}^0 = \mathbf{w}_1 \qquad \text{[cf. (1.24)]}$$

The point

$$\hat{\boldsymbol{\eta}}^1 = \boldsymbol{\eta}(\boldsymbol{\theta}^1) = \boldsymbol{\eta}(\boldsymbol{\theta}^0 + \boldsymbol{\delta}^0)$$

should now be closer to $\mathbf{y}$ than $\boldsymbol{\eta}(\boldsymbol{\theta}^0)$, and so we move to this better parameter value $\boldsymbol{\theta}^1 = \boldsymbol{\theta}^0 + \boldsymbol{\delta}^0$ and perform another iteration by calculating new residuals $\mathbf{z}^1 = \mathbf{y} - \boldsymbol{\eta}(\boldsymbol{\theta}^1)$, a new derivative matrix $\mathbf{V}^1$, and a new increment. This process is repeated until convergence is obtained, that is, until the increment is so small that there is no useful change in the elements of the parameter vector.

Example: Puromycin 4

To illustrate these calculations, consider the data from Example Puromycin 1, with the starting estimates $\boldsymbol{\theta}^0 = (205, 0.08)^T$. The data, along with the fitted values, residuals, and derivatives evaluated at $\boldsymbol{\theta}^0$, are shown in Table 2.1.

Collecting these derivatives into the derivative matrix $\mathbf{V}^0$, we then perform a *QR* decomposition, from which we generate $\mathbf{w}_1 = \mathbf{Q}_1^T \mathbf{z}^0$ and then solve for $\boldsymbol{\delta}^0$ using $\mathbf{R}_1 \boldsymbol{\delta}^0 = \mathbf{w}_1$. In this case, $\boldsymbol{\delta}^0 = (8.03, -0.017)^T$ and the sum of squares at $\boldsymbol{\theta}^1 = \boldsymbol{\theta}^0 + \boldsymbol{\delta}^0$ is $S(\boldsymbol{\theta}^1) = 1206$, which is much smaller than $S(\boldsymbol{\theta}^0) = 3155$. We therefore move to $\boldsymbol{\theta}^1 = (213.03, 0.063)^T$ and perform another iteration. ■

Example: BOD 1

As a second example, we consider data on biochemical oxygen demand (BOD) from Marske (1967), reproduced in Appendix 1, Section A1.4. The data are plotted in Figure 2.5. For these data, the model

$$f(x, \boldsymbol{\theta}) = \theta_1 (1 - e^{-\theta_2 x}) \tag{2.8}$$

is considered appropriate.

Using the starting estimates $\boldsymbol{\theta}^0 = (20, 0.24)^T$, for which $S(\boldsymbol{\theta}^0) = 128.2$, produces an increment to $\boldsymbol{\theta}^1 = (13.61, 0.52)^T$ with $S(\boldsymbol{\theta}^1) = 145.2$. In this case, the sum of squares has increased and so we must modify the increment as discussed below. ■

Table 2.1 Residuals and derivatives for Puromycin data at $\boldsymbol{\theta} = (205, 0.08)^T$.

n	x_n	y_n	η_n^0	z_n^0	v_{n1}^0	v_{n2}^0
1	0.02	76	41.00	35.00	0.2000	−410.00
2	0.02	47	41.00	6.00	0.2000	−410.00
3	0.06	97	87.86	9.14	0.4286	−627.55
4	0.06	107	87.86	19.14	0.4286	−627.55
5	0.11	123	118.68	4.32	0.5789	−624.65
6	0.11	139	118.68	20.32	0.5789	−624.65
7	0.22	159	150.33	8.67	0.7333	−501.11
8	0.22	152	150.33	1.67	0.7333	−501.11
9	0.56	191	179.38	11.62	0.8750	−280.27
10	0.56	201	179.38	21.62	0.8750	−280.27
11	1.10	207	191.10	15.90	0.9322	−161.95
12	1.10	200	191.10	8.90	0.9322	−161.95

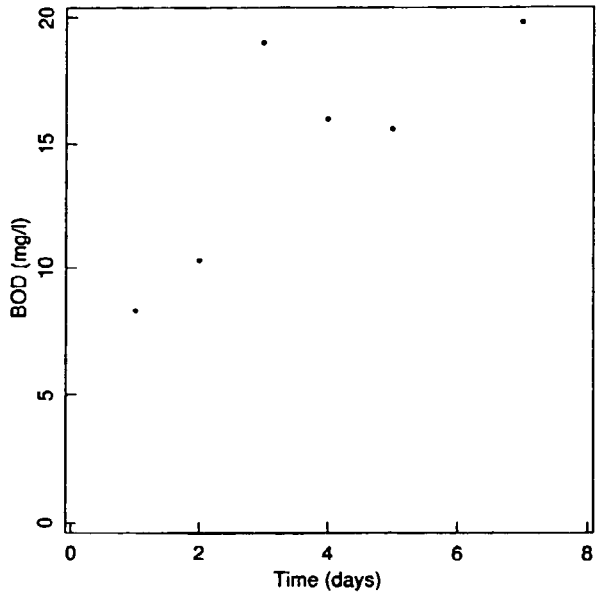

Figure 2.5 Plot of BOD versus time

2.2.1.1 Step Factor

As seen in the last example, the Gauss–Newton increment can produce an *increase* in the sum of squares when the requested increment extends beyond the region where the linear approximation is valid. Even in these circumstances, however, the linear approximation will be a close approximation to the actual surface for a sufficiently small region around $\boldsymbol{\eta}(\boldsymbol{\theta}^0)$. Thus a small step in the direction $\boldsymbol{\delta}^0$ should produce a decrease in the sum of squares. We therefore introduce a *step factor* λ, and calculate

$$\boldsymbol{\theta}^1 = \boldsymbol{\theta}^0 + \lambda\boldsymbol{\delta}^0$$

where λ is chosen to ensure that

$$S(\boldsymbol{\theta}^1) < S(\boldsymbol{\theta}^0) \tag{2.9}$$

A common method of selecting λ is to start with $\lambda = 1$ and halve it until (2.9) is satisfied. This modification to the Gauss–Newton algorithm was suggested in Box (1960) and Hartley (1961).

Example: BOD 2

For the data and starting estimates in Example BOD 1, the value $\lambda = 0.5$ gave a reduced sum of squares, 94.2, at $\boldsymbol{\theta} = (16.80, 0.38)^T$. ■

Pseudocode for the Gauss–Newton algorithm for nonlinear least squares is given in Appendix 3, Section A3.1, together with implementations in GAUSS™, S, and SAS/IML™.

2.2.2 The Geometry of Nonlinear Least Squares

Geometrically a Gauss–Newton iteration consists of:

(1) approximating $\boldsymbol{\eta}(\boldsymbol{\theta})$ by a Taylor series expansion at $\boldsymbol{\eta}^0 = \boldsymbol{\eta}(\boldsymbol{\theta}^0)$,
(2) generating the residual vector $\mathbf{z}^0 = \mathbf{y} - \boldsymbol{\eta}^0$,
(3) projecting the residual $\mathbf{z}^0$ onto the tangent plane to give $\hat{\boldsymbol{\eta}}^1$,
(4) mapping $\hat{\boldsymbol{\eta}}^1$ through the linear coordinate system to produce the increment $\boldsymbol{\delta}^0$, and finally
(5) moving to $\boldsymbol{\eta}(\boldsymbol{\theta}^0 + \lambda\,\boldsymbol{\delta}^0)$.

The first step actually involves two distinct approximations:

(1) the *planar* assumption, in which we approximate the expectation surface $\boldsymbol{\eta}(\boldsymbol{\theta})$ near $\boldsymbol{\eta}(\boldsymbol{\theta}^0)$ by its tangent plane at $\boldsymbol{\eta}(\boldsymbol{\theta}^0)$, and
(2) the *uniform coordinate* assumption, in which we impose a linear coordinate system $\mathbf{V}(\boldsymbol{\theta} - \boldsymbol{\theta}^0)$ on the approximating tangent plane.

We give geometrical interpretations of these steps and assumptions in the following examples.

Example: Rumford 3

For the 2-case Rumford data set of Example Rumford 2, we plot $\mathbf{y}$ and a portion of the expectation surface in Figure 2.6. The expectation surface is a curved line, and the points corresponding to $\theta = 0.01, 0.02, \ldots, 0.2$ are unevenly spaced.

For the initial estimate $\theta^0 = 0.05$, a Gauss–Newton iteration involves the linear approximation

$$\boldsymbol{\eta}(\theta) \approx \boldsymbol{\eta}^0 + \mathbf{v}\,\delta$$

where $\delta = (\theta - 0.05)$, $\boldsymbol{\eta}^0$ is the expectation vector at $\theta = 0.05$,

$$\boldsymbol{\eta}^0 = \begin{bmatrix} 60 + 70e^{-4\theta} \\ 60 + 70e^{-41\theta} \end{bmatrix} = \begin{bmatrix} 117.31 \\ 69.01 \end{bmatrix}$$

and $\mathbf{v}$ is the derivative vector at $\theta = 0.05$,

$$\mathbf{v} = \begin{bmatrix} -70(4)e^{-4\theta} \\ -70(41)e^{-41\theta} \end{bmatrix} = \begin{bmatrix} -229.25 \\ -369.47 \end{bmatrix}$$

The Taylor series approximation, consisting of the tangent plane and the linear coordinate system, is shown as a solid line in Figure 2.6. This replaces the curved expectation surface with the nonlinear parameter coordinates by a linear surface with a uniform coordinate system on it.

Next we use linear least squares to obtain the point $\hat{\boldsymbol{\eta}}^1$ on the tangent line which is closest to $\mathbf{y}$. We then calculate the *apparent* parameter incre-

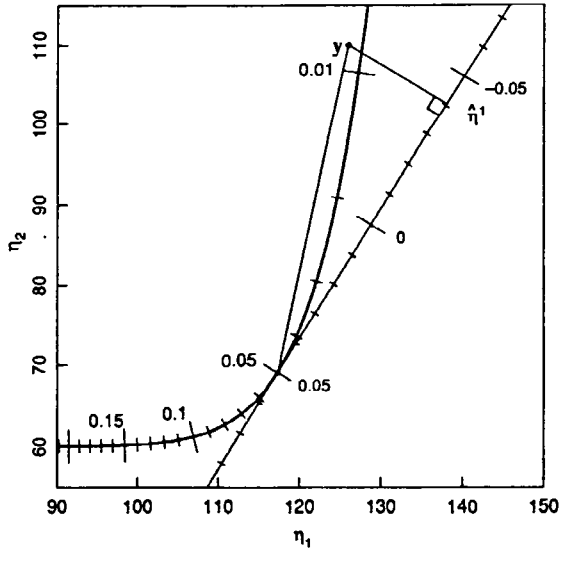

Figure 2.6 A geometric interpretation of calculation of the Gauss–Newton increment using the 2-case Rumford data. A portion of the expectation surface (heavy solid line) is shown in the response space together with the observed response $\mathbf{y}$. Also shown is the projection $\hat{\boldsymbol{\eta}}^1$ of $\mathbf{y}-\boldsymbol{\eta}(0.05)$ onto the tangent plane at $\boldsymbol{\eta}(0.05)$ (solid line). The tick marks indicate true positions on the expectation surface and linear approximation positions on the tangent plane.

ment δ^0 corresponding to $\hat{\boldsymbol{\eta}}^1$ and from this obtain $\theta^1 = \theta^0 + \delta^0$. For this example,

$$\mathbf{z}^0 = \begin{bmatrix} 126 \\ 110 \end{bmatrix} - \begin{bmatrix} 117.31 \\ 69.01 \end{bmatrix} = \begin{bmatrix} 8.69 \\ 40.99 \end{bmatrix}$$

so $\hat{\boldsymbol{\eta}}^1 = (138.1, 102.5)^T$, $\delta^0 = -0.091$, and $\theta^1 = 0.05 - 0.091 = -0.041$.

It is clear that the linear approximation increment is too large, since $\theta^1 = -0.041$, whereas we can see from the points on the expectation surface that $\hat{\theta}$ is near 0.01. We must therefore use a step factor to reduce the increment before proceeding. ■

Example: Puromycin 5

For a two parameter example, we consider the data and the starting values from Example Puromycin 4. Since the response space is 12-dimensional, we cannot picture it directly, but we can represent the salient features in the 3-dimensional space spanned by the tangent plane and the residual vector. We do this in Figure 2.7, where we show a portion of the curved expectation surface, the residual vector, and the approximating tangent plane. It can be seen that the expectation surface is only slightly curved, and so is

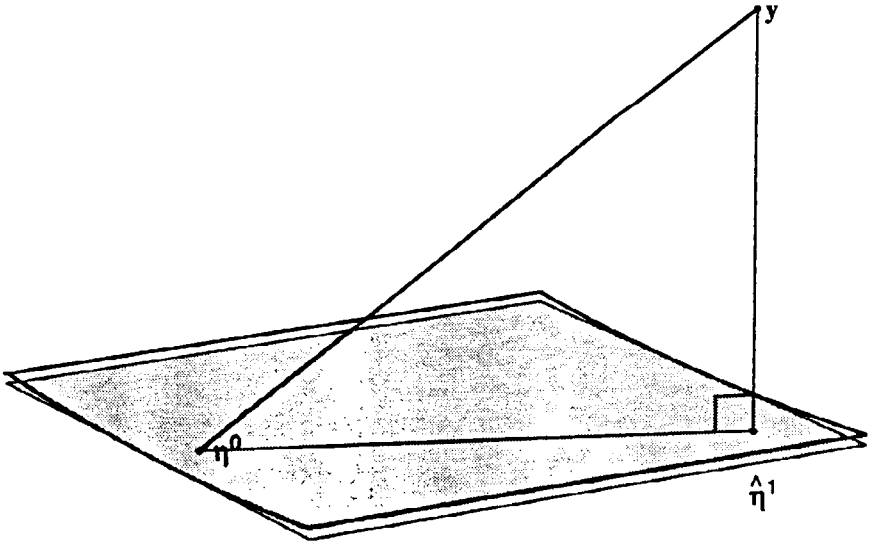

Figure 2.7 A geometric interpretation of calculation of the Gauss–Newton increment using the full Puromycin data set. We show the projection of a portion of the expectation surface into the subspace spanned by the tangent plane at $\boldsymbol{\eta}^0$ (shaded) and the residual vector $\mathbf{y}-\boldsymbol{\eta}^0$. The region on the expectation surface is bordered by the heavy solid lines. Also shown is the projection $\hat{\boldsymbol{\eta}}^1$ of the residual vector onto the tangent plane.

well approximated by the tangent plane.

In Figure 2.8*a* we show the parameter curves for $\theta_1 = 200, 210, 220, 230$ and $\theta_2 = 0.06, 0.07, \ldots, 0.1$ projected onto the tangent plane, and in Figure 2.8*b* the corresponding linear approximation lines on the tangent plane. It can be seen that the linear approximation lines match the true parameter curves very well. Also shown on the tangent planes are the points $\boldsymbol{\eta}^0$ and $\hat{\boldsymbol{\eta}}^1$, and in Figure 2.8*a* the projection of the curve $\boldsymbol{\eta}(\boldsymbol{\theta}^0 + \lambda\boldsymbol{\delta}^0)$ for $0 \le \lambda \le 1$. The points corresponding to $\lambda = 0.25, 0.5$, and 1 ($\boldsymbol{\eta}^1$) are marked.

Because the planar and uniform coordinate assumptions are both valid, the points $\hat{\boldsymbol{\eta}}^1$ and $\boldsymbol{\eta}^1$ are close together and are much closer to $\mathbf{y}$ than $\boldsymbol{\eta}^0$. In this case, a full step ($\lambda = 1$) can be taken resulting in a decrease in the sum of squares as shown in Example Puromycin 4. ■

Example: BOD 3

As a second two-parameter example, we consider the data and starting values from Example BOD 1. In Figure 2.9 we show a portion of the curved expectation surface, the residual vector, and the approximating tangent plane in the space spanned by the tangent plane and the residual vector. It can be seen that the expectation surface is moderately curved, but is still apparently well approximated by the tangent plane. In this ex-

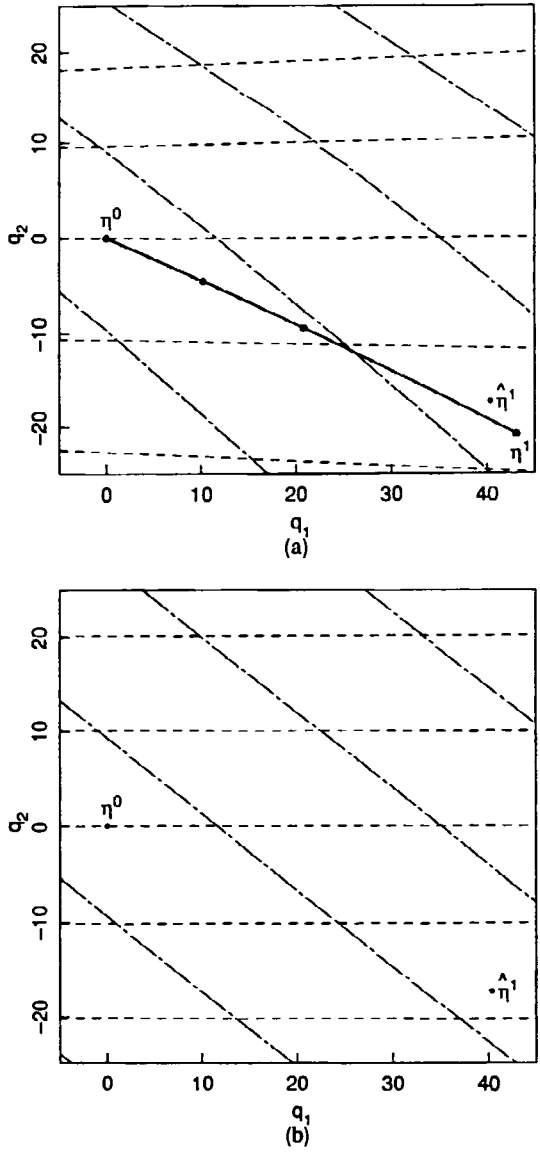

Figure 2.8 A geometric interpretation of calculation of the Gauss–Newton increment using the full Puromycin data set (continued). The points $\boldsymbol{\eta}^0$ and $\hat{\boldsymbol{\eta}}^1$ are shown in the tangent planes together with the parameter curves in part *a* and the linear approximation parameter lines in part *b*. In part *a* we also show the projection $\boldsymbol{\eta}^1$ of the point $\boldsymbol{\eta}(\boldsymbol{\theta}^0+\boldsymbol{\delta}^0)$. The curve (heavy solid line) joining $\boldsymbol{\eta}^0$ to $\boldsymbol{\eta}^1$ is the projection of $\boldsymbol{\eta}(\boldsymbol{\theta}^0+\lambda\boldsymbol{\delta}^0)$ for $0 \le \lambda \le 1$. The points corresponding to $\lambda = 0.25$ and 0.5 are marked.

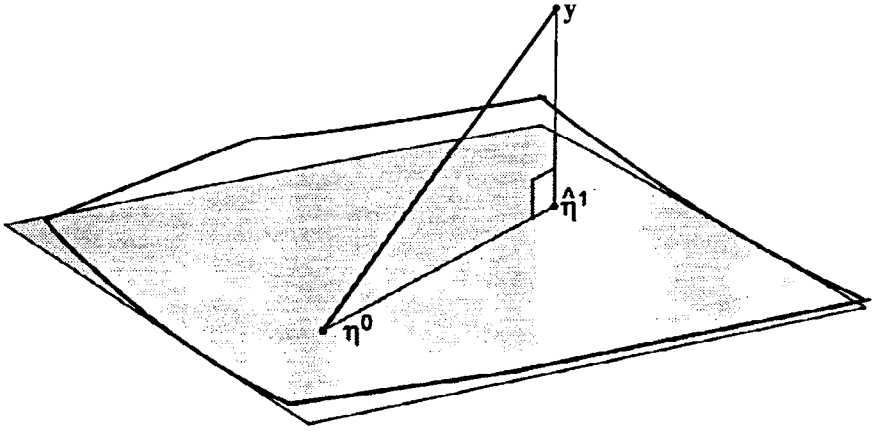

Figure 2.9 A geometric interpretation of calculation of the Gauss–Newton increment using the BOD data set. We show the projection of a portion of the expectation surface into the subspace spanned by the tangent plane at $\boldsymbol{\eta}^0$ (shaded) and the residual vector $\mathbf{y}-\boldsymbol{\eta}^0$. The region on the expectation surface is bordered by the heavy solid lines. Also shown is the projection $\hat{\boldsymbol{\eta}}^1$ of the residual vector onto the tangent plane.

ample, the edge of the finite expectation surface is shown as the angled solid line along the top edge of the surface.

In Figure 2.10*a* we show the parameter curves for $\theta_1 = 20, 30, \ldots$ and $\theta_2 = 0.2, 0.4, \ldots$ projected onto the tangent plane. In Figure 2.10*b* we show the corresponding linear approximation lines on the tangent plane. In this case, the linear approximation lines do not match the true parameter curves well at all. Also shown on the tangent planes are the points $\boldsymbol{\eta}^0$ and $\hat{\boldsymbol{\eta}}^1$, and in Figure 2.10*a* the projection of the curve $\boldsymbol{\eta}(\boldsymbol{\theta}^0 + \lambda\boldsymbol{\delta}^0)$ for $0 \le \lambda \le 1$. The points corresponding to $\lambda = 0.25, 0.5$, and 1 ($\boldsymbol{\eta}^1$) are marked.

Because the uniform coordinate assumption is not valid this far from $\boldsymbol{\theta}^0$, the points $\hat{\boldsymbol{\eta}}^1$ and $\boldsymbol{\eta}^1$ are widely separated, and in fact $\boldsymbol{\eta}^1$ is farther from $\hat{\boldsymbol{\eta}}^1$ than is $\boldsymbol{\eta}^0$. In this case, the reduced step, $\lambda = 0.5$, is successful, as was shown in Example BOD 2. ■

To summarize, geometrically we are using local information to generate a tangent plane with a linear coordinate system dictated by the derivative vectors, projecting the residual vector onto that tangent plane, and then mapping the tangent plane coordinates to the parameter plane using the linear mapping.

2.2.3 Convergence

We have indicated that the Gauss–Newton iterative method is continued until the values of $\boldsymbol{\theta}$ on successive iterations stabilize. This can be measured by the size of each parameter increment relative to the previous parameter value, which

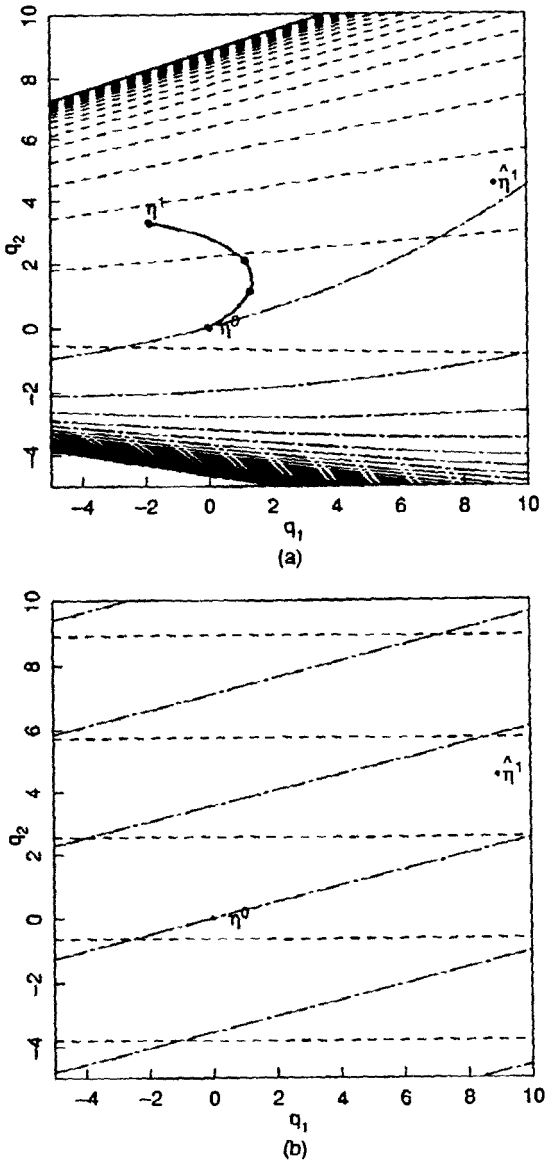

Figure 2.10 A geometric interpretation of calculation of the Gauss–Newton increment using the BOD data set (continued). The points $\boldsymbol{\eta}^0$ and $\hat{\boldsymbol{\eta}}^1$ are shown in the tangent planes together with the parameter curves in part *a* and the linear approximation parameter lines in part *b*. In part *a* we also show the projection $\boldsymbol{\eta}^1$ of the point $\boldsymbol{\eta}(\boldsymbol{\theta}^0+\boldsymbol{\delta}^0)$. The curve (heavy solid line) joining $\boldsymbol{\eta}^0$ to $\boldsymbol{\eta}^1$ is the projection of $\boldsymbol{\eta}(\boldsymbol{\theta}^0+\lambda\boldsymbol{\delta}^0)$ for $0\le\lambda\le 1$. The points corresponding to $\lambda=0.25$ and 0.5 are marked.

is the basis for one of the common criteria used to declare convergence (Bard, 1974; Draper and Smith, 1981; Jennrich and Sampson, 1968; Kennedy and Gentle, 1980; Ralston and Jennrich, 1978). Another criterion for convergence used, for example, in SAS (SAS Institute Inc., 1985), is that the relative change in the sum of squares on successive iterations be small. Himmelblau (1972) recommends that both these criteria be used, since compliance with one does not imply compliance with the other. However, compliance even with both relative change criteria does not guarantee convergence, as discussed in Bates and Watts (1981b). Kennedy and Gentle (1980) mention a relative step size criterion as well as relative change in the sum of squares and gradient size criteria. Chambers (1977) quotes several other criteria, including the size of the gradient, the size of the Gauss–Newton step, and the fact that the residual vector should be orthogonal to the derivative vectors; but no scale is suggested.

The main criticism of these criteria is that they indicate lack of progress rather than convergence. In most cases, of course, lack of progress occurs because a minimum is encountered: nevertheless, situations can occur where the parameter increment and sum of squares convergence criteria indicate lack of progress and yet a minimum has not been reached.

Examination of the geometry of nonlinear least squares provides a better procedure for determining convergence (Bates and Watts, 1981b). We know that a critical point is reached whenever the residual vector $\mathbf{y} - \boldsymbol{\eta}(\boldsymbol{\theta})$ is orthogonal to the expectation surface and therefore to the tangent plane to the expectation surface at $\boldsymbol{\eta}(\boldsymbol{\theta})$. We can thus adopt orthogonality of the residual vector to the tangent plane as a convergence criterion.

In practice, it would be unusual to obtain exact orthogonality in the presence of numerical roundoff, and we do not want to waste effort calculating small changes in the parameter vector while trying to achieve perfect orthogonality. We therefore need to establish a *tolerance level* which we can use to declare the residual vector to be "sufficiently orthogonal." One way to do this is to consider the statistical variability in the least squares estimates.

If we assume that the tangent plane forms a good approximation to the expectation surface near $\hat{\boldsymbol{\theta}}$, so a likelihood region for $\boldsymbol{\theta}$ roughly corresponds to a disk on the tangent plane with a radius proportional to $\sqrt{S(\hat{\boldsymbol{\theta}})}$, then we can measure the relative offset of the current parameter values from the exact least squares estimates by calculating the ratio of the length of the component of the residual vector in the tangent plane to $\sqrt{S(\hat{\boldsymbol{\theta}})}$. When this ratio is small, the numerical uncertainty of the least squares estimates is negligible compared to the statistical uncertainty of the parameters.

Unfortunately, this criterion involves the unknown least squares vector $\hat{\boldsymbol{\theta}}$. We therefore modify the criterion by substituting the current estimate, $\boldsymbol{\theta}^i$, for $\hat{\boldsymbol{\theta}}$, and measure the scaled length of the tangent plane component of the residual vector relative to the scaled length of the orthogonal component of the residual vector at $\boldsymbol{\theta}^i$. This leads to a *relative offset convergence criterion*

$$\frac{\| \mathbf{Q}_1^T(\mathbf{y} - \boldsymbol{\eta}(\boldsymbol{\theta}^i)) \| / \sqrt{P}}{\| \mathbf{Q}_2^T(\mathbf{y} - \boldsymbol{\eta}(\boldsymbol{\theta}^i)) \| / \sqrt{N-P}} \tag{2.10}$$

where $\mathbf{Q}_1$ and $\mathbf{Q}_2$ are the first P and last $N-P$ columns respectively of the matrix $\mathbf{Q}$ from a QR decomposition of $\mathbf{V}$. The criterion is related to the cotangent of the angle that the residual vector makes with the tangent plane, so that a small relative offset corresponds to an angle near 90°.

To declare convergence, we require the relative offset to be less than 0.001, reasoning that any inferences will not be affected materially by the fact that the current parameter vector is less than 0.1% of the radius of the confidence region disk from the least squares point.

Example: Rumford 4

We illustrate the convergence criterion and its development with the 2-observation Rumford example. We wish to test whether the parameter value $\theta = 0.01$ could be considered a point of convergence. Figure 2.11 shows a portion of the expectation surface, the observation point $\mathbf{y}$, and the tangent plane at $\boldsymbol{\eta}(0.01)$. Also shown is the component of the residual vector in the tangent plane, $\mathbf{Q}_1^T\mathbf{z}$, and the component orthogonal to the tangent plane, $\mathbf{Q}_2^T\mathbf{z}$. The tangent plane component is large relative to the orthogo-

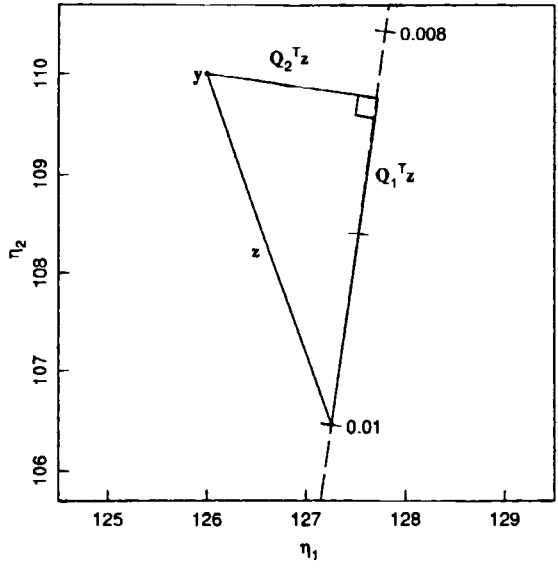

Figure 2.11 A geometric interpretation of relative offset using the 2-case Rumford data. A portion of the expectation surface (dashed line) is shown in the expectation space together with the residual vector $\mathbf{z}$ and its projections into the tangent plane ($\mathbf{Q}_1^T\mathbf{z}$) and orthogonal to the tangent plane ($\mathbf{Q}_2^T\mathbf{z}$).

nal component, having a relative offset of 1.92, and so we conclude that the residual vector at $\theta = 0.01$ is not sufficiently orthogonal for us to accept $\theta = 0.01$ as the converged value. ■

Convergence implies that the best estimates of the parameters have been obtained, under the assumption that the model is adequate. Before characterizing the precision of the estimates using inference intervals or regions, therefore, we should check the residuals for signs of model inadequacy. A complete discussion of the practical aspects of nonlinear regression is given in Chapter 3, but in the interests of completeness in analyzing the Puromycin and BOD data, we simply plot the residuals versus the fitted values and using probability plots before continuing.

Example: Puromycin 6

Convergence for the Puromycin data was declared at $\hat{\boldsymbol{\theta}} = (212.7, 0.0641)^{\mathrm{T}}$, with $s^2 = 119.5$ on 10 degrees of freedom. Studentized residuals from the least squares fit are plotted in Figure 2.12 versus fitted values in part *a* and as a normal probability plot in part *b*. Although there is one relatively large residual, the overall fit appears adequate, and so we proceed to develop parameter inference regions. ■

Example: BOD 4

Convergence for the BOD data was declared at $\hat{\boldsymbol{\theta}} = (19.143, 0.5311)^{\mathrm{T}}$, with $s^2 = 6.498$ on 4 degrees of freedom. Studentized residuals from the least squares fit are plotted in Figure 2.13 versus fitted values in part *a* and as a normal probability plot in part *b*. Since the residuals are well behaved, we proceed to develop parameter inference regions. ■

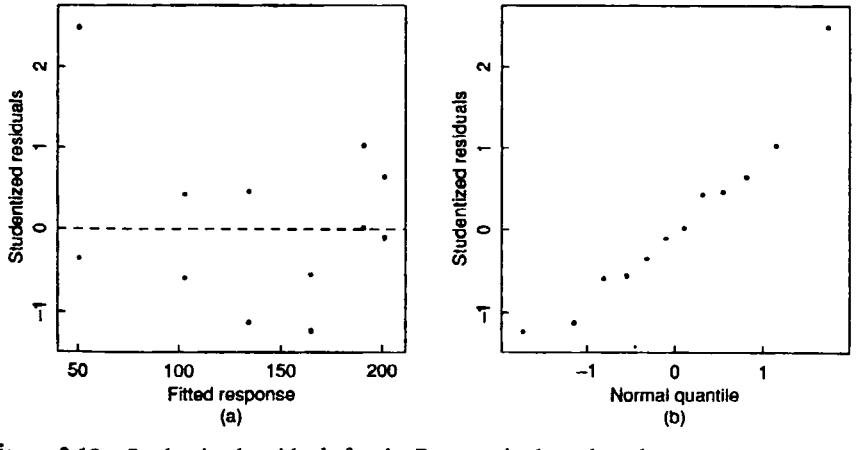

Figure 2.12 Studentized residuals for the Puromycin data plotted versus fitted values in part *a* and versus normal quantiles in part *b*.

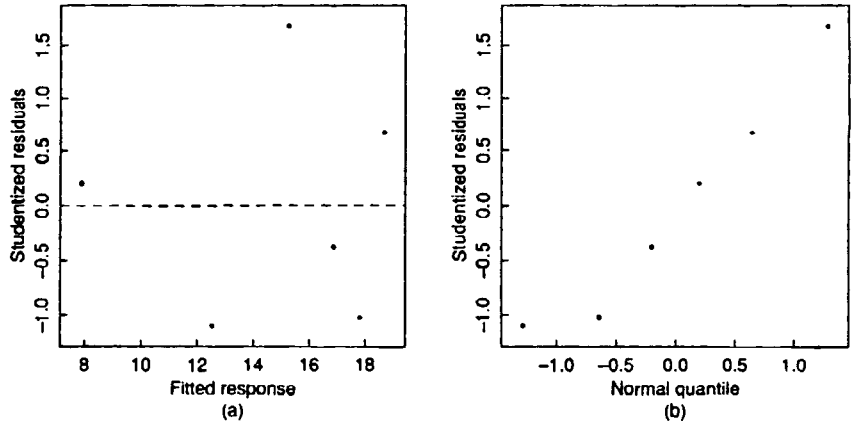

Figure 2.13 Studentized residuals for the BOD data plotted versus fitted values in part *a* and versus normal quantiles in part *b*.

2.3 Nonlinear Regression Inference Using the Linear Approximation

In the Gauss–Newton algorithm for calculating $\hat{\boldsymbol{\theta}}$, the derivative matrix $\mathbf{V}$ is evaluated at each iteration and used to calculate the increment and the convergence criterion. It is natural, then, to apply the linear approximation to *inference* for nonlinear models with the derivative matrix evaluated at the least squares parameter estimates. This yields approximate likelihood, confidence, or Bayesian HPD regions, based on

$$\boldsymbol{\eta}(\boldsymbol{\theta}) = \boldsymbol{\eta}(\hat{\boldsymbol{\theta}}) + \hat{\mathbf{V}}(\boldsymbol{\theta} - \hat{\boldsymbol{\theta}}) \tag{2.11}$$

2.3.1 Approximate Inference Regions for Parameters

Recall that in the linear case, a $1-\alpha$ parameter inference region can be expressed as [cf. (1.9)]

$$(\boldsymbol{\beta} - \hat{\boldsymbol{\beta}})^{\mathrm{T}}\mathbf{X}^{\mathrm{T}}\mathbf{X}(\boldsymbol{\beta} - \hat{\boldsymbol{\beta}}) \leq Ps^2F(P, N-P; \alpha) \tag{2.12}$$

Geometrically this region results because the expectation surface is a plane and the residual vector is orthogonal to that plane, so the region of plausible values on the expectation plane is a disk. Taking the disk through the linear mapping relating points on the expectation plane to points on the parameter plane, then maps the disk to an ellipsoid on the parameter plane.

Approximate inference regions for a nonlinear model are defined, by analogy with equation (2.12), as

$$(\boldsymbol{\theta} - \hat{\boldsymbol{\theta}})^{\mathrm{T}} \hat{\mathbf{V}}^{\mathrm{T}} \hat{\mathbf{V}} (\boldsymbol{\theta} - \hat{\boldsymbol{\theta}}) \leq P s^2 F(P, N-P; \alpha) \tag{2.13}$$

or equivalently

$$(\boldsymbol{\theta} - \hat{\boldsymbol{\theta}})^{\mathrm{T}} \hat{\mathbf{R}}_1^{\mathrm{T}} \hat{\mathbf{R}}_1 (\boldsymbol{\theta} - \hat{\boldsymbol{\theta}}) \leq P s^2 F(P, N-P; \alpha) \tag{2.14}$$

where the derivative matrix $\hat{\mathbf{V}} = \hat{\mathbf{Q}}_1 \hat{\mathbf{R}}_1$ is evaluated at $\hat{\boldsymbol{\theta}}$. The boundary of this inference region (2.14) is [cf. (1.28)]

$$\{\boldsymbol{\theta} = \hat{\boldsymbol{\theta}} + \sqrt{P s^2 F(P, N-P; \alpha)}\ \hat{\mathbf{R}}_1^{-1} \mathbf{d} \mid \|\mathbf{d}\| = 1\} \tag{2.15}$$

Similarly, the approximate standard error for θ_p is s times the length of the pth row of $\hat{\mathbf{R}}_1^{-1}$ [cf. (1.33)]. Approximate correlations and standard errors for the parameters are easily calculated by factoring $\hat{\mathbf{R}}_1^{-1}$ into a diagonal matrix [cf. (1.34)] giving the lengths of the rows of $\hat{\mathbf{R}}^{-1}$ and a matrix with unit length rows as described in Section 1.2.3. The parameter approximate correlation matrix is calculated as in (1.35).

Example: Puromycin 7

Convergence for the Puromycin data was declared at $\hat{\boldsymbol{\theta}} = (212.7, 0.0641)^{\mathrm{T}}$, with $s^2 = 119.5$ on 10 degrees of freedom and

$$\hat{\mathbf{R}}_1 = \begin{bmatrix} -2.4441 & 1568.7 \\ 0 & 1320.3 \end{bmatrix}$$

The 95 and 99% approximate joint inference regions were obtained by evaluating (2.15) with $\mathbf{d} = (\cos\omega, \sin\omega)^{\mathrm{T}}$ and are plotted in Figure 2.14. To calculate approximate marginal inference intervals, we factor

$$\hat{\mathbf{R}}_1^{-1} = \begin{bmatrix} -0.4092 & 0.4861 \\ 0 & 0.0007574 \end{bmatrix}$$

$$= \begin{bmatrix} 0.6354 & 0 \\ 0 & 0.0007574 \end{bmatrix} \begin{bmatrix} -0.6439 & 0.7651 \\ 0 & 1.0000 \end{bmatrix}$$

so the approximate standard errors are 6.95 and 8.28×10^{-3} and the approximate correlation between θ_1 and θ_2 is 0.77. A 95% approximate marginal inference interval for θ_2, for example, is

$$0.0641 \pm \sqrt{119.5}\,(0.0007574)\ t(10; 0.025)$$

or 0.0641 ± 0.0185. The 95% marginal inference intervals for both parameters are shown as dashed lines in Figure 2.14. ■

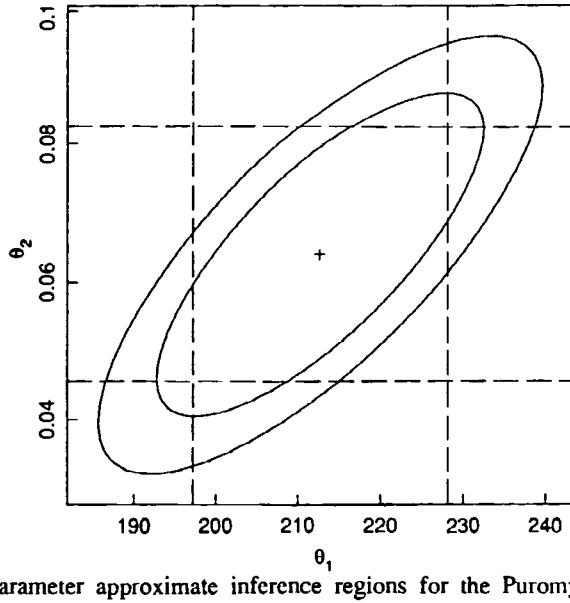

Figure 2.14 Parameter approximate inference regions for the Puromycin data. We show the least squares estimates (+), the parameter joint 95 and 99% inference regions (solid lines), and the marginal 95% inference intervals (dashed lines).

Example: BOD 5

Convergence for the BOD data was declared at $\hat{\boldsymbol{\theta}} = (19.143, 0.5311)^T$, with $s^2 = 6.498$ on 4 degrees of freedom and

$$\hat{\mathbf{R}}_1 = \begin{bmatrix} -1.9556 & -20.4986 \\ 0 & -12.5523 \end{bmatrix}$$

giving approximate standard errors of 2.50 and 0.203.

The 95 and 99% approximate joint inference regions are plotted in Figure 2.15 together with the 95% approximate marginal intervals. Note that the regions include negative values for θ_2, and such values are not physically meaningful. The approximate correlation between θ_1 and θ_2 is -0.85. ■

When there are more than two parameters, it is not possible to plot the joint approximate inference region, and so it is common to summarize the inferential situation by quoting the approximate marginal inference intervals and the parameter correlation matrix and by making pairwise plots of the inference region. More exact methods for summarizing the inferential situtation are presented in Chapter 6.

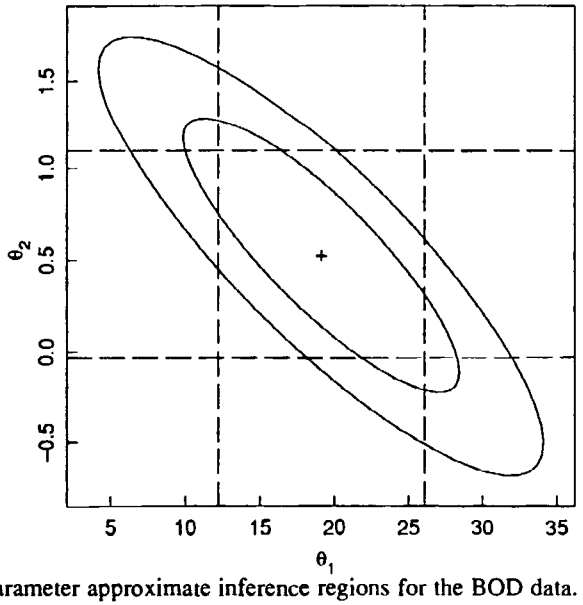

Figure 2.15 Parameter approximate inference regions for the BOD data. We show the least squares estimates (+), the parameter joint 95 and 99% inference regions (solid lines), and the marginal 95% inference intervals (dashed lines).

Example: Isomerization 1

Data on the reaction rate of the catalytic isomerization of *n*-pentane to isopentane versus the partial pressures of hydrogen, *n*-pentane, and isopentane as given in Carr (1960) are presented in Appendix 1, Section A1.5, and plotted in Figure 2.16. A proposed model function for these data is

$$f(\mathbf{x},\boldsymbol{\theta}) = \frac{\theta_1\theta_3(x_2 - x_3/1.632)}{1+\theta_2 x_1 + \theta_3 x_2 + \theta_4 x_3}$$

Parameter estimates and summary statistics are given in Table 2.2, and residual plots versus the partial pressures and the fitted values in Figure 2.17. The plots show the residuals are generally well behaved. The summary statistics suggest potential difficulties, since some of the correlations are extremely high and some of the standard errors produce approximate 95% intervals which include negative values, but the parameters must be positive to be physically meaningful. The pairwise plots of the parameter approximate 95% inference region, given in Figure 2.18, clearly extend into negative parameter regions. ■

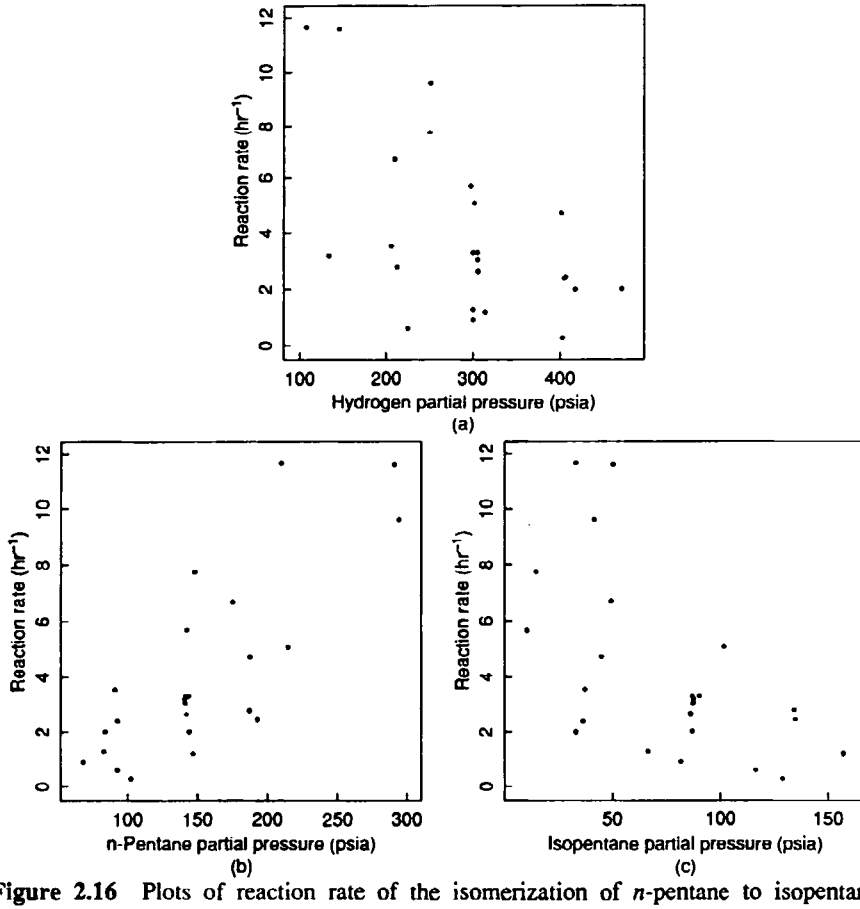

Figure 2.16 Plots of reaction rate of the isomerization of *n*-pentane to isopentane versus the partial pressures of hydrogen in part *a*, *n*-pentane in part *b*, and isopentane in part *c*.

Table 2.2 Parameter summary for the isomerization data.

Parameter	Estimate	Standard Error	Approximate Correlation Matrix			
θ_1	35.92	8.21	1.000			
θ_2	0.0708	0.1783	−0.805	1.000		
θ_3	0.0377	0.0998	−0.840	0.998	1.000	
θ_4	0.167	0.415	−0.790	0.998	0.995	1.000

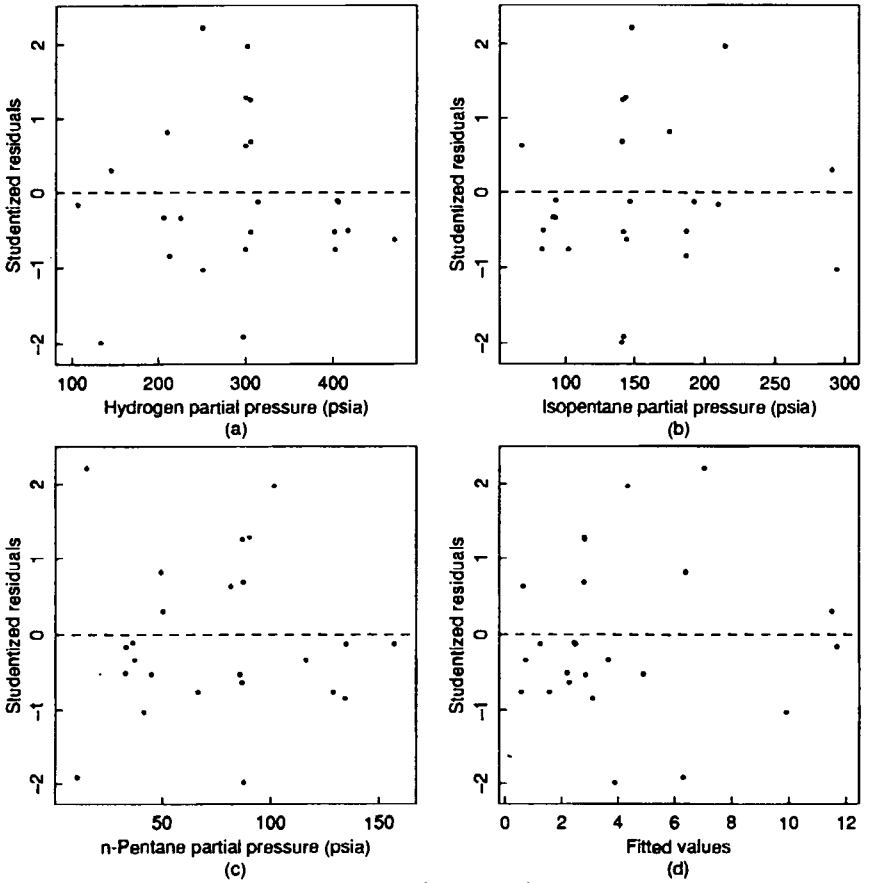

Figure 2.17 Studentized residuals for the isomerization data are plotted versus the partial pressures of hydrogen in part *a*, isopentane in part *b*, and *n*-pentane in part *c*, and versus the fitted values in part *d*.

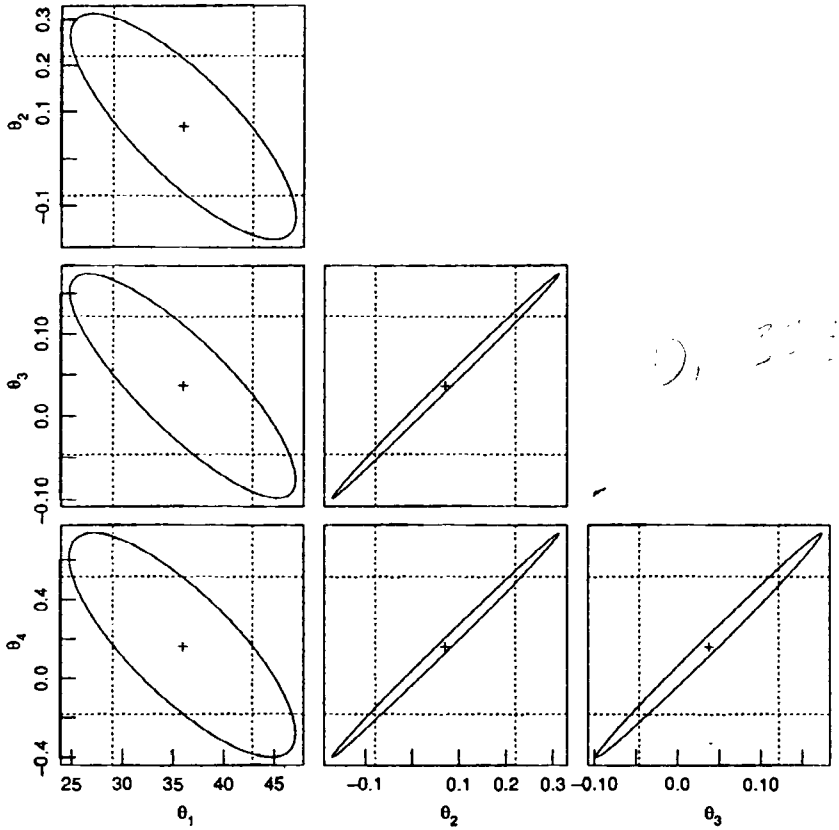

Figure 2.18 Pairwise plots of the parameter approximate 95% inference region for the isomerization data. For each pair of parameters we show the least squares estimates (+), the parameter approximate joint 95% inference region (solid line), and the approximate marginal 95% inference intervals (dotted lines).

2.3.2 Approximate Inference Bands for the Expected Response

Linear approximation inference intervals and bands for the expected response in nonlinear regression can be generated using the analogs of the equation for linear regression, (1.11) and (1.12). In those equations, we simply replace the estimated value $\mathbf{x}_0^T\hat{\boldsymbol{\beta}}$ by $f(\mathbf{x}_0,\hat{\boldsymbol{\theta}})$, the matrix $\mathbf{X}$ by $\hat{\mathbf{V}}$, and the derivative vector $\mathbf{x}_0$ by

$$\mathbf{v}_0 = \left.\frac{\partial f(\mathbf{x}_0,\boldsymbol{\theta})}{\partial \boldsymbol{\theta}^T}\right|_{\hat{\boldsymbol{\theta}}}$$

The $1-\alpha$ approximate inference interval is then

$$f(\mathbf{x}_0, \hat{\boldsymbol{\theta}}) \pm s \, \| \mathbf{v}_0^T \hat{\mathbf{R}}_1^{-1} \| \, t(N-P; \alpha/2) \qquad \text{[cf. (1.36)]}$$

and the $1-\alpha$ approximate inference band is

$$f(\mathbf{x}, \hat{\boldsymbol{\theta}}) \pm s \, \| \mathbf{v}^T \hat{\mathbf{R}}_1^{-1} \| \sqrt{P \, F(P, N-P; \alpha)} \qquad \text{[cf. (1.37)]}$$

Example: Puromycin 8

For the Puromycin data, the estimated response at $x = 0.4$ is 183.3 and the derivative vector is $\mathbf{v} = (0.8618, -394.9)^T$, so that, using $\hat{\mathbf{R}}_1^{-1}$ from Example Puromycin 6, $\mathbf{v}^T \hat{\mathbf{R}}_1^{-1} = (-0.3526, 0.1198)$. The inference band at $x = 0.4$ is then (171.6, 195.0). A plot of the approximate 95% inference band is given in Figure 2.19. The band gradually widens from zero width at $x = 0$ to a constant width as $x \to \infty$. ■

Example: BOD 6

The estimated response function for the BOD data and the approximate 95% inference band is plotted in Figure 2.20. The band widens from zero width at $x = 0$, narrows around $x = 4$ and then gradually approaches a constant width as $x \to \infty$. ■

Inference bands for nonlinear models behave quite differently from those for linear models. In the above examples, because the functions are constrained

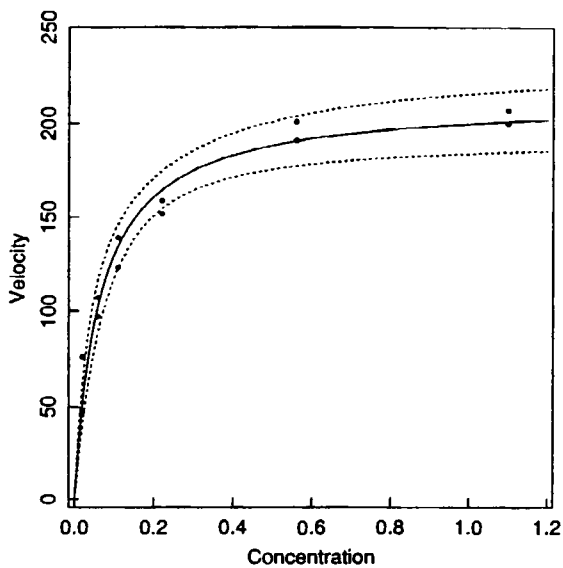

Figure 2.19 Approximate 95% inference band for the Puromycin data. The fitted expectation function is shown as a solid line, and the 95% inference band is shown as a pair of dotted lines.

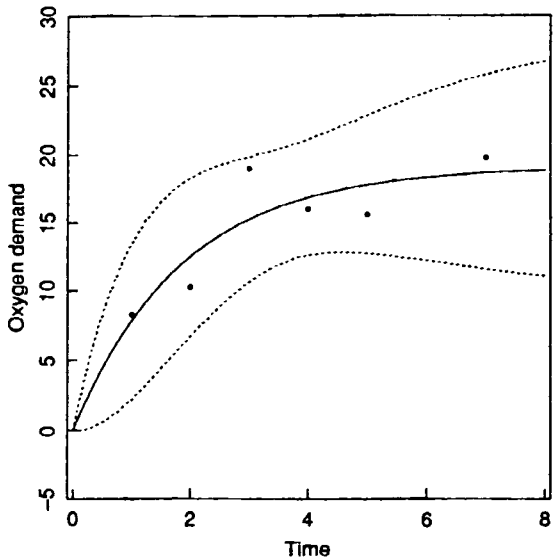

Figure 2.20 Approximate 95% inference band for the BOD data. The fitted expectation function is shown as a solid line, and the 95% inference band is shown as a pair of dotted lines.

to go through the origin, the bands reduce to 0 there. Also, because the model functions approach horizontal asymptotes, the inference bands approach asymptotes. These characteristics differ from those of the inference bands for linear models as exemplified in Figure 1.3. There it is seen that the bands are narrowest near the middle of the data, and expand without limit.

2.4 Nonlinear Least Squares via Sums of Squares

Sums of squares occur explicitly in linear and nonlinear least squares because of the assumptions of normality, independence, and constant variance of the disturbances. It is therefore natural to view linear and nonlinear regression via sums of squares, which can help in understanding these two topics. The likelihood approach is especially closely linked to sum of squares contours, because the loglikelihood function is directly proportional to the sum of squares function $S(\boldsymbol{\theta})$.

An important characteristic of linear models is that the sum of squares function $S(\boldsymbol{\beta})$ is quadratic. Because of this, contours of constant sums of squares are well-behaved regular curves or surfaces, such as ellipses and ellipsoids, and so the loglikelihood function can be completely summarized by:

the minimum value of the sum of squares function, $S(\hat{\boldsymbol{\beta}})$,

the location of the minimum of the sum of squares function, $\hat{\boldsymbol{\beta}}$, and the second derivative (Hessian) of the sum of squares function,

$$\frac{\partial^2 S(\boldsymbol{\beta})}{\partial\boldsymbol{\beta}\partial\boldsymbol{\beta}^{\mathrm{T}}} = \mathbf{X}^{\mathrm{T}}\mathbf{X}$$

Furthermore, all these quantities can be determined analytically. For nonlinear models, however, the sum of squares function is not regular or well behaved, and so it is difficult to summarize the loglikelihood function.

2.4.1 The Linear Approximation

Linear approximations of the expectation function are used to determine increments while seeking the least squares estimates, and to determine approximate inference regions when convergence has been achieved. The linear approximation to $\boldsymbol{\eta}(\boldsymbol{\theta})$ based at $\boldsymbol{\theta}^0$, (2.6), produces a linear approximation to the residual vector $\mathbf{z}(\boldsymbol{\theta})$, (2.7), and hence a *quadratic* approximation $\tilde{S}(\boldsymbol{\theta})$ to the sum of squares function $S(\boldsymbol{\theta})$, since

$$\begin{aligned} S(\boldsymbol{\theta}) &= \| \mathbf{y} - \boldsymbol{\eta}(\boldsymbol{\theta}) \|^2 \\ &= \mathbf{z}(\boldsymbol{\theta})^{\mathrm{T}}\mathbf{z}(\boldsymbol{\theta}) \approx \tilde{S}(\boldsymbol{\theta}) \\ &= [\mathbf{z}^0 - \mathbf{V}^0(\boldsymbol{\theta}-\boldsymbol{\theta}^0)]^{\mathrm{T}}[\mathbf{z}^0 - \mathbf{V}^0(\boldsymbol{\theta}-\boldsymbol{\theta}^0)] \\ &= \mathbf{z}^{0\mathrm{T}}\mathbf{z}^0 - 2\mathbf{z}^{0\mathrm{T}}\mathbf{V}^0(\boldsymbol{\theta}-\boldsymbol{\theta}^0) + (\boldsymbol{\theta}-\boldsymbol{\theta}^0)^{\mathrm{T}}\mathbf{V}^{0\mathrm{T}}\mathbf{V}^0(\boldsymbol{\theta}-\boldsymbol{\theta}^0) \\ &= S(\boldsymbol{\theta}^0) - 2[\mathbf{y} - \boldsymbol{\eta}(\boldsymbol{\theta}^0)]^{\mathrm{T}}\mathbf{V}^0(\boldsymbol{\theta}-\boldsymbol{\theta}^0) + (\boldsymbol{\theta}-\boldsymbol{\theta}^0)^{\mathrm{T}}\mathbf{V}^{0\mathrm{T}}\mathbf{V}^0(\boldsymbol{\theta}-\boldsymbol{\theta}^0) \end{aligned} \tag{2.16}$$

The location of the minimum of $\tilde{S}(\boldsymbol{\theta})$ is

$$\boldsymbol{\theta}^1 = \boldsymbol{\theta}^0 + (\mathbf{V}^{0\mathrm{T}}\mathbf{V}^0)^{-1}\mathbf{V}^{0\mathrm{T}}\mathbf{z}^0$$

which gives the Gauss–Newton increment.

Note that the quadratic approximation (2.16) is not the second order Taylor series approximation to $S(\boldsymbol{\theta})$ based at $\boldsymbol{\theta}^0$. The Hessian in the Taylor series approximation includes a term involving the second order partial derivatives of the model function with respect to the parameters (see Section 3.5.1).

Contours of the approximate sum of squares function (2.16) are ellipsoids centered at $\boldsymbol{\theta}^1$ and of the form

$$(\boldsymbol{\theta}-\boldsymbol{\theta}^1)^{\mathrm{T}}\mathbf{V}^{0\mathrm{T}}\mathbf{V}^0(\boldsymbol{\theta}-\boldsymbol{\theta}^1) = c$$

Of particular interest is the approximating contour

$$(\boldsymbol{\theta}-\boldsymbol{\theta}^1)^{\mathrm{T}}\mathbf{V}^{0\mathrm{T}}\mathbf{V}^0(\boldsymbol{\theta}-\boldsymbol{\theta}^1) = \mathbf{z}^{0\mathrm{T}}\mathbf{V}^0(\mathbf{V}^{0\mathrm{T}}\mathbf{V}^0)^{-1}\mathbf{V}^{0\mathrm{T}}\mathbf{z}^0$$

which passes through $\boldsymbol{\theta}^0$. If this contour is close to the actual sum of squares contour which passes through $\boldsymbol{\theta}^0$, then we can expect that $\boldsymbol{\theta}^1$ will be close to the optimal value of $\boldsymbol{\theta}$.

Example: Rumford 5

In Figure 2.21 we plot the sum of squares function, $S(\theta)$, for the Rumford data as a solid line. Superimposed on the plot is the approximating quadratic, $\bar{S}(\theta)$, obtained by taking a linear Taylor series approximation to the expectation function at $\theta^0 = 0.02$, shown as a dashed line.

A careful examination of $S(\theta)$ shows that it is not a parabola but is asymmetric, with a steeper rise to the left of the minimum than to the right. The closeness of $S(\theta)$ to a parabola indicates the small degree of nonlinearity of this model–data set combination. The minimum of the approximating parabola is at 0.008, and so the Gauss–Newton increment is $0.008 - 0.02 = -0.012$. ■

Example: Puromycin 9

In Figure 2.22 we plot sum of squares contours, $S(\boldsymbol{\theta})$, for the Puromycin data, shown as solid lines, and the location of the minimum, shown as +. Also shown, as a dashed line, is the ellipse derived from the linear approximation to the expectation function at $\boldsymbol{\theta}^0 = (205, 0.08)^T$. The approximating paraboloid has the same value and curvature at $\boldsymbol{\theta}^0$ as the true sum of squares surface, and so the location of the minimum of the paraboloid, denoted by *, is used as the apparent minimum of the true sum of squares surface. The Gauss increment is therefore the vector joining the starting point $\boldsymbol{\theta}^0$ to the point indicated by *.

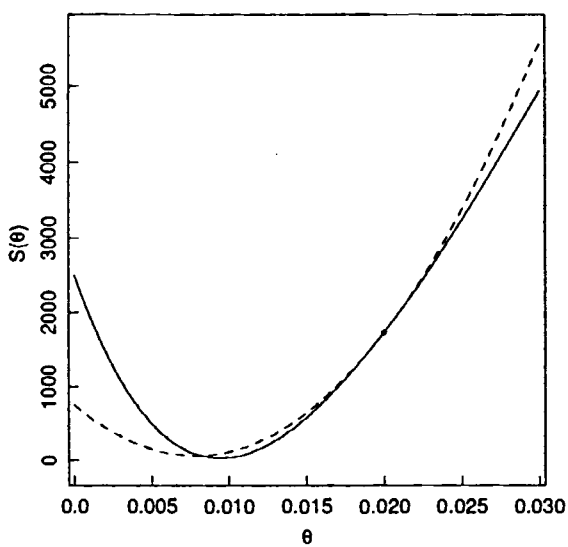

Figure 2.21 Sum of squares function for the Rumford data. The true sum of squares curve is shown as a solid line, and the parabola from the linear approximation at $\theta^0 = 0.02$ is shown as a dashed line.

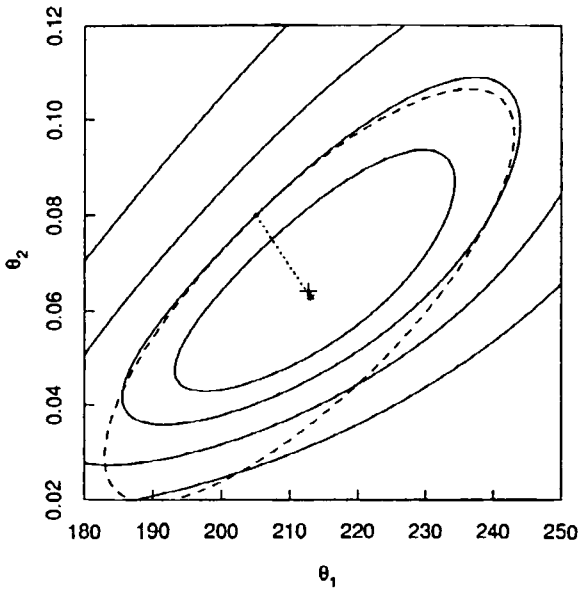

Figure 2.22 Sum of squares contours for the Puromycin data. True sum of squares contours are shown as solid lines, and the elliptical approximate contour from the linear approximation at $\boldsymbol{\theta}^0 = (205, 0.08)^T$ is shown as a dashed line. The location of the minimum sum of squares (+) and the center of the ellipse (*) are also shown. The dotted line is the Gauss–Newton increment.

Because the model–data set combination is not badly nonlinear, the sums of squares contours are quite elliptical, and the minimum of the approximating paraboloid is near the minimum of the true sum of squares surface. ■

Example: BOD 7

In Figure 2.23 we plot sum of squares contours, $S(\boldsymbol{\theta})$, for the BOD data, shown as solid lines, and location of the minimum, shown as +. Also shown, as a dashed line, is a portion of the ellipse derived from the linear approximation to the expectation function at $\boldsymbol{\theta}^0 = (20, 0.24)^T$. The center of the ellipse is indicated by *.

In this example, the ellipse is a poor approximation to the true contour. The center of the ellipse is not close to the minimum of the true sum of squares surface and furthermore has a true sum of squares greater than that at $\boldsymbol{\theta}^0$. ■

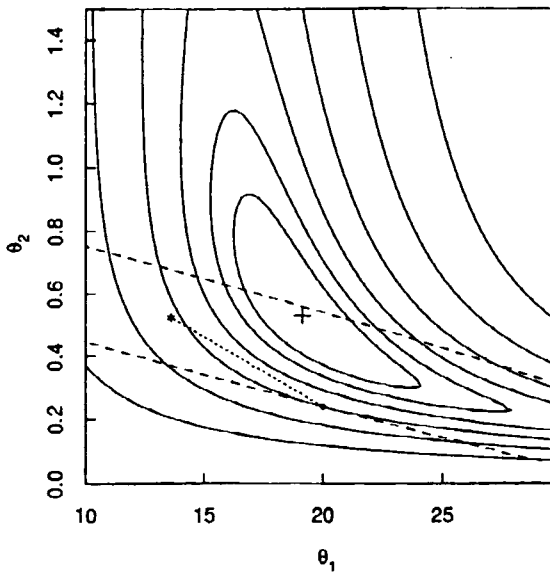

Figure 2.23 Sum of squares contours for the BOD data. True sum of
are shown as solid lines, and a portion of the elliptical approximate
linear approximation at $\boldsymbol{\theta}^0 = (20, 0.24)^T$ is shown as a dashed line. Th
minimum sum of squares (+) and the center of the ellipse (*) are also sh
line is the Gauss–Newton increment.

2.4.2 Overshoot

The next iteration is carried out from the location of the appare
the sum of squares surface—provided, of course, that $S(\boldsymbol{\theta}^1)$ is
In the Rumford example and in the Puromycin example, because
ty is moderate, the sum of squares at $\boldsymbol{\theta}^1$ is less than that at $\boldsymbol{\theta}^0$,
proceed to iterate from $\boldsymbol{\theta}^1$. For the BOD example, however, the
at $\boldsymbol{\theta}^1$ is greater than that at $\boldsymbol{\theta}^0$, so we have overshot the minin
porating a step factor, so that only a fraction of the increment
find a point with a smaller sum of squares, as described in Sectio

2.5 Use of the Linear Approximation

In this chapter we have used the linear approximation in two way

(1) to obtain a Gauss–Newton increment, and
(2) to obtain linear approximation inference regions.

For (1), the linear approximation is useful because the increment it generates can be checked by comparing $S(\boldsymbol{\theta}^0+\boldsymbol{\delta}^0)$ to $S(\boldsymbol{\theta}^0)$. If the sum of squares increases, we modify the increment with a step factor. Furthermore, the approximation is updated at each iteration.

For (2), the linear approximation provides inference regions which are easy to calculate and present for any number of parameters. However, the regions are based on only one approximation (at $\hat{\boldsymbol{\theta}}$), and we cannot easily check their adequacy.

The extent to which the approximate regions adequately delineate the regions of reasonable parameter values is determined by the adequacy of the linear approximation to the expectation function. We have noted in Section 2.2.2 that the linear approximation involves two distinct components: the *planar assumption* whereby the expectation surface is approximated by the tangent plane, and the *uniform coordinate assumption* whereby the true parameter coordinate system is approximated by a uniform system. Both these aspects influence the adequacy of the approximation for inference; they are discussed more fully in Chapter 6, where we present profile likelihood methods for determining and displaying more accurate inference regions, and in Chapter 7, where we present methods for measuring nonlinearity.

We hasten to warn the reader that *linear approximation regions can be extremely misleading.*

Exercises

2.1 Write a computer routine in a language of your choice to perform nonlinear least squares using the Gauss–Newton approach. Take the function, its derivatives with respect to the parameters, and starting values as input to the routine. If necessary, use the pseudocode in Appendix 3, Section A3.1 for guidance.

2.2 Use a nonlinear least squares routine to fit a model of the form $\beta_1+\beta_2(\text{age})^\alpha$ to the ln(PCB) data. Use starting values of $(-2.4, 2.3, 0.33)^T$ (the least squares estimates for β_1, β_2 for $\alpha=0.33$ from Example PCB 2).

2.3 (a) Plot the expectation surface for the Rumford model, using the design $\mathbf{x}=(7, 28)^T$. Mark the points on the expectation surface corresponding to the values $\theta=0, 0.01, \ldots, 0.1, 0.2, \ldots, 1.0, \infty$. Compare this expectation surface with the one based on the design $\mathbf{x}=(4, 41)^T$ plotted in Figure 2.3. Which design has smaller overall intrinsic nonlinearity? Which design has smaller overall parameter effects nonlinearity?

(b) Plot the expectation surface for the Rumford model, using the design $\mathbf{x}=(12, 14)^T$. Mark the points on the expectation surface corresponding to the values $\theta=0, 0.01, \ldots, 0.1, 0.2, \ldots, 1.0, \infty$. Compare this expectation surface with the one based on the design $\mathbf{x}=(4, 41)^T$ plotted in Figure 2.3 and with that from part (a). Which design has smallest overall intrinsic nonlinearity? Which design has smallest overall parameter effects nonlinearity?

(c) What kind of design would have zero intrinsic nonlinearity everywhere? Why?

(d) Would the design in part (c) have zero parameter effects nonlinearity? Why?

2.4 (a) Plot the expectation surface for the linear model $\ln(\text{PCB}) = \beta \ln(\text{age})$ for the design age = 5, 10. Mark the points on the surface corresponding to $\beta = 0, 1, 2, 3$.

(b) Compare this expectation surface and its properties with those of the nonlinear Rumford model shown in Figure 2.3.

(c) Compare this expectation surface and its properties with those of the nonlinear Rumford model plotted in Problem 2.3.

2.5 (a) Generate the expectation vector, the residual vector, the sum of squares $S(\boldsymbol{\theta}^0)$, and the derivative matrix $\mathbf{V}^0$ for the data and model from Appendix 4, Section A4.1, at the starting values $\boldsymbol{\theta}^0 = (2.20, 0.26)^{\mathrm{T}}$.

(b) Calculate the increment $\boldsymbol{\delta}^0$ and $S(\boldsymbol{\theta}^1)$, where $\boldsymbol{\theta}^1 = \boldsymbol{\theta}^0 + \lambda\boldsymbol{\delta}^0$, for $\lambda = 0.25, 0.50$, and 1.0. Is a step factor less than 1 necessary in this case?

2.6 (a) Use the fact that, for the model in Problem 2.5, θ_1 is conditionally linear, and generate and plot exact sum of squares contours for the data in Appendix 4, Section A4.1. (That is, for any specified value of θ_2, it is possible to use linear least squares to obtain the conditional estimate $\tilde{\theta}_1$ and to calculate the values of θ_1 which produce a specified sum of squares. By specifying the sum of squares to be that corresponding to a contour value, it is possible to generate the exact coordinates of points on the contour.) Let θ_2 go from 0.12 to 0.3 in steps of 0.01, and use contour values corresponding to 50, 75, and 95% confidence levels. Mark the location of the minimum on the plot.

(b) Compare these contours with those in Figure 2.23. Which data set suffers most from nonlinearity?

(c) Since the data are from the same type of experiment with the same model, how can this difference be explained?

2.7 Plot the point corresponding to $\boldsymbol{\theta}^0$ and the increment $\boldsymbol{\delta}^0$ from Problem 2.5 on the contour plot from Problem 2.6. Mark the points corresponding to the values $\lambda = 0.25, 0.5$, and 0.75 on the increment vector. Is a step factor less than 1 necessary in this case?

2.8 (a) Use the data, model, and starting values from Problem 2.5 in a nonlinear estimation routine to obtain the least squares parameter estimates.

(b) Calculate and plot the linear approximation joint and marginal inference regions on the plot from Problem 2.6.

(c) Are the linear approximation inference regions accurate in this case?

CHAPTER 3.

Practical Considerations in Nonlinear Regression

"Rationally, let it be said in a whisper, experience is certainly worth more than theory."

– Amerigo Vespucci

Nonlinear estimation, like all data analysis procedures, involves many practical considerations. In this chapter, we discuss some techniques which help ensure a successful nonlinear analysis. The topics include model specification, preliminary analysis, determination of starting values, transformations of parameters and variables, other iteration schemes, convergence, assessment of fit and modification of models, correlated residuals, accumulated data, comparison of models, parameters as functions of other variables, and presentation of results. A case study in which we illustrate many of the techniques presented in this chapter is given in Section 3.13. The important practical problem of designing experiments for nonlinear models is discussed in the final section.

3.1 Model Specification

An important step in any nonlinear analysis is specification of the model, which includes specifying both the expectation function and the characteristics of the disturbance.

3.1.1 The Expectation Function

Ideally, physical, biological, chemical, or other theoretical considerations will lead to a *mechanistic* model for the expectation function. The analyst's job is then to find the simplest form of the model and the parameter estimates which

provide an adequate fit of the model to the data, subject to the assumptions about the disturbance. Note that it is not necessary for the expectation function to be stated as an explicit function of the parameters and the control variables. In Chapter 5 we discuss an important class of models, known as compartment models, in which the expected response is given by the solution to a set of linear differential equations. Special techniques, developed in that chapter, can be used to avoid solving explicitly for the expectation function in terms of the parameters and independent variables.

In other situations, the expectation function may be the solution to a nonlinear differential equation or an integral equation which has no analytic solution. Then the value of the expectation function must be determined numerically for any given parameter values for a regular nonlinear least squares program to be used. In such situations, numerical parameter derivatives or a derivative-free optimization procedure will often have to be used to calculate the least squares estimates. However, as discussed in Caracotsios and Stewart (1985), when an expectation function is obtained from the solution to a set of ordinary differential equations, the parameter derivatives of the expectation function can be determined from the sensitivity functions for the system of differential equations. These functions are evaluated numerically at the same time as the solution of the differential equations is evaluated.

Example: α-Pinene 1

The decomposition of α-pinene was investigated by Fuguitt and Hawkins (1945, 1947), who reported the concentrations of five reactants as a function of time, at a series of reaction temperatures. In Appendix 1, Section A1.6, we present the data for the run at 189.5°C.

We discuss these data in Chapters 4 and 5 and fit a model which is specified by a set of linear differential equations. As discussed in Chapter 5, the parameters in such models can be estimated very easily, due to the ease with which they can be specified and the ease with which the responses and the derivatives with respect to the parameters can be evaluated. As will be also shown in Chapter 5, however, the linear differential equation model does not provide an adequate fit to the α-pinene data.

Stewart and Sorensen (1981) analyzed the complete data set reported by Fuguitt and Hawkins (1945, 1947), and proposed a model consisting of a set of five nonlinear differential equations

$$\frac{df_1}{dt} = -(\theta_1 + \theta_2)f_1 - 2\theta_3 f_1^2$$

$$\frac{df_2}{dt} = -\theta_4 f_2 + \theta_5 f_4$$

$$\frac{df_3}{dt} = \theta_1 f_1$$

$$\frac{df_4}{dt} = \theta_2 f_1 + \theta_4 f_2 - \theta_5 f_4 - 2\theta_6 f_4^2 + 2\theta_7 f_5$$

$$\frac{df_5}{dt} = \theta_8 f_1^2 + \theta_6 f_4^2 - \theta_7 f_5$$

where f_i, $i = 1, \ldots, 5$, represent the theoretical responses at time t.

There is no analytic solution to this set of differential equations, and so we must use numerical procedures. For given values of $\boldsymbol{\theta} = (\theta_1, \ldots, \theta_8)^T$, the differential equations would be integrated numerically using, say, a Runge–Kutta integration routine (Conte and de Boor, 1980). The numerical estimates of the responses, $\mathbf{f}(t)$, and the observed responses $\mathbf{y}(t)$, at the observation times, could then be used to calculate residuals from which an appropriate estimation criterion can be evaluated.

We discuss the choice of estimation criterion for multiresponse data in Chapter 4. Methods for obtaining derivatives of the response functions at the observation times by means of the "sensitivity functions"

$$\frac{\partial f_i(t)}{\partial \theta_p} \qquad i = 1, \ldots, 5 \quad p = 1, \ldots, P$$

are given in Caracotsios and Stewart (1985). The derivative matrix $\mathbf{V}$ can then be calculated from the sensitivity functions. ■

In other situations, a mechanistic model may not be advanced by the researcher, in which case the statistician will be called upon to suggest an equation. One approach is to ask the researcher to search through the literature to see if models have been proposed. If not, the statistician and the researcher can apply their modeling skills and develop a plausible mechanistic model. Failing this, the statistician must formulate a model which has the same sort of behavior as the data. If the data rise monotonically to an asymptote, perhaps a Michaelis–Menten, exponential rise, or logistic model might be appropriate. If the data peak and then decay towards zero, perhaps a double exponential, a Michaelis–Menten model with a quadratic term in the denominator, or a gamma function would be suitable.

Finally, if there are several sets of data, it may be possible to use the self-modeling approach of Lawton, Sylvestre, and Maggio (1972). This approach has been used in modeling spirometer curves which give the volume of air expelled from the lungs as a function of time for a number of subjects, and in modeling the creatine phosphokinase serum levels in patients suffering myocardial infarctions (Armstrong et al., 1979).

3.1.2 The Disturbance Term

All nonlinear estimation programs are based on specific assumptions about the disturbance term, usually that the disturbance is additive and normally distributed with zero mean, constant variance, and independence between cases (see

Section 1.3). Checking assumptions on the disturbance term is considerably easier and more sensitive if the data include replications at some or all of the design points. It is helpful if the experimental runs have been randomized, although many nonlinear experiments involve sequential measurements of the response, so that randomization may not be feasible.

At the initial stage, it is generally possible to check only one of the assumptions on the disturbance, namely constancy of variance. If there are replications, one can simply plot the data and look to see if the spread of the data tends to systematically increase or decrease with respect to any of the predictor variables. Alternatively, one can use an analysis of variance program to obtain averages and estimated variances and standard deviations for the replicated responses and then plot the variances or standard deviations versus the average, again looking for any systematic relationship, as discussed in Section 1.3. If none is apparent, then it may be tentatively assumed that the variance is constant and the analysis can proceed; if there is a relationship, then oftentimes a simple power transformation such as square root, logarithm, or inverse will stabilize the variance. Even without replications, some visual indication of constancy of variance can be gained from a data plot but this is not as definitive as when replications are available.

Note that transforming the data also involves transforming the expectation function. Thus, if there is a well-justified expectation function for the response but the data should be transformed to induce constant variance, then the same transformation should be applied to the expectation function to preserve the fundamental relationship. (See Section 3.9 for an example.) This is discussed more fully in Carroll and Ruppert (1984), where the Box–Cox transformations (Section 1.3.2) are applied to both the observed responses and the expected responses using the same transformation parameter λ. The optimal value of λ is determined by maximum likelihood. Alternatively, one can use weighted least squares (Draper and Smith, 1981) if a reasonable decision can be made about how the variance changes with respect to the response.

After a model has been fitted, it is possible to perform further checks on the disturbance assumptions by examining the residuals, as described in Sections 1.3, 3.7, and 3.8. It is also possible to check adequacy of the model and to compare rival models, as discussed in Section 3.10.

3.2 Preliminary Analysis

Having decided on a suitable expectation function (or set of plausible expectation functions) and a transformation of the data (and the expectation function, if necessary), we need to provide a computer program with the expectation function in some form and, unless numerical derivatives or derivative-free methods are used, its derivatives with respect to the parameters. Naturally, the expectation function and derivatives must be *correctly specified* and *correctly coded*, but (as most nonlinear analysts know from experience) a great many errors oc-

cur at this stage.

One way to ensure that the function is correctly specified and correctly coded is to use a separate program or even a calculator to evaluate the function at one or two distinct design points then compare these values with those from the nonlinear estimation routine. The same technique can be used for the derivatives, of course, but a better procedure is to compare the analytic derivatives from the routine with numerical derivatives obtained from finite differences of the expectation function (see Section 3.5.3). These comparisons are done on the basis of the relative differences between the derivatives calculated in the two ways. If v_{np} is the analytic derivative for case n and parameter p while $\tilde{v}_{np}$ is the finite difference approximation, then the relative difference is

$$\frac{|v_{np}-\tilde{v}_{np}|}{|v_{np}|} \qquad \text{if } v_{np} \neq 0$$

$$|v_{np}-\tilde{v}_{np}| \qquad \text{if } v_{np} = 0$$

Verifying that the relative differences are small not only provides a check on the derivatives, but, indirectly, a check on the expectation function, because a discrepancy between the numerical derivatives and the analytic derivatives can be due to either incorrect specification or coding of the analytic derivatives, or due to incorrect specification or coding of the expectation function, or both.

When coding the function, and especially when deriving and coding the derivatives, it is good practice to use temporary variables and the chain rule for derivatives, as demonstrated below. This helps avoid algebraic errors, which can occur when trying to reduce a function to its simplest form.

Example: Isomerization 2

For the isomerization data of Example Isomerization 1, the function

$$f(\mathbf{x},\boldsymbol{\theta}) = \frac{\theta_1\theta_3(x_2 - x_3/1.632)}{1+\theta_2 x_1 + \theta_3 x_2 + \theta_4 x_3}$$

is considered appropriate. To code the function and its derivatives, suppose the variables x_1, x_2, x_3 are coded as `X(1)`, `X(2)`, `X(3)`, and the parameters as `THETA(1)`, `THETA(2)`, `THETA(3)`, and `THETA(4)`. Then we can code the function simply and accurately by introducing the temporary variables

```
NUMX  = X(2) - X(3)/1.632
DENOM = 1.0 + THETA(2)*X(1) + THETA(3)*X(2)
        + THETA(4)*X(3)
RATIO = NUMX/DENOM
```

so the function becomes

```
F = THETA(1)*THETA(3)*RATIO
```

Next, introducing the temporary variable

```
FD = - F/DENOM
```

the derivatives become (denoting $\partial f/\partial\theta_1$ by F1 and so on),

```
F1 = THETA(3)*RATIO
F2 = FD*X(1)
F3 = THETA(1)*RATIO + FD*X(2)
F4 = FD*X(3)
```

■

It is also important to check that the data being analyzed are valid. That is, one must always ensure that the correct numerical values of the response and predictor variables have been entered into the machine. Probably the most effective way to check this is to plot the response versus each predictor variable, making sure that the response behaves the way it should with respect to each of the predictor variables.

3.3 Starting Values

One of the best things one can do to ensure a successful nonlinear analysis is to obtain good starting values for the parameters—values from which convergence is quickly obtained.

Several simple but useful principles for determining starting values can be used:

(1) interpret the behavior of the expectation function in terms of the parameters analytically or graphically;
(2) interpret the behavior of derivatives of the expectation function in terms of the parameters analytically or graphically;
(3) transform the expectation function analytically or graphically to obtain simpler, preferably linear, behavior;
(4) reduce dimensions by substituting values for some parameters or by evaluating the function at specific design values; and
(5) use conditional linearity.

We discuss each of these techniques in turn, and illustrate them with specific examples. For further discussion on obtaining starting values, see Ratkowsky (1983).

3.3.1 Interpreting the Expectation Function Behavior

One of the advantages of nonlinear regression is that the parameters in the expectation function are usually meaningful to the scientist or researcher. This meaning can be graphical, physical, biological, chemical, or in some other appropriate form, and can be very helpful in determining starting values. Initial

estimates for some of the parameters may be available from related experiments. Also, plotting a nonlinear expectation function using various values for the parameters is an extremely beneficial exercise, because in this way one becomes familiar with the function and how the parameters affect its behavior.

Sometimes starting values can be obtained by considering the behavior near the origin or at other special design values. For example, letting $x = 0$ gives the initial value of $\theta_1 + \theta_2$ for the model $f(x,\boldsymbol{\theta}) = \theta_1 + \theta_2 e^{-\theta_3 x}$, and letting $x \to \infty$ gives the asymptote θ_1 (assuming $\theta_3 > 0$).

Example: Puromycin 9

In the Michaelis–Menten expectation function, $f = \theta_1 x/(\theta_2 + x)$, the parameter θ_1 is the asymptotic velocity of the enzymatic reaction, and so can be estimated by the maximum observed data value, $y_{\max}$, or by eye from a plot. Graphically, θ_1 represents the asymptotic value of f as $x \to \infty$. Similarly, θ_2 represents the half-concentration, i.e. the value of x such that when the concentration reaches that value the velocity is one-half its ultimate value. For the Puromycin data, $y_{\max} = 207$ provides a good starting value for θ_1. From a plot of the data (Figure 2.1), or simply from a listing, it can be seen that the observed velocity reaches $y_{\max}/2$ at a concentration of about 0.06 and so this value can be used as a starting value for θ_2. ■

3.3.2 Interpreting Derivatives of the Expectation Function

Sometimes rates of change of the function at specified design values can be used to obtain parameter starting estimates. For example, the derivative with respect to x of the Michaelis–Menten model at $x = 0$ is θ_1/θ_2, and so by estimating the rate at $x = 0$ from the ratio of differences of adjacent y values over differences of adjacent x values, and dividing this rate into $y_{\max}$, we can obtain a starting value for θ_2. For Puromycin data, we obtain $\theta_2 = 207/(61/0.02) = 0.068$.

Similarly, derivatives at special values of x, such as limits or points of inflection, can be used. For example, for the double exponential model

$$f = \theta_1 e^{-\theta_2 x} + \theta_3 e^{-\theta_4 x}$$

assuming $\theta_2 > \theta_4$, the function behaves like a simple exponential $\theta_3 e^{-\theta_4 x}$ for large x and like $\theta_3 + \theta_1 e^{-\theta_2 x}$ for small x. Thus, the rate of change at small x provides an estimate of θ_2, and at large x an estimate of θ_4.

3.3.3 Transforming the Expectation Function

Transformations of the expectation function can often be used to obtain starting values. For instance, for the Michaelis–Menten model with a linear or quadratic denominator, simply taking the reciprocal of the function produces a model which can be rewritten as a linear model. Linear least squares can be used on the reciprocal data to estimate the linear parameters, which can then be used to

obtain starting values for $\boldsymbol{\theta}$. The model from Example Isomerization 1,

$$f(\mathbf{x}, \boldsymbol{\theta}) = \frac{\theta_1\theta_3(x_2 - x_3/1.632)}{1 + \theta_2 x_1 + \theta_3 x_2 + \theta_4 x_3}$$

is also transformably linear, since

$$\frac{x_2 - x_3/1.632}{f(\mathbf{x}, \boldsymbol{\theta})} = \frac{1}{\theta_1\theta_3} + \frac{\theta_2}{\theta_1\theta_3}x_1 + \frac{1}{\theta_1}x_2 + \frac{\theta_4}{\theta_1\theta_3}x_3$$

A linear regression (with a constant term) of $(x_2 - x_3/1.632)/y$ on x_1, x_2, and x_3 would yield starting values

$$\theta_1^0 = \frac{1}{\hat{\beta}_2} \qquad \theta_2^0 = \frac{\hat{\beta}_1}{\hat{\beta}_0} \qquad \theta_3^0 = \frac{\hat{\beta}_2}{\hat{\beta}_0} \qquad \theta_4^0 = \frac{\hat{\beta}_3}{\hat{\beta}_0}$$

For the model $f(\mathbf{x},\boldsymbol{\theta}) = \exp[-\theta_1 x_1 \exp(-\theta_2/x_2)]$, used in a chemical kinetics example (Bard, 1974, p. 124), taking logarithms twice gives

$$\ln\ln f = \ln x_1 + \ln(-\theta_1) - \frac{\theta_2}{x_2}$$

and one could again use linear least squares to obtain starting values.

Graphical transformations are also very effective. Plotting f versus x on semilog paper or plotting $\ln f$ versus x on regular graph paper often reveals the true nature of the data or enables one to see when one portion of the model is dominant, and hence where one can measure a rate and associate it with a particular parameter.

For example, the double exponential model

$$f(x,\boldsymbol{\theta}) = \theta_1 e^{-\theta_2 x} + \theta_3 e^{-\theta_4 x}$$

with $\theta_2 > \theta_4$ is approximately $\ln f = \ln\theta_3 - \theta_4 x$ at large x, which gives a straight line on a semilog plot. A simple fit can then be made by eye to obtain values for θ_3 and θ_4. These values can then be used to calculate values of $\theta_3 e^{-\theta_4 x}$ at all values of x, and hence residuals $\tilde{y} = y - \theta_3 e^{-\theta_4 x}$ can be derived. Plotting $\tilde{y}$ versus x on semilog paper then enables one to estimate θ_1 and θ_2. This process, known as *peeling*, can be used when the expectation function is a sum of several exponentials.

Example: Sulfisoxazole 1

To demonstrate the technique of peeling, we consider sulfisoxazole data given in Kaplan et al. (1972) and described in Appendix 1, Section A1.7. In this experiment, sulfisoxazole was administered to a subject intravenously, blood samples were taken at specified times, and the concentration of sulfisoxazole in the plasma was measured. The data are plotted in Figure 3.1.

Plotting the sulfisoxazole concentration on a log scale versus x as in Figure 3.2*a* reveals monotonic decay with straight line behavior for large x,

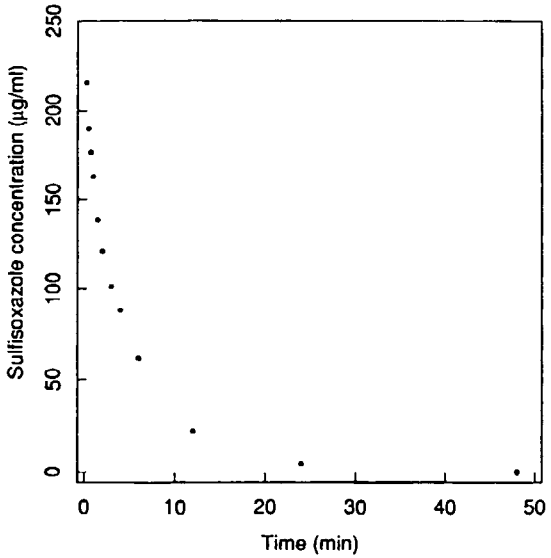

Figure 3.1 Plot of sulfisoxazole concentration in plasma versus time.

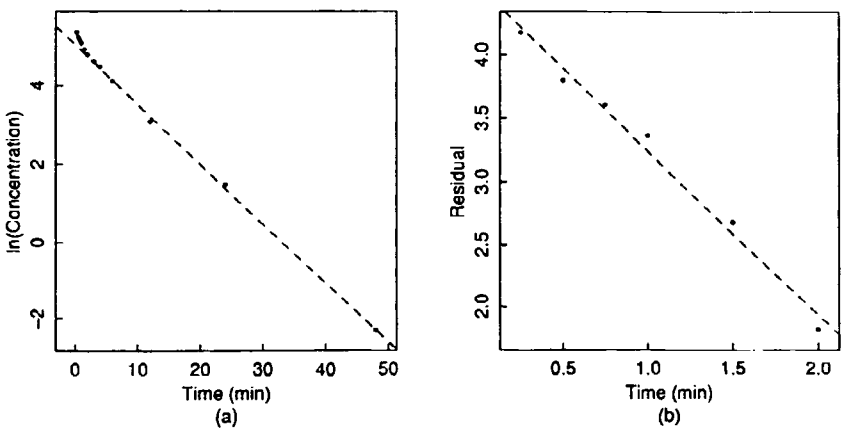

Figure 3.2 Curve peeling using the Sulfisoxazole data. In part *a* we show the data, plotted on a log scale, together with a straight line fit (dashed line) to the last six points. In part *b* we show, on a log scale, the residuals for the first six data points from the straight line fit in part *a*. The dashed line is the fitted line through these (log) residuals.

which suggests a model of the form

$$f(x,\boldsymbol{\theta}) = \theta_1 e^{-\theta_2 x} + \theta_3 e^{-\theta_4 x}$$

with all positive parameters. Fitting a straight line to the last six (log) data values gives an intercept of 5.05 and a slope of −0.153, so that the starting values are $\theta_3^0 = e^{5.05} = 156$ and $\theta_4^0 = 0.153$. Calculating the residuals

$$\tilde{y}_n = y_n - 156\,e^{-0.153x_n}$$

and plotting $\ln\tilde{y}$ versus x for the first six data values, as in Figure 3.2*b*, again reveals straight line behavior. Fitting a straight line to these (log) residuals gives an intercept of 4.55 and a slope of -1.31, so that the starting values are $\theta_1^0 = e^{4.55} = 95$ and $\theta_2 = 1.31$. ■

3.3.4 Reducing Dimensions

Peeling is an example of the general technique of reducing dimensions in order to obtain starting values. In this technique one estimates parameters successively, each estimated parameter making it easier to estimate the remaining ones. As another example of reducing parameter dimensions, consider the model $f = \theta_1 + \theta_2 e^{-\theta_3 x}$, where θ_3 is positive. Then the limiting value of the response when $x \to \infty$ is θ_1 and the value at $x = 0$ is $\theta_1 + \theta_2$. Depending on whether the data is increasing or decreasing, we can use $y_{\max}$ or $y_{\min}$ to get the starting value θ_1^0, and then use the difference $y(0) - \theta_1^0$ to get θ_2^0. We perform a linear regression (without a constant term) of $\ln[(y - \theta_1^0)/\theta_2^0]$ on x to obtain θ_3^0. Alternatively, once θ_1^0 and θ_2^0 are determined, we could substitute these values into the function and evaluate $(1/x)\ln[(y - \theta_1^0)/\theta_2^0]$ at selected values of x to obtain θ_3^0.

Sometimes we can reduce the dimensionality of the model and indirectly reduce the number of parameters. For example, with the model $f(\mathbf{x},\boldsymbol{\theta}) = \exp[-\theta_1 x_1 \exp(-\theta_2/x_2)]$, if there are some very large values of x_2, then the model is approximately $f(x_1,\boldsymbol{\theta}) = e^{-\theta_1 x_1}$, so it is easy to obtain a starting estimate for θ_1 by taking logarithms of the responses at large x_2. Similarly the model $f(\mathbf{x},\boldsymbol{\theta}) = \theta_1\theta_2 x_1/(1 + \theta_2 x_1 + \theta_3 x_2)$ reduces to a Michaelis–Menten type when x_2 is small, so it is easy to obtain starting values.

3.3.5 Conditional Linearity

In many model functions, several of the parameters are conditionally linear (see Section 2.1) and linear regression can be used to get starting values for these parameters conditional on the nonlinear parameters. Alternatively, special algorithms which exploit the conditional linearity, described in Section 3.5.5, can be used. These algorithms only require starting estimates for the nonlinear parameters. As an example of conditional linearity, in

$$f(x,\boldsymbol{\theta}) = \theta_1 + \theta_2 e^{-\theta_3 x}$$

both θ_1 and θ_2 are conditionally linear, so it is possible to use linear least squares to estimate θ_1^0 and θ_2^0 once an estimate for θ_3^0 has been obtained. A detailed example involving conditionally linear parameters is given in Section 3.6.

3.4 Parameter Transformations

As will be shown in Chapters 6 and 7, transforming the parameters in a nonlinear regression model can produce a much better linear approximation. This has the beneficial effects of making approximate inference regions better and speeding convergence to the least squares value. Parameter transformations can also be used to enforce constraints on the values of the parameters.

Note that transformations of parameters are very different from transformations of the responses. Transformations of the response distort the response space and create a new expectation surface, thereby affecting the disturbances and the validity of the assumptions on the disturbances. In contrast, transformations of the parameters merely relabel points in the parameter space and on the existing expectation surface. Consequently they do not affect the assumptions about the deterministic or the stochastic parts of the model, although they do affect the validity of the linear approximation and inferences based on it.

The use of parameter transformations to improve validity of the linear approximation is discussed in Chapter 7; here we focus on transformations to impose constraints on parameters and to improve convergence.

3.4.1 Constrained Parameters

The parameters in most nonlinear models are restricted to regions which make sense scientifically. For example, in the Michaelis–Menten model and in the isomerization model, all the parameters must be positive, and in exponential models, the parameters in the exponent usually must be positive.

It is often possible to ignore the restrictions when fitting the model and simply examine the converged parameter estimates to see if they satisfy the constraints. If the model fits the data well, the parameter estimates should be in a meaningful range. Sometimes, though, it may be dangerous to allow the parameter estimates to go into proscribed regions during the iterations because the parameter values may begin to oscillate wildly or cause numerical overflows. In these situations, one should impose the constraints throughout the estimation process.

General techniques for optimizing functions whose parameters are constrained, called *nonlinear programming*, are beyond the scope of this book. See, for example, Gill, Murray, and Wright (1981) or Bard (1974) for details. Fortunately, the types of constraints that are applied to the parameters of a nonlinear regression model are usually simple enough to be handled by parameter transformations. For example, if θ_p must be positive, we reparametrize to $\phi_p = \ln \theta_p$, so throughout the iterations the value of $\theta_p = e^{\phi_p}$ remains positive.

An *interval* constraint on a parameter, say

$$a \le \theta \le b$$

can be enforced by a logistic transformation of the form

$$\theta = a + \frac{b-a}{1+e^{-\phi}}$$

while an *order* constraint on parameters $\theta_j, \ldots, \theta_k$, say

$$a \le \theta_j \le \theta_{j+1} \le \cdots \le \theta_k \le b$$

can be enforced by a transformation given in Jupp (1978).

The order constraint can be used to ensure a unique optimum in a model with exchangeable parameters. As an example of such a model, consider the double exponential model

$$f(x,\boldsymbol{\theta}) = \theta_1 e^{-\theta_2 x} + \theta_3 e^{-\theta_4 x} \qquad 0 \le \theta_2, \theta_4$$

where the pairs of parameters (θ_1,θ_2) and (θ_3,θ_4) are *exchangeable*—that is, exchanging the parameter pair (θ_1,θ_2) with the pair (θ_3,θ_4) will not alter the values of the expected responses. Exchangeable parameters can create nasty optimization problems because the linear approximation cannot account for that kind of symmetry.

In this example, we remove the exchangeability by requiring

$$0 \le \theta_2 \le \theta_4$$

and enforce this with the transformation

$$\theta_2 = e^{\phi_2}$$

$$\theta_4 = e^{\phi_2}(1+e^{\phi_4})$$

Since θ_1 and θ_3 are conditionally linear parameters, their optimal values are uniquely determined when θ_2 and θ_4 are distinct. Thus we only need to keep θ_2 and θ_4 ordered to eliminate the exchangeability.

3.4.2 Facilitating Convergence

Parameter transformations can facilitate convergence because they prevent the parameters from venturing into proscribed regions. Transformations can also improve convergence by making the parameter lines behave more uniformly on the expectation surface so that the Gauss increment is more accurate. Joint variable–parameter transformations can also be used to improve the estimation situation by improving conditioning of the derivative matrix V. Frequently this is done by *centering* or *scaling* the data. For example, the simple model $f(x,\boldsymbol{\theta}) = \theta_1 e^{-\theta_2 x}$ has derivatives

$$\frac{\partial f}{\partial \theta_1} = e^{-\theta_2 x}$$

$$\frac{\partial f}{\partial \theta_2} = -x\theta_1 e^{-\theta_2 x}$$

and the derivative vectors tend to be collinear when the values of x are all posi-

tive. Rewriting the model as

$$f(x,\boldsymbol{\theta}) = \theta_1 e^{-\theta_2(x - x_0 + x_0)}$$

and reparametrizing with

$$\phi_1 = \theta_1 e^{-\theta_2 x_0}$$

$$\phi_2 = \theta_2$$

gives $f(x,\boldsymbol{\phi}) = \phi_1 e^{-\phi_2(x - x_0)}$, and now the derivatives with respect to $\boldsymbol{\phi}$ will be more nearly orthogonal. A useful choice is $x_0 = \bar{x}$.

Scaling the variables and the parameters can also improve conditioning by making the derivative matrix have column vectors which are more nearly equal in length.

Other transformations can be useful, depending on the context of the problem. For example, in chemical kinetics it is often useful to revise the model so that reciprocal absolute temperature is used rather than temperature T. Combining this with centering would then modify a term involving temperature to the form $1/T - 1/T_0$.

The effect of parameter transformations on parameter effects nonlinearities and the adequacy of linear approximation inference regions is discussed in Chapter 7.

3.5 Other Iterative Techniques

The Gauss–Newton iterative algorithm for nonlinear least squares, described in Section 2.2.1, is a simple, useful method for finding $\hat{\boldsymbol{\theta}}$. Some modifications to this method, as well as alternative methods, have been suggested—primarily to deal with ill-conditioning of the derivative matrix $\mathbf{V}$ and to avoid having to code and specify the derivatives.

3.5.1 A Newton–Raphson Method

The Gauss–Newton method for estimating nonlinear parameters can be considered as a special case of the more general Newton–Raphson method (Bard, 1974) which uses a local quadratic approximation to the objective function. Near $\boldsymbol{\theta}^0$, we approximate

$$S(\boldsymbol{\theta}) \approx S(\boldsymbol{\theta}^0) + \boldsymbol{\omega}^{\mathrm{T}}(\boldsymbol{\theta} - \boldsymbol{\theta}^0) + (\boldsymbol{\theta} - \boldsymbol{\theta}^0)^{\mathrm{T}} \frac{\boldsymbol{\Omega}}{2} (\boldsymbol{\theta} - \boldsymbol{\theta}^0)$$

where

$$\boldsymbol{\omega} = \frac{\partial S}{\partial \boldsymbol{\theta}}$$

is the *gradient* of $S(\boldsymbol{\theta})$ evaluated at $\boldsymbol{\theta}^0$ and

$$\mathbf{\Omega} = \frac{\partial^2 S}{\partial \boldsymbol{\theta}\, \partial \boldsymbol{\theta}^{\mathrm{T}}}$$

is the *Hessian* of $S(\boldsymbol{\theta})$ evaluated at $\boldsymbol{\theta}^0$. The approximating sum of squares function will have a stationary point when its gradient is zero—that is, when

$$\boldsymbol{\omega} + \mathbf{\Omega}(\boldsymbol{\theta} - \boldsymbol{\theta}^0) = \mathbf{0}$$

and this stationary point will be a minimum if $\mathbf{\Omega}$ is positive definite (all its eigenvalues positive). If $\mathbf{\Omega}$ is positive definite, the Newton–Raphson step is

$$\boldsymbol{\delta}^0 = -\mathbf{\Omega}^{-1}\boldsymbol{\omega}$$

For the function

$$S(\boldsymbol{\theta}) = (\mathbf{y} - \boldsymbol{\eta})^{\mathrm{T}}(\mathbf{y} - \boldsymbol{\eta})$$

the gradient is

$$\boldsymbol{\omega} = -2\mathbf{V}^{\mathrm{T}}(\mathbf{y} - \boldsymbol{\eta})$$

and the Hessian is

$$\mathbf{\Omega} = 2\mathbf{V}^{\mathrm{T}}\mathbf{V} - 2\frac{\partial \mathbf{V}^{\mathrm{T}}}{\partial \boldsymbol{\theta}^{\mathrm{T}}}(\mathbf{y} - \boldsymbol{\eta})$$

where $\mathbf{V}$ is the derivative matrix. The Gauss–Newton increment is therefore equivalent to the Newton–Raphson increment with the second derivative term $\partial \mathbf{V}^{\mathrm{T}}/\partial \boldsymbol{\theta}^{\mathrm{T}}$ set to zero.

Dennis, Gay, and Welsch (1981) describe a nonlinear least squares routine which develops a quasi-Newton approximation (Dennis and Schnabel, 1983) to the second term in the Hessian. This extends the Gauss–Newton algorithm and makes it closer to the Newton–Raphson algorithm, which has the advantage that the approximating Hessian should be closer to the actual Hessian than the single term $\mathbf{V}^{\mathrm{T}}\mathbf{V}$ used in the Gauss–Newton algorithm. However, the term $\mathbf{V}^{\mathrm{T}}\mathbf{V}$ is necessarily positive definite (or at least positive semidefinite), since the eigenvalues of $\mathbf{V}^{\mathrm{T}}\mathbf{V}$ are the squares of the singular values of $\mathbf{V}$. Adding another term on to this to form an approximating Hessian can destroy the positive definiteness, in which case the Newton–Raphson algorithm must be modified to restore positive definiteness in the Hessian.

3.5.2 The Levenberg–Marquardt Compromise

A condition that can cause erratic behavior of Gauss–Newton iterations is singularity of the derivative matrix $\mathbf{V}$ caused by collinearity of the columns. When $\mathbf{V}$ is nearly singular, $\boldsymbol{\delta}$ can be very large, causing the parameters to go into undesirable regions of the parameter space.

One solution to the problem of near-singularity is to perform the calculations for the increment in a numerically stable way, which is why we recommend using the *QR* decomposition rather than the normal equations. We also

recommend using double precision or extended precision arithmetic for the calculations, where feasible, and using joint variable–parameter transformations as discussed in Section 3.4.

Another general method for dealing with near-singularity is to modify the Gauss–Newton increment to

$$\boldsymbol{\delta}(k) = (\mathbf{V}^{\mathrm{T}}\mathbf{V} + k\mathbf{I})^{-1}\mathbf{V}^{\mathrm{T}}(\mathbf{y} - \boldsymbol{\eta}) \tag{3.1}$$

as suggested in Levenberg (1944), or to

$$\boldsymbol{\delta}(k) = (\mathbf{V}^{\mathrm{T}}\mathbf{V} + k\mathbf{D})^{-1}\mathbf{V}^{\mathrm{T}}(\mathbf{y} - \boldsymbol{\eta}) \tag{3.2}$$

as suggested in Marquardt (1963), where k is a conditioning factor and $\mathbf{D}$ is a diagonal matrix with entries equal to the diagonal elements of $\mathbf{V}^{\mathrm{T}}\mathbf{V}$. This is called the *Levenberg–Marquardt compromise* because the direction of $\boldsymbol{\delta}(k)$ is intermediate between the direction of the Gauss–Newton increment ($k \to 0$) and the direction of *steepest descent* $\mathbf{V}^{\mathrm{T}}(\mathbf{y} - \boldsymbol{\eta}) / \| \mathbf{V}^{\mathrm{T}}(\mathbf{y} - \boldsymbol{\eta}) \|$ $(k \to \infty)$.

Note that Levenberg recommends inflating the diagonal of $\mathbf{V}^{\mathrm{T}}\mathbf{V}$ by an additive factor, while Marquardt recommends inflating the diagonal by a multiplicative factor $1 + k$. Marquardt's method produces an increment which is invariant under scaling transformations of the parameters, so that if the scale for one component of the parameter vector is doubled, the increment calculated, and the corresponding component of the increment halved, the result will be the same as calculating the increment in the original scale. In Levenberg's method, this is not true. Box and Kanemasu (1984) showed, however, that if one requires invariance of the increment under linear transformations of the parameter space, the resulting increment is the Gauss–Newton increment with a step factor.

The Levenberg–Marquardt compromise is more difficult to implement than the Gauss–Newton algorithm, since one must decide how to manipulate both the conditioning factor k and the step factor λ; nevertheless it is implemented in many nonlinear least squares programs. Although we presented the increment in terms of the inverse of an augmented $\mathbf{V}^{\mathrm{T}}\mathbf{V}$ matrix, the actual calculations for the increment should be done using a QR decomposition of $\mathbf{V}$ and applying updates from a diagonal matrix using the Givens rotations (Dongarra et al., 1979, Chapter 10; Golub and Pereyra, 1973), since the Levenberg increment (3.1) is the least squares solution to the system with derivative matrix

$$\begin{bmatrix} \mathbf{V} \\ \sqrt{k}\,\mathbf{I} \end{bmatrix}$$

and response vector

$$\begin{bmatrix} \mathbf{y} - \boldsymbol{\eta} \\ \mathbf{0} \end{bmatrix}$$

For the Marquardt increment (3.2), the derivative matrix is changed to

$$\begin{bmatrix} \mathbf{V} \\ \sqrt{k}\,\mathbf{D}^{1/2} \end{bmatrix}$$

3.5.3 Numerical Derivatives

We have assumed that implementations of the algorithms we have described use analytic derivatives with respect to the parameters. Obtaining these derivatives and coding them is usually the most tedious and error-prone stage in a nonlinear analysis.

As a general rule we recommend using analytic derivatives for accuracy, although it is convenient to use programs which use numerical derivatives from finite differences. Such convenience is not obtained without cost, however, because numerical derivatives can be inaccurate and they usually increase the computing time necessary to obtain convergence. Furthermore, if second derivatives are required to investigate the effect of nonlinearity on inferences, the numerical second derivatives evaluated from numerical first derivatives can be very inaccurate. Other problems with numerical derivatives involve the choice of step size to determine the finite differences, and whether to use central or forward differences.

With forward differences, for the pth parameter we evaluate the model function using the current values of all the parameters except for the pth, which is incremented to $\theta_p(1+\varepsilon)$. Dividing the differences between the function values by the fractional amount $\varepsilon\theta_p$ gives an approximate derivative. This requires $1+P$ evaluations of the expected response vector at each iteration. Using central differences would require evaluation of the model function at $\theta_p(1\pm\varepsilon)$ in addition to the central value, so the total number of evaluations would be $1+2P$. Dennis and Schnabel (1983) recommend setting ε equal to the square root of the relative machine precision (that is, the square root of the smallest number which, when added to 1.0 in the floating point arithmetic of the computer, produces a number greater than 1.0).

3.5.4 Derivative-Free Methods

There are derivative-free methods which do not simply use numerical approximations to derivatives. Ralston and Jennrich (1978) introduced one such routine, DUD (Doesn't Use Derivatives), which is based on using a secant plane approximation to the expectation surface rather than a tangent plane approximation.

To use DUD, one must provide starting values $\boldsymbol{\theta}^0$. The program then automatically produces a further set of P parameter vectors by displacing each parameter in turn by 10%. These parameter vectors are then used to calculate expectation vectors $\boldsymbol{\eta}_1, \boldsymbol{\eta}_2, \ldots,$ giving a secant plane which matches the expectation surface at $P+1$ points. A set of linear coordinates is generated on the

secant plane, and the projection of $\mathbf{y}$ onto the secant plane is made and mapped into the parameter plane. This information is used to calculate a new $\boldsymbol{\theta}$ vector, say $\boldsymbol{\theta}'$, for which $\boldsymbol{\eta}(\boldsymbol{\theta}')$ is closer to $\mathbf{y}$ than any of the other parameter vectors. The parameter vector $\boldsymbol{\theta}$ corresponding to the $\boldsymbol{\eta}$ which is farthest from $\mathbf{y}$ is then replaced by $\boldsymbol{\theta}'$, and the process continued until convergence is achieved.

Example: Rumford 6

DUD can be illustrated very effectively using a two-observation example such as in Example Rumford 2. To simplify arithmetic and to provide a better scale for the figure, we provide the necessary two $(=P+1)$ starting values rather than using the automatic 10% displacement. The two starting values are chosen to be $\theta^1=0.02$ and $\theta^2=0.10$. Figure 3.3 shows the expectation surface $\boldsymbol{\eta}(\boldsymbol{\theta})$ together with the secant line $\mathbf{l}$ through the points $\boldsymbol{\eta}(\theta^1)$ and $\boldsymbol{\eta}(\theta^2)$. We now introduce a linear scale parameter α on $\boldsymbol{\theta}$ such that $\boldsymbol{\theta}=\boldsymbol{\theta}^1+T\alpha$, where $T=(\theta^2-\theta^1)$ and so $\alpha=0$ at θ^1 and $\alpha=1$ at θ^2. We also impose a linear scale on $\mathbf{l}$ such that $\mathbf{l}(\alpha)=\boldsymbol{\eta}(\theta^1)+\mathbf{H}\alpha$, where $\mathbf{H}=\boldsymbol{\eta}(\theta^2)-\boldsymbol{\eta}(\theta^1)$. The linear coordinate system is also shown in Figure 3.3.

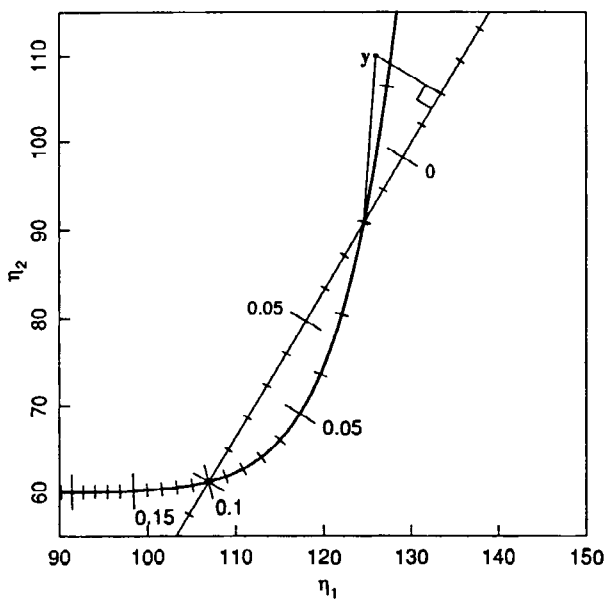

Figure 3.3 A geometric interpretation of the calculation of the DUD increment using the 2-case Rumford data. A portion of the expectation surface (heavy solid line) is shown in the response space together with the observed response $\mathbf{y}$. Also shown is the projection of $\mathbf{y}-\boldsymbol{\eta}(0.02)$ onto the secant plane joining $\boldsymbol{\eta}(0.02)$ and $\boldsymbol{\eta}(0.10)$ (solid line). The tick marks indicate true positions on the expectation surface and linear approximation positions on the secant plane.

For this example, $T = \theta^2 - \theta^1 = 0.08$, $\theta = \theta^1 + T\alpha$, so

$$\alpha = \frac{\theta - \theta^1}{T}$$

$$\mathbf{H} = \begin{bmatrix} 60 + 70\, e^{-4(0.1)} \\ 60 + 70\, e^{-41(0.1)} \end{bmatrix} - \begin{bmatrix} 60 + 70\, e^{-4(0.02)} \\ 60 + 70\, e^{-41(0.02)} \end{bmatrix}$$

$$= \begin{bmatrix} 106.92 \\ 61.16 \end{bmatrix} - \begin{bmatrix} 124.62 \\ 90.83 \end{bmatrix}$$

$$= \begin{bmatrix} -17.70 \\ -29.67 \end{bmatrix}$$

and

$$\mathbf{l} = \boldsymbol{\eta}(\theta^1) + \mathbf{H}\alpha$$

$$= \begin{bmatrix} 124.62 \\ 90.83 \end{bmatrix} + \begin{bmatrix} -17.70 \\ -29.67 \end{bmatrix} \alpha$$

We now use linear least squares to project the residual vector

$$\mathbf{y} - \mathbf{l}(0) = \begin{bmatrix} 126 \\ 110 \end{bmatrix} - \begin{bmatrix} 124.62 \\ 90.83 \end{bmatrix}$$

$$= \begin{bmatrix} 1.38 \\ 19.17 \end{bmatrix}$$

onto $\mathbf{l}$ to obtain

$$\hat{\alpha} = (\mathbf{H}^{\mathrm{T}}\mathbf{H})^{-1}\mathbf{H}^{\mathrm{T}}(\mathbf{y} - \mathbf{l}(0))$$

For this example

$$\hat{\alpha} = -0.49$$

so new value of θ is

$$\theta_{\text{new}} = 0.02 + T(-0.49)$$

$$= 0.02 + 0.08(-0.49)$$

$$= -0.019$$

Evaluating the sum of squares at this point reveals that this new point is farther from $\mathbf{y}$ than either of the two starting points, and so a step factor λ is introduced to search along the increment vector to determine a better point. Incorporating λ as

$$\theta_{\text{trial}} = \theta_{\text{new}}\lambda + \theta_{\text{old}}(1 - \lambda)$$

gives, for this example,

$$\theta_{\text{trial}} = (-0.019)\lambda + 0.02(1-\lambda)$$

and the minimum occurs at $\lambda = 0.5$ with $\theta_{\text{trial}} = 0.0005$. The point $\theta^2 = 0.10$ is then replaced by $\theta^3 = 0.0005$ and the process is repeated using the pair (θ^1, θ^3). ■

In the general case of P parameters, at the ith iteration we use the values of $\boldsymbol{\eta}(\boldsymbol{\theta})$ at $\boldsymbol{\theta}_1^i, \boldsymbol{\theta}_2^i, \ldots, \boldsymbol{\theta}_{P+1}^i$ to determine the secant plane as the P-dimensional plane which passes through $\boldsymbol{\eta}(\boldsymbol{\theta}_p^i)$, $p = 1, \ldots, P+1$. For convenience, we assume that $\boldsymbol{\theta}_{P+1}^i$ corresponds to the point closest to $\mathbf{y}$; we then determine the $P \times P$ matrix $\mathbf{T}$ by setting its pth column equal to $\boldsymbol{\theta}_p^i - \boldsymbol{\theta}_{P+1}^i$, and the $N \times P$ matrix $\mathbf{H}$ by setting its pth column equal to $\boldsymbol{\eta}(\boldsymbol{\theta}_p^i) - \boldsymbol{\eta}(\boldsymbol{\theta}_{P+1}^i)$. Then, formally,

$$\hat{\boldsymbol{\alpha}} = (\mathbf{H}^{\mathrm{T}}\mathbf{H})^{-1}\mathbf{H}^{\mathrm{T}}[\mathbf{y} - \boldsymbol{\eta}(\boldsymbol{\theta}_{P+1}^i)]$$

$$\boldsymbol{\theta}_{\text{new}} = \boldsymbol{\theta}_{P+1}^i + \mathbf{T}\hat{\boldsymbol{\alpha}}$$

and

$$\boldsymbol{\theta}_{\text{trial}} = \boldsymbol{\theta}_{\text{new}}\lambda + \boldsymbol{\theta}_{P+1}^i(1-\lambda)$$

Note that Ralston and Jennrich (1978) allow the step factor to be negative, by choosing λ from a sequence of values $1, 1/2, -1/4, 1/8, -1/16, \ldots$. At convergence the linear approximation parameter covariance matrix is given by $s^2\mathbf{T}(\mathbf{H}^{\mathrm{T}}\mathbf{H})^{-1}\mathbf{T}^{\mathrm{T}}$, where s^2 is the usual variance estimate. Note that the matrix $\mathbf{T}$ may be ill conditioned by the time convergence is achieved and so the linear approximation standard errors and correlations may not be reliable.

3.5.5 Removing Conditionally Linear Parameters

One way of simplifying a nonlinear regression problem is to eliminate conditionally linear parameters. As mentioned in Sections 2.1 and 3.3.5, the optimal values of the conditionally linear parameters, for fixed values of the nonlinear parameters, can be determined by linear least squares. If we partition the parameter vector $\boldsymbol{\theta}$ into the conditionally linear parameters $\boldsymbol{\beta}$ of dimension P_1 and the nonlinear parameters $\boldsymbol{\phi}$ of dimension P_2 with $P = P_1 + P_2$, the expected responses can be written

$$\boldsymbol{\eta}(\boldsymbol{\beta}, \boldsymbol{\phi}) = \mathbf{A}(\boldsymbol{\phi})\boldsymbol{\beta}$$

where the $N \times P_1$ matrix $\mathbf{A}$ depends only on the nonlinear parameters. For any value of $\boldsymbol{\phi}$, the conditional estimate of $\boldsymbol{\beta}$ is

$$\hat{\boldsymbol{\beta}}(\boldsymbol{\phi}) = \mathbf{A}^{+}(\boldsymbol{\phi})\,\mathbf{y}$$

where $\mathbf{A}^{+} = (\mathbf{A}^{\mathrm{T}}\mathbf{A})^{-1}\mathbf{A}^{\mathrm{T}}$ is the pseudoinverse of $\mathbf{A}$. The associated expected responses are

$$\hat{\boldsymbol{\eta}}(\boldsymbol{\phi}) = \mathbf{A}(\boldsymbol{\phi})\mathbf{A}^{+}(\boldsymbol{\phi})\,\mathbf{y}$$

Golub and Pereyra (1973) formulated a Gauss–Newton algorithm to minimize the reduced sum of squares function

$$S_2(\boldsymbol{\phi}) = \| \mathbf{y} - \mathbf{A}(\boldsymbol{\phi})\hat{\boldsymbol{\beta}}(\boldsymbol{\phi}) \|^2$$

that depends only on the nonlinear parameters. In particular, they give the derivative of $\mathbf{A}^{+}(\boldsymbol{\phi})$ with respect to $\boldsymbol{\phi}$, which is the key ingredient in the algorithm. The expression for this derivative is used in Chapter 4, where we present a Gauss–Newton algorithm for multiresponse parameter estimation.

One difficulty with using projection over the conditionally linear parameters is that additional information about the parameters must be given by the user. The user must specify which parameters are conditionally linear as well as specifying the derivatives of the entries of $\mathbf{A}$ with respect to $\boldsymbol{\phi}$. This often results in more difficulty than simply ignoring the conditional linearity. There are some structured problems, however—such as spline regression with knot positions allowed to vary, as described in Jupp (1978)—where the division between conditionally linear and nonlinear parameters is inherent in the specification of the problem, so the Golub–Pereyra method can be used to advantage. These methods are discussed further in Kaufman (1975) and Bates and Lindstrom (1986).

3.6 Obtaining Convergence

Obtaining convergence is sometimes difficult. If you are having trouble, check the following:

Is the expectation function correctly specified?
Is the expectation function correctly coded?
Are the derivatives correctly specified?
Are the derivatives correctly coded?
Are the data entered correctly?
Are all the observations reasonable?
Is the response variable correctly identified?
Do the starting values have the correct values?
Do the starting values correspond to the correct parameters?

If the answer to all these questions is yes, look carefully at the outpu from the optimization program. Most good programs can produce detailed ou put on each iteration to help find out what is wrong. Check to see that the initi sum of squares, $S(\boldsymbol{\theta}^0)$, is smaller than the sum of squares of the responses. not, then the fitted function is worse than no function and, in spite of yo checks, you probably have an incorrect expectation function, or incorrect dat or incorrect starting values. You may even be trying to fit an x variable rath

than the response y.

Look at the parameter values. Do the starting values have the correct magnitudes? Correct signs? And are they assigned to the correct parameters?

Next, look at the parameter increments. Are they all of roughly the same magnitude relative to the parameters? Does the increment, when added to the parameter vector, place the parameter vector in a bad region in the parameter space? For example, are any necessarily positive parameters driven negative? Do any of the parameters become unreasonably large or small? If so, could there be an error in the derivative functions? Try using numerical derivatives at a few design points to check the analytic derivatives. Would different starting values for some of the parameters help? Is there a transformation of the parameters which could help?

Sometimes convergence is not achieved because the model has too many parameters. Look at the parameter values to see whether any of them are being driven to extreme values corresponding to a simpler model function. Also look at combinations of the parameter increments to see, for example, if pairs of them tend to move together, suggesting collinearity or possibly overparametrization. If there is a suspicion of overparametrization, try simplifying the expectation function, even temporarily—it may be that a simpler model will produce better parameter estimates, so that eventually the full model can be fitted.

Check to see that there are enough data in all regions of the design space so that valid parameter estimates can be obtained. For example, when fitting a transition type model in which there is, say, linear behavior to the left of a point and different linear behavior to the right (Bacon and Watts, 1971; Hinkley, 1969; Watts and Bacon, 1974), it is often the case that there are lots of data values to define the behavior away from the join point, but not many near the join point. In this situation, the parameter which describes the sharpness of transition will be poorly estimated, and so convergence may be slow.

When dealing with a comprehensive model which involves combining data from several experiments, it is generally good practice to fit each data set with a possibly simpler restricted model, and gradually extend the model by incorporating more data sets and parameters. An example of this is given in Ziegel (1985). Conversely, a large data set which has several reasonably distinct operating regions can be blocked into small subsets on that basis, so that a reduced model can be fitted to each subset and the results used to provide starting estimates for a model for the full data set, as illustrated below.

Example: Lubricant 1

To illustrate the process of getting starting values and obtaining convergence for a complicated nonlinear model function, we consider data on the kinematic viscosity of a lubricant as a function of temperature (x_1) and pressure (x_2). The data, discussed in Linssen (1975), are reproduced in Appendix 1, Section A1.8, and plotted in Figure 3.4. The model function is

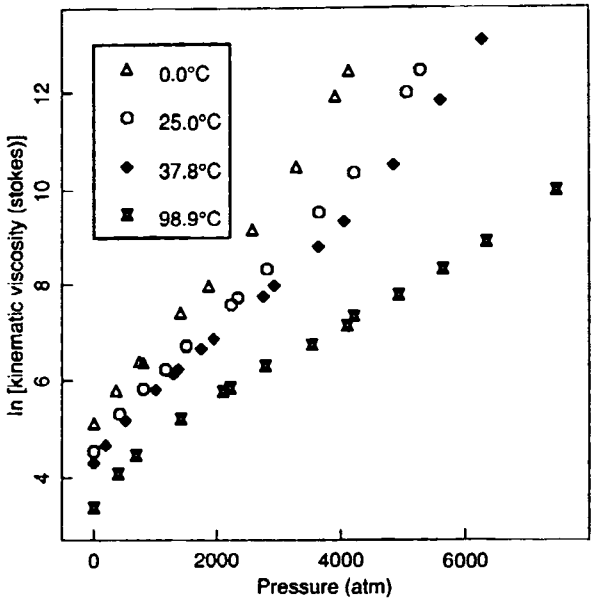

Figure 3.4 Plot of the logarithm of the kinematic viscosity of a lubricant versus pressure for four different temperatures.

$$f(\mathbf{x},\boldsymbol{\theta}) = \frac{\theta_1}{\theta_2 + x_1} + \theta_3 x_2 + \theta_4 x_2^2 + \theta_5 x_2^3 + (\theta_6 + \theta_7 x_2^2)\, x_2 \exp\left[\frac{-x_1}{\theta_8 + \theta_9 x_2^2}\right] \tag{3.2}$$

To begin, we note that six of the nine parameters are conditionally linear, which is most helpful. Also, to improve conditioning, as discussed in Section 3.4.1, we scale the pressure data x_2 by dividing by 1000 and avoid confusion by writing $w_2 = x_2/1000$.

To obtain a starting estimate for θ_2, we use the data for $w_2 = 0.001$ and assume that for this low value of scaled pressure, the model is a function of x_1 only. Taking reciprocals and using linear least squares as described in Section 3.3.3 gives $\theta_1^0 = 983$ and $\theta_2^0 = 192$.

Now we exploit the conditional linearity in the model because we can use linear least squares to obtain starting estimates for the remaining parameters once we have reasonable estimates for θ_8 and θ_9. Thus we concentrate on getting estimates for only these two. We simplify the situation even more by assuming that when w_2 is small, the model function is essentially linear in w_2, so that

$$f(\mathbf{x},\boldsymbol{\theta}) \approx \frac{\theta_1}{\theta_2 + x_1} + \theta_3 w_2 + \theta_6 w_2 \, e^{-x_1/\theta_8}$$

That is, we can ignore the terms involving θ_4, θ_5, θ_7, and θ_9. By examining the plot, we see that the data for each temperature follow quite straight lines for $w_2 < 2$, so we choose this for the range. Also, for fixed values of x_1, the leading term and the exponential term are constant and we may rearrange the model as

$$\begin{aligned} y' &= \theta_3 w_2 + \theta_6 w_2 \, g \\ &= w_2 \beta \end{aligned}$$

where

$$y' = y - \frac{983}{192 + x_1}$$

$$g = e^{-x_1/\theta_8}$$

and

$$\beta = \theta_3 + \theta_6 g$$

Regressing y' on w_2 for each of the four temperatures 0, 25, 37.8, 98.9 gives β values of 1.57, 1.49, 1.39, 1.37. We now use the β values and the relation $g = e^{-x_1/\theta_8}$ to obtain estimates for θ_3 and θ_6 by noting that when $x_1 = 0$ we have $g = 1$, so $\beta = \theta_3 + \theta_6$, and when $x_1 \to \infty$, $\beta = \theta_3$. We therefore estimate the sum of the two parameters as 1.57 (the value of β at $x_1 = 0$), and assuming that the lower asymptote has almost been reached at the highest temperature, we choose θ_3 to be 1.35, which is a bit smaller than 1.37 (the value of β at $x_1 = 98.9$). The value for θ_6 is then estimated as $1.57 - 1.35 = 0.22$. Finally, since $\beta = \theta_3 + \theta_6 g$, so $(\beta - \theta_3)/\theta_6 = g$, we regressed

$$\ln\left(\frac{\beta - 1.35}{0.22}\right)$$

on x_1 to give $\theta_8 = 35.5$.

Using these parameter estimates for θ_2 and θ_8, we performed a nonlinear regression on the data for small w_2 values to get more refined estimates, $\theta_2 = 202$ and $\theta_8 = 35.90$. We then used these estimates for θ_2 and θ_8, and the data for all w_2 values, to estimate all the parameters with $\theta_9 = 0$. The new values were $\theta_2 = 209$ and $\theta_8 = 47.55$. Finally, we used these values plus the starting value $\theta_9 = 0$ to converge on the full model. The final parameter estimates were

$$\hat{\boldsymbol{\theta}} = (1053, 206.1, 1.464, -0.259, 0.0224, 0.398, 0.09354, 56.97, -0.463)^{\mathrm{T}}$$

with a residual sum of squares of 0.08996. ■

3.7 Assessing the Fit and Modifying the Model

In any nonlinear analysis, it is necessary to assess the fit of the model to the data and to assess the appropriateness of the assumptions about the disturbances. To do so, we use the same techniques as in linear regression, namely sensibleness of parameter values, comparison of mean squares and extra sums of squares, and plots of residuals. If there are any inadequacies in the model, or if any of the assumptions do not seem to be appropriate, then the model must be modified and the analysis continued until a satisfactory result is obtained.

In nonlinear estimation, it is possible to converge to parameter values which are obviously, or perhaps suspiciously, wrong. This is because we may have converged to a local minimum, or got stalled because of some awkward behavior of the expectation surface. Assessment of any fitted model should therefore begin with a careful consideration of the parameter estimates and whether they make sense scientifically. If the parameters do not make sense, check to see that the correct starting values were used. Also check to see that the program did not simply terminate due to lack of progress or too many iterations, but that convergence was actually achieved. One should also scan the iteration progress information to see if convergence occurred smoothly. Some programs have special facilities for fixing some parameters while allowing others to vary, and others have poor convergence criteria. It is incumbent on the user to understand fully the program being used and to appreciate its idiosyncrasies. "Caveat emptor" is as true for nonlinear estimation packages as it is for anything else in life.

If the program has proceeded smoothly to an apparently legitimate convergence point, but the parameters are not reasonable, check the expectation function and its coding, the derivatives and their codings, the starting values, and the data, as in Section 3.6. Is the response variable correctly specified? Are the residuals well behaved?

If these checks are satisfactory but the parameter vector is not, try a fairly different starting vector. If you then converge to the same point, it may be that the data are trying to tell you that the expectation function is not appropriate. At this stage it may well be helpful to discuss things with the researcher or a colleague; as often happens, in the course of such a discussion you may discover a simple, "obvious" error.

When convergence to reasonable values has been reached, check the parameter approximate standard errors and approximate t ratios [calculated as (parameter estimate) / (approximate standard error)]. If a t ratio is not significant, consider deleting that parameter from the expectation function and refitting the model, as discussed more fully in Section 3.10.

Generally, the simpler the model the better (Ockham's razor: see quotation, p.1).

Also check the parameter approximate correlation matrix to see whether any parameters are excessively highly correlated, since high correlations may indicate overparametrization (a model which is too complicated for the data set).

Exactly what constitutes a "high" correlation is somewhat dependent on the type of data and model being considered. In general, correlations above 0.99 in absolute value should be investigated. Try simplifying the expectation function in a scientifically sensible way or transforming the variables and parameters to reduce collinearities (Section 3.4). For further discussion on simplifying models, see Section 3.8. Further information on variability of parameter estimates and nonlinear dependencies between parameter estimates can be obtained using the techniques of Chapter 6.

When a simple, adequate expectation function has been found, a plot of the fitted values overlaid with the observed responses is an excellent way to assess the fit. Plots of the residuals versus the fitted values and the control variables are also powerful aids. The residuals should also be plotted against other, possibly lurking factors to help detect model inadequacies. For further discussion, see Draper and Smith (1981), Joiner (1981), or Cook and Weisberg (1983). Particular attention should be paid to whether the residuals have a uniform spread, since any nonsystematic behavior is suggestive of nonconstant variance. If there is nonconstant variance, consider transforming the data to induce constant variance, and transforming the model function to maintain the integrity of the model, possibly using the approach in Carroll and Ruppert (1984) to optimize the transformation parameter, or try using weighted least squares.

Nonrandom behavior of the residuals, as evidenced by plots of the residuals against the regressor variables or other variables, tends to indicate lack of adequacy of the expectation function. In such cases, try expanding the model in a scientifically sensible way to eliminate the nonrandom behavior. For example, add "incremental" parameters to account for differences between subjects or days, or between groups of subjects or days, as discussed in Section 3.10. When dealing with sums of exponentials, perhaps add a constant term to allow for decay to a nonzero asymptote.

Probability plots of the residuals should be made to verify the normal assumption about the disturbances. If there is pronounced lack of normality, try to decide whether it is due to a small number of outliers or whether it is due to inadequacy of the expectation function. For obvious outliers, check that the data have been correctly recorded and correctly entered into the computer. If they have been correctly entered, discuss with the experimenter the propriety of deleting them. Perhaps there are good nonstatistical reasons for removing them—for example, a contaminated sample. If you are considering such editing, it may be helpful to present the experimenter with information concerning the influence of the possible outliers, such as parameter estimates, standard deviations, fitted values, and residual mean squares with and without the suspicious data points.

If the residuals are clearly nonnormal, consider transforming the data and the model (Carroll and Ruppert, 1984) or changing the criterion from least squares to a "robust" estimation criterion (Huber, 1981). Note, however, that the use of criteria other than least squares will usually require special software.

Assessment of adequacy of the expectation function is easier if there are replications, because it will have been possible to check for, or transform to,

stable variance before fitting the model. Replications also allow one to test for lack of fit of the model by comparing the ratio of the lack of fit mean square with the replication mean square with the appropriate F distribution value, as discussed in Sections 1.3.2, 3.10, and 3.12.

3.8 Correlated Residuals

Whenever time or distance is involved as a factor in a regression analysis, it is prudent to check the assumption of independent disturbances. Correlation of the disturbances can be detected from a *time series* plot of the residuals versus time (or order of the experiments) or from a *lag* plot of the residual on the nth case versus the residual on the $(n-1)$th case. Tendencies for the residuals to stay positive or negative in runs on the time series plot, or nonrandom scatter of the residuals when plotted on the lag plot, can reveal nonindependence or correlation of the disturbances.

Example: Chloride 1

Sredni (1970) analyzed data on chloride ion transport through blood cell walls. The data, derived from Sredni's thesis, are listed in Appendix 1, Section A1.9, and plotted in Figure 3.5. The observation y_n gives the chloride concentration (in percent) at time x_n (in minutes).

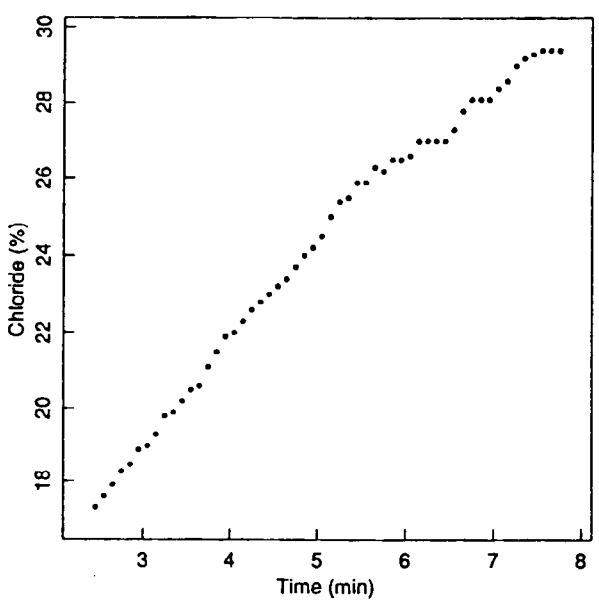

Figure 3.5 Plot of chloride concentration versus time for the chloride transport data.

The model function

$$f(x_n, \boldsymbol{\theta}) = \theta_1(1 - \theta_2 e^{-\theta_3 x_n})$$

was derived from the theory of ion transport, where θ_1 represents the final percentage concentration of chlorine, θ_3 is a rate constant, and θ_2 accounts for the unknown initial and final concentrations of the chlorine and the unknown initial reaction time. As usual, it was assumed that the disturbances had zero mean and constant variance and were independent.

An initial estimate for θ_1 was obtained by extrapolating the data to large time, giving $\theta_1^0 = 35$. Dividing y_n by θ_1^0 and linearizing the equation by rearranging terms and taking logarithms allowed us to estimate the remaining parameters by linear regression, to give $\boldsymbol{\theta}^0 = (35, 0.91, 0.22)^T$. Convergence was obtained to $\hat{\boldsymbol{\theta}} = (39.09, 0.828, 0.159)^T$ with a residual sum of squares of 1.88. A time series plot of the residuals, shown in Figure 3.6*a*, shows runs in the residuals. Similarly, the lag plot shown in Figure 3.6*b*, shows positive correlation. We are thus alerted to the possibility that the disturbances are not independent, or that there is some deficiency in the form of the expectation function. ■

When the disturbances are not independent, the model for the observations must be altered to account for dependence. Common forms for dependence, or *autocorrelation*, of disturbances are *moving average* or *autoregressive* models of variable order (Box and Jenkins, 1976). Simple examples of such forms are a moving average process of order 1 where

$$Z_n = \varepsilon_n - \omega_1 \varepsilon_{n-1}$$

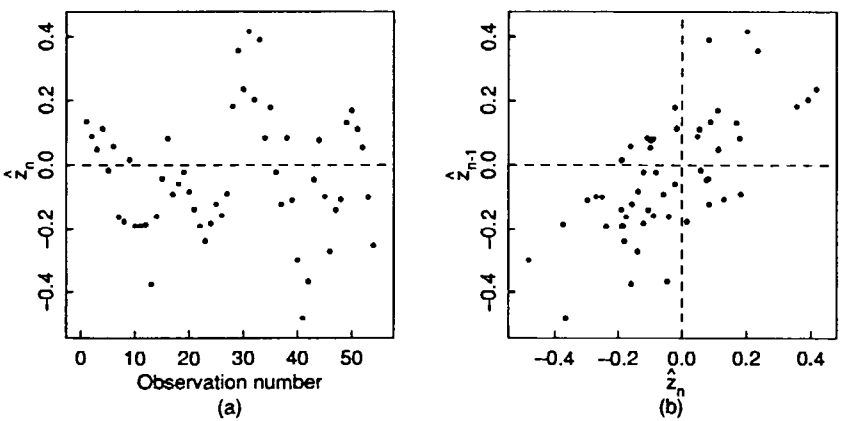

Figure 3.6 Plots of the residuals $\hat{z}$ from the original nonlinear least squares fit to the chloride data. The residuals are plotted as a time series in part *a* and as a lag plot in part *b*.

or an autoregressive process of order 1 where

$$Z_n = \varepsilon_n + \phi_1 Z_{n-1}$$

and the ε_n, $n = 1, 2, \ldots, N$, are independent random disturbances with zero mean and constant variance, or more simply, *white noise*.

In regression situations, when the data are equally spaced in time, it is relatively easy to determine an appropriate form for the dependence of the disturbances by calculating and plotting the *residual autocorrelation function*,

$$r_k = \sum_{n=k+1}^{N} \frac{\hat{z}_n \hat{z}_{n-k}}{Ns^2} \qquad k = 1, 2, \ldots$$

versus the lag k. In the definition of r_k, s^2 is the variance estimate, and the residuals are assumed to have zero average. The residual autocorrelation function is usually calculated out to $k \approx N/5$. If the residual autocorrelation function is consistently within the range $\pm 2/\sqrt{N}$ after lag 2 or 3, then the model may be identified as a moving average process of order 1 or 2. If the residual autocorrelation function tends to decay gradually to zero, then the process may be identified as an autoregressive process. Alternatively, to determine the order of the autoregressive process, it may be necessary to calculate the *partial autocorrelation function* (Box and Jenkins, 1976). For regression situations where time is not the only factor, or the most important factor, first order autoregressive processes are often adequate.

Example: Chloride 2

The residual autocorrelation function for the chloride data was calculated

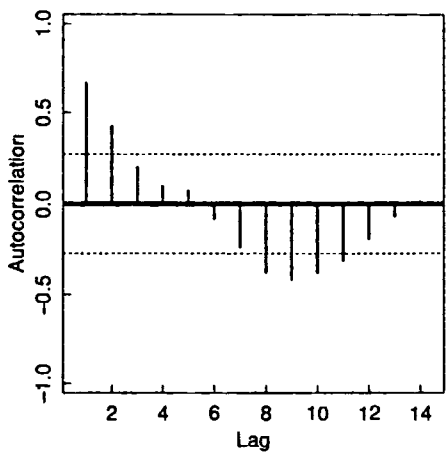

Figure 3.7 Autocorrelation function of the residuals from the original nonlinear least squares fit to the chloride data. The dotted lines enclose the interval in which approximately 95% of the correlations would be expected to lie if the true correlations were 0.

and plotted as in Figure 3.7. The correlation estimates decay towards zero, falling within the limits $\pm 2/\sqrt{N}$ (shown as dotted horizontal lines) quite quickly. On the basis of this plot, it was decided that a first order autoregressive process would adequately model the dependence in the residuals.

The model to be fitted is now of the form $Y_n = f(x_n, \boldsymbol{\theta}) + Z_n$, where $Z_n = \varepsilon_n + \phi Z_{n-1}$. To estimate the parameters $\boldsymbol{\theta}$ and ϕ, we reduce the problem to an ordinary nonlinear least squares problem by subtracting ϕ times the equation for Y_{n-1} from Y_n, as

$$Y_n - \phi Y_{n-1} = f(x_n, \boldsymbol{\theta}) - \phi f(x_{n-1}, \boldsymbol{\theta}) + Z_n - \phi Z_{n-1}$$

or

$$Y_n = \phi Y_{n-1} + f(x_n, \boldsymbol{\theta}) - \phi f(x_{n-1}, \boldsymbol{\theta}) + \varepsilon_n$$

Starting values for $\boldsymbol{\theta}$ were taken from $\hat{\boldsymbol{\theta}}$ above, and the starting value for ϕ was taken as the lag one correlation estimate, $r_1 = 0.67$. Convergence was obtained to $(\boldsymbol{\theta}^T, \phi) = (37.58, 0.849, 0.178, 0.69)$ with a residual sum of squares of 0.98. The residuals $\hat{\varepsilon}$ from this fit are well behaved, as shown in Figure 3.8 and the residual autocorrelation function, shown in Figure 3.9, was uniformly small. ■

In general, as in the above example, the main effect of accounting for dependence is to reduce the residual variance and reduce the correlation in the residuals: the model parameter estimate $\hat{\boldsymbol{\theta}}$ does not change much. However, the model parameters are better estimated because they have smaller standard errors and because the method of least squares has been applied correctly, since the assumptions are satisfied. For a more complicated application of this technique,

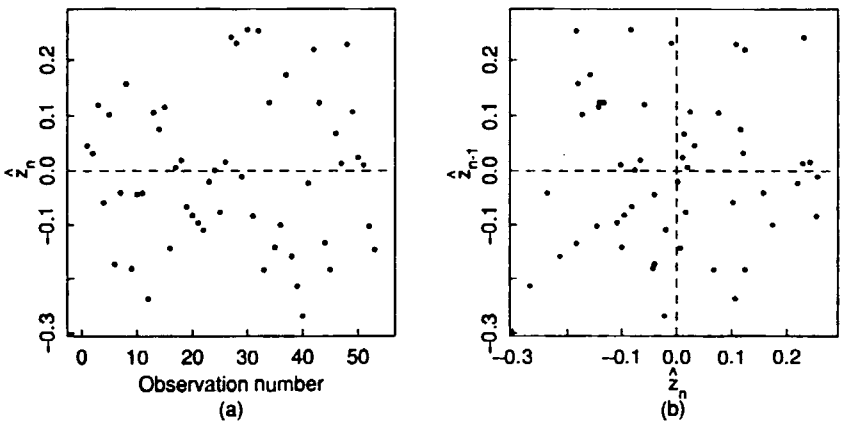

Figure 3.8 Plots of the residuals $\hat{z}$ from the nonlinear least squares fit to the chloride data using $\phi = 0.69$. The residuals are plotted as a time series in part *a* and as a lag plot in part *b*.

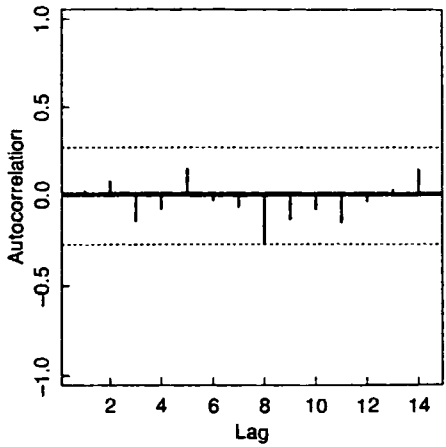

Figure 3.9 Autocorrelation function of the residuals from the nonlinear least squares fit to the chloride data using $\phi = 0.69$. The dotted lines enclose the interval in which approximately 95% of the correlations would be expected to lie if the true correlations were 0.

see Watts and Bacon (1974).

3.9 Accumulated Data

In some studies, when it is impractical to measure instantaneous concentrations, *accumulated* responses are recorded.

Example: Ethyl acrylate 1

An experiment to study the metabolism of ethyl acrylate was performed by giving rats a single bolus of radioactively tagged ethyl acrylate. Each rat was given a measured dose of the compound via stomach intubation and placed in an enclosed cage from which the air could be drawn through a bubble chamber. The exhaled air was bubbled through the chamber, and at a specified time the bubble chamber was replaced by a fresh one, so that the measured response was the accumulated CO_2 during the time interval. Preliminary analysis of the data revealed that normalizing each animal's response by dividing by the actual dose received would permit combination of the data so that a single model could be fitted to the data for all the rats. Furthermore, the variability in the normalized data was such that it was necessary to take logarithms of the data to produce constant variance across the time points. The starting points and lengths of the accumulation intervals and the averages for the nine rats, normalized by actual dose, are given in Appendix 1, Section A1.10 (Watts, deBethizy, and Stiratelli, 1986), and the cumulative CO_2 data are plotted in Figure 3.10. ■

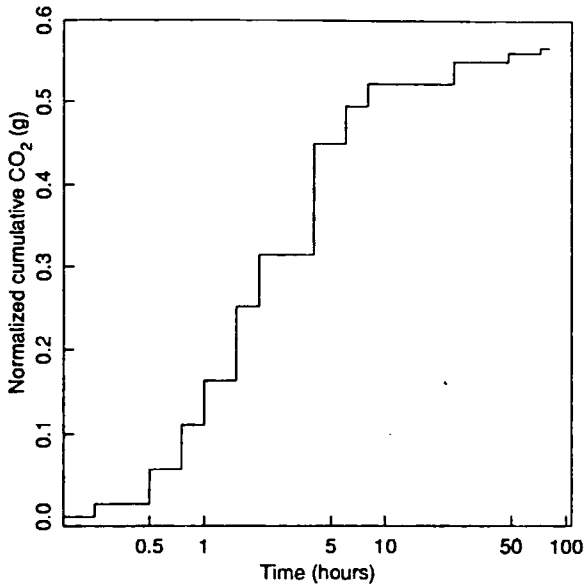

Figure 3.10 Plot of cumulative exhaled CO_2 amounts versus collection interval end point for the ethyl acrylate data.

Two methods for the analysis of such data were given in Renwick (1982). The first method uses peeling of the "approximate concentration" data obtained by dividing the accumulated amount by the accumulation time interval. The second method uses the cumulative total, extrapolated to infinite time, and then peeling of the differences [*extrapolated* – (*cumulative total*)]. This is called the "sigma–minus" method.

We do not recommend either of these methods, and specifically decry use of the sigma–minus method because it is so sensitive to variations in the extrapolated value. It can be shown, for example, that small percentage changes in the extrapolated value, say less than 2%, can cause changes in the rate constants in excess of 100%. Furthermore, both methods are based on peeling, which requires excessive subjective judgement. Instead of the abovementioned methods, we recommend direct analysis of the accumulated data using integrated responses as described below. In addition to avoiding the disadvantages of the other methods, this method has the advantage that it provides measures of precision of the estimates in the form of parameter approximate standard errors and correlations.

3.9.1 Estimating the Parameters by Direct Integration

Suppose that the theoretical response to the input stimulus at time t is $f(t, \boldsymbol{\theta})$. Then the accumulated output in the interval t_{n-1} to t_n is

$$F_n = \int_{t_{n-1}}^{t_n} f(t, \boldsymbol{\theta})\, dt$$

We therefore use the integrated function values F_n and the observed accumulated data pairs (y_n, t_n) to estimate the parameters. We rewrite the model in terms of the factors $x_{1n} = t_{n-1}$, the start of the interval, and $x_{2n} = t_n - t_{n-1}$, the length of the interval, so the model for the amount accumulated in an interval is $F(\mathbf{x}_n, \boldsymbol{\theta})$, where $\mathbf{x}_n = (x_{1n}, x_{2n})^{\mathrm{T}}$.

To determine a tentative form for $f(t, \boldsymbol{\theta})$, we plot the approximate rates y_n / x_{2n} versus $x_{1n} + x_{2n}/2$ on semilog paper and use peeling to obtain *starting* estimates for the parameters. The final estimation is done using nonlinear least squares. Note that if the variance is not constant, it may be necessary to transform the data and the function, as in the following example.

Example: Ethyl acrylate 2

The CO_2 data are reproduced in Table 3.1 together with the derived quantities (interval midpoint $x_{1n} + x_{2n}/2$ and approximate rate y_n / x_{2n}) which are plotted in Figure 3.11. We can see from the figure that an appropriate model for the data involves three exponentials (two to account for the peak, and another to account for the change in slope of the decay from the peak). Because the radioactivity prior to injection must be zero, the concentration at $t = 0$ must be zero. A plausible model for the concentration at time t is therefore

$$f(t, \boldsymbol{\theta}) = -(\theta_4 + \theta_5) e^{-\theta_1 t} + \theta_4 e^{-\theta_2 t} + \theta_5 e^{-\theta_3 t}$$

An appropriate model for the accumulated data in the collection interval starting at t_{n-1} is then

$$F_n = -\frac{\theta_4 + \theta_5}{\theta_1}(e^{-\theta_1 t_{n-1}} - e^{-\theta_1 t_n}) + \frac{\theta_4}{\theta_2}(e^{-\theta_2 t_{n-1}} - e^{-\theta_2 t_n}) + \frac{\theta_5}{\theta_3}(e^{-\theta_3 t_{n-1}} - e^{-\theta_3 t_n})$$

or

$$F(\mathbf{x}, \boldsymbol{\theta}) = -\frac{\theta_4 + \theta_5}{\theta_1} e^{-\theta_1 x_1}(1 - e^{-\theta_1 x_2}) + \frac{\theta_4}{\theta_2} e^{-\theta_2 x_1}(1 - e^{-\theta_2 x_2}) + \frac{\theta_5}{\theta_3} e^{-\theta_3 x_1}(1 - e^{-\theta_3 x_2})$$

Because of the nonconstant variance, the logarithms of F were fitted to the

Table 3.1 Collection intervals and averages of normalized exhaled CO_2 for the ethyl acrylate data together with the derived quantities: interval midpoint and approximate rate

Collection Interval (hr)			Derived Quantities	
Start x_1	Length x_2	CO_2 (g)	Interval Midpoint	Approx. Rate
0.0	0.25	0.01563	0.125	0.0625
0.25	0.25	0.04190	0.375	0.1676
0.5	0.25	0.05328	0.625	0.2131
0.75	0.25	0.05226	0.875	0.2090
1.0	0.5	0.08850	1.25	0.1770
1.5	0.5	0.06340	1.75	0.1268
2.0	2.0	0.13419	3.0	0.0671
4.0	2.0	0.04502	5.0	0.0225
6.0	2.0	0.02942	7.0	0.0147
8.0	16.0	0.02716	16.0	0.0017
24.0	24.0	0.01037	36.0	0.0004
48.0	24.0	0.00602	60.0	0.0003

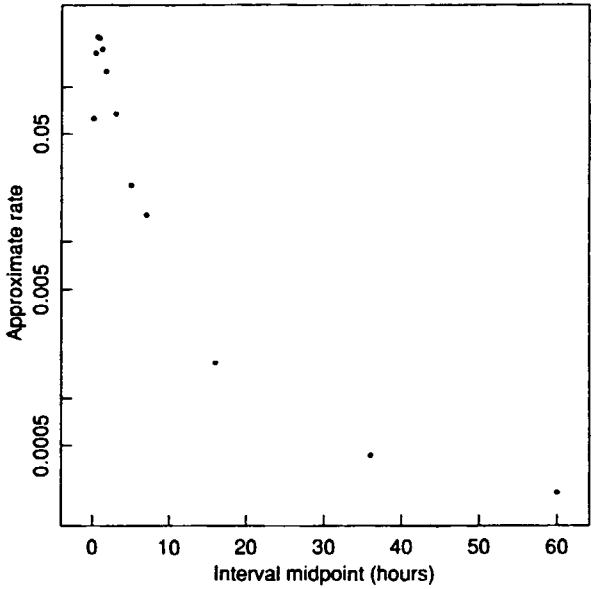

Figure 3.11 Approximate CO_2 exhalation rate versus collection interval midpoint for the ethyl acrylate data.

logarithms of the data. The results of this analysis together with the starting estimates are presented in Table 3.2.

In an analysis of the logarithmic data for the individual rats, due attention was paid to the behavior of the residuals. The triple rate constant model fitted the data very well. ■

Table 3.2 Parameter summary for the 3-exponential model fitted to the ethyl acrylate data.

		Nonlinear Least Squares	
Parameter	Start	Estimate	Approx. Std. Err.
θ_1	4.461	3.025	0.752
θ_2	0.571	0.481	0.038
θ_3	0.0434	0.0258	0.0096
θ_4	0.355	0.310	0.049
θ_5	0.0034	0.0011	0.0005

Example: Saccharin 1

As a second example of treating accumulated data, we analyze the saccharin data in Renwick (1982). In this experiment, the measured response was the amount of saccharin accumulated in the urine of a rat after receiving a single bolus of saccharin. The data are recorded in Appendix 1, Section A1.11, and plotted in Figure 3.12.

The function involved only two rate constants, and the response was modeled as

$$f(t,\boldsymbol{\theta}) = \theta_3 e^{-\theta_1 t} + \theta_4 e^{-\theta_2 t}$$

so

$$F(\mathbf{x},\boldsymbol{\theta}) = \frac{\theta_3}{\theta_1} e^{-\theta_1 x_1}(1 - e^{-\theta_1 x_2}) + \frac{\theta_4}{\theta_2} e^{-\theta_2 x_1}(1 - e^{-\theta_2 x_2})$$

As in the ethyl acrylate example, the integrated model was fitted to the logarithms of the accumulated data to stabilize variance.

The curve peeling and the sigma–minus method results from Renwick (1982) are given in columns 2 and 3 of Table 3.3, and the results using the direct integration method are given in column 4. Note the considerable differences between the results based on peeling and those obtained by nonlinear least squares. Note too, that the peeling and sigma–minus

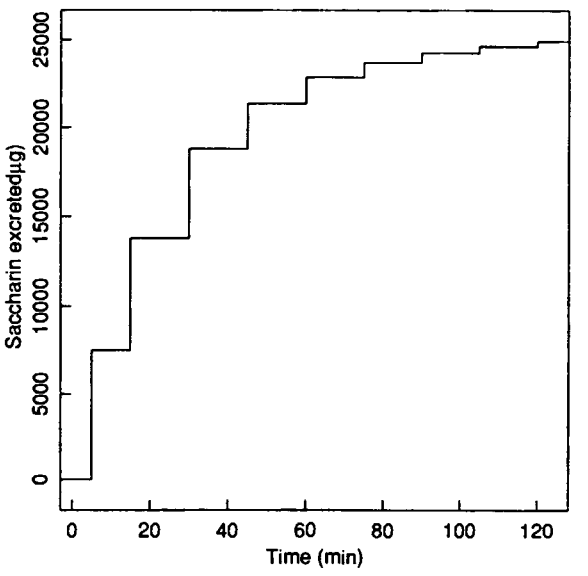

Figure 3.12 Plot of cumulative excreted amount versus collection interval end point for the saccharin data.

Table 3.3 Parameter summary for the saccharin data, comparing estimates obtained using the sigma–minus method, using the approximate rate method, and using nonlinear least squares to fit the integrated response function.

			Estimate by Nonlinear Least Squares	
Parameter	Peeling[a]	Sigma–Minus[a]	Value	Approx. Std. Err.
θ_1	0.0710	0.0833	0.122	0.031
θ_2	0.0234	0.0255	0.0279	0.003
θ_3	830	932	1345	249
θ_4	270	314	402	98

[a] From Renwick (1982).

methods do not provide parameter standard errors.

There were two very large residuals from the nonlinear least squares fit, at $x_1 = 5$ and $x_1 = 105$. A second analysis was done by simply combining the observations at $x_1 = 5$ and $x_1 = 15$ and at $x_1 = 90$ and $x_1 = 105$, as shown in Table 3.4. The residuals from this fit were very well behaved,

Table 3.4 Collection intervals and excreted amounts for original and combined saccharin data.

Original			Combined		
Collection Interval (hr)			Collection Interval (hr)		
Start x_1	Length x_2	Saccharin (μg)	Start x_1	Length x_2	Saccharin (μg)
0	5	7518	0	5	7518
5	10	6275	5	25	11264
15	15	4989			
30	15	2580	30	15	2580
45	15	1485	45	15	1485
60	15	861	60	15	861
75	15	561	75	15	561
90	15	363	90	30	663
105	15	300			

and the residual variance was reduced to 0.0071 from 0.0158. The parameter estimates (standard errors in parentheses) were $\theta_1 = 0.154(0.035)$, $\theta_2 = 0.030(0.002)$, $\theta_3 = 1506(233)$, and $\theta_4 = 472(70)$. ■

3.10 Comparing Models

In some situations there may be more than one function which could be used as a model. For example, in fitting a double exponential model,

$$f(x,\boldsymbol{\theta}) = \theta_1 e^{-\theta_2 x} + \theta_3 e^{-\theta_4 x}$$

θ_4 could be 0, in which case the model reduces to

$$f(x,\boldsymbol{\theta}) = \theta_1 e^{-\theta_2 x} + \theta_3$$

or θ_3 could be 0, in which case the model reduces to

$$f(x,\boldsymbol{\theta}) = \theta_1 e^{-\theta_2 x}$$

In this situation of *nested* models, we would be interested in finding the simplest model which adequately fits the data.

In other situations, we might compare *non-nested* models—for example, model 1

$$f(x,\boldsymbol{\theta}) = \theta_1(1 - e^{-\theta_2 x})$$

versus model 2

$$f(x,\boldsymbol{\theta}) = \frac{\theta_1 x}{\theta_2 + x}$$

both of which start at $f = 0$ when $x = 0$ and approach the asymptote θ_1 as $x \to \infty$. In these situations, one model may give a superior fit to the data, and we would like to select that model.

3.10.1 Nested Models

To decide which is the simplest nested model to fit a data set adequately, we proceed as in the linear case and use a likelihood ratio test (Draper and Smith, 1981). Because of the spherical normal assumption, this leads to an assessment of the extra sum of squares due to the extra parameters involved in going from the partial to the full model.

Letting S denote the sum of squares, ν the degrees of freedom, and P the number of parameters, with subscripts f and p for the *full* and *partial* models and a subscript e for *extra*, the calculations can be summarized as in Table 3.5. To complete the analysis, we compare the ratio s_e^2/s_f^2 to $F(\nu_e,\nu_f;\alpha)$ and accept the partial model if the calculated mean square ratio is lower than the table value. Otherwise, we retain the extra terms and use the full model. Illustrations of the

Table 3.5 Extra sum of squares analysis for nested models.

Source	Sum of Squares	Degrees of Freedom	Mean Square	F Ratio
Extra parameters	$S_e = S_p - S_f$	$\nu_e = P_f - P_p$	$s_e^2 = S_e/\nu_e$	s_e^2/s_f^2
Full model	S_f	$\nu_f = N - P_f$	$s_f^2 = S_f/\nu_f$	
Partial model	S_p	$N - P_p$		

use of the extra sum of squares analysis are given below in Example Puromycin 10 and in Section 3.11.

Note that for linear least squares, the extra sum of squares analysis is exact because the data vector **y** is being projected onto linear subspaces of the response space to determine S_p and S_f. Mathematically, the partial model expectation plane is a linear subspace of the full model expectation plane. Residual vectors can then be decomposed into orthogonal components and, from the fact that the full model residual vector has a squared length which is distributed as a $\sigma^2\chi^2$ random variable with $N - P$ degrees of freedom, it follows that the squared lengths of the components are also distributed as $\sigma^2\chi^2$ random variables with degrees of freedom equal to the dimensions of the linear subspaces.

For nonlinear models, as we might expect, the analysis is only approximate because the calculated mean square ratio will not have an exact F distribution. However, the distribution of the mean square ratio is only affected by intrinsic nonlinearity and not by parameter effects nonlinearity, and, as shown in Chapter 7, the intrinsic nonlinearity is generally small. When the partial model is inadequate, the effect of intrinsic nonlinearity on the analysis can be large but the partial model will be rejected anyway: it is only when the fitted values are very close that the form of the distribution is critical. In these cases, the intrinsic nonlinearity will usually have a small effect because the expected responses being compared are close together on the expectation surface.

3.10.2 Incremental Parameters and Indicator Variables

Many nested models can be parametrized in terms of incremental parameters. An *incremental parameter* accounts for a change in a parameter between blocks of cases and is associated with an indicator variable. An advantage of using incremental parameters is that a preliminary evaluation of the need for the full model can be made directly from the regression output without having to do additional computation. The use of incremental parameters is most easily described by means of an example.

Example: Puromycin 10

In the Puromycin experiment, two blocks of experiments were run. In one the enzyme was treated with puromycin (Table A1.3*a*), and in the other the same enzyme was untreated (Table A1.3*b*). It was hypothesized that the Puromycin should affect the maximum velocity parameter θ_1, but not the half-velocity parameter θ_2. The two data sets are plotted in Figure 3.13.

To determine if the θ_2 parameter is unchanged, we use an extra sum of squares analysis, which requires fitting a full and a partial model. The full model corresponds to completely different sets of parameters for the treated data and the untreated data, while the partial model corresponds to different θ_1 parameters but the same θ_2 parameter. To combine the full and partial models, we introduce the *indicator variable*

$$x_2 = \begin{cases} 0 & \text{untreated} \\ 1 & \text{treated} \end{cases}$$

and let x_1 be the substrate concentration. The combined model is then written

$$f(\mathbf{x},\boldsymbol{\theta}) = \frac{(\theta_1 + \phi_1 x_2)x_1}{(\theta_2 + \phi_2 x_2) + x_1} \tag{3.4}$$

where θ_1 is the maximum velocity for the untreated enzyme, ϕ_1 is the in-

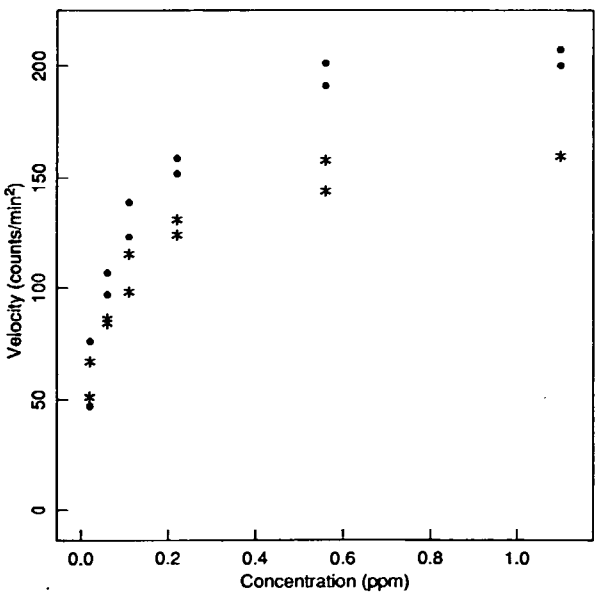

Figure 3.13 Plot of enzyme velocity data versus substrate concentration. The data for the enzyme treated (not treated) with Puromycin are shown as • (*).

cremental maximum velocity due to the treatment, θ_2 is the (possibly common) "half-velocity" point, and ϕ_2 is the change in the half-velocity due to the treatment. Since we expect ϕ_1 to be nonzero, we are interested in testing whether ϕ_2 could be zero.

The model (3.4) was fitted and the results of this fit are shown in Table 3.6. It appears that ϕ_2 could be zero, since it has a small t ratio, and so we fit the partial model (3.4) with $\phi_2 = 0$. The results of this fit are given in Table 3.7 and the extra sum of squares analysis is presented in Table 3.8. In this well-designed experiment, which includes replications, it is also

Table 3.6 Parameter summary for the 4-parameter Michaelis–Menten model fitted to the combined Puromycin data set.

Parameter	Estimate	Approx. Std. Err.	t Ratio	Correlation Matrix			
θ_1	160.3	6.90	23.2	1.00			
θ_2	0.0477	0.00828	5.8	0.77	1.00		
ϕ_1	52.4	9.55	5.5	−0.72	−0.56	1.00	
ϕ_2	0.0164	0.0114	1.4	−0.56	−0.72	0.77	1.00

Table 3.7 Parameter summary for the 3-parameter Michaelis–Menten model fitted to the combined Puromycin data set.

Parameter	Estimate	Approx. Std. Err.	t Ratio	Correlation Matrix		
θ_1	166.6	5.81	28.7	1.00		
θ_2	0.058	0.00591	9.8	0.61	1.00	
ϕ_1	42.0	6.27	6.7	−0.54	0.06	1.00

Table 3.8 Extra sum of squares analysis for the 3- and 4-parameter Michaelis–Menten model fitted to the combined Puromycin data set.

Source	Sum of Squares	Degrees of Freedom	Mean Square	F Ratio	p Value
Extra	186	1	186.	1.7	0.21
4-parameter	2055	19	108.2		
3-parameter	2241	20			

possible to analyze for lack of fit of the partial model as shown in Table 3.9. These summary calculations, together with plots of the residuals (not shown), suggest that a model which has a common half-velocity parameter and a higher asymptotic velocity for the treated enzyme is adequate. ■

In the above example, the t ratios for the incremental parameters permit reliable inferences to be made concerning changes from one block to another. We recommend, however, that the extra sum of squares analysis always be used, since it is unaffected by parameter effects nonlinearity (see Chapter 7) and is therefore more exact than the t test in the nonlinear case. We only use the t ratios to suggest which incremental parameters might be zero and should be investigated further: the actual decision on whether to retain a parameter should be based on an extra sum of squares analysis or a profile t analysis (see Chapter 6).

In summary, incremental parameters provide a direct and simple procedure for determining whether changes in parameters occur between different blocks. Clearly, incremental parameters can also be used to advantage in linear least squares to determine changes in parameters between blocks, since then the t tests are exact. Even for linear least squares, however, we recommend fitting the reduced model and using the extra sum of squares analysis to make any final decisions concerning inclusion or deletion of parameters, so as to avoid problems with multicollinearity and inflation of variances. Incremental parameters can also be used when there are more than two blocks by introducing additional indicator variables or, possibly, by rewriting the parameters as functions of other variables as in Section 3.11.

3.10.3 Non-nested Models

When trying to decide which of several *non-nested* models is best, the first approach should be to the researcher. That is, if there are scientific reasons for preferring one model over the others, strong weight should be given to the researcher's reasons because the primary aim of data analysis is to explain or account for the behavior of the data, not simply to get the best fit.

Table 3.9 Lack of fit analysis for the 3-parameter Michaelis–Menten model fitted to the combined Puromycin data set.

Source	Sum of Squares	Degrees of Freedom	Mean Square	F Ratio	p Value
Lack of fit	1144	9	127.3	1.3	0.35
Replication	1097	11	99.7		
Residuals	2241	20			

If the researcher cannot provide convincing reasons for choosing one model over others, then statistical analyses can be used, the most important of which is probably an analysis of the residuals. Generally the model with the smallest residual mean square and the most random-looking residuals should be chosen. The residuals should be plotted versus the predicted values, the control variables, time order, and any other (possibly lurking) variables; see Section 3.7.

3.11 Parameters as Functions of Other Variables

In many situations, the parameters in a mechanistic model will depend on other variables. For example, in chemical kinetic studies, we may have data from several experiments in which the operating conditions have been varied, and it may be thought that the rate constants should depend in some systematic way on the operating conditions. We would then like to fit a model which incorporates the dependence of the *kinetic parameters* $\boldsymbol{\theta}$ on some *process variables*, say $\mathbf{w}$, and some *process parameters*, $\boldsymbol{\phi}=(\phi_1,\ldots,\phi_L)^{\mathrm{T}}$. That is, $\boldsymbol{\theta}=\boldsymbol{\theta}(\mathbf{w},\boldsymbol{\phi})$. The expectation function is then $f(\mathbf{x},\boldsymbol{\theta})=f(\mathbf{x},\boldsymbol{\theta}(\mathbf{w},\boldsymbol{\phi}))$.

To estimate the parameters in such an extended model, we could express the function in terms of the regular variables $\mathbf{x}$, the process variables $\mathbf{w}$, and the process parameters $\boldsymbol{\phi}$, determine the derivatives with respect to $\boldsymbol{\phi}$, and then use a Gauss–Newton algorithm to converge to $\hat{\boldsymbol{\phi}}$. It is more efficient, however, to build on what we already have and proceed as follows:

(1) At each level of $\mathbf{w}$, estimate the kinetic parameters $\boldsymbol{\theta}$ in the regular model.

(2) Plot the parameter estimates $\hat{\theta}_p$ versus $\mathbf{w}$ to determine a plausible form for the relationship of $\hat{\theta}_p$ to $\mathbf{w}$ and to obtain starting estimates for the process parameters $\boldsymbol{\phi}$.

(3) Use the chain rule for derivatives to determine the derivatives with respect to $\boldsymbol{\phi}$, exploiting the existing derivatives with respect to $\boldsymbol{\theta}$, as

$$\frac{\partial\eta_n}{\partial\phi_l}=\sum_{p=1}^{P}\frac{\partial\eta_n}{\partial\theta_p}\frac{\partial\theta_p}{\partial\phi_l}$$

for $l=1,2,\ldots,L$, where L is the total number of process parameters.

An application of this method is described in Section 5.5.

Example: Puromycin 11

Suppose in the research on Puromycin (Example Puromycin 10) there were, say, four treatment levels of Puromycin instead of just two (treated and untreated). We could then proceed by incorporating three indicator variables to account for changes in the parameters due to different treatments. However, if the Puromycin treatments consist of different doses, it might be possible to write

$$f(x,\boldsymbol{\theta}) = \frac{\theta_1(w)x}{\theta_2(w)+x}$$

where a possible form of θ_1 and θ_2 is

$$\theta_1 = \phi_{10} + \phi_{11}\, w$$

$$\theta_2 = \phi_{20} + \phi_{21}\, w$$

In this example, the (regular) variable is x, the substrate concentration, and the process variable is w, the Puromycin concentration.

Now suppose that at Puromycin concentration w_1 we get estimates $\hat{\theta}_{11}$ and $\hat{\theta}_{21}$, at concentration w_2, we get estimates $\hat{\theta}_{12}$ and $\hat{\theta}_{22}$, and so on, and that a plot of $\hat{\theta}_2$ versus w looks essentially flat, which suggests $\theta_2 = \text{constant}$. Then we would choose $\phi_{20} = \hat{\theta}_2$. Suppose further that the plot of $\hat{\theta}_1$ versus w reveals a straight line relationship, $\theta_1 = \phi_{10} + \phi_{11} w$. We could then use linear regression of $\hat{\theta}_1$ on w to get starting estimates for ϕ_{10} and ϕ_{11}.

The model to be fitted to the combined data vector would be

$$f(x,w,\boldsymbol{\phi}) = \frac{\theta_1(w)x}{\theta_2(w)+x} = \frac{(\phi_{10}+\phi_{11}w)x}{\phi_{20}+x}$$

■

3.12 Presenting the Results

As in all statistical analyses, the results from a nonlinear regression analysis should be presented clearly and succinctly. This is usually done most effectively by considering the needs and abilities of the prospective audience. The report should always include a summary of the main findings and conclusions.

The summary should include a statement of the final model, the parameter estimates and their standard errors, and an interpretation of the model and the parameters in the context of the original problem.

In the main body of the report, it is useful to state the original problem and possibly a derivation of the general form of mechanistic model proposed. Plots of the data should be given, and any preliminary analyses should be discussed, particularly if they involved transformation of the data or the expectation function. A listing of the data should always be included (perhaps in an appendix), but otherwise plots should be used for effective communication.

The initial model should be presented with a brief description of the steps taken to reduce or extend it, if necessary referring to detailed analyses in appendices. The final model, together with parameter estimates and their approximate standard errors and correlation matrix should be stated, along with a plot of the data, the fitted expectation function, and an approximate confidence band for the

expectation function. Pairwise plots of the parameter inference region, and possibly profile t plots, as described in Chapter 6, should be given. Of great importance is an interpretation of the expectation function and the parameter values relative to the original problem, and especially any new findings, such as the need for additional variables in the model or the non-necessity of any variables or parameters.

Finally, conclusions and recommendations should be made, especially concerning possible future experiments or development of the research.

For further tips on report writing, see Ehrenberg (1981), Ehrenberg (1982), and Watts (1981). The preparation and presentation of graphical material is covered in Tufte (1983), Cleveland (1984, 1985), and Chambers et al. (1983).

3.13 Nitrite Utilization: A Case Study

To illustrate the techniques presented in this chapter, we present an analysis of data on the utilization of nitrite in bush beans as a function of light intensity (Elliott and Peirson, 1986). Portions of primary leaves from three 16-day-old bean plants were subjected to eight levels of light intensity ($\mu E/m^2 s$), and the nitrite utilization (nmol/g hr) was measured. The experiment was repeated on a different day, resulting in the data listed in Appendix 1, Section A1.12.

The experimenters did not have a theoretical mechanism to explain the behavior, but they thought that nitrite utilization should be zero at zero light intensity, and should tend to an asymptote as light intensity increased.

3.13.1 Preliminary Analysis

From a plot of the data (Figure 3.14) it can be seen that there was a difference in the nitrite utilization between experiments on the two days, particularly at higher light intensities. There is also a tendency for the response to drop at high light intensity. Note too that, even though the response ranges from 200 to 20 000 nmol/g hr, the variance is effectively constant; there is no need to transform to stabilize variance. To verify the apparent stable variance, we performed a two way analysis of variance using indicator variables for days and for light intensities, with the results shown in Tables 3.10 and 3.11.

For our purposes the most useful information from the two way analysis of variance is the replication sum of squares and mean square, which can be used for testing lack of fit. We note, however, that the lack of a significant day×intensity interaction suggests that some of the model parameters may be equal for the two days, although the significant day effect tends to corroborate the observed difference between the heights of the maxima on the two days. A plot of the replication standard deviations versus the replication averages, shown

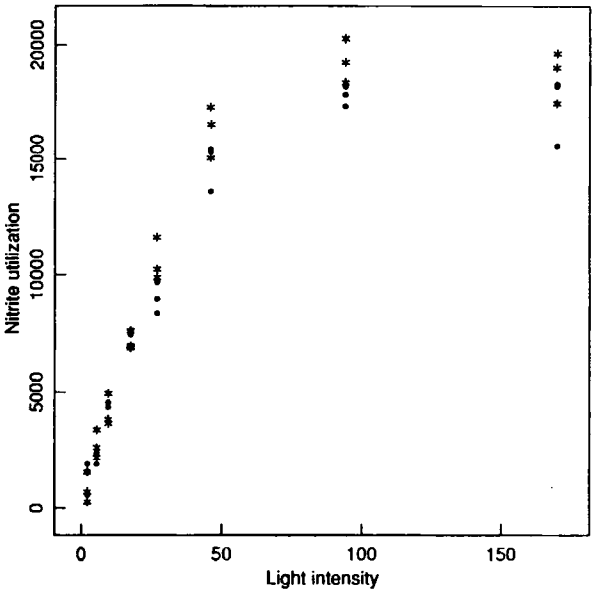

Figure 3.14 Plot of nitrite utilization by bean plants versus light intensity for day 1 (*) and day 2 (•).

Table 3.10 Two way analysis of variance for the nitrite utilization data.

Source	Sum of Squares (10^6)	Degrees of Freedom	Mean Square (10^6)	F Ratio	p Value
Days	4.23	1	4.23	6.1	0.02
Intensity	2040	7	291.5	420.	0.00
Days × intensity	10.07	7	1.44	2.1	0.08
Replication	22.21	32	0.694		

Table 3.11 Replication averages and standard deviations for the nitrite utilization data.

	Day 1		Day 2	
Intensity	Average	Standard Deviation	Average	Standard Deviation
2.2	826	652	1 327	694
5.5	2 702	623	2 541	758
9.6	4 136	719	4 619	296
17.5	7 175	401	7 554	86
27.0	10 567	908	9 019	650
46.0	16 302	1154	14 753	1082
94.0	19 296	963	17 786	430
170.0	18 719	1117	17 374	1408

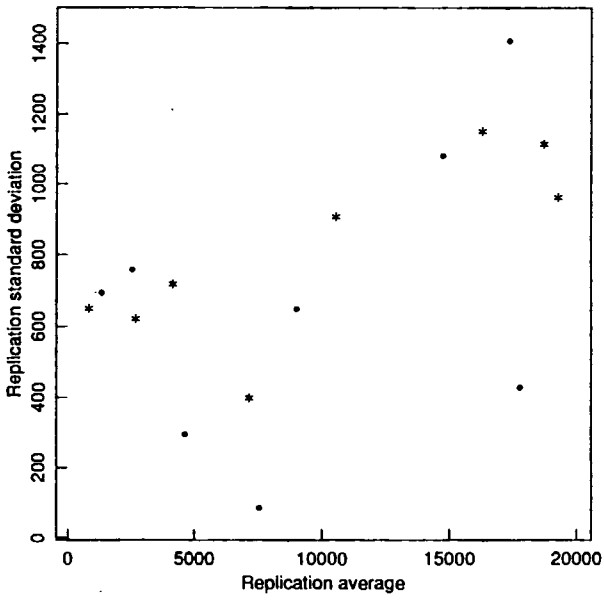

Figure 3.15 Replication standard deviations plotted versus replication averages for the nitrite utilization data. Day 1 data are shown as * and day 2 data as •.

in Figure 3.15, verified our earlier assessment that the variance is stable since there is no systematic relation, and so we proceed to model fitting.

Note that the analysis of variance is used here only as a screening tool. It is not intended as a final analysis of these data, since the underlying additive linear model assumed in an analysis of variance is not appropriate.

3.13.2 Model Selection

Because the researchers did not have a model in mind, it was necessary to select one on the basis of the behavior of the data. The Michaelis–Menten model

$$f(x,\boldsymbol{\theta}) = \frac{\theta_1 x}{\theta_2 + x}$$

and the simple exponential rise model

$$f(x,\boldsymbol{\theta}) = \theta_1(1 - e^{-\theta_2 x})$$

were selected because they met the researcher's beliefs that nitrite utilization was zero at zero light intensity and tended to an asymptote as the light intensity increased. To simplify the description, we give details for the Michaelis–Menten model analysis, and only present summaries for the exponential rise model.

Since there are 24 observations for each day from this well-designed experiment, it would be reasonable to fit a separate model for each day. We would like to think, however, that the same parameter values, or at least some of the same parameter values, would be valid for both days, and so we proceed to fit a model for day 1 with incremental parameters for day 2. That is, we write

$$f(x,\boldsymbol{\theta}) = \frac{(\theta_1 + \phi_1 x_2)x_1}{(\theta_2 + \phi_2 x_2) + x_1}$$

where x_1 is the light intensity and x_2 is an indicator variable

$$x_2 = \begin{cases} 0 & \text{day 1} \\ 1 & \text{day 2} \end{cases}$$

as described in Section 3.10.

3.13.3 Starting Values

Since the maximum value on day 1 is about 20 000, and on day 2 is about 18 000, we choose $\theta_1^0 = 25\,000$ and $\phi_1^0 = -3000$. The response reaches about 12 500 at a light intensity of about 34 for day 1 and 35 for day 2, which gives $\theta_2^0 = 34$ and $\phi_2^0 = 1$.

3.13.4 Assessing the Fit

Convergence was achieved at the values shown in Table 3.12.

It appears from the t ratios that both the incremental parameters could be estimates of zero, and so a common model could be fitted. However, if we do a lack of fit analysis on this model as in Table 3.13, we see that this four-parameter model is not adequate. (The same conclusion was reached for the ex-

Table 3.12 Parameter summary for the 4-parameter Michaelis–Menten model fitted to the nitrite utilization data.

Parameter	Estimate	Standard Error	t Ratio	Correlation Matrix			
θ_1	24743	1241	19.9	1.00			
θ_2	35.27	4.66	7.6	0.88	1.00		
ϕ_1	−2329	1720	−1.4	−0.72	−0.64	1.00	
ϕ_2	−2.174	6.63	−0.3	−0.62	−0.70	0.88	1.00

Table 3.13 Lack of fit analysis for the 4-parameter Michaelis–Menten model fitted to the nitrite utilization data.

Source	Sum of Squares (10^6)	Degrees of Freedom	Mean Square (10^6)	F Ratio	p Value
Lack of fit	64.30	12	5.36	7.72	0.00
Replications	22.21	32	0.694		
Residuals	86.51	44			

ponential rise model, in this case with a lack of fit ratio of 3.2, corresponding to a p value of 0.00.)

A plot of the residuals versus light intensity, as in Figure 3.16, reveals nonrandom behavior, with negative residuals at small and large intensities and positive ones in the middle. The model must therefore be modified to allow the nitrite utilization to drop with increasing light intensity, rather than leveling off as suggested by the researchers.

3.13.5 Modifying the Model

To alter the Michaelis–Menten expectation function to rise to a peak and then fall, we added a quadratic term to the denominator to produce the quadratic Michaelis–Menten model,

$$f(x,\boldsymbol{\theta}) = \frac{\theta_1 x}{\theta_2 + x + \theta_3 x^2}$$

which, with incremental parameters and an indicator variable for the different days, becomes

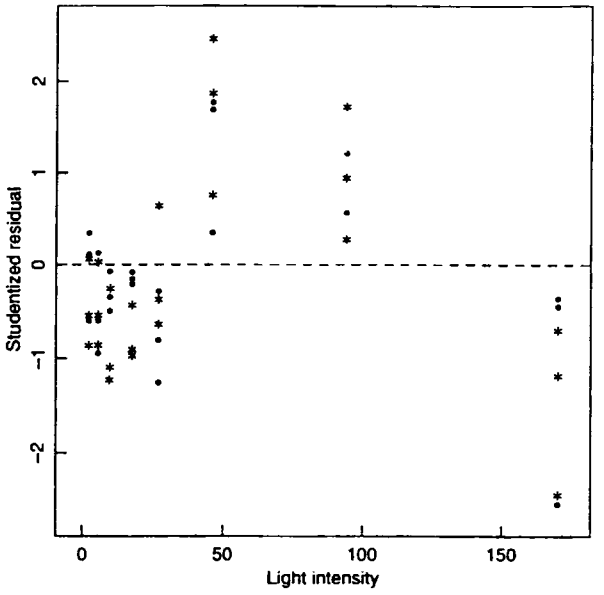

Figure 3.16 Studentized residuals from the 4-parameter Michaelis–Menten model plotted versus light intensity. Day 1 data are shown as * and day 2 data as •.

$$f(\mathbf{x},\boldsymbol{\theta}) = \frac{(\theta_1 + \phi_1 x_2)x_1}{(\theta_2 + \phi_2 x_2) + x_1 + (\theta_3 + \phi_3 x_2)x_1^2}$$

(For the exponential rise model, we replaced the unit term by an exponential to produce the exponential difference model,

$$f = \theta_1(e^{-\theta_3 x} - e^{-\theta_2 x})$$

This model, augmented with increment parameters and an indicator variable, was also used to fit the data.)

Starting values for the parameters were obtained by taking reciprocals of the function and the data and using linear least squares for the quadratic Michaelis–Menten model. Taking reciprocals worked for the day 2 data, giving $\boldsymbol{\theta} = (107\,411, 234, 0.024)^{\mathrm{T}}$, but gave some negative values for the day 1 data. We therefore used the day 2 starting values with slight perturbations to get starting values for the 6-parameter model of $\boldsymbol{\theta}^0 = (110\,000, 234, 0.024)^{\mathrm{T}}$ and $\boldsymbol{\phi}^0 = (-10\,000, 23, 0.002)^{\mathrm{T}}$. (For the exponential difference model, we guessed that the two rate constants might be in the ratio 1:5 and used the estimate for θ_2 to give $\theta_3 = 0.006$. We then estimated θ_1 by evaluating

$$\theta_1 = \frac{y}{e^{-0.006x} - e^{-0.030x}}$$

for several x values. This gave $\theta_1^0 = 37\,000$ for the day 1 data and 35 000 for the day 2 data, from which we got $\phi_1^0 = -2000$.)

3.13.6 Assessing the Fit

Quick convergence was achieved to the parameter estimates given in Table 3.14 for the quadratic Michaelis–Menten model. All the incremental parameters have nonsignificant approximate t ratios, which suggests that the parameters could be zero, and so a simpler model may be adequate. The extremely high parameter approximate correlations also lead one to suspect that the model may be overparametrized. The residual sum of squares (32.02×10^6 on 42 df) is only about a third of that for the previous model. (Similar conclusions were reached for the 6-parameter exponential difference model.)

The residuals for this model, plotted versus light intensity in Figure 3.17, are clearly well behaved and give no evidence of inadequacy of the model.

3.13.7 Reducing the Model

To determine what simplifications could be made in the quadratic Michaelis–Menten model, we set ϕ_2 and ϕ_3 to zero, still retaining ϕ_1 to account for a difference between days. For starting values, we simply used the relevant converged values from the 6-parameter model.

3.13.8 Assessing the Fit

The results for the 4-parameter quadratic model are given in Table 3.15. The extra sum of squares analysis for the 4-parameter versus the 6-parameter quadratic model, shown in Table 3.16, does not show a significant degradation of the fit with elimination of ϕ_2 and ϕ_3. The residuals, when plotted versus light intensity as in Figure 3.18, attest to the adequacy of the model. Furthermore, a lack of fit analysis, shown in Table 3.17, suggests that the model is adequate.

Table 3.14 Parameter summary for the 6-parameter quadratic Michaelis–Menten model fitted to the nitrite utilization data.

Parameter	Estimate	Standard Error	t Ratio	Correlation Matrix				
θ_1	89 846	37 583	2.4	1.00				
θ_2	186.7	90.1	2.1	1.00	1.00			
θ_3	0.01626	0.00922	1.8	1.00	0.99	1.00		
ϕ_1	−38 956	40 020	−1.0	−0.94	−0.94	−0.94	1.00	
ϕ_2	−83.23	96.8	−0.9	−0.93	−0.93	−0.92	1.00	1.00
ϕ_3	−0.00846	0.0993	−0.9	−0.93	−0.92	−0.93	1.00	0.99

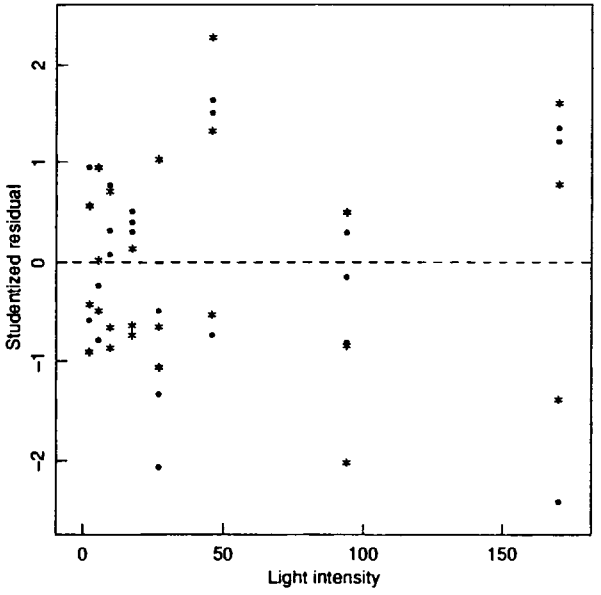

Figure 3.17 Studentized residuals from the 6-parameter quadratic Michaelis–Menten model plotted versus light intensity. Day 1 data are shown as * and day 2 data as •.

Table 3.15 Parameter summary for the 4-parameter quadratic Michaelis–Menten model fitted to the nitrite utilization data.

Parameter	Estimate	Standard Error	t Ratio	Correlation Matrix			
θ_1	70096	16443	4.3	1.00			
θ_2	139.4	39.3	3.6	1.00	1.00		
θ_3	0.01144	0.00404	2.8	0.99	0.99	1.00	
ϕ_1	−5381	1915	−2.8	−0.69	−0.66	−0.66	1.00

Table 3.16 Extra sum of squares analysis for the 6-parameter versus the 4-parameter quadratic Michaelis–Menten model fitted to the nitrite utilization data.

Source	Sum of Squares (10^6)	Degrees of Freedom	Mean Square (10^6)	F Ratio	p Value
Extra	0.82	2	0.41	0.54	0.59
6-parameter	32.02	42	0.762		
4-parameter	32.84	44	0.746		

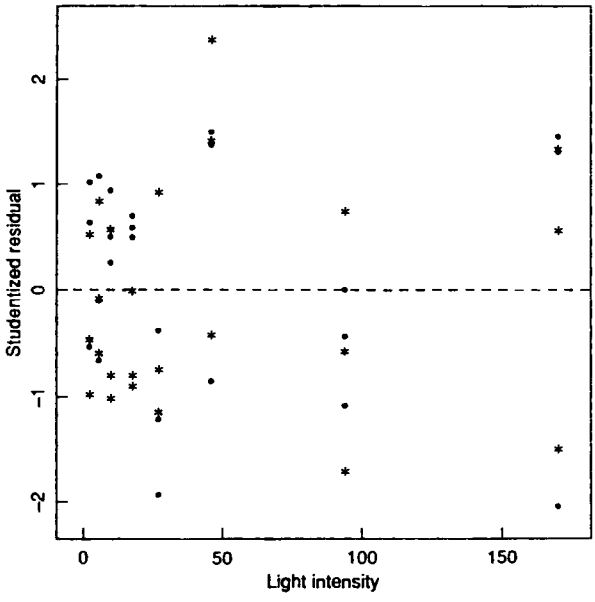

Figure 3.18 Studentized residuals from the 4-parameter quadratic Michaelis–Menten model plotted versus light intensity. Day 1 data are shown as * and day 2 data as •.

Table 3.17 Lack of fit analysis for the 4-parameter quadratic Michaelis–Menten model fitted to the nitrite utilization data.

Source	Sum of Squares (10^6)	Degrees of Freedom	Mean Square (10^6)	F Ratio	p Value
Lack of fit	10.63	12	0.886	1.28	0.28
Replications	22.21	32	0.694		
Residuals	32.84	44	0.746		

Note that the parameter ϕ_1 is now apparently significantly different from 0, with an approximate t ratio of -2.8, confirming our earlier suspicion that there was a difference between days. This parameter was not significantly different from 0 in the 6-parameter model, which is further evidence for the 6-parameter model being overparametrized and hence the parameter approximate standard errors being artificially inflated, causing nonsignificant t ratios.

The parameter approximate correlation matrix for the quadratic Michaelis–Menten 4-parameter model shown in Table 3.15 reveals that several of the correlations are very large. This is not unusual in nonlinear regression, and is induced by a combination of the form of the expectation function and the design used. For example, for a Michaelis–Menten model, no matter how good the design is, it is impossible to obtain zero correlation between the parameters because it is impossible to force the derivatives to be orthogonal. To see this, we note that the first column of the derivative matrix, $\mathbf{v}_1$, has elements $x/(\theta_2 + x)$, and the second column, $\mathbf{v}_2$, has elements $-\theta_1 x/(\theta_2 + x)^2$. All the elements in $\mathbf{v}_1$ are positive and all the elements in $\mathbf{v}_2$ are negative, and so the two vectors $\mathbf{v}_1$ and $-\mathbf{v}_2$ will always tend to point in the same direction in the response space. Consequently, they will tend to be collinear.

As a final check on the model, the 3-parameter Michaelis–Menten model

$$f = \frac{(\theta_1 + \phi_1 x_2)x_1}{\theta_2 + x_1}$$

could be fitted and compared with the 4-parameter quadratic Michaelis–Menten model using an extra sum of squares analysis to further substantiate the necessity for the parameter θ_3. This was not done because the residuals for the original 3-parameter Michaelis–Menten model were so badly behaved.

(Similar results and conclusions were reached for the exponential difference model: that is, a 4-parameter model with common exponential parameters and scale factor, plus an incremental parameter for day 2, was found to give an adequate fit. Summary information on the fit is given in Table 3.18, and comparison with the 6-parameter model in Table 3.19. The lack of fit analysis is given in Table 3.20. In this case, the lack of fit ratio was 1.46, still not significant, but slightly larger than for the quadratic Michaelis–Menten model.)

Table 3.18 Parameter summary for the 4-parameter exponential difference model fitted to the nitrite utilization data.

Parameter	Estimate	Standard Error	t Ratio	Correlation Matrix			
θ_1	35 115	8940	3.9	1.00			
θ_2	0.01845	0.00317	5.8	−0.99	1.00		
θ_3	0.00325	0.00120	2.7	0.99	−0.97	1.00	
ϕ_1	−2686	1006	−2.7	−0.71	0.67	−0.68	1.00

Table 3.19 Extra sum of squares analysis for the 6-parameter versus the 4-parameter exponential difference model fitted to the nitrite utilization data.

Source	Sum of Squares (10^6)	Degrees of Freedom	Mean Square (10^6)	F Ratio	p Value
Extra	0.37	2	0.19	0.23	0.80
6-parameter	33.97	42	0.809		
4-parameter	34.34	44	0.780		

Table 3.20 Lack of fit analysis for the 4-parameter exponential difference model fitted to the nitrite utilization data.

Source	Sum of Squares (10^6)	Degrees of Freedom	Mean Square (10^6)	F Ratio	p Value
Lack of fit	12.13	12	1.011	1.46	0.19
Replications	22.21	32	0.694		
Residuals	34.34	44	0.780		

3.13.9 Comparing the Models

To compare the nested models we have used incremental parameters and the extra sum of squares principal, but they can not be used to compare the quadratic Michaelis–Menten and the exponential difference models. Our first approach was to the researchers, asking them whether one model was preferred on scientific grounds. In this case, the researchers had no preference, and so we simply presented them with the results for both models. Because the lack of fit ratio and the residual mean squares were smaller, we had a slight preference for

the Michaelis–Menten model. In Figure 3.19 we show the nitrite utilization data together with the fitted curve and the approximate 95% confidence bands for the 4-parameter quadratic Michaelis–Menten model.

3.13.10 Reporting the Results

A brief report was prepared for Professors Elliott and Peirson, along the lines of Section 3.12. The major finding of interest was the need for a model which rose to a peak rather than to an asymptote. This was not expected, at least at such a low light level. As part of our report, we recommended additional experiments be run, especially at higher light intensities, in order to verify the need for a model which rises to a peak rather than approaching an asymptote, and to help discriminate between the two competing models. It was further suggested that future experiments involve fewer levels at low light intensity to reduce effort.

3.14 Experimental Design

So far we have concentrated more on the analysis of data than on the design of experiments to produce good data, although we believe that good experimental

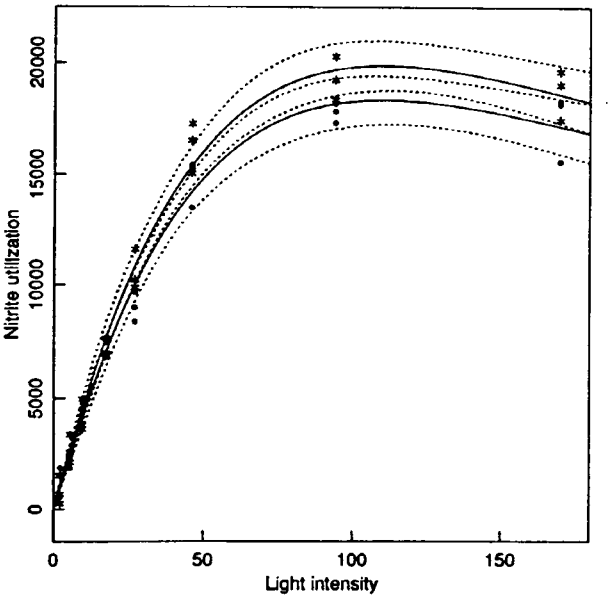

Figure 3.19 Plot of nitrite utilization versus light intensity together with the fitted curves (solid lines) and the 95% approximate inference bands (dotted). Data for day 1 are shown as * and for day 2 as •.

design is vital to scientific progress. The reason for the prime importance of experimental design is that *the information content of the data is established when the experiment is performed*, and no amount of sensitive data analysis can recover information which is not present in the data.

One reason for our emphasizing analysis rather than design is that we usually have to deal with data that have been obtained without the benefit of good statistical design. Another reason is that, while good experimental design is extremely valuable, it is necessary to know how to analyze data in order to appreciate what "good experimental design" is.

3.14.1 General Considerations

Experimentation is fundamental to scientific learning, which we may characterize as *reducing ignorance*. At any stage of research, we are in a position of having data, and of being able to explain part of that data, and as the research proceeds, we are able to account for, or explain, more of the data. For example, a chemical engineer trying to learn about how a particular product is produced would know very little initially about the factors and the chemical reactions involved. As she proceeds, planning and running experiments under various conditions, she would endeavor to find out, at each stage, what the important factors are, and how they affect the response. Initially, she would be involved in empirical "screening designs" to try to isolate those factors which are most influential in affecting the response, probably using *factorial* or *fractional factorial* designs (Box, Hunter, and Hunter, 1978). If she was interested in optimizing some characteristic, she might then proceed to *response surface* designs (Box, Hunter, and Hunter, 1978; Box and Draper, 1987). Later on, perhaps to fine tune the product or to gain better understanding of the mechanisms involved, she would move from empirical models and their associated strategies to mechanistic (usually nonlinear) models. It is this aspect of experimental design which we consider in this section.

We assume initially that the experimenter has a well-defined *form* for the expectation function relating the factors to the response, and that the objectives of the experiments are to provide the necessary and adequate information to:

(1) estimate the parameters of interest in the model with
  accuracy (i.e. small bias),
  precision (i.e. small variance), and
(2) verify the assumptions about
  the expectation function,
  the disturbance model.

As was the case for estimation, it is helpful first to discuss the linear situation. Accordingly, in the following section we present a brief review of experimental design for linear expectation functions. For a more comprehensive presentation, see Box, Hunter, and Hunter (1978), Davies (1956), and Cochran

and Cox (1957); and for general considerations on the planning of experiments, Box and Draper (1959) and Draper and Smith (1981). A thorough review of optimal designs is given in St. John and Draper (1975), Cochran (1973), and Steinberg and Hunter (1984). Hamilton and Watts (1985) discussed designs using second order derivatives, and the geometry of experimental designs was discussed in Silvey and Titterington (1973).

Before considering the more technical details of experimental design, we offer some comments which help ensure attainment of the general objectives (1) and (2) above.

With regard to providing accurate and precise estimates of the parameters, it is helpful to recognize that an experimental design involves choosing the values of the factors for a selected number of experimental cases (or runs). It is therefore important that the number of cases be large enough to ensure attainment of the specific objectives of the experiment. For example, if an expectation function involves five parameters, there will have to be at least five distinct experimental conditions. It is equally important to limit the number of experiments done at any one time. That is, one should not construct an extremely large design and then proceed slavishly to follow that design to its completion. Due account should be taken of what is learned at each stage of the experiment, and this information should be exploited in the design of the next stage. The number of experiments which should be run in a *block* will depend on the number of factors and the type of experiment being run, of course, but blocks of size 10 to 20 are usually informative and manageable.

The choices of the factor settings should be such that they are in useful and appropriate ranges of the factors. That is, the factors should be located near sensible values which will permit use of the parameter estimates in future investigations, and the levels of each factor should be spread out enough so that the effect of each factor will be revealed in spite of the inherent variability of the response.

With regard to verifying the assumptions about the expectation function, it is important to provide *replications* to enable testing for lack of fit or inadequacy of the expectation function. It is also important, when possible, to *randomize* the order of the experiments, to ensure that the expectation function is appropriate. (If there are unsuspected factors operating, randomizing will tend to cause their effects to appear as increased variability rather than as incorrect parameter estimates, as discussed in Section 1.3.)

With regard to verifying the assumptions about the disturbance model, replications are again important. As discussed in Section 1.3, replications enable one to test for constancy of variance and to determine a variance stabilizing transformation if the variance is deemed not constant. Randomizing will also tend to ensure that all of the assumptions concerning the disturbances will be appropriate, as discussed in Section 1.3. Once again, we see the importance and power of randomizing.

In summary, *statistical analysis* is concerned with the efficient extraction and presentation of the information embodied in a data set, while *statistical experimental design* is concerned first with ensuring that the important necessary

information is embodied in a data set, and second with making the extraction and presentation of that information easy.

3.14.2 The Determinant Criterion

Consider the linear model (1.1)

$$Y = \mathbf{X}\boldsymbol{\beta} + Z$$

with the usual assumptions (1.2) and (1.3) about the disturbances Z,

$$\mathrm{E}[Z] = \mathbf{0}$$

$$\mathrm{Var}[Z] = \sigma^2\mathbf{I}$$

For a linear regression model, a row of the derivative matrix X depends only on the choice of the K design variables, where the design variables determine such characteristics as when the run is taken, at what pressure, at what temperature, etc. An individual entry in the derivative matrix is calculated from the values of the design variables. For any choice of the design variables generating a derivative matrix X, the parameters $\boldsymbol{\beta}$ will have a joint inference region whose volume is proportional to $|\mathbf{X}^{\mathrm{T}}\mathbf{X}|^{-1/2}$. Thus, a logical choice of design criterion is to choose the design points so that the volume of the joint inference region is minimized (Wald, 1943). Since the power $-1/2$ is inconsequential, Wald proposed maximizing the determinant $D = |\mathbf{X}^{\mathrm{T}}\mathbf{X}|$, and designs which satisfy this criterion are called *D-optimal* designs. The criterion is referred to as the *determinant criterion.*

From a geometric point of view, the determinant criterion implies that we should choose the columns of X so that each vector is as long as possible ($\|\mathbf{x}_p\|^2$ is as large as possible, $p = 1, 2, \ldots, P$), and try to make the vectors orthogonal ($\mathbf{x}_p^{\mathrm{T}}\mathbf{x}_q = 0$, $p \neq q$). The former ensures that the expectation plane will be well supported in the response space, and that the parameter lines will be widely spaced on the expectation plane. Consequently the disturbances, whose variance is beyond our control, will have small effect, thereby producing a joint region in the parameter space with small volume. The latter ensures that the parameter estimates associated with the factors will not be correlated. That is, changes in the response will be correctly associated with changes in the appropriate causative factor, and not attributed to other factors.

The two requirements of long length and orthogonality of the derivative vectors ensure that a disk on the expectation plane will map to a small ellipse in standard position on the parameter plane.

The determinant criterion was applied to nonlinear expectation functions by Box and Lucas (1959) who used, in place of the X matrix, the derivative matrix $\mathbf{V}^0$ evaluated at some initial parameter estimates $\boldsymbol{\theta}^0$. That is, in nonlinear design, the D-optimal criterion is modified to maximize

$$D = |\mathbf{V}^{0\,\mathrm{T}}\mathbf{V}^0| \tag{3.5}$$

The design of an experiment depends on the stage at which the researcher is in an investigation. When only the form of the model is known, but not the parameter values, as could be the case in enzyme kinetics or in biochemical oxygen demand studies, the researcher would be concerned with choosing the values of the factors to produce good parameter estimates. These are called "starting designs." Later on in an investigation, the researcher might wish to design an experiment to improve the precision of estimates of some or all of the parameters, exploiting data already obtained. Such designs are called "sequential designs," and, when special interest is attached to a subset of the parameters, "subset designs."

3.14.3 Starting Designs

Box and Lucas (1959) proposed starting designs consisting of P points for a P-parameter model, and therefore simplified the criterion (3.5) to that of maximizing $|\mathbf{V}^0|$. Geometrically, the determinant criterion ensures that the expectation surface is such that large regions on the tangent plane at $\boldsymbol{\eta}(\boldsymbol{\theta}^0)$ map to small regions in the parameter space. When more than P points are to be chosen, the D-optimal design usually results in replications of P distinct design points (Box, 1968), and these design points are those that would be chosen as D-optimal with $N = P$. We therefore consider starting designs as having only P runs.

Example: Puromycin.12

To illustrate the choice of a starting design, we consider the case of enzyme kinetics, which are assumed to follow a Michaelis–Menten model. We assume that the maximum allowable substrate concentration is specified as $x_{\max}$, and that initial estimates of the parameters $\boldsymbol{\theta}^0$ are given.

The derivatives of the expectation function, evaluated at the initial parameter estimates $\boldsymbol{\theta}^0$, are

$$\frac{x}{\theta_2^0 + x} \qquad \frac{-\theta_1^0 x}{(\theta_2^0 + x)^2}$$

and so the determinant to be maximized is

$$|\mathbf{V}^0| = \begin{vmatrix} \dfrac{x_1}{\theta_2^0+x_1} & \dfrac{-\theta_1^0 x_1}{(\theta_2^0+x_1)^2} \\ \dfrac{x_2}{\theta_2^0+x_2} & \dfrac{-\theta_1^0 x_2}{(\theta_2^0+x_2)^2} \end{vmatrix}$$

$$= \frac{\theta_1^0 x_1 x_2 \, |x_1 - x_2|}{(\theta_2^0+x_1)^2(\theta_2^0+x_2)^2}$$

The modulus of this determinant is maximized when

$$x_1 = x_{\max} \quad \text{and} \quad x_2 = \frac{\theta_2^0}{1+2(\theta_2^0/x_{\max})} \simeq \theta_2^0$$

The determinant criterion therefore places the design points so as to tie down the asymptote (θ_1) by performing one experiment at the maximum concentration, and to tie down the half-concentration by performing the other experiment near the assumed half-concentration.

It is instructive to compare the D-optimal design with the dilution design used by Treloar (1974). The dilution design used $x_{\max} = 1.1$ and five dilutions by approximately one-half, with duplications, giving a total of 12 runs. With the same number of runs, the D-optimal design would consist of 6 replications at $x_{\max}$ and 6 replications at $x_2 = \theta_2^0/[1+2(\theta_2^0/x_{\max})]$. We take $\theta_2^0 = 0.1$ as a reasonable starting estimate, and so the design is $x_1 = 1.1$, $x_2 = 0.085$. In Figure 3.20 we plot the linear approximation 95% confidence region for the dilution design and data together with the linear approximation confidence region for the D-optimal design assuming that both designs gave the same parameter estimates and residual variance. We see that the D-optimal design does indeed give a smaller joint confidence region and smaller confidence intervals. In addition, the correlation between the parameters is lower. However, the gain in precision from using the D-optimal design would have to be balanced against any loss of information about lack of fit.

Note that the design does not depend on the conditionally linear parameter θ_1, which is true in general for conditionally linear parameters, as shown in Section 3.14.6. ■

The determinant criterion provides an objective basis for determining P-point designs for P-parameter models, but the design strategy should not be applied blindly. The criterion was derived on the basis that the expectation function is *known*, and provides only P design points to estimate the P parameters. Replications at these P design points are useful because they provide informa-

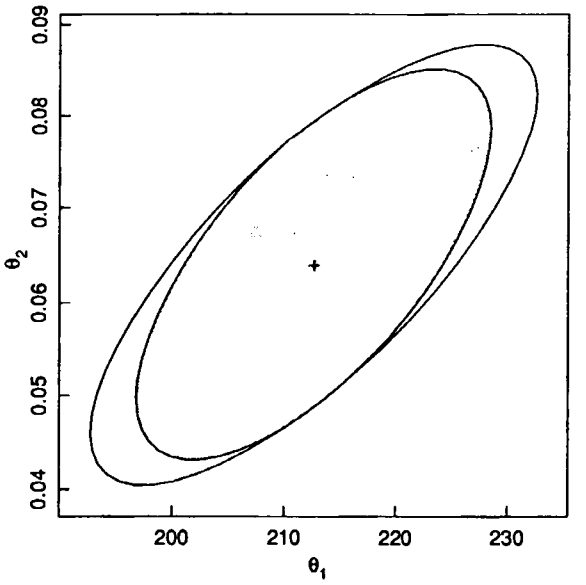

Figure 3.20 Comparison of 95% approximate inference regions for two designs for the Puromycin data. The larger region results from the dilution design used, and the shaded region results from a D-optimal design.

tion concerning constancy of variance, but they cannot provide information about lack of fit. It might be useful, therefore, to perform additional experiments at other design points in order to detect lack of fit. In light of these considerations, the dilution design strategy is eminently sensible, especially given its high level of performance as demonstrated in the above example.

3.14.4 Sequential Designs

In many situations, some experiments will already have been done to check if the equipment is functioning properly, or to screen possible models, as described in Box and Hunter (1965). In other situations, it may be possible to perform and analyze the result from a single experiment quite rapidly. In these situations, it is possible to obtain even better parameter estimates by designing the experiments sequentially; that is, an experimental run is designed, the data are collected and analyzed, and the design for the next run is obtained by maximizing $|\mathbf{V}_1^{\mathrm{T}}\mathbf{V}_1|$ with respect to the design variables, $\mathbf{x}_{N+1}$, where

$$\mathbf{V}_1 = \begin{bmatrix} \mathbf{V}_0 \\ \mathbf{v}_{N+1} \end{bmatrix}$$

and $\mathbf{v}_{N+1}$ is the gradient vector $\partial f/\partial \boldsymbol{\theta}^{\mathrm{T}}$ evaluated at the least squares estimates

from the N runs already made.

Example: Isomerization 3

To illustrate sequential design, we consider the model and data set from Example Isomerization 1. The correlations between the parameters are very high, and the linear approximation confidence regions include negative values for the equilibrium constants. We would therefore like to design experiments to provide better precision in the parameter estimates.

The design points are determined by the values of the partial pressure of hydrogen, x_1, the partial pressure of n-pentane, x_2, and the partial pressure of isopentane, x_3. In the previous runs these variables have ranged from about 100 to 400 for x_1, 75 to 350 for x_2, and 30 to 150 for x_3, so we use these limits to define a reasonable region within which to design further runs. We begin by evaluating the sequential D-optimal design criterion at the original design points and at sequential design points at the corners of the region. This gives the values in Table 3.21. The combination which optimizes the D-optimal criterion is low x_1 (100), high x_2 (350), and low x_3 (30). Examination of nearby values confirms that the corner is a local optimum, and since a coarse grid search of the design region did not reveal any optima in the interior, we choose this corner as the design point for the next run. ■

Table 3.21 Sequential D-optimal design criteria for the isomerization model, evaluated at the corners of the design region.

Factor			Criterion
x_1	x_2	x_3	D 10^6
100	100	30	4.63
400	100	30	1.95
100	350	30	9.44
400	350	30	3.99
100	100	150	1.82
400	100	150	1.82
100	350	150	3.98
400	350	150	2.42

3.14.5 Subset Designs

When only a subset of the parameters $\boldsymbol{\theta}$ is of interest, the design criterion is modified as suggested in Box (1971) and Hill and Hunter (1974). We assume that the parameters have been ordered so the first P_1 parameters are the nuisance parameters and the trailing P_2 parameters are the parameters of interest, and we partition the vector $\boldsymbol{\theta}^{\mathrm{T}}$ as $(\boldsymbol{\theta}_1^{\mathrm{T}} \mid \boldsymbol{\theta}_2^{\mathrm{T}})$, and the matrix $\mathbf{V}^0$ as $[\mathbf{V}_1^0 \mid \mathbf{V}_2^0]$. Then the variance–covariance matrix of the P_2 parameters is proportional to $\mathbf{D}_{2,2}$, where

$$\begin{aligned}\mathbf{D} &= (\mathbf{V}^{0\,\mathrm{T}}\mathbf{V}^0)^{-1} \\ &= \begin{bmatrix} \mathbf{V}_1^{0\,\mathrm{T}}\mathbf{V}_1^0 & \mathbf{V}_1^{0\,\mathrm{T}}\mathbf{V}_2^0 \\ \mathbf{V}_2^{0\,\mathrm{T}}\mathbf{V}_1^0 & \mathbf{V}_2^{0\,\mathrm{T}}\mathbf{V}_2^0 \end{bmatrix}^{-1} \\ &= \begin{bmatrix} \mathbf{D}_{1,1} & \mathbf{D}_{1,2} \\ \mathbf{D}_{1,2}^{\mathrm{T}} & \mathbf{D}_{2,2} \end{bmatrix}\end{aligned}$$

and so the D-optimal criterion is changed to minimization of

$$D_S = |\mathbf{D}_{2,2}|$$

which is equivalent to maximizing

$$\frac{|\mathbf{V}^{0\mathrm{T}}\mathbf{V}^0|}{|\mathbf{V}_1^{0\mathrm{T}}\mathbf{V}_1^0|}$$

Example: Isomerization 4

To illustrate subset design, we consider the model, data set, and design region from Example Isomerization 3, and treat the situation in which we wish to improve the estimates of θ_2, θ_3, and θ_4. Evaluation of D_S at the corners of the same region gives the results in Table 3.22, which produce similar conclusions and the same design point as in Example Isomerization 3. ■

3.14.6 Conditionally Linear Models

It is awkward to have to specify initial estimates of the parameters $\boldsymbol{\theta}$ before an experimental design can be obtained, since, after all, the purpose of the experiment is to determine parameter estimates. In Examples Puromycin 12 and Isomerization 3, we saw that the D-optimal design was not affected by the value of a conditionally linear parameter. For most models with conditionally linear parameters, the locations of the D-optimal design points do not depend on the conditionally linear parameters (Hill, 1980; Khuri, 1984), so the design problem

Table 3.22 Sequential D-optimal subset design criteria for the isomerization model, evaluated at the corners of the design region.

Factor			Criterion
x_1	x_2	x_3	D_S 10^6
100	100	30	8.77
400	100	30	3.90
100	350	30	13.11
400	350	30	7.08
100	100	150	3.69
400	100	150	3.68
100	350	150	7.39
400	350	150	4.70

is simpler.

The easiest type of conditionally linear model to demonstrate this for is that with only one conditionally linear parameter, so the function can be written

$$f(\mathbf{x},\boldsymbol{\theta}) = \theta_1\, g(\mathbf{x},\boldsymbol{\theta}_{-1})$$

for some function g where $\boldsymbol{\theta}_{-1} = (\theta_2, \ldots, \theta_P)^{\mathrm{T}}$. This includes the Michaelis–Menten, BOD, and isomerization models. The gradient of the model function can then be written

$$\frac{\partial f}{\partial \boldsymbol{\theta}^{\mathrm{T}}} = \left[g(\mathbf{x},\boldsymbol{\theta}_{-1}), \frac{\partial g}{\partial \boldsymbol{\theta}_{-1}^{\mathrm{T}}} \right] \begin{bmatrix} 1 & \mathbf{0} \\ \mathbf{0} & \theta_1 \mathbf{I} \end{bmatrix} \tag{3.6}$$

which isolates the dependence of θ_1 from any dependence upon $\mathbf{x}$. Using (3.6), the derivative matrix $\mathbf{V}$ can be written

$$\mathbf{V} = \mathbf{H}(\mathbf{x},\boldsymbol{\theta}_{-1})\,\mathbf{B}(\theta_1) \tag{3.7}$$

where

$$\mathbf{B}(\theta_1) = \begin{bmatrix} 1 & \mathbf{0} \\ \mathbf{0} & \theta_1 \mathbf{I} \end{bmatrix}$$

is $P \times P$, so the D-optimal criterion is

$$\begin{aligned} |\mathbf{V}^{\mathrm{T}}\mathbf{V}| &= |\mathbf{B}^{\mathrm{T}}\mathbf{H}^{\mathrm{T}}\mathbf{H}\,\mathbf{B}| \\ &= |\mathbf{B}|^2\, |\mathbf{H}^{\mathrm{T}}\mathbf{H}| \end{aligned}$$

and, again, the dependence of θ_1 is isolated from $\mathbf{x}$. Therefore, the design does

not depend upon θ_1.

In general, for conditionally linear models of the form

$$f(\mathbf{x},\boldsymbol{\theta}) = \theta_1 g_1(\mathbf{x},\boldsymbol{\theta}_{-\mathbf{L}}) + \cdots + \theta_L g_L(\mathbf{x},\boldsymbol{\theta}_{-\mathbf{L}})$$

where $\boldsymbol{\theta}_{-\mathbf{L}} = (\theta_{L+1}, \ldots, \theta_P)^{\mathrm{T}}$, the D-optimal design will not depend on the conditionally linear parameters $(\theta_1, \ldots, \theta_L)^{\mathrm{T}}$ if $\mathbf{V}$ can be factored as in (3.7), provided $\mathbf{B}$ is square. The condition that the matrix $\mathbf{B}$ is square was not explicitly stated in Hill (1980), nor was it emphasized in Khuri (1984), where it was shown that conditionally linear parameters will usually affect subset designs. This occurs because, for subset designs, the design criterion involves the *ratio* of determinants of components of $\mathbf{V}$, and so the simple factorization above usually does not occur even if $\mathbf{B}$ is square. Khuri (1984) gives conditions under which the conditionally linear parameters do not affect designs for subsets of parameters.

In the common situation where each component of $\boldsymbol{\theta}_{-\mathbf{L}}$ enters into only one of the functions g_i, $i = 1, \ldots, L$, the derivatives can be factored as in (3.7). For example, D-optimal designs for the sum of exponentials model

$$f(x,\boldsymbol{\theta}) = \theta_1 e^{-\theta_2 x} + \theta_3 e^{-\theta_4 x} + \cdots + \theta_{P-1} e^{-\theta_P x}$$

do not depend on the conditionally linear parameters.

3.14.7 Other Design Criteria

Precise parameter estimation is not the only objective used for experimental design. Methods have been proposed for constructing designs for discriminating between possible model functions (Box and Hill, 1974) and for balancing the objectives of model discrimination and precise parameter estimation (Hill, Hunter, and Wichern, 1968). The review article (Steinberg and Hunter, 1984) describes many of these criteria. We also list several of the references for different experimental design criteria for single response and multiresponse nonlinear models in the bibliography.

Exercises

3.1 Use the data from Appendix 4, Section A4.2 to fit the logistic model

$$f(x,\boldsymbol{\theta}) = \theta_1 + \frac{\theta_2}{1 + e^{-\theta_4(x-\theta_3)}}$$

(a) Plot the data versus $x = \log_{10}$ (NIF concentration). Note that you will have to make a decision about how to incorporate the zero concentration data. You may want to incorporate the actual NTD concentrations also.

(b) Give graphical interpretations of the parameters in the model, and use the plot to obtain starting values for each data set.

(c) Use the starting values in a nonlinear least squares routine to find the least squares estimates for the parameters for each data set.
(d) Use incremental parameters and indicator variables to fit all of the data sets together.
(e) Simplify the model by letting some of the parameters be common to all of the data sets. Use extra sum of squares analyses to determine a simple adequate model.
(f) Write a short report about this analysis and your findings.

3.2 Use the data from Appendix 1, Section A1.14 to determine an appropriate sum of exponentials model.
(a) Plot the data on semilog paper and use the plot to determine the number of exponential terms to fit to the data.
(b) Use curve peeling to determine starting estimates for the parameters.
(c) Use the starting estimates from part (b) to fit the postulated model from part (a).

3.3 (a) Use the plot from Problem 2.6 and sketch in the curve of steepest descent from the point $\boldsymbol{\theta}^0$. Hint: The direction of steepest descent is perpendicular to the contours.
(b) Is the direction of the Gauss–Newton increment close to the initial direction of steepest descent?
(c) Calculate and plot the Levenberg increment using a conditioning factor of $k=4$.
(d) Calculate and plot the Marquardt increment using a conditioning factor of $k=4$.
(e) Comment on the relative directions of the Gauss–Newton, Levenberg and Marquardt increment vectors.

3.4 Use the data from Appendix 4, Section A4.3 to determine an appropriate model and to estimate the parameters.
(a) Plot the concentration versus time on semilog paper, and use the plot to determine the number of exponential terms necessary to fit the data.
(b) Use the plot and the method of curve peeling to determine starting values for the parameters.
(c) Use a nonlinear estimation routine to estimate the parameters.

3.5 Use a nonlinear estimation routine and the data and model from Appendix 4, Section A4.4 to estimate the parameters. Take note of the number of iterations required and any difficulties you encounter in each attempt.
(a) Use any approach you think is appropriate to obtain starting values for the parameters in the model.
(b) Use your starting values in a nonlinear estimation routine to estimate the parameters. If you achieve convergence, examine the parameter approximate correlation matrix, and comment on the conditioning of the model.
(c) Reparametrize the model by centering the factor $1/x_3$, and use the equivalent starting values from part (a) to estimate the parameters. If you achieve convergence, examine the parameter approximate correla-

tion matrix, and comment on the conditioning of the model. What effect does this reparametrization have on the number of iterations to convergence?

(d) Reparametrize the model in part (a) using $\theta_1 = e^{\phi_1}$ and $\theta_2 = e^{\phi_2}$ and the equivalent starting values from part (a) to estimate the parameters. If you achieve convergence, examine the parameter approximate correlation matrix, and comment on the conditioning of the model. What effect does this reparametrization have on the number of iterations to convergence?

(e) Reparametrize the model in part (b) using the same parametrization as in part (c) and the equivalent starting values from part (a) to estimate the parameters. If you achieve convergence, examine the parameter approximate correlation matrix, and comment on the conditioning of the model. What effect does this reparametrization have on the number of iterations to convergence?

3.6 Use a nonlinear estimation routine and the data and model from Appendix 4, Section A4.5 to estimate the parameters. Take note of the number of iterations required and any difficulties you encounter in each attempt.

(a) Use any approach you think is appropriate to obtain starting values for the parameters in the model.

(b) Use your starting values in a nonlinear estimation routine to estimate the parameters. If you achieve convergence, examine the parameter approximate correlation matrix, and comment on the conditioning of the model.

(c) Reparametrize the model in part (a) using $\theta_2 e^{-\theta_3 x} = e^{-\phi_3(x-\phi_2)}$. If you achieve convergence, examine the parameter approximate correlation matrix, and comment on the conditioning of the model. What effect does this reparametrization have on the number of iterations to convergence?

3.7 (a) Show that the theoretical D-optimal starting design for the logistic model of Problem 3.1 consists of $\mathbf{x} = (-\infty, \theta_3 - 1.044/\theta_4, \theta_3 + 1.044/\theta_4, +\infty)^T$.

(b) Interpret the choice of the design points graphically by plotting the logistic function versus x and plotting the location of the design points on the x-axis.

(c) Plot the derivatives with respect to the parameters versus x and use these plots to help interpret the choice of the design points.

CHAPTER 4.

Multiresponse Parameter Estimation

"Better is the enemy of the good."

– Voltaire

In some experimental situations it is possible to measure more than one response for each case. In the analysis of such experiments, information from all the measured responses can be combined to provide more precise parameter estimation and to determine more realistic models. The information must be combined so as to reflect reasonable assumptions on the behavior of the disturbance terms in the measurements.

A determinant parameter estimation criterion for multiresponse data was derived by Box and Draper (1965) under the assumptions that the disturbance terms in different cases are uncorrelated but the disturbance terms for different responses in the same case have a fixed, unknown variance–covariance matrix. In this chapter, we discuss this criterion and present a generalization of the Gauss–Newton method to optimize it. We also describe a convergence criterion for this optimization method, and discuss modifications which should be made to the method when there are singularities in the data or residual matrix.

4.1 The Multiresponse Model

We assume there are M responses measured on each of N experimental runs and that the models for the M responses depend on a total of P parameters, $\boldsymbol{\theta}$, and write

$$Y_{nm} = f_m(\mathbf{x}_n, \boldsymbol{\theta}) + Z_{nm} \qquad n = 1, \ldots, N \quad m = 1, \ldots, M \tag{4.1}$$

where Y_{nm} is the random variable associated with the measured value of the mth response for the nth case, f_m is the model function for the mth response depending on some or all of the experimental settings $\mathbf{x}_n$ and on some or all of the

parameters $\boldsymbol{\theta}$, and Z_{nm} is the disturbance term.

Example: α-Pinene 2

Box et al. (1973) reported a multiresponse analysis of some α-pinene data originally analyzed by Fuguitt and Hawkins (1947). In the experiment, α-pinene, a component of turpentine, was purified and heated to produce by-products. Two sets of measurements were made, at temperatures of 189.5 and 204.5°C. In each experiment, the relative concentrations of α-pinene and three by-products were measured at each of eight times. The relative concentration of a fourth by-product was imputed from the other concentrations. In this example, there are $M = 5$ responses and $N = 8$ cases. The data for 189.5°C are listed in Appendix 1, Section A1.6, and plotted in Figure 4.1. ■

Example: s-PMMA 1

The behavior of the complex dielectric coefficient of a polymer can be used to help understand the molecular structure of the polymer. Physically, a disk of the polymer is inserted between the two metal electrodes of the dielectric cell which forms one arm of a four armed electrical bridge. The bridge is powered by an oscillating voltage whose frequency (f, in hertz) can be changed over a wide range (say 5 to 500 000 Hz), and bridge balance is achieved using capacitance and conductance standards. The com-

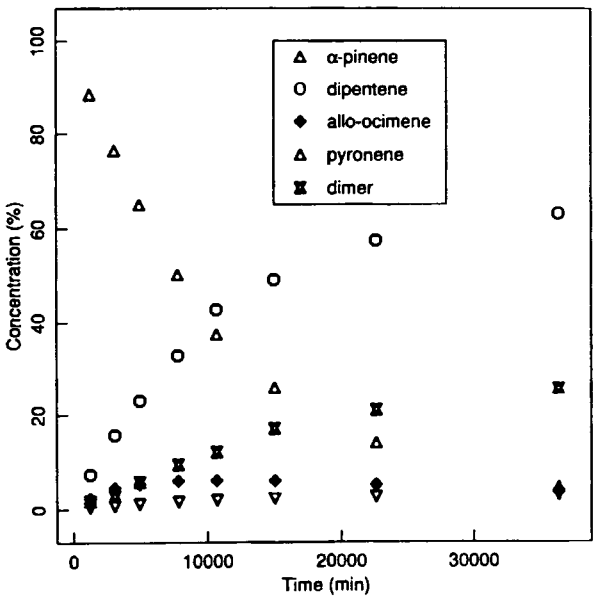

Figure 4.1 Plot of the concentrations of α-pinene and its by-products versus time at 189.5°C.

plex dielectric constant is then calculated using changes from the standards relative to the cell dielectric constant. Measurements are made by simultaneously adjusting the capacitance (real) and the conductance (imaginary) arms of the bridge when it is excited at a specific frequency and temperature.

The complex dielectric constant is written $\varepsilon^* = \varepsilon' - i\varepsilon''$, where ε' is the real component, ε'' is the imaginary component, and i denotes $\sqrt{-1}$. Havriliak and Negami (1967) analyzed the dielectric relaxation data for 21 polymers, and proposed a general model of the form

$$\varepsilon^* = \varepsilon_\infty + \frac{\varepsilon_0 - \varepsilon_\infty}{\left[1 + (i2\pi f/f_0)^\alpha\right]^\beta}.$$

In Figure 4.2*a* and *b* we plot the imaginary component y_{imag} and the real component y_{real}, versus frequency for syndiotactic poly(methylmethacrylate) (s-PMMA) at 86.7°F, and, as recommended in Cole and Cole (1941), in Figure 4.2*c* we plot these components in the complex plane. In this example, there are $M = 2$ responses, $N = 23$ cases, and $P = 5$ parameters. The data are listed in Appendix 1, Section A1.13. ■

As with uniresponse parameter estimation discussed in the previous chapters, in the analysis of experimental data we assume that the N experimental design variables $\mathbf{x}_n$, $n = 1, \ldots, N$, are fixed and known, so we can form the $N \times M$ observation matrix $\mathbf{Y}$ with (n,m)th element y_{nm} and the $N \times M$ expected response matrix $\mathbf{H}(\boldsymbol{\theta})$ with (n,m)th element $f_m(\mathbf{x}_n, \boldsymbol{\theta})$. From $\mathbf{Y}$ and $\mathbf{H}(\boldsymbol{\theta})$, we create the residual matrix

$$\mathbf{Z}(\boldsymbol{\theta}) = \mathbf{Y} - \mathbf{H}(\boldsymbol{\theta}) \tag{4.2}$$

The parameter estimates $\hat{\boldsymbol{\theta}}$ are given by the values of $\boldsymbol{\theta}$ which optimize some criterion based on $\mathbf{Z}(\boldsymbol{\theta})$ in the same way that the least squares estimates in uniresponse parameter estimation minimize $\|\mathbf{z}(\boldsymbol{\theta})\|^2$. The criterion will depend on assumptions about the disturbance. For example, if we make the stringent assumption that the Z_{nm} are normally distributed and independent with the same variance σ^2, then least squares is appropriate and we find $\hat{\boldsymbol{\theta}}$ which minimizes the sum of squared residuals of all NM responses. That is, the estimation criterion would be to minimize the *trace* of $\mathbf{Z}^T\mathbf{Z}$, $\text{tr}(\mathbf{Z}^T\mathbf{Z})$.

The assumptions leading to the trace criterion may not be realistic. It could be reasonable to assume that the variances of different measurements on the same response are constant, but not that the variances of different responses are equal. Furthermore, assuming independent disturbances for different measurements in the same experimental run may not be justified. For example, in chemical experiments where the concentrations of a number of different chemical species are measured from the same sample, if only the relative concentrations can be determined, different measurements on the same sample may be correlated. Similarly, for dielectric determinations, errors in the frequency set-

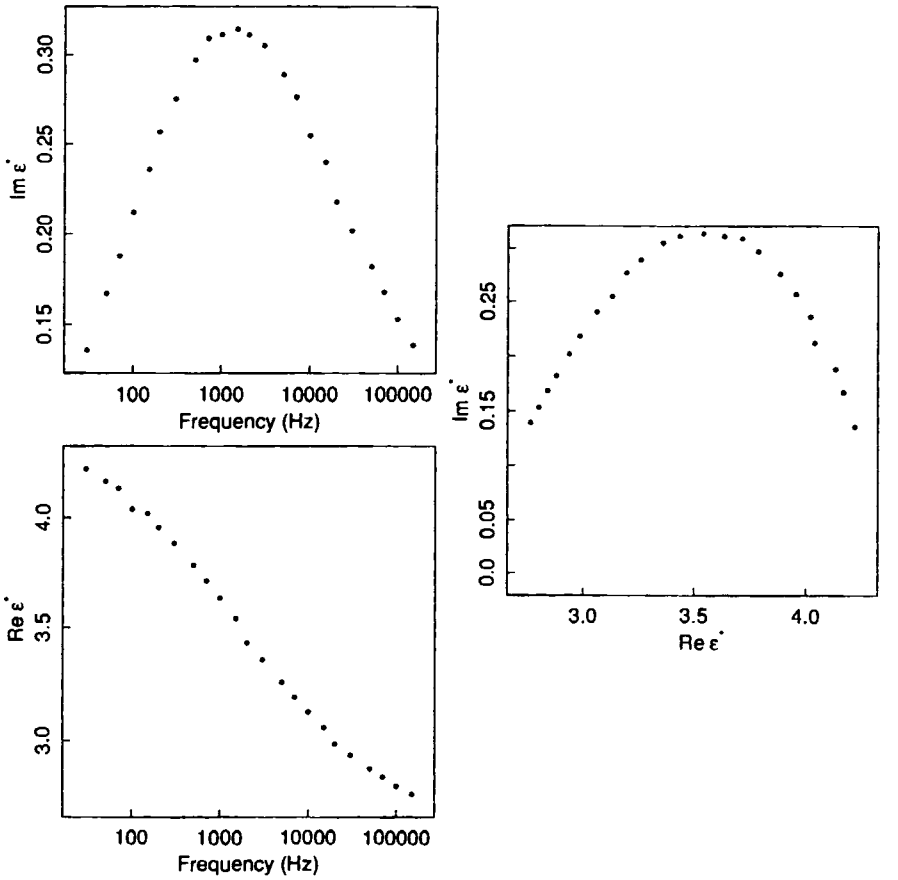

Figure 4.2 Plots of the real and imaginary components of the dielectric constant ε^* (dimensionless) versus frequency (on a logarithmic scale) and in the complex plane for the s-PMMA dielectric data.

tings can induce errors in both components.

Following Box and Draper (1965), the model used to describe the disturbance term is a normal distribution with

$$E[Z_{nm}] = 0$$

and

$$E[Z_{nm}Z_{ri}] = \begin{cases} \{\Sigma\}_{mi} & n = r \\ 0 & n \neq r \end{cases}$$

where Σ is a fixed $M \times M$ covariance matrix. That is, we assume that measurements from different experiments are independent but measurements from the

same experiment are correlated. The joint probability density function for the N observations, conditional on all the unknown parameters, is then

$$\begin{aligned} p(\mathbf{Y} \mid \boldsymbol{\theta}, \boldsymbol{\Sigma}) &\propto |\boldsymbol{\Sigma}|^{-N/2} \exp\left[-\frac{\operatorname{tr}[(\mathbf{Y}-\mathbf{H})\boldsymbol{\Sigma}^{-1}(\mathbf{Y}-\mathbf{H})^{\mathrm{T}}]}{2}\right] \\ &= |\boldsymbol{\Sigma}^{-1}|^{N/2} \exp\left[-\frac{\operatorname{tr}(\mathbf{Z}\boldsymbol{\Sigma}^{-1}\mathbf{Z}^{\mathrm{T}})}{2}\right] \end{aligned} \tag{4.3}$$

where the vertical bars denote a determinant.

4.1.1 The Determinant Criterion

A parameter estimation criterion under these assumptions can be derived using a likelihood or Bayesian argument. The loglikelihood function for the parameters $\boldsymbol{\theta}$ and $\boldsymbol{\Sigma}^{-1}$ is

$$L(\boldsymbol{\theta}, \boldsymbol{\Sigma}^{-1}) = k + \frac{N}{2}\ln|\boldsymbol{\Sigma}^{-1}| - \frac{\operatorname{tr}(\mathbf{Z}\boldsymbol{\Sigma}^{-1}\mathbf{Z}^{\mathrm{T}})}{2} \tag{4.4}$$

where k is an unimportant constant. To maximize the loglikelihood function we write the last term as $\operatorname{tr}(\mathbf{Z}^{\mathrm{T}}\mathbf{Z}\boldsymbol{\Sigma}^{-1})$ and differentiate the entire expression with respect to the elements σ^{mi} of $\boldsymbol{\Sigma}^{-1}$. Using the result (Bard, 1974, p. 296)

$$\frac{\partial \ln|\boldsymbol{\Sigma}^{-1}|}{\partial \sigma^{mi}} = \{\boldsymbol{\Sigma}\}_{mi} \tag{4.5}$$

allows us to write

$$\frac{\partial L(\boldsymbol{\theta}, \boldsymbol{\Sigma}^{-1})}{\partial \sigma^{mi}} = \frac{N}{2}\{\boldsymbol{\Sigma}\}_{mi} - \frac{1}{2}\{\mathbf{Z}^{\mathrm{T}}\mathbf{Z}\}_{mi}$$

Setting this derivative to zero provides the conditional estimates

$$\{\hat{\boldsymbol{\Sigma}}(\boldsymbol{\theta})\}_{mi} = \frac{\{\mathbf{Z}^{\mathrm{T}}\mathbf{Z}\}_{mi}}{N}$$

or

$$\hat{\boldsymbol{\Sigma}}(\boldsymbol{\theta}) = \frac{\mathbf{Z}^{\mathrm{T}}\mathbf{Z}}{N}$$

which, when substituted into (4.4), gives the conditional loglikelihood function

$$L(\boldsymbol{\theta}, \hat{\boldsymbol{\Sigma}}(\boldsymbol{\theta})) = k' - \frac{N}{2}\ln|\mathbf{Z}^{\mathrm{T}}\mathbf{Z}| \tag{4.6}$$

The maximum likelihood estimates are then obtained by minimizing $|\mathbf{Z}^{\mathrm{T}}\mathbf{Z}|$ with respect to $\boldsymbol{\theta}$.

A Bayesian argument was used by Box and Draper (1965) to derive the marginal posterior density for $\boldsymbol{\theta}$ by integrating over the unknown variances and

covariances after incorporating an noninformative prior of the form

$$p(\boldsymbol{\Sigma}, \boldsymbol{\theta}) \propto |\boldsymbol{\Sigma}|^{-(M+1)/2}$$

The marginal posterior density is then

$$p(\boldsymbol{\theta} \mid \mathbf{Y}) \propto |\mathbf{Z}^{\mathrm{T}}\mathbf{Z}|^{-N/2} \tag{4.7}$$

and so the posterior density is maximized when the determinant is minimized. Thus, the likelihood and Bayesian approaches lead to the same criterion.

As pointed out in Box and Tiao (1973), (4.6) and (4.7) are remarkably general results, since they do not depend on whether the expectation functions are linear or nonlinear, whether the parameters are common to more than one response, or whether the design variables are common to more than one response. Furthermore, a scale change on any of the responses will not affect the estimates, and linear combinations of the responses can be used in place of the original responses.

Geometrically, $|\mathbf{Z}^{\mathrm{T}}\mathbf{Z}|$ corresponds to the square of the volume of the M-dimensional parallelepiped spanned by the residual vectors, $\mathbf{z}_m$, $m = 1, \ldots, M$, in the N-dimensional case space. Minimizing the determinant corresponds to minimizing the volume enclosed by the residual vectors.

4.1.2 Inferences for Multiresponse Estimation

To draw inferences about parameters in multiresponse estimation, we use the Bayesian formulation and assume that $|\mathbf{Z}^{\mathrm{T}}\mathbf{Z}|$ can be adequately represented by a quadratic Taylor series near $\hat{\boldsymbol{\theta}}$ to give an approximate marginal posterior density function. From (4.7),

$$p(\boldsymbol{\theta} \mid \mathbf{Y}) \dot{\propto} \left[1 + (\boldsymbol{\theta} - \hat{\boldsymbol{\theta}})^{\mathrm{T}} \frac{\boldsymbol{\Omega}}{2|\hat{\mathbf{Z}}^{\mathrm{T}}\hat{\mathbf{Z}}|} (\boldsymbol{\theta} - \hat{\boldsymbol{\theta}}) \right]^{-N/2} \tag{4.8}$$

where $\boldsymbol{\Omega}$ is the Hessian of the determinant evaluated at $\hat{\boldsymbol{\theta}}$. This approximation has the form of a P-variate Student's T density with location parameter $\hat{\boldsymbol{\theta}}$, degrees of freedom $N - P$, scale factor

$$s^2 = |\hat{\mathbf{Z}}^{\mathrm{T}}\hat{\mathbf{Z}}|/(N - P) \tag{4.9}$$

and covariance matrix $2s^2\boldsymbol{\Omega}^{-1}$ (Box and Tiao, 1973). An approximate $1 - \alpha$ HPD region for the parameters is given by

$$(\boldsymbol{\theta} - \hat{\boldsymbol{\theta}})^{\mathrm{T}} \frac{\boldsymbol{\Omega}}{2} (\boldsymbol{\theta} - \hat{\boldsymbol{\theta}}) \leq P s^2 F(P, N - P; \alpha) \tag{4.10}$$

so that the square of the volume in the parameter space enclosed by the joint region is proportional to the determinant of the Hessian.

Because we are approximating $|\mathbf{Z}^{\mathrm{T}}\mathbf{Z}|$, the approximations (4.8) and (4.10) may be very poor: additional research needs to be done to assess the adequacy of these approximations even for cases where the model functions are

linear. More accurate HPD regions can be written as either

$$\frac{(|\mathbf{Z}^{\mathrm{T}}\mathbf{Z}| - |\hat{\mathbf{Z}}^{\mathrm{T}}\hat{\mathbf{Z}}|)/P}{s^2} < F(P, N-P; \alpha) \tag{4.11}$$

or

$$\ln[p(\hat{\boldsymbol{\theta}} \mid \mathbf{Y})] - \ln[p(\boldsymbol{\theta} \mid \mathbf{Y})] < \frac{1}{2}\chi^2(P;\alpha) \tag{4.12}$$

(Box and Tiao, 1973), where $\chi^2(P;\alpha)$ is the upper α percentile of the χ^2 distribution with P degrees of freedom. Such regions would have to be determined numerically and displayed in contour plots, and therefore suffer from the disadvantages inherent in exact confidence and likelihood regions for uniresponse models, as discussed in Chapter 6. Nevertheless, the methods of Chapter 6 (profile t and profile trace plots) can be used for multiresponse problems.

An approximate $1-\alpha$ HPD interval for the parameter θ_p is given by

$$\hat{\theta}_p \pm t(N-P;\alpha/2)\, s\sqrt{2\{\boldsymbol{\Omega}^{-1}\}_{pp}} \tag{4.13}$$

and an approximate $1-\alpha$ HPD band for the mth expectation function $f_m(\mathbf{x},\boldsymbol{\theta})$ is

$$f_m(\mathbf{x},\hat{\boldsymbol{\theta}}) \pm s\sqrt{2\,\mathbf{v}_m^{\mathrm{T}}\boldsymbol{\Omega}^{-1}\mathbf{v}_m}\,\sqrt{P\,F(P, N-P;\alpha)}$$

where $\mathbf{v}_m$ is the gradient of f_m with respect to $\boldsymbol{\theta}$ evaluated at $\mathbf{x}$ and $\hat{\boldsymbol{\theta}}$.

4.1.3 Dimensional Considerations in Multiresponse Estimation

Note that the determinant criterion implies two important constraints on the number of observations, N, the number of responses, M, and the number of parameters, P.

First, M can not exceed N, since otherwise the determinant is identically zero. To see this, note that the rank of the $N\times M$ matrix $\mathbf{Z}$ cannot exceed the minimum of (N,M), and when $N<M$ the rank of the $M\times M$ matrix $\mathbf{Z}^{\mathrm{T}}\mathbf{Z}$ is less than M and hence the determinant is identically zero. Another way of seeing this is to recall from the geometric interpretation that $|\mathbf{Z}^{\mathrm{T}}\mathbf{Z}|$ gives the square of the volume, in the N-dimensional case space, enclosed by the residual vectors (columns of $\mathbf{Z}$). If the case dimension N does not at least equal the response dimension M, then the volume is zero. For example, the volume of a rectangle is zero.

Second, in general P must be less than N, since otherwise the criterion can be made zero by fitting any one response perfectly, or even by fitting a linear combination of the responses perfectly. That is, if there is an M-vector $\mathbf{v}$ such that $\mathbf{Z}(\boldsymbol{\theta})\mathbf{v} = \mathbf{0}$ for some $\boldsymbol{\theta}$, then the determinant will be zero at that value of $\boldsymbol{\theta}$ regardless of how well the remaining responses have been fitted.

The reasoning leading to the constraint $N>P$ provides justification for the use of $N-P$ for the residual degrees of freedom proposed above. It would seem that with NM data values there should be $NM-P$ degrees of freedom for

the residuals, as suggested in Bard (1974), but in fact, near the optimum the value of the determinant is controlled by the linear combination of responses corresponding to the smallest singular value of $\mathbf{Z}$, and this vector has dimension N. The vector corresponding to this singular value therefore has $N-P$ degrees of freedom.

In summary, the number of cases, N, should exceed the maximum of M and P to ensure a successful analysis.

A great advantage in using multiresponse data is the increased precision of parameter estimates relative to those obtained from uniresponse data. However, we cannot attribute this increased precision to additional denominator degrees of freedom when multiple responses are used. The increased precision is due to the combination of different types of information from the responses.

One difficulty with the use of multiresponse data is that all problems become nonlinear optimization problems. That is, even if the expectation functions are linear in the parameters, iterative methods must be used to obtain the estimates which minimize the determinant criterion. The problem of obtaining the best estimates is also more difficult than in the uniresponse nonlinear case, since the Hessian need not be positive definite. Further discussion on these aspects of optimizing the determinant is given in Section 4.2.3.

Another difficulty with multiresponse estimation is that inference regions for the parameters based on (4.10) or (4.13) are only approximate, even when all the expectation functions are linear in the parameters. The accuracy of these approximations is questionable. On the other hand, inference regions from multiresponse estimation are usually much smaller than those from uniresponse estimation, and so approximate multiresponse regions may in fact be better than approximate uniresponse regions for nonlinear models.

In spite of the difficulties, multiresponse estimation is a valuable technique and should be used whenever multiresponse data are available. The reduction in size of the parameter inference regions, together with the extra ability to discriminate between rival models, is well worth any additional effort required.

4.2 A Generalized Gauss–Newton Method

One advantage of least squares as a criterion is that specialized methods can be used to exploit properties of the criterion and to provide standard optimization algorithms. In this section, we describe a Gauss–Newton method for minimizing the determinant criterion.

To evaluate the determinant, following Bates and Watts (1987), we take a QR decomposition of $\mathbf{Z}(\boldsymbol{\theta})$,

$$\mathbf{Z}(\boldsymbol{\theta}) = \mathbf{QR} = \mathbf{Q}_1\mathbf{R}_1$$

Then, since

$$
\begin{aligned}
|\mathbf{Z}(\boldsymbol{\theta})^{\mathrm{T}}\mathbf{Z}(\boldsymbol{\theta})| &= |\mathbf{R}_1^{\mathrm{T}}\mathbf{R}_1| \\
&= |\mathbf{R}_1|^2 \\
&= \prod_{m=1}^{M} \{\mathbf{R}_1\}_{mm}^2
\end{aligned}
$$

we have an easy way to evaluate the determinant criterion for any $\boldsymbol{\theta}$.

4.2.1 The Gradient and Hessian of the Determinant

The decomposition of $\mathbf{Z}(\boldsymbol{\theta})$ as $\mathbf{Q}_1\mathbf{R}_1$ is also helpful in evaluating the gradient and Hessian of the determinant criterion. To simplify notation we omit the dependence on $\boldsymbol{\theta}$ and use a subscript enclosed in parentheses to denote differentiation, as

$$
\frac{\partial \mathbf{Z}}{\partial \theta_p} = \mathbf{Z}_{(p)}
$$

Using the result (1.1.34) from Fedorov (1972), we have

$$
\frac{\partial |\mathbf{Z}^{\mathrm{T}}\mathbf{Z}|}{\partial \theta_p} = |\mathbf{Z}^{\mathrm{T}}\mathbf{Z}| \operatorname{tr}\left[(\mathbf{Z}^{\mathrm{T}}\mathbf{Z})^{-1}\frac{\partial(\mathbf{Z}^{\mathrm{T}}\mathbf{Z})}{\partial \theta_p}\right] \tag{4.14}
$$

with

$$
\frac{\partial(\mathbf{Z}^{\mathrm{T}}\mathbf{Z})}{\partial \theta_p} = \mathbf{Z}^{\mathrm{T}}\mathbf{Z}_{(p)} + \mathbf{Z}_{(p)}^{\mathrm{T}}\mathbf{Z} \tag{4.15}
$$

so the gradient $\boldsymbol{\omega} = \partial|\mathbf{Z}^{\mathrm{T}}\mathbf{Z}|/\partial\boldsymbol{\theta}^{\mathrm{T}}$ has components

$$
\begin{aligned}
\{\boldsymbol{\omega}\}_p &= 2|\mathbf{Z}^{\mathrm{T}}\mathbf{Z}| \operatorname{tr}[(\mathbf{Z}^{\mathrm{T}}\mathbf{Z})^{-1}\mathbf{Z}^{\mathrm{T}}\mathbf{Z}_{(p)}] \\
&= 2|\mathbf{Z}^{\mathrm{T}}\mathbf{Z}| \operatorname{tr}[\mathbf{R}_1^{-1}\mathbf{R}_1^{-\mathrm{T}}\mathbf{R}_1^{\mathrm{T}}\mathbf{Q}_1^{\mathrm{T}}\mathbf{Z}_{(p)}] \\
&= 2|\mathbf{Z}^{\mathrm{T}}\mathbf{Z}| \operatorname{tr}[\mathbf{R}_1^{-1}\mathbf{Q}_1^{\mathrm{T}}\mathbf{Z}_{(p)}] \\
&= 2|\mathbf{Z}^{\mathrm{T}}\mathbf{Z}| \operatorname{tr}[\mathbf{Z}^{+}\mathbf{Z}_{(p)}]
\end{aligned} \tag{4.16}
$$

where $\mathbf{Z}^{+} = \mathbf{R}_1^{-1}\mathbf{Q}_1^{\mathrm{T}}$ is the pseudoinverse of $\mathbf{Z}$.

To obtain the second derivative or Hessian terms, we write

$$
g = \ln|\mathbf{Z}^{\mathrm{T}}\mathbf{Z}|
$$

so that

$$
|\mathbf{Z}^{\mathrm{T}}\mathbf{Z}| = e^{g} \tag{4.17}
$$

and

$$
g_{(p)} = 2 \operatorname{tr}[\mathbf{Z}^{+}\mathbf{Z}_{(p)}] \tag{4.18}
$$

and then use the expressions for the derivative of the pseudoinverse (Golub and Pereyra, 1973) to obtain

$$g_{(pq)} = 2\{-\mathrm{tr}[\mathbf{Z}^+\mathbf{Z}_{(p)}\mathbf{Z}^+\mathbf{Z}_{(q)}] + \mathrm{tr}[\mathbf{Z}^+(\mathbf{Z}^+)^{\mathrm{T}}\mathbf{Z}_{(p)}^{\mathrm{T}}(\mathbf{I}-\mathbf{Z}\mathbf{Z}^+)\mathbf{Z}_{(q)}] + \mathrm{tr}[\mathbf{Z}^+\mathbf{Z}_{(pq)}]\} \tag{4.19}$$

From (4.17), a second derivative term for $|\mathbf{Z}^{\mathrm{T}}\mathbf{Z}|$ is then

$$\frac{\partial^2 |\mathbf{Z}^{\mathrm{T}}\mathbf{Z}|}{\partial\theta_p\partial\theta_q} = |\mathbf{Z}^{\mathrm{T}}\mathbf{Z}|[g_{(p)}g_{(q)} + g_{(pq)}] \tag{4.20}$$

Alternative expressions for the gradient and Hessian of $|\mathbf{Z}^{\mathrm{T}}\mathbf{Z}|$ are obtained by expanding (4.16) as

$$\begin{aligned}\{\boldsymbol{\omega}\}_p &= |\mathbf{Z}^{\mathrm{T}}\mathbf{Z}|\,\mathrm{tr}[(\mathbf{Z}^{\mathrm{T}}\mathbf{Z})^{-1}(\mathbf{Z}^{\mathrm{T}}\mathbf{Z}_{(p)} + \mathbf{Z}_{(p)}^{\mathrm{T}}\mathbf{Z})] \\ &= |\mathbf{Z}^{\mathrm{T}}\mathbf{Z}|\,\mathrm{tr}[\mathbf{U}_p]\end{aligned} \tag{4.21}$$

where $\mathbf{U}_p = (\mathbf{Z}^{\mathrm{T}}\mathbf{Z})^{-1}(\mathbf{Z}^{\mathrm{T}}\mathbf{Z}_{(p)} + \mathbf{Z}_{(p)}^{\mathrm{T}}\mathbf{Z})$. Differentiating (4.21) with respect to θ_q gives

$$\begin{aligned}\frac{\partial^2 |\mathbf{Z}^{\mathrm{T}}\mathbf{Z}|}{\partial\theta_q\partial\theta_p} &= \{\boldsymbol{\omega}\}_q\mathrm{tr}[\mathbf{U}_p] + |\mathbf{Z}^{\mathrm{T}}\mathbf{Z}|\{-\mathrm{tr}[\mathbf{U}_q\mathbf{U}_p] + \mathrm{tr}[(\mathbf{Z}^{\mathrm{T}}\mathbf{Z})^{-1}(\mathbf{Z}_{(q)}^{\mathrm{T}}\mathbf{Z}_{(p)} + \mathbf{Z}_{(p)}^{\mathrm{T}}\mathbf{Z}_{(q)})] \\ &\quad + \mathrm{tr}[(\mathbf{Z}^{\mathrm{T}}\mathbf{Z})^{-1}(\mathbf{Z}^{\mathrm{T}}\mathbf{Z}_{(pq)} + \mathbf{Z}_{(pq)}^{\mathrm{T}}\mathbf{Z})]\} \\ &= |\mathbf{Z}^{\mathrm{T}}\mathbf{Z}|\{\mathrm{tr}[\mathbf{U}_q]\mathrm{tr}[\mathbf{U}_p] - \mathrm{tr}[\mathbf{U}_q\mathbf{U}_p] + \mathrm{tr}[(\mathbf{Z}^{\mathrm{T}}\mathbf{Z})^{-1}(\mathbf{Z}_{(q)}^{\mathrm{T}}\mathbf{Z}_{(p)} + \mathbf{Z}_{(p)}^{\mathrm{T}}\mathbf{Z}_{(q)})] \\ &\quad + \mathrm{tr}[(\mathbf{Z}^{\mathrm{T}}\mathbf{Z})^{-1}(\mathbf{Z}^{\mathrm{T}}\mathbf{Z}_{(pq)} + \mathbf{Z}_{(pq)}^{\mathrm{T}}\mathbf{Z})]\}\end{aligned} \tag{4.22}$$

4.2.2 An Approximate Hessian

The last term in the expression for $g_{(pq)}$ requires second derivatives of the model functions. We prefer to avoid calculating second derivatives, especially since the Hessian matrix is being used primarily to determine an increment, and so we make the same assumption as in the Gauss–Newton method for nonlinear least squares. That is, we assume that the model functions can be locally approximated by linear functions and set $\mathbf{Z}_{(pq)}$ to zero. The *approximate Hessian* matrix $\boldsymbol{\Omega}$ is therefore calculated with entries

$$\begin{aligned}\{\boldsymbol{\Omega}\}_{pq} &= 4|\mathbf{Z}^{\mathrm{T}}\mathbf{Z}|\,\mathrm{tr}[\mathbf{Z}^+\mathbf{Z}_{(p)}]\,\mathrm{tr}[\mathbf{Z}^+\mathbf{Z}_{(q)}] \\ &\quad + 2|\mathbf{Z}^{\mathrm{T}}\mathbf{Z}|\{-\mathrm{tr}[\mathbf{Z}^+\mathbf{Z}_{(p)}\mathbf{Z}^+\mathbf{Z}_{(q)}] + \mathrm{tr}[\mathbf{Z}^+(\mathbf{Z}^+)^{\mathrm{T}}\mathbf{Z}_{(p)}^{\mathrm{T}}(\mathbf{I}-\mathbf{Z}\mathbf{Z}^+)\mathbf{Z}_{(q)}]\}\end{aligned} \tag{4.23}$$

These can be collected into $\boldsymbol{\Omega}$ and used with the gradient vector $\boldsymbol{\omega}$ to form the increment $\boldsymbol{\delta} = -\boldsymbol{\Omega}^{-1}\boldsymbol{\omega}$ in a Newton–Raphson iterative scheme to optimize $|\mathbf{Z}^{\mathrm{T}}\mathbf{Z}|$. Since only first derivatives of the model functions are used, this is a generalization of the Gauss–Newton method for nonlinear least squares.

Some rearrangement of the terms in (4.16) and (4.19) can be used to simplify the calculations of $\boldsymbol{\omega}$ and $\boldsymbol{\Omega}$ (Bates and Watts, 1984). In particular, we can use the relationship $\mathrm{tr}(\mathbf{AB}) = \mathrm{tr}(\mathbf{BA})$ to change (4.16) to

$$\begin{aligned}\{\boldsymbol{\omega}\}_p &= 2|\mathbf{Z}^{\mathrm{T}}\mathbf{Z}|\ \mathrm{tr}[\mathbf{Q}_1^{\mathrm{T}}\mathbf{Z}_{(p)}\mathbf{R}_1^{-1}] \\ &= 2|\mathbf{Z}^{\mathrm{T}}\mathbf{Z}| \sum_{m=1}^{M} g_{p,mm}\end{aligned}$$

where $g_{p,mm}$ is the (m,m)th element of the $N\times M$ matrix

$$\mathbf{G}_p = \mathbf{Q}^{\mathrm{T}}\mathbf{Z}_{(p)}\mathbf{R}_1^{-1} \tag{4.24}$$

This does not change the gradient calculation substantially, but now (4.23) can be rewritten to give

$$\begin{aligned}\{\boldsymbol{\Omega}\}_{pq} &= 4|\mathbf{Z}^{\mathrm{T}}\mathbf{Z}| \sum_{m=1}^{M} g_{p,mm} \sum_{m=1}^{M} g_{q,mm} \\ &\quad + 2|\mathbf{Z}^{\mathrm{T}}\mathbf{Z}|\{-\mathrm{tr}[\mathbf{Q}_1^{\mathrm{T}}\mathbf{Z}_{(p)}\mathbf{R}_1^{-1}\mathbf{Q}_1^{\mathrm{T}}\mathbf{Z}_{(q)}\mathbf{R}_1^{-1}] \\ &\qquad + \mathrm{tr}[\mathbf{R}_1^{-1}\mathbf{Q}_1^{\mathrm{T}}\mathbf{Q}_1\mathbf{R}_1^{-\mathrm{T}}\mathbf{Z}_{(p)}^{\mathrm{T}}\mathbf{Q}_2\mathbf{Q}_2^{\mathrm{T}}\mathbf{Z}_{(q)}]\} \\ &= 4|\mathbf{Z}^{\mathrm{T}}\mathbf{Z}| \sum_{m=1}^{M} g_{p,mm} \sum_{m=1}^{M} g_{q,mm} \\ &\quad + 2|\mathbf{Z}^{\mathrm{T}}\mathbf{Z}|\left[-\sum_{m=1}^{M}\sum_{i=1}^{M} g_{p,mi}g_{q,im} + \mathrm{tr}[(\mathbf{Q}_2^{\mathrm{T}}\mathbf{Z}_{(p)}\mathbf{R}_1^{-1})^{\mathrm{T}}(\mathbf{Q}_2^{\mathrm{T}}\mathbf{Z}_{(q)}\mathbf{R}_1^{-1})]\right] \\ &= 4|\mathbf{Z}^{\mathrm{T}}\mathbf{Z}| \sum_{m=1}^{M} g_{p,mm} \sum_{m=1}^{M} g_{q,mm} \\ &\quad + 2|\mathbf{Z}^{\mathrm{T}}\mathbf{Z}|\left[-\sum_{m=1}^{M}\sum_{i=1}^{M} g_{p,mi}g_{q,im} + \sum_{m=M+1}^{N}\sum_{i=1}^{M} g_{p,mi}g_{q,mi}\right]\end{aligned} \tag{4.25}$$

Equation (4.25) permits very efficient evaluation of $\boldsymbol{\Omega}$, because once the QR decomposition of $\mathbf{Z}$ is done and the matrices $\mathbf{G}_p$, $p = 1, \ldots, P$, are formed, it is only necessary to collect a few inner products. As discussed in Appendix 2, although $\mathbf{Q}^{\mathrm{T}}$ occurs as a factor in (4.24), the matrix $\mathbf{Q}$ is not explicitly formed; instead, a product such as $\mathbf{Q}^{\mathrm{T}}\mathbf{Z}_{(p)}$ is formed by applying Householder transformations to $\mathbf{Z}_{(p)}$.

4.2.3 Calculations for Each Iteration

At each iteration, the current value of the parameter vector, $\boldsymbol{\theta}^0$, is used to evaluate $|\mathbf{Z}^{\mathrm{T}}\mathbf{Z}|$, the gradient $\boldsymbol{\omega}$, and the approximate Hessian $\boldsymbol{\Omega}$. If $\boldsymbol{\Omega}$ is positive definite, the increment is calculated by solving

$$\boldsymbol{\Omega}\boldsymbol{\delta}^0 = -\boldsymbol{\omega} \tag{4.26}$$

for $\boldsymbol{\delta}^0$ and setting

$$\boldsymbol{\theta}^1 = \boldsymbol{\theta}^0 + \lambda\boldsymbol{\delta}^0$$

where λ is a step size factor chosen to ensure that $|\mathbf{Z}(\boldsymbol{\theta}^1)^T\mathbf{Z}(\boldsymbol{\theta}^1)| < |\mathbf{Z}(\boldsymbol{\theta}^0)^T\mathbf{Z}(\boldsymbol{\theta}^0)|$. The solution to (4.26) is accomplished most efficiently by taking a Cholesky decomposition of $\boldsymbol{\Omega}$ (Dongarra et al., 1979, Chapter 8) as

$$\boldsymbol{\Omega} = \mathbf{C}^T\mathbf{C} \tag{4.27}$$

where $\mathbf{C}$ is $P \times P$ and upper triangular.

Unlike the Gauss–Newton method for nonlinear least squares, the generalized Gauss–Newton method for multiresponse data need not result in a positive definite $\boldsymbol{\Omega}$. One of the situations in which negative eigenvalues of the Hessian can occur is when there are multiple minima for the determinant criterion, such as in the case study of Section 5.5.

When $\boldsymbol{\Omega}$ is not positive definite, the quadratic approximation to $|\mathbf{Z}^T\mathbf{Z}|$ does not have a minimum and $\mathbf{C}$ cannot be calculated. As in Section 3.5, we restore positive definiteness to the Hessian by inflating the diagonal and modifying the increment to be the solution of

$$(\boldsymbol{\Omega} + k\mathbf{I})\boldsymbol{\delta}^0 = -\boldsymbol{\omega}$$

where k is large enough to make $\boldsymbol{\Omega} + k\mathbf{I}$ positive definite. Such a k can be calculated by determining the eigenvalues of $\boldsymbol{\Omega}$ and setting k to twice the magnitude of the most negative eigenvalue, or by using a modified Cholesky decomposition (Dennis and Schnabel, 1983).

4.2.4 A Multiresponse Convergence Criterion

To decide whether we have convergence at a particular parameter vector $\boldsymbol{\theta}^0$, we reason as in Section 2.2.3 and compare the magnitude of the increment at that point with the statistical variability in the estimates. The statistical variability is accounted for in the elliptical regions of (4.10), and so we take a linear transformation of the parameters to make the regions spherical. With such a transformation, the length of the increment from $\boldsymbol{\theta}^0$ is simply $\|\mathbf{C}\boldsymbol{\delta}\|$, where $\mathbf{C}$ is the Cholesky factor from (4.27), and the region is simply a disk with radius proportional to $s\sqrt{P\,F(P, N-P; \alpha)}$. The convergence criterion is then (Bates and Watts, 1987)

$$\frac{\|\mathbf{C}\boldsymbol{\delta}\|^2/P}{2s^2} < \varepsilon^2$$

where ε is the tolerance level and s^2 is the scale factor (4.9). When the criterion is small, it indicates that the requested increment is negligible relative to the statistical variability. The value of ε can be set at 0.001, reasoning as in Section

2.2.3.

Pseudocode for multiresponse parameter estimation is presented in Appendix 3, Section A3.3.

4.3 Practical Considerations

As in uniresponse estimation, care should be taken in selecting the model and obtaining starting estimates for the parameters. After convergence, residuals for all the responses should be examined using plots as described in Chapter 3. However, multiresponse modeling involves additional practical considerations, as discussed below.

4.3.1 Obtaining Starting Values

The techniques for obtaining starting estimates for uniresponse models described in Chapter 3 can be used for multiresponse models by applying the procedures to each response and then combining the estimates to give starting values for the complete parameter vector. Graphical analyses can be especially helpful, as illustrated in the following example.

Example: s-PMMA 2

Starting estimates for the parameters in the expectation function for the complex dielectric coefficient can be obtained from graphical considerations, following Havriliak and Negami (1967). They showed that the real and imaginary components can be written

$$\varepsilon' = \varepsilon_\infty + (\varepsilon_0 - \varepsilon_\infty)R^{-\beta}\cos\beta\phi$$

$$\varepsilon'' = (\varepsilon_0 - \varepsilon_\infty)R^{-\beta}\sin\beta\phi$$

where

$$R^2 = \left[1 + (2\pi f/f_0)^\alpha \cos(\pi\alpha/2)\right]^2 + \left[(2\pi f/f_0)^\alpha \sin(\pi\alpha/2)\right]^2$$

and

$$\phi = \arctan\left[\frac{(2\pi f/f_0)^\alpha \sin(\pi\alpha/2)}{1 + (2\pi f/f_0)^\alpha \cos(\pi\alpha/2)}\right]$$

The parameters ε_0 and ε_∞ are the limiting low and high frequency intercepts of the locus with the real axis, when the function is plotted in the complex plane. Furthermore, the limiting angle the high frequency locus makes with the real axis is $\psi_L = \pi\alpha\beta/2$, and the angle bisector of ψ_L from $(\varepsilon_\infty, 0)$ intersects the locus at the frequency $\tilde{f}$ for which $2\pi\tilde{f}/f_0 = 1$. And finally, α is related to ψ_L through

$$\psi_L = -\pi\alpha \frac{\ln\left[\dfrac{\tilde{R}}{\varepsilon_0 - \varepsilon_\infty}\right]}{\ln\left[2 + 2\cos(\pi\alpha/2)\right]}$$

where $\tilde{R}$ is the length of the line from $(\varepsilon_\infty, 0)$ to $\varepsilon^*(\tilde{f})$.

To obtain starting values for the s-PMMA data, we plotted the data in the complex plane, as in Figure 4.2*c*, but this time we made the scales of the real and imaginary parts equal so that angles and distances would be correct. We extrapolated the right hand portion of the curve to the real axis to give the starting value $\varepsilon_0^0 = 4.40$, and extrapolated the left hand portion to the real axis to give the starting value $\varepsilon_\infty^0 = 2.36$. Next, we measured the angle of the left hand extrapolation line to the real axis to give the limiting angle estimate $\psi_L = 19°$. The bisector of this angle intercepts the data between the points corresponding to 200 and 300 Hz, so we took the value of $(\ln f_0)^0 = \ln[2\pi(250)] = 7.36$. The length $\tilde{R}$ was measured to be 1.6, and using this value together with that of the limiting angle, we solved for $\alpha^0 = 0.53$ and, finally, $\beta^0 = 0.40$. ■

4.3.1.1 Starting Estimates for Multiresponse Models Described by Systems of Linear Differential Equations

For multiresponse models described by systems of differential equations, such as in Example α-Pinene 1 or α-Pinene 2, one can exploit the relation between the rates and the responses to develop a simple procedure for determining starting values (Bates and Watts, 1985; Varah, 1982). The general approach is to derive estimates for the rates and then solve the simpler linear or nonlinear set of equations rather than using numerical integration to solve the differential equations. In Varah (1982), cubic spline fits were made to the data and rates were obtained by differentiating the spline fits. A cruder approach is to use simple differences to obtain rate estimates, as was used in Example Ethyl acrylate 2, and illustrated below for multiresponse data.

Example: α-Pinene 3

A linear kinetic model was proposed in Box et al. (1973) for the α-pinene data, of the form

$$\frac{d\gamma_1}{dt} = -(\theta_1 + \theta_2)\gamma_1$$

$$\frac{d\gamma_2}{dt} = \theta_1\gamma_1$$

$$\frac{d\gamma_3}{dt} = \theta_2\gamma_1 - (\theta_3 + \theta_4)\gamma_3 + \theta_5\gamma_5$$

$$\frac{d\gamma_4}{dt} = \theta_3\gamma_3$$

$$\frac{d\gamma_5}{dt} = \theta_4\gamma_3 - \theta_5\gamma_5$$

The explicit solution to this set of linear differential equations was given in Box et al. (1973), and involves long complicated expressions.

An alternative form is the matrix equation

$$\begin{bmatrix} \dot{\gamma}_1 \\ \dot{\gamma}_2 \\ \dot{\gamma}_3 \\ \dot{\gamma}_4 \\ \dot{\gamma}_5 \end{bmatrix} = \begin{bmatrix} -\theta_1-\theta_2 & 0 & 0 & 0 & 0 \\ \theta_1 & 0 & 0 & 0 & 0 \\ \theta_2 & 0 & -\theta_3-\theta_4 & 0 & \theta_5 \\ 0 & 0 & \theta_3 & 0 & 0 \\ 0 & 0 & \theta_4 & 0 & -\theta_5 \end{bmatrix} \begin{bmatrix} \gamma_1 \\ \gamma_2 \\ \gamma_3 \\ \gamma_4 \\ \gamma_5 \end{bmatrix}$$

or

$$\dot{\boldsymbol{\gamma}} = \mathbf{A}\boldsymbol{\gamma}$$

where $\mathbf{A}$ is the system transfer matrix, and a dot denotes differentiation with respect to time. Further discussion of linear differential equation models is given in Chapter 5.

To derive an expression useful for obtaining starting values, we rewrite the matrix equation as

$$\begin{bmatrix} \dot{\gamma}_1 \\ \dot{\gamma}_2 \\ \dot{\gamma}_3 \\ \dot{\gamma}_4 \\ \dot{\gamma}_5 \end{bmatrix} = \begin{bmatrix} -\theta_1\gamma_1-\theta_2\gamma_1 \\ \theta_1\gamma_1 \\ \theta_2\gamma_1-\theta_3\gamma_3-\theta_4\gamma_3+\theta_5\gamma_5 \\ \theta_3\gamma_3 \\ \theta_4\gamma_3-\theta_5\gamma_5 \end{bmatrix} = \mathbf{X}(t)\boldsymbol{\theta}$$

where

$$\mathbf{X}(t) = \begin{bmatrix} -\gamma_1 & -\gamma_1 & 0 & 0 & 0 \\ \gamma_1 & 0 & 0 & 0 & 0 \\ 0 & \gamma_1 & -\gamma_3 & -\gamma_3 & \gamma_5 \\ 0 & 0 & \gamma_3 & 0 & 0 \\ 0 & 0 & 0 & \gamma_3 & -\gamma_5 \end{bmatrix}$$

At any time t, therefore, if we have estimates for the rates and the concentrations, we could estimate $\boldsymbol{\theta}$ by linear regression of $\dot{\boldsymbol{\gamma}}$ on $\mathbf{X}$. Collecting the estimated rates for each time into a vector gives the "response" vector for the linear regression. Similarly, we calculate $\mathbf{X}(t)$ matrices for each time, using the average concentrations, and stack them to form the $\mathbf{X}$

matrix.

For example, the estimated rates at $t = 1230$ are

$$(-9.47, 5.93, 1.87, 0.33, 1.43)^{\mathrm{T}} \times 10^{-3}$$

and the average concentrations, inserted into the appropriate matrix, are

$$\begin{bmatrix} -94.2 & -94.2 & 0 & 0 & 0 \\ 94.2 & 0 & 0 & 0 & 0 \\ 0 & 94.2 & -1.15 & -1.15 & 0.88 \\ 0 & 0 & 1.15 & 0 & 0 \\ 0 & 0 & 0 & 1.15 & -0.88 \end{bmatrix}$$

Finally, we stack the vectors from each time to form a single vector, stack the matrices to form a single matrix, and then perform a simple linear regression with no intercept term to get the starting estimates. The starting values so obtained are

$$\boldsymbol{\theta}^0 = (5.84, 2.65, 1.63, 27.77, 4.61)^{\mathrm{T}} \times 10^{-5}$$

Because the parameters are rate constants, which are necessarily positive, we fit the model in the parameters $\phi_p = \ln \theta_p$ (see Section 3.4.1). ■

When some of the responses are not measured, it is still possible to use approximate rates provided other information, such as a mass balance, is substituted. In addition to providing starting values, the approximate rate method provides useful information on the estimation situation, and can even be used for parameter estimation (Varah, 1982), although, when estimating parameters, one should ensure that the implicit assumptions on the distribution of the noise terms are reasonable.

4.3.2 Assessing the Fit

As in any statistical analysis, it is extremely important to assess the fit. Generally, the best type of assessment involves plotting the residuals for all responses versus the design variables, versus each other, and versus the fitted responses, plus overlay plots of the data and the fitted responses. These plots are especially important in that they can reveal whether the program has converged to a spurious optimum due to dependencies in the data or in the residuals.

Example: s-PMMA 3

Convergence output for the s-PMMA data is given in Table 4.1. The residuals for the real and imaginary components are plotted versus frequency in Figure 4.3. The imaginary residuals are quite well behaved, but the real residuals are grouped and have a strong trend with frequency.

As discussed in Havriliak and Watts (1987), this behavior can be explained by considering the way in which the frequencies are set in an ex-

Table 4.1 Parameter summary for the s-PMMA data.

Parameter	Estimate	Approx. Std.Error	Approximate Correlation Matrix				
ε_0	4.320	0.011	1.00				
ε_∞	2.522	0.018	0.75	1.00			
$\ln f_0$	7.956	0.084	0.46	0.74	1.00		
α	0.531	0.010	−0.57	−0.71	−0.93	1.00	
β	0.554	0.030	0.53	0.84	0.95	−0.95	1.00

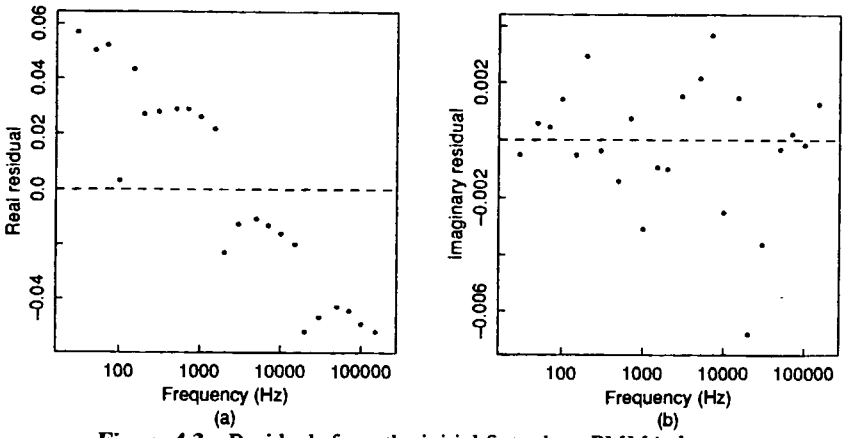

Figure 4.3 Residuals from the initial fit to the s-PMMA data.

periment. When the frequency of an oscillator is made to cover an extremely large range (in this example, from 30 to 150 000 Hz), it is done by manipulating two dials, a *units* dial which covers a range of, say, 2 to 20, and a *decade* dial which changes the frequency by multiples of 10. Thus, to set the frequency to 150 Hz, the operator would set the units dial to 15 and the decade dial to ×10; and to set the frequency to 30 000 Hz, the operator would set the units dial to 3 and the decade dial to ×10 000. In this experiment, the capacitance of the polymer sample was apparently large enough to affect the frequency of the oscillator, so that the actual frequency delivered was not that indicated on the dials. At high frequencies the fitted values were too large, and at low frequencies the fitted values were too small, suggesting that the indicated frequencies were below the actual, with the discrepancy (indicated − actual) increasing with each decade increase.

A decade correction was therefore made to the indicated frequencies so that when the decade was increased, the frequency was multiplied by $10 \times K$. Assuming the first decade was correct, the second decade would have actual frequencies of $K\times$ the indicated values, the third decade $K^2\times$ the indicated values, and so on. Rather than incorporate the decade factor

K as a parameter in the model, we performed a search by selecting values for K, modifying the indicated frequencies, fitting the model and examining the residuals, and choosing that value of K which gave the best behaved residuals. For this data set, a decade correction of $K = 1.25$ was found.

The convergence output for the decade-corrected data is given in Table 4.2. The major changes were a reduction in the determinant and in the variance estimate of the real residuals by a factor of about 10. The residuals for the real and imaginary components are plotted versus frequency in Figure 4.4, from which it can be seen that the imaginary residuals are very well behaved, with perhaps two or three outliers. The real residuals are much better behaved now, with no trend. There is, however, one obvious outlier and one other possible outlier. Plotting the imaginary residuals versus the real residuals more clearly discloses two outliers. Since the residuals are bad in both the real and imaginary components, we simply delete these two cases. If only one residual were bad, we could treat the observation which gave rise to the bad residual as missing, and proceed as in Section 4.4.

Analysis of the decade-corrected and edited data set produced the results in Table 4.3. Removing the two unusual cases reduced the parameter and variable variances, but the parameter estimates were not materially affected. The residuals from this fit are very well behaved, as can be seen from Figure 4.5.

We also analyzed the data by estimating K rather than obtaining it from a search. The optimum value was $\hat{K} = 1.24$; the other parameter estimates and their approximate standard errors changed slightly. ■

Example: α-Pinene 4

The starting values in Example α-Pinene 2 were used together with the techniques described in Chapter 5 for obtaining the expectation function and derivatives, and convergence was obtained for the five response data set as shown in Table 4.4. In Figure 4.6 we show a plot of the data and the fitted responses. The fitted curves do not follow the data very well, sug-

Table 4.2 Parameter summary for the decade-corrected s-PMMA data.

Parameter	Estimate	Approx. Std.Error	Approximate Correlation Matrix				
ε_0	4.400	0.007	1.00				
ε_∞	2.447	0.013	0.58	1.00			
$\ln f_0$	8.228	0.091	0.68	0.84	1.00		
α	0.486	0.008	−0.86	−0.68	−0.91	1.00	
β	0.571	0.026	0.76	0.85	0.99	−0.95	1.00

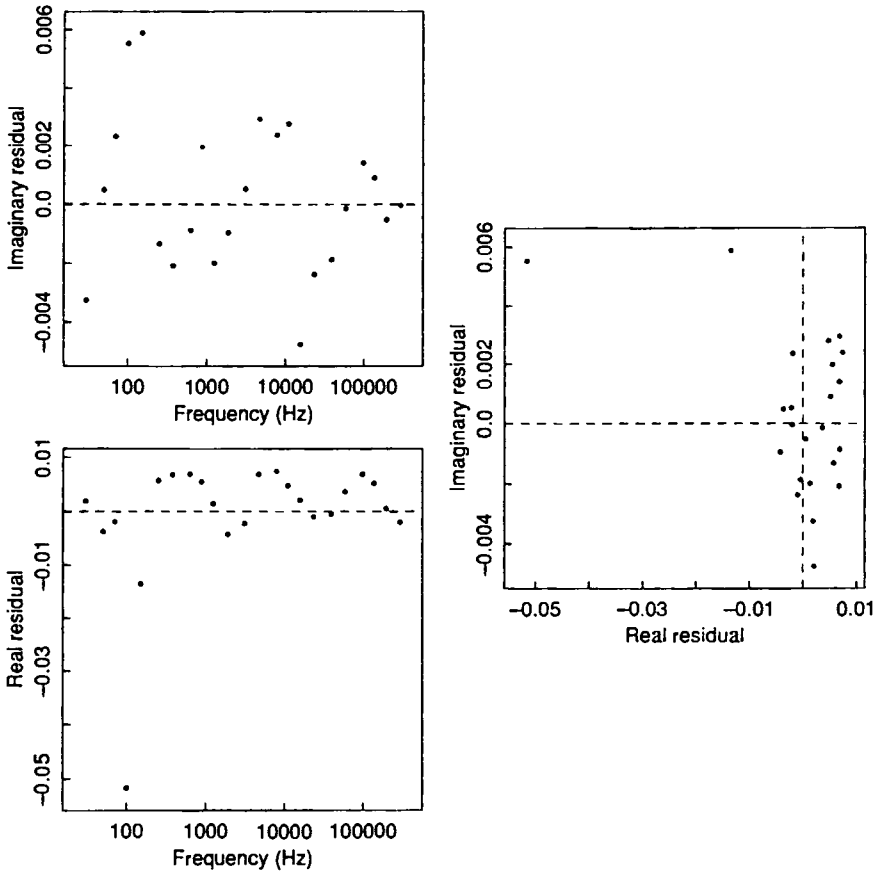

Figure 4.4 Residuals from the fit to the decade-corrected s-PMMA data.

Table 4.3 Parameter summary for the decade-corrected and edited s-PMMA data.

Parameter	Estimate	Approx. Std.Error	Approximate Correlation Matrix				
ε_0	4.398	0.006	1.00				
ε_∞	2.451	0.010	0.53	1.00			
$\ln f_0$	8.245	0.074	0.63	0.91	1.00		
α	0.487	0.007	−0.86	−0.75	−0.90	1.00	
β	0.571	0.021	0.74	0.91	0.98	−0.95	1.00

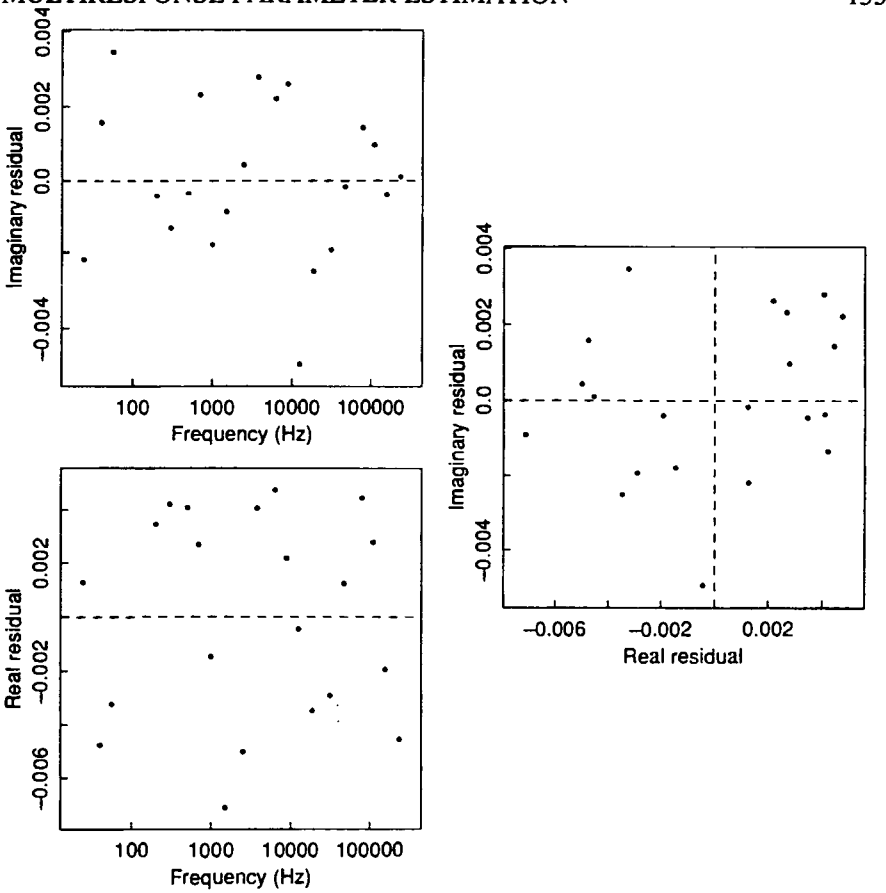

Figure 4.5 Residuals from the fit to the decade-corrected and edited s-PMMA data.

Table 4.4 Parameter summary for the α-pinene data using five responses.

Parameter		θ	Logarithm Scale						
From	To	(10^{-5})	φ	Std.Error	Correlation				
1	2	3.74	−10.19	0.085	1.00				
1	3	1.95	−10.85	0.073	0.84	1.00			
3	4	1.65	−11.01	0.104	−0.20	−0.41	1.00		
3	5	27.01	−8.217	0.128	0.00	−0.00	0.85	1.00	
5	3	2.61	−10.55	0.195	0.68	0.78	−0.01	0.40	1.00

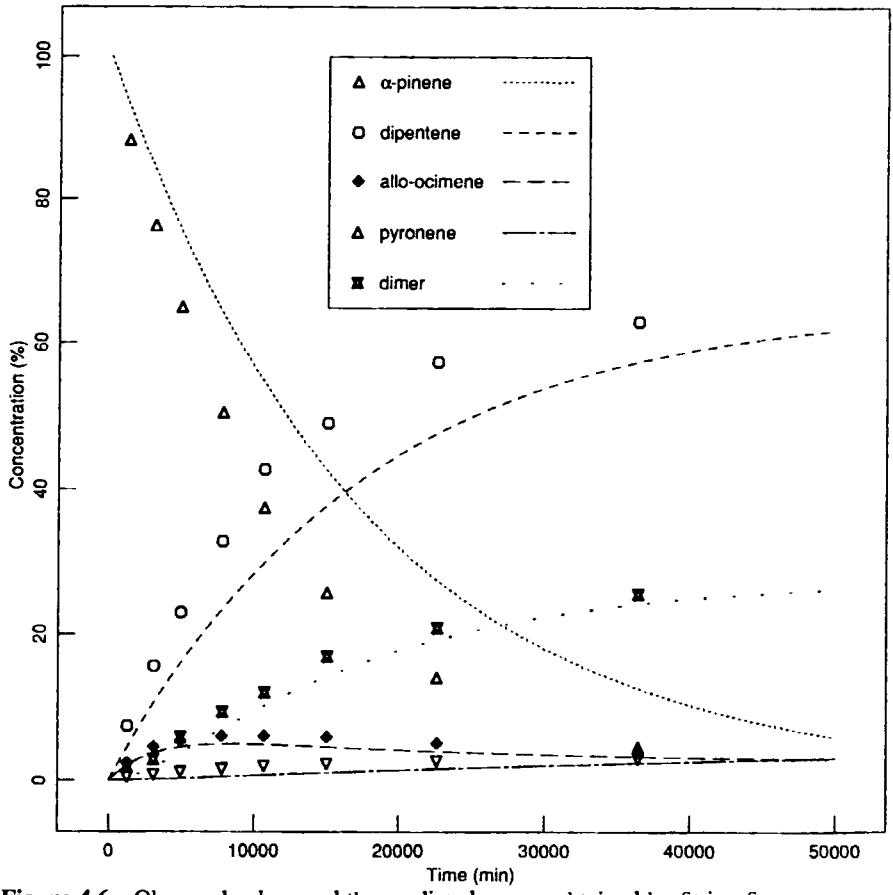

Figure 4.6 Observed values and the predicted curves obtained by fitting five responses to the α-pinene data

gesting that convergence to a spurious optimum has occurred. As will be shown in the next section, this has occurred because there are dependencies in the data. ■

4.3.3 Dependencies Among Responses

Convergence to a spurious optimum due to dependencies in the response data is an important problem which can easily arise in multiresponse estimation, but which can not happen in uniresponse estimation. Data dependencies can occur, for example, because the responses are constrained through mass balances or because one or more responses are not measured but are imputed from other measured responses. If dependencies occur in the data or in the expected responses, then the estimation procedure must be modified so as to avoid con-

vergence to spurious optima (Box et al., 1973; McLean et al., 1979).

To detect dependencies in a multiresponse data set, Box et al. (1973) used an eigenvalue analysis of the inner product of the centered data matrix, $(\mathbf{Y}-\overline{\mathbf{Y}})^{\mathrm{T}}(\mathbf{Y}-\overline{\mathbf{Y}})$, where $\overline{\mathbf{Y}}$ is the matrix of response averages obtained by replacing each column of $\mathbf{Y}$ by the average of the column. They then compared the eigenvalues with an estimate of the roundoff sum of squares, $(N-1)u^2/12$, where u is the rounding unit of the data. Any eigenvalues which were of the same magnitude as the roundoff sum of squares were assumed to be associated with linear dependencies in the data.

This approach can reveal singularities due to conditions that cause a linear combination of the responses from all cases to be a constant (for example, a mass balance), but, as described in McLean et al. (1979), analysis of the centered *data* matrix can fail to detect singularities in the *residual* matrix, and hence one may still be trying to converge with a "defective" data set. As was also pointed out by these authors, in certain circumstances linear dependencies among the data need not cause singularities in the residual matrix $\mathbf{Z}(\boldsymbol{\theta})$, so removal of singularities detected through analysis of the centered data matrix can cause unnecessary loss of precision in the parameter estimates. Therefore, it is necessary to search for singularities in both the centered data matrix and the residual matrix.

As an example where there can be singularities in $\mathbf{Z}$ but no singularities in $\mathbf{Y}-\overline{\mathbf{Y}}$, following McLean et al. (1979), we consider a chemical reaction in which two responses are measured. The two responses are normalized so that the total for the nth case is γ_n^0, the initial concentration of the first chemical. Unless the initial concentrations are all the same, the matrix $\mathbf{Y}-\overline{\mathbf{Y}}$ will not be singular. However, if the reaction follows first order kinetics so that $f_{n1}=\gamma_n^0 e^{-\theta t_n}$ and $f_{n2}=\gamma_n^0(1-e^{-\theta t_n})$, then the residual matrix $\mathbf{Z}$ with nth row

$$(z_{n1}, z_{n2})=(y_{n1}-f_{n1}, y_{n2}-f_{n2})$$

involves the linear dependency $z_{n1}+z_{n2}=0$ for all n, and the residual matrix is singular. It would be futile, therefore, to try to estimate the parameter $\boldsymbol{\theta}$ using a multiresponse estimation criterion.

As an example where there can be singularities in $\mathbf{Y}-\overline{\mathbf{Y}}$ but no singularities in $\mathbf{Z}$, suppose that in the example above, the two responses are obtained from chromatograph area fractions, so the measurement for y_{n1} is

$$y_{n1}=a_1+b_1\left[\frac{\text{area}_{n1}}{\text{area}_{n1}+\text{area}_{n2}}\right]$$

and that for y_{n2} is

$$y_{n2}=a_2+b_2\left[\frac{\text{area}_{n2}}{\text{area}_{n1}+\text{area}_{n2}}\right]$$

where a_1, b_1, a_2, and b_2 are calibration constants. Then a linear dependency will exist in the data of the form $b_2y_{n1}+b_1y_{n2}=\text{constant}$ for all n, and so $\mathbf{Y}-\overline{\mathbf{Y}}$

will be singular. However, unless for every case

$$\gamma_n^0\left[b_1+(b_2-b_1)e^{-\theta t_n}\right]=a_2b_1+a_1b_2+b_1b_2$$

the residual matrix will not be singular because of the linear dependence in the data.

Singularities in $\mathbf{Y}-\overline{\mathbf{Y}}$ and in $\mathbf{Z}$ can be detected by performing an eigenvalue–eigenvector decomposition of the inner product, as proposed by Box et al. (1973), but we prefer to arrange the rounding units in the columns of $\mathbf{Y}$ to be approximately equal and then take singular value decompositions of $\mathbf{Y}-\overline{\mathbf{Y}}$ and $\mathbf{Z}$ (Dongarra et al., 1979, Chapter 11). As explained there, singular values on the order of the rounding unit indicate singularity and should prompt the analyst to search for dependencies in the data.

A singular value decomposition of the centered data matrix, and of the residual matrix using the initial parameter values, should be done at the beginning of the analysis so as to avoid unnecessary calculations caused by dealing with a defective data set which involves linear dependencies. If small singular values are obtained, the corresponding singular vectors should be examined to reveal what is causing the dependencies. If the dependency can be explained (e.g., a mass balance, or a response has been imputed from other measured responses) and the offending responses identified, they should be removed and a multiresponse analysis performed on the reduced data set. If a dependency can not be explained, then the multiresponse analysis should be modified to take account of the dependency as described in Section 4.3.4. The residual matrix at the converged parameter values should also be analyzed for singular values so as to detect possible dependencies in the residuals. Further comments on detecting and eliminating linear dependencies are given in McLean et al. (1979).

Example: s-PMMA 4

For the decade-corrected and edited s-PMMA data, the singular values of the centered data matrix are 0.278 and 2.161, and since the rounding units in the data are both 0.001, neither of these singular values is small enough to suggest a linear dependency. The singular values of the residual matrix at the converged values are 0.009 and 0.017 and neither of these is small enough to cause concern. ■

Example: α-Pinene 5

The centered data matrix for the α-pinene data, has the singular value decomposition

Singular value	0.04	0.13	1.10	5.08	98.30
	−0.17	0.48	−0.30	0.06	−0.81
	−0.21	0.49	−0.61	−0.22	0.54
Singular vectors	−0.16	0.43	0.64	−0.61	0.01
	0.93	0.36	−0.01	0.00	0.02
	−0.19	0.46	0.36	0.76	0.23

which clearly indicates dependencies in the data because the two small singular values are of the same magnitude as the rounding unit in the data (0.1, see Appendix 1, Section A1.6).

The residual matrix at the starting estimates has the singular value decomposition

Singular value	0.06	0.14	0.46	1.63	42.70
	0.34	−0.30	−0.28	0.26	0.81
	0.39	−0.26	−0.39	0.55	−0.57
Singular vectors	0.60	−0.27	0.75	−0.08	−0.07
	−0.50	−0.86	0.08	−0.05	−0.06
	0.36	−0.20	−0.45	−0.79	−0.12

which also reveals two dependencies.

As noted by Box et al. (1973), from careful reading of the paper by Fuguitt and Hawkins (1947), the response y_4 was not in fact measured, but was imputed as 3% of the amount of converted y_1, i.e., $y_4 = 0.03(100 - y_1)$. The first singular vector of the centered data matrix reflects this dependency and so the imputed data for y_4 should not be used in estimation. The second singular vector, consisting of almost equal entries, reflects a mass balance dependency, i.e., the data must sum to 100%. This occurs because the system is a conservative one, as can easily be seen, since all the columns of the system matrix **A** sum to zero. The singular vectors of the residual matrix do not reflect these dependencies, so that while the singular value decomposition of **Z** does suggest that there are dependencies, it does not reveal their nature.

Because there are two small singular values, suggesting two linear dependencies in the data, only three responses should be retained for parameter estimation. ■

When linear dependencies are found, the problem of choosing an appropriate subset of the responses must be addressed. One approach is to retain those responses which the researcher thinks are most reliable. It may not be possible to select the responses on this basis, however, and so we follow Box et al. (1973) and use a linear combination of the responses instead. In either situation, it would be helpful to have a procedure for estimating parameters in the presence of dependencies. Accordingly, in the following section we describe a procedure for estimating parameters in the presence of linear dependencies.

4.3.4 Linear Combinations of Responses

Suppose there are d linear dependencies, and there are no missing values in the data matrix. To deal with linear dependencies, we generate an $N \times (M-d)$ reduced residual matrix $\mathbf{ZB}$ by combining the d linear dependency vectors into an $M \times d$ dependency matrix $\mathbf{D}$, performing a QR decomposition on $\mathbf{D}$, and letting the rotation matrix $\mathbf{B}$ be the $M-d$ columns of $\mathbf{Q}$ which are orthogonal to the dependency vectors.

Example: α-Pinene 6

For the α-pinene data, we have decided that response 4 should not be used in estimation, and that there is a mass balance relation in the data. The dependency matrix is therefore

$$\mathbf{D} = \begin{bmatrix} 0 & 1 \\ 0 & 1 \\ 0 & 1 \\ 1 & 1 \\ 0 & 1 \end{bmatrix}$$

Performing a QR decomposition produces $\mathbf{B}$ as the last three columns of $\mathbf{Q}$. Again, as discussed in Appendix 2, although $\mathbf{Q}$ is required to obtain $\mathbf{B}$, $\mathbf{Q}$ is not explicitly formed; a product such as $\mathbf{Z}_{(p)}\mathbf{B}$ is formed by applying Householder transformations to $\mathbf{Z}_{(p)}^{\mathrm{T}}$, retaining the last $M-d$ rows to give $(\mathbf{Z}_{(p)}\mathbf{B})^{\mathrm{T}}$, and then transposing the result. ■

To minimize $|(\mathbf{ZB})^{\mathrm{T}}(\mathbf{ZB})|$ using the generalized Gauss–Newton method of Section 4.2, we need $(\mathbf{ZB})_{(p)}$. This is easily obtained because $\mathbf{B}$ is independent of $\boldsymbol{\theta}$, and so

$$(\mathbf{ZB})_{(p)} = \mathbf{Z}_{(p)}\mathbf{B}$$

Thus, the terms in the determinant, the gradient and the approximate Hessian for the reduced data set can be calculated by simply using $\mathbf{Z}$ and $\mathbf{Z}_{(p)}$, $p = 1, \ldots, P$.

Example: α-Pinene 7

Using the starting values from Example α-Pinene 4 and three (rotated) responses, we obtained the results in Table 4.5.

The overlay plot of the data and fitted curves in Figure 4.7 gives no evidence of inadequacy of the fitted model. However, the residuals, shown in Figure 4.8, are not well behaved, with a large negative residual for response 3 and a trend and a large positive residual for response 2. There is also a preponderance of negative residuals. Also the approximate confidence limits on ϕ_3 are very wide, suggesting that it is badly estimated and that θ_3 could be zero. We temporarily ignore the defective residuals, and try to see if a simpler model would be adequate. ■

Table 4.5 Parameter summary for the α-pinene data using three rotated responses.

Parameter		θ	Logarithm Scale						
From	To	(10^{-5})	φ	Std.Error	Correlation				
1	2	5.94	−9.731	0.021	1.00				
1	3	2.86	−10.47	0.042	−0.20	1.00			
3	4	0.453	−12.31	3.92	−0.37	0.91	1.00		
3	5	31.12	−8.072	0.124	−0.22	0.51	0.45	1.00	
5	3	5.79	−9.757	0.21	0.10	0.16	0.16	0.78	1.00

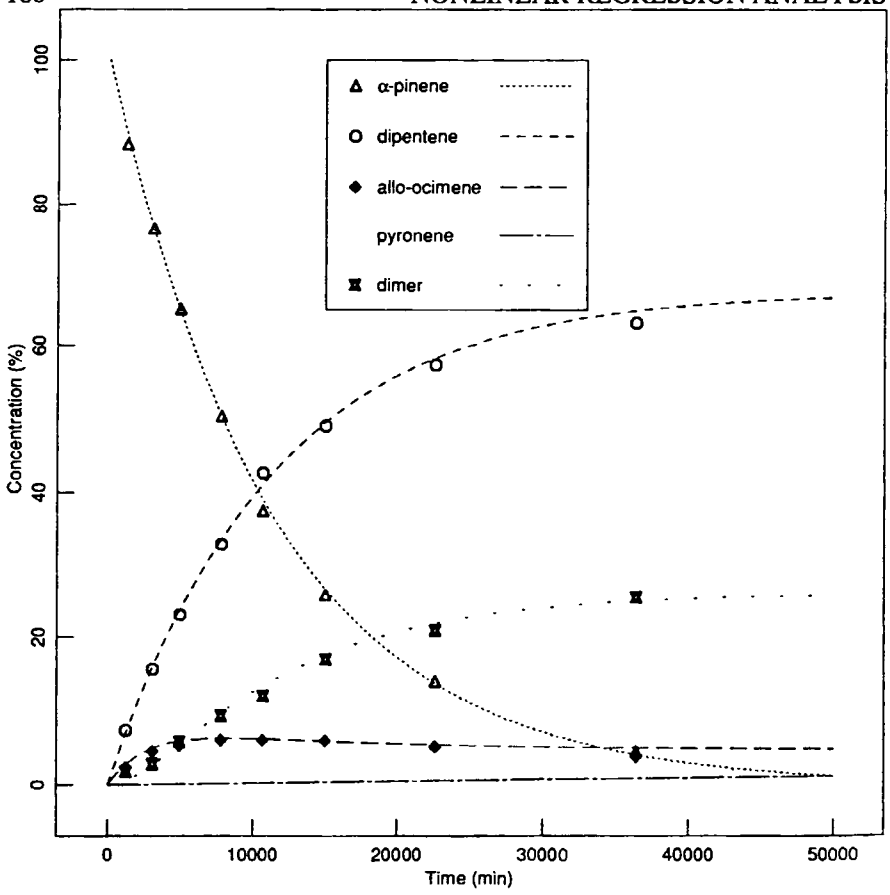

Figure 4.7 Observed values and the predicted curves obtained by fitting three rotated responses to the α-pinene data.

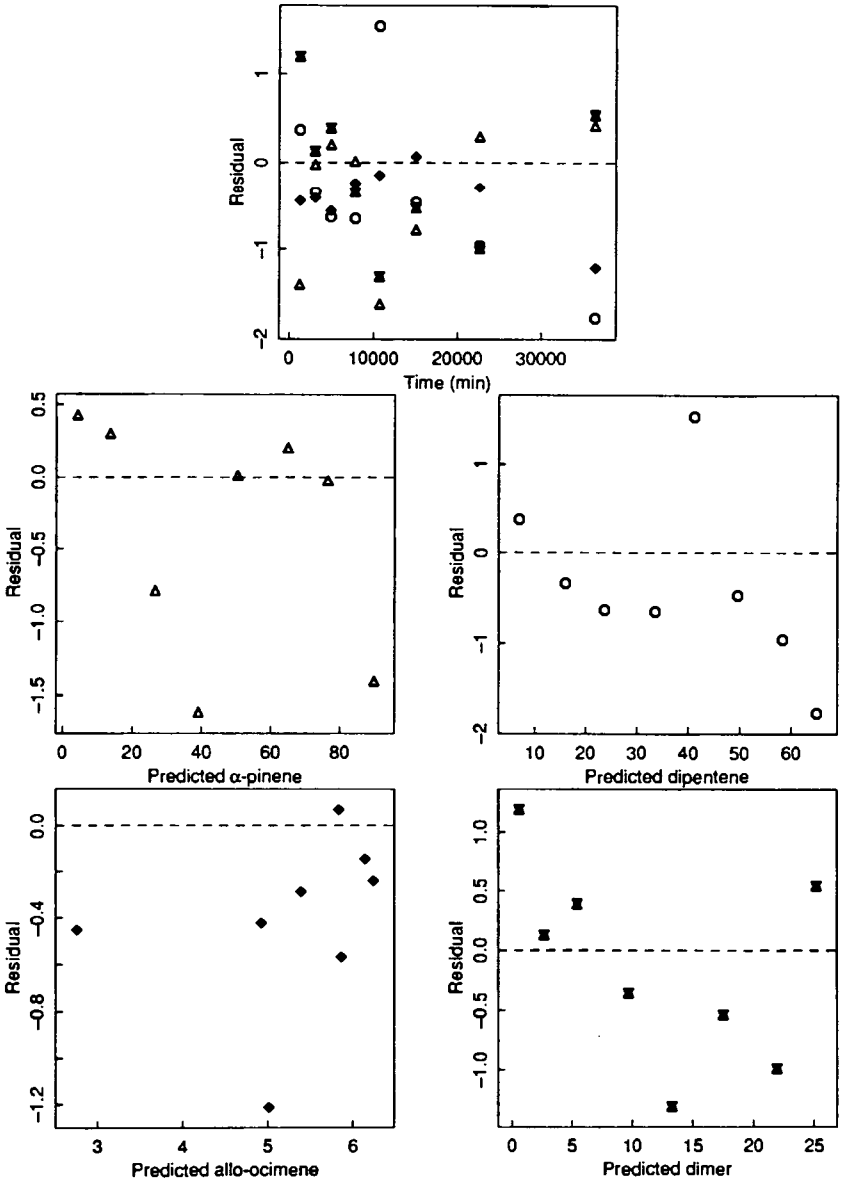

Figure 4.8 Residuals from the three rotated response fit to the α-pinene data plotted versus time and versus predicted response.

Linear combinations of responses can be used to check for consistency of information by analyzing subsets of the responses, as suggested in Box and Draper (1965). We simply let **B** be the matrix derived from an identity matrix by deleting columns corresponding to the unused responses.

Example: α-Pinene 8

Suppose we wished to estimate the parameters using only the responses y_1, y_2, and y_5. Then we would use as the rotation matrix

$$\mathbf{B} = \begin{bmatrix} 1 & 0 & 0 \\ 0 & 1 & 0 \\ 0 & 0 & 0 \\ 0 & 0 & 0 \\ 0 & 0 & 1 \end{bmatrix}$$

■

4.3.5 Comparing Models

Nested models can be compared using an "extra determinant" analysis in the same way that uniresponse nested models were compared using an extra sum of squares analysis (Section 3.10). That is, we compare the ratio of the change in the determinant divided by the change in the degrees of freedom with the scaled determinant for the complete model as in (4.11).

Example: α-Pinene 9

The model for the α-pinene reaction includes a path from species 3 to species 4, but as seen in Example α-Pinene 6, the logarithm of the rate constant associated with that path has a large standard error, suggesting that this path could be eliminated. Fitting the data without this path, but still retaining only three (rotated) responses, gives the results in Table 4.6. Combining these results with the results in Table 4.5 allows us to perform an extra determinant analysis as in Table 4.7. According to this analysis, the extra path is not necessary.

The predicted response curves are plotted in Figure 4.9. The residuals for this model are almost identical to those from the previous fit, and so we could reanalyze the data, treating the observations with the large residuals as missing. ■

Table 4.6 Parameter summary for the α-pinene data using three rotated responses, eliminating pyronene production.

Parameter		θ	Logarithm Scale					
From	To	(10^{-5})	φ	Std.Error	Correlation			
1	2	5.94	−9.73	0.018	1.00			
1	3	2.82	−11.28	0.016	0.44	1.00		
3	5	30.75	−8.09	0.093	−0.07	0.26	1.00	
5	3	5.72	−9.77	0.182	0.16	0.05	0.81	1.00

Table 4.7 Extra determinant analysis of the 4-parameter model versus the 5-parameter model for the α-pinene data.

Source	Determinant	Degrees of Freedom	Mean Det.	F Ratio	*p* Value
Extra	0.60	1	0.60	0.06	0.822
Full model	28.39	3	9.46		
partial model	28.99	4			

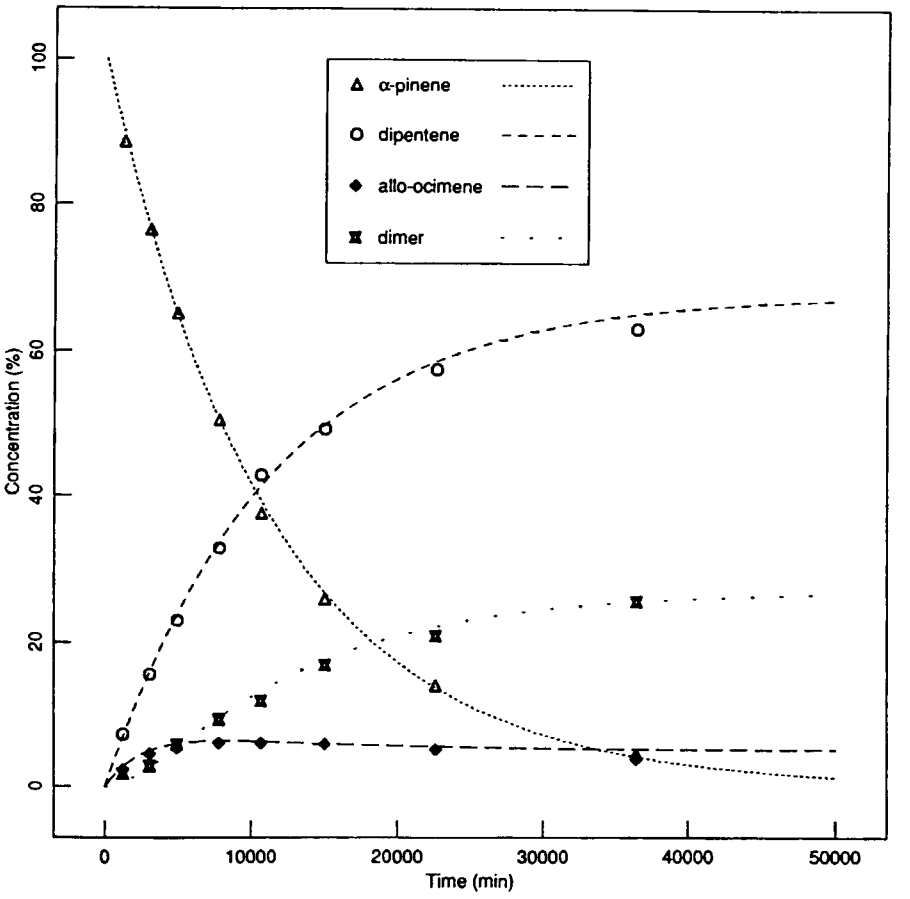

Figure 4.9 Observed values and the predicted curves obtained by fitting three rotated responses to the α-pinene data, eliminating pyronene production.

4.4 Missing Data

Missing data are a source of difficulty in statistics. In uniresponse linear or nonlinear regression analysis, if the value of a predictor variable is missing, or if the response itself is missing, the residual cannot be calculated and the only course is to delete the case. In multiresponse estimation, however, it is possible to have all the predictor variables recorded and some, but not all, of the responses recorded. In such situations, it is still possible to use the recorded response values even though there are incomplete data for that case.

Stewart and Sorensen (1981) gave a Bayesian approach for multiresponse data with missing values based on the posterior density for $\boldsymbol{\theta}$ and $\boldsymbol{\Sigma}$ conditional on the recorded data. The total number of parameters to be estimated is $P+M(M+1)/2$. Point estimates for $\boldsymbol{\theta}$ and $\boldsymbol{\Sigma}$ are obtained by minimizing the negative of the logarithm of the posterior density,

$$S(\boldsymbol{\theta},\boldsymbol{\Sigma}) = (M+1)\ln|\boldsymbol{\Sigma}| + \sum_{n=1}^{N}\ln|\boldsymbol{\Sigma}_n| + \sum_{n=1}^{N}\sum_{m=1}^{M}\sum_{i=1}^{M}\sigma_n^{mi}\{Y_{nm}-f_{nm}(\boldsymbol{\theta})\}\{Y_{ni}-f_{ni}(\boldsymbol{\theta})\}$$

where $\boldsymbol{\Sigma}_n$ is obtained from $\boldsymbol{\Sigma}$ by substituting

$$\delta_{mi} = \begin{cases} 1 & m=i \\ 0 & m\neq i \end{cases}$$

whenever the data for case (n,m) or (n,i) is missing, and the term σ_n^{mi} is the (m,i)th entry of $\boldsymbol{\Sigma}_n^{-1}$.

This approach is complicated, requiring sophisticated minimization algorithms and careful checks on the data and the model formulation so as to avoid an indeterminate problem. It is also necessary to ensure that all the variances are positive and that the estimated matrices $\boldsymbol{\Sigma}$ and $\boldsymbol{\Sigma}_n$ remain positive definite

Another approach, suggested by Box, Draper, and Hunter (1970), is to treat the missing responses as parameters (say, $\mathbf{y}^*$) and optimize the determinant criterion over $\boldsymbol{\theta}$ and $\mathbf{y}^*$ simultaneously. As noted (Bard, 1974; Stewart and Sorensen, 1981), this approach is not feasible when there are many missing values, since then the total number of model and missing response parameters can exceed the number of cases.

When the total number of parameters is acceptable, we recommend a two stage procedure in which the model parameters and the residuals corresponding to the missing values are estimated alternately. We use missing residuals instead of missing responses because zero is a good starting estimates for a missing residual, and because the missing residuals tend to be uncorrelated with the model parameters. In the first stage, the missing residuals are fixed and the model parameters are estimated using a generalized Gauss–Newton algorithm. The algorithm must be modified because after each function evaluation, the entries in $\mathbf{Z}(\boldsymbol{\theta})$ corresponding to missing data must be replaced by their current

values. Also, the corresponding entries in $\mathbf{Z}_{(p)}$ must be replaced by zeros, since those residuals do not depend on the model parameters.

In the second stage, $\boldsymbol{\theta}$ is held fixed and the determinant is minimized with respect to the missing residuals. The generalized Gauss–Newton method can also be used here, since the derivatives of $\mathbf{Z}$ with respect to a missing residual consist of zeros everywhere except for a one in the location of the missing residual.

Example: s-PMMA 5

Recall from Example s-PMMA 3 that the residuals at 100 and 150 Hz were anomalous, and so we deleted those cases. We now illustrate the two stage approach for fitting multiresponse data with missing observations by treating the y_{real} values as missing and the y_{imag} values as good.

We begin with initial estimates $\boldsymbol{\theta}=(4.40, 2.45, 8.25, 0.49, 0.57)^{\mathrm{T}}$ and set the missing residuals, $\{\mathbf{Z}\}_{4,1}$ and $\{\mathbf{Z}\}_{5,1}$, to zero. Converging on the parameters gives $\boldsymbol{\theta}=(4.41, 2.45, 8.24, 0.48, 0.57)^{\mathrm{T}}$ with a determinant of 4.500×10^{-8}. We now fix $\boldsymbol{\theta}$ and optimize the determinant with respect to $\{\mathbf{Z}\}_{4,1}$ and $\{\mathbf{Z}\}_{5,1}$. This gives estimates 0.00248 and 0.00270 and a determinant of 4.373×10^{-8}.

Fixing these residuals and optimizing with respect to $\boldsymbol{\theta}$ produces minor changes in $\boldsymbol{\theta}$ (e.g., $\ln f_0$ changes from 8.237 to 8.252). Optimizing the residuals again gives estimates 0.00252 and 0.00277 and a determinant of 4.371×10^{-8}. In the next stage, the values of the parameters do not change, so convergence is achieved. ■

Example: α-Pinene 10

As discussed in Examples α-Pinene 7 and α-Pinene 9, the residuals exhibited trends with respect to the fitted value for response 2 and response 4, and unequal distributions of the residuals with respect to sign. There were also two possible outliers, $\hat{z}_{5,2}$ and $\hat{z}_{8,3}$. To see if the trends or unequal distributions could be caused by these outliers, we reanalyzed the data using the 4-parameter model and treating the corresponding observations as missing. A summary of the results is given in Table 4.8. The main effect is that $\ln\theta_4$ changes by 0.317, which corresponds to a factor of 1.37 for θ_4. The residuals, not shown, were very similar to those from the fit to the complete data set, plotted in Figure 4.8, so the imbalance in signs and the trends do not appear to be caused by the two residuals we characterized as outliers. We therefore interpret the nonrandom behavior of the residuals as indicating a fundamental inadequacy in the form of the model. This finding is in accord with that of Stewart and Sorensen (1981), who analyzed the complete data set reported by Fuguitt and Hawkins (1945, 1947). The model proposed by Stewart and Sorensen (1981) consisted of the set of nonlinear differential equations presented in Example α-pinene 1 of Chapter 3. ■

Table 4.8 Summary of the effects of treating two observations as missing in the α-pinene data.

	Data Set			
	Complete		Incomplete	
Quantity	Estimate	Std. Err.	Estimate	Std. Err.
$\ln \theta_1$	−9.729	0.018	−9.740	0.013
$\ln \theta_2$	−10.478	0.016	−10.475	0.019
$\ln \theta_3$	−8.087	0.093	−8.229	0.105
$\ln \theta_4$	−9.769	0.183	−10.086	0.265
$\hat{z}_{5,2}$	1.528		−0.562	0.138
$\hat{z}_{8,3}$	−1.214		−1.804	0.381
Determinant	28.99		24.44	

Exercises

4.1 Write a computer routine in a language of your choice to calculate the determinant, the gradient of the determinant, and the approximate Hessian of the determinant, for a multiresponse estimation routine. If necessary, use the pseudocode in Appendix 3, Section A3.3 for guidance.

4.2 Use the data for responses 1 and 2 in the α-pinene data set, Appendix 4, Section A4.6, to fit the multiresponse model

$$\boldsymbol{\gamma}(t) = \begin{bmatrix} e^{-(\theta_1+\theta_2)t} \\ \dfrac{\theta_1}{\theta_1+\theta_2}\left[1-e^{-(\theta_1+\theta_2)t}\right] \end{bmatrix}$$

Assume the initial concentration of α-pinene (response 1) is 100% and of dipentene (response 2) is 0%.

(a) Use the approximate rate procedure of Section 4.3.1 to obtain starting estimates for the parameters.

(b) Use a nonlinear estimation routine to obtain the parameter estimates. Replace the missing value for response 1 at time 16 020 by 0 to obtain the parameter estimates.

(c) Use the procedure in Section 4.4 to estimate the parameters and the missing value.

4.3 Perform a singular value decomposition of the centered data matrix for the data from Appendix 4, Section A4.7, to determine if there are any linear dependencies in the data.

4.4 For the data and model of Problem 4.2, the parameter estimates and summary statistics from part (b) are as follows:

		Logarithm Scale			
Parameter	Estimate	$\ln\theta$	Std. Error	Correlation Matrix	
θ_1	0.000221	−8.417	0.0085	1.00	
θ_2	0.000139	−8.881	0.0059	0.69	1.00

(a) Calculate joint and marginal 95% inference regions for the parameters using equations (4.9) and (4.12).

(b) Use a grid of values of $\ln\theta_1$ from −8.46 to −8.38 in steps 0.005 and $\ln\theta_2$ from −8.904 to −8.854 in steps of 0.002, and calculate the determinant at each point. Join points of equal value to delineate contours.

(c) Plot the joint 95% inference region from part (a) on the contour plot in part (b). Is the linear approximation region accurate in this case?

4.5 Use the data and model from Appendix 4, Section A4.7 to fit a multiresponse model. Reduce the model to a simple form by eliminating parameters which could be zero. Your analysis to Problem 4.3 should have alerted you to the fact that there was a dependency in the data. In fact, the water component y_6 was imputed from a mass balance equation, and so this response should not be used in fitting the model. Because of this, it is convenient to estimate the parameters θ_6 and β_6 from the parameter constraint equations.

CHAPTER 5.

Models Defined by Systems of Differential Equations

"The universe is like a safe to which there is a combination, but the combination is locked up in the safe."

– Peter de Vries

An important special class of nonlinear models is that in which the responses are described by a linear system of ordinary differential equations. These models are used in chemical kinetics (Froment and Bischoff, 1979) and in pharmacokinetics (Godfrey, 1983), where they are called *compartment* models. Because they are used in so many areas, it is worthwhile to have special techniques to make their analysis easier. Accordingly, in this chapter we present efficient methods for estimating parameters in compartment models and for developing and testing competing models. Techniques for dealing with systems of nonlinear differential equations are discussed in Bard (1974) and Caracotsios and Stewart (1985).

5.1 Compartment Models and System Diagrams

A common use of compartment models is in pharmacokinetics, where the exchange of materials in biological systems is studied. A system is divided into compartments, and it is assumed that the rates of flow of drugs between compartments follow first order kinetics, so that the rate of transfer to a receiving, or *sink*, compartment is proportional to the concentration in the supplying, or *source*, compartment. The transfer coefficients, which are assumed constant with respect to time, are called *rate constants*.

Example: Tetracycline 1

As an example of a compartment model, we consider data on the concentration of tetracycline hydrochloride in serum. A tetracycline compound was administered to a subject orally, and the concentration of tetracycline hydrochloride in the serum was measured over a period of 16 hours (Wagner, 1967). The data are recorded in Appendix 1, Section A1.14, and plotted in Figure 5.1.

The biological system can be modeled by a gut compartment into which the chemical is introduced, a blood compartment which absorbs the chemical from the gut, and an elimination path. Assuming first order kinetics, the concentrations $(\gamma_1(t), \gamma_2(t))^T$ of tetracycline hydrochloride in the two compartments can be described by the following pair of differential equations:

$$\begin{aligned} \frac{d\gamma_1(t)}{dt} &= \dot{\gamma}_1 = -\theta_1\gamma_1(t) \\ \frac{d\gamma_2(t)}{dt} &= \dot{\gamma}_2 = \theta_1\gamma_1(t) - \theta_2\gamma_2(t) \end{aligned} \tag{5.1}$$

where the dot denotes differentiation with respect to time.

The system can be represented graphically as a compartment or system diagram as in Figure 5.2. ■

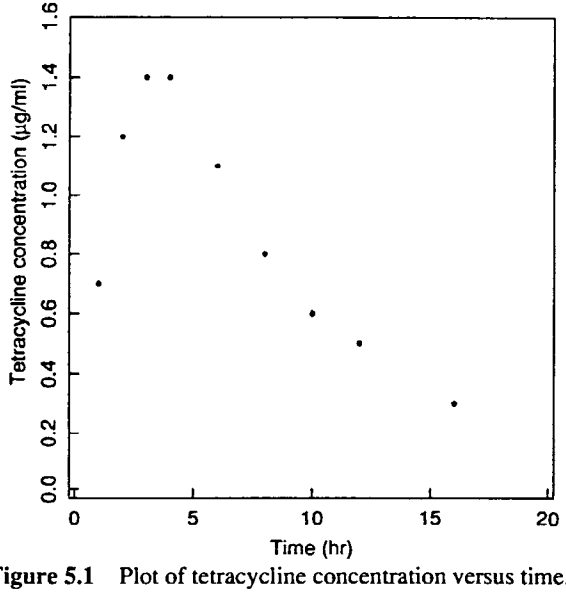

Figure 5.1 Plot of tetracycline concentration versus time.

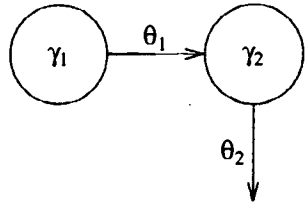

Figure 5.2 A compartment or system diagram for the tetracycline model.

Chemical reactions can also be described by linear systems of first order differential equations. In this context, the chemical species of the reaction constitute the compartments, the original species being termed "parents," and the product species "daughters."

Example: Oil shale 1

As a chemical example, we consider the pyrolysis of oil shale described by Ziegel and Gorman (1980). Oil shale contains organic material which is organically bonded to the structure of the rock. To extract oil from the rock, heat is applied so the technique is called pyrolysis.

During pyrolysis, the benzene organic material, called kerogen, decomposes to oil and bitumen, and there are unmeasured by-products of insoluble organic residues and light gases. Ziegel and Gorman, using data obtained from Hubbard and Robinson (1950), estimated the rate constants in several candidate models. The data obtained by Hubbard and Robinson are listed in Appendix 1, Section A1.15.

The final model fitted by Ziegel and Gorman to the 400°C data using multiresponse estimation techniques can be represented by the system diagram in Figure 5.3, which corresponds to the set of linear differential equations,

$$\begin{aligned} \frac{d\gamma_1}{dt} &= -(\theta_1+\theta_4)\gamma_1 \\ \frac{d\gamma_2}{dt} &= \theta_1\gamma_1-(\theta_2+\theta_3)\gamma_2 \\ \frac{d\gamma_3}{dt} &= \theta_4\gamma_1+\theta_2\gamma_2 \end{aligned} \tag{5.2}$$

In this equation, γ_1 denotes kerogen, γ_2 bitumen, and γ_3 oil.

The model implies that kerogen decomposes to bitumen with rate constant θ_1 and to oil with rate constant θ_4, and that bitumen decomposes to oil with rate constant θ_2 and to unmeasured by-products with rate constant θ_3. ■

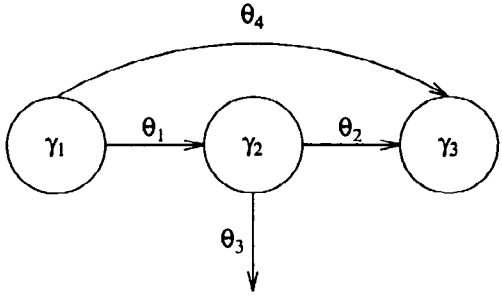

Figure 5.3 System diagram for the oil shale pyrolysis model.

In the general compartment model consisting of K compartments, we write the concentrations at time t as $\boldsymbol{\gamma}(t) = (\gamma_1(t), \ldots, \gamma_K(t))^T$. Assuming first order kinetics with rate constants $\theta_1, \theta_2, \ldots, \theta_P$, the concentrations obey the linear system of differential equations

$$\frac{d\boldsymbol{\gamma}}{dt} = \dot{\boldsymbol{\gamma}}(t) = \mathbf{A}\boldsymbol{\gamma}(t) + \boldsymbol{\iota}(t) \tag{5.3}$$

where $\mathbf{A}$ is the $K \times K$ system *transfer matrix* containing the rate constants and $\boldsymbol{\iota}(t)$ is a vector function representing input to the system.

Although more complicated inputs may be used (Bates, Wolf, and Watts, 1985), in this book we consider only two input functions. One is a continuous infusion of material or *step input* into the system,

$$\boldsymbol{\iota}(t) = \begin{cases} \boldsymbol{\iota} & t \geq 0 \\ \mathbf{0} & t < 0 \end{cases}$$

where $\boldsymbol{\iota}$ is a constant vector. The other is a bolus or instantaneous injection, and although it can be considered as an impulse or Dirac δ-function input, it is simpler to consider it as determining a vector of initial conditions $\boldsymbol{\gamma}(0) = \boldsymbol{\gamma}_0$.

Example: Tetracycline 2

For the tetracycline example, the input is a bolus in the gut, and the transfer matrix $\mathbf{A}$ can be readily obtained by inspection of the differential equations (5.1) or from the system diagram (Figure 5.2), as

$$\mathbf{A} = \begin{bmatrix} -\theta_1 & 0 \\ \theta_1 & -\theta_2 \end{bmatrix}$$

The initial concentration of tetracycline hydrochloride in the gut is unknown, but the concentration in the serum is assumed to be zero, so we incorporate another parameter θ_3 and write $\boldsymbol{\gamma}_0 = (\theta_3, 0)^T$. ■

Example: Oil shale 2

For the model (5.2) suggested by Ziegel and Gorman (1980),

$$\mathbf{A} = \begin{bmatrix} -\theta_1-\theta_4 & 0 & 0 \\ \theta_1 & -\theta_2-\theta_3 & 0 \\ \theta_4 & \theta_2 & 0 \end{bmatrix}$$

The recorded measurements for bitumen and oil are percentages of the initial amount of kerogen, so we take $\boldsymbol{\gamma}_0 = (100, 0, 0)^T$. Ziegel and Gorman (1980) found it necessary to incorporate a fifth parameter in the model to account for the unknown dead time before the reaction began. ■

5.2 Estimating Parameters in Compartment Models

Several methods can be used to estimate parameters in compartment models. The most obvious is to obtain the analytic solution to the system of differential equations and then use the expectation function corresponding to the compartment for which data are available in a standard nonlinear estimation program. A second approach is to use a standard nonlinear estimation program, but calculate the function by solving the equations using numerical integration. A third approach (Anderson, 1983) is to recognize that the responses $\gamma_1, \gamma_2, \ldots, \gamma_K$ generally consist of weighted sums of exponential functions of time, with the exponents related to the system rate constants $\boldsymbol{\theta}$. One can then fit a general sum of exponentials model and derive estimates for the rate constants and other parameters. This is not efficient, especially when the fitting is done using the process of *peeling* (see Sections 3.3 and 3.9). A fourth and superior *matrix exponential* approach, proposed by Jennrich and Bright (1976), generates the solution to the system of equations by calculating values for the model function $\boldsymbol{\gamma}(t)$ and its derivatives directly, given values of $\boldsymbol{\theta}$, t, and $\mathbf{u}(t)$.

The matrix exponential approach is superior to the analytic solution approach because it avoids the difficult and sometimes impossible task of deriving explicit expressions for the model function and its derivatives. In addition, it is possible to obtain the derivatives with respect to the parameters in the same way as the expectation function itself. It is superior to the numerical integration approach because it is faster and more accurate. And finally, it is superior to the sum of exponentials approach because it avoids having to solve for the rate constants in terms of the exponent and weight coefficients, and because the correct number of parameters is incorporated directly into the model.

In the matrix exponential approach, if only one compartment is observed, the expectation function $f(t, \boldsymbol{\theta})$ is simply the appropriate element of the vector $\boldsymbol{\gamma}(t)$, and, as discussed in Section 4.3.4, the function and its derivatives can be obtained from the general solution by multiplying the expected response matrix $\mathbf{H}$, and the derivative of the expected response matrix with respect to the parameters, by a $K \times 1$ vector which is 0 except for a 1 in the appropriate row. For ex-

ample, for the tetracycline data, the concentration of tetracycline hydrochloride in the serum is measured, and so $\eta = \gamma_2$; this response is therefore used in estimating θ_1 and θ_2, and the expected response matrix is multiplied by the vector $(0,1)^T$. In the oil shale example, oil and bitumen concentrations are available, and so the multiresponse expectation matrix $\mathbf{H} = (\gamma_2, \gamma_3)$ can be used to estimate the system parameters using the methods discussed in Chapter 4. In this case, the expected responses and their derivatives with respect to the parameters will be multiplied by the 3×2 rotation matrix $\mathbf{B}$, which consists of a row of zeros stacked above a 2×2 identity matrix.

5.2.1 Solving Systems of Linear Differential Equations

The general solution to (5.3) can be written

$$\gamma(t) = e^{\mathbf{A}t}\gamma_0 + e^{\mathbf{A}t} * \mathbf{u}(t) \tag{5.4}$$

where the matrix exponential $e^{\mathbf{A}t}$ represents the convergent power series

$$e^{\mathbf{A}t} = \mathbf{I} + \frac{\mathbf{A}t}{1!} + \frac{(\mathbf{A}t)^2}{2!} + \cdots \tag{5.5}$$

and the * denotes convolution,

$$e^{\mathbf{A}t} * \mathbf{u}(t) = \int_0^t e^{\mathbf{A}(t-u)}\mathbf{u}(u)\,du \tag{5.6}$$

The vector function is integrated componentwise.

Suppose $\mathbf{A}$ is *diagonalizable*, so there is a nonsingular matrix of eigenvectors, $\mathbf{U}$, and a diagonal matrix of eigenvalues, $\mathbf{\Lambda} = \mathrm{diag}(\lambda_1, \ldots, \lambda_K)$, such that

$$\mathbf{A} = \mathbf{U}\mathbf{\Lambda}\mathbf{U}^{-1}$$

Then

$$e^{\mathbf{A}t} = \mathbf{U}e^{\mathbf{\Lambda}t}\mathbf{U}^{-1}$$

with

$$e^{\mathbf{\Lambda}t} = \mathrm{diag}(e^{\lambda_1 t}, \ldots, e^{\lambda_K t})$$

General computational methods for evaluating the convolution integral are given in Appendix 5, and pseudocode is given in Appendix 3.

To develop the matrix exponential solution, we consider the special situation in which $\mathbf{A}$ is diagonalizable and the input is a bolus, so the system (5.3) can be written

$$\begin{aligned} \dot{\gamma} &= \mathbf{A}\gamma \qquad t > 0 \\ \gamma(0) &= \gamma_0 \end{aligned} \tag{5.7}$$

Then (5.7) becomes

$$\dot{\boldsymbol{\gamma}} = \mathbf{A}\boldsymbol{\gamma}$$
$$= \mathbf{U}\boldsymbol{\Lambda}\mathbf{U}^{-1}\boldsymbol{\gamma}$$

Premultiplying both sides of the equation by $\mathbf{U}^{-1}$, and letting $\boldsymbol{\xi} = \mathbf{U}^{-1}\boldsymbol{\gamma}$, gives

$$\dot{\boldsymbol{\xi}} = \boldsymbol{\Lambda}\boldsymbol{\xi}$$

which is a set of independent first order differential equations

$$\dot{\xi}_k = \lambda_k \xi_k \qquad k = 1, 2, \ldots, K$$

with solutions

$$\xi_k(t) = e^{\lambda_k t}\,\xi_k(0)$$

where $\xi_k(0)$ is the kth element of $\mathbf{U}^{-1}\boldsymbol{\gamma}_0$. Reverting to $\boldsymbol{\gamma} = \mathbf{U}\boldsymbol{\xi}$ gives

$$\boldsymbol{\gamma}(t) = \mathbf{U}e^{\boldsymbol{\Lambda}t}\mathbf{U}^{-1}\boldsymbol{\gamma}_0 = e^{\mathbf{A}t}\boldsymbol{\gamma}_0 \tag{5.8}$$

Thus, for a bolus or impulse input, the convolution integral (5.6) reduces to (5.8).

Example: Tetracycline 3

For the tetracycline example, $\boldsymbol{\gamma}_0 = (\theta_3, 0)^{\mathrm{T}}$, and

$$\mathbf{A} = \begin{bmatrix} -\theta_1 & 0 \\ \theta_1 & -\theta_2 \end{bmatrix} \tag{5.9}$$

For this simple system, we can calculate eigenvalues and eigenvectors of the transfer matrix (5.9) and use these to obtain explicit analytic expressions for the responses. Thus,

$$\boldsymbol{\Lambda} = \begin{bmatrix} -\theta_1 & 0 \\ 0 & -\theta_2 \end{bmatrix}$$

and

$$\mathbf{U} = \begin{bmatrix} 1 & 0 \\ \dfrac{\theta_1}{\theta_2 - \theta_1} & -\theta_1 \end{bmatrix}$$

so

$$\mathbf{U}^{-1} = \begin{bmatrix} 1 & 0 \\ \dfrac{1}{\theta_2 - \theta_1} & -\dfrac{1}{\theta_1} \end{bmatrix}$$

and, using (5.8), the responses are

$$\gamma = \begin{bmatrix} \theta_3 e^{-\theta_1 t} \\ \dfrac{\theta_3\theta_1(e^{-\theta_1 t} - e^{-\theta_2 t})}{\theta_2 - \theta_1} \end{bmatrix}$$

■

5.2.1.1 Dead Time

For the oil shale data, it was noted that the system does not respond immediately to the input, so a "dead time," t_0, must be incorporated into the model. We then modify (5.3) to

$$\begin{aligned} \dot{\gamma}(\tau) &= A\gamma(\tau) + \iota(\tau) \\ \gamma(0) &= \gamma_0 \end{aligned} \tag{5.10}$$

where $\tau = (t - t_0)_+$, that is,

$$\tau = \begin{cases} t - t_0 & t > t_0 \\ 0 & t \le t_0 \end{cases}$$

where t_0 can be known or unknown. The general solution is then

$$\gamma(\tau) = \begin{cases} \gamma_0 & \tau \le 0 \\ e^{A\tau}\gamma_0 + e^{A\tau} * \iota(\tau) & \tau > 0 \end{cases} \tag{5.11}$$

Example: Tetracycline 4

The tetracycline data also shows evidence of dead time in the system. Fitting the model (5.1) gives the parameter estimates in Table 5.1. A plot of the data and the fitted response versus time, in Figure 5.4, shows a poor fit, since the fitted curve is too squat.

Allowing for dead time with a fourth parameter produces the estimates in Table 5.2 and the fitted curve plotted in Figure 5.5. This fit is better, especially for small time values. An extra sum of squares analysis, as in Table 5.3, confirms the need for dead time in the model. ■

Table 5.1 Parameter summary for the tetracycline model without dead time.

		Logarithm Scale		
Parameter	Value	$\ln\theta$	Std. Error	Correlation Matrix
θ_1	0.1830	−1.698	0.244	1.00
θ_2	0.4345	−0.8335	0.272	−0.96 1.00
$\gamma_1(0)$	5.996	1.791	0.318	−0.98 0.99 1.00

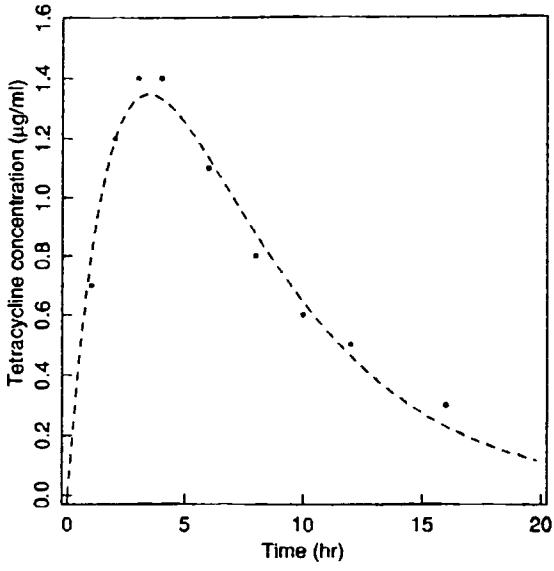

Figure 5.4 Plot of the tetracycline data and the fitted response curve for the model without dead time.

Table 5.2 Parameter summary for the tetracycline model with dead time.

		Logarithm Scale					
Parameter	Value	$\ln\theta$	Std. Error	Correlation Matrix			
θ_1	0.1488	−1.905	0.097	1.00			
θ_2	0.7158	−0.3343	0.176	−0.86	1.00		
$\gamma_1(0)$	10.10	2.312	0.198	−0.92	0.99	1.00	
t_0	0.4123		0.095	−0.54	0.81	0.77	1.00

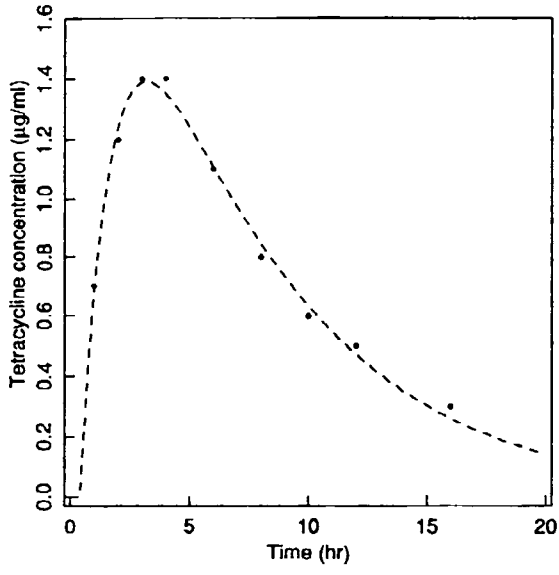

Figure 5.5 Plot of the tetracycline data and the fitted response curve for the model with dead time.

Table 5.3 Extra sum of squares analysis for dead time in the tetracycline model.

Source	Sum of Squares	Degrees of Freedom	Mean Square	F Ratio	p Value
Extra	0.02560	1	0.02560	12.736	0.016
4-parameter	0.01005	5	0.00201		
3-parameter	0.03565	6			

5.2.1.2 Cessation of Infusion

With continuous infusion there is sometimes another critical time, t_f, when the infusion is stopped. In pharmacokinetic studies, the period $0 < t \leq t_f$ is called the *on-infusion* stage, and the period $t > t_f$ is called the *off-infusion* stage. If there are measurements in the off-infusion stage, the model function during off-infusion, say $\boldsymbol{\gamma}_{\text{off}}(t)$, is evaluated by using the on-infusion model function evaluated at t_f, as the initial condition vector in a new system with $\boldsymbol{\iota} = \mathbf{0}$. Thus, assuming the initial conditions are zero, for the on-infusion stage we have

$$\boldsymbol{\gamma}_{\text{on}}(t) = e^{\mathbf{A}t} * \boldsymbol{\iota}(t) \qquad t \leq t_f$$

and for the off-infusion stage we have

$$\boldsymbol{\gamma}_{\text{off}}(t) = e^{\mathbf{A}(t-t_f)} \boldsymbol{\gamma}_{\text{on}}(t_f) \qquad t > t_f$$

5.2.2 Derivatives of the Expectation Function

To estimate the parameters using a Gauss–Newton procedure, we must evaluate the derivatives with respect to the parameters. As shown by Jennrich and Bright (1976), a great advantage of systems of linear differential equations is that these derivatives can be evaluated in the same manner as the model function itself. They differentiated the general solution (5.11) directly to get the gradient terms, but in Bates and Watts (1985), we exploited the interchangability of differentiation with respect to time and with respect to a parameter to generate another set of linear system of differential equations which can be solved directly.

As in Chapter 4, we use a subscript in parentheses to denote differentiation with respect to a parameter and write, for example,

$$\frac{\partial \boldsymbol{\gamma}(\tau)}{\partial \theta_p} = \boldsymbol{\gamma}_{(p)} \qquad p = 1, 2, \ldots, P$$

If only τ depends on θ_p, the derivative of $\boldsymbol{\gamma}(\tau)$ with respect to θ_p can be evaluated directly from (5.10) using the chain rule, so

$$\boldsymbol{\gamma}_{(p)}(\tau) = \tau_{(p)}[\mathbf{A}\boldsymbol{\gamma}(\tau) + \boldsymbol{\iota}] \tag{5.12}$$

When $\mathbf{A}$, $\boldsymbol{\gamma}_0$, or $\boldsymbol{\iota}$, but not τ, depends on θ_p, we get the derivative $\boldsymbol{\gamma}_{(p)}(\tau)$ by differentiating (5.10) with respect to θ_p to obtain

$$\dot{\boldsymbol{\gamma}}_{(p)}(\tau) = \mathbf{A}\boldsymbol{\gamma}_{(p)}(\tau) + \mathbf{A}_{(p)}\boldsymbol{\gamma}(\tau) + \boldsymbol{\iota}_{(p)}$$

This is simply another linear system of differential equations with driving function $\mathbf{A}_{(p)}\boldsymbol{\gamma}(\tau) + \boldsymbol{\iota}_{(p)}$, for which the solution is

$$\begin{aligned} \boldsymbol{\gamma}_{(p)}(\tau) &= e^{\mathbf{A}\tau}\boldsymbol{\gamma}_{(p)}(0) + e^{\mathbf{A}\tau} * [\mathbf{A}_{(p)}\boldsymbol{\gamma}(\tau) + \boldsymbol{\iota}_{(p)}] \\ &= e^{\mathbf{A}\tau}\boldsymbol{\gamma}_{(p)}(0) + e^{\mathbf{A}\tau} * \boldsymbol{\iota}_{(p)} + e^{\mathbf{A}\tau} * \mathbf{A}_{(p)} e^{\mathbf{A}\tau}\boldsymbol{\gamma}_0 + e^{\mathbf{A}\tau} * \mathbf{A}_{(p)} e^{\mathbf{A}\tau} * \boldsymbol{\iota} \end{aligned} \tag{5.13}$$

To get a general expression for θ_p determining any of τ, $\mathbf{A}$, $\boldsymbol{\gamma}_0$, and $\boldsymbol{\iota}$, we combine (5.13) and (5.12) to give the expression

$$\boldsymbol{\gamma}_{(p)}(\tau) = e^{\mathbf{A}\tau}\boldsymbol{\gamma}_{(p)}(0) + e^{\mathbf{A}\tau} * [\mathbf{A}_{(p)}\boldsymbol{\gamma}(\tau) + \boldsymbol{\iota}_{(p)}] + \tau_{(p)}[\mathbf{A}\boldsymbol{\gamma}(\tau) + \boldsymbol{\iota}] \tag{5.14}$$

which is true for an impulse or step input.

It is easy to evaluate $\mathbf{A}_{(p)}$, $\boldsymbol{\gamma}_{(p)}(0) = \partial\boldsymbol{\gamma}_0/\partial\theta_p$, $\boldsymbol{\iota}_{(p)}$, and $\tau_{(p)}$, since the elements of the derivatives are always -1, $+1$, or 0.

Note that the method can be extended to higher order derivatives: in particular, the derivative with respect to θ_p and θ_q is

$$\boldsymbol{\gamma}_{(pq)}(\tau) = e^{\mathbf{A}\tau} * (\mathbf{A}_{(p)}\boldsymbol{\gamma}_{(q)}(\tau)) + e^{\mathbf{A}\tau} * (\mathbf{A}_{(q)}\boldsymbol{\gamma}_{(p)}(\tau)) \tag{5.15}$$

since the elements of $\mathbf{A}_{(pq)}$, $\boldsymbol{\gamma}_{(pq)}(0)$, $\boldsymbol{\iota}_{(pq)}$, and $\tau_{(pq)}$ are all 0.

Example: Tetracycline 5

For the tetracycline example with delay time, we have $\tau=(t-\theta_4)_+$, $\gamma_0=(\theta_3, 0)^T$ and

$$\mathbf{A}=\begin{bmatrix}-\theta_1 & 0\\ \theta_1 & -\theta_2\end{bmatrix}$$

so that

$$\mathbf{A}_{(1)}=\begin{bmatrix}-1 & 0\\ 1 & 0\end{bmatrix}, \quad \mathbf{A}_{(2)}=\begin{bmatrix}0 & 0\\ 0 & -1\end{bmatrix}, \quad \mathbf{A}_{(3)}=\mathbf{A}_{(4)}=\begin{bmatrix}0 & 0\\ 0 & 0\end{bmatrix}$$

$$\gamma_{(1)}(0)=\gamma_{(2)}(0)=\gamma_{(4)}(0)=\begin{bmatrix}0\\ 0\end{bmatrix}, \quad \gamma_{(3)}(0)=\begin{bmatrix}1\\ 0\end{bmatrix}$$

$$\tau_{(1)}=\tau_{(2)}=\tau_{(3)}=0, \quad \tau_{(4)}=\begin{cases}-1 & \tau\geq 0\\ 0 & \tau<0\end{cases}$$

and all second derivatives of these quantities are zero. ■

The functions $\gamma_{(p)}(\tau)$, $p=1,\ldots,P$, are called the *sensitivity functions* of the system (Caracotsios and Stewart, 1985) and can be evaluated for any τ and $\boldsymbol{\theta}$ using (5.14) and the results of Appendix 5. Pseudocode for fitting compartment models is given in Appendix 3.

5.3 Practical Considerations

In this section we discuss some practical considerations related to fitting compartment models.

5.3.1 Parameter Transformations

A property of compartment models is that the rate constants, initial concentrations, and infusion rates must be positive. As discussed in Section 3.4, an effective way to ensure positive values is to use logarithms of the parameters in the model. This also enables linear approximation inference intervals for some important derived quantities to be obtained easily.

For example, the *half-life*, $t_{1/2}$, associated with the rate constant θ is $\ln 2/\theta \approx 0.693/\theta$. Then

$$\begin{aligned}\ln t_{1/2} &= \ln\ln 2-\ln\theta\\ &= -0.367-\ln\theta\end{aligned}$$

and the width of a linear approximation inference interval for $\ln t_{1/2}$ is the same

as the width of the interval for $\ln \theta$.

Another derived quantity of interest in pharmacological studies is the *volume of distribution* in a compartment. With a bolus injection, the dose, say D, in the initial compartment is known, but the concentration γ_0 is estimated. These are related by

$$\gamma_0 = \frac{D}{V_i}$$

where V_i is the volume of distribution for the injection compartment. Again, the logarithms of γ_0 and V_i are linearly related, $\ln V_i = \ln D - \ln \gamma_0$, and linear approximation confidence intervals on the logarithms have the same width.

A third derived quantity of interest in pharmacological studies is the *area under the curve* (AUC). For many simple compartment models this is equal to the initial concentration in the injection compartment, say $\gamma_1(0)$, divided by the elimination rate, say θ_1, so $\text{AUC} = \gamma_1(0)/\theta_1$. Again, $\ln \text{AUC}$ is linearly related to $\ln \gamma_1(0)$ and $\ln \theta_1$, so linear approximation confidence intervals for $\ln \text{AUC}$ are easily calculated.

In chemical kinetics, sometimes data are collected under different experimental conditions, and the analyst would like to combine the data in order to fit a more general model, as discussed in Section 3.11 and demonstrated in Section 5.5. In these cases, it is often assumed that the rate constants depend on the absolute temperature T according to an Arrhenius relation ($\theta \propto e^{-k/T}$) multiplied by products of pressures P_i raised to powers. For these models, the logarithms of the rate constants are linear functions of $1/T$ and $\ln P_i$, which provides another rationale for using logarithms.

An apparent disadvantage of using logarithms is that we cannot use linear approximation inference intervals to indicate whether a parameter could be zero, because they will never contain points corresponding to zero. However, a logarithm which is tending to a large negative value suggests that the parameter might be zero, and by using the matrix exponential method it is straightforward to eliminate that path or term in the compartment model, and then compare the reduced model with the original model using an extra sum of squares analysis. Besides, as explained in Section 3.10, the extra sum of squares test is more valid than the approximate t test for nonlinear regression.

5.3.2 Identifiability

A problem in fitting compartment models *when only one response is observed* is that some configurations result in exchangable parameters. This can cause problems in estimation, as mentioned in Section 3.4.1, because discrete sets of parameters give the same predicted responses. The parameters in such models are said to be *locally* identifiable rather than *globally* (uniquely) identifiable (Godfrey, 1983). For example, in the system of Figure 5.6 with $\boldsymbol{\gamma}_0 = (1, 0, 0)^{\mathrm{T}}$, the same $\gamma_3(t)$ curve results for the parameter pair (a, b) as for (b, a), so when only the third compartment is measured, the parameters θ_1 and θ_2 are exchang-

able.

A worse problem, though, is *unidentifiable* models, where continuous *sets* of parameters give the same predictions. For example, the system of Figure 5.7 produces the same $\gamma_1(t)$ curve for any set of parameters which satisfy

$$\theta_1 + \theta_2 = a$$

$$\theta_3 + \theta_4 = b$$

$$\theta_1\theta_3 + \theta_1\theta_4 + \theta_2\theta_4 = c$$

Thus continuous subspaces of the parameter space give the same predictions, so there are no unique parameter estimates for this system if only γ_1 is observed. However, if either θ_1 or θ_4 is zero, the system is identifiable.

A straightforward way to check the local identifiability of a compartment model with only one observed response is to fix a set of design times and generate the parameter derivative matrices at a number of different parameter values. If the matrices are all computationally singular, the model can be assumed to be unidentifiable. Note that we must use several parameter values, since a particular derivative matrix could be computationally singular due to an unfortunate choice of parameter values.

The ambiguity of compartment models when only one compartment is observed provides motivation for multiresponse experiments. The additional information not only provides better estimates of the parameters, but permits better discrimination between competing models.

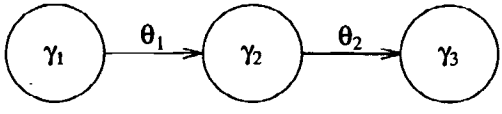

Figure 5.6 A system which has exchangable parameters when only γ_3 is observed.

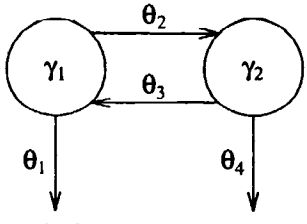

Figure 5.7 A system which is unidentifiable when only γ_1 is observed.

5.3.3 Starting Values

Obtaining starting values for compartment models can be difficult in the uniresponse case. Peeling (see Section 3.3) can be used, but an alternative procedure is to start with a simple model, such as a 1-compartment model, and extend it.

A plot of the data can be used to estimate the initial concentration and the single rate constant, and a plot of the residuals can then reveal how the model should be extended. The parameter estimates from the 1-compartment model can then be used to derive estimates for the rate constants in the new model. The model is extended as necessary, gradually adding compartments and paths, and using parameter estimates from the current model to obtain starting estimates for the next.

5.4 Lipoproteins: A Case Study

The ease with which compartment models can be fitted using the matrix exponential approach enables an analyst to try many different models on the same data set, and so engage in highly effective model development. To demonstrate this process, we consider the lipoprotein data in Table 23.1 of Anderson (1983), reproduced in Appendix 1, Section A1.16. The single response is the percentage concentration of a tracer in the serum of a baboon given a bolus injection at time 0. It is assumed that there is an initial concentration of 100% in compartment 1 and zero in all other compartments.

5.4.1 Preliminary Analysis

The data are plotted in Figure 5.8, from which it can be seen that there is a decrease in concentration through time, indicating elimination from the serum compartment. From a semilog plot of concentration versus time, it is apparent that there are at least 2 compartments, but to begin developing a model we fit a 1-compartment elimination model, as shown in Figure 5.9.

5.4.2 One Compartment

We see from the plot that the concentration has reached 46% by time 0.5 day, and so the starting value for the rate constant is

$$\theta = \frac{-\ln 0.46}{0.5}$$

$$\approx 1.55$$

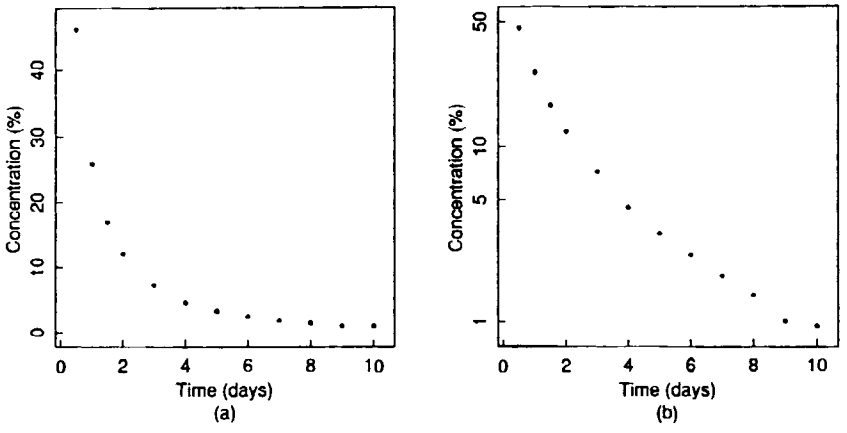

Figure 5.8 Plot of the lipoprotein concentration versus time, on a linear scale in part *a*, and on a logarithmic scale in part *b*.

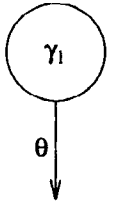

Figure 5.9 A 1-compartment elimination model.

Convergence to $\hat{\theta} = 1.31$ was achieved with a residual sum of squares of 133 on 11 degrees of freedom.

5.4.3 Two Compartments

The residuals, plotted against time in Figure 5.10, have a noticeable pattern, suggesting that the model initially underestimates and then overestimates the concentration. This pattern is consistent with the presence of another compartment with a system diagram as in Figure 5.11, possibly with θ_2 and θ_3 equal. It is easy to fit such a 2-parameter model first and use the estimates to provide starting values for a 3-parameter model.

To get starting estimates for the 2-parameter model, we let $\theta_1 + \theta_2 = 1.31$ from the 1-compartment model fit, and try $\boldsymbol{\theta}^0 = (1.0, 0.31)^T$. Convergence was obtained to $\hat{\boldsymbol{\theta}} = (0.992, 0.663)^T$ with a residual sum of squares of 2.65 on 10 degrees of freedom. Allowing θ_2 and θ_3 to differ, we used starting estimates $\boldsymbol{\theta}^0 = (0.99, 0.67, 0.65)^T$, which yielded $\hat{\boldsymbol{\theta}} = (1.022, 0.662, 0.820)^T$ with a residual sum of squares of 1.26 on 9 degrees of freedom.

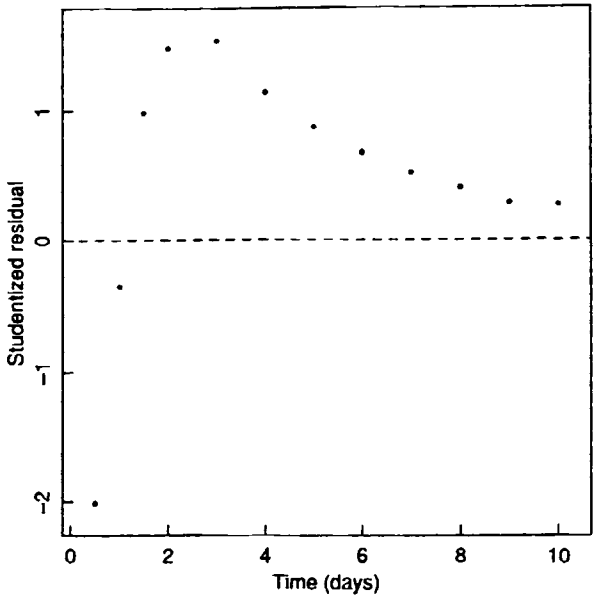

Figure 5.10 Residuals from a 1-compartment model fitted to the lipoprotein data.

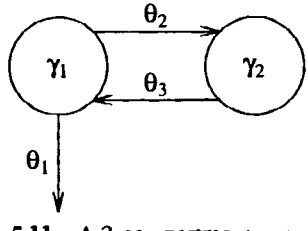

Figure 5.11 A 2-compartment open model.

5.4.4 Three Compartments

The residuals from the 3-parameter model, plotted in Figure 5.12, still display a pattern, so we continue to extend the model. We can extend it in a number of different ways: if the experimenter was uncertain how the concentrations were normalized to produce $\gamma_1(0) = 100$, we could introduce a parameter to represent this initial value, or we could introduce a delay time into the model, or (as seems more appropriate in this case) we could introduce another compartment. Even when introducing a third compartment, however, we must decide how to do so. The simplest extensions are the *catenary* system (in which the compartments are chained together), and the *mamillary* system (in which each "daughter" compartment communicates only with the central "mother" compartment.) A catenary system is shown in Figure 5.13, and a mamillary system is shown in

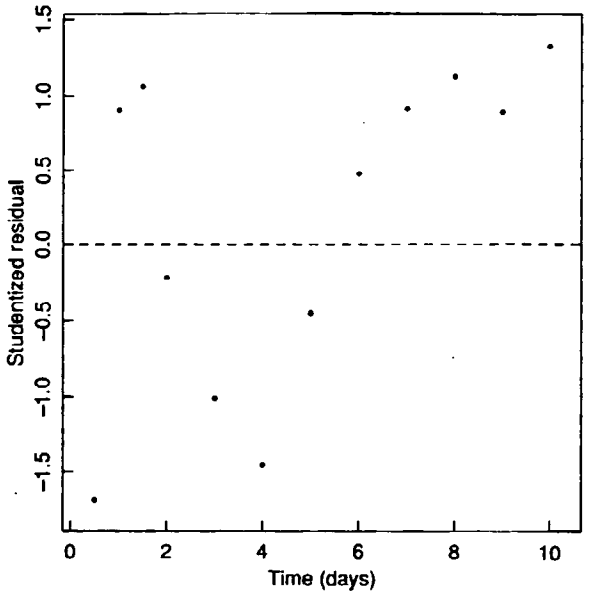

Figure 5.12 Residuals from a 2-compartment model fitted to the lipoprotein data.

Figure 5.14.

To fit these systems, we could use 5, 4, or 3 parameters by assuming some of the parameters equal. We chose to fit the 5-parameter models and examine the fits to determine a simple adequate model.

For the catenary model we added two parameters with values smaller than, and distinct from, the current parameter estimates to produce the starting estimates

$$\boldsymbol{\theta}^0 = (1.00, 0.66, 0.82, 0.5, 0.2)^T$$

from which we converged to

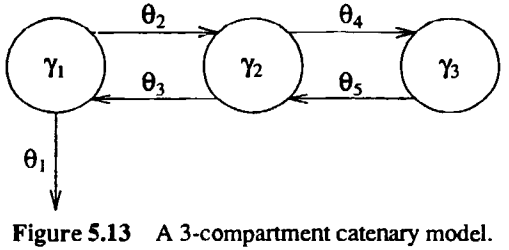

Figure 5.13 A 3-compartment catenary model.

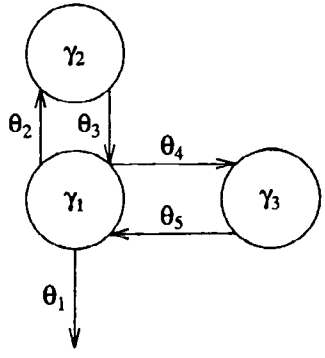

Figure 5.14 A 3-compartment mamillary model.

$$\hat{\boldsymbol{\theta}} = (0.990, 0.762, 1.015, 0.240, 0.352)^T$$

with a residual sum of squares of 0.043 on 7 degrees of freedom.

Using the same starting values, the mamillary model converged to

$$\hat{\boldsymbol{\theta}} = (0.990, 0.532, 1.340, 0.231, 0.267)^T$$

with the same residual sum of squares as the catenary model. The residuals (for both models) are shown in Figure 5.15, and are well behaved.

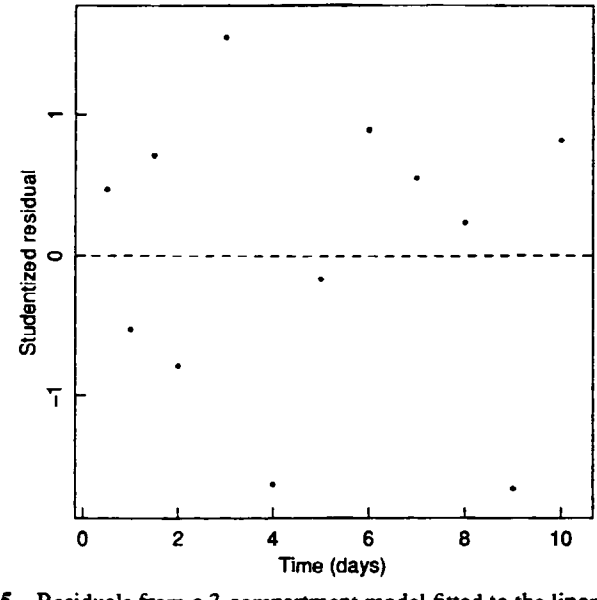

Figure 5.15 Residuals from a 3-compartment model fitted to the lipoprotein data.

It is not an accident that the same residuals and the same sum of squares occur for these two models, since they are equivalent when compartment 1 is the only one measured. Thus, for this data set, the model is not identifiable. Writing $\boldsymbol{\phi}$ for the parameters of the catenary model and $\boldsymbol{\theta}$ for the mamillary model parameters, the equivalence is given by

$$\begin{aligned}
\phi_1 &= \theta_1 \\
\phi_2 &= \theta_2 + \theta_4 \\
\phi_3 + \phi_4 + \phi_5 &= \theta_3 + \theta_5 \\
\phi_3\phi_5 &= \theta_3\theta_5 \\
\phi_2\phi_4 + \phi_2\phi_5 &= \theta_2\theta_5 + \theta_3\theta_4
\end{aligned}$$

5.4.5 Three Compartments, Common Parameters

The extra sum of squares due to extending the model from two to three compartments was highly significant [an extra sum of squares ratio of 97 to be compared with an $F(2,7)$ distribution]. We now try to simplify the model by letting some parameters be equal. We take starting values from the 5-parameter fits using the average of the pair of rate constants with the smallest difference relative to the standard error of the difference, so that, for both models, we equate θ_4 and θ_5. For the catenary model, we converged to $\hat{\boldsymbol{\theta}} = (0.967, 0.778, 0.948, 0.224)^T$ with a residual sum of squares of 0.062, and for the mamillary model, to $\hat{\boldsymbol{\theta}} = (0.978, 0.558, 1.27, 0.213)^T$ with a residual sum of squares of 0.050. The parameter estimates and approximate standard errors strongly suggest that none of the other parameters are equal, and so we do not reduce the models further.

Normal plots and plots of the residuals versus time and versus the fitted response (not shown) did not show inadequacy of the 4-parameter models. The judgement of which model to use must then be based on extra sum of squares analyses and the opinion of the experimenter as to which model is better. Extra sum of squares analyses for the nested models are shown in Table 5.4.

5.4.6 Conclusions

The conclusion of this analysis is that the data can be adequately fitted by a 3-compartment model in either the catenary or mamillary configuration. For five rate constants, the two models are equivalent: for four rate constants, slightly better results are obtained with the mamillary configuration. Whether or not equal rate constants is physically sensible must be decided by the experimenter on the basis of theory or on the basis of further experimental results.

Table 5.4 Extra sum of squares analyses for compartment models fitted to the lipoprotein data. The models with 4 parameters are the 3-compartment catenary (model 1) and the 3-compartment mamillary (model 2), each with two of the rate constants contrained to be equal. The 5-parameter 3-compartment model is model 3.

Source	Sum of Squares (10^{-6})	Degrees of Freedom	Mean Square (10^{-7})	F Ratio	p Value
Extra	1.857	1	18.57	3.0	0.13
Model 3	4.339	7	6.20		
Model 1	6.196	8			
Extra	0.682	1	6.82	1.1	0.33
Model 3	4.339	7	6.20		
Model 2	5.021	8			

5.5 Oil Shale: A Case Study

As an example of multiresponse parameter estimation using compartment models, we return to the oil shale data obtained by Hubbard and Robinson (1950). This case study also demonstrates the use of process parameters to model kinetic parameters (see Section 3.11).

5.5.1 Preliminary Analysis

In Figure 5.16 we plot the two measured responses, oil and bitumen, versus time for the six temperatures. One thing to note from these plots is that kerogen decomposition occurs more rapidly with increased temperature; at 673 K there is a substantial fraction of bitumen after 100 minutes, but at 773 K there is only a small fraction after 10 minutes. This strongly suggests that the rate constants depend on temperature.

A common form of rate constant dependence upon temperature is the Arrhenius relation

$$k_i(T) = k_{i,0}\, e^{-E_i/RT} \tag{5.16}$$

where $k_i(T)$ is the rate constant at temperature T, $k_{i,0}$ is the preexponential term, E_i is the activation energy for the reaction, R is the universal gas constant of 1.987 cal/g-mole K, and T is the temperature in kelvins.

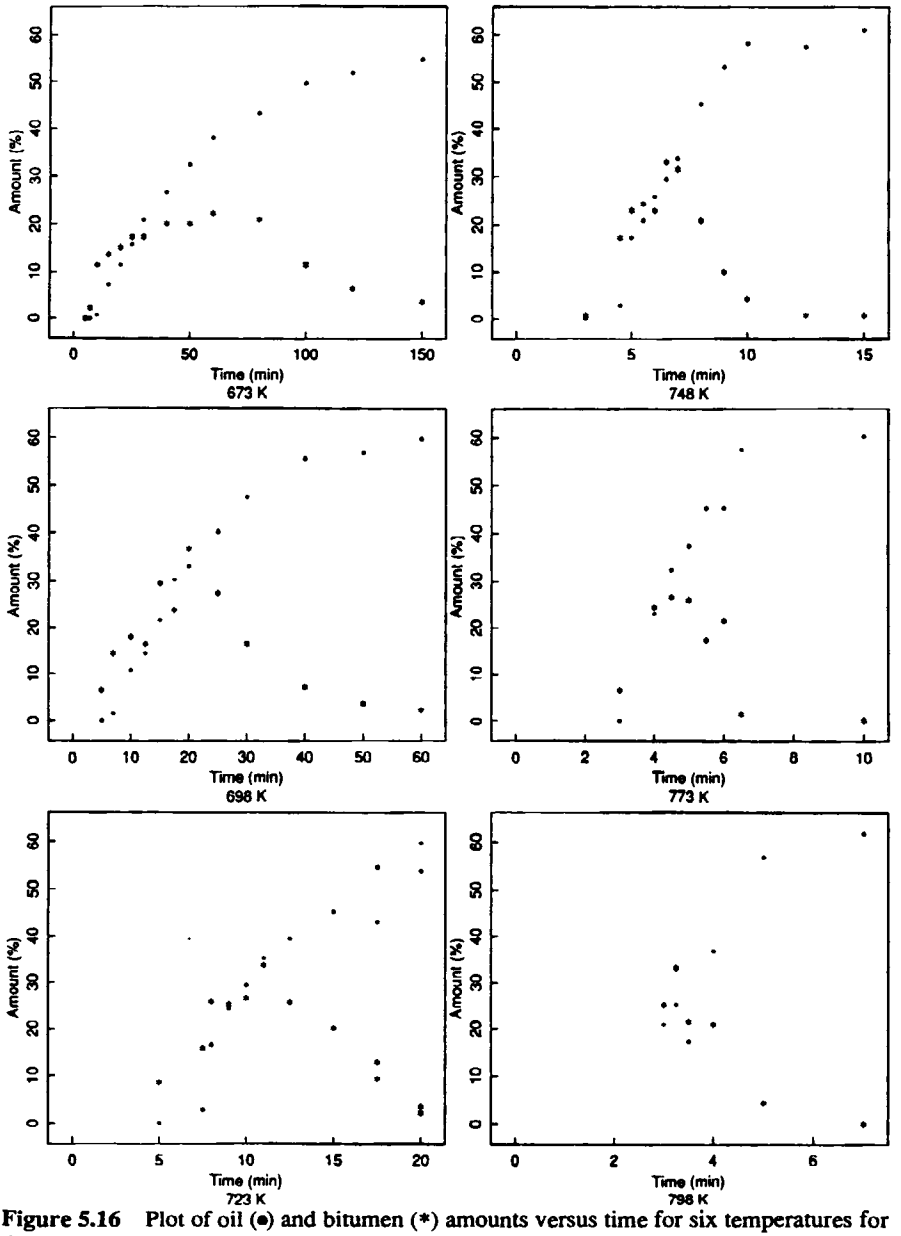

Figure 5.16 Plot of oil (•) and bitumen (*) amounts versus time for six temperatures for the oil shale pyrolysis data.

Estimating the activation energies and the preexponential terms usually results in highly correlated estimates, since the range of the observed temperatures is small relative to the mean temperature. To reduce the correlations, we

center the temperatures about an intermediate temperature, T_0, as discussed in Section 3.4.2, and write (5.16) as

$$k_i(T) = k_i(T_0)\exp\left[-\frac{E_i}{R}\left(\frac{1}{T}-\frac{1}{T_0}\right)\right]$$

Then

$$\ln k_i(T) = \ln k_i(T_0) - \frac{E_i}{R}\left(\frac{1}{T}-\frac{1}{T_0}\right) \tag{5.17}$$

$$= \phi_i - \frac{E_i}{R}\left(\frac{1}{T}-\frac{1}{T_0}\right)$$

so the logarithms of the rate constants depend linearly on the scaled inverse temperature.

5.5.2 Starting Values for the 673 K Data

To determine starting values for the process parameters, we first fit the kinetic model to the data at each individual temperature. This means that we must find starting estimates for the kinetic parameters, which can be done by modifying the approximate rate method described in Section 4.3.1.

For these data sets, only bitumen and oil have been measured at each time. The kerogen percentage is not measured, nor can it be inferred from a mass balance, since the by-products, coke and gas, are not measured either. However, we know that at time 0 the kerogen percentage is 100 while the percentage of the other species is zero. Substituting these values into the model

$$\frac{d\gamma_1}{dt} = -(\theta_1+\theta_4)\gamma_1$$

$$\frac{d\gamma_2}{dt} = \theta_1\gamma_1 - (\theta_2+\theta_3)\gamma_2$$

$$\frac{d\gamma_3}{dt} = \theta_4\gamma_1 + \theta_2\gamma_2$$

at time 0 produces

$$\frac{d\gamma_2(0)}{dt} = \theta_1\gamma_1(0)$$

$$= 100\,\theta_1$$

and

$$\frac{d\gamma_3(0)}{dt} = 100\,\theta_4$$

and we can use approximate rates from early observations of γ_2 and γ_3 to obtain starting estimates θ_1^0 and θ_4^0. From these, we can infer a percentage of kerogen as

$$\gamma_1(t) \approx 100\,e^{-(\theta_1^0+\theta_4^0)t}$$

and use the approximate rate method of Section 4.3.1 to obtain starting estimates θ_2^0 and θ_3^0.

The plot of the 673 K data in Figure 5.16 reveals evidence of dead time in the reactions, as described in Ziegel and Gorman (1980). We therefore use the first two nonzero observations of γ_2 and γ_3 to calculate θ_1^0 and θ_4^0 as

$$\theta_1^0 = \frac{1}{\gamma_1(0)}\left.\frac{d\gamma_2}{dt}\right|_0$$

$$= \frac{1}{100}\,\frac{11.5-2.2}{3}$$

$$= 0.031$$

and

$$\theta_4^0 = \frac{1}{100}\,\frac{7.2-0.7}{5}$$

$$= 0.013$$

A starting estimate of the dead time, $t_0^0 = 6$ minutes, is read from Figure 5.16. Using these values in the approximate rate procedure produces starting estimates of 0.0131 for θ_2^0 and 0.0286 for θ_3^0.

5.5.3 Fitting the Individual Temperature Data

The generalized Gauss–Newton algorithm converged to the parameter estimates shown in Table 5.5 with a determinant value of 428.

The converged values for the 673 K data can be used as starting estimates for the 698 K data, except for the dead time which we estimate from Figure 5.16 to be 5 minutes. Convergence was obtained to the results shown in Table 5.6.

To obtain starting estimates for the kinetic parameters at the other temperatures, we assume that an Arrhenius relation holds and fit linear models to the logarithms of the rate constants as a function of scaled inverse temperature. Extrapolations of these linear fits are used to get starting estimates for the kinetic parameters at the next temperature. Since the dead time decreases with in-

Table 5.5 Parameter summary for the oil shale data at 673 K.

		Logarithm Scale						
Parameter	Value	$\ln\theta$	Std. Error	Correlation Matrix				
θ_1	0.0172	−4.064	0.1219	1.00				
θ_2	0.00891	−4.721	0.2524	0.85	1.00			
θ_3	0.0200	−3.912	0.1117	0.30	0.64	1.00		
θ_4	0.0105	−4.557	0.0645	−0.71	−0.89	−0.36	1.00	
t_0	7.772		0.5263	−0.07	−0.34	−0.09	0.64	1.00

Table 5.6 Parameter summary for the oil shale data at 698 K.

		Logarithm Scale						
Parameter	Value	$\ln\theta$	Std. Error	Correlation Matrix				
θ_1	0.0784	−2.546	0.1648	1.00				
θ_2	0.0473	−3.051	0.2270	0.46	1.00			
θ_3	0.0510	−2.975	0.1560	0.02	0.75	1.00		
θ_4	0.0249	−3.694	0.2290	−0.48	−0.91	−0.47	1.00	
t_0	6.247		0.5065	−0.09	−0.53	−0.17	0.76	1.00

creasing temperature, we also regress t_0 on scaled inverse temperature and extrapolate to get starting estimates.

Care must be taken when fitting the 723 K data because there are two optima for the determinant criterion, as shown in Table 5.7. A plot of the data and

Table 5.7 Parameter summary for the oil shale data at 723 K, showing two optima.

Parameter	Optimum 1	Optimum 2
θ_1	0.2637	0.1596
θ_2	0.08496	0.1512
θ_3	0.1587	0.1020
θ_4	0.1248	0.02706
t_0	6.775	4.526
Determinant	28 309	53 422

the two sets of fitted curves, as in Figure 5.17, reveals that a tradeoff is being made: the oil concentration is best fitted with a dead time 6.8 minutes, while the bitumen concentration is best fitted with a dead time of 4.5 minutes. The optimum with the larger dead time has a smaller determinant, but from the plots and from consideration of the data at other temperatures, it appears that the predictions with the smaller dead time are better.

Individual fits were made to the data at the remaining temperatures and are recorded in Table 5.8.

5.5.4 Starting Estimates for the Process Parameters

To get starting estimates for the process parameters in the Arrhenius relation, we introduced the negative scaled inverse temperature variable

$$T_{\text{inv}} = \frac{-1000}{1.987}\left(\frac{1}{T} - \frac{1}{723}\right)$$

which centers about the middle temperature 723 K and includes a factor of 1000 to convert the units of the activation energy from cal/g-mole to the more convenient kcal/g-mole. The negative sign is used so that increasing T increases

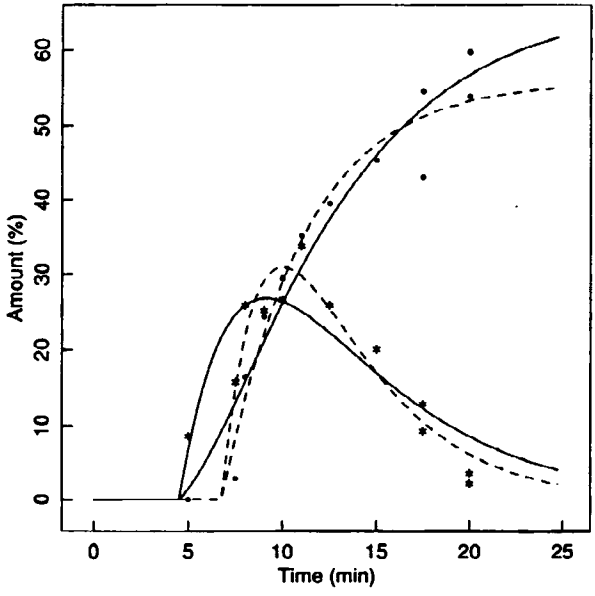

Figure 5.17 Plot of oil (•) and bitumen (*) amounts versus time for the temperatures for the oil shale data at 723 K. The fitted curves for a dead time of 4.5 minutes are shown as solid lines, and the fitted curves for a dead time of 6.8 minutes are shown as dashed lines.

Table 5.8 Parameter summary for the oil shale data at all temperatures together with the scaled inverse temperature variable and the parameters from a linear regression of each kinetic parameter on scaled inverse temperature.

Temperature (K)	$\ln\theta_1$	$\ln\theta_2$	$\ln\theta_3$	$\ln\theta_4$	t_0	T_{inv}
673	−4.064	−4.720	−3.912	−4.557	7.771	−0.0517
698	−2.546	−3.051	−2.975	−3.694	6.247	−0.0249
723	−1.835	−1.889	−2.283	−3.610	4.526	0.0000
748	−0.801	−1.252	−1.264	−2.082	4.082	0.0233
773	−0.447	−0.853	−0.803	−1.623	2.938	0.0450
798	0.287	−0.120	−0.297	−0.998	2.849	0.0654
Intercept:	−1.907	−2.335	−2.221	−3.056	5.146	
Slope:	35.73	37.27	31.37	31.09	−43.14	

T_{inv}.

The slopes and intercepts from linear regressions of each kinetic parameter on T_{inv}, included in Table 5.8, were used as starting estimates for the scaled preexponential and activation energies in the Arrhenius model. A plot of dead time versus T_{inv} indicated that a linear model for t_0 versus T_{inv} was also reasonable.

5.5.5 Fitting the Complete Data Set

We simultaneously fitted the data for both responses at all six temperatures to a model with ten process parameters, consisting of four rate constants (i.e., preexponential terms) and the dead time t_0 at 723 K, plus four activation energies and the slope of t_0 versus T_{inv}.

The final parameter summary is given in Table 5.9. Estimates of each of the kinetic parameters from the individual temperature data are plotted versus T_{inv} in Figure 5.18 together with the estimated Arrhenius relation from the process model. Each of the individual estimates is shown with bars representing approximate 95% HPD intervals. The process model for t_0 does not appear to follow the individual estimates well, but we note that t_0 is much more precisely determined at higher values of T_{inv}, where the Arrhenius relation fits the data well. Plots of the fitted curves versus time are overlaid with the original data in Figure 5.19. For low temperatures and early times, the model does not fit well.

Table 5.9 Parameter summary for the complete oil shale data set.

	Est.	Approx. Std. Error	Approximate Correlation Matrix								
ϕ_1	−1.920	0.079	1.00								
ϕ_2	−2.277	0.127	0.38	1.00							
ϕ_3	−2.195	0.076	0.52	0.09	1.00						
ϕ_4	−3.024	0.164	−0.02	−0.84	0.25	1.00					
t_0	4.406	0.227	0.50	−0.15	0.44	0.52	1.00				
E_1	38.14	1.956	0.08	−0.12	0.03	0.19	0.19	1.00			
E_2	34.25	3.303	−0.06	−0.17	−0.02	0.07	0.00	0.54	1.00		
E_3	34.41	1.848	0.01	−0.07	−0.16	0.10	0.14	0.45	0.30	1.00	
E_4	36.13	3.864	0.18	0.02	0.10	0.16	0.21	−0.25	−0.84	0.01	1.00
β	−24.67	3.311	−0.43	0.13	−0.39	−0.45	−0.96	−0.08	−0.01	−0.07	−0.12

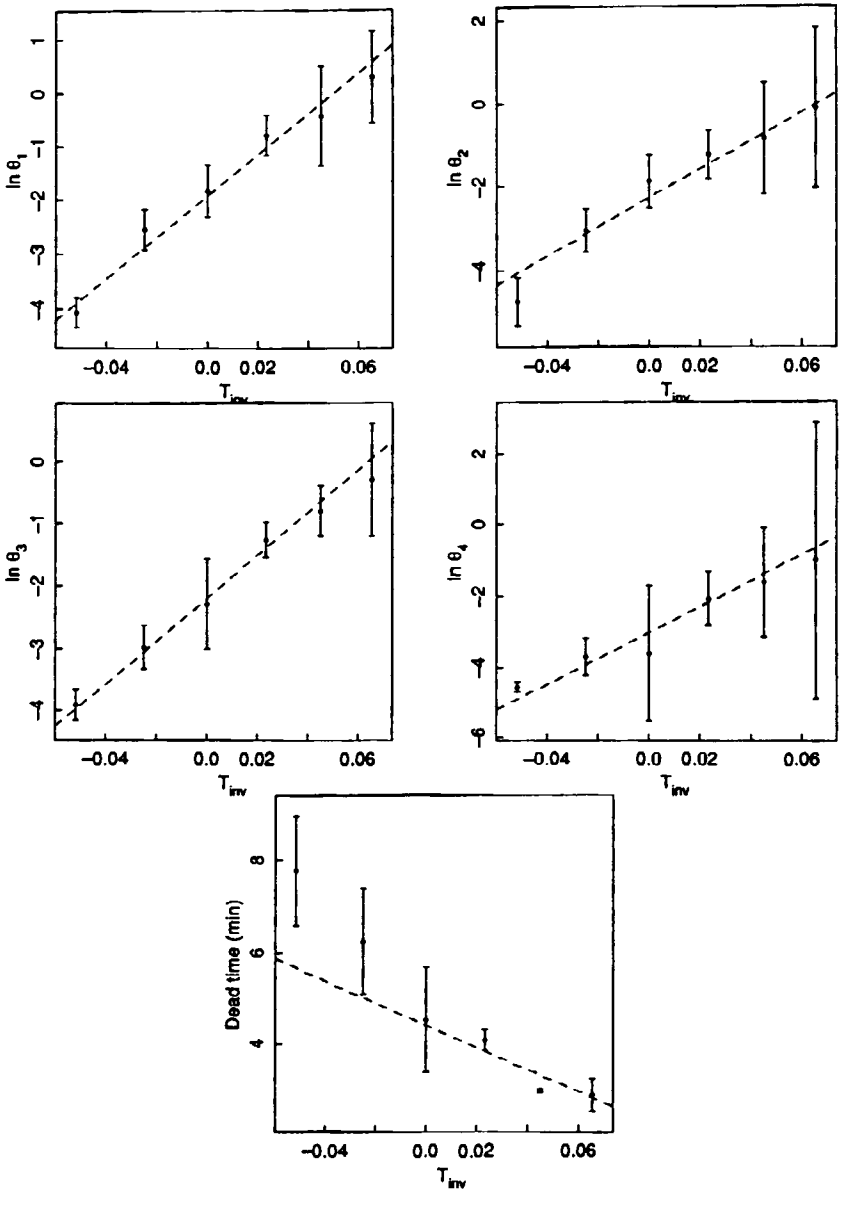

Figure 5.18 Plots of kinetic parameter estimates and Arrhenius model fits for the oil shale data. The kinetic parameter estimates and their approximate 95% inference intervals are shown as solid lines. The Arrhenius model fits are shown as dashed lines.

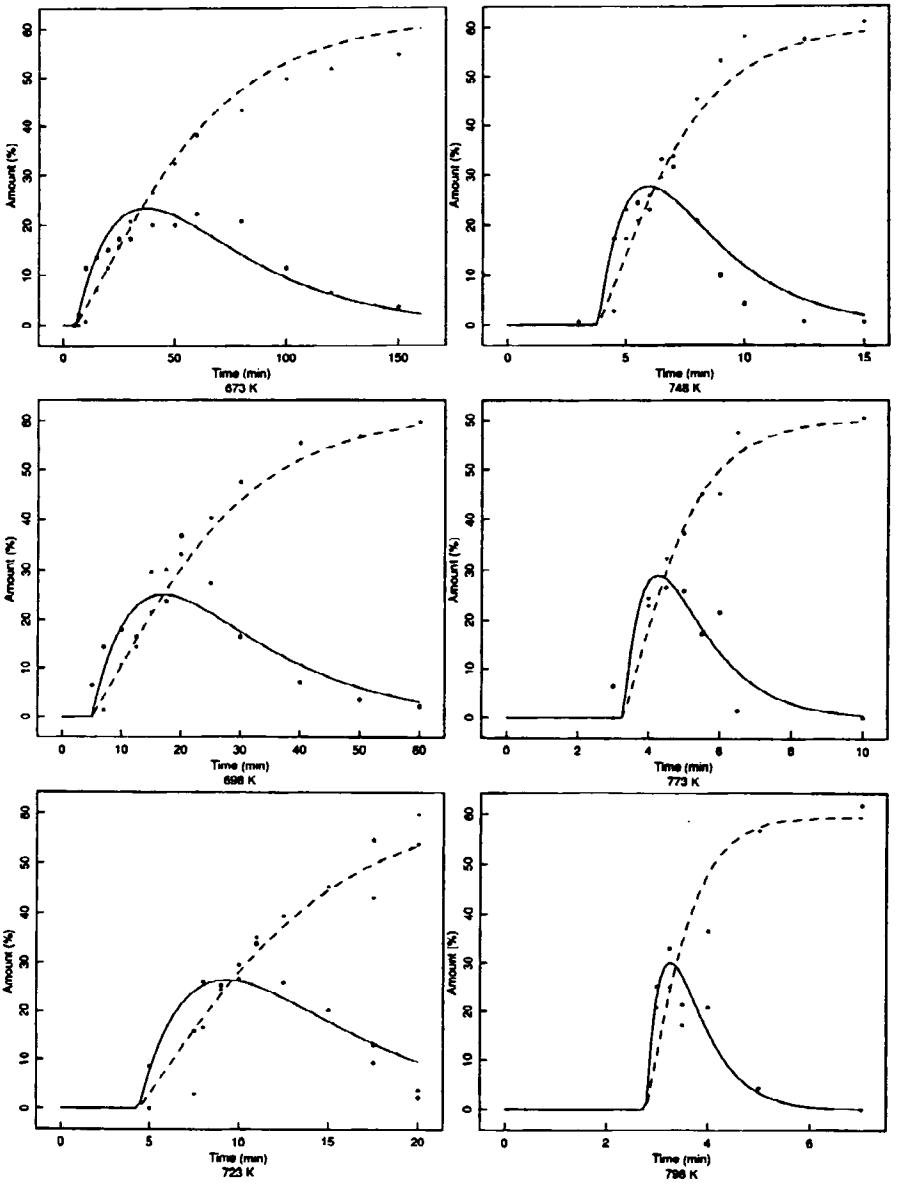

Figure 5.19 Plot of oil (•) and bitumen (*) amounts versus time for six temperatures for the oil shale pyrolysis data together with the fitted curves. The fitted curves for oil are shown as dashed lines, and those for bitumen as solid lines.

5.5.6 Conclusions

We have fitted the process model to the multiresponse data over a range of temperatures. The fitted parameters have reasonable values, and the assumptions on the disturbances do not appear inappropriate. However, the assumed kinetic model does have deficiencies, and so we should consult experts on chemical kinetics to try to formulate a better model. One obvious change in the model is to allow for different dead times for bitumen and for oil, with $t_0^{\text{oil}} > t_0^{\text{bitumen}}$.

Exercises

5.1 (a) Write a computer routine in a language of your choice to solve systems of linear differential equations, using the pseudocode of Appendix 3, Section A3.4. Assume that the transfer matrix A is diagonalizable.

(b) Extend the subroutine to evaluate derivatives of the expectation functions with respect to the parameters for bolus and step inputs.

5.2 (a) Show that the system matrix A for the chemical reaction with system diagram

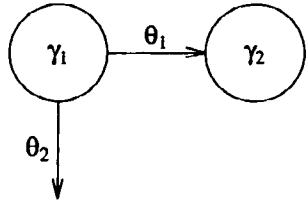

has eigenvalues $(-(\theta_1+\theta_2), 0)^T$ and eigenvectors

$$\mathbf{U} = \begin{bmatrix} \theta_1+\theta_2 & 0 \\ -\theta_1 & 1 \end{bmatrix}$$

with

$$\mathbf{U}^{-1} = \begin{bmatrix} \dfrac{1}{\theta_1+\theta_2} & 0 \\ \dfrac{\theta_1}{\theta_1+\theta_2} & 1 \end{bmatrix}$$

(b) Use the results from part (a) to show that the response at time t to an initial concentration of 100% in response 1 and 0% concentration in response 2 is

$$\boldsymbol{\gamma}(t) = \begin{bmatrix} e^{-(\theta_1+\theta_2)t} \\ \dfrac{\theta_1}{\theta_1+\theta_2}\left[1-e^{-(\theta_1+\theta_2)t}\right] \end{bmatrix}$$

5.3 Use the data from Appendix 4, Section A4.8 to fit a compartment model.

5.4 (a) Use the results from Example Tetracycline 5 to derive the derivatives of the model function with respect to the parameters.

(b) Verify that the derivatives in part (a) are correct by differentiating the explicit solutions for the functions given in Example Tetracycline 3.

5.5 Use a multiresponse parameter estimation criterion to fit the model from Example α-pinene 2, to the α-pinene data at 204.5°C given in Appendix 4, Section A4.6.

(a) Use the method of Section 4.3 to determine starting values.

(b) Use an extra determinant analysis to decide whether the path from allo-ocimene to pyronene is necessary.

CHAPTER 6.

Graphical Summaries of Nonlinear Inference Regions

"What can we know? or what
can we discern,
When error chokes the windows
of the mind?"

– Sir John Davies

So far we have assumed that linear approximations provide adequate summaries of the inferential results of a nonlinear analysis. Unfortunately, in many nonlinear analyses they will be woefully inadequate. In this chapter we present improved graphical methods for summarizing the inferential results of a nonlinear analysis, and in Chapter 7 methods for assessing the severity of the nonlinearity in an estimation situation.

6.1 Likelihood Regions

6.1.1 Joint Parameter Likelihood Regions

The spherical normal assumption for the disturbance $\mathbf{Z}$ in the model (2.2) dictates that statistical inference using the likelihood approach is closely linked to the geometry of the expectation surface in the response space. For linear and nonlinear models with the spherical normal assumption, a likelihood contour consists of all values of $\boldsymbol{\theta}$ for which $\boldsymbol{\eta}(\boldsymbol{\theta})$ is a fixed distance from $\mathbf{y}$, that is, all $\boldsymbol{\theta}$ for which $S(\boldsymbol{\theta})$ equals a constant. To associate a "confidence" level with a contour, by analogy with the linear model (1.39), we let the nominal $1-\alpha$ joint likelihood region be all values of $\boldsymbol{\theta}$ such that

$$S(\boldsymbol{\theta}) \le S(\hat{\boldsymbol{\theta}})\left[1+\frac{P}{N-P}F(P, N-P; \alpha)\right] \tag{6.1}$$

As with the linear model, this is the intersection of the expectation surface with a sphere centered at $\mathbf{y}$. Now, however, the surface is not planar and there is no easy way to map the points on the expectation surface back to the parameter space even if we could determine those points on the intersection.

When $P = 2$, we can determine a likelihood contour in $\boldsymbol{\theta}$ by standard contouring methods, that is, by evaluating $S(\boldsymbol{\theta})$ for a grid of $\boldsymbol{\theta}$ values and approximating the contour by straight line segments in the grid.

Example: Puromycin 13

Figure 6.1 shows nominal 80 and 95% likelihood contours for the Puromycin parameters. The contours are nearly elliptical and concentric, and the least squares estimate $\hat{\boldsymbol{\theta}}$ is well centered in the region. The linear approximation ellipses, shown as dashed lines, provide quite good approximate regions. ■

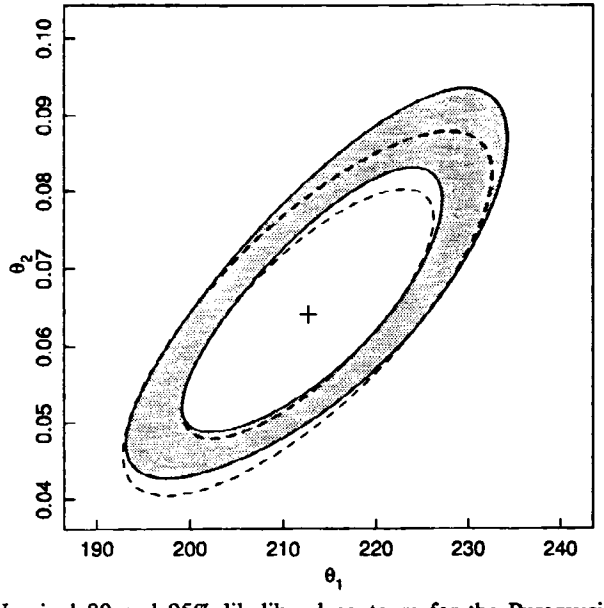

Figure 6.1 Nominal 80 and 95% likelihood contours for the Puromycin parameters. The dashed lines are the linear approximation ellipses, and the least squares estimate is indicated by +.

Example: BOD 7

Figure 6.2 shows nominal 80 and 95% likelihood contours for the BOD parameters, together with the linear approximation ellipses. These contours are not at all elliptical; in fact, the contours are more like hyperbolas, extending to ∞ in the positive θ_2 direction. The linear approximation ellipses are completely inadequate.

The occurrence of hyperbolic contours can be explained by looking at the data and the behavior of the model function, $f = \theta_1(1 - e^{-\theta_2 x})$. From Figure 6.3, where we plot the data and the estimated model function, we see that the data are very scattered and consequently the fitted model is not well determined.

Analyzing the model function, as $\theta_2 \to \infty$, the model reduces to $f = \theta_1$, and becomes insensitive to changes in θ_2. For large θ_2, therefore, the conditional estimate of θ_1 is $\bar{y}$. Setting $\boldsymbol{\theta} = (\bar{y}, \infty)^T$, which corresponds to fitting the data by the horizontal line in Figure 6.3, produces a sum of squares of 107.2. Since the data are so noisy, this fit is not significantly worse than the best fit of the nonlinear model, having an F ratio of

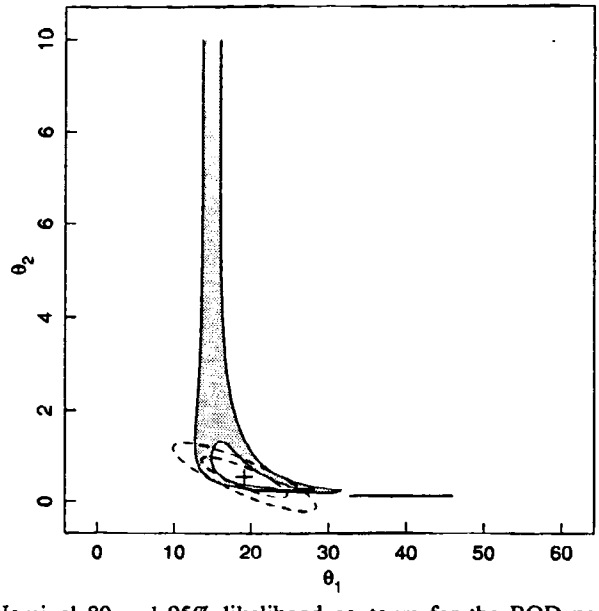

Figure 6.2 Nominal 80 and 95% likelihood contours for the BOD parameters. The dashed lines are the linear approximation ellipses, and the least squares estimate is indicated by +.

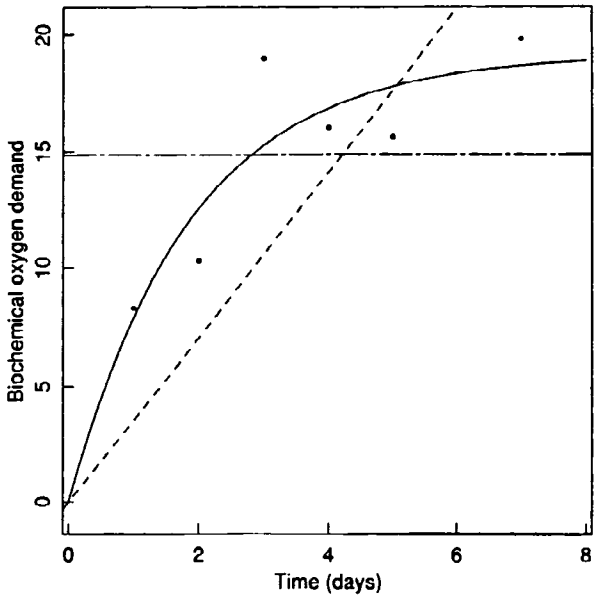

Figure 6.3 Estimated response curves for the BOD data. The solid line is the least squares response curve. The dashed line is the limiting curve as $\theta_2 \to 0$ and the dot–dashed line is the limiting curve as $\theta_2 \to \infty$.

$$\frac{[S((\bar{y},\infty)^{\mathrm{T}}) - S(\hat{\boldsymbol{\theta}})]/P}{S(\hat{\boldsymbol{\theta}})/(N-P)} = \frac{(107.21 - 25.99)/2}{25.99/4}$$

$$= 6.25$$

and a probability level of 94%. Thus, any likelihood contours at a nominal level greater than 94% will be open.

As $\theta_2 \to 0$, the model function reduces to

$$f(x,\boldsymbol{\theta}) = \theta_1 \theta_2 x$$

which gives a straight line through the origin with slope 3.52, as shown in Figure 6.3. Since the residual sum of squares for this straight line is 135.82, corresponding to an F ratio of 8.45 and a probability level of 96%, the likelihood contour will be open on the right for any nominal level greater than 96%.

For this example, then, the large scatter in the data and the form of the model function combine to produce hyperbolic-like contours which, for large enough confidence level, will be open. Consequently, the likelihood regions are not well approximated by linear approximation regions. ■

Determining the shape of badly distorted contours like those in Figure 6.2 can take several tries. We evaluated an initial grid of likelihood values and found that the contour went beyond the grid, so we changed the limits and reevaluated the grid, repeating the procedure until we obtained a satisfactory plot. The contours in Figure 6.2 illustrate another deficiency of standard contouring methods. The nominal 95% contour appears to have two disjoint pieces—the main body and a thin region centered near $\boldsymbol{\theta} = (40, 0)^T$. In fact, this contour should be one continuous curve, and the two pieces are an artifact of the way that the curve is traced by a computer program. Contouring programs typically have difficulty with long, thin segments of contours.

This discussion has focused on 2-parameter models, but nonlinear models with many more parameters occur and, unfortunately, standard contouring methods are not easily extended beyond $P = 2$. One approach for multiparameter models is to try to evaluate the likelihood on a P-dimensional grid. This can be expensive, since the amount of computing effort and the amount of storage required for the grid grows exponentially with P. Also, the analyst must choose the bounds of the grid before evaluating a contour, and these bounds may not encompass the entire contour, or they may be so wide that the resolution over the region of interest is poor. In this case, the analyst would have to guess at a new set of bounds and reevaluate the contour, thereby adding to the expense of the process. Even when the grid is evaluated, approximation of the contour and display of the approximation in many dimensions is difficult.

One way of avoiding multidimensional grids is to evaluate the sum of squares function on a series of 2-dimensional grids corresponding to each pair of parameters. This requires one grid for the (θ_1, θ_2) pair, one grid for the (θ_1, θ_3) pair, and so on, for a total of $P(P-1)/2$ grids. Contours on the 2-dimensional grids can be easily calculated and displayed, and from these contours the analyst can gain insight into the multidimensional shape of the likelihood region. However, it is not clear which likelihood or sum of squares to evaluate at each point in these 2-dimensional grids. Two choices are to evaluate the *conditional likelihood* function by varying a pair of parameters while holding the others fixed at their least squares estimates, or to evaluate the 2-dimensional *profile likelihood* function by finding the minimum sum of squares over all the other coordinates for each point on the grid.

Both these approaches have disadvantages. On the one hand, the conditional likelihood function does not always present a comprehensive view of the likelihood contour, since it only shows selected cross-sections of the contour, and the global behavior of the contour can be quite different from the sectional behavior. On the other hand, evaluating the profile likelihood requires solving a $(P-2)$-dimensional nonlinear least squares problem for each of the points on the $P(P-1)/2$ grids, which could be computationally expensive. To mitigate these difficulties, we propose making profile t plots and profile pair sketches as described in the next section.

6.1.2 Profile t Plots, Profile Traces, and Profile Pair Sketches

To develop marginal likelihood intervals for nonlinear model parameters, we begin by relating a linear model interval to the sum of squares function. For a linear model, a $1-\alpha$ marginal interval for β_p can be written in terms of the studentized parameter

$$\frac{\beta_p - \hat{\beta}_p}{\mathrm{se}(\hat{\beta}_p)} = \delta(\beta_p)$$

as

$$-t(N-P;\alpha/2) \le \delta(\beta_p) \le t(N-P;\alpha/2)$$

But the studentized parameter can also be written

$$\frac{\beta_p - \hat{\beta}_p}{\mathrm{se}(\hat{\beta}_p)} = \mathrm{sign}(\beta_p - \hat{\beta}_p)\sqrt{\tilde{S}(\beta_p) - S(\hat{\boldsymbol{\beta}})}\,/s \tag{6.2}$$

where

$$\tilde{S}(\beta_p) = \min_{\boldsymbol{\beta}_{-p}} S((\beta_p, \boldsymbol{\beta}_{-p}^{\mathrm{T}})^{\mathrm{T}}) = S((\beta_p, \tilde{\boldsymbol{\beta}}_{-p}^{\mathrm{T}})^{\mathrm{T}}) \tag{6.3}$$

is the profile sum of squares function and $\tilde{\boldsymbol{\beta}}_{-p} = (\tilde{\beta}_1, \ldots, \tilde{\beta}_{p-1}, \tilde{\beta}_{p+1}, \ldots, \tilde{\beta}_P)^{\mathrm{T}}$ is the least squares estimate of $\boldsymbol{\beta}_{-p}$ conditional on β_p. The notation $(\beta_p, \tilde{\boldsymbol{\beta}}_{-p}^{\mathrm{T}})^{\mathrm{T}}$ indicates the vector with elements $(\tilde{\beta}_1, \ldots, \tilde{\beta}_{p-1}, \beta_p, \tilde{\beta}_{p+1}, \ldots, \tilde{\beta}_P)$. (The derivation of (6.2) is assigned as Problem 6.2.)

For a nonlinear model, we define the *profile t* function, $\tau(\theta_p)$, as

$$\tau(\theta_p) = \mathrm{sign}(\theta_p - \hat{\theta}_p)\sqrt{\tilde{S}(\theta_p) - S(\hat{\boldsymbol{\theta}})}\,/s \tag{6.4}$$

using the same notation. By analogy with the linear model, we define a nominal $1-\alpha$ likelihood interval for θ_p as the set of all θ_p for which

$$-t(N-P;\alpha/2) \le \tau(\theta_p) \le t(N-P;\alpha/2)$$

The profile t function is similar to the χ statistic used by Bliss and James (1966).

Plots of the profile t function provide exact likelihood intervals for individual parameters and, in addition, reveal how nonlinear the estimation situation is. To see this, suppose the model were linear. Then a plot of $\tau(\theta_p)$ versus θ_p would be a straight line. In particular, as seen from (6.2), a plot of $\tau(\theta_p)$ versus the studentized parameter, $\delta(\theta_p) = (\theta_p - \hat{\theta}_p)/\mathrm{se}(\hat{\theta}_p)$, would be a straight line through the origin with unit slope. For a nonlinear model, a plot of $\tau(\theta_p)$ versus $\delta(\theta_p)$ will be curved, the amount of curvature giving information about the nonlinearity of the model.

Example: Puromycin 14

To make the profile t plot for θ_1 for the Puromycin data, we let $\delta(\theta_1) = 0.2, 0.4, \ldots,$ and for each value we converged on θ_2. This gave a series of values for θ_1, $\tilde{\theta}_2(\theta_1)$, and $\tau(\theta_1)$. Repeating the process to the left of the estimate gave the necessary data to plot $\tau(\theta_1)$ versus θ_1 as in Figure 6.4*a*.

In this figure, we have included a straight line with slope 1 (dashed), corresponding to the linear case, and axes in scales of δ and nominal confidence level, which make it easy to read off likelihood intervals. The nominal 99% likelihood interval for θ_1 is [191.1, 236.7], which is well approximated by the (symmetric) linear approximation interval [190.7, 234.7]. The profile t plot is only slightly curved, suggesting that the nonlinearity is slight.

The profile t plot for θ_2 is shown in Figure 6.4*b*, from which we see that the likelihood intervals are slightly skewed to the right. The nominal 99% likelihood interval for θ_2 is [0.0408, 0.0972], which is well approximated by the linear approximation interval, [0.0379, 0.0903]. The nonlinearity for θ_2 is somewhat worse than that for θ_1, but it is still small. ■

Example: BOD 8

Profile t plots for the BOD parameters are given in Figure 6.5*a* and *b*. The plots are badly curved and tend to asymptotes, indicating severe nonlinearity. The likelihood intervals are skewed and do not close on the right for levels above 98%. These observations are in accord with those made from the contour plot in Figure 6.2. The nominal 95% likelihood intervals are [14.05, 37.77] for θ_1 and [0.132, 1.77] for θ_2, which are very different from the linear approximation intervals, [12.2, 26.1] and

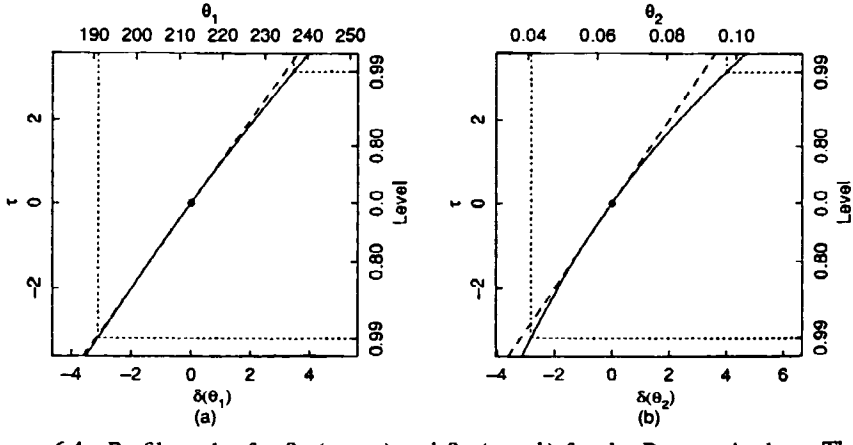

Figure 6.4 Profile t plot for θ_1 (part *a*) and θ_2 (part *b*) for the Puromycin data. The curve (solid) is the profile t, and the line (dashed) is the linear approximation. Dotted lines show the construction of a 99% marginal likelihood interval.

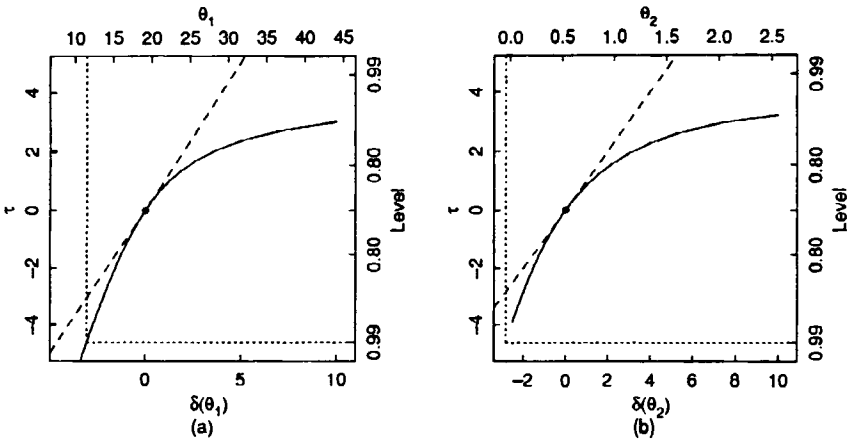

Figure 6.5 Profile t plot for θ_1 (part a) and θ_2 (part b) for the BOD data. The curve (solid) is the profile t, and the line (dashed) is the linear approximation. Dotted lines show the construction of a 99% marginal likelihood interval which extends to $+\infty$ in both cases, and is undefined on the left for θ_2.

[−0.033, 1.095]. ■

6.1.2.1 Profile Traces

Another useful plot is the likelihood *profile trace* obtained by plotting the components of the conditional maximum $\tilde{\boldsymbol{\theta}}_{-p}$ as a function of θ_p. For example, after evaluating the profile likelihood for θ_1, we can plot $\tilde{\theta}_2$ versus θ_1, $\tilde{\theta}_3$ versus θ_1, and so on, up to $\tilde{\theta}_P$ versus θ_1. Next, we evaluate the profile likelihood for θ_2 and plot $\tilde{\theta}_1$ versus θ_2, $\tilde{\theta}_3$ versus θ_2, and so on, up to $\tilde{\theta}_P$ versus θ_2. We continue to work through the parameters θ_3 to θ_P, calculating the conditional minima of the other parameters, and plotting the profile traces. Finally, we combine the plots of $\tilde{\theta}_q$ versus θ_p and $\tilde{\theta}_p$ versus θ_q, to generate the pairwise profile traces. As before, it is convenient to do the calculations using studentized parameters.

Plots of the profile traces provide useful information on how the parameters interact. For a linear model with studentized parameters, the profile traces on a plot of $\delta(\theta_q)$ versus $\delta(\theta_p)$ consist of straight lines intersecting at (0, 0) with slopes of $\{\mathbf{C}\}_{pq}$ for the trace of $\tilde{\delta}(\theta_q)$ on $\delta(\theta_p)$ and $1/\{\mathbf{C}\}_{pq}$ for the trace of $\tilde{\delta}(\theta_p)$ on $\delta(\theta_q)$, where $\mathbf{C}$ is the parameter correlation matrix. If the correlation between the parameters is zero, the angle between the profile traces is 90°.

For nonlinear models, the profile traces will be curved, the curving of the lines providing information on how the parameter estimates affect one another and on the shape of the projection of the likelihood contours onto the (θ_p, θ_q) plane. If the contours are long and thin, the profile traces will be close together; if the contours are fat, the profile traces will tend to be perpendicular; and if the contours are nearly elliptical, the profile traces will be straight.

Example: Puromycin 15

The profile traces for the Puromycin parameters are plotted in Figure 6.6, superimposed on the likelihood contours from Figure 6.1. We see that the profile traces are only slightly curved and, because they do not intersect at too sharp an angle, the contours should be fairly fat ellipses. Because the profile traces are quite straight, linear approximation regions should give good approximations to the joint likelihood regions. Inspection of the actual contours reveals that this is the case.

We also see that the profile traces intersect the contours where they are parallel to the coordinate axes, which graphically demonstrates that the likelihood profile traces are plots of the conditional likelihood values. ■

Example: BOD 9

The profile traces for the BOD parameters are plotted in Figure 6.7, superimposed on the likelihood contours. We see that the profile traces are badly curved, intersect at a sharp angle, and are coincident over a long range, indicating that the contours are long, tapering, and markedly nonelliptical. It is clear that the model–data set combination is highly nonlinear, and that linear approximation inference regions will be unsatisfactory, as was noted in Example BOD 7. The plots of the contours bear this out. ■

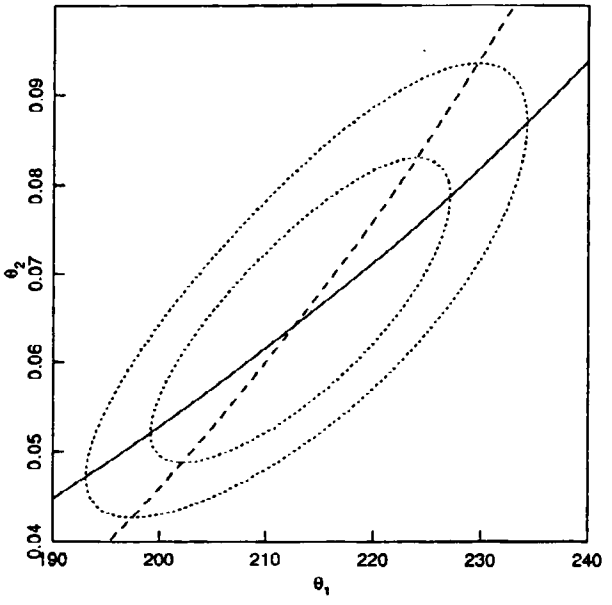

Figure 6.6 Likelihood profile traces for the Puromycin parameters, showing $\bar{\theta}_2$ on θ_1 (solid) and $\bar{\theta}_1$ on θ_2 (dashed). Nominal 80 and 95% likelihood contours (dotted) have been added to show that the solid lines intersect the contours at the vertical tangents to the contours and the dashed lines intersect the contours at the horizontal tangents.

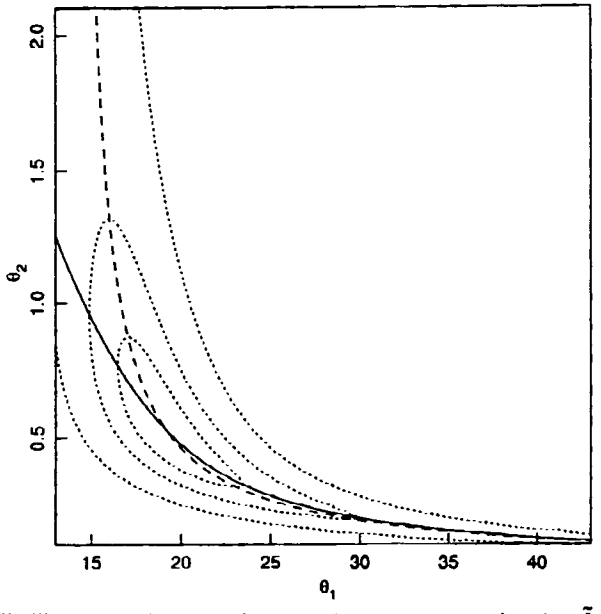

Figure 6.7 Likelihood profile traces for the BOD parameters, showing $\tilde{\theta}_2$ on θ_1 (solid) and $\tilde{\theta}_1$ on θ_2 (dashed). Nominal 50, 80, and 95% likelihood contours (dotted) have been added to show that the profile traces intersect the contours at the vertical or horizontal tangents to the contours.

6.1.2.2 Profile Pair Sketches

As stated earlier, it is not generally feasible to determine and plot likelihood contours for models with several parameters. However, we can use the profile sums of squares and the profile traces to create very accurate approximations to the 2-dimensional projections of the likelihood region and thus get a visual indication of the extent of the region and the nonlinear dependence of parameter estimates upon each other. To determine the projections of the 95% contour on the (θ_1, θ_2) plane, for example, we use the profile sum of squares for θ_1 to find where the contour intersects the trace of $\tilde{\theta}_2$ on θ_1. This gives two points on the contour. In addition, we know that the tangent to the contour must be vertical at these points, since they represent the bounds of the contour in the θ_1 direction. Similarly, from the profile sum of squares for θ_2 and from the trace of $\tilde{\theta}_2$ on θ_1, we determine two more points on the contour and we know that the contour will have horizontal tangents at these points.

By using all of this information—the profile t plots, the points on the contour, the directions of the tangent to the contour at these points, and the fact that the contour is bounded by the parameter values at these points—we can create a very accurate interpolation of a contour using the methods described in Appendix 6. We call these interpolated curves *profile pair sketches*.

Example: Puromycin 16

The coordinates on the traces corresponding to nominal 50, 80, 95, and 99% confidence levels for the Puromycin parameters are plotted in Figure 6.8*a* together with the contour sketches based on those points. The sketches and the exact contours are plotted in Figure 6.8*b*, from which it can be seen that the sketches are extremely accurate at all levels. This is in contrast to the linear approximation ellipses, shown in Figure 6.1, which deviate noticeably from the true contours. ■

Example: BOD 10

The coordinates corresponding to nominal 50, 80, and 90% confidence levels for the BOD parameters are plotted in Figure 6.9*a* together with the interpolated contours. Comparing the sketched contours with the exact contours in Figure 6.9*b* shows that even with these badly behaved contours, the sketches provide entirely adequate characterizations of the joint region. ■

When there are more than two parameters, a similar procedure is followed to generate the sketches. For example, with three parameters, for each of a set of values of θ_1 we converge to $\tilde{\boldsymbol{\theta}}_{-1} = (\tilde{\theta}_2(\theta_1), \tilde{\theta}_3(\theta_1))^T$, to produce $\tilde{S}(\theta_1)$. This information is used to calculate $\tau(\theta_1)$, the coordinates of the profile traces $\tilde{\theta}_2(\theta_1)$ and $\tilde{\theta}_3(\theta_1)$, and the coordinates of some of the points on the joint likelihood contour for (θ_1, θ_2) and for (θ_1, θ_3). Next, we choose a set of values for θ_2 and converge to $\tilde{\boldsymbol{\theta}}_{-2} = (\tilde{\theta}_1(\theta_2), \tilde{\theta}_3(\theta_2))^T$, this time producing $\tau(\theta_2)$, the coordinates of the profile traces $\tilde{\theta}_1(\theta_2)$ and $\tilde{\theta}_3(\theta_2)$, and the coordinates of some of the points on the joint likelihood contour for (θ_1, θ_2) and for (θ_2, θ_3). Then a range of values

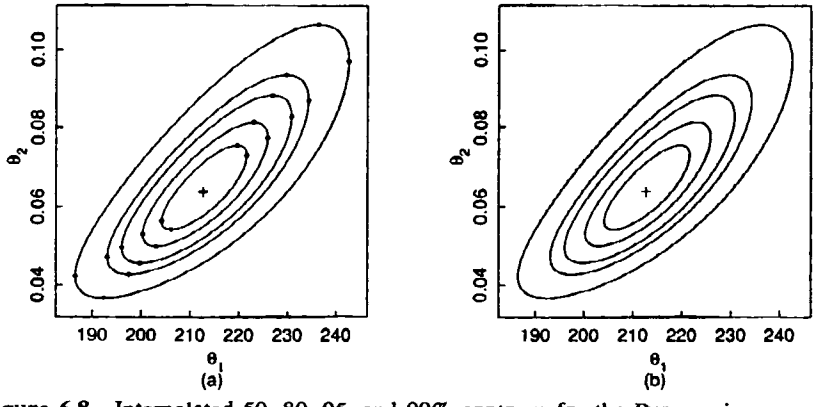

Figure 6.8 Interpolated 50, 80, 95, and 99% contours for the Puromycin parameters. Shown in part *a* are the interpolated contours with the points on the profile traces used to construct them, and in part *b*, the interpolated contours overlaid with the exact contours (dotted lines). On this scale, the exact contours cannot be distinguished from the interpolated contours.

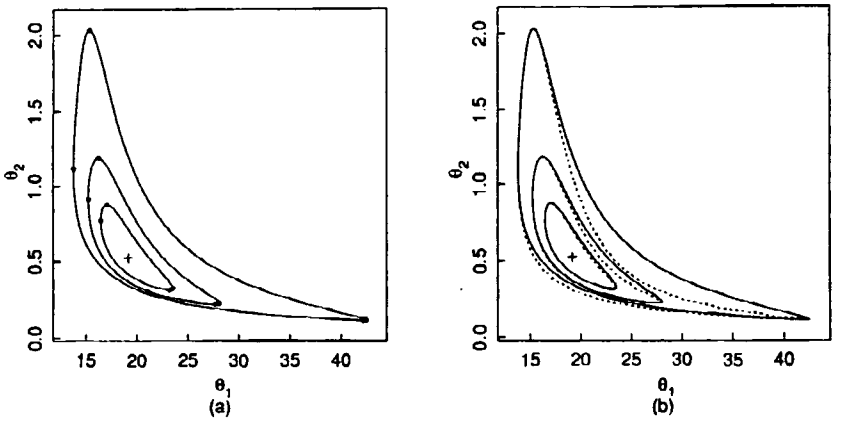

Figure 6.9 Interpolated 50, 80, and 90% contours for the BOD parameters. Shown in part *a* are the interpolated contours with the points on the profile traces used to construct them, and in part *b*, the interpolated contours overlaid with the exact contours (dotted lines).

of θ_3 is chosen and we converge to $\tilde{\boldsymbol{\theta}}_{-3} = (\tilde{\theta}_1(\theta_3), \tilde{\theta}_2(\theta_3))$, this time producing $\tau(\theta_3)$, the coordinates of the profile traces $\tilde{\theta}_1(\theta_3)$ and $\tilde{\theta}_2(\theta_3)$, and the coordinates of some of the points on the joint likelihood contour for (θ_1, θ_3) and for (θ_2, θ_3). We then plot the interpolated contours for each pair of parameters. If the profile traces are fairly straight and distinct in both the original and the τ coordinates, the contour will be fairly elliptical and the sketches will be very accurate. If the traces are curved in the original coordinates and tend to be coincident in the τ coordinates over an appreciable range, then the contours will be decidedly nonelliptical in the original coordinates and the sketches may not be accurate.

Example: Isomerization 5

Profile *t* plots for the isomerization data are shown in Figure 6.10, from which it can be seen that the parameters are very poorly determined. There is no upper bound on the likelihood intervals for the equilibrium constants even for nominal levels of 50%, so that effectively the only information about these parameters is that they are positive. Profile traces for some of the parameters, plotted in Figure 6.11, enable us to see why the equilibrium constants are so poorly determined.

The profile traces of θ_1 versus θ_3, shown in Figure 6.11*a*, look like a pair of sharply curved hyperbolas. These can be explained by noting that θ_1 appears only with θ_3 in the form of a product, and so values for which $\theta_1\theta_3 = \text{constant}$ will produce similar residual sums of squares, and therefore, hyperbolic traces.

The traces of the equilibrium constant θ_3 versus θ_2 shown in Figure 6.11*b* (and those for θ_4 versus θ_3, not shown) consist of a pair of coincident straight lines through the origin. This allows us to see why there is no

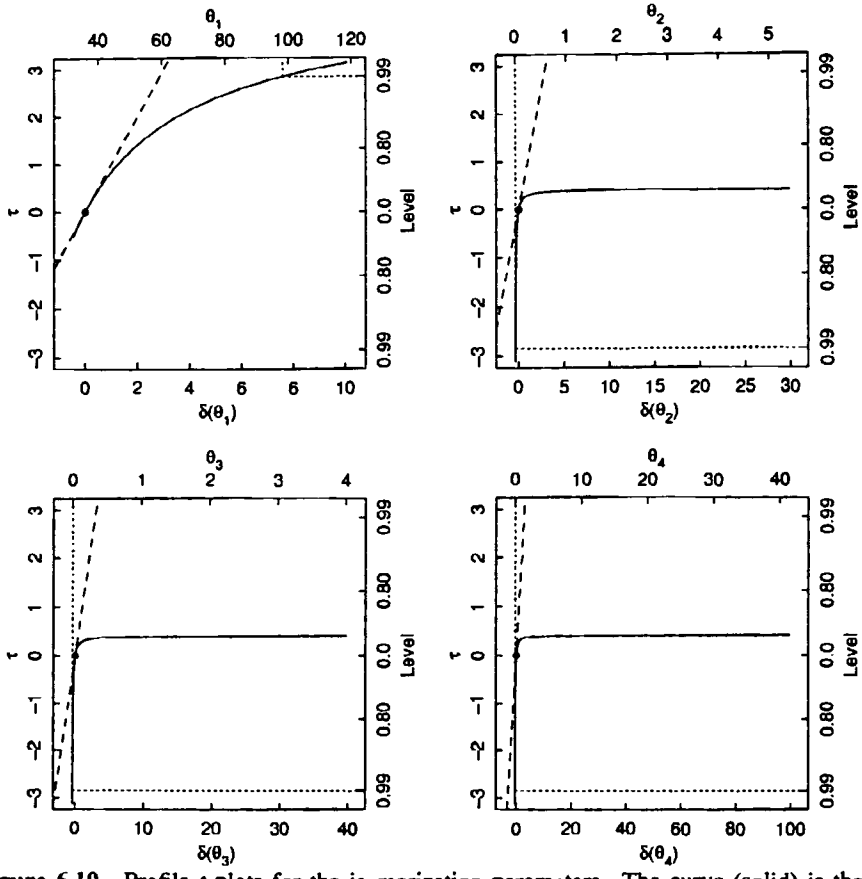

Figure 6.10 Profile t plots for the isomerization parameters. The curve (solid) is the profile t, and the line (dashed) is the linear approximation. Dotted lines show the construction of a 99% likelihood interval, which extends to $+\infty$ in three cases and which is not defined on the left for θ_1.

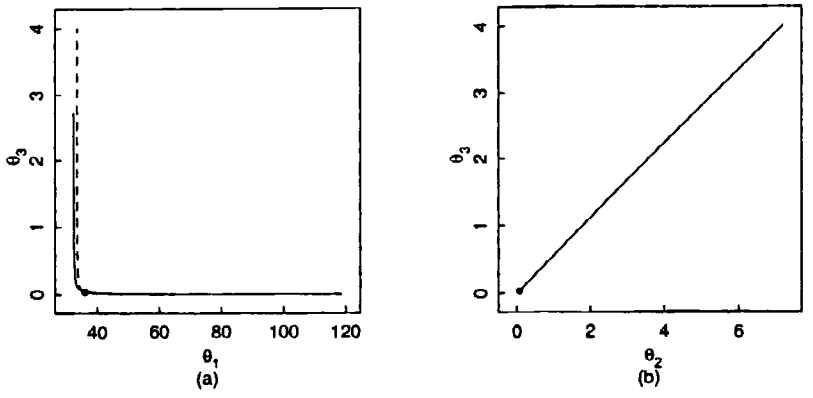

Figure 6.11 Profile traces for θ_1 versus θ_3 (part *a*) and θ_2 versus θ_3 (part *b*) in the isomerization data model. The traces of $\tilde{\theta}_3$ on θ_2 and $\tilde{\theta}_2$ on θ_3 are coincident.

upper bound on the likelihood intervals for the equilibrium constants. When the denominator in

$$f(\mathbf{x},\boldsymbol{\theta}) = \frac{\theta_1\theta_3(x_2 - x_3/1.632)}{1+\theta_2 x_1 + \theta_3 x_2 + \theta_4 x_3}$$

is substantially greater than one, the model is approximately

$$f(\mathbf{x},\boldsymbol{\theta}) \approx \frac{\theta_1\theta_3(x_2 - x_3/1.632)}{\theta_2 x_1 + \theta_3 x_2 + \theta_4 x_3}$$

and scaling θ_2, θ_3, and θ_4 by the same factor without changing θ_1 produces essentially the same predictions and residual sums of squares.

We have not bothered to plot profile pair sketches, because of the extremely bad behavior of the profile t plots and the profile traces. This behavior reveals that very little information has been gained so far. Additional experiments would have to be performed so that meaningful parameter estimates with reasonable inference regions could be obtained.

Box and Hill (1974) presented a different analysis of these data by writing the model

$$f(\mathbf{x},\boldsymbol{\beta}) = \frac{x_2 - x_3/1.632}{\beta_1 + \beta_2 x_1 + \beta_3 x_2 + \beta_4 x_3} \tag{6.5}$$

using an obvious reparametrization. (This form of reparametrization has been recommended by Ratkowsky (1985) for use with models consisting of ratios of polynomials.) This gave the estimates $\hat{\boldsymbol{\beta}} = (0.739, 0.0523, 0.0278, 0.123)^{\mathrm{T}}$. The profile t plots shown in Figure 6.12 are much better behaved than those for the $\boldsymbol{\theta}$ parameters, producing almost perfectly symmetric likelihood regions. The profile traces (not shown) are also straight, and the

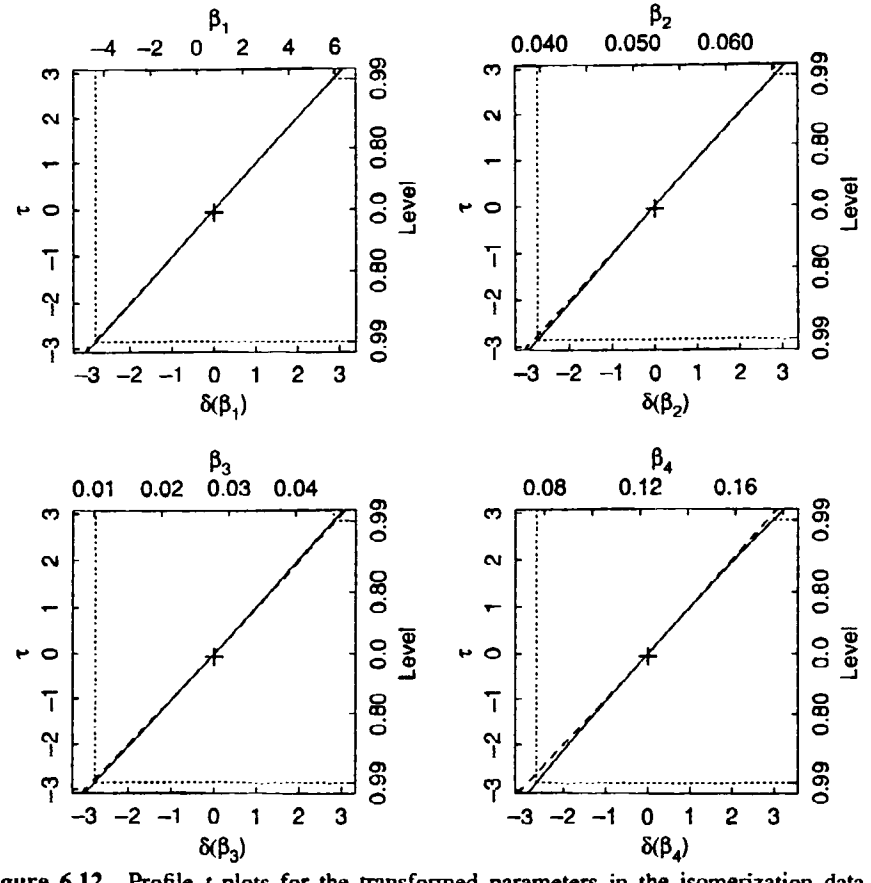

Figure 6.12 Profile t plots for the transformed parameters in the isomerization data model. The solid lines are the profile t curves, and the dashed lines are the linear approximation. Dotted lines show the construction of 99% marginal likelihood intervals.

profile pair sketches are remarkably elliptical, so that individual and joint linear approximation regions and summaries are extremely accurate for the $\boldsymbol{\beta}$ parameters. We note that the likelihood interval for β_1 included negative values even for moderate confidence levels. Since this parameter only has physical meaning when it is positive, we are still alerted to the fact that the data set is of limited value. ■

6.1.3 Comments

Using profile t plots, profile traces, and profile pair sketches to summarize the inferential results of a nonlinear analysis has much to recommend it. The computations for the profile t and profile traces are very efficient because we start

from the least squares estimates of the previous calculation, and because the problem is always of reduced dimension $P-1$. Also, at each value of the parameter of interest, we simultaneously generate the profile t value and the converged values of the vector $\tilde{\theta}_{-p}$, which also provides most of the data necessary for sketching the profile pairs. Profile t functions can also be used to determine exact likelihood intervals and bands for the expectation function. For all these calculations, only minor modifications to standard nonlinear regression software are necessary. Pseudocode for generating profile t plots and profile traces is given in Appendix 3.

The approach also provides important detailed information about the estimation situation. In addition to providing exact likelihood intervals for each parameter, the profile t plots reveal how nonlinear each parameter is. This can help guide the analyst towards nonlinear reparametrizations to be used for future data sets with the same model function. Such reparametrizations could be used to provide accurate linear approximation marginal and joint parameter regions, and so obviate the need for plots. A reparametrization could also be used to accelerate convergence. (For example, we recommend using the reparametrization suggested by Ratkowsky (1985) during estimation, since it simplifies the determination of starting values for the parameters and accelerates convergence. However, we recommend that the estimates and likelihood intervals be reported in terms of the original parameters, since these are physically meaningful to chemists and chemical engineers. If a reparametrization can be determined which has all the attributes of near linearity, assured convergence, and meaningfulness to the researcher, then of course, that should be used.)

Note that for univariate reparametrizations in which, say, ϕ_p is a function only of θ_p, the profile t plot (and associated profile traces) for ϕ_p can be obtained directly from the profile t plot (and associated profile traces) for θ_p: there is no need to reparametrize the model function or reestimate the parameters. This, of course, is a consequence of invariance of the likelihood function.

The profile t function can be used to determine likelihood intervals for the expectation function at any point $\mathbf{x}_0$ by reparametrizing the model function so that a new parameter, say ϕ_1, is the response at $\mathbf{x}_0$. The remaining parameters can be chosen as $\phi_p=\theta_p$, $p=2,\ldots,P$, and derivatives of the expectation function with respect to the new parameters can be determined simply by using the chain rule. To determine a likelihood interval for the response at a particular point we find the values of ϕ_1 such that $\tau(\phi_1)=\pm t(N-P;\alpha/2)$, and to determine a likelihood band for the fitted response function at any $\mathbf{x}$, we find the values of ϕ_1 such that $\tau(\phi_1)=\pm F(P,N-P;\alpha)$.

The profile traces and the profile pair sketches provide important information on the pairwise behavior of the parameters, which can also be used in the search for effective reparametrizations. Perhaps more importantly, however, the plots collectively provide insights into the experimental situation, so that steps can be taken to design experiments which will generate better data. For example, for the BOD data, future experiments should include more replications at each sampling time in order to reduce the scatter in the data, and some observations should be taken at about 36 hours (instead of just 24 and 48) to provide vi-

tal information about the rate constant θ_2. Similarly, for the isomerization data, more informative data must be obtained about the converted parameter θ_1. Nonlinear design techniques using the subset design criterion (Section 3.14) would be useful here.

6.2 Bayes Regions

Inferences about nonlinear models using the Bayesian approach involve the same difficulties as the likelihood approach, with the additional complexity of choosing a prior density for the parameters.

6.2.1 Choice of Bayes Prior on the Parameters

In the Bayesian analysis of a linear regression model, described in Section 1.1.4, a prior density

$$p(\boldsymbol{\beta},\sigma) \propto \sigma^{-1}$$

is often used. This does not correspond to an actual probability density, since the integral of this density over the parameter σ or $\boldsymbol{\beta}$ is infinite, but the use of such "uninformative" or "improper" priors can be justified because the posterior density obtained by multiplying the prior by the likelihood function *is* a proper density. That is, the posterior density has a finite integral over all possible parameter values and can be normalized so that the integral is unity. This follows because, for linear models, whenever $\|\boldsymbol{\beta}\| \to \infty$, $\|\boldsymbol{\eta}(\boldsymbol{\beta})\| \to \infty$, and since $\mathbf{y}$ is fixed, this means that $\|\mathbf{z}\| \to \infty$, so $l(\boldsymbol{\beta},\sigma|\mathbf{y}) \to 0$. [Technically, more is required for the finite integral: we must have $l(\boldsymbol{\beta},\sigma|\mathbf{y})$ going to zero "quickly," which it does.]

An uninformative prior can usually be considered to be the limit of proper priors that are more and more diffuse (for example, a limit of multivariate normal priors on $\boldsymbol{\beta}$ with variance–covariance matrices consisting of a fixed matrix multiplied by a factor that approaches infinity). In this limiting process, quantities calculated from the posterior densities, such as highest posterior density (HPD) regions, approach finite limits smoothly. However, for nonlinear models it is not always true that locally uniform priors produce proper posterior densities. Nonlinear models frequently have asymptotes, so $\|\boldsymbol{\theta}\| \to \infty$ does not imply that $\|\boldsymbol{\eta}(\boldsymbol{\theta})\| \to \infty$ or $l(\boldsymbol{\theta},\sigma|\mathbf{y}) \to 0$. [For example, as $\theta \to \infty$ the Rumford model approaches a finite limit, the point $(60, \ldots, 60)^{\mathrm{T}}$.] This means that when an improper prior on the parameters is used, the posterior density will also be improper. Even if one regards the uninformative prior as being the limit of a sequence of proper prior densities, the situation is not improved because the properties of the posterior density do not approach a finite limit satisfactorily. For example, if one were to apply a uniform prior density on θ for the Rumford model over the interval $0 \le \theta < k$ and let k approach infinity while calculating a

95% HPD interval for each value of k, the right hand end points of the HPD intervals would go to infinity.

Consideration of the Rumford example enables us to see how to avoid obtaining improper posterior densities: instead of putting a locally uniform prior on the parameter space, we should put a locally uniform prior *on the expectation surface* to represent an uninformative prior (Bates, 1978). For linear models, a locally uniform prior in the parameter space produces a locally uniform prior on the expectation plane, so this prior is consistent with standard practice for the linear model. For a nonlinear model, the uninformative prior on $\boldsymbol{\theta}$ is proportional to the Jacobian of the mapping to the expectation plane, so we set

$$p(\boldsymbol{\theta}) \propto \frac{dA}{d\boldsymbol{\theta}}$$
$$= |\mathbf{V}^{\mathrm{T}}\mathbf{V}|^{1/2}$$

where dA represents an element of area on the expectation surface.

For the Rumford example, the expectation surface is finite, so a uniform prior density over the expectation surface will be a proper prior density and hence the posterior density will be a proper density. When the expectation surface has infinite extent, so the uninformative prior is not a proper density, the likelihood will force the posterior density to be proper because the surface extends to infinity. (Mathematically it is possible to get surfaces of infinite extent which are restricted to a finite region in the response space, but such pathological cases would not occur as expectation surfaces.)

We could also justify a locally uniform prior on the expectation surface by arguing that prior ignorance about the responses corresponds to a locally uniform prior on the sample space for the responses. This induces a locally uniform prior over the expectation surface as the prior for the model parameters $\boldsymbol{\theta}$. Note that this choice makes the prior *independent of the parametrization* used in the model function, since the Jacobian for the transformation cancels out.

Example: Puromycin 17

Contours of the prior density $p(\boldsymbol{\theta})$ for the model and design of the Puromycin data are shown in Figure 6.13. The prior density has been scaled so that it attains a maximum value of 1 over a region which covers the area of appreciable likelihood for these data. This prior gives greater weight to smaller θ_2 values, but the changes in the weights are small. For these data, the likelihood (whose contours were shown in Figure 6.1) will clearly dominate the prior in determining the posterior density, and so the contours of the posterior density look almost identical to the contours of the likelihood function. (The maximum and minimum value of the prior density over this region have a ratio of about 10, while the maximum and minimum likelihood values have a ratio of about 10^{195}.) ■

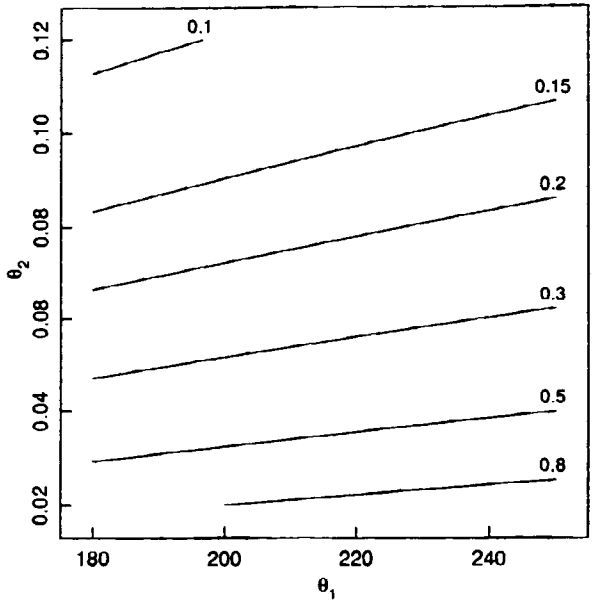

Figure 6.13 Contours of relative prior density for the parameters in the Puromycin data model. The prior density has been scaled so it attains a maximum of 1 over the region shown.

Example: BOD 11

Contours of prior density for the model and design of the BOD data are shown in Figure 6.14. As before, the prior density has been scaled so that it has a maximum of 1 over the region which includes most of the area of appreciable likelihood. In this example, we cannot include all the parameter values with appreciable likelihood, since that region is unbounded, as demonstrated in Example BOD 7. The prior varies considerably over the region, reaching zero for $\theta_2 = 0$. The prior is very small for large values of θ_2, which correspond to the region of the expectation surface where the parameter curves are approaching a limit as described in Example BOD 7. The very small prior values discount the parameter values in that area. ■

To complete the prior density, we must specify the joint prior for $\boldsymbol{\theta}$ and σ. Following Box and Tiao (1973), we choose independent priors for $\boldsymbol{\theta}$ and σ with $p(\sigma) \propto \sigma^{-1}$, so the joint prior density is

$$\begin{aligned} p(\boldsymbol{\theta},\sigma) &\propto p(\boldsymbol{\theta})\,p(\sigma) \\ &= |\mathbf{V}^{\mathrm{T}}\mathbf{V}|^{1/2}\,\sigma^{-1} \end{aligned} \tag{6.6}$$

It is noteworthy that the prior density does not depend on the parametrization, but it is equally noteworthy that the prior depends on the design used by

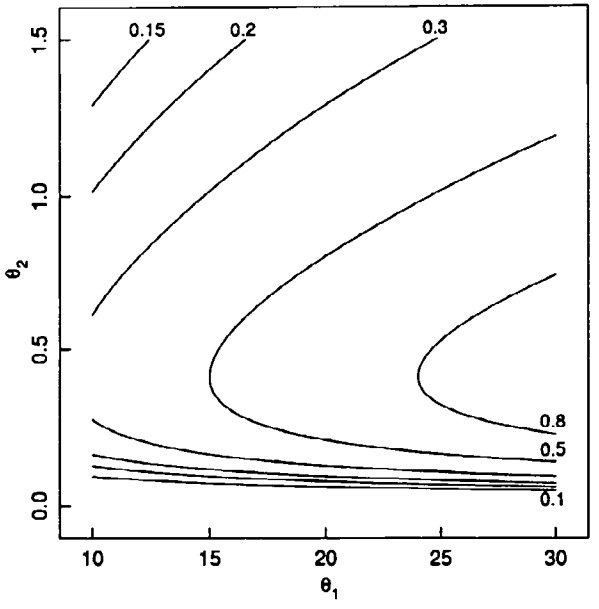

Figure 6.14 Contours of relative prior density for the parameters in the BOD data model. The prior density has been scaled so it attains a maximum of 1 over the region shown.

the experimenter. This makes good sense, since no scientific experiment is done in the complete absence of knowledge, and the prior subtly expresses the current knowledge of the experimenter through the design.

To illustrate, suppose one wished to measure BOD of a river, and the model function $f=\theta_1(1-e^{-\theta_2 x})$ was considered appropriate. The BOD, and consequently the parameters, would depend on the season of the year, the latitude of the river, the rate of flow of the river, the number and types of sources of pollution along the river, the type of river bed, and so on. For fast-flowing northern mountain rivers with no immediate pollution sources, the rate constant θ_2 would likely be very small, and so samples taken from the river should be analyzed at rather long intervals and over a long time, say every three days for three weeks. For a sluggish meandering river in an industrial area, on the other hand, the rate constant θ_2 would likely be large, and so the samples should be analyzed at shorter intervals and over a shorter time, say every twelve hours for five days. These considerations clearly affect the design and, in turn, the prior on the parameters.

6.2.2 Joint HPD Regions

After choosing a prior density, we form the posterior density by multiplying the prior by the likelihood function. Thus the posterior density, $p(\boldsymbol{\theta},\sigma \mid \mathbf{y})$, becomes

$$p(\boldsymbol{\theta},\sigma \mid \mathbf{y}) \propto |\mathbf{V}^{\mathrm{T}}\mathbf{V}|^{1/2}\,\sigma^{-(N+1)} \exp\left[-\frac{S(\boldsymbol{\theta})}{2\sigma^2}\right]$$

where $S(\boldsymbol{\theta})$ is the residual sum of squares at $\boldsymbol{\theta}$. As shown in Box and Tiao (1973), the marginal posterior density of $\boldsymbol{\theta}$ is obtained by integrating the joint posterior over the nuisance parameter σ to yield

$$\begin{aligned} p(\boldsymbol{\theta} \mid \mathbf{y}) &= \int_0^\infty p(\boldsymbol{\theta},\sigma \mid \mathbf{y})\, d\sigma \\ &\propto |\mathbf{V}^{\mathrm{T}}\mathbf{V}|^{1/2}\,[S(\boldsymbol{\theta})]^{-N/2} \end{aligned} \tag{6.7}$$

An HPD region will be bounded by a contour of this posterior density function, or equivalently, by a contour of

$$\frac{S(\boldsymbol{\theta})}{|\mathbf{V}^{\mathrm{T}}\mathbf{V}|^{1/N}}$$

To assign a probability value to the region, we must determine the level of contour. The exact method for determining a $1-\alpha$ HPD region is to integrate (6.7) over all possible values of $\boldsymbol{\theta}$, obtain the constant of proportionality, and then integrate the normalized posterior within contours of the posterior density until we find the one with the required probability content.

All the integrations in this exact procedure make it too computationally intensive for general use, but fortunately there is a convenient approximation to the probability content of a contour. For any expectation surface, a set of *geodesic* parameters exists, say $\boldsymbol{\phi}$, for which the prior density will be approximately constant near $\hat{\boldsymbol{\phi}}$. That is,

$$|\mathbf{V}_{\boldsymbol{\phi}}^{\mathrm{T}}\mathbf{V}_{\boldsymbol{\phi}}| \approx \text{constant} \tag{6.8}$$

where

$$\mathbf{V}_{\boldsymbol{\phi}} = \frac{d\boldsymbol{\eta}}{d\boldsymbol{\phi}^{\mathrm{T}}}$$

If the expectation surface is perfectly flat or, more generally, if it has zero Gaussian curvature everywhere (O'Neill, 1966), (6.8) is an equality.

Besides having a locally uniform prior density, the $\boldsymbol{\phi}$ parameters also have an easily expressed likelihood function, since when the expectation surface is reasonably flat over the region of nonnegligible likelihood, the sum of squares function $S_{\boldsymbol{\phi}}(\boldsymbol{\phi})$ is quadratic in $\boldsymbol{\phi}$. That is,

$$\begin{aligned} p_{\boldsymbol{\phi}}(\boldsymbol{\phi} \mid \mathbf{y}) &\propto [S_{\boldsymbol{\phi}}(\boldsymbol{\phi})]^{-N/2} \\ &\approx \left[S_{\boldsymbol{\phi}}(\hat{\boldsymbol{\phi}}) + \tfrac{1}{2}(\boldsymbol{\phi}-\hat{\boldsymbol{\phi}})^{\mathrm{T}} \left.\frac{\partial^2 S_{\boldsymbol{\phi}}}{\partial\boldsymbol{\phi}\partial\boldsymbol{\phi}^{\mathrm{T}}}\right|_{\hat{\boldsymbol{\phi}}} (\boldsymbol{\phi}-\hat{\boldsymbol{\phi}}) \right]^{-N/2} \end{aligned}$$

which is in the form of a multivariate T density (Box and Tiao, 1973). Thus, an approximate $1-\alpha$ HPD region consists of all values of $\boldsymbol{\phi}$ enclosed by the con-

tour $S_\phi(\boldsymbol{\phi})$ determined by

$$\frac{[S_\phi(\boldsymbol{\phi})-S_\phi(\hat{\boldsymbol{\phi}})]/P}{S_\phi(\hat{\boldsymbol{\phi}})/(N-P)} \le F(P, N-P; \alpha)$$

In terms of $\boldsymbol{\theta}$, the HPD region becomes a contour in $S(\boldsymbol{\theta})/|\mathbf{V}^T\mathbf{V}|^{1/N}$, and so the approximate $1-\alpha$ HPD region in $\boldsymbol{\theta}$ is bounded by the contour

$$\frac{S(\boldsymbol{\theta})}{|\mathbf{V}^T\mathbf{V}|^{1/N}} = \frac{S(\hat{\boldsymbol{\theta}})}{|\hat{\mathbf{V}}^T\hat{\mathbf{V}}|^{1/N}}\left[1+\frac{P}{N-P}F(P, N-P; \alpha)\right]$$

Computationally, it is more convenient to determine contours of $|\mathbf{V}^T\mathbf{V}|^{1/N}/S(\boldsymbol{\theta})$, since sometimes $|\mathbf{V}^T\mathbf{V}| = 0$ on the boundary of the parameter region, as in Example BOD 11.

Example: Puromycin 18

The approximate 80 and 95% HPD regions for the Puromycin parameters are shown in Figure 6.15, together with the corresponding likelihood regions (dotted lines). The HPD contours are very similar to the likelihood contours but are slightly more symmetric about the least squares estimate, since large values of θ_2 are given less weight. ■

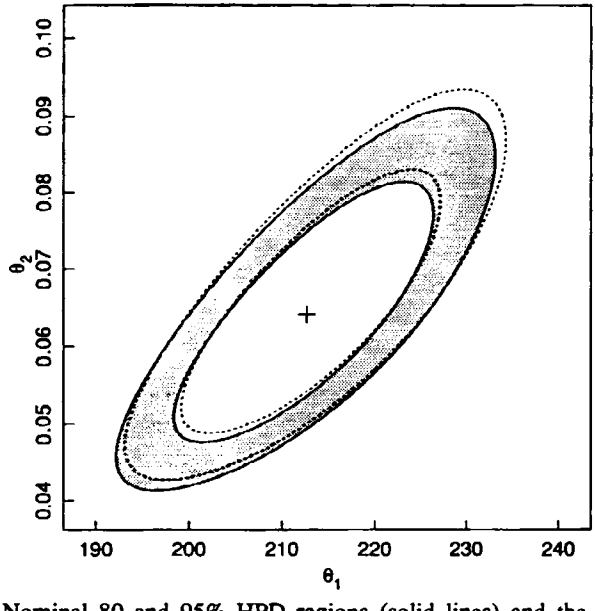

Figure 6.15 Nominal 80 and 95% HPD regions (solid lines) and the corresponding likelihood regions (dotted) for the Puromycin parameters.

Example: BOD 12

The approximate 80 and 95% HPD regions for the BOD parameters are shown in Figure 6.16 together with portions of the corresponding likelihood regions (dotted lines). The HPD contours are closed in the θ_2 direction, unlike the corresponding likelihood contours, but they are still decidedly nonelliptical. ■

Sketches could be made of the pairwise projections of HPD regions using the same approach as for likelihood regions. Instead of minimizing the conditional sum of squares, however, we determine the posterior profile traces by minimizing $S(\boldsymbol{\theta})/|\mathbf{V}^{\mathrm{T}}\mathbf{V}|^{1/N}$. Minimizing this is much more difficult than minimizing the profile sum of squares, but fortunately the *locus* of the minima, say $\boldsymbol{\theta}^*_{-p}(\theta_p)$ (i.e., the posterior profile trace) will be essentially the same as $\tilde{\boldsymbol{\theta}}_{-p}(\theta_p)$ (the likelihood trace) because the term $|\mathbf{V}^{\mathrm{T}}\mathbf{V}|^{1/N}$ will usually vary more slowly than the term $S(\boldsymbol{\theta})$. It is therefore easy to evaluate the posterior density along the likelihood trace and so generate sketches of the projections of HPD regions using the methods of Appendix 6.

In theory, Bayesian marginal inferences are straightforward: the posterior density is simply integrated over the nuisance parameters, as in eliminating σ. If θ_1 is the single parameter of interest and $\boldsymbol{\theta}_{-1}$ represents the nuisance parameters, the marginal density for θ_1 is

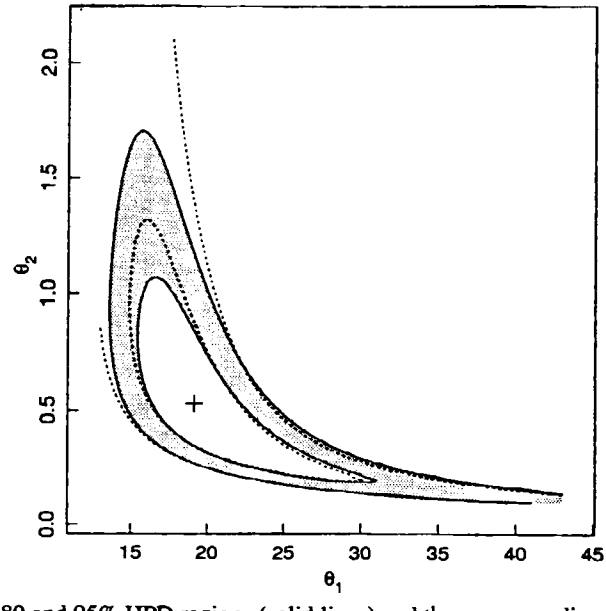

Figure 6.16 80 and 95% HPD regions (solid lines) and the corresponding likelihood regions (dotted) for the BOD parameters.

$$p_{\theta_1}(\theta_1) \propto \int p_{\boldsymbol{\theta}}(\theta_1, \boldsymbol{\theta}_{-1}^{\mathrm{T}})\, d\boldsymbol{\theta}_{-1}$$

This method of eliminating components of $\boldsymbol{\theta}$ would generally require a prohibitive amount of numerical integration, so approximations based on the density conditional on the parameter of interest are used. A first approximation is to use the analogue of the profile likelihood,

$$\int p_{\boldsymbol{\theta}}(\theta_1, \boldsymbol{\theta}_{-1}^{\mathrm{T}})\, d\boldsymbol{\theta}_{-1} \propto p_{\boldsymbol{\theta}}(\theta_1, \boldsymbol{\theta}_{-1}^{*}(\theta_1))$$

where $\boldsymbol{\theta}_{-1}^{*}(\theta_1)$ is the value which maximizes $p_{\boldsymbol{\theta}}(\theta_1, \boldsymbol{\theta}_{-1})$ over $\boldsymbol{\theta}_{-1}$ for that value of θ_1. That is, the marginal density for θ_1 is assumed to be proportional to the maximum value of the conditional density on θ_1. To obtain more accurate intervals, a quadratic approximation could be used in which the integral of the joint density is replaced by the product of its maximum value and a measure of its spread at the maximum, as discussed in Tierney and Kadane (1986).

6.3 Exact Sampling Theory Confidence Regions

Sampling theory methods for linear regression can be extended to provide joint confidence regions for parameters in nonlinear regression models. We only do this for completeness, however, because *we do not recommend the approach.*

The method involves hypotheses of the form

$$\mathrm{H}_0 : \boldsymbol{\theta} = \boldsymbol{\theta}_0$$

versus

$$\mathrm{H}_A : \boldsymbol{\theta} \neq \boldsymbol{\theta}_0$$

where, as in the linear model, the test is based on the relative lengths of tangential and orthogonal components of the residual vector $\mathbf{z}_0 = \mathbf{y} - \boldsymbol{\eta}(\boldsymbol{\theta}_0)$. For linear models, the tangent plane is independent of $\boldsymbol{\theta}$ and the length of the orthogonal component of the residual vector is fixed. For nonlinear models, however, the tangent plane changes with the value of $\boldsymbol{\theta}$ and so does the length of the orthogonal component.

Even with a nonlinear model, this test provides a locally most powerful, unbiased test of the hypothesis, and under the assumptions on the model, the confidence region

$$\frac{\| \mathbf{Q}_1^{\mathrm{T}}(\boldsymbol{\theta})\mathbf{z}(\boldsymbol{\theta}) \|^2 / P}{\| \mathbf{Q}_2^{\mathrm{T}}(\boldsymbol{\theta})\mathbf{z}(\boldsymbol{\theta}) \|^2 / (N-P)} \leq F(P, N-P; \alpha) \tag{6.9}$$

is an exact $1-\alpha$ confidence region. In (6.9), $\mathbf{Q}_1(\boldsymbol{\theta})$ and $\mathbf{Q}_2(\boldsymbol{\theta})$ are the orthogonal parts of the QR decomposition of $\mathbf{V}(\boldsymbol{\theta})$, the derivative matrix evaluated at $\boldsymbol{\theta}$. When there is an independent variance estimate s_r^2 with ν_r degrees of freedom, an alternative form of the confidence region is

$$\| Q_1^T(\boldsymbol{\theta})\mathbf{z}(\boldsymbol{\theta}) \|^2 \le P s_r^2 F(P, \nu_r; \alpha)$$

Example: Puromycin 19

Figure 6.17 shows portions of the 80, 95, and 99% exact confidence regions for the Puromycin parameters. The 80% region is quite elliptical and nicely centered about the least squares estimate $\hat{\boldsymbol{\theta}}$, but the 95 and 99% regions are very badly behaved, neither region appearing to close.

Comparing Figure 6.17 with Figures 6.1 and 6.15, we see that the confidence regions are larger and less well behaved than the corresponding likelihood or HPD regions. The fact that the confidence regions do not close for moderate confidence levels for this well-behaved example is particularly damaging testimony against using exact confidence regions. ■

Example: BOD 13

The 80 and 95% exact confidence regions for the BOD data set are shown in Figure 6.18. Again, the contours at moderate confidence levels are open and are very badly behaved relative to the likelihood and HPD contours. The "shoulders" on the contours near $\theta_2 = 1.4$ are not an artifact of the contouring program, but appear to be a genuine feature of the contours. ■

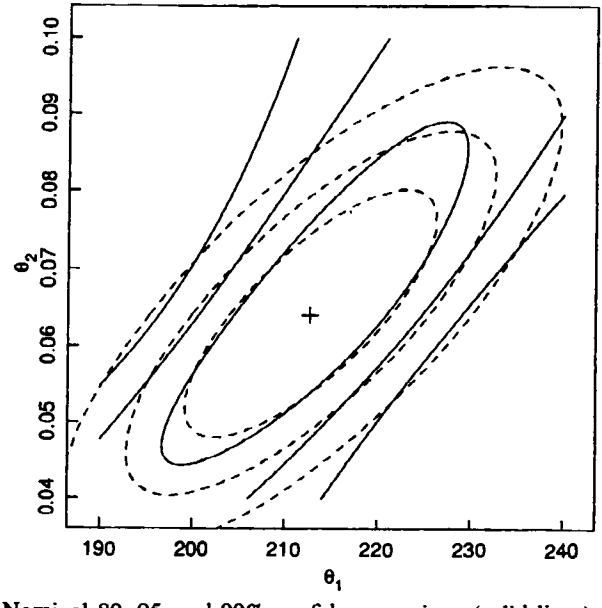

Figure 6.17 Nominal 80, 95, and 99% confidence regions (solid lines) and the linear approximation ellipses (dashed) for the Puromycin parameters.

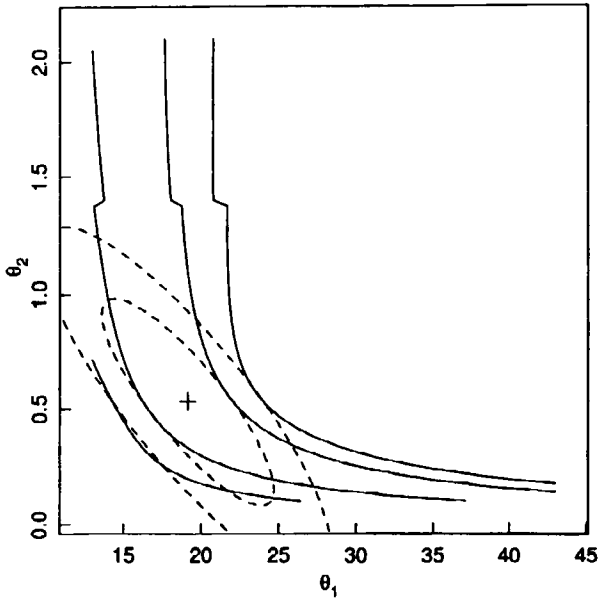

Figure 6.18 Nominal 80 and 95% confidence regions (solid lines) and the linear approximation ellipses (dashed) for the BOD parameters.

As pointed out in Beale (1960), sampling theory confidence regions have undesirable properties because they are determined by values of a ratio in which both the numerator and the denominator vary with $\boldsymbol{\theta}$. The ratio in (6.9) can be small because the tangential component is small or because the orthogonal component is large. When the expectation surface bends, the ratio often falls below the critical value for points which are very far away from the least squares values because the tangent plane has tilted.

Example: Rumford 7

It is instructive to examine exact confidence regions in more detail geometrically. For the 2-case Rumford example, a 50% confidence region for the parameter θ is defined as the set of all parameter values θ for which the F ratio does not exceed $F(1,1;0.50)=1.0$. That is, a point θ^0 is included in the 50% confidence region if the angle that the residual vector makes with the tangent line exceeds 45°. For this example, the region will include values close to the least squares point $\hat{\theta}=0.00832$, and will also include values close to 0.1. Figure 6.19 illustrates the situation for $\theta^0=0.1$, for which the angle between the residual vector and the tangent line is about 54°. (The shaded region enclosed by the 45° lines indicates the exclusion region for residual vectors at $\theta=0.1$.)

In fact, plotting the F ratio versus θ, as in Figure 6.20, shows that the F ratio decreases to a minimum around $\hat{\theta}$, goes through a maximum,

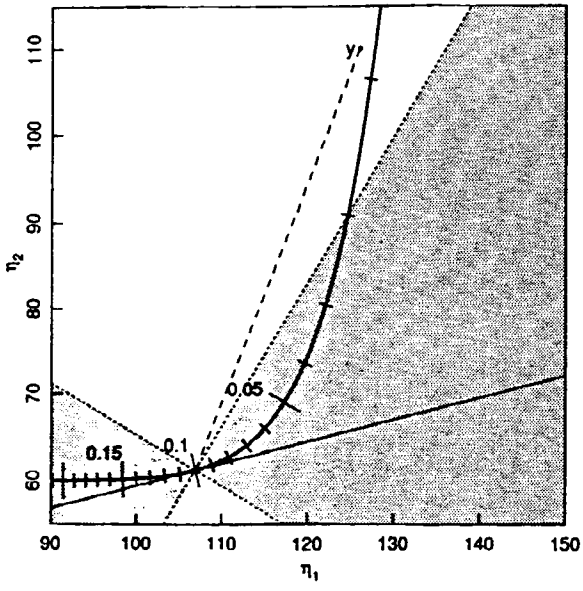

Figure 6.19 Test to determine if $\theta = 0.1$ should be included in a 50% confidence set for the 2-case Rumford data. The heavy solid line is the expectation curve; the light solid line is the tangent at $\boldsymbol{\eta}(0.1)$. The dotted lines at 45° to the tangent delimit the exclusion region (shaded) for residual vectors at $\theta = 0.1$. Since the residual vector (dashed line) forms an angle of more than 45° to the tangent, $\theta = 0.1$ is included in the 50% confidence set.

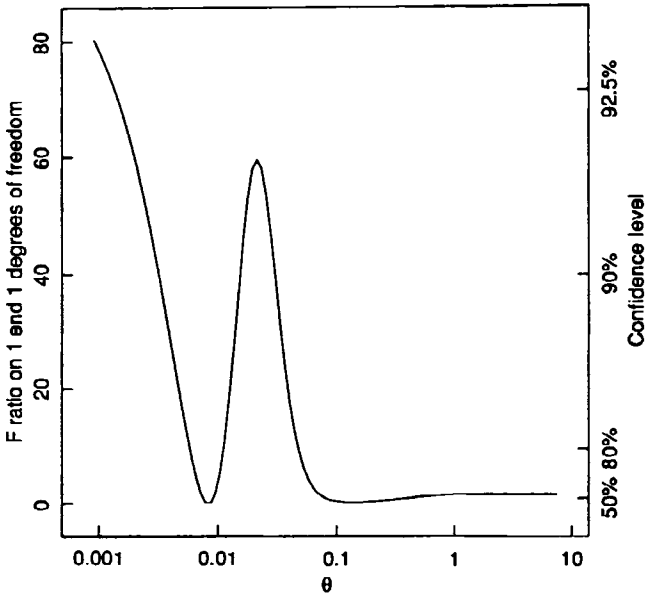

Figure 6.20 Plot of the F ratio versus θ for the 2-case Rumford example.

reaches another minimum near 0.1, and then remains small as $\theta \to \infty$. Some confidence intervals (actually "confidence sets") derived in this way are given in Table 6.1.

It may seem unreasonable to calculate confidence intervals for a 2-case data set, because there is only one degree of freedom for residuals. But the same behavior occurs with the full data set. The F ratios, plotted in Figure 6.21, have a minimum at $\hat{\theta}$ (= 0.00942), reach a maximum, and decrease again as $\theta \to \infty$, which produces confidence sets as in Table 6.2. ■

We see that even for a simple 1-parameter model, exact confidence regions can consist of disjoint portions which include parameter values whose residual vectors are much longer than the residual vector at $\hat{\boldsymbol{\theta}}$. Moreover, even without producing confidence regions in disjoint portions, the method is subject

Table 6.1 Confidence sets for the 2-case Rumford example.

Confidence Level (%)	Set		
50	[0.0076, 0.0091]	and	[0.0813, 0.3869]
80	[0.0058, 0.0111]	and	[0.0475, ∞]
90	[0.0032, 0.0154]	and	[0.0302, ∞]
95	[0, ∞]		

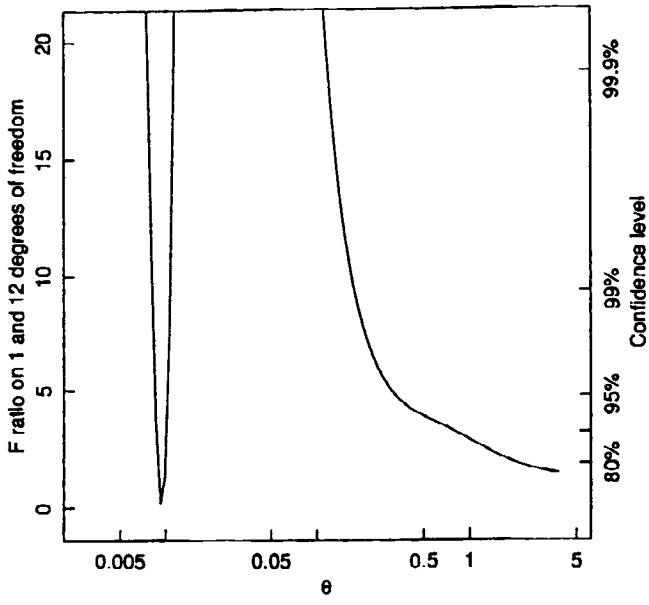

Figure 6.21 Plot of the F ratio versus θ for the Rumford data.

Table 6.2 Confidence sets for the Rumford data.

Confidence Level (%)	Set
50	[0.0092, 0.0094]
80	[0.0089, 0.0100] and [2.0947, ∞]
90	[0.0087, 0.0101] and [0.8224, ∞]
95	[0.0085, 0.0103] and [0.3261, ∞]

to enclosing clearly inappropriate parameter values in the confidence sets.

Marginal inferences are difficult to formulate using sampling theory because the method for constructing joint or marginal confidence regions for the parameters in a linear model does not generalize to nonlinear models except when conditional linearity can be exploited (Hamilton, 1986). As described in Section 1.2.3 for linear models, the method involves decomposing the residual vector for a representative point on the subplane defined by $\beta_2 = c$ into three components: one *orthogonal to* the expectation plane, one *in* the expectation plane and *orthogonal to* the subplane, and one *parallel to* the subplane. For a nonlinear model, both the expectation surface and the subsurface generated by a constraint such as $\theta_2 = c$ are nonlinear, and there is no general decomposition giving three orthogonal components. In theory, marginal confidence regions could be computed, but a reference distribution would have to be computed for each model, each data set, and each parameter value, and so there would be no

straightforward way to obtain marginal confidence regions using standard (F or t) distributions.

The only instance where the approach from linear models can be used is when there are conditionally linear parameters. If the model reduces to a linear model when a subset of the parameters is held fixed, then exact marginal confidence regions for the nonlinear parameters can be calculated. For example, the model

$$f(x, \boldsymbol{\theta}) = \theta_1 + \theta_2 e^{\theta_3 x}$$

reduces to a linear model when θ_3 is held fixed. Thus confidence intervals for θ_3 can be determined using a t distribution, as described in Halperin (1963) and Williams (1962).

6.4 Comparison of the Likelihood, Bayes, and Sampling Theory Approaches

Four methods for summarizing joint and marginal inference regions have been given. In Chapter 2 we discussed linear approximations, and in this chapter we presented profile t and profile pair plots, Bayes joint and marginal HPD procedures, and sampling theory procedures. The linear approximation methods are the easiest to use, and most nonlinear regression programs produce the linear approximation standard errors for the parameters and the approximate correlation matrix for the parameters in addition to the parameter estimates. The major disadvantage of linear approximations is that the validity of the approximation over the region of interest is not known. This approximation involves both the *planar* assumption and the *uniform coordinate* assumption, one or both of which could be invalid—as shown in the next chapter, it is usually the uniform coordinate assumption.

The other approaches to inference produce joint regions defined by contours. Determining and displaying exact contours is generally too expensive when $P > 2$, but displaying profile t plots, profile traces, and profile pair sketches is eminently practical. This approach requires a minor amount of extra computation over the linear approximation approach but provides valuable information on the behavior of the marginal and joint regions. Fortunately, the calculations only require slight modifications of standard nonlinear programs. The confidence level associated with likelihood regions is not well defined, but in contrast to the linear approximation intervals, the likelihood regions require only the planar assumption.

Similarly, examination of the approximate marginal and joint HPD regions provides much more information than does the linear approximation. The Bayes prior moderates the tendency of likelihood contours to open as the model function approaches an asymptote, making the Bayes intervals more satisfactory. The probability associated with the HPD intervals is based on an approximation to the expectation surface that, like the likelihood approach, only requires

the planar assumption. The Bayes approach has stronger justification for the probability content or level of a region than the likelihood approach.

It is noteworthy that the prior density does not depend on the parametrization, but it is equally noteworthy that the prior depends on the design used by the experimenter. As demonstrated in Section 6.2.1, however, this makes good sense, since no scientific experiment is done in the complete absence of knowledge, and the prior expresses the current knowledge of the experimenter through the design.

The sampling theory approach, which uses the ratio of lengths of components of the residual vector rather than the total length of the residual vector to determine the region, can result in regions which include inappropriate parameter values. In addition, the difficulty of defining marginal regions for a general case makes this approach completely unsuitable.

To summarize, when a nonlinear regression is performed, we recommend producing the linear approximation standard errors and correlations, and profile t plots, profile traces, and profile pair sketches for either the likelihood function or the Bayesian posterior density.

Exercises

6.1 Write a computer routine in a language of your choice to generate profile t and profile trace plots. Use the nonlinear subroutine from Problem 2.1.

6.2 Use Lagrange multipliers to show analytically that the profile t value for a parameter in a linear model can be written as in equation (6.2).

6.3 (a) Use the data and model from Appendix 4, Section A4.1 to make profile t and profile trace plots for the parameters. Does this model–data set–parametrization combination suffer from bad nonlinearity?

(b) Use the profile t plots to determine nominal 50, 75, and 95% intervals for the parameters.

(c) Plot the points on the profile traces corresponding to the 50, 75, and 95% nominal confidence level in the (θ_1, θ_2) plane. Using the information concerning the tangents of the contours at these points, sketch the joint regions.

(d) Compare your sketch with the exact sum of squares contours from Problem 2.6. Comment on the accuracy of the sketch.

6.4 Use the data from Appendix 4, Section A4.3 and the model fitted in Problem 3.4 to make profile t and profile trace plots for the parameters.

6.5 Use the data and model from Appendix 4, Section A4.4 to make profile t and profile trace plots for the parameters.

(a) Use the model with the factor $1/x_3$ centered.

(b) Reparametrize the model using $\theta_1 = e^{\phi_1}$ and $\theta_2 = e^{\phi_2}$, and plot the profile t values. Is is necessary to recalculate the t values or the trace values?

6.6 (a) Use the data and model from Appendix 4, Section A4.5 to make profile

t and profile trace plots for the parameters.

(b) Reparametrize the model in part (a) using $\theta_2 e^{-\theta_3 x} = e^{-\phi_3(x-\phi_2)}$. Is it necessary to recalculate the t values or the trace values? Which ones?

(c) Comment on the effects of this transformation on the profile t plots and on the profile trace plots.

6.7 (a) Calculate and plot contours of the Bayesian prior density for the exponential rise model of Example BOD 11 but using the design with $\mathbf{x} = (2, 10)^{\mathrm{T}}$. (This is the optimal experimental design for this model, assuming that the true parameter value is $\theta_2 = 0.5$ and that $x_{\max} = 10$.) Use the same region for $\boldsymbol{\theta}$ as was used in Figure 6.14.

(b) Compare this prior with the prior shown in Figure 6.14.

(c) Calculate and plot contours for the prior corresponding to n replications of the optimal design, where $n = 2, 4, 8$. Comment on the effect of increasing the number of replications.

CHAPTER 7.

Curvature Measures of Nonlinearity

"The great tragedy of Science: the slaying of a beautiful hypothesis by an ugly fact."

– Thomas Huxley

In Chapter 2 we presented linear approximation inference intervals and regions for parameters in nonlinear regression models, and in Chapter 6 we discussed improved methods for summarizing inferences about the parameters. An important assumption used in the development of these methods is that the expectation surface is flat (the planar assumption), so that the tangent plane provides an accurate approximation. In this chapter, we develop relative curvature measures of the nonlinearity of an estimation situation, and discuss how they can be used to indicate the adequacy of the linear approximation in a particular case. We then apply the curvature measures to 67 real data set–model combinations to gain some idea of how serious the two kinds of nonlinearity are in practice. Finally, we discuss more direct assessment of intrinsic nonlinearity to provide practical justification for assuming planarity.

As discussed in Section 2.5, linear approximation inference regions can be obtained from a first order Taylor series approximation to the expectation function evaluated at $\hat{\boldsymbol{\theta}}$. The $1-\alpha$ region is

$$(\boldsymbol{\theta}-\hat{\boldsymbol{\theta}})^{\mathrm{T}}\hat{\mathbf{V}}^{\mathrm{T}}\hat{\mathbf{V}}(\boldsymbol{\theta}-\hat{\boldsymbol{\theta}}) \leq Ps^2F(P, N-P; \alpha) \tag{7.1}$$

where $\hat{\mathbf{V}}$ is the derivative matrix evaluated at $\hat{\boldsymbol{\theta}}$.

Geometrically, the linear approximation inference region (7.1) assumes that, over the region of interest, the mapping of $\boldsymbol{\theta}$ to $\boldsymbol{\eta}(\boldsymbol{\theta})$ is

$$\hat{\boldsymbol{\eta}} + \hat{\mathbf{V}}(\boldsymbol{\theta} - \hat{\boldsymbol{\theta}})$$

This approximation, as pointed out by Beale (1960) and as discussed in Section 2.5, will be good only if the expectation surface is sufficiently flat to be replaced by the tangent plane, and if straight, parallel equispaced lines in the parameter space map into nearly straight, parallel equispaced lines on the expectation sur-

face. In that event, we can assume that the expectation surface inference region is a sphere of radius $\sqrt{Ps^2F(P, N-P; \alpha)}$ on the tangent plane and that the mapping of the tangent plane to the parameter space is linear.

To determine how planar the expectation surface is, and how uniform the parameter lines are on the tangent plane, we use second derivatives of the expectation function to derive *curvature measures* of *intrinsic* and *parameter effects nonlinearity*. The curvatures can also be used to investigate reparametrizations of expectation functions so as to obtain models which have more valid linear approximation parameter inference regions.

7.1 Velocity and Acceleration Vectors

A fundamental feature of linear models is that second and higher order derivatives of the expectation function with respect to the parameters are zero. It is logical, therefore, to attempt to measure the nonlinearity of a model by investigating second order derivatives of the expectation function (Bates, 1978; Bates and Watts, 1980; Beale, 1960). For clarity, we introduce a dot notation to distinguish between first and second derivatives. Thus for a nonlinear model $\boldsymbol{\eta}(\boldsymbol{\theta})$, the $N \times P$ derivative matrix is written as $\dot{\mathbf{V}}$ with elements

$$\{\dot{\mathbf{V}}\}_{np} = \frac{\partial f(\mathbf{x}_n, \boldsymbol{\theta})}{\partial \theta_p} \tag{7.2}$$

and the $N \times P \times P$ second derivative array is written as $\ddot{\mathbf{V}}$ with elements

$$\{\ddot{\mathbf{V}}\}_{npq} = \frac{\partial^2 f(\mathbf{x}_n, \boldsymbol{\theta})}{\partial \theta_p \, \partial \theta_q} \tag{7.3}$$

In (7.2) and (7.3), n runs from 1 to N while p and q run from 1 to P. In matrix notation,

$$\dot{\mathbf{V}} = \frac{\partial \boldsymbol{\eta}}{\partial \boldsymbol{\theta}^{\mathrm{T}}}$$

where each row of $\dot{\mathbf{V}}$ is the gradient of one coordinate of $\boldsymbol{\eta}(\boldsymbol{\theta})$ with respect to $\boldsymbol{\theta}$. Alternatively, we may regard $\dot{\mathbf{V}}$ as consisting of vectors $\dot{\mathbf{v}}_p, p = 1, 2, \ldots, P$.

Also,

$$\ddot{\mathbf{V}} = \frac{\partial^2 \boldsymbol{\eta}}{\partial \boldsymbol{\theta} \, \partial \boldsymbol{\theta}^{\mathrm{T}}}$$

where each face $\ddot{\mathbf{V}}_n$ of $\ddot{\mathbf{V}}$ is a complete $P \times P$ second derivative matrix, or Hessian, of one element of $\boldsymbol{\eta}(\boldsymbol{\theta})$ with respect to $\boldsymbol{\theta}$. As above, we may regard the Hessian array as consisting of vectors $\ddot{\mathbf{v}}_{pq}$, $p, q = 1, 2, \ldots, P$.

The vectors $\dot{\mathbf{v}}$ are, of course, the tangent vectors, and they are also called *velocity* vectors, since they give the rate of change of $\boldsymbol{\eta}$ with respect to each parameter. Accordingly, the vectors $\ddot{\mathbf{v}}$ are called *acceleration* vectors, since

they give the rates of change of the velocity vectors with respect to the parameters. That is,

$$\ddot{\mathbf{v}}_{pq} = \frac{\partial \dot{\mathbf{v}}_p}{\partial \theta_q}$$

Example: Puromycin 21

For the Michaelis–Menten expectation function

$$f(x,\boldsymbol{\theta}) = \frac{\theta_1 x}{\theta_2 + x}$$

the elements in $\dot{\mathbf{V}}$ are

$$\{\dot{\mathbf{V}}\}_{n1} = \frac{x_n}{\theta_2 + x_n}$$

$$\{\dot{\mathbf{V}}\}_{n2} = \frac{-\theta_1 x_n}{(\theta_2 + x_n)^2}$$

Evaluating these functions at each x_n value for a particular parameter pair $\boldsymbol{\theta}$ produces the matrix $\dot{\mathbf{V}}$.

The elements in $\ddot{\mathbf{V}}$ can also be evaluated, as

$$\{\ddot{\mathbf{V}}\}_{n11} = 0$$

$$\{\ddot{\mathbf{V}}\}_{n12} = \frac{-x_n}{(\theta_2 + x_n)^2}$$

$$\{\ddot{\mathbf{V}}\}_{n21} = \{\ddot{\mathbf{V}}\}_{n12}$$

$$\{\ddot{\mathbf{V}}\}_{n22} = \frac{2\theta_1 x_n}{(\theta_2 + x_n)^3}$$

For the Puromycin data, the concentrations and the velocity and acceleration vectors at $\hat{\boldsymbol{\theta}}$ are given in Table 7.1. ■

7.1.1 Tangential and Normal Accelerations

The acceleration vectors can be decomposed into components *in* and *orthogonal to* the tangent plane. Because there are only $P(P+1)/2$ distinct acceleration vectors, the acceleration vectors will span a subspace of maximum dimension $P(P+1)/2$ in the response space, so the maximum dimension of the combined tangent and acceleration spaces is $P(P+3)/2$ (Hamilton, 1980). In many cases the combined dimension is only slightly larger than P, say $P+P'$.

Table 7.1 Velocity and acceleration vectors for the Puromycin data evaluated at $\hat{\boldsymbol{\theta}} = (212.7, 0.0641)^T$.

	Velocity		Acceleration		
Conc.	$\dot{\mathbf{v}}_1$	$\dot{\mathbf{v}}_2$	$\ddot{\mathbf{v}}_{11}$	$\ddot{\mathbf{v}}_{12}$	$\ddot{\mathbf{v}}_{22}$
0.02	0.237812	−601.458	0	−2.82773	14 303.4
0.02	0.237812	−601.458	0	−2.82773	14 303.4
0.06	0.483481	−828.658	0	−3.89590	13 354.7
0.06	0.483481	−828.658	0	−3.89590	13 354.7
0.11	0.631821	−771.903	0	−3.62907	8 867.4
0.11	0.631821	−771.903	0	−3.62907	8 867.4
0.22	0.774375	−579.759	0	−2.72571	4 081.4
0.22	0.774375	−579.759	0	−2.72571	4 081.4
0.56	0.897292	−305.807	0	−1.43774	980.0
0.56	0.897292	−305.807	0	−1.43774	980.0
1.10	0.944936	−172.655	0	−0.81173	296.6
1.10	0.944936	−172.655	0	−0.81173	296.6

Example: Puromycin 22

For the Michaelis–Menten model, $\ddot{\mathbf{v}}_{11} \equiv \mathbf{0}$ because θ_1 is a conditionally linear parameter. This conditional linearity causes the acceleration vector $\ddot{\mathbf{v}}_{12} = \ddot{\mathbf{v}}_{21}$ to be a simple multiple of $\dot{\mathbf{v}}_2$, so that the only acceleration vector which is not in the tangent plane is $\ddot{\mathbf{v}}_{22}$. The tangent space has dimension 2, the acceleration space has dimension 2, and the combined tangent and acceleration spaces have dimension 3.

In Figure 7.1 we show the projection of the tangent vectors and the acceleration vectors into the combined tangent and acceleration space for the Puromycin data. To provide a clearer figure, we have scaled the response by dividing by 100 and scaled the concentrations by multiplying by 10. Note that only the vector $\ddot{\mathbf{v}}_{22}$ has a component outside the tangent plane, and that this component is small. ■

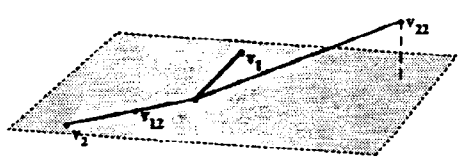

Figure 7.1 Projection of the scaled velocity and acceleration vectors for the Puromycin data at $\hat{\boldsymbol{\theta}} = (212.7, 0.0641)^T$ in the 3-dimensional space spanned by these vectors. The tangent plane is shaded.

To determine the tangential and normal components of an acceleration vector, we project the acceleration vectors into the tangent plane and into the space normal to the tangent space but spanned by the acceleration vectors. This is easily accomplished by gathering the $P(P+1)/2$ nonredundant acceleration vectors into a matrix $\ddot{\mathbf{W}}$ and combining them with the tangent vectors in $\dot{\mathbf{V}}$ to give

$$\mathbf{D} = (\dot{\mathbf{V}}, \ddot{\mathbf{W}}) \tag{7.4}$$

We then perform a QR decomposition on $\mathbf{D}$, as $\mathbf{D} = (\mathbf{Q}_1 \mid \mathbf{Q}'_1 \mid \mathbf{Q}_2)\mathbf{R}$, and multiply the array $\ddot{\mathbf{V}}$ by $(\mathbf{Q}_1 \mid \mathbf{Q}'_1)^{\mathrm{T}}$ to give

$$\ddot{\mathbf{A}} = [(\mathbf{Q}_1 \mid \mathbf{Q}'_1)^{\mathrm{T}}][\ddot{\mathbf{V}}] \tag{7.5}$$

where $\mathbf{Q}_1$ is the first P columns of $\mathbf{Q}$ and $\mathbf{Q}'_1$ is the next P' columns of $\mathbf{Q}$. This provides a compact $(P+P')\times P\times P$ *acceleration array* $\ddot{\mathbf{A}}$ with P faces in the tangent space and P' faces in the acceleration space. (The square bracket notation indicates that the summation is over the numerator index: that is, the element in the nth face, pth row, and qth column of the product $\mathbf{A} = [\mathbf{B}][\mathbf{C}]$, where $\mathbf{B}$ is an $N_1 \times N_2$ matrix and $\mathbf{C}$ is an $N_2 \times N_3 \times N_4$ array, is

$$\{\mathbf{A}\}_{npq} = \sum_{i=1}^{N_2} \{\mathbf{B}\}_{ni} \{\mathbf{C}\}_{ipq}$$

and $\mathbf{A}$ is an $N_1 \times N_3 \times N_4$ array.)

Example: Puromycin 23

To illustrate these calculations, we use the velocity and acceleration vectors from Example Puromycin 21, Table 7.1, to form the matrix $\mathbf{D}$. Performing a QR decomposition on $\mathbf{D}$ gives

$$\mathbf{R}_1 = [(\mathbf{Q}_1 \mid \mathbf{Q}'_1)^{\mathrm{T}}][\mathbf{D}] = \begin{bmatrix} \mathbf{R}_{11} & \mathbf{R}_{12} \\ \mathbf{0} & \mathbf{R}_{22} \end{bmatrix}$$

$$= \begin{bmatrix} -2.44 & 1568.7 & 0 & 7.378 & -16185.7 \\ 0 & 1320.3 & 0 & 6.210 & -25030.4 \\ 0 & 0 & 0 & 0 & 8369.1 \end{bmatrix}$$

The left upper 2×2 matrix, $\mathbf{R}_{11}$, is simply $\hat{\mathbf{R}}_1$ from the QR decomposition of $\dot{\mathbf{V}}$ (cf. Example Puromycin 7), and the right upper 2×3 matrix, $\mathbf{R}_{12}$, gives the projection of the acceleration vectors into the tangent plane, $[\mathbf{Q}_1^{\mathrm{T}}][\ddot{\mathbf{W}}]$. The 1×3 lower right matrix, $\mathbf{R}_{22}$, gives the projection of that part of the acceleration vector which is orthogonal to the tangent space but in the space spanned by the acceleration vectors, $[\mathbf{Q}'^{\mathrm{T}}_1][\ddot{\mathbf{W}}]$. In this example, this extra space has dimension $P' = 1$.

Reforming the elements of $\mathbf{R}_{12}$ and $\mathbf{R}_{22}$ into a $3\times 2\times 2$ acceleration array $\ddot{\mathbf{A}}$ gives

$$\ddot{\mathbf{A}} = \begin{bmatrix} 0 & 7.378 \\ 7.378 & -16185.7 \end{bmatrix} \begin{bmatrix} 0 & 6.210 \\ 6.210 & -25030.4 \end{bmatrix} \begin{bmatrix} 0 & 0 \\ 0 & 8369.1 \end{bmatrix}$$

These are the values which, when scaled as in Example Puromycin 22, were used to generate Figure 7.1. ■

The extent to which the acceleration vectors lie outside the tangent plane measures how much the expectation surface deviates from a plane, and hence measures the nonplanarity of the expectation surface. We call this nonplanarity *intrinsic nonlinearity* because, as discussed in Chapter 2, it does not depend on the parametrization chosen for the expectation function, but only on the design and the expression for the expectation function. The projections of the acceleration vectors in the tangent plane necessarily depend on the parametrization, and measure the nonuniformity of the parameter lines on the tangent plane. This nonuniformity is called *parameter effects nonlinearity* or, more simply, *parameter effects*.

Because the elements in the array $\ddot{\mathbf{A}}$ provide information on the parameter effects and intrinsic nonlinearities, we write the first P faces of $\ddot{\mathbf{A}}$ as $\mathbf{A}^{\theta}$, to denote the parameter effects acceleration array, and the last P' faces as $\mathbf{A}^{\iota}$, to denote the intrinsic acceleration array.

Example: Rumford 8

In Figure 7.2*a* we show the expectation surface (curve) $\boldsymbol{\eta}(\theta)$ for the Rumford model with the design $\mathbf{x} = (4, 41)^{\mathrm{T}}$ and the parametrization

$$f = 60 + 70\, e^{-x\theta}$$

The marks on the expectation curve correspond to

$$\theta = 0.01, 0.02, \ldots, 0.08, 0.1, 0.2, \ldots, 0.9, 1.0$$

and as pointed out in Chapter 2, equally spaced values of θ map to unequally spaced values on $\boldsymbol{\eta}$. This is a manifestation of the parameter effects nonlinearity, while the curving of the line is a manifestation of intrinsic nonlinearity.

In Figure 7.2*b* we show the expectation surface $\boldsymbol{\eta}(\phi)$ for the Rumford model with the same design and the reparametrization $\phi = \log_{10}\theta$,

$$f = 60 + 70 \exp(-x\, 10^{\phi})$$

The marks on the expectation curve correspond to the values

$$\phi = -2.0, -1.9, -1.8, \ldots, -0.1, 0$$

so that the same range of θ is covered. Note that the expectation curves are identical, and that the only change is a relabeling of the points on the curve. It is because the curve does not change with the parametrization that we call the nonlinearity *intrinsic*. Note, too, that points which are equally spaced in the ϕ space still map to unequally spaced points on the expecta-

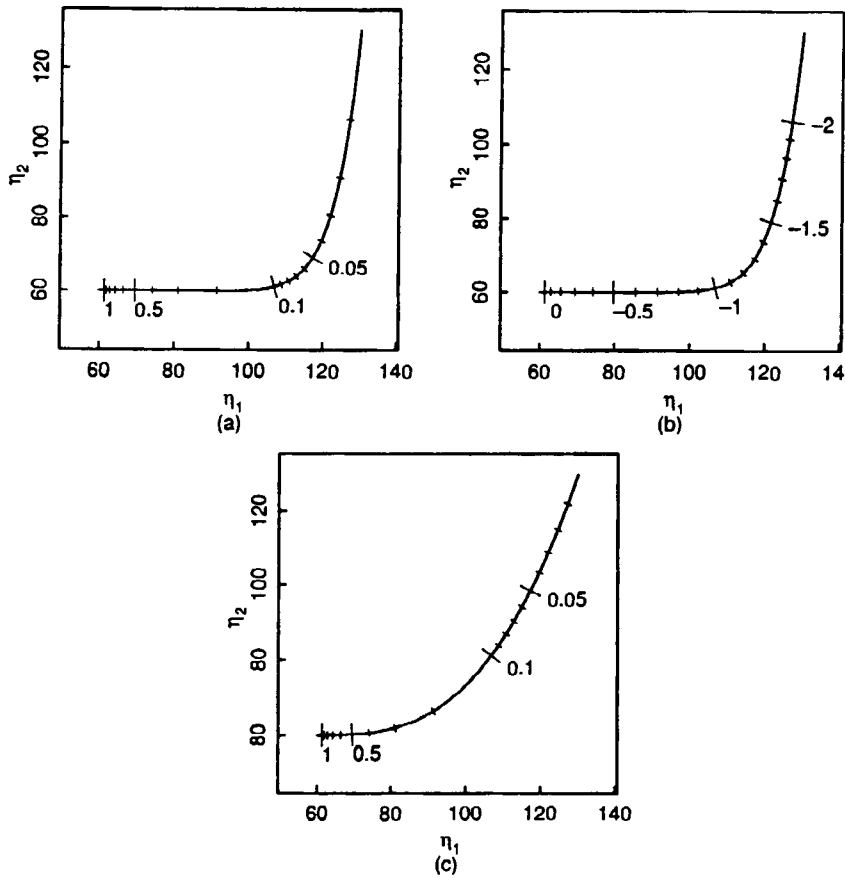

Figure 7.2 Plot of the expectation surface (curve) for the 2-case Rumford example. In part *a*, the design is $(4,41)^T$ and the parameter is the original parameter θ. In part *b*, the same design is used but the parameter is $\phi = \log_{10}\theta$. In part *c*, the original parameter θ is used, but the design is changed to $(4,12)^T$.

tion curve, but the nonuniformity in the spacing on η is not as severe as it was for the θ parametrization. The ϕ parametrization is therefore said to have smaller parameter effects nonlinearity.

In Figure 7.2*c* we show the expectation surface $\eta(\theta)$ for the Rumford model with the θ parametrization and the design $\mathbf{x} = (4, 12)^T$. The main feature to notice is that the expectation surface is different from that in Figure 7.2*a* and *b* because the design has been changed. ■

Reparametrizing a model not only affects the mapping of the parameter lines to the expectation surface but also the tangent and acceleration vectors, and consequently the parameter effects nonlinearity.

Example: Rumford 9

Shown in Figure 7.3 are the expectation surface and the acceleration and the tangent vectors at a point on the surface. As in Example Puromycin 22, we have scaled the parameters and the design variable to provide a clearer figure. The design variable is scaled by 0.1, and the parameter θ by 10. In this scaling, the point is $\theta = 1.0$ ($\phi = 0.0$) for the $(0.4, 4.1)^T$ design, corresponding to $\theta = 0.1$ ($\phi = -1.0$) for the $(4, 41)^T$ design in the original scaling.

Note that the tangent vectors are in the same direction, as they must be for them both to be tangent to the same curve. The *lengths* of the tangent vectors are very different, however, and the acceleration vectors are different not only in length, but also in orientation. Both these differences are due to the reparametrization, and so we see some of the effects of parameter nonlinearity. ■

7.1.2 The Acceleration in an Arbitrary Direction

The velocity and acceleration vectors only provide information about the expectation surface corresponding to changes along the parameter axes in the parameter space. To measure the velocity and acceleration near $\hat{\boldsymbol{\theta}}$ in an arbitrary direction $\mathbf{u}$ in the parameter space, we introduce a distance parameter b and let

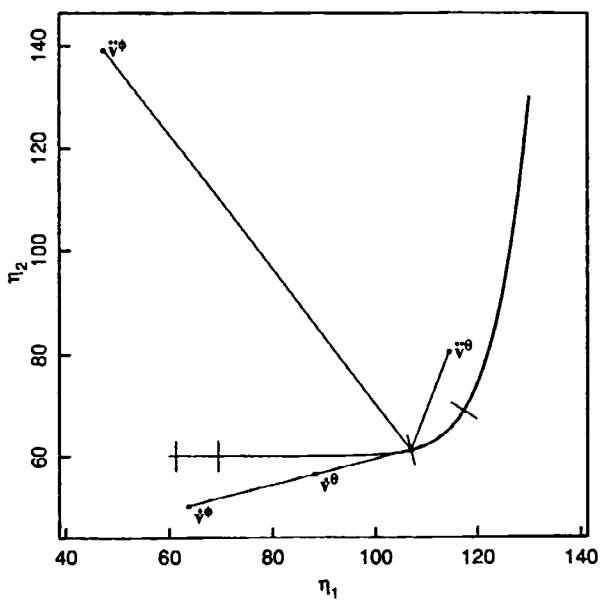

Figure 7.3 Scaled velocity and acceleration vectors at $\theta = 1$ for the 2-case Rumford example using the parameter θ and the parameter $\phi = \log_{10}\theta$.

$\boldsymbol{\theta}=\hat{\boldsymbol{\theta}}+b\mathbf{u}$, where $\mathbf{u}$ is a $P\times 1$ unit vector. Mapping the line $\boldsymbol{\theta}(b)=\hat{\boldsymbol{\theta}}+b\mathbf{u}$ to the expectation surface generates a curve $\boldsymbol{\eta}_{\mathbf{u}}(b)=\boldsymbol{\eta}(\hat{\boldsymbol{\theta}}+b\mathbf{u})$ through the point $\boldsymbol{\eta}(\hat{\boldsymbol{\theta}})$. The tangent and acceleration vector to that curve at $\hat{\boldsymbol{\theta}}$ are obtained by differentiating with respect to b and evaluating the derivatives at $b=0$. Thus,

$$\left.\frac{d\boldsymbol{\eta}_{\mathbf{u}}}{db}\right|_0 = \sum_{p=1}^{P} \left.\frac{\partial\boldsymbol{\eta}}{\partial\theta_p}\right|_{\hat{\boldsymbol{\theta}}} \left.\frac{d\theta_p}{db}\right|_0$$

$$= \sum_{p=1}^{P} \dot{\mathbf{v}}_p u_p$$

or, more compactly,

$$\dot{\boldsymbol{\eta}}_{\mathbf{u}} = \dot{\mathbf{V}}\mathbf{u} \tag{7.6}$$

Similarly, the acceleration vector corresponding to the direction $\mathbf{u}$ is

$$\left.\frac{d^2\boldsymbol{\eta}_{\mathbf{u}}}{db^2}\right|_0 = \sum_{q=1}^{P} \left.\frac{\partial\sum_{p=1}^{P}\dot{\mathbf{v}}_p u_p}{\partial\theta_q}\right|_{\hat{\boldsymbol{\theta}}} \left.\frac{d\theta_q}{db}\right|_0$$

$$= \sum_{p=1}^{P}\sum_{q=1}^{P} \ddot{\mathbf{v}}_{pq} u_p u_q \tag{7.7}$$

which can also be written compactly as

$$\ddot{\boldsymbol{\eta}}_{\mathbf{u}} = \mathbf{u}^{\mathrm{T}}\ddot{\mathbf{V}}\mathbf{u} \tag{7.8}$$

From (7.6) we see that the velocity corresponding to the direction $\mathbf{u}$ is just a linear combination of the velocity vectors $\dot{\mathbf{v}}$, and from (7.7) and (7.8) that the acceleration is also just a linear combination of the acceleration vectors $\ddot{\mathbf{v}}$. In (7.8), the $N\times 1$ vector $\ddot{\boldsymbol{\eta}}_{\mathbf{u}}$ is formed by pre- and postmultiplying the $N\times P\times P$ array by a $1\times P$ and a $P\times 1$ vector. Each coordinate of $\ddot{\boldsymbol{\eta}}_{\mathbf{u}}$ is of the form $\mathbf{u}^{\mathrm{T}}\ddot{\mathbf{V}}_n\mathbf{u}$, where $\ddot{\mathbf{V}}_n$ is the nth face of the array $\ddot{\mathbf{V}}$.

Since our primary interests are accelerations in and normal to the tangent plane, we can represent them more compactly by reducing $\ddot{\mathbf{V}}$ to $\ddot{\mathbf{A}}$ as in (7.5). In this case, the acceleration corresponding to the direction $\mathbf{u}$ becomes

$$\mathbf{Q}^{\mathrm{T}}\ddot{\boldsymbol{\eta}}_{\mathbf{u}} = \mathbf{u}^{\mathrm{T}}\ddot{\mathbf{A}}\mathbf{u} \tag{7.9}$$

or

$$\mathbf{Q}^{\mathrm{T}}\ddot{\boldsymbol{\eta}}_{\mathbf{u}} = \sum_{p=1}^{P}\sum_{q=1}^{P} \{\ddot{\mathbf{A}}\}_{pq} u_p u_q \tag{7.10}$$

where $\{\ddot{\mathbf{A}}\}_{pq}$ is the $(P+P')\times 1$ vector in the array $\ddot{\mathbf{A}}$. Note that these are simply columns from the matrix $\mathbf{R}_1$ from the QR decomposition of $\mathbf{D}$, equation (7.4). Writing the matrix

$$\begin{bmatrix} \mathbf{R}_{12} \\ \mathbf{R}_{22} \end{bmatrix} = \left[\mathbf{r}_{11}, \mathbf{r}_{12}, \mathbf{r}_{22}, \ldots, \mathbf{r}_{pp} \right] \tag{7.11}$$

then (7.10) can be expressed as

$$\mathbf{Q}^{\mathrm{T}} \ddot{\boldsymbol{\eta}}_{\mathbf{u}} = \sum_{p=1}^{P} \mathbf{r}_{pp} u_p^2 + 2 \sum_{p=1}^{P} \sum_{q=p+1}^{P} \mathbf{r}_{pq} u_p u_q \tag{7.12}$$

which is a convenient form for calculation.

Example: Puromycin 24

To illustrate the calculations involved in (7.12), we calculate the acceleration corresponding to the direction $\mathbf{u} = (0.6, 0.8)^{\mathrm{T}}$. Using (7.12) and the values in $\mathbf{R}_1$ from Example Puromycin 23,

$$\begin{aligned} \mathbf{Q}^{\mathrm{T}} \ddot{\boldsymbol{\eta}}_{\mathbf{u}} &= (0.6)^2 \mathbf{r}_{11} + (0.8)^2 \mathbf{r}_{22} + 2(0.6)(0.8) \mathbf{r}_{12} \\ &= 0.36 \begin{bmatrix} 0 \\ 0 \\ 0 \end{bmatrix} + 0.64 \begin{bmatrix} -16185.7 \\ -25030.4 \\ 8369.1 \end{bmatrix} + 0.96 \begin{bmatrix} 7.378 \\ 6.210 \\ 0 \end{bmatrix} \\ &= \begin{bmatrix} -10351.8 \\ -16013.5 \\ 5356.2 \end{bmatrix} \end{aligned}$$

■

7.2 Relative Curvatures

Although accelerations are indicators of nonlinearity, they are not useful measures of it, because they depend on scaling of the data and the parameters. In the Rumford example, for instance, measuring the temperature on the Celsius instead of the Farenheit scale, or measuring the time in hours instead of minutes, would produce different accelerations. To avoid this dependence, we convert the accelerations to *relative curvatures*.

The *curvature* $c_{\mathbf{u}}$ in the direction $\mathbf{u}$ at a point is defined as the ratio of the length of the acceleration vector to the squared length of the tangent vector,

$$c_{\mathbf{u}} = \frac{\| \ddot{\boldsymbol{\eta}}_{\mathbf{u}} \|}{\| \dot{\boldsymbol{\eta}}_{\mathbf{u}} \|^2}$$

For parameter effects curvature, we have

$$c_{\mathbf{u}}^{\theta} = \frac{\| \ddot{\boldsymbol{\eta}}_{\mathbf{u}}^{\theta} \|}{\| \dot{\boldsymbol{\eta}}_{\mathbf{u}} \|^2} \tag{7.13}$$

and for intrinsic curvature,

$$c_{\mathbf{u}}^{\iota} = \frac{\| \ddot{\boldsymbol{\eta}}_{\mathbf{u}}^{\iota} \|}{\| \dot{\boldsymbol{\eta}}_{\mathbf{u}} \|^2} \tag{7.14}$$

Multiplying the acceleration and tangent vectors by $\mathbf{Q}^{\mathrm{T}}$ does not change the magnitude of either the denominator or the numerator, and so we use the more compact array $\mathbf{A}^{\theta}$ to calculate the numerator in (7.13) using

$$\| \mathbf{u}^{\mathrm{T}} \mathbf{A}^{\theta} \mathbf{u} \|^2 = \sum_{p=1}^{P} (\mathbf{u}^{\mathrm{T}} \ddot{\mathbf{A}}_p \mathbf{u})^2$$

and the numerator in (7.14) using

$$\| \mathbf{u}^{\mathrm{T}} \mathbf{A}^{\iota} \mathbf{u} \|^2 = \sum_{p=P+1}^{P+P'} (\mathbf{u}^{\mathrm{T}} \ddot{\mathbf{A}}_p \mathbf{u})^2$$

The denominators are calculated using

$$\begin{aligned} \| \dot{\boldsymbol{\eta}}_{\mathbf{u}} \|^2 &= \| \dot{\mathbf{V}} \mathbf{u} \|^2 \\ &= \mathbf{u}^{\mathrm{T}} \mathbf{R}_{11}^{\mathrm{T}} \mathbf{R}_{11} \mathbf{u} \\ &= \| \mathbf{R}_{11} \mathbf{u} \|^2 \end{aligned}$$

where $\mathbf{R}_{11}$ is from the QR decomposition of $\mathbf{D}$, (7.4).

To simplify calculation of the curvatures, we arrange that $\| \dot{\boldsymbol{\eta}}_{\mathbf{u}} \|^2 = 1$ for any $\mathbf{u}$ with $\| \mathbf{u} \| = 1$ by linearly tranforming to orthogonal parameters

$$\boldsymbol{\phi} = \mathbf{R}_{11}(\boldsymbol{\theta} - \hat{\boldsymbol{\theta}}) \tag{7.15}$$

Furthermore, since curvatures are measured in units of 1/response, their values depend on the scaling of the data. To remove this dependence, we convert to dimensionless *relative curvatures* by multiplying the response and the curvatures by $s\sqrt{P}$. The final result is a *relative curvature array*

$$\mathbf{C} = \mathbf{R}_{11}^{-\mathrm{T}} \ddot{\mathbf{A}} \mathbf{R}_{11}^{-1} s\sqrt{P} \tag{7.16}$$

which consists of a $P \times P \times P$ *parameter effects relative curvature array* $\mathbf{C}^{\theta}$, given by the first P faces of $\mathbf{C}$ and a $P' \times P \times P$ *intrinsic relative curvature array* $\mathbf{C}^{\iota}$, given by the last P' faces of $\mathbf{C}$.

An important consequence of scaling by $s\sqrt{P}$ is that the sum of squares contour bounding a nominal $1-\alpha$ likelihood region on the tangent plane is simply a disk of radius $\sqrt{F(P, N-P; \alpha)}$, and the likelihood region itself, determined from (6.1), becomes all values of $\boldsymbol{\theta}$ for which the (scaled) sum of squares equals $1 + [P/(N-P)]F(P, N-P; \alpha)$. This affords a convenient scale of measurement for the curvatures.

Example: Puromycin 25

For the Puromycin data, $s = 10.93$, $P = 2$,

$$\mathbf{R}_{11}^{-1} = \begin{bmatrix} -0.4092 & 0.4861 \\ 0 & 0.0007574 \end{bmatrix}$$

and, from Example Puromycin 23,

$$\ddot{\mathbf{A}} = \begin{bmatrix} 0 & 7.378 \\ 7.378 & -16185.7 \end{bmatrix} \begin{bmatrix} 0 & 6.210 \\ 6.210 & -25030.4 \end{bmatrix} \begin{bmatrix} 0 & 0 \\ 0 & 8369.1 \end{bmatrix}$$

so that

$$\mathbf{C} = \begin{bmatrix} 0.000 & -0.035 \\ & -0.059 \end{bmatrix} \begin{bmatrix} 0.000 & -0.030 \\ & -0.151 \end{bmatrix} \begin{bmatrix} 0.000 & 0.000 \\ & 0.074 \end{bmatrix}$$

where the first two matrices give $\mathbf{C}^{\theta}$, and the third, $\mathbf{C}^{\iota}$. Since each face of $\mathbf{C}$ is symmetric, we only display the upper triangular part; for example, in the above array, $c_{212} = -0.030 = c_{221}$.

Because the curvatures are small, we expect that the tangent plane would provide a good approximation to the expectation surface and that projections of the parameter curves on the tangent plane would be quite uniform. In Figure 7.4*a* we show projections of the $\boldsymbol{\phi}$ parameter curves on the tangent plane. As expected, the curves are quite straight, parallel, and equispaced.

Also shown in Figure 7.4*a* is the tangent plane disk of radius $\sqrt{F(2,10;0.05)} = 2.02$. Since the region is not too large, the parameter curves are well behaved within it and we would expect a linear approximation region to give a good approximation to the true likelihood region. This

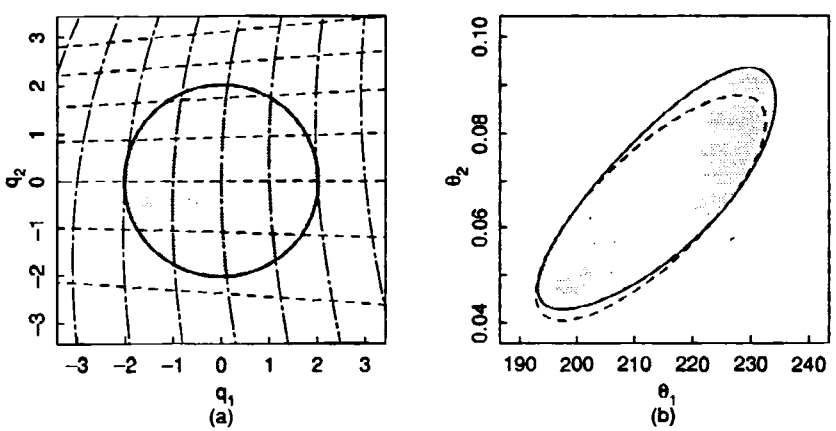

Figure 7.4 Likelihood regions for the parameters in the Puromycin model. In part *a*, the parameter curves for the parameters $\boldsymbol{\phi} = \mathbf{R}_{11}(\boldsymbol{\theta} - \hat{\boldsymbol{\theta}})$ are projected onto the tangent plane with the 95% likelihood disk, assuming the expectation surface is planar, shaded. In part *b*, this region is transformed to the $\boldsymbol{\theta}$ parameter space and shaded. The ellipse shown as a dashed line in part *b* is from the linear approximation.

is indeed the case, as demonstrated in Figure 7.4*b*, where we show the linear approximation region (dashed line) and the likelihood region (solid line) determined from the (scaled) sum of squares contour $S(\boldsymbol{\theta}) = 1 + (2/10)4.10 = 1.82$. ■

The relative curvature array **C** is not unique, since any transformation to orthogonal parameters $\boldsymbol{\phi}$ could be used, and any orthogonal rotation of the response space could be used, provided the tangent and its orthogonal are kept distinct. The parameter transformation given by $\mathbf{R}_{11}$ is convenient.

An algorithm for calculating the relative curvature array was presented in Bates, Hamilton, and Watts (1983). They combine $\dot{\mathbf{V}}$ and the nonredundant $\ddot{\mathbf{V}}$ vectors into a matrix **D**, the first P columns of which contain the first derivative vectors $\dot{\mathbf{v}}_p$ and the remaining $P(P+1)/2$ columns the second derivative vectors $\ddot{\mathbf{v}}_{pq}$ stored in symmetric storage mode; that is, in the order $11, 12, 22, 13, \ldots, PP$. They then use a pivoted QR decomposition (Dongarra et al., 1979, Chapter 9) to write $\mathbf{D} = \mathbf{QRE}$, where **Q** is $N \times N$ orthogonal, **E** is a $P(P+3)/2$ square permutation matrix in which the upper left $P \times P$ submatrix is the identity, and **R** is upper trapezoidal with the upper-left $P \times P$ submatrix being upper triangular. They assume $\dot{\mathbf{V}}$ is nonsingular but do not require **D** to be so.

Partitioning **R** as

$$\mathbf{R} = \begin{bmatrix} \mathbf{R}_{11} & \mathbf{R}_{12} \\ \mathbf{0} & \mathbf{R}_{22} \\ \mathbf{0} & \mathbf{0} \end{bmatrix}$$

provides $\mathbf{R}_{11}$, which is used to produce $\boldsymbol{\phi}$, $\mathbf{R}_{12}$, which is used to produce $\mathbf{C}^{\theta}$, and $\mathbf{R}_{22}$, which is used to produce $\mathbf{C}^{\iota}$. The number of nonzero rows in **R** is the dimension of the combined tangent and acceleration spaces. The first P columns of **Q**, $\mathbf{Q}_1$, form an orthogonal basis for the tangent space and the next P' columns, $\mathbf{Q}'_1$, form an orthogonal basis for the normal acceleration space.

To calculate the curvature arrays, each $P \times P$ face of the 3-dimensional array formed by expanding the second derivative columns from the symmetric storage mode must be postmultiplied by $\mathbf{R}_{11}^{-1}$ and premultiplied by $\mathbf{R}_{11}^{-\mathrm{T}}$. These two multiplications are replaced by a single postmultiplication of the last $P(P+1)/2$ columns of **R** by a matrix composed of products of elements of $\mathbf{R}_{11}^{\mathrm{T}}$, which creates the symmetric storage version of the curvature array with dimension $(P+P') \times P(P-1)/2$ (Bates, Hamilton, and Watts, 1983). This *relative curvature matrix* gives a more compact representation of the curvatures, with the first P rows revealing the parameter effect relative curvature terms and the last P' rows the intrinsic curvature terms. Alternatively, each column gives a curvature vector for a particular parameter pair.

Example: Puromycin 26

From Example Puromycin 25, the curvature matrix is

$$\begin{bmatrix} 0 & -0.035 & -0.059 \\ 0 & -0.030 & -0.151 \\ 0 & 0 & 0.074 \end{bmatrix}$$

For this model and data set, all the relative curvatures are small, and so the estimation situation is probably not badly affected by the nonlinearity. ■

7.2.1 Interpreting Terms in the Curvature Arrays

7.2.1.1 Intrinsic Curvatures

The geometric interpretation of intrinsic curvature is that it is the reciprocal of the radius of the circle which best approximates the expectation surface in the direction η_u. Thus, if the planar assumption is good, the intrinsic curvature will be small.

Example: Rumford 10

In Figure 7.5 we show the expectation curve for the Rumford model with

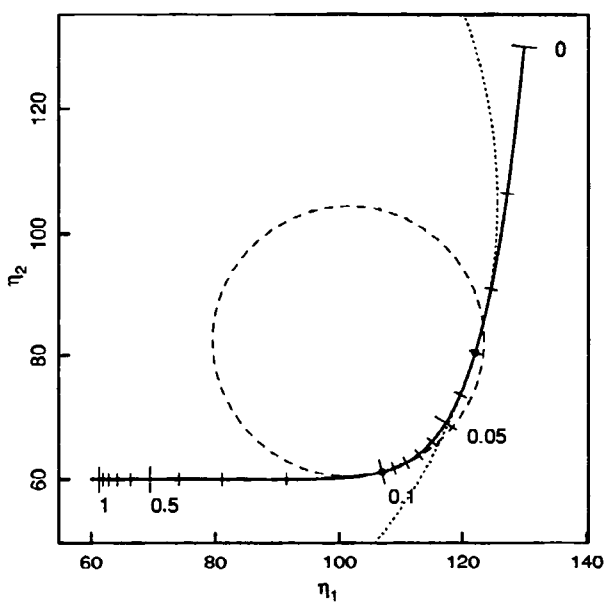

Figure 7.5 Approximating circles to the expectation surface for the 2-case Rumford example. The dashed circle is the approximation to the surface based on the intrinsic curvature at $\theta = 0.1$. The dotted circle is the approximation to the surface based on the intrinsic curvature at $\theta = 0.03$.

the design $\mathbf{x} = (4, 41)^T$, together with portions of the approximating circles at points corresponding to $\theta = 0.1$ and $\theta = 0.03$. For $\theta = 0.1$ the circle has a curvature of $1706/37490 = 0.046$ with a radius of $1/0.046 = 22$, and for $\theta = 0.03$ the larger circle has a curvature 0.0115 with a radius of $1/0.0115 = 87$. ■

Example: Puromycin 27

In Figure 7.6 we show the expectation surface in the space spanned by the tangent vectors and the residual vector for the Puromycin data. The surface is extremely flat, and so the tangent plane provides an excellent approximation to the expectation surface near $\hat{\boldsymbol{\theta}}$. This is expected, given the magnitudes of the entries in the intrinsic curvature array

$$\mathbf{C}^{\iota} = \begin{bmatrix} 0.000 & 0.000 \\ & 0.074 \end{bmatrix}$$

■

7.2.1.2 *Parameter Effects Curvatures*

Each of the terms c_{npq} in the relative curvature array has a geometric interpretation, which helps in understanding nonlinearity (Bates and Watts, 1981a). To interpret the terms c_{npq}, we consider a 2-parameter example.

The tangential components of the scaled velocity and acceleration vectors evaluated at $\boldsymbol{\phi} = \mathbf{0}$ are

$$\dot{\mathbf{v}}_1(\boldsymbol{\phi} = \mathbf{0}) = \mathbf{q}_1$$

$$\dot{\mathbf{v}}_2(\boldsymbol{\phi} = \mathbf{0}) = \mathbf{q}_2$$

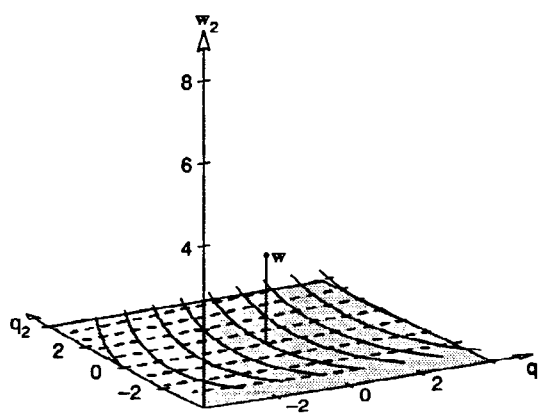

Figure 7.6 Projection of the parameter curves from the orthogonal parameters $\boldsymbol{\phi} = \mathbf{R}_{11}(\boldsymbol{\theta} - \hat{\boldsymbol{\theta}})$ for the Puromycin data model into the 3-dimensional subspace spanned by the tangent plane vectors, $\mathbf{q}_1$ and $\mathbf{q}_2$, and the rotated residual vector, $\mathbf{w}$. The tangent plane is shaded.

and

$$\ddot{\mathbf{v}}_{11} = c_{111}\mathbf{q}_1 + c_{211}\mathbf{q}_2$$

$$\ddot{\mathbf{v}}_{12} = c_{112}\mathbf{q}_1 + c_{212}\mathbf{q}_2$$

$$\ddot{\mathbf{v}}_{22} = c_{122}\mathbf{q}_1 + c_{222}\mathbf{q}_2$$

At another point $\boldsymbol{\phi} = \boldsymbol{\delta}$ the new tangent vectors will be approximately

$$\dot{\mathbf{v}}_1(\boldsymbol{\delta}) \approx \dot{\mathbf{v}}_1(\mathbf{0}) + \delta_1 \left.\frac{\partial \dot{\mathbf{v}}_1}{\partial \phi_1}\right|_{\boldsymbol{\phi}=\mathbf{0}} + \delta_2 \left.\frac{\partial \dot{\mathbf{v}}_1}{\partial \phi_2}\right|_{\boldsymbol{\phi}=\mathbf{0}}$$

$$= \mathbf{q}_1 + \delta_1 \ddot{\mathbf{v}}_{11} + \delta_2 \ddot{\mathbf{v}}_{12}$$

and

$$\dot{\mathbf{v}}_2(\boldsymbol{\delta}) \approx \mathbf{q}_2 + \delta_1 \ddot{\mathbf{v}}_{21} + \delta_2 \ddot{\mathbf{v}}_{22}$$

Collecting terms in $\mathbf{q}_1$ and $\mathbf{q}_2$ gives

$$\dot{\mathbf{v}}_1(\boldsymbol{\delta}) = \mathbf{q}_1(1 + \delta_1 c_{111} + \delta_2 c_{112}) + \mathbf{q}_2(\delta_1 c_{211} + \delta_2 c_{212})$$

$$\dot{\mathbf{v}}_2(\boldsymbol{\delta}) = \mathbf{q}_1(\delta_1 c_{112} + \delta_2 c_{122}) + \mathbf{q}_2(1 + \delta_1 c_{212} + \delta_2 c_{222})$$

Thus, c_{111} gives the change in the $\mathbf{q}_1$ direction of the $\dot{\mathbf{v}}_1$ vector due to a unit change in ϕ_1: that is, terms of the form c_{ppp} cause the vector $\dot{\mathbf{v}}_p$ to change length. We therefore refer to c_{ppp} as *compansion* terms since they cause compression or expansion of scale along a ϕ_p parameter line. The term c_{211} gives the change in the $\mathbf{q}_2$ direction of the $\dot{\mathbf{v}}_1$ vector due to a unit change in ϕ_1: that is, terms of the form c_{qpp} $(q \neq p)$ cause changes in the $\mathbf{q}_q$ direction of the ϕ_p parameter lines as we move along them. We refer to these as *arcing* terms. The term c_{212} gives the change in the $\mathbf{q}_2$ direction of the $\dot{\mathbf{v}}_2$ vector due to a unit change in ϕ_1: that is, terms of the form c_{qpq} cause changes in the $\mathbf{q}_q$ direction of the ϕ_p parameter curves as we move across the ϕ_q parameter curves. We call these *fanning* terms, since the ϕ_p parameter lines will appear to fan out from a common point on the $\mathbf{q}_p$ axis. Since $c_{qqp} = c_{qpq}$, terms of the form c_{qqp} also cause ϕ_p fanning.

With two parameters, only compansion, arcing, and fanning can occur; with more than two parameters, only one more type of parameter effect can occur—when all the subscripts are different. A term such as c_{npq} causes a change in the $\mathbf{q}_n$ direction of the $\dot{\mathbf{v}}_p$ tangent vector due to a unit change in ϕ_q. We refer to these as *torsion* terms, since they cause a twisting of the (ϕ_p, ϕ_q) parameter surface, where a parameter surface—analogous to a parameter curve—is the set of points generated by holding all ϕ_p's except two constant and varying those two.

The interpretation of the individual elements in $\mathbf{C}$ also helps to interpret the parameter effects curvature in a particular direction. For a direction $\mathbf{u}$ which is parallel to a parameter axis, $c_{\mathbf{u}}^{\theta}$ is the square root of the sum of squares of the

compansion term and all the arcing terms for that parameter. This is also the case for a general **u**: $c_{\mathbf{u}}^{\theta}$ measures a combination of the arcing and compansion in the direction **u**.

Example: BOD 14

For the BOD data, the parameter effects curvature array is

$$\mathbf{C}^{\theta} = \begin{bmatrix} 0.000 & -0.157 \\ & 2.100 \end{bmatrix} \begin{bmatrix} 0.000 & -0.096 \\ & 0.497 \end{bmatrix}$$

Examination of the terms in $\mathbf{C}^{\theta}$ reveals the following:

(1) the ϕ_2 parameter lines will be perfectly uniformly spaced along the ϕ_1 lines, since the ϕ_1 term c_{111} is zero;
(2) the ϕ_1 parameter curves will be markedly nonuniformly spaced along the ϕ_2 lines, since the ϕ_2 compansion term c_{222} is large (0.497);
(3) the ϕ_2 parameter lines will be markedly curved, because the ϕ_1 arcing term c_{122} is extremely large (2.100);
(4) the ϕ_1 parameter lines will be straight, because the ϕ_2 arcing term c_{211} is zero;
(5) the ϕ_2 parameter lines will show modest fanning, because the ϕ_1 fanning term $c_{121} = c_{112}$ is quite small (−0.157);
(6) the ϕ_1 parameter lines will show modest fanning, because the ϕ_2 fanning term $c_{221} = c_{212}$ is quite small (−0.096).

In Figure 7.7 we show the BOD parameter curves projected onto the tangent plane. We recall that a parameter curve is associated with the parameter which is varying, so the short dash curves, corresponding to fixed ϕ_2, are actually ϕ_1 parameter curves, and the long–short dash curves, corresponding to fixed ϕ_1, are actually ϕ_2 parameter curves. Thus by referring to Figure 7.7, we can see that the parameter curves behave in the way predicted.

Note that the 95% likelihood disk extends beyond the expectation surface and that linear approximation parameter lines would not adequately approximate the true parameter curves within the disk. ■

7.2.2 Reparametrization

In Section 7.1 we saw that a transformation of parameters can make great changes in the parameter effects nonlinearity, and in Chapter 6 we saw that such transformations can greatly improve profile likelihood plots. Unfortunately, there is little guidance available as to the choice of a reparametrization and its effects in a particular situation. As shown in Bates and Watts (1981a), transfor-

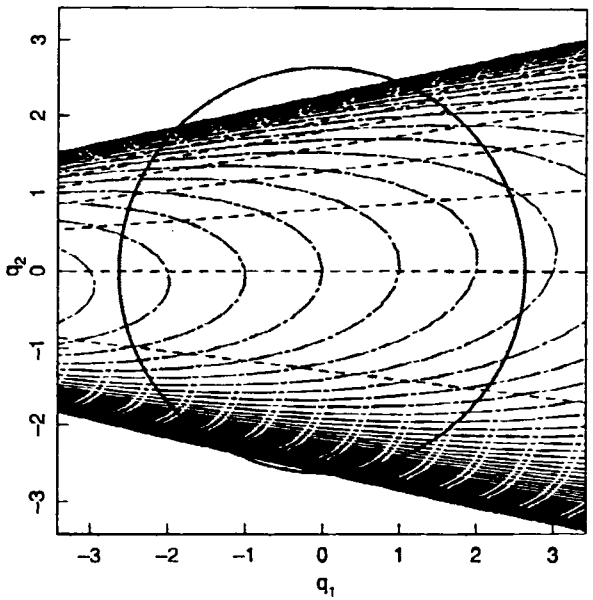

Figure 7.7 Parameter curves for the orthogonal parameters $\phi = \mathbf{R}_{11}(\boldsymbol{\theta} - \hat{\boldsymbol{\theta}})$ for the BOD data. The parameter curves are projected onto the tangent plane, and the circular region corresponding to a 95% likelihood contour (assuming the expectation surface is planar) is shaded. The parameter curves for ϕ_1 are indicated by short dashes, and the ϕ_2 parameter curves by long–short dashes.

mations which are recommended for certain types of parameters and models can decrease the parameter effects nonlinearity for one data set and increase them for another. Consequently, it may be necessary to experiment with several transformations to find a suitable one, as done, for example, in Ratkowsky (1983).

It would be tedious to evaluate parameter transformations by finding the parameter effects curvature array for a particular expectation function–data set combination under a reparametrization by (1) restating the model in terms of the new parameters, (2) recalculating all the derivatives, and (3) determining the $\mathbf{C}$ array. Fortunately this work can be avoided.

Suppose we wish to determine the parameter effects array, $\mathbf{C}^{\boldsymbol{\beta}}$, corresponding to a reparametrization in which the new parameters $\boldsymbol{\beta}$ are nonlinear transformations of $\boldsymbol{\theta}$,

$$\boldsymbol{\beta} = \mathbf{G}(\boldsymbol{\theta})$$

or

$$\beta_p = \mathbf{G}_p(\boldsymbol{\theta}) \qquad p = 1, 2, \ldots, P$$

We assume the inverse transformation is

$$\boldsymbol{\theta} = \mathbf{D}(\boldsymbol{\beta})$$

or

$$\theta_p = \mathbf{D}_p(\boldsymbol{\beta}) \quad p = 1, 2, \ldots, P$$

and write the $P \times P$ Jacobian matrices as $\dot{\mathbf{D}}$ and $\dot{\mathbf{G}}$ with (n,p)th elements $\partial \mathbf{D}_n / \partial \beta_p$ and $\partial \mathbf{G}_n / \partial \theta_p$ respectively.

The $P \times P \times P$ second derivative arrays are written as $\ddot{\mathbf{D}}$ and $\ddot{\mathbf{G}}$ with elements $\partial^2 \mathbf{D}_n / \partial \beta_p \partial \beta_q$ and $\partial^2 \mathbf{G}_n / \partial \theta_p \partial \theta_q$ respectively: a term with subscript npq resides in the nth face, pth row, and qth column. [It may be helpful to note that the nth row of $\dot{\mathbf{G}}$ is the gradient of $\mathbf{G}_p$, $\partial \mathbf{G}_p / \partial \boldsymbol{\theta}^{\mathrm{T}}$, and that the pth row of the nth face of $\ddot{\mathbf{G}}$ is the gradient of $\partial \mathbf{G}_n / \partial \theta_p$, $(\partial / \partial \boldsymbol{\theta}^{\mathrm{T}}) \partial \mathbf{G}_n / \partial \theta_p$.]

Using the chain rule for differentiation, the new tangent vectors at the least squares estimates $\hat{\boldsymbol{\beta}} = \mathbf{G}(\hat{\boldsymbol{\theta}})$ are

$$\begin{aligned}
\dot{\mathbf{b}}_p &= \left. \frac{\partial \boldsymbol{\eta}}{\partial \beta_p} \right|_{\hat{\boldsymbol{\beta}}} \\
&= \sum_{q=1}^{P} \left[\left. \frac{\partial \boldsymbol{\eta}}{\partial \theta_q} \right|_{\hat{\boldsymbol{\theta}}} \right] \{\dot{\mathbf{D}}\}_{qp} \\
&= \sum_{q=1}^{P} \dot{\mathbf{v}}_q \{\dot{\mathbf{D}}\}_{qp}
\end{aligned}$$

where $\dot{\mathbf{v}}_q$ is the qth column of $\dot{\mathbf{V}}$. Equivalently, we have

$$\begin{aligned}
\dot{\mathbf{B}} &= (\dot{\mathbf{b}}_1, \dot{\mathbf{b}}_2, \ldots, \dot{\mathbf{b}}_P) \\
&= \dot{\mathbf{V}} \dot{\mathbf{D}} \\
&= \mathbf{Q}_1 \mathbf{R}_1 \dot{\mathbf{D}}
\end{aligned} \tag{7.17}$$

Similarly the new second derivative vectors are

$$\begin{aligned}
\ddot{\mathbf{b}}_{pq} &= \left. \frac{\partial^2 \boldsymbol{\eta}}{\partial \beta_p \partial \beta_q} \right|_{\hat{\boldsymbol{\beta}}} \\
&= \frac{\partial}{\partial \beta_q} \left[\sum_{r=1}^{P} \dot{\mathbf{v}}_r \{\dot{\mathbf{D}}\}_{rp} \right] \\
&= \sum_{r=1}^{P} \dot{\mathbf{v}}_r \{\ddot{\mathbf{D}}\}_{rpq} + \sum_{r=1}^{P} \sum_{s=1}^{P} \{\dot{\mathbf{D}}\}_{rp} \ddot{\mathbf{v}}_{rs} \{\dot{\mathbf{D}}\}_{sq}
\end{aligned}$$

where $\ddot{\mathbf{v}}_{rs}$ is the (r,s)th vector in the array $\ddot{\mathbf{V}}$. Thus

$$\ddot{\mathbf{B}} = \dot{\mathbf{D}}^{\mathrm{T}}\ddot{\mathbf{V}}\dot{\mathbf{D}} + [\dot{\mathbf{V}}][\ddot{\mathbf{D}}] \tag{7.18}$$

so

$$\mathbf{A}^{\beta} = [\mathbf{Q}_1^{\mathrm{T}}][\ddot{\mathbf{B}}] = \dot{\mathbf{D}}^{\mathrm{T}}\mathbf{A}^{\theta}\dot{\mathbf{D}} + [\mathbf{R}_1][\ddot{\mathbf{D}}]$$

where, again, the square brackets imply that the summation involved in the multiplication is over the numerator index. Now

$$\mathbf{C}^{\theta} = \mathbf{R}_1^{-\mathrm{T}}\mathbf{A}^{\theta}\mathbf{R}_1^{-1}$$

and the equivalent expression for $\mathbf{C}^{\beta}$ is, from (7.17),

$$\mathbf{C}^{\beta} = (\mathbf{R}_1\dot{\mathbf{D}})^{-\mathrm{T}}\mathbf{A}^{\beta}(\mathbf{R}_1\dot{\mathbf{D}})^{-1}$$

so

$$\begin{aligned}
\mathbf{C}^{\beta} &= (\mathbf{R}_1\dot{\mathbf{D}})^{-\mathrm{T}}[\mathbf{R}_1][\ddot{\mathbf{D}}](\mathbf{R}_1\dot{\mathbf{D}})^{-1} + \mathbf{R}_1^{-\mathrm{T}}\mathbf{A}^{\theta}\mathbf{R}_1^{-1} \\
&= (\mathbf{R}_1\dot{\mathbf{D}})^{-\mathrm{T}}[\mathbf{R}_1][\ddot{\mathbf{D}}](\mathbf{R}_1\dot{\mathbf{D}})^{-1} + \mathbf{C}^{\theta} \\
&= [\mathbf{R}_1][\mathbf{R}_1^{-\mathrm{T}}\dot{\mathbf{D}}^{-\mathrm{T}}\ddot{\mathbf{D}}\dot{\mathbf{D}}^{-1}\mathbf{R}_1^{-1}] + \mathbf{C}^{\theta} \\
&= -[\mathbf{R}_1][\mathbf{R}_1^{-\mathrm{T}}\mathbf{T}\mathbf{R}_1^{-1}] + \mathbf{C}^{\theta}
\end{aligned} \tag{7.19}$$

The quantity $\mathbf{T}$ is called the *transformation curvature array*,

$$\mathbf{T} = -\dot{\mathbf{D}}^{-\mathrm{T}}\ddot{\mathbf{D}}\dot{\mathbf{D}}^{-1} \tag{7.20}$$

since it is in the form of a curvature, that is, acceleration/velocity^2.

Thus, the array $\mathbf{C}^{\beta}$ equals the original array $\mathbf{C}^{\theta}$ minus an adjustment,

$$\mathbf{C}^{\beta} = \mathbf{C}^{\theta} - [\mathbf{R}_1][\mathbf{R}_1^{-\mathrm{T}}\mathbf{T}\mathbf{R}_1^{-1}]$$

Now $\mathbf{T}$ is given in terms of derivatives with respect to $\boldsymbol{\beta}$, and it is more convenient to have it in terms of the original parameters $\boldsymbol{\theta}$. By writing

$$\boldsymbol{\beta} = \mathbf{G}(\mathbf{D}(\boldsymbol{\beta}))$$

and differentiating with respect to $\boldsymbol{\beta}$, we have

$$\frac{\partial\boldsymbol{\beta}}{\partial\boldsymbol{\beta}^{\mathrm{T}}} = \mathbf{I} = \dot{\mathbf{G}}\dot{\mathbf{D}}$$

and

$$\frac{\partial^2\boldsymbol{\beta}}{\partial\boldsymbol{\beta}\,\partial\boldsymbol{\beta}^{\mathrm{T}}} = \mathbf{0} = \dot{\mathbf{D}}^{\mathrm{T}}\ddot{\mathbf{G}}\dot{\mathbf{D}} + [\dot{\mathbf{G}}][\ddot{\mathbf{D}}]$$

and so, from (7.20),

$$\mathbf{T} = [\dot{\mathbf{G}}^{-1}][\ddot{\mathbf{G}}]$$

Finally, we have the result

$$\mathbf{C}^{\beta} = \mathbf{C}^{\theta} - [\mathbf{R}_1][\mathbf{R}_1^{-\mathrm{T}}[\dot{\mathbf{G}}^{-1}][\ddot{\mathbf{G}}]\mathbf{R}_1^{-1}] \tag{7.21}$$

Example: Puromycin 28

The Michaelis–Menten model is a ratio of polynomials, and so, as noted at the end of Section 6.1.2, reparametrizing in the form

$$f = \frac{x}{\beta_1 + \beta_2 x}$$

should reduce the parameter effects (although for this example, they are already small). The reparametrization in this case is

$$\boldsymbol{\beta} = \begin{bmatrix} \dfrac{\theta_2}{\theta_1} \\ \dfrac{1}{\theta_1} \end{bmatrix}$$

and so

$$\dot{\mathbf{G}} = \begin{bmatrix} \dfrac{-\theta_2}{\theta_1^2} & \dfrac{1}{\theta_1} \\ \dfrac{-1}{\theta_1^2} & 0 \end{bmatrix}$$

and

$$\ddot{\mathbf{G}} = \begin{bmatrix} \dfrac{2\theta_2}{\theta_1^3} & \dfrac{-1}{\theta_1^2} \\ \dfrac{-1}{\theta_1^2} & 0 \end{bmatrix} \quad \begin{bmatrix} \dfrac{2}{\theta_1^3} & 0 \\ 0 & 0 \end{bmatrix}$$

The product $\mathbf{T} = [\dot{\mathbf{G}}^{-1}][\ddot{\mathbf{G}}]$ is then

$$\mathbf{T} = \begin{bmatrix} \dfrac{-2}{\theta_1} & 0 \\ 0 & 0 \end{bmatrix} \begin{bmatrix} 0 & \dfrac{-1}{\theta_1} \\ \dfrac{-1}{\theta_1} & 0 \end{bmatrix}$$

Finally, substituting the parameter values and performing the remaining multiplications and subtractions as in (7.21) gives

$$\mathbf{C}^{\beta} = \begin{bmatrix} 0.000 & -0.035 \\ & -0.059 \end{bmatrix} \begin{bmatrix} 0.000 & -0.030 \\ & -0.151 \end{bmatrix} - \begin{bmatrix} 0.000 & 0.003 \\ & -0.027 \end{bmatrix} \begin{bmatrix} 0.000 & 0.002 \\ & -0.005 \end{bmatrix}$$

$$= \begin{bmatrix} 0.000 & -0.038 \\ & -0.032 \end{bmatrix} \begin{bmatrix} 0.000 & -0.032 \\ & -0.146 \end{bmatrix}$$

As expected, the change in the parameter effects is slight. ■

Example: Isomerization 6

For the isomerization data,

$$C^{\theta} = \begin{bmatrix} 0.000 & -0.110 & -0.256 & 0.361 \\ & -0.064 & 1.762 & -18.157 \\ & & 8.180 & -48.275 \\ & & & 119.610 \end{bmatrix} \quad \begin{bmatrix} 0.000 & -0.032 & 0.000 & 0.000 \\ & -0.264 & 0.269 & -4.898 \\ & & 0.008 & -0.004 \\ & & & 0.008 \end{bmatrix}$$

$$\begin{bmatrix} 0.000 & 0.000 & -0.032 & 0.000 \\ & 0.013 & -0.102 & -0.004 \\ & & 0.413 & -4.919 \\ & & & 0.009 \end{bmatrix} \quad \begin{bmatrix} 0.000 & 0.000 & 0.000 & -0.032 \\ & 0.020 & -0.004 & -0.102 \\ & & -0.001 & 0.265 \\ & & & -9.826 \end{bmatrix}$$

so that the parameter effects nonlinearities are disastrous. If we reparametrize using the $\boldsymbol{\beta}$ parameters of Example Isomerization 5, it is clear from the discussion in Chapter 6 that the parameter effects will be reduced to an extremely small amount. Using the above techniques we find the following parameter effects array for the $\boldsymbol{\beta}$ parameters:

$$C^{\beta} = \begin{bmatrix} -0.069 & 0.011 & -0.007 & 0.006 \\ & -0.062 & 0.001 & 0.004 \\ & & -0.060 & 0.003 \\ & & & -0.052 \end{bmatrix} \quad \begin{bmatrix} 0.011 & -0.062 & 0.001 & 0.004 \\ & -0.032 & -0.016 & 0.007 \\ & & -0.015 & 0.005 \\ & & & -0.039 \end{bmatrix}$$

$$\begin{bmatrix} -0.007 & 0.001 & -0.060 & 0.003 \\ & -0.016 & -0.015 & 0.005 \\ & & 0.018 & -0.005 \\ & & & -0.035 \end{bmatrix} \quad \begin{bmatrix} 0.006 & 0.004 & 0.003 & -0.052 \\ & 0.007 & 0.005 & -0.039 \\ & & -0.005 & -0.035 \\ & & & -0.088 \end{bmatrix}$$

The parameter effects are reduced to negligible values, as expected from the analysis in Chapter 6. ■

Two important points should be noted. First, the transformation curvature array $\mathbf{T}$ is expressed in terms of the original parameters $\boldsymbol{\theta}$, so we do not have to determine the inverse transformation. Second, a new array C^{β} is calculated from the array C^{θ} and the matrix $\mathbf{R}_1$ from previous calculations, a total of only $P^2(P+3)/2$ values. Equation (7.21) is therefore an extremely efficient expression for computing the effect of a transformation.

7.3 RMS Curvatures

An appreciation of the terms in the curvature array is helpful to understanding nonlinearity, but for data analysis we need a simple overall measure of nonlinearity so that we can assess the quality of a linear approximation in a particu-

lar situation. For this purpose, we use the *root mean square* (RMS) curvature which is the square root of the average over all directions of the squared curvature. We denote the RMS parameter effects curvature by c^{θ} and the RMS intrinsic curvature by c^{ι}. Formal expressions for a general RMS curvature are developed below: the results for parameter effects or intrinsic curvature are obtained by simply inserting superscripts $^{\theta}$ and $^{\iota}$ in the resulting equations and selecting the appropriate range of the index n.

7.3.1 Calculating RMS Curvatures

The curvature corresponding to the direction $\mathbf{u}$ on the tangent plane is

$$c_{\mathbf{u}} = \| \mathbf{u}^{\mathrm{T}}\mathbf{C}\mathbf{u} \| = \sqrt{\sum_n (\mathbf{u}^{\mathrm{T}}\mathbf{C}_n\mathbf{u})^2}$$

where $\mathbf{C}_n$ is the nth face of $\mathbf{C}$. The mean square curvature is then obtained by integrating $c_{\mathbf{u}}^2$ over all directions $\mathbf{u}$ and dividing by the surface area A of the P-dimensional sphere. That is,

$$c^2 = \frac{1}{A}\int \sum_n (\mathbf{u}^{\mathrm{T}}\mathbf{C}_n\mathbf{u})^2 \, dA \tag{7.22}$$

where dA is the element of surface area on the sphere. This integral can be expressed as a sum of integrals, giving the final result (Bates and Watts, 1980)

$$c^2 = \frac{1}{P(P+2)}\sum_n \left[2\sum_{p=1}^{P}\sum_{q=1}^{P} c_{npq}^2 + \left(\sum_{p=1}^{P} c_{npp} \right)^2 \right] \tag{7.23}$$

In (7.22) and (7.23), the index n goes from 1 to P for c^{θ} and from $P+1$ to at most $P(P+3)/2$ for c^{ι}.

The mean square curvature for 2-parameter models can be expressed as a 1-dimensional integral over an angle ω, since then $\mathbf{u} = [\cos\omega, \sin\omega]^{\mathrm{T}}$. Equation (7.22) then becomes

$$c^2 = \frac{1}{2\pi}\sum_n \int_0^{2\pi} \left[c_{n11}\cos^2\omega + 2c_{n12}\sin\omega\cos\omega + c_{n22}\sin^2\omega \right]^2 d\omega$$

After expanding the square in the integral, all terms involving odd powers of sines or cosines integrate to 0. The remaining integrals contribute the amounts $\frac{3}{8}c_{n11}^2$, $\frac{3}{8}c_{n22}^2$, $\frac{1}{4}c_{n11}c_{n22}$, and $\frac{1}{2}c_{n12}^2$, which agrees with (7.23).

Example: Puromycin 29

For 2-parameter models with a conditionally linear parameter, such as the Michaelis–Menten model, the intrinsic curvature array always consists of one face, the only nonzero entry of which is c_{322} if θ_1 is the conditionally linear parameter. Thus, the mean square intrinsic curvature is just $\frac{3}{8}c_{322}^2$.

Furthermore, because the 11 vector in $\mathbf{C}^{\theta}$ is $\mathbf{0}$, the mean square parameter effects curvature is just $\sqrt{\frac{1}{2}\,\|\mathbf{c}_{12}^{\theta}\|^2 + \frac{3}{8}\,\|\mathbf{c}_{22}^{\theta}\|^2}$. ■

RMS curvature measures are not very meaningful as they stand, because we do not know what constitutes a "large" value. A convenient scale of reference can be established by comparing the RMS curvature with that of the confidence disk at a specified level, say 95%. Thus, an RMS curvature will be considered small if it is much less than the curvature of the 95% confidence disk, that is, if $c \ll 1/\sqrt{F}$, or equivalently, if $c\sqrt{F} \ll 1$, where $F = F(P, N-P; 0.05)$

Having established a reference scale, we still must determine how small $c\sqrt{F}$ should be to be acceptable. Following Bates and Watts (1980), we consider an expectation surface with radius $1/c$ and determine the deviation of the surface from the tangent plane at a distance $\sqrt{F}$ from the tangent point. This deviation, expressed as a percentage of the radius of the confidence disk, is $100(1-\sqrt{1-c\sqrt{F}})/c\sqrt{F}$, so that a value of $c\sqrt{F} = 0.1$ causes the surface to deviate by 5% of the radius of the confidence at the edge of the confidence disk; a value of $c\sqrt{F} = 0.2$ causes a deviation of 10%; 0.3, 15%; and 0.4, 21%. If we accept a deviation of no more than 15%, then we will declare an analysis as having unacceptable curvature if at least one value of $c\sqrt{F}$ is greater than 0.3.

Example: Puromycin 30

For the Puromycin data, we calculate $c^{\iota} = 0.045$ and $c^{\theta} = 0.105$, so that $c^{\iota}\sqrt{F} = 0.09$ and $c^{\theta}\sqrt{F} = 0.21$. The RMS parameter effects curvature is about twice as large as the intrinsic in this case, but even the parameter effects curvature is acceptable according to the criterion above. By referring to Figure 7.4*a*, we can get a visual appreciation of the extent of the parameter effects when the magnitude of $c^{\theta}\sqrt{F}$ is 0.2. ■

Example: BOD 15

For the BOD data, we calculate $c^{\iota} = 0.184$ and $c^{\theta} = 1.328$, so $c^{\iota}\sqrt{F} = 0.49$ and $c^{\theta}\sqrt{F} = 3.50$. In this case, both the intrinsic and parameter effects curvatures are judged to be large, but the parameter effects are extremely bad. By referring to Figure 7.7, we can get a visual appreciation of the extent of the parameter effects when the magnitude of $c^{\theta}\sqrt{F}$ is 3.5. ■

Example: Isomerization 7

For the isomerization data, $c^{\iota} = 0.048$ and $c^{\theta} = 48.39$, so $c^{\iota}\sqrt{F} = 0.81$ and $c^{\theta}\sqrt{F} = 81.92$. The parameter effects curvature is huge in this case, so that linear approximation inference regions will be completely unreliable. This is in accord with our findings in Chapter 6, where we saw that the profile *t* plots were badly curved and the profile traces were badly behaved. ■

7.3.2 RMS Curvatures in Practice

In this subsection, we discuss RMS curvatures for 67 data set–model combinations. The data sets were gathered from published papers, textbooks, and researchers, and were carefully selected to be real, not simulated, so as to reflect what actually occurs in practice. Some of the data sets were used with more than one expectation function, so there are only 37 distinct data sets and 19 expectation functions. A key to the expectation functions and data sets is given in Appendix 7.

In Table 7.2 we present the RMS intrinsic and parameter effects $c\sqrt{F}$ values for $\alpha = 0.05$ for the 67 data set–model combinations studied. In the table, N is the total number of observations, P is the number of parameters in the model, and ν is the number of degrees of freedom for replications. In Figure 7.8*a* we present a scatterplot of the parameter effects versus intrinsic $c\sqrt{F}$ values, and in Figure 7.8*b* and *c* we show histograms of those values, all on log scales. The solid line on Figure 7.8*a* is the line of equality, so that it is easily seen that the intrinsic curvature is smaller, and in almost all cases very much smaller, than the parameter effects curvature. Figure 7.8*a* also reveals that there is a positive correlation between intrinsic and parameter effects nonlinearity.

Referring to the histograms, it can be seen that the intrinsic curvature (Figure 7.8*b*) is generally not large (about 93% of the analyses have a $c^{\iota}\sqrt{F}$ value less than 0.3, which corresponds to a 15% deviation of the expectation surface from the tangent plane). Parameter effects curvatures, on the other hand, are often bad (in only 10% of the analyses is $c^{\theta}\sqrt{F}$ less than 0.3, which corresponds to a deviation of less than 15% from uniform coordinates, and in about 80% of the cases, the $c^{\theta}\sqrt{F}$ value is greater than 1.0, which corresponds to a deviation of a parameter curve from a straight line in excess of 100%).

These results, based on real data sets from a variety of sources, lead one to conclude that linear approximation inference regions, which require the uniform coordinates assumption, can be very misleading in many practical situations. They also lend strong support to the validity of the planarity assumption which was used in deriving the profile t and profile pair plots in Chapter 6. To further substantiate the validity of the planar assumption, we investigate the effects of intrinsic nonlinearity in more detail in the next section.

7.4 Direct Assessment of the Effects of Intrinsic Nonlinearity

We have seen in the previous section that RMS intrinsic curvatures are generally small, and so there is some justification for assuming that the planar assumption will be valid. To give further justification, we look at the effects of nonlinearity from a different viewpoint, by considering that the construction of a likelihood region involves two stages. In the first stage, we determine the intersection of the expectation surface with the appropriate likelihood sphere cen-

Table 7.2 Scaled RMS curvatures relative to a 95% confidence disk radius and extreme axis ratios for a collection of models and real data sets.

P	Model*	Data Set*	N	ν	$c^0\sqrt{F}$	$c^1\sqrt{F}$	Axis Ratios Min.	Axis Ratios Max.
2	A	1	7	0	0.12	0.05	1.00	1.00
		2	11	5	0.26	0.12	1.00	1.08
		3	12	6	0.21	0.09	1.00	1.05
	B	4	7	0	1.02	0.10	1.00	1.04
		5	8	0	1.04	0.06	0.99	1.00
		6	6	0	3.09	0.09	0.96	1.00
		7	6	0	4.55	0.26	0.97	1.00
		8	6	0	1.33	0.11	1.00	1.02
		9	6	0	1.63	0.17	1.00	1.04
		10	6	0	1.17	0.27	1.00	1.13
		11	6	0	3.50	0.49	1.00	1.01
		12	4	0	1.91	0.10	1.00	1.02
	C	13	44	26	0.93	0.10	1.00	1.01
	D	14	38	17	0.02	0.01	1.00	1.00
	E	15	43	21	46.28	0.11	0.98	1.00
3	F	16	9	0	93.49	0.13	0.92	1.00
		17	15	0	11.21	0.14	0.87	1.00
		18	9	0	2.66	0.17	0.91	1.00
		19	15	0	30.43	0.14	0.88	1.00
		20	27	7	1.18	0.16	1.00	1.06
		21	6	0	2.10	0.32	1.00	1.06
		22	4	0	25.67	3.11	0.89	1.00
		23	13	0	1.80	0.04	1.00	1.04
	G	16	9	0	0.65	0.07	0.97	1.01
		17	15	0	2.24	0.14	0.95	1.01
		18	9	0	0.55	0.12	1.00	1.05
		19	15	0	1.52	0.11	0.98	1.04
		24	7	0	2.65	0.25	0.99	1.06
		25	7	0	2.26	0.22	0.99	1.03
		26	7	0	3.47	0.22	1.00	1.01
		27	7	0	2.36	0.26	1.00	1.06
		28	7	0	3.64	0.22	0.99	1.02

* The key to the data set numbers and models is given in Appendix 7.

Table 7.2 continued

P	Model	Data Set	N	v	$c^{\theta}\sqrt{F}$	$c^{1}\sqrt{F}$	Axis Ratios Min.	Axis Ratios Max.
3	H	16	9	0	2.27	0.09	0.95	1.02
		17	15	0	0.62	0.22	0.95	1.10
		18	9	0	0.64	0.13	0.97	1.06
		19	15	0	0.76	0.21	0.95	1.17
		24	7	0	5.11	0.19	1.00	1.01
		25	7	0	4.80	0.18	0.98	1.02
		26	7	0	9.35	0.19	0.97	1.02
		27	7	0	5.02	0.23	0.97	1.06
		28	7	0	12.51	0.20	0.96	1.04
	I	24	7	0	42.21	0.17	0.97	1.00
		25	7	0	88.93	0.18	0.94	1.00
		26	7	0	410.78	0.19	0.94	1.00
		27	7	0	147.59	0.21	0.93	1.00
	J	24	7	0	1.03	0.15	1.00	1.01
		25	7	0	0.89	0.14	0.99	1.00
		26	7	0	1.70	0.16	0.98	1.00
		27	7	0	1.38	0.21	0.97	1.00
		28	7	0	2.48	0.20	0.96	1.00
	K	29	5	0	4.70	0.10	1.00	1.01
		30	5	0	4.76	0.24	1.00	1.05
	L	31	40	32	1.17	0.14	1.00	1.01
4	M	32	24	0	81.92	0.08	0.95	1.01
	N	33	57	2	0.68	0.11	1.00	1.03
		34	57	2	2.13	0.53	0.86	1.03
	O	16	9	0	27.52	0.17	0.95	1.08
		17	15	0	20.26	0.19	0.93	1.05
		18	9	0	0.94	0.09	0.97	1.01
		19	15	0	16.12	0.16	0.97	1.09
	P	16	9	0	55.26	0.22	0.99	1.06
		17	15	0	58.45	0.27	0.91	1.09
		18	9	0	39.00	0.31	0.88	1.07
		19	15	0	52.16	0.23	0.89	1.03
5	Q	35	33	0	29.49	0.01	1.00	1.01
6	R	36	24	1	13.52	0.47	0.96	1.07
9	S	37	53	2	0.30	0.10	0.95	1.02

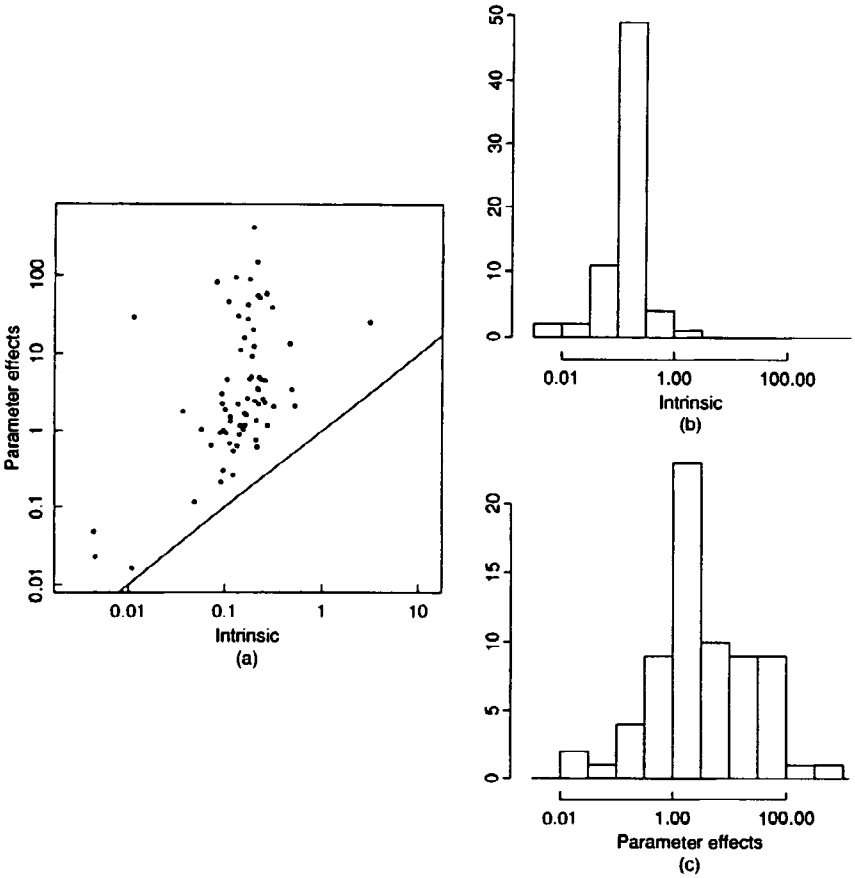

Figure 7.8 Histograms and scatterplots of scaled intrinsic and parameter effects curvatures for real data sets. In part *a*, a scatterplot of the parameter effects versus intrinsic curvature is given. The solid line is the line of equality. Histograms of the curvatures are given in parts *b* and *c*.

tered on $\mathbf{y}$, and in the second we map the coordinates of that intersection into the parameter space. A linear approximation confidence region is then obtained by performing an approximation at each of these stages. At the first stage, we replace the true expectation surface by a plane, thereby producing a disk on the tangent plane, and at the second stage we approximate the mapping of the disk to the parameter plane by a linear mapping. If the intrinsic nonlinearity is large, so that a tangent plane does not provide an adequate approximation, we can use a quadratic approximation (Hamilton, 1980; Hamilton, Watts, and Bates, 1982).

To obtain a quadratic approximation, consider a point $\boldsymbol{\theta}$ in the parameter space. This point maps through the nonlinear transformation, $\boldsymbol{\eta}(\boldsymbol{\theta})$, to the point on the tangent plane with coordinates

$$\boldsymbol{\tau} = \mathbf{Q}_1^{\mathrm{T}}[\boldsymbol{\eta}(\boldsymbol{\theta}) - \boldsymbol{\eta}(\hat{\boldsymbol{\theta}})]$$

The coordinates $\boldsymbol{\tau}$ provide a natural reference system for the expectation surface, in particular, a local set of coordinates with no parameter effects nonlinearity.

An approximation to the expectation surface by a quadratic surface centered at $\boldsymbol{\eta}(\hat{\boldsymbol{\theta}})$ is

$$\boldsymbol{\eta}(\boldsymbol{\tau}) = \boldsymbol{\eta}(\hat{\boldsymbol{\theta}}) + \mathbf{Q}_1\boldsymbol{\tau} + \frac{[\mathbf{Q}'_1][\boldsymbol{\tau}^{\mathrm{T}}\mathbf{C}^{\mathrm{l}}\boldsymbol{\tau}]}{2}$$

where $\mathbf{C}$ is the relative curvature array and $\mathbf{Q}_1$ and $\mathbf{Q}'_1$ are obtained from the QR decomposition of the matrix $\mathbf{D}$ consisting of the first derivative and nonredundant second derivative vectors (see Section 7.1). Recall from Section 7.1.1 that the square brackets denote matrix multiplication in which the summation is over the numerator index.

An approximate expectation surface likelihood region and its projection onto the tangent plane can then be defined by rewriting equation (6.1) as

$$\frac{\mathbf{z}^{\mathrm{T}}\mathbf{z}}{\hat{\mathbf{z}}^{\mathrm{T}}\hat{\mathbf{z}}} = \left[1 + \frac{P}{N-P}F(P, N-P; \alpha)\right] \tag{7.24}$$

and replacing the exact residual vector $\mathbf{z}(\boldsymbol{\theta}) = \mathbf{y} - \boldsymbol{\eta}$ with the approximate residual vector $\tilde{\mathbf{z}} = \mathbf{y} - \tilde{\boldsymbol{\eta}}(\boldsymbol{\tau})$, where $\boldsymbol{\tau}$ is a point on the tangent plane in the coordinates given by the columns of $\mathbf{Q}$. Now the approximate residual vector at the point $\tilde{\boldsymbol{\eta}}(\boldsymbol{\tau})$ is

$$\tilde{\mathbf{z}} = \hat{\mathbf{z}} - \mathbf{Q}_1\boldsymbol{\tau} - \frac{[\mathbf{Q}'_1][\boldsymbol{\tau}^{\mathrm{T}}\mathbf{C}^{\mathrm{l}}\boldsymbol{\tau}]}{2}$$

and so

$$\begin{aligned} \mathbf{z}^{\mathrm{T}}\mathbf{z} &\simeq \tilde{\mathbf{z}}^{\mathrm{T}}\tilde{\mathbf{z}} \\ &= \hat{\mathbf{z}}^{\mathrm{T}}\hat{\mathbf{z}} + \boldsymbol{\tau}^{\mathrm{T}}(\mathbf{I} - \mathbf{B})\boldsymbol{\tau} + \frac{(\boldsymbol{\tau}^{\mathrm{T}}\mathbf{C}^{\mathrm{l}}\boldsymbol{\tau})^{\mathrm{T}}(\boldsymbol{\tau}^{\mathrm{T}}\mathbf{C}^{\mathrm{l}}\boldsymbol{\tau})}{4} \end{aligned} \tag{7.25}$$

where $\mathbf{B} = [(\mathbf{Q}'^{\mathrm{T}}_1\hat{\mathbf{z}})^{\mathrm{T}}][\mathbf{C}^{\mathrm{l}}]$ is the $P \times P$ matrix obtained from the inner product of the rotated residual vector $\mathbf{Q}'^{\mathrm{T}}_1\hat{\mathbf{z}}$ and the intrinsic curvature array. The matrix $\mathbf{B}$ is called the *effective residual curvature matrix*, because it gives the effective normal curvatures in the direction of the residual vector $\hat{\mathbf{z}}$ (Hamilton, Watts, and Bates, 1982).

Neglecting the term in (7.25) which involves fourth powers of the length of $\boldsymbol{\tau}$ and inserting the first two terms into (7.24) gives the approximate expectation surface region

$$\boldsymbol{\tau}^{\mathrm{T}}(\mathbf{I} - \mathbf{B})\boldsymbol{\tau} = F(P, N-P; \alpha) \tag{7.26}$$

Thus the tangent plane projection of the expectation surface likelihood region is approximately an ellipsoid, since, as shown below, $\mathbf{I} - \mathbf{B}$ is positive definite.

Beale (1960) also noted that sum of squares contours were approximately ellipsoidal in the $\boldsymbol{\tau}$ coordinates. [Hamilton, Watts, and Bates (1982) obtained similar approximations to (7.26) for confidence regions; however, for reasons given in Chapter 6, we do not recommend using confidence regions for nonlinear models.]

The tangent plane ellipsoids depend on the residual vector–expectation surface configuration through the effective residual curvature matrix $\mathbf{B}$, whose entries give the projections of the acceleration vectors on the residual vector. If the expectation surface curves towards the residual vector, all the projections are positive and all the eigenvalues of $\mathbf{B}$ are positive. Consequently, the tangent plane ellipsoid is larger than the linear approximation sphere. This is intuitively correct because when the expectation surface is curving towards the residual vector, more points on the expectation surface are nearer the observation point than if the expectation surface is a plane. Similar reasoning holds when the expectation surface curves away from the residual vector, causing the eigenvalues of $\mathbf{B}$ to be negative and the tangent plane ellipsoid to be smaller.

Example: BOD 16

Since the model for the BOD data is a 2-parameter model with a conditionally linear parameter, the normal acceleration space has dimension 1. For these data,

$$\mathbf{C}^{\iota} = \begin{bmatrix} 0 & 0 \\ 0 & 0.301 \end{bmatrix}$$

and $\mathbf{Q}'^{\mathrm{T}}_{1}\hat{\mathbf{z}} = 0.056$, so

$$\mathbf{B} = \begin{bmatrix} 0 & 0 \\ 0 & 0.017 \end{bmatrix}$$

(Whenever the normal acceleration space is 1-dimensional, $\mathbf{B}$ is a multiple of the single face in $\mathbf{C}^{\iota}$.) The effective residual curvature is extremely small, indicating that the expectation surface curves only slightly towards the observed response. ■

Box and Coutie (1956) recommended using

$$(\boldsymbol{\theta} - \hat{\boldsymbol{\theta}})^{\mathrm{T}}\mathbf{W}(\boldsymbol{\theta} - \hat{\boldsymbol{\theta}})$$

as an approximate confidence region for $\boldsymbol{\theta}$, where

$$\mathbf{W} = \frac{1}{2} \left. \frac{\partial^2 S}{\partial \boldsymbol{\theta}\, \partial \boldsymbol{\theta}^{\mathrm{T}}} \right|_{\hat{\boldsymbol{\theta}}}$$

In our notation,

$$\mathbf{W} = \dot{\mathbf{V}}^{\mathrm{T}}\dot{\mathbf{V}} - [\hat{\mathbf{z}}^{\mathrm{T}}][\ddot{\mathbf{V}}]$$
$$= \mathbf{R}_{11}^{\mathrm{T}}(\mathbf{I}-\mathbf{B})\mathbf{R}_{11}$$

so the inference region based on the second derivatives of the sum of squares function may be considered the image, in parameter space, of the ellipsoidal tangent plane likelihood region (7.26), assuming no parameter effects nonlinearity and with a linear mapping from the tangent plane to the parameter plane. Since $S(\hat{\boldsymbol{\theta}})$ is a local minimum, it also follows that $\mathbf{W}$, and hence $\mathbf{I}-\mathbf{B}$, is positive definite.

A direct assessment of the effect of intrinsic nonlinearity on likelihood regions can be made by calculating how much the tangent plane inference ellipsoids differ from the linear approximation spheres. We do this by calculating the ratios of the lengths of the axes of the ellipsoid to the radius of the linear approximation sphere. The ratio for the pth axis is simply $\rho_p = (1-\lambda_p)^{-1/2}$, where λ_p is the pth eigenvalue of $\mathbf{B}$, and so the *extreme axis length ratios*, ρ_1 and ρ_P, can be used as direct indicators of the effects of intrinsic nonlinearity.

The last two columns of Table 7.2 give the extreme axis length ratios for the 67 data set–model combinations, and Figure 7.9 presents histograms of these ratios. From the data and the histograms we see that the effect of intrinsic nonlinearity on likelihood regions is extremely small, with 95% of the minimum axis ratios exceeding 0.9 and 80% exceeding 0.95. Similarly, 97% of the maximum axis ratios are less than 1.1 and 70% are less than 1.05. The deviation of an ellipsoid from a sphere by 5 or 10% is quite small, and so we conclude that the planar assumption, unlike the uniform coordinates assumption, will usually be accurate and reliable. For this reason we recommend summarizing the in-

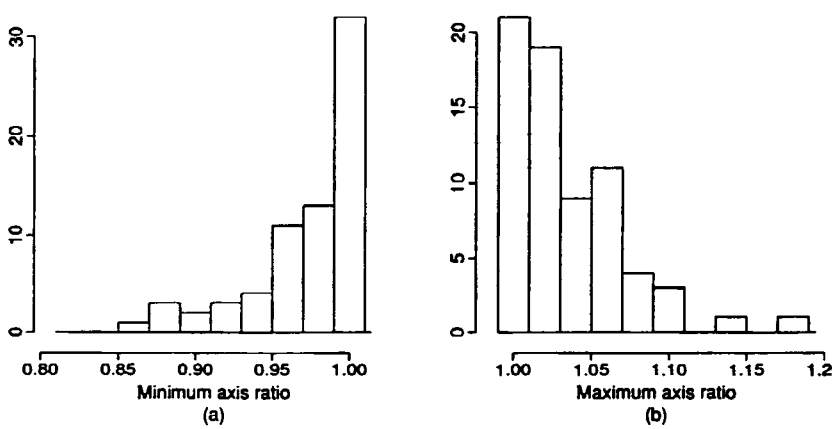

Figure 7.9 Histograms of the minimum and maximum axis ratios for the 67 real data examples.

ferential results of a nonlinear analysis by profile t and profile pair plots, since they only require the planar assumption.

Exercises

7.1 (a) Use the data from Appendix 4, Section A4.1, to calculate the velocity and the acceleration vectors at $\hat{\boldsymbol{\theta}} = (2.498, 0.2025)^{\mathrm{T}}$.

(b) Gather the velocity and nonredundant acceleration vectors into a matrix $\mathbf{W}$, and perform a QR decomposition on $\mathbf{W}$. Use the matrices $\mathbf{R}_{12}$ and $\mathbf{R}_{22}$ to construct the acceleration array.

(c) Calculate the relative curvatures as in equation (7.16), where, for this data set, $s\sqrt{P} = 0.0661\sqrt{2} = 0.935$.

7.2 (a) Use the methods of Section 7.2.2 to determine the effects of reparametrizing the model in Problem 7.1 with $\boldsymbol{\beta} = \ln \boldsymbol{\theta}$, that is, writing

$$f(x, \boldsymbol{\theta}) = \theta_1 (1 - e^{-\theta_2 x})$$

as

$$f(x, \boldsymbol{\beta}) = e^{\beta_1} [1 - \exp(-e^{\beta_2} x)]$$

(b) Calculate the RMS parameter effects curvature for both situations.

(c) Which parametrization should provide better linear approximation inference intervals?

(d) Calculate 50, 75, and 95% linear approximation intervals for β_1 and β_2 and convert them to intervals on θ_1 and θ_2. Compare the linear approximation 50, 75, and 95% inference intervals for the $\boldsymbol{\theta}$ parameters, after reexpression, with the corresponding likelihood intervals determined from the plot from Problem 6.3.

7.3 Suppose that an image is projected onto a screen which is tilted to the line of projection.

(a) Show that the nonlinear transformation corresponding to this projection consists only of fanning terms. Why is this so?

(b) What is the image of a circle? Does the orientation matter?

(c) What is the image of a square? Does the orientation matter?

APPENDIXES

APPENDIX 1.

Data Sets Used in Examples

A1.1 PCB

Data on the concentrations of polychlorinated biphenyl (PCB) residues in a series of lake trout from Cayuga Lake, NY, were reported in Bache et al. (1972) and are reproduced in Table A1.1. The ages of the fish were accurately known, because the fish are annually stocked as yearlings and distinctly marked as to

Table A1.1 PCB concentration versus age for lake trout.

Age (years)	PCB Conc. (ppm)	Age (years)	PCB Conc. (ppm)
1	0.6	6	3.4
1	1.6	6	9.7
1	0.5	6	8.6
1	1.2	7	4.0
2	2.0	7	5.5
2	1.3	7	10.5
2	2.5	8	17.5
3	2.2	8	13.4
3	2.4	8	4.5
3	1.2	9	30.4
4	3.5	11	12.4
4	4.1	12	13.4
4	5.1	12	26.2
5	5.7	12	7.4

Copyright 1972 by the AAAS. Reproduced from *SCIENCE*, 1972, **117**, 1192–1193, with permission of the authors.

year class. Each whole fish was mechanically chopped, ground, and thoroughly mixed, and 5-gram samples taken. The samples were treated and PCB residues in parts per million (ppm) were estimated using column chromatography.

A linear model

$$f(x, \boldsymbol{\beta}) = \beta_1 + \beta_2 x$$

is proposed where f is predicted ln(PCB concentration) and x is $\sqrt[3]{\text{age}}$.

A1.2 Rumford

Data on the amount of heat generated by friction were obtained by Count Rumford in 1798. A bore was fitted into a stationary cylinder and pressed against the bottom by means of a screw. The bore was turned by a team of horses for 30 minutes, after which Rumford "suffered the thermometer to remain in its place nearly three quarters of an hour, observing and noting down, at small intervals of time, the temperature indicated by it" (Roller, 1950). (See Table A1.2.)

A model based on Newton's law of cooling was proposed as

$$f(x, \theta) = 60 + 70\, e^{-\theta x}$$

where f is predicted temperature and x is time.

Table A1.2 Temperature versus time for Rumford cooling experiment.

Time (min)	Temperature (°F)	Time (min)	Temperature (°F)
4	126	24	115
5	125	28	114
7	123	31	113
12	120	34	112
14	119	37.5	111
16	118	41	110
20	116		

Reprinted with permission from "The Early Development of the Concepts of Temperature and Heat: The Rise and Decline of the Caloric Theory." by Duane Roller, Harvard University Press, 1950.

A1.3 Puromycin

Data on the "velocity" of an enzymatic reaction were obtained by Treloar (1974). The number of counts per minute of radioactive product from the reaction was measured as a function of substrate concentration in parts per million (ppm) and from these counts the initial rate, or "velocity," of the reaction was calculated (counts/min^2). The experiment was conducted once with the enzyme treated with Puromycin, [(a) in Table A1.3] and once with the enzyme untreated (b). The velocity is assumed to depend on the substrate concentration according to the Michaelis–Menten equation. It was hypothesized that the ultimate velocity parameter (θ_1) should be affected by introduction of the Puromycin, but not the half-velocity parameter (θ_2).

Table A1.3 Reaction velocity versus substrate concentration for the Puromycin experiment.

Substrate Concentration	Velocity (counts/min^2)	
(ppm)	(a) Treated	(b) Untreated
0.02	76	67
	47	51
0.06	97	84
	107	86
0.11	123	98
	139	115
0.22	159	131
	152	124
0.56	191	144
	201	158
1.10	207	160
	200	

Copyright 1974 by M. A. Treloar. Reproduced from "Effects of Puromycin on Galactosyltransferase of Golgi Membranes," Master's Thesis, University of Toronto. Reprinted with permission of the author.

The Michaelis–Menten model is

$$f(x, \boldsymbol{\theta}) = \frac{\theta_1 x}{\theta_2 + x}$$

where f is predicted velocity and x is substrate concentration.

A1.4 BOD

Data on biochemical oxygen demand (BOD) were obtained by Marske (1967). To determine the BOD, a sample of stream water was taken, injected with soluble organic matter, inorganic nutrients, and dissolved oxygen, and subdivided into BOD bottles. Each bottle was innoculated with a mixed culture of microorganisms, sealed, and incubated at constant temperature, and then the bottles were opened periodically and analyzed for dissolved oxygen concentration, from which the BOD was calculated in milligrams per liter (mg/l). (See Table A1.4.) The values shown are the averages of two analyses on each bottle.

A model was derived based on exponential decay with a fixed rate constant as

$$f(x, \boldsymbol{\theta}) = \theta_1 (1 - e^{\theta_2 x})$$

where f is predicted biochemical oxygen demand and x is time.

Table A1.4 Biochemical oxygen demand versus time.

Time (days)	Biochemical Oxygen Demand (mg/l)	Time (days)	Biochemical Oxygen Demand (mg/l)
1	8.3	4	16.0
2	10.3	5	15.6
3	19.0	7	19.8

Copyright 1967 by D. Marske. Reproduced from "Biochemical Oxygen Demand Data Interpretation Using Sum of Squares Surface," M.Sc. Thesis, University of Wisconsin–Madison. Reprinted with permission of the author.

A1.5 Isomerization

Data on the reaction rate of the catalytic isomerization of *n*-pentane to isopentane versus the partial pressures of hydrogen, *n*-pentane, and isopentane were given in Carr (1960) and are reproduced in Table A1.5. Isomerization is a chemical process in which a complex chemical is converted into more simple units, called isomers: catalytic isomerization employs catalysts to speed the reaction. The reaction rate depends on various factors, such as partial pressures of the products and the concentration of the catalyst. The differential reaction

Table A1.5 Reaction rate for isomerization of *n*-pentane to isopentane.

Partial Pressure (psia)			Reaction Rate
Hydrogen	*n*-Pentane	Isopentane	(hr^{-1})
205.8	90.9	37.1	3.541
404.8	92.9	36.3	2.397
209.7	174.9	49.4	6.694
401.6	187.2	44.9	4.722
224.9	92.7	116.3	0.593
402.6	102.2	128.9	0.268
212.7	186.9	134.4	2.797
406.2	192.6	134.9	2.451
133.3	140.8	87.6	3.196
470.9	144.2	86.9	2.021
300.0	68.3	81.7	0.896
301.6	214.6	101.7	5.084
297.3	142.2	10.5	5.686
314.0	146.7	157.1	1.193
305.7	142.0	86.0	2.648
300.1	143.7	90.2	3.303
305.4	141.1	87.4	3.054
305.2	141.5	87.0	3.302
300.1	83.0	66.4	1.271
106.6	209.6	33.0	11.648
417.2	83.9	32.9	2.002
251.0	294.4	41.5	9.604
250.3	148.0	14.7	7.754
145.1	291.0	50.2	11.590

Copyright 1960 by the American Chemical Society. Reprinted with permission from *Industrial and Engineering Chemistry*, 52, 391–396.

rate was expressed as grams of isopentane produced per gram of catalyst per hour (hr^{-1}), and the instantaneous partial pressure of a component was calculated as the mole fraction of the component times the total pressure, in pounds per square inch absolute (psia).

A common form of model for the reaction rate is the Hougen–Watson model (Hougen and Watson, 1947), of which the following is a special case,

$$f(\mathbf{x},\boldsymbol{\theta}) = \frac{\theta_1\theta_3(x_2 - x_3/1.632)}{1+\theta_2 x_1 + \theta_3 x_2 + \theta_4 x_3}$$

where f is predicted reaction rate, x_1 is partial pressure of hydrogen, x_2 is partial pressure of isopentane, and x_3 is partial pressure of n-pentane.

A1.6 α-Pinene

Data on the thermal isomerization of α-pinene, a component of turpentine, were reported in Fuguitt and Hawkins (1947). In this experiment, the relative concentrations (%) of α-pinene and three by-products were measured at each of eight times, and the relative concentration of a fourth by-product was imputed from the other concentrations. (See Table A1.6.) The initial concentration of α-pinene was 100%.

A linear kinetic model, shown in Figure A1.1, was proposed in Box et al. (1973). This model provides for the production of dipentene and alloocimene, which in turn yields α- and β-pyronene and a dimer.

Table A1.6 Relative concentrations of products versus time for thermal isomerization of α-pinene at 189.5°C.

Time (min)	α-Pinene (%)	Dipentene (%)	Alloocimene (%)	Pyronene (%)	Dimer (%)
1 230	88.35	7.3	2.3	0.4	1.75
3 060	76.4	15.6	4.5	0.7	2.8
4 920	65.1	23.1	5.3	1.1	5.8
7 800	50.4	32.9	6.0	1.5	9.3
10 680	37.5	42.7	6.0	1.9	12.0
15 030	25.9	49.1	5.9	2.2	17.0
22 620	14.0	57.4	5.1	2.6	21.0
36 420	4.5	63.1	3.8	2.9	25.7

Copyright 1947 by the American Chemical Society. Reprinted with permission from *Journal of the American Chemical Society*, **69**, 319–322.

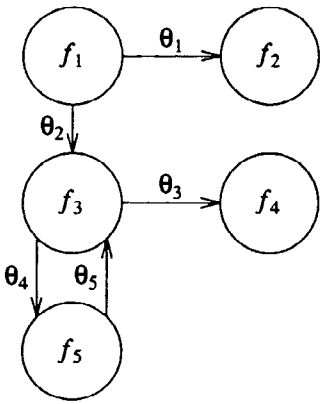

Figure A1.1 System diagram for α-pinene model where f_1 is α-pinene concentration, f_2 is dipentene concentration, f_3 is alloocimene concentration, f_4 is pyronene concentration, and f_5 is dimer concentration.

A1.7 Sulfisoxazole

Data on the metabolism of sulfisoxazole were obtained by Kaplan et al. (1972) and are reproduced in Table A1.7. In this experiment, sulfisoxazole was administered to a subject intravenously, blood samples were taken at specified times, and the concentration of sulfisoxazole in the plasma in micrograms per milliliter (μg/ml) was measured.

Table A1.7 Sulfisoxazole concentration versus time.

Time (min)	Sulfisoxazole Conc. (μg/ml)	Time (min)	Sulfisoxazole Conc. (μg/ml)
0.25	215.6	3.00	101.2
0.50	189.2	4.00	88.0
0.75	176.0	6.00	61.6
1.00	162.8	12.00	22.0
1.50	138.6	24.00	4.4
2.00	121.0	48.00	0.1

Reproduced from the *Journal of the American Pharmaceutical Association*, 1972, **61**, 773–778, with permission of the copyright owner, the American Pharmaceutical Association.

For the intravenous data, a 2-compartment model was proposed, which we write as a sum of two exponentials,

$$f(x,\boldsymbol{\theta}) = \theta_1 e^{-\theta_2 x} + \theta_3 e^{-\theta_4 x}$$

where f is predicted sulfisoxazole concentration and x is time.

A1.8 Lubricant

Data on the kinematic viscosity of a lubricant, in stokes, as a function of temperature (°C), and pressure in atmospheres (atm), were obtained (see Table A1.8) and an empirical model was proposed for the logarithm of the viscosity, as discussed in Linssen (1975).

The proposed model is

$$f(\mathbf{x},\boldsymbol{\theta}) = \frac{\theta_1}{\theta_2 + x_1} + \theta_3 x_2 + \theta_4 x_2^2 + \theta_5 x_2^3 + (\theta_6 + \theta_7 x_2^2)\, x_2 \exp\left[\frac{-x_1}{\theta_8 + \theta_9 x_2^2}\right]$$

where f is predicted ln(viscosity), x_1 is temperature, and x_2 is pressure.

A1.9 Chloride

Data on the rate of transport of sulfite ions from blood cells suspended in a salt solution were obtained by W. H. Dennis and P. Wood at the University of Wisconsin, and analyzed by Sredni (1970). The chloride concentration (%) was determined from a continuous curve generated from electrical potentials. (See Table A1.9.)

A model was derived from the theory of ion transport as

$$f(x,\boldsymbol{\theta}) = \theta_1 (1 - \theta_2 e^{-\theta_3 x})$$

where f is predicted chloride concentration and x is time.

A1.10 Ethyl Acrylate

Data on the metabolism of ethyl acrylate were obtained by giving rats a bolus of radioactively tagged ethyl acrylate (Watts, deBethizy, and Stiratelli, 1986). Each rat was given a measured dose of the compound via stomach intubation and placed in an enclosed cage from which the air could be drawn through a bubble chamber. The exhalate was bubbled through the chamber, and at a specified time the bubble chamber was replaced by a fresh one, so that the measured response was the accumulated CO_2 during the collection interval. The response reported in Table A1.10 is the average, for nine rats, of the amount of

Table A1.8 Logarithm of lubricant viscosity versus pressure and temperature.

T = 0°C		T = 25°C	
Pressure (atm)	ln[viscosity (s)]	Pressure (atm)	ln[viscosity (s)]
1.000	5.10595	1.000	4.54223
740.803	6.38705	805.500	5.82452
1407.470	7.38511	1505.920	6.70515
363.166	5.79057	2339.960	7.71659
1.000	5.10716	422.941	5.29782
805.500	6.36113	1168.370	6.22654
1868.090	7.97329	2237.290	7.57338
3285.100	10.47250	4216.890	10.3540
3907.470	11.92720	5064.290	11.9844
4125.470	12.42620	5280.880	12.4435
2572.030	9.15630	3647.270	9.52333
		2813.940	8.34496

T = 37.8°C		T = 98.9°C	
Pressure (atm)	ln[viscosity (s)]	Pressure (atm)	ln[viscosity (s)]
516.822	5.17275	1.000	3.38099
1737.990	6.64963	685.950	4.45783
1008.730	5.80754	1423.640	5.20675
2749.240	7.74101	2791.430	6.29101
1375.820	6.23206	4213.370	7.32719
191.084	4.66060	2103.670	5.76988
1.000	4.29865	402.195	4.08766
2922.940	7.96731	1.000	3.37417
4044.600	9.34225	2219.700	5.83919
4849.800	10.51090	3534.750	6.72635
5605.780	11.82150	4937.710	7.76883
6273.850	13.06800	6344.170	8.91362
3636.720	8.80445	7469.350	9.98334
1948.960	6.85530	5640.940	8.32329
1298.470	6.11898	4107.890	7.13210

Reprinted with permission of H. N. Linssen.

Table A1.9 Chloride ion concentration versus time.

Time (min)	Conc. (%)	Time (min)	Conc. (%)	Time (min)	Conc. (%)
2.45	17.3	4.25	22.6	6.05	26.6
2.55	17.6	4.35	22.8	6.15	27.0
2.65	17.9	4.45	23.0	6.25	27.0
2.75	18.3	4.55	23.2	6.35	27.0
2.85	18.5	4.65	23.4	6.45	27.0
2.95	18.9	4.75	23.7	6.55	27.3
3.05	19.0	4.85	24.0	6.65	27.8
3.15	19.3	4.95	24.2	6.75	28.1
3.25	19.8	5.05	24.5	6.85	28.1
3.35	19.9	5.15	25.0	6.95	28.1
3.45	20.2	5.25	25.4	7.05	28.4
3.55	20.5	5.35	25.5	7.15	28.6
3.65	20.6	5.45	25.9	7.25	29.0
3.75	21.1	5.55	25.9	7.35	29.2
3.85	21.5	5.65	26.3	7.45	29.3
3.95	21.9	5.75	26.2	7.55	29.4
4.05	22.0	5.85	26.5	7.65	29.4
4.15	22.3	5.95	26.5	7.75	29.4

Reproduced from J. Sredni, "Problems of Design, Estimation, and Lack of Fit in Model Building," Ph.D. Thesis, University of Wisconsin–Madison, 1970, with permission of the author.

Table A1.10 Collection intervals and averages of normalized exhaled CO_2.

Collection Interval (hr)		CO_2
Start	Length	(g)
0.0	0.25	0.01563
0.25	0.25	0.04190
0.5	0.25	0.05328
0.75	0.25	0.05226
1.0	0.5	0.08850
1.5	0.5	0.06340
2.0	2.0	0.13419
4.0	2.0	0.04502
6.0	2.0	0.02942
8.0	16.0	0.02716
24.0	24.0	0.01037
48.0	24.0	0.00602

Reproduced with permission.

accumulated CO_2 normalized by actual dose, in units of grams CO_2 per gram acrylate per gram rat. An empirical model with three exponential terms was determined from inspection of plots of the data and physical reasoning. Logarithms of the integrated function were fitted to logarithms of the data, using the refinements of Section 3.9.

The integrated model is written

$$F(\mathbf{x},\boldsymbol{\theta}) = -\frac{\theta_4+\theta_5}{\theta_1}e^{-\theta_1 x_1}(1-e^{-\theta_1 x_2}) + \frac{\theta_4}{\theta_2}e^{-\theta_2 x_1}(1-e^{-\theta_2 x_2}) + \frac{\theta_5}{\theta_3}e^{-\theta_3 x_1}(1-e^{-\theta_3 x_2})$$

where F is predicted CO_2 exhaled during an interval, x_1 is interval starting time, and x_2 is interval duration.

A1.11 Saccharin

Data on the metabolism of saccharin compounds were obtained by Renwick (1982). In this experiment, a rat received a single bolus of saccharin, and the amount of saccharin excreted was measured by collecting urine in contiguous time intervals. The measured response was the level of radioactivity of the urine, which was converted to amount of saccharin in micrograms (μg). (See Table A1.11.) An empirical compartment model with two exponential terms

Table A1.11 Collection intervals and excreted saccharin amounts.

Collection Interval (min)		Saccharin
Start	Length	(μg)
0	5	7518
5	10	6275
15	15	4989
30	15	2580
45	15	1485
60	15	861
75	15	561
90	15	363
105	15	300

From "Pharmacokinetics in Toxicology," by A. G. Renwick, in *Principles and Methods of Toxicology*, A. Wallace Hayes, Ed., Raven Press, 1982. Reprinted with permission of the publisher.

was determined from inspection of plots of the data. Logarithms of the integrated function were fitted to logarithms of the data, using the refinements of Section 3.9.

The integrated model is written

$$F(\mathbf{x},\boldsymbol{\theta}) = \frac{\theta_3}{\theta_1} e^{-\theta_1 x_1}(1-e^{-\theta_1 x_2}) + \frac{\theta_4}{\theta_2} e^{-\theta_2 x_1}(1-e^{-\theta_2 x_2})$$

where F is predicted saccharin excreted during an interval, x_1 is interval starting time, and x_2 is interval duration.

A1.12 Nitrite Utilization

Data on the utilization of nitrite in bush beans as a function of light intensity were obtained by J. R. Elliott and D. R. Peirson of Wilfrid Laurier University. Portions of primary leaves from three 16-day-old bean plants were subjected to eight levels of light intensity measured in microeinsteins per square metre per second ($\mu E/m^2$ s) and the nitrite utilization in nanomoles of NO_2^- per gram per hour (nmol/g hr) was measured. The experiment was repeated on a different day. (See Table A1.12.)

An empirical model was suggested to satisfy the requirements of zero nitrite utilization at zero light intensity and approach to an asymptote as light intensity increased. Two models were fitted which rose to a peak and then began

Table A1.12 Nitrite utilization versus light intensity.

Light Intensity ($\mu E/m^2$ s)	Nitrite Utilization (nmol/g hr) Day 1	Day 2
2.2	256	549
	685	1 550
	1 537	1 882
5.5	2 148	1 888
	2 583	3 372
	3 376	2 362
9.6	3 634	4 561
	4 960	4 939
	3 814	4 356
17.5	6 986	7 548
	6 903	7 471
	7 636	7 642
27.0	9 884	9 684
	11 597	8 988
	10 221	8 385
46.0	17 319	13 505
	16 539	15 324
	15 047	15 430
94.0	19 250	17 842
	20 282	18 185
	18 357	17 331
170.0	19 638	18 202
	19 043	18 315
	17 475	15 605

Reprinted with permission of J. R. Elliott and D. R. Peirson.

to decline, as described in Section 3.12. These models are

$$f(x, \boldsymbol{\theta}) = \frac{\theta_1 x}{\theta_2 + x + \theta_3 x^2}$$

and

$$f(x, \boldsymbol{\theta}) = \theta_1(e^{-\theta_3 x} - e^{-\theta_2 x})$$

where f is predicted nitrite utilization and x is light intensity.

A1.13 s-PMMA

Data on the dielectric behavior of syndiotactic poly(methylmethacrylate) (s-PMMA) were obtained by Havriliak and Negami (1967). A disk of the polymer was inserted between the two metal electrodes of a dielectric cell which formed one arm of a four-armed electrical bridge. The bridge was powered by an oscillating voltage whose frequency f could be changed from 5 to 500 000 hertz (Hz), and bridge balance was achieved using capacitance and conductance standards. The complex dielectric constant was calculated using changes from the standards relative to the cell dielectric constant. Measurements were made by simultaneously adjusting the capacitance (real) and the conductance (imaginary) arms of the bridge when it was excited at a specific frequency. The measured responses were the relative capacitance and relative conductance (dimensionless). (See Table A1.13.)

Table A1.13 Real and imaginary dielectric constant versus frequency for s-PMMA at 86.7°F.

Frequency	Relative Impedance		Frequency	Relative Impedance	
(Hz)	Real	Imag	(Hz)	Real	Imag
30	4.220	0.136	3 000	3.358	0.305
50	4.167	0.167	5 000	3.258	0.289
70	4.132	0.188	7 000	3.193	0.277
100	4.038	0.212	10 000	3.128	0.255
150	4.019	0.236	15 000	3.059	0.240
200	3.956	0.257	20 000	2.984	0.218
300	3.884	0.276	30 000	2.934	0.202
500	3.784	0.297	50 000	2.876	0.182
700	3.713	0.309	70 000	2.838	0.168
1 000	3.633	0.311	100 000	2.798	0.153
1 500	3.540	0.314	150 000	2.759	0.139
2 000	3.433	0.311			

From "Analytic Representation of Dielectric Constants: A Complex Multiresponse Problem," by S. Havriliak, Jr. and D. G. Watts, in *Design, Data, and Analysis*, Colin L. Mallows, Ed., Wiley, 1987. Reprinted with permission of the publisher.

The model is an empirical generalization of two models based on theory. It is written

$$f(x,\boldsymbol{\theta}) = \theta_2 + \frac{\theta_1 - \theta_2}{\left[1 + \left[i2\pi x\, e^{-\theta_3}\right]^{\theta_4}\right]^{\theta_5}}$$

where f is predicted relative complex impedance and x is frequency.

A1.14 Tetracycline

Data on the metabolism of tetracycline were presented in Wagner (1967). In this experiment, a tetracycline compound was administered orally to a subject and the concentration of tetracycline hydrochloride in the serum in micrograms per milliliter (μg/ml) was measured over a period of 16 hours. (See Table A1.14.)

A 2-compartment model was proposed, and dead time was incorporated as

$$f(x,\boldsymbol{\theta}) = \theta_3[e^{-\theta_1(x-\theta_4)} - e^{-\theta_2(x-\theta_4)}]$$

where f is predicted tetracycline hydrochloride concentration and x is time.

Table A1.14 Tetracycline concentration versus time.

Time (hr)	Tetracycline Conc. (μg/ml)	Time (hr)	Tetracycline Conc. (μg/ml)
1	0.7	8	0.8
2	1.2	10	0.6
3	1.4	12	0.5
4	1.4	16	0.3
6	1.1		

From "Use of Computers in Pharmacokinetics," by J.G. Wagner, in *Journal of Clinical Pharmacology and Therapeutics*, 1967, 8, 201. Reprinted with permission of the publisher.

A1.15 Oil Shale

Data on the pyrolysis of oil shale were obtained by Hubbard and Robinson (1950) and are reproduced in Table A1.15. Oil shale contains organic matter which is organically bonded to the structure of the rock: to extract oil from the rock, heat is applied, and so the technique is called pyrolysis. During pyrolysis, the benzene organic material, called kerogen, decomposes chemically to oil and bitumen, and there are unmeasured by-products of insoluble organic residues and light gases. The responses measured were the concentrations of oil and bitumen (%). The initial concentration of kerogen was 100%. Ziegel and Gorman (1980) proposed a linear kinetic model with the system diagram in Figure A1.2.

A1.16 Lipoproteins

Data on lipoprotein metabolism were reported in Anderson (1983). The response was the concentration, in percent, of a tracer in the serum of a baboon given a bolus injection. Measurements were made at half-day and day intervals. (See Table A1.16.) An empirical compartment model with two exponential terms was proposed, based on inspection of plots of the data. The system diagram of the final 3-compartment catenary model fitted in Section 5.4 is given in Figure A1.3. (A mammary model was also fitted, as discussed in Section 5.4.) It is assumed that the initial concentration in compartment 1 is 100% and that the only response measured is the concentration in compartment 1.

Table A1.15 Relative concentration of bitumen and oil versus time and temperature for pyrolysis of oil shale.

T = 673 K			T = 698 K		
Time	Concentration (%)		Time	Concentration (%)	
(min)	Bitumen	Oil	(min)	Bitumen	Oil
5	0.0	0.0	5.0	6.5	0.0
7	2.2	0.0	7.0	14.4	1.4
10	11.5	0.7	10.0	18.0	10.8
15	13.7	7.2	12.5	16.5	14.4
20	15.1	11.5	15.0	29.5	21.6
25	17.3	15.8	17.5	23.7	30.2
30	17.3	20.9	20.0	36.7	33.1
40	20.1	26.6	25.0	27.3	40.3
50	20.1	32.4	30.0	16.5	47.5
60	22.3	38.1	40.0	7.2	55.4
80	20.9	43.2	50.0	3.6	56.8
100	11.5	49.6	60.0	2.2	59.7
120	6.5	51.8			
150	3.6	54.7			

T = 723 K			T = 748 K		
Time	Concentration (%)		Time	Concentration (%)	
(min)	Bitumen	Oil	(min)	Bitumen	Oil
5.0	8.6	0.0	3.0	0.7	0.0
7.5	15.8	2.9	4.5	17.3	2.9
8.0	25.9	16.5	5.0	23.0	17.3
9.0	25.2	24.4	5.5	24.4	20.9
10.0	26.6	29.5	6.0	23.0	25.9
11.0	33.8	35.2	6.5	33.1	29.5
12.5	25.9	39.5	7.0	31.6	33.8
15.0	20.1	45.3	8.0	20.9	45.3
17.5	12.9	43.1	9.0	10.1	53.2
17.5	9.3	54.6	10.0	4.3	58.2
20.0	3.6	59.7	12.5	0.7	57.5
20.0	2.2	53.9	15.0	0.7	61.1

Table A1.15 continued

T = 773 K			T = 798 K		
Time	Concentration (%)		Time	Concentration (%)	
(min)	Bitumen	Oil	(min)	Bitumen	Oil
3.0	6.5	0.0	3.00	25.2	20.9
4.0	24.4	23.0	3.25	33.1	25.2
4.5	26.6	32.4	3.50	21.6	17.3
5.0	25.9	37.4	4.00	20.9	36.7
5.5	17.3	45.3	5.00	4.3	56.8
6.0	21.6	45.3	7.00	0.0	61.8
6.5	1.4	57.5			
10.0	0.0	60.4			

From "A Thermal Decomposition Study of Colorado Oil Shale," Hubbard, A.B. and Robinson, W.E., U.S. Bureau of Mines, Rept. Invest. No. 4744, 1950.

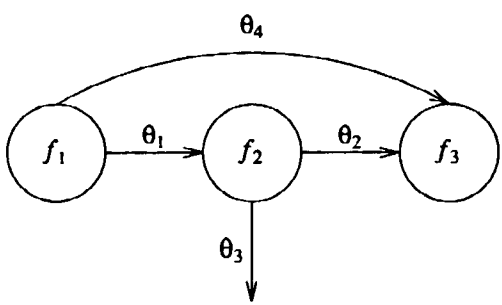

Figure A1.2 System diagram for oil shale model where f_1 is kerogen, f_2 is bitumen, and f_3 is oil.

Table A1.16 Lipoprotein tracer concentration versus time.

Time (days)	Tracer Conc. (%)	Time (days)	Tracer Conc. (%)
0.5	46.10	5.0	3.19
1.0	25.90	6.0	2.40
1.5	17.00	7.0	1.82
2.0	12.10	8.0	1.41
3.0	7.22	9.0	1.00
4.0	4.51	10.0	0.94

From *Compartmental Modeling and Tracer Kinetics*, D. H. Anderson, p 211, 1983, Springer–Verlag. Reproduced with permission of the author and the publisher.

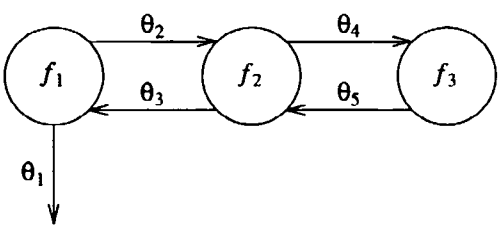

Figure A1.3 System diagram for the tetracycline model where f_1 is the concentration in the sampled compartment. The other compartments do not have a physical interpretation.

APPENDIX 2.

QR Decompositions Using Householder Transformations

To compute the *QR* decomposition of an $N \times P$ matrix $\mathbf{X}$, we use Householder transformations (Householder, 1958), a generalization of reflections in the plane. These are $N \times N$ matrices of the form

$$\mathbf{H}_{\mathbf{u}} = \mathbf{I} - 2\mathbf{u}\mathbf{u}^{\mathrm{T}}$$

where $\mathbf{I}$ is the $N \times N$ identity matrix and $\mathbf{u}$ is an N-dimensional unit vector (that is, $\|\mathbf{u}\| = \sqrt{\mathbf{u}^{\mathrm{T}}\mathbf{u}} = 1$). $\mathbf{H}_{\mathbf{u}}$ is symmetric and orthogonal, since

$$\mathbf{H}_{\mathbf{u}}^{\mathrm{T}} = \mathbf{I}^{\mathrm{T}} - 2\mathbf{u}\mathbf{u}^{\mathrm{T}} = \mathbf{H}_{\mathbf{u}}$$

and

$$\mathbf{H}_{\mathbf{u}}^{\mathrm{T}}\mathbf{H}_{\mathbf{u}} = \mathbf{I} - 4\mathbf{u}\mathbf{u}^{\mathrm{T}} + 4\mathbf{u}\mathbf{u}^{\mathrm{T}}\mathbf{u}\mathbf{u}^{\mathrm{T}} = \mathbf{I}$$

Multiplying a vector $\mathbf{y}$ by $\mathbf{H}_{\mathbf{u}}$, as

$$\mathbf{H}_{\mathbf{u}}\mathbf{y} = \mathbf{y} - 2\mathbf{u}\mathbf{u}^{\mathrm{T}}\mathbf{y}$$

corresponds to reflecting $\mathbf{y}$ about the line through the origin perpendicular to $\mathbf{u}$, as shown in Figure A2.1. By choosing

$$\mathbf{u} = \frac{\mathbf{y} - \|\mathbf{y}\|\mathbf{e}_1}{\|(\mathbf{y} - \|\mathbf{y}\|\mathbf{e}_1)\|} \tag{A2.1}$$

or

$$\mathbf{u} = \frac{\mathbf{y} + \|\mathbf{y}\|\mathbf{e}_1}{\|(\mathbf{y} + \|\mathbf{y}\|\mathbf{e}_1)\|} \tag{A2.2}$$

where $\mathbf{e}_1 = (1,0,\ldots,0)^{\mathrm{T}}$, the Householder transformation can be made to take the vector $\mathbf{y}$ to the x axis; that is, in the new (rotated) coordinate system, the vector $\mathbf{H}_{\mathbf{u}}\mathbf{y}$ has coordinates $(\pm\|\mathbf{y}\|,0,\ldots,0)^{\mathrm{T}}$.

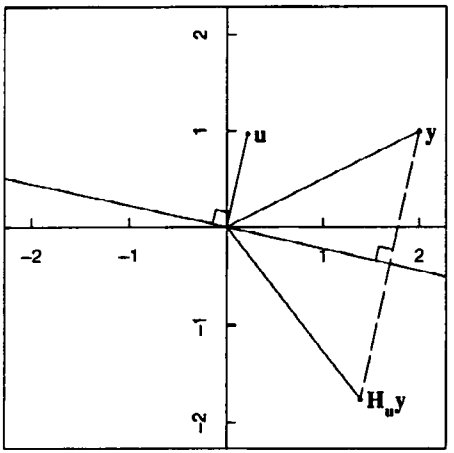

Figure A2.1 A Householder transformation showing the reflection about the line perpendicular to **u** of the vector **y** to form $\mathbf{H}_u\mathbf{y}$.

Example: PCB 14

To perform the *QR* decomposition of the matrix

$$\mathbf{X} = \begin{bmatrix} 1 & 1.26 \\ 1 & 1.82 \\ 1 & 2.22 \end{bmatrix}$$

from Example PCB 3, we choose a transformation $\mathbf{H}_{\mathbf{u}_1}$ to take the first column $\mathbf{x}_1$ of $\mathbf{X}$ to the x axis using (A2.1) and obtain

$$\mathbf{u}_1 = \frac{(1,1,1)^T - \sqrt{3}(1,0,0)^T}{1.5925} = \frac{(-0.7321,1,1)^T}{1.5925}$$

so that

$$\mathbf{X}_1 = \mathbf{H}_{\mathbf{u}_1}\mathbf{X} = \begin{bmatrix} 1.7321 & 3.0600 \\ 0 & -0.6388 \\ 0 & -0.2388 \end{bmatrix}$$

We now perform a second rotation, orthogonal to the first, by choosing $\mathbf{u}_2$ so that $\mathbf{H}_{\mathbf{u}_2}$ zeros the rows below the diagonal of the second column of $\mathbf{X}_1$ without changing the first column. To ensure that we do not change the first column, we make the first element of $\mathbf{u}_2$ be zero. The vector $\mathbf{u}_2$ is therefore chosen to be

$$\mathbf{u}_2 = \frac{(0,-0.6388,-0.2388)^T - 0.6820(0,1,0)^T}{1.3422}$$

which gives

$$\mathbf{R} = \mathbf{H}_{\mathbf{u}_2}\mathbf{H}_{\mathbf{u}_1}\mathbf{X} = \begin{bmatrix} 1.7321 & 3.0600 \\ 0 & 0.6820 \\ 0 & 0 \end{bmatrix}$$

■

As shown in the above example, the matrix $\mathbf{R}$ is produced at the same time as the Householder reflection vectors $\mathbf{u}_1, \ldots, \mathbf{u}_P$ are obtained. The corresponding $\mathbf{Q}$ is determined from $\mathbf{R} = \mathbf{Q}^T\mathbf{X}$, that is, $\mathbf{Q}^T = \mathbf{H}_{\mathbf{u}_P} \cdots \mathbf{H}_{\mathbf{u}_1}$. Because Householder transformations are symmetric, this gives

$$\mathbf{Q} = \mathbf{H}_{\mathbf{u}_1}^T \cdots \mathbf{H}_{\mathbf{u}_P}^T = \mathbf{H}_{\mathbf{u}_1} \cdots \mathbf{H}_{\mathbf{u}_P}$$

Note that $\mathbf{Q}$ is almost never calculated explicitly, as any multiplications by $\mathbf{Q}$ or $\mathbf{Q}^T$ are performed by applying Householder transformations in the appropriate order. A Householder transformation $\mathbf{H}_{\mathbf{u}}$ is applied to a vector $\mathbf{y}$ by subtracting $2\mathbf{u}\mathbf{u}^T\mathbf{y}$ from $\mathbf{y}$ and only requires calculating one inner product and subtracting a multiple of a vector from another vector.

For linear and nonlinear regression, it is sometimes convenient to perform a QR decomposition of the matrix $\mathbf{X}$ augmented with the vector $\mathbf{y}$. The QR decomposition of $(\mathbf{X} \mid \mathbf{y})$ produces the vector $\mathbf{w}_1$ directly in the first P rows of the $(P+1)$st column of $\mathbf{R}$, [cf. (1.21)], from which the least squares estimate or the increment can be obtained [cf. (1.24)]. The $(P+1)$st entry of that column gives $\| \mathbf{w}_2 \|$, which can be used to test for convergence in nonlinear regression as discussed in Section 2.2.3, and, after convergence, to calculate the residual standard deviation.

Example: PCB 15

For the data from Example PCB 3 with

$$\mathbf{y} = \begin{bmatrix} 0.92 \\ 2.15 \\ 2.52 \end{bmatrix}$$

we calculate

$$\begin{aligned} \mathbf{Q}^T\mathbf{y} &= \mathbf{H}_{\mathbf{u}_2}(\mathbf{y} - 2\mathbf{u}_1\mathbf{u}_1^T\mathbf{y}) \\ &= \mathbf{H}_{\mathbf{u}_2}\begin{bmatrix} 3.2275 \\ -1.0024 \\ -0.6324 \end{bmatrix} \\ &= \begin{bmatrix} 3.2275 \\ 1.1601 \\ -0.2414 \end{bmatrix} \end{aligned}$$

■

Using Householder transformations is faster and numerically more stable than explicitly forming $\mathbf{Q}$, especially when N is large compared to P. In addi-

tion, using Householder transformations only requires storing the P vectors $\mathbf{u}_1, \mathbf{u}_2, \ldots, \mathbf{u}_P$, which can provide substantial savings in storage compared to storing the N^2 elements of $\mathbf{Q}$.

In actual implementations of the QR decomposition, such as the code in LINPACK (Dongarra et al., 1979, Chapter 9), the choice of (A2.1) or (A2.2) to define $\mathbf{u}$ is based on the sign of the first coordinate of $\mathbf{y}$. If this coordinate is negative, (A2.1) is used, and if it is positive, (A2.2) is used for numerical stability. For further discussion on the QR decomposition, see Dongarra et al. (1979) and Stewart (1973).

APPENDIX 3.

Pseudocode for Computing Algorithms

At several points in this book we have described how to compute estimates and summary results. To aid the reader in understanding the computing methods and to provide guidance in implementing them, we present pseudocode for the more important algorithms in this appendix.

A3.1 Nonlinear Least Squares

The Gauss–Newton algorithm for nonlinear least squares with a relative offset convergence criterion can be expressed in pseudocode as:

```
initialize iteration counter(0) and step factor λ=1
repeat {
   increment iteration counter
   error exit if maximum number of iterations exceeded
   evaluate residuals and derivatives
   decompose derivatives as QR
   error exit if R is computationally singular
   overwrite residuals by Q^T z
   solve for δ
   evaluate convergence criterion
   normal exit if (criterion < tolerance)
   repeat {
      evaluate residuals at θ+λδ
      break loop if (S(θ+λδ) < S(θ))
      halve λ
      error exit if (λ < minimum allowed)
   }
   overwrite S(θ) with S(θ+λδ)
   overwrite θ with θ+λδ
   double λ to maximum of 1
}
```

We implement this algorithm in three high level languages, S (Becker, Chambers, and Wilks, 1988), GAUSS (Edlefsen and Jones, 1986), and SAS/IML (SAS Institute Inc., 1985) in the following subsections.

A3.1.1 Implementation in S

One of the fundamental issues to be resolved in any implementation of nonlinear algorithms is the method of packaging the model function and the independent variables. In S we can use default values for arguments of functions for this. For example, we define the Michaelis–Menten model with the Puromycin data as:

```
Puromycin ← function(theta = (205., 0.08), derivs = F,
   conc = (0.02, 0.02, 0.06, 0.06, 0.11, 0.11, 0.22,
   0.22, 0.56, 0.56, 1.1, 1.1), rate = (76., 47., 97.,
   107., 123., 139., 159., 152., 191., 201., 207., 200.))
{
   denom ← theta[2] + conc
   res ← rate - (theta[1] * conc/denom)
   if(!derivs) return(res)
   grad ← matrix((conc/denom, - theta[1] * conc/denom^2), ncol = 2)
   list(residual = res, gradient = grad)
}
```

The function Puromycin has four arguments (theta, derivs, conc, rate) but the only arguments which are changed between calls are theta, the model parameters, and derivs, a logical value which indicates if derivatives are to be calculated. Any actual arguments specified for these two formal arguments will override the default values. Using conc, the observed concentrations, and rate, the observed reaction rates, as arguments is a convenient way of incorporating information about the observed response and the regressor variables with the expressions which define the residuals and the derivatives of the model function.

The Gauss–Newton nonlinear least squares algorithm is also specified as a function with default arguments to specify characteristics such as the maximum number of iterations and the minimum step factor. This function, which we call nlsfit, is:

```
nlsfit ← function(model, theta = eval(model[["theta"]]), maxiter = 25 * P,
   minfactor = 1/2^10, tolerance = 0.001, verbose = T)
{
   resid ← model(theta, derivs = F)
   newssq ← sum(resid^2)
   P ← length(theta)
   N ← length(resid)
   ndof ← N - P
   mult ← sqrt(ndof/P)
   iteration ← 0
```

```
    stepfactor ← 1.
    repeat {
      iteration ← iteration + 1
      if(iteration > maxiter)
        stop("Maximum number of iterations exceeded")
      oldssq ← newssq
      resgrad ← model(theta, derivs = T)
      qrstr ← qr(resgrad$gradient)
      if(qrstr$rank!=P) stop("Singular derivative matrix")
      qrslv ← qr.coefqty(qrstr, resgrad$residual)
      incr ← qrslv$coef
      converge ← mult * sqrt(sum(qrslv$qty[1:P]^2)
        /sum(qrslv$qty[ - (1:P)]^2))
      if(verbose) cat(iteration, "<", converge, ">", incr, fill = T)
      if(converge < tolerance) break
      repeat {
        trial ← theta + stepfactor * incr
        if(stepfactor < minfactor)
          stop("Step factor reduced below minimum")
        newssq ← sum(model(trial, derivs = F)^2)
        if(verbose) cat("  ", stepfactor,
          "(", newssq, ")", trial, fill = T)
        if(newssq <= oldssq) break
        stepfactor ← stepfactor/2
      }
      stepfactor ← min(1., 2 * stepfactor)
      theta ← trial
    }
    list(model = model, coef = theta, qr = qrstr,
      residuals = resgrad$residual, criterion = converge)
  }
```

The name nlsfit is chosen to correspond to lsfit, the S function for fitting linear regression models. Furthermore, the object returned by nlsfit is similar to the object returned by lsfit, so that other functions in S for summarizing the results of a linear least squares fit can be used for linear approximation summaries of the nonlinear least squares fit.

The S code very closely follows the pseudocode given above. An initial evaluation of the residuals at the starting values for theta is used to set the sum of squares for later comparisons. The length of this residual vector is the number of observations, N, which, along with the number of parameters, P, is used to calculate a multiplier, mult, for the convergence criterion. The S function qr performs the *QR* decomposition of a matrix, and the function qr.coefqty returns both the coefficient vector, which is $\boldsymbol{\delta}$ in our case, and $\mathbf{Q}^T\mathbf{y}$, which is $\mathbf{Q}^T\mathbf{z}$ in our case. The convergence criterion is calculated from the sum of squares of the first P elements of $\mathbf{Q}^T\mathbf{z}$ (using the notation 1:P), and the sum of squares of everything but the first P elements [using the notation −(1:P)].

If the argument verbose has the value T (true), diagnostic output is produced by the function cat during each iteration of the outer loop and each itera-

tion of the inner loop. Diagnostic output for the Puromycin data appears as:

```
PUR.out ← nlsfit(Puromycin)
1 < 2.8046 > 8.02889 -0.0171078
     1.0000 ( 1205.66 ) 213.029 0.0628922
2 < 0.204279 > -0.425519 0.00109553
     1.0000 ( 1195.48 ) 212.603 0.0639878
3 < 0.0103471 > 0.0720588 0.000120553
     1.0000 ( 1195.45 ) 212.675 0.0641083
4 < 0.00100142 > 0.0075058 1.17256e-05
     1.0000 ( 1195.45 ) 212.683 0.06412
5 < 9.65585e-05 > 0.000725621 1.13078e-06
```

The output from the outer loop consists of the iteration numbers at the left margin, followed by the convergence criterion, in angle brackets, followed by the requested increment. The output from the inner loop is indented and consists of the step factor, λ, followed by the residual sum of squares, in parentheses, followed by the parameter values.

A3.1.2 Implementation in GAUSS

The principal input to the GAUSS nlsfit procedure (proc) is the model function, which we code as in the **S** implementation, with two notable differences. First, the residuals and the derivative matrix are returned as an $N \times (P+1)$ matrix, because the current version of GAUSS (1.49b, revision 19) allows a proc to return only one matrix. Second, the raw data are specified as global variables so that they are available for other purposes. With these conditions, we define the Michaelis–Menten model with the Puromycin data as:

```
P_MYCIN.PRG;
let conc = .02 .02 .06 .06 .11 .11 .22 .22 .56 .56 1.1 1.1 ;
let rate =  76  47  97 107 123 139 159 152 191 201 207 200 ;
proc p_mycin( theta, derivs);
   local denom, resid, grad;
   denom = theta[2,1] + conc;
   resid  = rate  - ( theta[1,1] *  conc./denom );
   if not derivs;
      retp(resid);
   endif;
   grad = conc./denom ~ -theta[1,1] * conc./denom .^2;
   retp(resid~grad);
endp;
```

The GAUSS procedure nlsfit is similar to the **S** routine, but because GAUSS has no facilities for defining default arguments, we include the number of iterations, the minimum step factor, and the tolerance in the calling sequence. The procedure nlsfit returns the $P+2$ vector (theta|ssq|criterion), (the least squares estimates,

the sum of squares, and the convergence criterion, which is awkward to compute outside the procedure). If convergence is not achieved, an error code can be returned by using the error function. Diagnostic output is written when verbose is nonzero by calling the procedure diagnost. If desired, the residuals and derivative matrix could be returned to global variables by means of the varput function. The procedure is:

```
proc nlsfit(&model, theta, maxiter, minstep, tol, verbose);
local model:proc, mult, iter, stepsize, resgrad, res, incr, fullrank,
   criterion, ssq, trial, newssq;
res  = model( theta, 1);
nobs = rows( res );
npar = rows( theta );
mult = sqrt( (nobs - npar) ./ npar );
iter = 0;
stepsize = 1;
do while 1;
   iter = iter + 1;
   resgrad = model( theta, 1);
   ssq = sumc( resgrad[ .,1] .^ 2 );
   gosub qr_solv;
   pop incr;pop criterion;pop fullrank;
   if verbose;
      call diagnost(iter|"<"|criterion|">"|incr,1);
   endif;
   if not fullrank;
      "Singular derivative matrix";stop;
   elseif criterion < tol;
      retp(theta|ssq|criterion);
   elseif iter > maxiter;
      "Maximum iterations reached";stop;
   endif;
   gosub step;
   pop stepsize;pop theta;
endo;
```

The subroutine step, which follows, computes the new stepsize and the corresponding parameter vector and returns them to the body of the procedure, where they are "pop"ed into the appropriate variables. The code is:

```
step:
 do while 1;
   trial = theta + stepsize * iner;
   newssq = sumc( model( trial, 0 ) .^ 2 );
   if verbose;
      call diagnost(stepsize|"("|newssq|")"|trial,0);
   endif;
   if stepsize < minstep;
      " Stepsize reduced below minimum ";stop;
```

```
    elseif newssq < ssq;
      return( trial, minc( 1 | 2 * stepsize ));
    endif;
    stepsize = stepsize ./ 2 ;
  endo;
```

All that remains is to compute the *QR* decomposition in the subroutine qr_solv. GAUSS implements *QR* decompositions via the LINPACK routines (Dongarra et al., 1979) DQRDC and DQRSL using the loadexe/callexe commands. For iterative applications it is more efficient to preload the LINPACK code at startup: for discussion of how to do this, see the December 1986 GAUSS newsletter, vol. 2 no. 6. Code for the subroutine qr_solv using the callexe command is:

```
qr_solv:
 local flag, qraux, work, jpvt, qty, dum, job, info, grad,
    beta, karg, ss_tan, ss_orth;
 flag = 1;
 qraux = zeros( npar , 1 );
 work = qraux;
 jpvt = qraux;                @--- all columns free ---@
 qty = zeros( nobs, 1 );
 dum = 0;
 job = 100;                   @--- compute beta and Q'y---@
 info = 0;
 grad = submat(resgrad,0,seqa(2,1,npar))';
 res = resgrad[ .,1];
 callexe  gqrdc(grad,nobs,nobs,npar,qraux,jpvt,work,flag);
 beta = abs( diag( trim( grad', 0, nobs-npar)));
 karg = sumc( beta .> beta[1,1] * 1e-14 );
 beta = zeros(npar,1);
 callexe
    gqrsl(grad,nobs,nobs,karg,qraux,res,dum,qty,beta,dum,dum,job,info);
 beta = submat( sortc( beta ~ jpvt, 2 ), 0, 1 );
 ss_tan = sumc( submat( qty, seqa(1,1,npar), 0 ) .^2 );
 ss_orth = sumc(submat( qty, seqa( npar+1, 1, nobs - npar ), 0 ) .^2 );
 return( karg == npar, mult*sqrt(ss_tan./ss_orth) , beta);
 endp;
end;
```

With these procs, the program nlsfit(&p_mycin,205|.08,10,.001,.001,1); produces the output:

```
--------------Nonlinear estimation--------------

Starting values:      205.00000000        0.08000000
01 <     2.804604 >     8.028894    -0.017108
    1.000000 ( 1205.661845 )  213.028894     0.062892
02 <     0.204279 >    -0.425519     0.001096
    1.000000 ( 1195.477124 )  212.603375     0.063988
```

```
03 <    0.010347 >    0.072059    0.000121
    1.000000 ( 1195.449080 )  212.675434    0.064108
04 <    0.001001 >    0.007506    0.000012
    1.000000 ( 1195.448817 )  212.682940    0.064120
05 <    0.000097 >    0.000726    0.000001
```

A3.1.3 Implementation in SAS/IML

The principal input to the SAS/IML module nlsfit is the model function, which we code in a submodule called model. This submodule includes the data and code for the residuals and the derivatives. For the Michaelis–Menten model with the Puromycin data, we have:

```
start model(theta,res,grad,derivs);
 conc = { .02,.02,.06,.06,.11,.11,.22,.22,.56,.56,1.1,1.1};
 rate = { 76,47,97,107,123,139,159,152,191,201,207,200};
 denom = theta(|2,1|) + conc;
 res = rate -(theta(|1,1|) * conc / denom );
 if derivs = 1 then do;
 grad = (conc/denom)||(-theta(|1,1|)*conc/(denom ## 2));
 end;
finish;
```

In SAS/IML, the *QR* decomposition is achieved by means of the GSORTH function, which returns the **Q** and **R** matrices. The increment is determined using the solve function, incr=solve(rhat,resid), and the convergence criterion is calculated by invoking the Pythagorean decomposition of the total sum of squares.

Like GAUSS, SAS/IML lacks an explicit repeat/break structure, and so we use a do until loop to calculate the step factor. The condition newssq < oldssq is evaluated at the end of the loop, so it is not necessary to initialize newssq. The step factor, however, is half the appropriate value on exit from the loop, so we multiply by 4, to a maximum of 1.

The main loop is implemented as do iter = 1 to max. On exit from the loop a message is printed and the program stops. When convergence is obtained, the program links directly to the finish statement and returns. One feature worth noting is that both the residuals and the derivatives are initialized to their starting values at the top of the module. For each new iteration they are recalculated using the new parameters at the end of the main loop, saving a function evaluation.

If the verbose option is chosen, the reset noname option is set, and must be reset to its previous state after exit from the module. Diagnostic output is similar to that from the **S** function. Code for the nlsfit module is:

```
run model( theta, resid, grad, 1);
p = nrow( theta );
n = nrow( resid );
ndof = n – p;
mult = sqrt( ndof / p );
Stepsize = 1;
do iter = 1 to maxiter;
   oldssq = ssq(resid);
   call gsorth( qhat, rhat, rank, grad);
   if rank = 1 then do;
      print "singular derivative matrix";
      stop;
   end;
   tan = qhat' * resid;
   ss_tan = ssq( tan );
   incr = solve( rhat, tan );
   criterion = mult * sqrt( ss_tan /( oldssq – ss_tan ) );
   if verbose then
      print iter(|format=2.0|) criterion (incr');
   if criterion < tol then link returns;
   do until(newssq < oldssq);
      if stepsize < minstep then do;
         print "step factor reduced below minimum";
         stop;
      end;
      trial = theta + stepsize * incr;
      run model( trial, resid, grad, 0);
      newssq = ssq( resid );
      if verbose then
         print stepsize newssq (trial');
      stepsize = stepsize / 2;
   end;
   theta = trial;
   stepsize = min( 1 || 4 * stepsize );
   run model( theta, resid, grad, 1);
end;
print " Maximum number of iterations reached: program terminated";
stop;
returns: finish;
```

With these modules, the program

```
title NLSFIT to puromycin data;
PROC IML;
start model(theta,res,grad,derivs);
 ...
start nlsfit( theta, criterion, maxiter, minstep, tol, verbose);
 ...
theta = { 205, 0.08 };
run nlsfit(theta,criterion,10,.001,.001,1);
```

```
reset name;print theta;
```

produces the following output:

```
NLSFIT to puromycin data

  1      2.8046     8.0289  -0.0171
1.0000     1205.7      213.0   0.0629
  2      0.2043    -0.4255 .0010955
1.0000     1195.5      212.6   0.0640
  3      0.0103     0.0721  1.2E-04
1.0000     1195.4      212.7   0.0641
  4    .0010014   .0075058  1.2E-05
1.0000     1195.4      212.7   0.0641
  5     9.7E-05    7.3E-04  1.1E-06

          THETA      COL1

          ROW1      212.7
          ROW2     0.0641
```

A3.2 Linear Summaries and Studentized Residuals

It is straightfoward to calculate the linear summary for the parameter estimates using the method described in Section 1.2.3. Pseudocode for this is:

set $s = \sqrt{S(\hat{\boldsymbol{\theta}})/(N-P)}$
calculate $\mathbf{R}_1^{-1}$
calculate the length of each rows of $\mathbf{R}_1^{-1}$
divide each row of $\mathbf{R}_1^{-1}$ by its length to produce $\mathbf{L}$
multiply each row length by s to give the parameter standard errors
form the correlation matrix, $\mathbf{L}\mathbf{L}^{\mathrm{T}}$

To calculate the studentized residuals we need the diagonal of the "hat matrix" $\mathbf{Q}_1\mathbf{Q}_1^{\mathrm{T}}$, but this is just the squared length of the rows of $\mathbf{Q}_1$. Pseudocode for calculating the studentized residuals is:

form the matrix $\mathbf{Q}_1$ by applying the Householder transformations
which define $\mathbf{Q}$ to the first P columns of the $N \times N$ identity matrix
sum the squares of the elements of the rows of $\mathbf{Q}_1$ to get h_{nn}
divide the nth residual by $s\sqrt{1-h_{nn}}$

It is convenient to combine the two operations of calculating the linear summary values and the studentized residuals into a single function, say ls.summary, which acts on the object returned by nlsfit.

A3.3 Multiresponse Estimation

The algorithm for optimizing the multiresponse criterion is similar to the nonlinear least squares algorithm given in Section A3.1, the main difference being in calculation of the increment at each step. Pseudocode is:

```
initialize iteration counter(0) and step factor λ = 1
repeat {
   increment iteration counter
   error exit if maximum number of iterations exceeded
   evaluate residual matrix and derivative array
   calculate |Z^T Z|, ω, and Ω
   attempt the Cholesky decomposition Ω = C^T C
   if (Ω is not positive definite) then {
      criterion is LARGE (note 1)
      decompose as Ω = UDU^T (note 2)
      δ = -U(D + 2 d_1 I)^-1 U^T ω
   } else {
      solve C^T C δ = -ω for Cδ
      evaluate convergence criterion
      solve for δ
   }
   normal exit if (criterion < tolerance)
   repeat {
      evaluate Z at θ + λδ
      break loop if (|Z^T Z| < previous value)
      halve λ
      error exit if (λ < minimum allowed)
   }
   overwrite previous |Z^T Z| with current value
   overwrite θ with θ + λδ
   double λ to maximum of 1
}
```

Notes:

(1) When $\mathbf{\Omega}$ is not positive definite, the convergence criterion is set to a predetermined value which is greater than the tolerance, so convergence cannot be declared: this is because the determinant cannot be minimized at this point unless $\mathbf{\Omega}$ is positive definite.

(2) The decomposition $\mathbf{\Omega} = \mathbf{UDU}^{\mathrm{T}}$ is an eigenvalue–eigenvector decomposition of the symmetric matrix $\mathbf{\Omega}$. The diagonal matrix $\mathbf{D}$ has diagonal entries $d_1 \leq d_2 \leq \cdots \leq d_P$, while $\mathbf{U}$ is a $P \times P$ orthogonal matrix.

The calculation of $|\mathbf{Z}^{\mathrm{T}}\mathbf{Z}|$, $\boldsymbol{\omega}$, and $\mathbf{\Omega}$ from the residual matrix and the gradient array is as described in Section 4.2.2. The pseudocode is

```
decompose Z as QR
evaluate |Z^T Z| as the square of the product of the diagonal elements of R_1
for p = 1, 2, . . . , P {
   overwrite Z_(p) by G_p = Q^T Z_(p) R_1^-1
   calculate {ω}_p from diagonal of G_p
   for q = 1, 2, . . . , p {
      calculate {Ω}_pq as in (4.24)
      store {Ω}_qp = {Ω}_pq
   }
}
```

FORTRAN implementations of these algorithms are given in Bates and Watts (1984).

A3.4 Linear Systems of Differential Equations

Pseudocode for the methods described in Appendix 5 when **A** is diagonalizable is given here. Extensions for nondiagonalizable **A** or complex eigenvalues are obtained from the formulas in Sections A5.2 and A5.3.

Before presenting the pseudocode, however, we present a compact way of specifying the form of the system of linear differential equations and the way that the components of $\boldsymbol{\theta}$ enter the system. We define a parameter use matrix **J** as described in Bates and Watts (1985, Section 3.3). The matrix **J** consists of three columns: the entry in the first column is the parameter number, the entry in the second column is the source compartment, and the entry in the third column is the sink compartment. If the parameter is an initial condition instead of a rate constant, the value -1 is used in the third column: if the parameter is a dead time, the value 0 is used in the second and third column. For Example α-Pinene 3, which involves only rate constants, the parameter use matrix is

$$\mathbf{J} = \begin{bmatrix} 1 & 1 & 2 \\ 2 & 1 & 3 \\ 3 & 3 & 4 \\ 4 & 3 & 5 \\ 5 & 5 & 3 \end{bmatrix}$$

For Example α-Pinene 9, where the reaction path from 3 to 4 is dropped,

$$\mathbf{J} = \begin{bmatrix} 1 & 1 & 2 \\ 2 & 1 & 3 \\ 3 & 3 & 5 \\ 4 & 5 & 3 \end{bmatrix}$$

The last two columns of the parameter use matrix correspond to the first two columns of the parameter summary tables which we used in these examples.

In Example Tetracycline 2, the third parameter is the initial condition in compartment 1, so the parameter use matrix is

$$\mathbf{J} = \begin{bmatrix} 1 & 1 & 2 \\ 2 & 2 & 0 \\ 3 & 1 & -1 \end{bmatrix}$$

When dead time is involved, as in Example Tetracycline 4, the source and sink compartments are coded as 0, so the parameter use matrix is extended to

$$\mathbf{J} = \begin{bmatrix} 1 & 1 & 2 \\ 2 & 2 & 0 \\ 3 & 1 & -1 \\ 4 & 0 & 0 \end{bmatrix}$$

Pseudocode to generate the values of $\mathbf{A}$, $\boldsymbol{\gamma}_0$, t_0, and $\mathbf{A}_{(p)}$, $\boldsymbol{\gamma}_{(p)}(0)$, and $\partial t_0/\partial\theta_p$, $p = 1, \ldots, P$, from the parameter use matrix $\mathbf{J}$, the parameter vector $\boldsymbol{\theta}$, and the fixed part of the initial conditions, $\boldsymbol{\gamma}_{\text{fix}}$, is

```
initialize A to 0, γ0 to γfix
for p = 1, . . . , P
   initialize A(p) to 0, γ(p)(0) to 0
initialize dt0/dθ^T to 0
for j = 1, . . . , J {
   p = {J}j1
   φ = exp({θ}p)
   i = {J}j2
   k = {J}j3
   if (i = 0) {
      t0 = {θ}p
      {dt0/dθ^T}p = 1
   } else if (k = −1) {
      increment {γ0}i by φ
      increment {γ(p)(0)}i by φ
   } else {
      decrement {A}ii by φ
      decrement {A(p)}ii by φ
      if (k > 0) {
         increment {A}ki by φ
         increment {A(p)}ki by φ
      }
   }
}
```

In this code, logarithms of the rate parameters and the initial conditions are used, but the delay time parameter is not transformed.

Pseudocode to use these values to create the predicted responses $\mathbf{H}$ and the derivatives $\mathbf{H}_{(p)}$, $p = 1, \ldots, P$ at the times t_n, $n = 1, \ldots, N$, is

```
decompose A = UΛU^-1
if (any complex eigenvalues) error exit
decompose U with an LU decomposition and check condition (note 1)
if (condition unacceptable) error exit
solve Uξ_0 = γ_0 for ξ_0
for p = 1, . . . , P
   solve UC_(p) = A_(p)U for C_(p)
for n = 1, . . . , N {
   τ = t_n − t_0
   if (τ < 0) τ = 0
   for k = 1, . . . , K {
      {ξ}_k = e^(λ_k τ) {ξ_0}_k
      for j = 1, . . . , K {
         dif = λ_j − λ_k
         if (τ dif < ε)
            {B}_kj = τ e^(λ_k τ)
         else
            {B}_kj = (e^(λ_j τ) − e^(λ_k τ)) / dif
      }
   }
   store γ_n = Uξ
   for p = 1, . . . , P {
      ξ_(p)(τ) = e^(Λτ) ξ_(p)(0) + τ_(p) e^(Λτ) Λξ_0
      increment ξ_(p)(τ) by the componentwise product
         of C_(p) and B times ξ_0
      store γ_(p)n = Uξ_(p)(τ)
   }
}
```

Notes:

(1) The *LU* decomposition (Dongarra et al., 1979, Chapter 1) of U with an estimate of the condition of the matrix is used to determine if U is computationally singular and to solve linear systems based on U.

A3.5 Profile Calculations

A3.5.1 Generation of τ and the Profile Traces

To generate the values of τ and the profile traces, we assume that the components of $\hat{\boldsymbol{\theta}}$ and their approximate standard errors are known. For each component θ_p, we generate $\tau(\theta_p)$ and the profile trace $\tilde{\boldsymbol{\theta}}_{-p}(\theta_p)$ first to the left of $\hat{\theta}_p$, then to the right. We calculate the τ values until the absolute value exceeds $\tau_{\max} = \sqrt{F(P, N-P; \alpha)}$ where α is small, say $\alpha = 0.01$. In some cases, such as Example BOD 8 or Example Isomerization 5, the value of τ approaches an asymp-

tote which is less than τ_{max}, so we impose a condition on the maximum number of values k_{max} to be calculated on either side of $\hat{\theta}_p$, say $k_{max} = 30$. A nominal step size of $se(\hat{\theta}_p)/step$ with $step = 8$ is used to start the process, but thereafter the step size is determined from the slope of the curve τ versus t, with limits to prevent the step size from becoming too large.

Pseudocode for the calculation is:

```
for p = 1, . . . ,P {
   Δ = −se(θ̂_p)/step
   t = 0
   repeat {
      invslope = 1
      for k = 1, . . . ,k_max {
         t = t + invslope
         minimize S(θ) with θ_p = θ̂_p + Δ × t obtaining S̄(θ_p) and θ̄_−p
         invslope = abs( τ × s² / (se × z^T v_p) )
         record τ(θ_p) = sign(Δ) × √(S̄ − Ŝ / s), θ, and invslope
         invslope = min(4, max(invslope, 1/16))
         if (abs(τ) > τ_max) break loop
      }
      Δ = −Δ
      if (Δ < 0) break loop
   }
}
```

Minimizing $S(\boldsymbol{\theta})$ with $\theta_p = \hat{\theta}_p + \Delta \times k$ is done with a few simple modifications to the Gauss–Newton code. In addition to evaluating the residuals and derivatives we remove the pth column of the derivatives, then solve for the increment $\boldsymbol{\delta}_{-p}$ and form $\boldsymbol{\delta}$ from $\boldsymbol{\delta}_{-p}$ with zero in the pth position. Note that $\bar{\boldsymbol{\theta}}_{-p}$ is used as the starting value for the next iteration.

A3.5.2 Profile Pair Plots

In producing the profile pair plots, we first generate a vector of τ values, $\boldsymbol{\tau}_p$, $p = 1, \ldots, P$, of length n_p for each parameter, and the corresponding $n_p \times P$ matrix $\mathbf{M}_p$ of parameter values. Each of these matrices is transformed to the τ scale in the following steps:

```
for p = 1, 2, . . . ,P {
   store s_θ→τ,p, the interpolating spline for the pth
      column of M_p as a function of τ_p.
   store s_τ→θ,p, the interpolating spline for τ_p
      as a function of the pth column of M_p
   for q = 1, 2, . . . ,P  and q ≠ p {
      g_pq = s_θ→τ,p(pth column of M_q)
```

```
        overwrite g_pq by arccos(g_pq/τ_p)
        store s_{t→g,pq} the interpolating spline for
          g_pq as a function of τ_p
    }
}
```

When determining the splines $s_{\theta\to\tau,p}$ and $s_{\tau\to\theta,p}$ we include a zero entry in $\boldsymbol{\tau}_p$ with a corresponding row $\hat{\boldsymbol{\theta}}$ in $\mathbf{M}_p$. This entry and the corresponding row must be eliminated before the division by $\boldsymbol{\tau}_p$.

To interpolate the projection of the contours $S(\boldsymbol{\theta})=S^i$, $i=1,\ldots,m$, into the (θ_p,θ_q) plane, we convert the levels to the τ scale as

$$k^i=\sqrt{S^i-S(\hat{\boldsymbol{\theta}})}/s$$

and determine the angles for the points on the traces as described in Appendix 6. These four angle pairs are

$$\mathbf{p}_1=(0,s_{t\to g,pq}(+k^i))$$

$$\mathbf{p}_2=(\pi,s_{t\to g,pq}(-k^i))$$

$$\mathbf{p}_3=(s_{t\to g,qp}(+k^i),0)$$

$$\mathbf{p}_4=(s_{t\to g,qp}(-k^i),\pi)$$

We convert these angles to an average angle and a phase difference by

```
for j=1,...,4{
    a_j=({p_j}_1 + {p_j}_2)/2
    d_j={p_j}_1 - {p_j}_2
    if (d_j<0) {
        replace d_j by -d_j
        replace a_j by -a_j
    }
}
```

and for d_j as a function of a_j, determine $sp_{a\to d,pqi}$, an interpolating spline with period 2π. A sequence of K points (usually K is between 50 and 100) on the interpolating contour is evaluated using

```
for k=1,...,K {
    a = (k-1)×2π/(K-1) - π
    d = sp_{a→d,pqi}(a)
    τ_p = cos(a + d/2)
    τ_q = cos(a - d/2)
    θ_p = s_{τ→θ,p}(τ_p)
    θ_q = s_{τ→θ,q}(τ_q)
}
```

and plotted.

APPENDIX 4.

Data Sets Used in Problems

A4.1 BOD Data Set 2

Data on biochemical oxygen demand (BOD) were obtained by Marske (1967) as described in Appendix 1, Section A1.3. A second set of data is reported in Table A4.1.

A model was derived based on exponential decay with a fixed rate constant as

$$f(x, \boldsymbol{\theta}) = \theta_1 (1 - e^{\theta_2 x})$$

where f is predicted biochemical oxygen demand and x is time.

Table A4.1 Biochemical oxygen demand versus time.

Time (days)	Biochemical Oxygen Demand (mg/l)	Time (days)	Biochemical Oxygen Demand (mg/l)
1	0.47	5	1.60
2	0.74	7	1.84
3	1.17	9	2.19
4	1.42	11	2.17

Copyright 1967 by D. Marske. Reproduced from "Biochemical Oxygen Demand Data Interpretation Using Sum of Squares Surface," M. Sc. Thesis, University of Wisconsin–Madison. Reprinted with permission of the author.

A4.2 Nitrendipene

Data on binding of [^{3}H] nitrendipine to sites in rat heart homogenate were obtained by Abdollah (1986). In this study, experiments were performed to investigate the competition for binding to the sites between nitrendipene (NTD), a calcium channel antagonist, and nifedipine (NIF), another calcium channel antagonist. Heart tissue was homogenated and incubated with radioactively tagged NTD at molar concentration $\approx 5\times10^{-10}$ in the presence of different concentrations of NIF, which are given in Table A4.2 as $x = \log_{10}$(NIF concentration), except for the rows with (0), for which the actual concentration was 0. The NIF has greater binding ability and so displaces the NTD. Counts on radioactive material were obtained to determine how much material was bound under different conditions. When the NIF concentration is 0, all of the radioactive NTD is bound to the sites, and so a large count is recorded: as the NIF concentration increases, it displaces NTD and so lower counts are recorded. Although the nominal NTD concentration was 5×10^{-10}, the actual concentrations were 4.76, 5.11, 4.78, and 5.02×10^{-10} respectively, for the four tissue samples.

The proposed model is

$$f(x, \boldsymbol{\theta}) = \theta_1 + \frac{\theta_2}{1+\exp[-\theta_4(x-\theta_3)]}$$

where f is the predicted total count and x is $\log_{10}$(NIF concentration).

A4.3 Saccharin Data Set 2

Data on the concentration of saccharin in plasma were reported in Renwick (1982) and are reproduced in Table A4.3.

A4.4 Steady State Adsorption

Data on the disappearance of o-xylene as a function of oxygen concentration, inlet o-xylene concentration, and temperature, were obtained by Juusola (1971) and were further analyzed by Pritchard (1972). The data are reproduced in Table A4.4.

The postulated model is a steady state adsorption model written

$$f(\mathbf{x}, \boldsymbol{\theta}) = \frac{f_1 f_2}{f_1 + 2.2788 f_2}$$

$$f_1 = \theta_1 x_1 e^{-\theta_3/x_3}$$

$$f_2 = \theta_2 x_2 e^{-\theta_4/x_3}$$

Table A4.2 Radioactivity versus molar concentration of nifedipene for four tissue samples.

	Counts[a]			
$x = \log_{10}(\text{NIF})$[b]	Tissue Sample 1	2	3	4
(0)	6 696	4 403	6 133	5 327
(0)	6 211	5 042	5 688	6 274
(0)	6 385	*	6 544	5 210
−11	6 396	5 259	6 783	6 811
−11	6 283	5 598	6 194	6 751
−11	6 071	*	6 188	7 289
−10	6 545	4 868	5 674	7 214
−10	6 378	4 769	5 583	5 652
−10	5 932	*	6 027	5 700
−9	5 509	3 931	5 458	6 184
−9	6 573	4 503	5 482	5 175
−9	5 932	*	5 878	5 802
−8	4 763	2 588	4 173	3 582
−8	5 389	3 089	3 837	7 021
−8	4 131	*	4 852	4 187
−7	4 583	2 084	4 359	3 838
−7	3 815	3 665	3 936	3 273
−7	3 539	*	4 468	4 562
−6	3 211	2 149	3 110	4 004
−6	4 263	2 216	3 860	3 520
−6	3 537	*	4 297	4 581
−5	*	1 433	3 471	3 719
−5	*	1 926	3 674	2 915
−5	*	*	3 990	4 504
(0)	*	*	5 938	6 396
(0)	*	*	5 948	6 071

[a] Total counts for 5×10^{-10} Molar NTD additive. (Missing values coded as *.)

[b] (0) means NIF concentration = 0.

Copyright 1986 by S. Abdollah. Reproduced from "The Effect of Doxorbicin on the Specific Binding of [^3H] Nitrendipenes to Rat Heart Microsomes," M. Sc. Thesis, Queen's University. Reprinted with permission of the author.

Table A4.3 Saccharin concentration in plasma versus time.

Time (min)	Saccharin Conc. (μg/ml)	Time (min)	Saccharin Conc. (μg/ml)
0	0	60	14.1
5	184.3	75	8.0
15	102.0	90	5.7
30	50.5	105	4.0
45	24.9	120	2.9

From "Pharmacokinetics in Toxicology" by A. G. Renwick, in *Principles and Methods of Toxicology*, A. Wallace Hayes, Ed., Raven Press, 1982. Reprinted with permission of the publisher.

Table A4.4 Rate of oxidation of o-xylene versus oxygen concentration (gm-mole/l), inlet o-xylene concentration (g-mole/l), and temperature (K). The reaction rate is recorded as (g-mole/g-mole catalyst second) at standard catalyst age.

Oxygen	o-Xylene	Temp.	Rate	Oxygen	o-Xylene	Temp.	Rate
0.00502	0.000200	543	116	0.00249	0.000198	563	224
0.00499	0.000190	543	120	0.00571	0.000049	563	198
0.00504	0.000200	543	114	0.00555	0.000347	563	463
0.00505	0.000200	543	117	0.00549	0.000274	563	370
0.01000	0.000351	543	245	0.00554	0.000095	563	258
0.01010	0.000351	543	230	0.00507	0.000191	573	543
0.01030	0.000050	543	106	0.00502	0.000187	573	561
0.01040	0.000361	543	230	0.00505	0.000192	573	560
0.01010	0.000049	543	121	0.00506	0.000188	573	578
0.01010	0.000050	543	115	0.00500	0.000201	573	542
0.01010	0.000050	543	127	0.00100	0.000350	573	197
0.00570	0.000201	563	408	0.00505	0.000202	573	559
0.00552	0.000201	563	380	0.00306	0.000349	573	414
0.00551	0.000202	563	320	0.00502	0.000198	573	467
0.00551	0.000186	563	399	0.00504	0.000201	573	468
0.00554	0.000202	563	371	0.01017	0.000245	573	933
0.00553	0.000199	563	368	0.00499	0.000187	573	509
0.00108	0.000051	563	63	0.01000	0.000253	573	955
0.00707	0.000099	563	333	0.00496	0.000346	573	650
0.00554	0.000197	563	322	0.01000	0.000253	573	902
0.00605	0.000351	563	413	0.00502	0.000199	573	532
0.00552	0.000202	563	344	0.00399	0.000357	573	552
0.01016	0.000189	563	543	0.00107	0.000196	573	184
0.00552	0.000200	563	372	0.00499	0.000353	573	663
0.00603	0.000049	563	229	0.00503	0.000100	573	409
0.01000	0.000201	563	563	0.00251	0.000199	573	326
0.01010	0.000151	563	490	0.00499	0.000277	573	580
0.00805	0.000354	563	595	0.00906	0.000205	573	831
0.00552	0.000199	563	352				

Copyright 1971 by J. A. Juusola. Reproduced from "A Kinetic Mechanism for the Vapor-Phase Oxidation of o-xylene," Ph.D. Thesis, Queen's University. Reprinted with permission of the author.

where f is predicted reaction rate, x_1 is oxygen concentration, x_2 is o-xylene inlet concentration, and x_3 is temperature.

A4.5 Leaves

Data on the growth of leaves were reported in Heyes and Brown (1956) and are reproduced in Table A4.5.

One model for such growth data is the Richards model written

$$f(x, \boldsymbol{\theta}) = \frac{\theta_1}{(1+\theta_2 e^{-\theta_3 x})^{1/\theta_4}}$$

where f is predicted leaf length and x is time.

A4.6 α-Pinene Data Set 2

Data on the thermal isomerization of α-pinene at 204.5°C were reported in Fuguitt and Hawkins (1947) as described in Appendix 1, Section A1.6. (See Table A4.6.)

The linear kinetic model given in Figure A1.1 is also proposed for these data.

Table A4.5 Leaf length versus time.

Time (days)	Leaf Length (cm)	Time (days)	Leaf Length (cm)
0.5	1.3	8.5	16.4
1.5	1.3	9.5	18.3
2.5	1.9	10.5	20.9
3.5	3.4	11.5	20.5
4.5	5.3	12.5	21.3
5.5	7.1	13.5	21.2
6.5	10.6	14.5	20.9
7.5	16.0		

Table A4.6 Relative concentrations of products versus time for thermal isomerization of α-pinene at 204.5°C.

Time (min)	α-Pinene (%)	Dipentene (%)	Alloocimene (%)	Pyronene (%)	Dimer (%)
440	85.9	8.2	4.1	0.4	0.6
825	74.3	15.6	6.8	0.8	1.6
1200	65.1	21.5	7.7	1.0	3.4
1500	58.6	25.5	8.4	1.2	5.0
2040	48.1	31.9	8.5	1.6	8.2
3060	32.1	42.0	8.2	2.0	13.5
6060	11.2	54.7	6.9	2.7	21.9
16020		61.3	5.0	3.0	27.8

Copyright 1947 by the American Chemical Society. Reprinted with permission from *Journal of the American Chemical Society*, **69**, 319–322.

A4.7 Coal Liquefaction

Data on coal liquefaction were analyzed in Lythgoe (1986). The reaction conditions and inlet (x) and outlet (y) data are presented in Tables A4.7a, b, and c. The model formulated by Lythgoe can be represented as

$$y_1 = x_1 + \theta_1 x_8 - \phi_1 t$$

$$y_2 = x_2 + \theta_2 x_8 + \alpha_2 \phi_1 t - \phi_2 t$$

$$y_3 = x_3 + \theta_3 x_8 + \beta_3 \phi_2 t$$

$$y_4 = x_4 + \theta_4 x_8 + \beta_4 \phi_2 t$$

$$y_5 = x_5 + \theta_5 x_8 + \beta_5 \phi_2 t$$

$$y_6 = x_6 + \theta_6 x_8 + \beta_6 \phi_2 t$$

$$y_7 = x_7 + \theta_7 x_8 + \alpha_7 \phi_1 t + \beta_7 \phi_2 t$$

where

$$\phi_1 = \gamma_1 P[1+(F/100)]e^{-\gamma_2/T}$$

$$\phi_2 = \gamma_3[1+(F/100)]\mathrm{TR}_{\mathrm{feed}}\, e^{-\gamma_4/T}$$

Table A4.7a Reaction conditions for autoclave runs.

Run No.	Time (min)	Temp (K)	Pressure (MPa)	Fe_2O_3 (wt% maf)[a]	TR_{feed} (wt% maf)[a]
52	25	713.7	16.028	2.608	66.341
53	25	713.7	16.304	2.609	66.340
54	25	713.7	16.166	2.611	66.341
55	25	713.7	16.166	2.607	66.339
56	25	713.7	13.960	2.597	66.358
57	25	713.7	13.822	2.607	66.373
58	25	705.4	13.684	2.611	66.395
59	40	705.4	13.546	2.612	66.380
60	25	705.4	13.063	2.640	85.878
61	25	705.4	13.063	2.639	77.927
64	25	705.4	13.684	2.609	83.915
65	25	705.4	16.235	2.511	56.633
77	25	705.4	13.684	2.593	66.358
78	70	697.0	13.270	2.589	66.359
79	90	688.7	13.270	2.599	66.346
80	70	697.0	13.339	2.599	66.351
81	25	697.0	13.339	2.597	66.358
82	55	697.0	12.926	2.599	66.351
86	55	697.0	15.270	1.688	48.740
91	55	697.0	18.717	0.000	46.306
92	55	697.0	17.338	1.723	46.440
94	55	697.0	14.442	1.650	24.786
95	55	697.0	17.338	2.611	66.332

[a] wt% maf is 100 × (mass of material/mass of moisture-ash-free coal).

Table A4.7b Inlet compositions for autoclave runs (weight %).

Run No.	Unconv. Coal x_1	Thermal Resid. x_2	C_4–822K Dist. x_3	C_1–C_3 Gases x_4	Byproduct Gases x_5	Water x_6	Hydrogen x_7	Coal In x_8
52	0.015	22.308	41.013	0.180	0.008	0.820	2.029	33.627
53	0.015	22.306	41.009	0.180	0.007	0.820	2.040	33.623
54	0.015	22.316	41.027	0.184	0.016	0.820	1.984	33.638
55	0.015	22.308	41.013	0.180	0.008	0.820	2.030	33.627
56	0.015	22.384	41.133	0.180	0.009	0.821	1.726	33.731
57	0.015	22.381	41.130	0.180	0.008	0.822	1.746	33.719
58	0.015	22.390	41.134	0.180	0.007	0.823	1.730	33.722
59	0.015	22.388	41.142	0.180	0.007	0.823	1.717	33.728
60	0.015	28.726	35.106	0.181	0.009	0.819	1.694	33.450
61	0.015	26.043	37.783	0.185	0.017	0.818	1.719	33.419
64	0.012	23.684	45.926	0.151	0.006	0.688	1.310	28.223
65	0.014	18.764	43.472	0.173	0.011	2.812	1.622	33.132
77	0.015	22.423	41.217	0.000	0.000	0.822	1.733	33.790
78	0.015	22.388	41.147	0.184	0.019	0.820	1.689	33.738
79	0.015	22.389	41.166	0.179	0.007	0.822	1.676	33.747
80	0.015	22.416	41.207	0.000	0.000	0.823	1.757	33.783
81	0.015	22.418	41.209	0.000	0.000	0.822	1.753	33.783
82	0.015	22.387	41.154	0.180	0.009	0.822	1.693	33.740
86	0.000	17.879	41.423	0.000	0.000	2.137	1.880	36.682
91	0.000	16.896	39.141	0.000	0.000	4.805	2.670	36.489
92	0.000	16.879	39.110	0.000	0.000	4.998	2.669	36.345
94	0.000	9.017	51.088	0.000	0.000	1.570	1.946	36.380
95	0.018	20.634	37.928	0.000	0.000	7.618	2.696	31.106

Table A4.7c Outlet compositions for autoclave runs (weight %).

Run No.	Unconv. Coal y_1	Thermal Resid. y_2	C_4–822K Dist. y_3	C_1–C_3 Gases y_4	Byproduct Gases y_5	Water y_6	Hydrogen y_7
52	1.702	35.197	53.884	1.729	1.985	4.010	1.491
53	1.777	34.870	54.317	1.715	1.830	4.020	1.470
54	1.390	36.224	52.909	1.902	2.063	4.027	1.485
55	1.674	36.295	52.692	1.842	2.006	4.017	1.474
56	2.392	35.439	52.698	2.046	2.146	3.986	1.294
57	1.909	34.650	53.758	1.972	2.067	4.401	1.242
58	2.694	36.093	53.323	1.442	1.935	3.234	1.279
59	1.843	33.549	55.452	1.816	2.041	4.151	1.148
60	2.998	42.572	46.972	1.404	1.620	3.199	1.235
61	2.793	40.889	48.832	1.461	1.744	3.051	1.229
64	2.103	34.867	56.440	1.182	1.619	2.759	1.030
65	2.455	36.858	48.818	1.567	3.015	5.909	1.380
77	2.276	38.326	50.961	1.424	1.797	3.870	1.346
78	1.500	36.885	52.210	2.225	2.099	3.990	1.091
79	1.699	35.716	53.325	1.854	2.289	4.032	1.084
80	1.679	36.764	52.093	2.017	2.183	4.085	1.178
81	3.138	38.821	50.516	0.927	1.710	3.532	1.356
82	1.615	36.610	52.378	1.744	2.137	4.403	1.113
86	2.177	39.042	46.474	1.904	3.339	5.737	1.327
91	4.423	35.829	44.133	1.989	3.558	7.811	2.258
92	1.672	35.249	47.062	1.882	3.356	8.813	1.967
94	2.347	29.585	55.937	1.832	3.231	5.660	1.410
95	1.226	31.952	50.266	1.856	2.203	10.507	1.989

Copyright 1987 by S. C. Lythgoe. Reproduced from "A Model for the Thermal Dissolver of the Wilsonville Direct Coal Liquefaction Process," M. Sc. Thesis, Queen's University. Reprinted with permission of the author.

subject to the conditions

$$\theta_1 + \cdots + \theta_7 = 1$$

$$\alpha_2 + \alpha_7 = 1$$

$$\beta_3 + \cdots + \beta_7 = 1$$

In the model, the reaction condition variables are time, t; temperature, T; pressure, P; Fe_2O_3 concentration in the inlet feed, F; and thermal residual in the inlet feed, TR_{feed}. The inlet and outlet compositions are unconverted coal, (x_1, y_1); thermal residual, (x_2, y_2); C_4–822K distillate, (x_3, y_3); C_1–C_3 gases, (x_4, y_4); byproduct gases, (x_5, y_5); water, (x_6, y_6); hydrogen, (x_7, y_7); and coal in, x_8. Note that hydrogen is consumed and so the parameters θ_7, α_7, and β_7 are negative.

A4.8 Haloperidol

Data on plasma concentrations of Haloperidol were reported in Wagner (1975, pp. 60–63) and are reproduced in Table A4.8.

Table A4.8 Haloperidol concentration versus time.

Time (hr)	Haloperidol Conc. (ng/ml)	Time (hr)	Haloperidol Conc. (ng/ml)
0.17	2.99	4.00	0.945
0.33	4.82	6.00	0.679
0.67	2.86	8.00	0.619
1.00	2.23	12.00	0.462
1.50	1.65	24.00	0.336
2.00	1.33	48.00	0.178
3.00	1.05	72.00	0.084

From "Use of Computers in Pharmacokinetics," by J.G. Wagner, in *Journal of Clinical Pharmacology and Therapeutics*, 1967, **8**, 201. Reprinted with permission of the publisher.

APPENDIX 5.

Evaluating Matrix Exponentials and Convolutions

In Sections 5.1 and 5.2 we showed how to obtain response functions for systems of linear differential equations and how to find derivatives of the response functions with respect to the parameters. In this appendix, we present efficient methods for evaluating the functions, given a parameter vector $\boldsymbol{\theta}$, and N cases at observation times $t_1, t_2, \ldots, t_N$.

Expressions for the model function and derivatives of a compartment model have been given in terms of the matrix $e^{\mathbf{A}t}$ and convolutions with this matrix. In practice, it is recommended (Moler and Van Loan, 1978) that the eigenvalues and eigenvectors of $\mathbf{A}$ be used when evaluating $e^{\mathbf{A}t}$ at a number of different t values. It may seem computationally intensive to determine the eigenvalues of $\mathbf{A}$ for each value of $\boldsymbol{\theta}$ at which $\boldsymbol{\gamma}$ is to be evaluated, but this is not so, because the dimension K of $\mathbf{A}$ is usually small and $\mathbf{A}$ is usually sparse. This sparsity can be exploited to isolate some eigenvalues without the need for iterative calculations, as in Example Tetracycline 2, where the eigenvalues are already isolated on the diagonal of $\mathbf{A}$. Routines such as BALANC from EISPACK (Smith et al., 1976) isolate such eigenvalues by means of row and column interchanges, when possible.

The methods for computing the matrix exponential and the convolutions depend on whether $\mathbf{A}$ can be diagonalized and whether all the eigenvalues are real. A matrix $\mathbf{A}$ can be diagonalized if there is an invertible matrix $\mathbf{U}$ such that

$$\mathbf{A} = \mathbf{U}\boldsymbol{\Lambda}\mathbf{U}^{-1}$$

with $\boldsymbol{\Lambda}$ diagonal. The elements on the diagonal of $\boldsymbol{\Lambda}$ are the eigenvalues and the columns of $\mathbf{U}$ are the (right) eigenvectors of $\mathbf{A}$. Diagonalization is not always possible; for instance, if we set $\theta_1 = \theta_2$ in Example Tetracycline 2, then there is no invertible matrix $\mathbf{U}$ which will diagonalize $\mathbf{A}$. Because of roundoff in calculations, however, an eigenvector routine will usually return a matrix $\mathbf{U}$, even for nondiagonalizable matrices, but $\mathbf{U}$ will be badly conditioned. The condition of the returned $\mathbf{U}$ can be checked using routines from LINPACK (Dongarra et al., 1979) to determine if $\mathbf{A}$ is diagonalizable. Alternatively, the modification suggested in Moler and Van Loan (1978) for the EISPACK routines ORTHES, ORTRAN,

and HQR2 (Smith et al., 1976) can be used to compute the QR decomposition of $\mathbf{U}$ directly and the condition of $\mathbf{R}$ evaluated using LINPACK routines.

In Section A5.1 we present methods for when $\mathbf{A}$ is diagonalizable, in Section A5.2 for when $\mathbf{A}$ is nondiagonalizable, and in Section A5.3 for when $\mathbf{A}$ has complex eigenvalues.

A5.1 Diagonalizable A

When $\mathbf{A}$ can be diagonalized by a well-conditioned matrix $\mathbf{U}$, calculations of the matrix exponential and matrix convolutions can be transformed into scalar calculations, because all power series expressions will have internal products $\mathbf{U}^{-1}\mathbf{U}$ which cancel and the powers of $\mathbf{\Lambda}$ will be diagonal with the appropriate power of the λ_i on the diagonal. Thus,

$$\mathbf{A}^k = (\mathbf{U}\mathbf{\Lambda}\mathbf{U}^{-1}) \cdots (\mathbf{U}\mathbf{\Lambda}\mathbf{U}^{-1})(\mathbf{U}\mathbf{\Lambda}\mathbf{U}^{-1}) = \mathbf{U}\mathbf{\Lambda}^k\mathbf{U}^{-1} \tag{A5.1}$$

and so (5.6) becomes

$$e^{\mathbf{A}t} = \mathbf{U}e^{\mathbf{\Lambda}t}\mathbf{U}^{-1}$$

where $e^{\mathbf{\Lambda}t}$ is diagonal with entries $e^{\lambda_i t}$ on the diagonal.

Because there will be factors $\mathbf{U}$ and $\mathbf{U}^{-1}$ in many of the expressions we need, it is convenient to take a linear transformation of coordinates for $\boldsymbol{\gamma}$ and write

$$\boldsymbol{\xi}(t) = \mathbf{U}^{-1}\boldsymbol{\gamma}(t)$$

$$\boldsymbol{\xi}_0 = \mathbf{U}^{-1}\boldsymbol{\gamma}_0$$

$$\boldsymbol{\kappa} = \mathbf{U}^{-1}\boldsymbol{\iota}$$

Similarly, for the derivatives we write

$$\boldsymbol{\xi}_{(p)}(t) = \mathbf{U}^{-1}\boldsymbol{\gamma}_{(p)}(t)$$

$$\boldsymbol{\kappa}_{(p)} = \mathbf{U}^{-1}\boldsymbol{\iota}_{(p)}$$

$$\mathbf{C}_{(p)} = \mathbf{U}^{-1}\mathbf{A}_{(p)}\mathbf{U}$$

(The notation $\boldsymbol{\xi}_{(p)}$ and $\boldsymbol{\kappa}_{(p)}$ is convenient, but not strictly correct, since, for example, $\boldsymbol{\xi}_{(p)}$ is not the partial derivative of $\mathbf{U}^{-1}\boldsymbol{\gamma}(t)$ with respect to θ_p.)

Substituting $\mathbf{A} = \mathbf{U}\mathbf{\Lambda}\mathbf{U}^{-1}$ into (5.11) and (5.13) and premultiplying both sides of the equations by $\mathbf{U}^{-1}$ gives

$$\boldsymbol{\xi}(t) = e^{\mathbf{\Lambda}t}\boldsymbol{\xi}_0 + (e^{\mathbf{\Lambda}t} * \mathbf{I})\boldsymbol{\kappa}$$

and

$$\boldsymbol{\xi}_{(p)}(t) = e^{\mathbf{\Lambda}t}\boldsymbol{\xi}_{(p)}(0) + (e^{\mathbf{\Lambda}t} * \mathbf{C}_{(p)}e^{\mathbf{\Lambda}t})\boldsymbol{\xi}_0 + (e^{\mathbf{\Lambda}t} * \mathbf{I})\boldsymbol{\kappa}_{(p)} + (e^{\mathbf{\Lambda}t} * \mathbf{C}_{(p)}e^{\mathbf{\Lambda}t} * \mathbf{I})\boldsymbol{\kappa}$$

where $e^{\mathbf{\Lambda}t}$ is evaluated as above. The matrix $e^{\mathbf{\Lambda}t} * \mathbf{I}$ is also a diagonal matrix

with diagonal elements

$$\{e^{\Lambda t} * \mathbf{I}\}_{ii} = e^{\lambda_i t} * 1$$
$$= \begin{cases} \dfrac{e^{\lambda_i t} - 1}{\lambda_i} & \lambda_i \neq 0 \\ t & \lambda_i = 0 \end{cases}$$

Since the matrices $e^{\Lambda t} * \mathbf{C}_{(p)} e^{\Lambda t}$ and $e^{\Lambda t} * \mathbf{C}_{(p)} e^{\Lambda t} * \mathbf{I}$ are not diagonal, we must evaluate each element. But these elements can be expressed in terms of scalar convolutions as

$$\{e^{\Lambda t} * \mathbf{C}_{(p)} e^{\Lambda t}\}_{ij} = \{\mathbf{C}_{(p)}\}_{ij}\, e^{\lambda_i t} * e^{\lambda_j t}$$

and

$$\{e^{\Lambda t} * \mathbf{C}_{(p)} e^{\Lambda t} * \mathbf{I}\}_{ij} = \{\mathbf{C}_{(p)}\}_{ij}\, e^{\lambda_i t} * e^{\lambda_j t} * 1$$

To evaluate the scalar convolutions we use the fact that $f * g = g * f$ to arrange that $\lambda_i \leq \lambda_j$. We also note from the form of $\mathbf{A}$ that $\lambda_i \leq 0$ and $\lambda_j \leq 0$. Then

$$e^{\lambda_i t} * e^{\lambda_j t} = e^{\lambda_j t}(e^{(\lambda_i t - \lambda_j t)} * 1) = \begin{cases} \dfrac{e^{\lambda_i t} - e^{\lambda_j t}}{\lambda_i - \lambda_j} & \lambda_i < \lambda_j \\ te^{\lambda_i t} & \lambda_i = \lambda_j \end{cases}$$

and

$$e^{\lambda_i t} * e^{\lambda_j t} * 1 = \begin{cases} 1 * 1 * 1 & \lambda_i = \lambda_j = 0 \\ e^{\lambda_i t} * 1 * 1 & \lambda_i < \lambda_j = 0 \\ e^{\lambda_i t}(e^{-\lambda_i t} * 1 * 1) & \lambda_i = \lambda_j < 0 \\ e^{\lambda_i t} * \dfrac{e^{\lambda_j t} - 1}{\lambda_j} & \lambda_i < \lambda_j < 0 \end{cases}$$
$$= \begin{cases} \dfrac{t^2}{2} & \lambda_i = \lambda_j = 0 \\ \dfrac{e^{\lambda_i t} - (1 + \lambda_i t)}{\lambda_i^2} & \lambda_i < \lambda_j = 0 \\ \dfrac{1 - e^{\lambda_i t}(1 - \lambda_i t)}{\lambda_i^2} & \lambda_i = \lambda_j < 0 \\ \dfrac{1}{\lambda_i \lambda_j}\left[1 + \dfrac{\lambda_j e^{\lambda_i t} - \lambda_i e^{\lambda_j t}}{\lambda_i - \lambda_j}\right] & \lambda_i < \lambda_j < 0 \end{cases}$$

In practice, the condition $\lambda_i = \lambda_j$ is determined by comparing $|(\lambda_i - \lambda_j)t_{\max}|$ with the relative machine precision, where $t_{\max}$ is the maximum value of t for which the system is to be evaluated. If this difference is less than the relative machine precision, then the form for equality is used.

A5.2 Nondiagonalizable A

When **A** cannot be diagonalized, a method given by Bavely and Stewart (1979) is used to reduce **A** to block-diagonal form as

$$\mathbf{A} = \mathbf{UBU}^{-1}$$

where **B** is formed from r triangular blocks $\mathbf{B}_i$ of size K_i, $i = 1, \ldots, r$, on the diagonal, and in each block the diagonal elements are almost equal. We express each $\mathbf{B}_i$ as

$$\mathbf{B}_i = d_i\mathbf{I} + \mathbf{E}_i$$

where d_i is the average of the diagonal elements of $\mathbf{B}_i$, **I** is the identity matrix of size K_i, and $\mathbf{E}_i$ is the remainder. Since $\mathbf{E}_i$ is triangular with small entries on the diagonal, the K_ith power of $\mathbf{E}_i$ will be approximately zero.

These blocks are gathered into $K \times K$ matrices **D** and **E** to give

$$\mathbf{B} = \mathbf{D} + \mathbf{E}$$

where **D** is blockwise a multiple of the identity matrix, and

$$\mathbf{E}^J \approx \mathbf{0}$$

where J is the maximum of the K_i, $i = 1, \ldots, r$. Since **D** is blockwise a multiple of the identity matrix, it commutes with **E**; then

$$\mathbf{DE} = \mathbf{ED}$$

and so

$$e^{\mathbf{B}t} = e^{(\mathbf{D}+\mathbf{E})t} = e^{\mathbf{D}t}e^{\mathbf{E}t} = e^{\mathbf{E}t}e^{\mathbf{D}t}$$

(It is not generally true for matrices that the exponential of a sum is the product of the exponentials.)

Since **D** is diagonal, $e^{\mathbf{D}t}$ is also diagonal with diagonal elements of the form $e^{d_i t}$ along the ith block. The other term is evaluated by

$$e^{\mathbf{E}t} = \mathbf{I} + \mathbf{E}t + \frac{\mathbf{E}^2 t^2}{2!} + \cdots + \frac{\mathbf{E}^J t^J}{J!}$$

and the convolutions can be evaluated for each term in the series. For example,

$$e^{\mathbf{B}t} * \mathbf{I} = e^{\mathbf{D}t}(\mathbf{I} + \mathbf{E}t + \frac{\mathbf{E}^2 t^2}{2!} + \cdots + \frac{\mathbf{E}^J t^J}{J!}) * \mathbf{I}$$
$$= e^{\mathbf{D}t} * \mathbf{I} + \mathbf{E}t\, e^{\mathbf{D}t} * \mathbf{I} + \cdots + \frac{\mathbf{E}^J t^J e^{\mathbf{D}t} * \mathbf{I}}{J!}$$

The basic scalar convolution

$$t^k e^{-at} * 1 = \frac{k![1 - e^{-at}(1 + at + \cdots + a^k t^k / k!)]}{a^k}$$

is used to evaluate this matrix convolution with similar expressions for the other matrix convolutions such as

$$e^{\mathbf{B}t} * \mathbf{C}_{(p)} e^{\mathbf{B}t} * \mathbf{I}$$

A5.3 Complex Eigenvalues

In most simple compartment models, the eigenvalues will be real and the methods of the previous sections can be used. In fact, all the eigenvalues must be real whenever the greatest length of a cycle in the model is less than 3, where a cycle is a chain of distinct compartments in which there is transfer of material from the first to the second and so on until the last one, which transfers back to the first. The mammillary and catenary models described in Section 5.4 only have cycles of length 2.

A cycle of length 3 can be easily generated, for example, as in Figure A5.1, and this system could have complex eigenvalues. Complex eigenvalues and their corresponding eigenvectors always occur in conjugate pairs, so the values of the model function and its derivatives are real and can be calculated without having to resort to complex arithmetic. The basic method with real arithmetic is first to reduce **A** to a quasitriangular matrix and then to a quasidiagonal matrix. The quasitriangular matrix is triangular except for disjoint blocks of order 2 on the diagonal, where each block corresponds to a pair of complex conjugate eigenvalues. This reduction is accomplished using the *QR* method with implicit shifts as implemented in the subroutine HQR2 from EISPACK (Smith et al.,

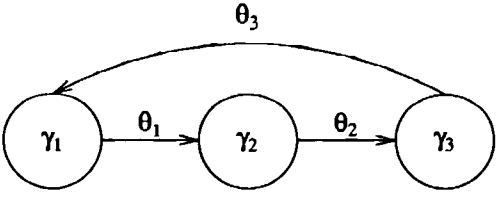

Figure A5.1 Cycle of length 3.

1976) or HQR3 (Stewart, 1976) and results in an orthogonal matrix **Q** such that

$$\mathbf{C} = \mathbf{Q}^{\mathrm{T}}\mathbf{A}\mathbf{Q}$$

is quasitriangular. Any 2×2 block on the diagonal of **C** is of the form

$$\begin{bmatrix} a & b \\ c & d \end{bmatrix}$$

with $(a-d)^2 + 4bc < 0$.

When the quasitriangular matrix **C** is produced, an attempt can be made to produce a quasidiagonal form using the method in Bavely and Stewart (1979) based on the subroutine SHRSLV (Bartels and Stewart, 1972). That is, a matrix **R** is calculated such that

$$\mathbf{D} = \mathbf{R}^{-1}\mathbf{C}\mathbf{R}$$

is diagonal except for 2×2 blocks on the diagonal corresponding to each complex conjugate pair. The matrix **R** is upper triangular with ones on the diagonal, and the blocks on the diagonal of **D** are the same as the corresponding blocks of **C**. If all the eigenvalues are real, the matrices **Q** and **R** produced in this manner are the *QR* decomposition of a matrix of eigenvectors of **A**.

If the matrix **A** has complex eigenvalues and is also nondiagonalizable, the matrix **R** cannot be calculated (or, in practice, will be very badly conditioned). In this case, the methods of this section must be combined with those of Section A5.2. Fortunately, nondiagonalizable matrices with complex eigenvalues occur very rarely, and so we do not give the explicit forms, as they are very complicated.

Assuming that a well-conditioned **R** can be calculated so

$$\mathbf{A} = \mathbf{Q}\mathbf{R}\mathbf{D}\mathbf{R}^{-1}\mathbf{Q}^{\mathrm{T}}$$

we form

$$\begin{aligned}
\boldsymbol{\xi}(t) &= \mathbf{R}^{-1}\mathbf{Q}^{\mathrm{T}}\boldsymbol{\gamma}(t) \\
\boldsymbol{\xi}_0 &= \mathbf{R}^{-1}\mathbf{Q}^{\mathrm{T}}\boldsymbol{\gamma}_0 \\
\boldsymbol{\kappa} &= \mathbf{R}^{-1}\mathbf{Q}^{\mathrm{T}}\boldsymbol{\iota} \\
\boldsymbol{\xi}_{(p)}(t) &= \mathbf{R}^{-1}\mathbf{Q}^{\mathrm{T}}\boldsymbol{\gamma}_{(p)}(t) \\
\boldsymbol{\kappa}_{(p)} &= \mathbf{R}^{-1}\mathbf{Q}^{\mathrm{T}}\boldsymbol{\iota}_{(p)}
\end{aligned}$$

and

$$\mathbf{C}_{(p)} = \mathbf{R}^{-1}\mathbf{Q}^{\mathrm{T}}\mathbf{A}_{(p)}\mathbf{Q}\mathbf{R}$$

as in Section A5.1. Evaluation of the model function and derivatives is then reduced to evaluating $e^{\mathbf{D}t}$ and convolutions such as $e^{\mathbf{D}t} * \mathbf{I}$ and $e^{\mathbf{D}t} * \mathbf{C}_{(p)}e^{\mathbf{D}t}$.

Both $e^{\mathbf{D}t}$ and $(e^{\mathbf{D}t} * \mathbf{I})$ are quasidiagonal with 2×2 blocks in the same positions as **D**, so we only need to consider what the results for each 2×2 block are, as 1×1 diagonal blocks were considered in Section A5.2. Each 2×2 block

will have the form

$$\mathbf{D}_i = \begin{bmatrix} a & b \\ c & d \end{bmatrix}$$

with $(a-d)^2 + 4bc < 0$. We calculate the quantities

$$\zeta = \frac{a+d}{2}$$

$$\delta = \frac{a-d}{2}$$

$$\rho = \sqrt{-\delta^2 - bc}$$

and the matrix

$$\mathbf{F}_i = \begin{bmatrix} \frac{\delta}{\rho} & \frac{b}{\rho} \\ \frac{c}{\rho} & \frac{-\delta}{\rho} \end{bmatrix}$$

to give

$$e^{\mathbf{D}_i t} = e^{\zeta t}[(\cos \rho t)\mathbf{I} + (\sin \rho t)\mathbf{F}_i]$$

and

$$e^{\mathbf{D}_i t} * \mathbf{I} = \mu\{[\cos \phi - e^{\zeta t}\cos(\rho t + \phi)]\mathbf{I} + [\sin \phi - e^{\zeta t}\sin(\rho t + \phi)]\mathbf{F}_i\}$$

where

$$\mu = (\zeta^2 + \rho^2)^{-1/2}$$

and

$$\phi = \tan^{-1}(-\rho/\zeta)$$

The phase angle ϕ is always in the first quadrant because ζ will be negative for a compartment model. That is, $0 < \phi \leq \pi/2$.

APPENDIX 6.

Interpolating Profile Pair Contours

To interpolate the (p,q) projection of a likelihood contour from points on the profile traces, we first transform from θ_p,θ_q to τ_p,τ_q coordinates using cubic splines. This transforms the likelihood surface so that, in the $\boldsymbol{\tau}$ coordinates, the surface is nearly a paraboloid with elliptical contours, and it is easy to interpolate points on these near-ellipses.

Example: Puromycin 28

The profile traces for the Puromycin parameters, shown in Figure 6.7, are plotted in the $\boldsymbol{\tau}$ coordinates in Figure A6.1, from which it can be seen that

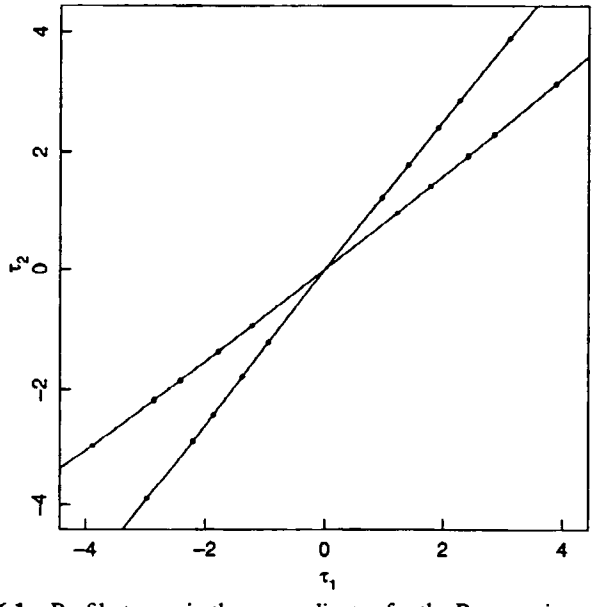

Figure A6.1 Profile traces in the $\boldsymbol{\tau}$ coordinates for the Puromycin parameters.

the profile traces are very nearly straight lines through the origin. Because the traces are straight, the contours will be nearly elliptical, and so the the likelihood surface is quite parabolic in these coordinates. The contours in the $\boldsymbol{\theta}$ coordinates will also be quite elliptical, because the profile t plots (Figure 6.4) are quite straight. This implies that the likelihood surface in the $\boldsymbol{\theta}$ coordinates is also quite parabolic. ■

Example: BOD 17

The profile traces for the BOD parameters, shown in Figure 6.8, are plotted in the $\boldsymbol{\tau}$ coordinates in Figure A6.2. The profile traces for the BOD parameters are curved and tend to a common asymptote in the lower right quadrant. For this example, the likelihood surface is not close to being an elliptical paraboloid, even in the $\boldsymbol{\tau}$ coordinates, and therefore we should not expect to produce very accurate contour interpolations. ■

To interpolate a particular contour, we scale the $\boldsymbol{\tau}$ coordinates by dividing by $\sqrt{P\,F(P, N-P; \alpha)}$ so that a nominal $1-\alpha$ joint likelihood contour in the scaled $\boldsymbol{\tau}$ coordinates is bounded by the square $-1 \le \tau_p,\ \tau_q \le 1$.

If the contour were a ellipse, it could be represented in the scaled coordinates in the parametric form

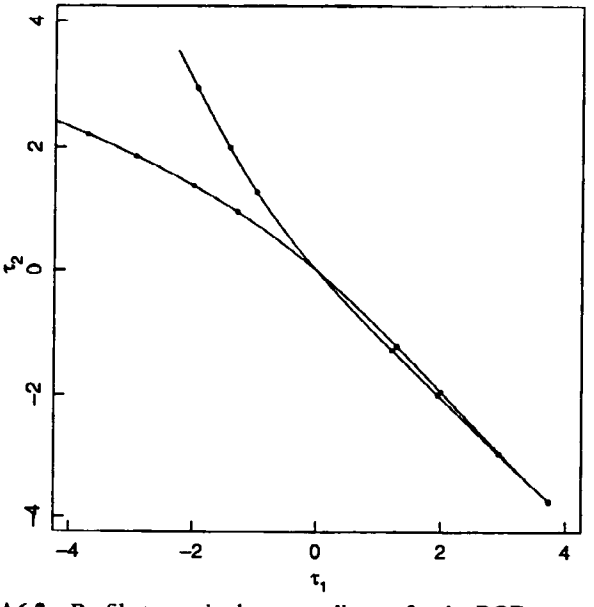

Figure A6.2 Profile traces in the $\boldsymbol{\tau}$ coordinates for the BOD parameters.

$$\tau_p = \cos(a + d/2)$$
$$\tau_q = \cos(a - d/2) \tag{A6.1}$$

where the angle a goes from $-\pi$ to π and the phase d is a constant. When the contour is not elliptical, the phase angle will vary. Therefore, to interpolate a contour given a set of points $(\tau_{p,r}, \tau_{q,r})$, $r = 1, \ldots, 4$, we could calculate the arccosines $s_{p,r} = \arccos \tau_{p,r}$ and $s_{q,r} = \arccos \tau_{q,r}$, form the averages and differences, and interpolate the differences as a function of the average. Finally we could transform back to τ_p and τ_q using (A6.1).

Example: Puromycin 29

The scaled τ coordinates for the points on the nominal 95% contour for the Puromycin parameters, derived from the profile traces, are given in Table A6.1 together with the arccosines and the averages and differences of the arccosines. Since this contour is nearly elliptical, the phase d should be almost constant and the angle a should extend over the range $-\pi$ to π. However, from the table we see that the differences of the arccosines vary in sign and the averages of the arccosines all lie between 0 and π. ■

Even for an ellipse, the differences of the arccosines will vary in sign and the averages of the arccosines will lie between 0 and π because the arccosine transformation only yields values in the range 0 to π. To obtain suitable values for a and d we note that, since $\cos(-x) = \cos x$, (A6.1) will yield the same τ_p and τ_q if the sign of the average *and* the sign of the difference is reversed. We therefore reverse the sign of any negative difference and its corresponding average to give a and d values suitable for interpolation with a periodic spline.

Example: Puromycin 30

The angle a and phase d for the points on the 95% contour for the Puromycin parameters are given in Table A6.1 and plotted in Figure A6.3*a*. Also shown is the interpolated phase, which is relatively constant, varying from

Table A6.1 Calculating the angle and phase for the Puromycin 95% contour.

Scaled		Arccosine				Angle	Phase
τ_1	τ_2	1	2	Avg.	Diff.	a	d
1.000	0.801	0.000	0.641	0.321	−0.641	−0.321	0.641
0.795	1.000	0.651	0.000	0.326	0.651	0.326	0.651
−1.000	−0.762	3.142	2.437	2.789	0.704	2.789	0.704
−0.769	−1.000	2.448	3.142	2.795	−0.693	−2.795	0.693

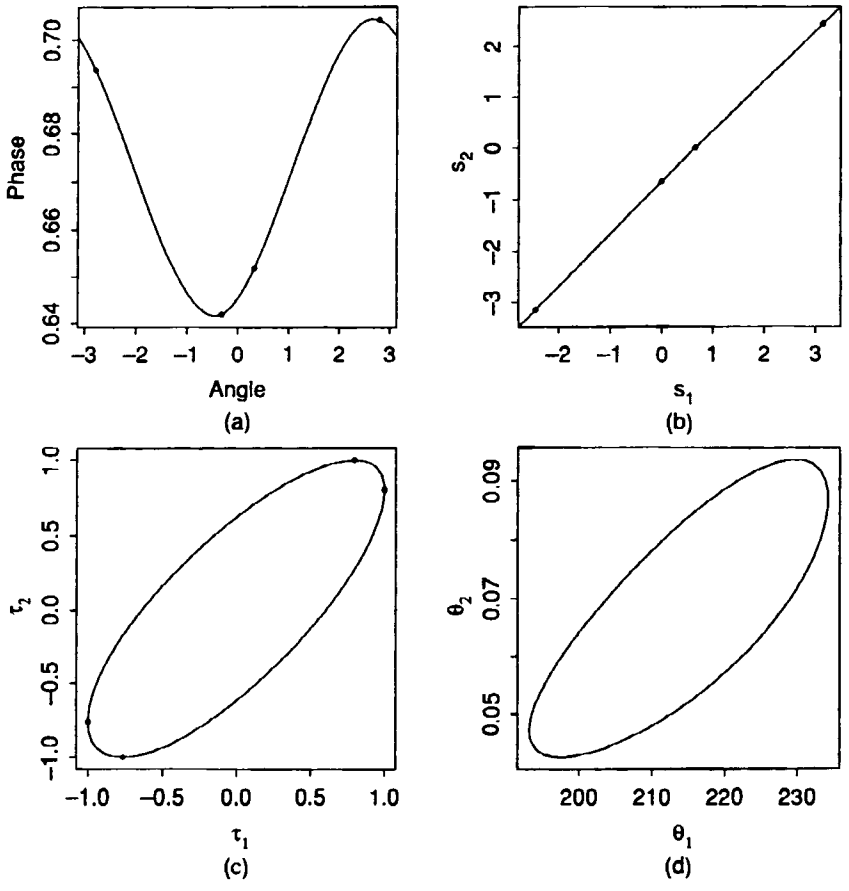

Figure A6.3 Interpolation of the 95% likelihood contour for the Puromycin parameters. The phases (•) corresponding to the points on the profile traces are shown in part *a* together with the interpolated curve, and the corresponding points (•) and interpolated values $a+d/2$ and $a-d/2$ are shown in part *b*. The points on the traces (•) and the interpolated contour are shown in the $\boldsymbol{\tau}$ coordinates in part *c*, and in the $\boldsymbol{\theta}$ coordinates in part *d*.

$0.64 < d < 0.71$. This implies that a plot of $a-d/2$ versus $a+d/2$ will be very close to a straight line, as demonstrated in Figure A6.3*b*. The relatively constant phase also implies that the contour is nearly elliptical in the (τ_1, τ_2) coordinates, as shown in Figure A6.3*c*. Finally, because the profile *t* plots for the Puromycin parameters are quite straight, the near ellipse in the $\boldsymbol{\tau}$ coordinates maps to a nearly elliptical contour in the $\boldsymbol{\theta}$ coordinates, as shown in Figure A6.3*d*. ■

Example: BOD 18

In Figure A6.4*a* we plot the phase d versus the angle a for the 90% contour for the BOD parameters, together with the interpolated curve. For this example, the phase is more variable so that a plot of $a-d/2$ versus $a+d/2$ will not be very straight, as is demonstrated in Figure A6.4*b*. This also implies that the contour will not be an ellipse in the (τ_1,τ_2) coordinates, which is demonstrated in Figure A6.4*c*. Finally, because the profile t plots for the BOD parameters are badly curved, the elongated ellipse in the τ coordinates maps to a tapered curved contour in the θ coordinates, as shown in

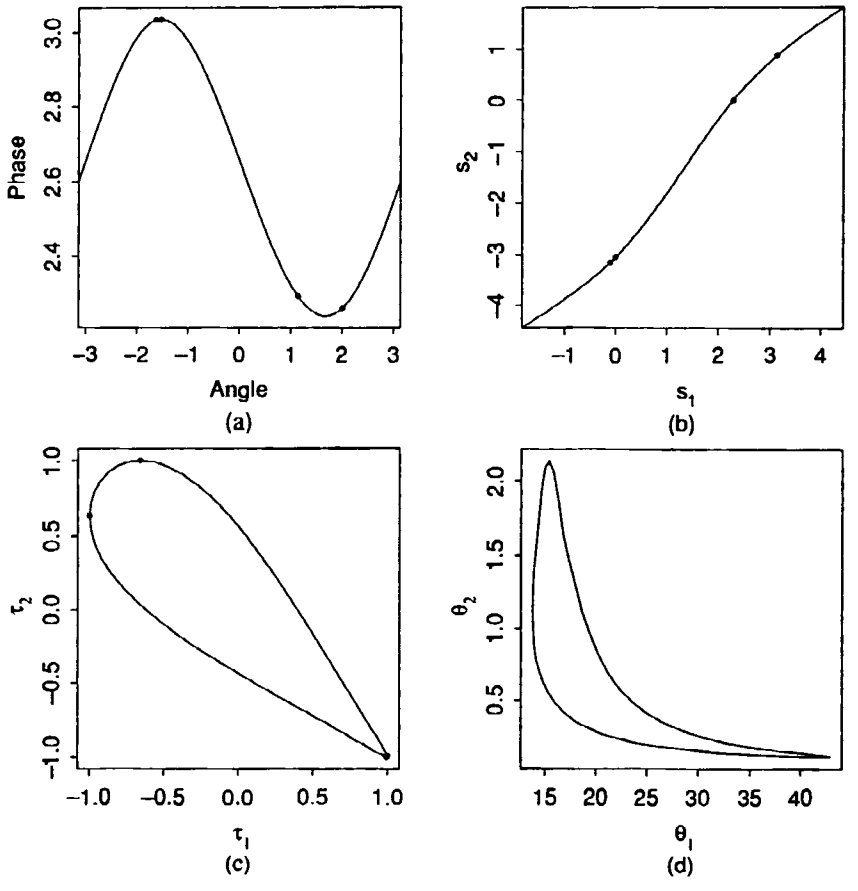

Figure A6.4 Interpolation of the 90% likelihood contour for the BOD parameters. The phases (•) corresponding to the points on the profile traces are shown in part *a* together with the interpolated curve, and the corresponding points (•) and interpolated values $a+d/2$ and $a-d/2$ are shown in part *b*. The points on the traces (•) and the interpolated contour are shown in the τ coordinates in part *c*, and in the θ coordinates in part *d*.

Figure A6.4*d*. This relatively poor performance was predicted from inspection of the profile trace plots; nevertheless, we find it rather remarkable that interpolated contours based on only four points can be so accurate. ■

In the above example it is clear from the profile t and profile trace plots that the true contours are badly behaved, and so interpolations based on only four intersection points of a contour with the traces will not be accurate. To generate more accurate contour plots, additional points on the contour must be calculated and used in the interpolation process. A procedure for adding points to generate accurate contour sketches based on traces is being developed.

APPENDIX 7.

Key to Data Sets

The model functions for the data sets in Section 7.3.2 are:

Model A: Michaelis–Menten model,

$$f(x,\boldsymbol{\theta}) = \frac{\theta_1 x}{\theta_2 + x}$$

Model B:

$$f(x,\boldsymbol{\theta}) = \theta_1\,[1 - \exp(-\theta_2 x)]$$

Model C:

$$f(x,\boldsymbol{\theta}) = \theta_1 + (0.49 - \theta_1)\exp[-\theta_2(x-8)]$$

Model D:

$$f(\mathbf{x},\boldsymbol{\theta}) = \exp\left\{-\theta_1 x_1 \exp\left[-\theta_2\left(\frac{1}{x_2} - \frac{1}{620}\right)\right]\right\}$$

Model E:

$$f(x,\boldsymbol{\theta}) = \theta_1 x^{\theta_2}$$

Model F: Asymptotic regression model,

$$f(x,\boldsymbol{\theta}) = \theta_1 + \theta_2 \exp(\theta_3 x)$$

Model G: Logistic model,

$$f(x,\boldsymbol{\theta}) = \frac{\theta_1}{1 + \theta_2 \exp(\theta_3 x)}$$

Model H: Gompertz growth model,

$$f(x,\boldsymbol{\theta}) = \theta_1 \exp[-\exp(\theta_2 - \theta_3 x)]$$

Model I:

$$f(x,\boldsymbol{\theta}) = \theta_1\,[1-\theta_2\exp(-\theta_3\,x)]$$

Model J: Log logistic growth model,

$$f(x,\boldsymbol{\theta}) = \theta_1 - \ln[1+\theta_2\exp(-\theta_3\,x)]$$

Model K:

$$f(x,\boldsymbol{\theta}) = \theta_1 + \theta_2/x^{\theta_3}$$

Model L:

$$f(x,\boldsymbol{\theta}) = \ln[\theta_1\exp(-\theta_2\,x)+(1-\theta_1)\exp(-\theta_3\,x)]$$

Model M:

$$f(\mathbf{x},\boldsymbol{\theta}) = \frac{\theta_1\,\theta_3\,(x_2 - x_3/1.632)}{1+\theta_2\,x_1+\theta_3\,x_2+\theta_4\,x_3}$$

Model N: Steady state adsorption model,

$$f(\mathbf{x},\boldsymbol{\theta}) = \frac{\theta_1\,x_1\exp(-\theta_3\,x_{\text{inv}})\,\theta_2\,x_2\exp(-\theta_4\,x_{\text{inv}})}{\theta_1\,x_1\exp(-\theta_3\,x_{\text{inv}})+2.28\,\theta_2\,x_2\exp(-\theta_4\,x_{\text{inv}})}$$

where

$$x_{\text{inv}} = \frac{1}{x_3+273} - \frac{1}{558}$$

Model O: Morgan–Mercer–Florin growth model,

$$f(x,\boldsymbol{\theta}) = \frac{\theta_2\,\theta_3+\theta_1\,x^{\theta_4}}{\theta_3+x^{\theta_4}}$$

Model P: Richards growth model,

$$f(x,\boldsymbol{\theta}) = \frac{\theta_1}{[1+\theta_2\exp(-\theta_3\,x)]^{1/\theta_4}}$$

Model Q:

$$f(x,\boldsymbol{\theta}) = \theta_1+\theta_2\exp(-\theta_4\,x)+\theta_3\exp(-\theta_5\,x)$$

Model R:

$$f(x,\boldsymbol{\theta}) = \frac{x\exp\left[\dfrac{\theta_1-\theta_2/x}{R}\right]}{1+\exp\left[\dfrac{\theta_3-\theta_4/x}{R}\right]+\exp\left[\dfrac{\theta_5-\theta_6/x}{R}\right]}$$

where

$$R = 1.98$$

Model S:

$$f(\mathbf{x},\boldsymbol{\theta}) = \frac{\theta_1}{\theta_2 + x_1} + \theta_3 x_2 + \theta_4 x_2^2 + \theta_5 x_2^3 + (\theta_6 + \theta_7 x_2^2)\, x_2 \exp\left[\frac{-x_1}{\theta_8 + \theta_9 x_2^2}\right]$$

References for the data sets are given in Table A7.1. Some of these data sets were used in the examples and exercises. The correspondence between the data set number and the section of Appendix 1 or Appendix 4 is given in Table A7.2.

Table A7.1 References for data sets in Section 7.3.2.

Data Set	Reference
1	Michaelis and Menten (1913)
2	Treloar (1974)
3	Treloar (1974)
4	Draper and Smith (1981), p. 522, problem L, set 1
5	Draper and Smith (1981), p. 522, problem L, set 2
6	Draper and Smith (1981), p. 522, problem L, set 3
7	Draper and Smith (1981), p. 522, problem L, set 4
8	Draper and Smith (1981), p. 522, problem L, set 5
9	Draper and Smith (1981), p. 522, problem L, set 6
10	Draper and Smith (1981), p. 522, problem L, set 7
11	Draper and Smith (1981), p. 522, problem L, set 8
12	Draper and Smith (1981), p. 522, problem L, set 9
13	Draper and Smith (1981), p. 476
14	Draper and Smith (1981), p. 519, problem H
15	Draper and Smith (1981), p. 519, problem M
16	Ratkowsky (1983), p. 88, set 1
17	Ratkowsky (1983), p. 88, set 2
18	Gregory (1956)
19	Heyes and Brown (1956)
20	Ratkowsky (1983), Appendix 5.A, set 1
21	Ratkowsky (1983), Appendix 5.A, set 2
22	Ratkowsky (1979), barley yields
23	Pimentel-Gomes (1953)
24	Draper and Smith (1981), p. 524, problem N, set 1
25	Draper and Smith (1981), p. 524, problem N, set 2
26	Draper and Smith (1981), p. 524, problem N, set 3
27	Draper and Smith (1981), p. 524, problem N, set 4
28	Draper and Smith (1981), p. 524, problem N, set 5
29	Draper and Smith (1981), p. 524, problem P, tensile strength
30	Draper and Smith (1981), p. 524, problem P, yield strength
31	Dierburg and Ewel (1982)
32	Carr (1960)
33	Pritchard (1972), model 1
34	Pritchard (1972), model 2
35	Osborne (1971)
36	Miller (1983)
37	Linssen (1975)

Table A7.2 Correspondence of data set numbers to sections of Appendix 1 or Appendix 4.

Data Set	Section.
2	A1.3, Table A1.3*b*
3	A1.3, Table A1.3*a*
5	A4.1
11	A1.4
19	A4.5
32	A1.5
33	A4.4
37	A1.8

References

Abdollah, Shirin (1986), *The Effect of Doxorubicin on the Specific Binding of [^{3}H] Nitrendipine to Rat Heart Microsomes.* Master's Thesis, Queen's University at Kingston.

Anderson, David H. (1983), *Compartmental Modeling and Tracer Kinetics.* Springer Verlag.

Ansley, Craig F. (1985), "Quick proofs of some regression theorems via the *QR* algorithm." *American Statistician*, **39**(1), 55–59.

Armstrong, P. W., D. G. Watts, D. C. Hamilton, M. A. Chiong, and J. O. Parker (1979), "Quantification of myocardial infarction: Template model for serial creatine kinase analysis." *Circulation*, **60**(4), 856–865.

Bache, C. A., J. W. Serum, W. D. Youngs, and D. J. Lisk (1972), "Polychlorinated biphenyl residues: Accumulation in Cayuga Lake trout with age." *Science*, **117**, 1192–1193.

Bacon, D. W., and D. G. Watts (1971), "Estimating the transition between two intersecting straight lines." *Biometrika*, **58**, 525–534.

Bard, Y. (1974), *Nonlinear Parameter Estimation.* New York: Academic Press.

Bartels, R. H., and G. W. Stewart (1972), "Algorithm 432, the solution of the matrix equation $AX - XB = C$." *Communications of the Association for Computing Machinery*, **15**(9), 820–826.

Bates, Douglas M. (1978), *Curvature Measures of Nonlinearity.* Ph.D. Thesis, Queen's University at Kingston.

Bates, D. M., D. C. Hamilton, and D. G. Watts (1983), "Calculation of intrinsic and parameter-effects curvatures for nonlinear regression models." *Communications in Statistics—Simulation and Computation*, **12**, 469–477.

Bates, Douglas M., and Mary J. Lindstrom (1986), "Nonlinear least squares with conditionally linear parameters," in *Proceedings of the Statistical Computing Section.* New York: American Statistical Association.

Bates, D. M., and D. G. Watts (1980), "Relative curvature measures of nonlinearity (with discussion)." *Journal of the Royal Statistical Society, Ser. B*, **42**(1), 1–25.

Bates, D. M., and D. G. Watts (1981a), "Parameter transformations for improved approximate confidence regions in nonlinear least squares." *Annals of Statistics*, **9**(6), 1152–1167.

Bates, D. M., and D. G. Watts (1981b), "A relative offset orthogonality convergence criterion for nonlinear least squares." *Technometrics*, **23**(2), 179–183.

Bates, D. M., and D. G. Watts (1984), "A multi-response Gauss–Newton algorithm." *Communications in Statistics—Simulation and Computation*, **13**(5), 705–715.

Bates, Douglas M., and Donald G. Watts (1985), "Multiresponse estimation with special application to systems of linear differential equations (with discussion)." *Technometrics*, **27**(4), 329–360.

Bates, Douglas M., and Donald G. Watts (1987), "A generalized Gauss–Newton procedure for multi-response parameter estimation." *SIAM Journal of Scientific and Statistical Computing*, 7(1), 49–55.

Bates, Douglas M., Dennis A. Wolf, and Donald G. Watts (1985), "Nonlinear least squares and first-order kinetics," in David Allen, Ed., *Proceedings of Computer Science and Statistics: Seventeenth Symposium on the Interface*. New York: North-Holland.

Bavely, Connice A., and G. W. Stewart (1979), "An algorithm for computing reducing subspaces by block diagonalization." *SIAM Journal of Numerical Analysis*, **16**(2), 359–367.

Beale, E. M. L. (1960), "Confidence regions in nonlinear estimation (with discussion)." *Journal of the Royal Statistical Society, Ser. B*, **22**, 41–88.

Becker, Richard A., John M. Chambers, and Allan R. Wilks (1988), *The New S Language: A Programming Environment For Data Analysis and Graphics*. Belmont, Calif.: Wadsworth.

Belsley, D. A., E. Kuh, and R. E. Welsch (1980), *Regression Diagnostics—Identifying Influential Data and Sources of Variation*. New York: Wiley.

Bliss, C. I., and A. T. James (1966), "Fitting the rectangular hyperbola." *Biometrics*, **22**, 573–602.

Box, G. E. P. (1960), "Fitting empirical data." *Annals of the New York Academy of Sciences*, **86**, 792–816.

Box, G. E. P., and G. A. Coutie (1956), "Applications of digital computers in the exploration of functional relationships." *Proceedings of the IEEE*, **103B** (Supplement no. 1), 100–107.

Box, George E. P., and David R. Cox (1964), "An analysis of transformations." *Journal of the Royal Statistical Society, Ser. B*, **26**, 211–252.

Box, G. E. P., and N. R. Draper (1959), "A basis for the selection of a response surface design." *Journal of the American Statistical Association*, **54**, 622–653.

Box, G. E. P., and N. R. Draper (1965), "The Bayesian estimation of common parameters from several responses." *Biometrika*, **52**, 355–365.

Box, George E. P., and Norman R. Draper (1987), *Empirical Model-Building and Response Surfaces*. New York: Wiley.

Box, G. E. P., and W. J. Hill (1974), "Correcting inhomogeneity of variance with power transformation weighting." *Technometrics*, **16**, 385–389.

Box, G. E. P., and W. G. Hunter (1965), "Sequential design of experiments for nonlinear models" in *IBM Scientific Computer Symposium in Statistics*, pp. 113–137.

Box, G. E. P., W. G. Hunter, and J. S. Hunter (1978), *Statistics for Experimenters*. New York: Wiley.

Box, G. E. P., W. G. Hunter, J. F. MacGregor, and J. Erjavec (1973), "Some problems associated with the analysis of multiresponse models." *Technometrics*, **15**(1), 33–51.

Box, George E. P., and Gwilym M. Jenkins (1976), *Time Series Analysis: Forecasting and Control* (revised edition). San Francisco: Holden-Day.

Box, George E. P., and Hiromitsu Kanemasu (1984), "Constrained nonlinear least squares," in Klaus Hinkelmann, Ed., *Contributions to Experimental Design, Linear Models, and Genetic Statistics: Essays in Honor of Oscar Kempthorne*. New York: Marcel Dekker.

Box, G. E. P., and H. L. Lucas (1959), "Design of experiments in non-linear situations." *Biometrika*, **46**, 77–90.

Box, G. E. P., and G. C. Tiao (1973), *Bayesian Inference in Statistical Analysis*. Reading, Mass.: Addison-Wesley.

Box, George E. P., and Paul W. Tidwell (1962), "Transformations of the independent

variables." *Technometrics*, **4**, 531–550.

Box, M. J. (1968), "The occurence of replications in optimal designs of experiments to estimate parameters in nonlinear models." *Journal of the Royal Statistical Society, Ser. B*, **30**, 290–302.

Box, M. J. (1971), "An experimental design criterion for precise parameter estimation of a subset of the parameters in a nonlinear model." *Biometrika*, **58**, 149–153.

Box, M. J., N. R. Draper, and W. G. Hunter (1970), "Missing values in multi-response nonlinear data fitting." *Technometrics*, **12**, 613–620.

Caracotsios, M., and W. E. Stewart (1985), "Sensitivity analysis of initial value problems with mixed ODE's and algebraic equations." *Computers and Chemical Engineering*, **9**(4), 359–365.

Carr, N. L. (1960), "Kinetics of catalytic isomerization of *n*-pentane." *Industrial and Engineering Chemistry*, **52**, 391–396.

Carroll, Raymond J., and David Ruppert (1984), "Power transformation when fitting theoretical models to data." *Journal of the American Statistical Association*, **79**(386), 321–328.

Chambers, J. M. (1977), *Computational Methods for Data Analysis*. New York: Wiley.

Chambers, John M., William S. Cleveland, Beat Kleiner, and Paul A. Tukey (1983), *Graphical Methods for Data Analysis*. Belmont, Calif.: Wadsworth.

Cleveland, William S. (1984), "Graphs in scientific publications." *American Statistician*, **38**(4), 261–269.

Cleveland, William S. (1985), *Elements of Graphing Data*. Belmont, Calif.: Wadsworth.

Cochran, W. G. (1973), "Experiments for nonlinear functions." *Journal of the American Statistical Association*, **68**, 771–778.

Cochran, W. G., and G. M. Cox (1957), *Experimental Designs*. New York: Wiley.

Cole, K. S., and R. H. Cole (1941), "Dispersion and absorption in dielectrics I: Alternating current characteristics." *Journal of Physical Chemistry*, **9**, 341–351.

Conte, Samuel D., and Carl de Boor (1980), *Elementary Numerical Analysis, an Algorithmic Approach* (third edition). New York: McGraw-Hill.

Cook, R. D., and S. Weisberg (1982), *Residuals and Influence in Regression*. London: Chapman and Hall.

Cook, R. D., and S. Weisberg (1983), "Diagnostics for heteroscedasticity in regression." *Biometrika*, **70**(1), 1–10.

Daniel, C., and F. S. Wood (1980), *Fitting Equations to Data* (second edition). New York: Wiley.

Davies, O. L., Ed. (1956), *The Design and Analysis of Industrial Experiments* (second edition). Edinburgh: Oliver and Boyd.

Dennis, Jr., J. E., D. M. Gay, and R. E. Welsch (1981), "An adaptive nonlinear least-squares algorithm." *ACM Transactions on Mathematical Software*, **7**, 348–368.

Dennis, Jr., J. E., and Robert B. Schnabel (1983), *Numerical Methods for Unconstrained Optimization and Nonlinear Equations*. Englewood Cliffs, N. J.: Prentice Hall.

Dierburg, F., and K. C. Ewel (1982), "The effects of treated sewage effluent on decomposition and organic matter accumulation in cypress domes," in K. C. Ewel and H. T. Odum, Eds., *Cypress Domes*. Florida University Press.

Dongarra, J. J., J. R. Bunch, C. B. Moler, and G. W. Stewart (1979), *Linpack Users' Guide*. Philadelphia: SIAM.

Draper, N. R., and H. Smith (1981), *Applied Regression Analysis* (second edition). New York: Wiley.

Edlefsen, Lee E., and Samuel D. Jones (1986), *GAUSS™ Programming Language Manual*. Kent, Wash.: Aptech Systems Inc..

Ehrenberg, A. S. C. (1981), "The problem of numeracy." *American Statistician*, **35**(2),

67–71.

Ehrenberg, A. S. C. (1982), "Writing technical reports or papers." *American Statistician*, **36**(4), 326–329.

Elliot, J. R., and D. R. Pierson (1986), Private communication.

Fedorov, V. V. (1972), *Theory of Optimal Experiments*. New York: Academic Press. (Translated by W. J. Studden and E. M. Klimko.)

Fisher, R. A. (1935), *Design of Experiments*. London: Oliver and Boyd.

Froment, Gilbert F., and Kenneth B. Bischoff (1979), *Chemical Reactor Analysis and Design*. New York: Wiley.

Fuguitt, R. E., and J. E. Hawkins (1945), "The liquid-phase thermal isomerization of α-pinene." *Journal of the American Chemical Society*, **67**, 242–245.

Fuguitt, R. E., and J. E. Hawkins (1947), "Rate of the thermal isomerization of α-pinene in the liquid phase." *Journal of the American Chemical Society*, **69**, 319–322.

Gill, P. E., W. Murray, and M. H. Wright (1981), *Practical Optimization*. New York: Academic Press.

Godfrey, Keith (1983), *Compartmental Models and Their Application*. New York: Academic Press.

Golub, G. H., and V. Pereyra (1973), "The differentiation of pseudo-inverses and nonlinear least squares problems whose variables separate." *Journal of SIAM*, **10**, 413–432.

Gregory, F. G. (1956), "General aspects of leaf growth," in F. L. Milthorpe, Ed., *The Growth of Leaves*. London: Butterworth.

Halperin, M. (1963), "Confidence interval estimation in nonlinear regression." *Journal of the Royal Statistical Society, Ser. B*, **25**, 330–333.

Hamilton, D. C. (1980), *Experimental Design for Nonlinear Regression Models*. Ph.D. Thesis, Queen's University at Kingston.

Hamilton, D. C. (1986), "Confidence regions for parameter subsets in nonlinear regression." *Biometrika*, **73**(1), 57–64.

Hamilton, David C., and Donald G. Watts (1985), "A quadratic design criterion for precise estimation in nonlinear regression models." *Technometrics*, **27**(3), 241–250.

Hamilton, D. C., D. G. Watts, and D. M. Bates (1982), "Accounting for intrinsic nonlinearity in nonlinear regression parameter inference regions." *Annals of Statistics*, **10**(2), 386–393.

Hartley, H. O. (1961), "The modified Gauss–Newton method for the fitting of non-linear regression functions by least squares." *Technometrics*, **3**, 269–280.

Havriliak, Stephen Jr., and S. Negami (1967), "A complex plane representation of dielectric and mechanical relaxation processes in some polymers." *Polymer*, **8**, 161–205.

Havriliak, Stephen Jr., and Donald G. Watts (1987), "Estimating dielectric constants: A complex multiresponse problem," in C. Mallows, Ed., *Data, Design, and Analysis*. New York: Wiley.

Heyes, J. K., and R. Brown (1956), "Growth and cellular differentiation," in F. L. Milthorpe, Ed., *The Growth of Leaves*. London: Butterworth.

Hill, P. D. H. (1980), "D-optimal designs for partially nonlinear regression models." *Technometrics*, **22**(2), 275–276.

Hill, W. J., and W. G. Hunter (1974), "Design of experiments for subsets of the parameters." *Technometrics*, **16**, 425–434.

Hill, W. J., W. G. Hunter, and D. W. Wichern (1968), "A joint design criterion for the dual problem of model discrimination and parameter estimation." *Technometrics*, **10**, 145–160.

Himmelblau, D. M. (1972), "A uniform evaluation of unconstrained optimization techniques," in F. A. Lootsma, Ed., *Numerical Methods for Nonlinear Optimization*.

London: Academic Press.

Hinkley, D. V. (1969), "Inference about the intersection in two-phase regression." *Biometrika*, **56**, 495–504.

Hocking, R. R. (1983), "Developments in linear regression methodology: 1959–1982 (with discussion)." *Technometrics*, **25**(3), 219–249.

Hougen, O. A., and K. M. Watson (1947), *Chemical Reaction Principles*. New York: Wiley.

Householder, A. S. (1958), "Unitary triangularization of a nonsymmetric matrix." *Journal of the Association for Computing Machinery*, **5**, 339–342.

Hubbard, A. B., and W. E. Robinson (1950), "A thermal decomposition study of colorado oil shale." U.S. Bureau of Mines, Rept. Invest. No. 4744.

Huber, P. J. (1981), *Robust Statistics*. New York: Wiley.

Jennrich, R. I., and P. B. Bright (1976), "Fitting systems of linear differential equations using computer generated exact derivatives (with discussion)." *Technometrics*, **18**(4), 385–399.

Jennrich, R. I., and P. F. Sampson (1968), "An application of stepwise regression to nonlinear estimation." *Technometrics*, **10**(1), 63–72.

Joiner, B. L. (1981), "Lurking variables: Some examples." *American Statistician*, **35**, 227–233.

Jupp, David L. B. (1978), "Approximation to data by splines with free knots." *SIAM Journal of Numerical Analysis*, **15**(2), 328–343.

Juusola, J. A. (1971), *A Kinetic Mechanism for the Vapor-phase Oxidation of o-Xylene over a Vanadium Oxide Catalyst*. Ph. D. thesis, Queen's University at Kingston.

Kaplan, Stanley A., Robert E. Weinfeld, Charles W. Abruzzo, and Margaret Lewis (1972), "Pharmacokinetic profile of sulfisoxazole following intravenous, intramuscular, and oral administration to man." *Journal of Pharmaceutical Sciences*, **61**, 773–778.

Kaufman, Linda (1975), "A variable projection method for solving separable nonlinear least squares problems." *BIT*, **15**, 49–57.

Kennedy, Jr., W. J., and J. E. Gentle (1980), *Statistical Computing*. New York: Marcel Dekker.

Khuri, A. I. (1984), "A note on D-optimal designs for partially nonlinear regression models." *Technometrics*, **26**(1), 59–61.

Lawton, W. H., E. A. Sylvestre, and M. S. Maggio (1972), "Self modeling nonlinear regression." *Technometrics*, **14**(3), 513–532.

Levenberg, K. (1944), "A method for the solution of certain nonlinear problems in least squares." *Quarterly of Applied Mathematics*, **2**, 164–168.

Linssen, H. N. (1975), "Nonlinearity measures: a case study." *Statistica Neerlandica*, **29**, 93–99.

Lythgoe, Steven C. (1986), *A model for the Thermal Dissolver of the Wilsonville Direct Coal Liquefaction Process*. Master's Thesis, Queen's University at Kingston.

Marquardt, D. W. (1963), "An algorithm for the estimation of non-linear parameters." *Journal of SIAM*, **11**, 431–441.

Marske, Donald (1967), *Biochemical Oxygen Demand Data Interpretation Using Sum of Squares Surface*. M.S. Thesis, University of Wisconsin—Madison.

McLean, D. D., D. J. Pritchard, D. W. Bacon, and J. Downie (1979), "Singularities in multiresponse modelling." *Technometrics*, **21**(3), 291–298.

Michaelis, L., and M. L. Menten (1913), "Kinetik der Invertinwirkung." *Biochemische Zeitschrift*, **49**, 333.

Miller, Allan (1983), "BMD P3R – A warning." CSIRO–DMS Newsletter, Sydney, Australia: CSIRO.

Moler, Cleve, and Charles Van Loan (1978), "Nineteen dubious ways to compute the exponential of a matrix." *SIAM Review*, **20**(4), 801–836.

Montgomery, Douglas C., and Elizabeth A. Peck (1982), *Introduction to Linear Regression Analysis*. New York: Wiley.

O'Neill, Barrett (1966), *Elementary Differential Geometry*. New York: Academic Press.

Osborne, M. R. (1971), "Some aspects of non-linear least squares calculations," in F. A. Lootsma, Ed., *Numerical Methods for Non-linear Optimization*. New York: Academic Press.

Pimentel-Gomes, F. (1953), "The use of Mitscherlich's regression law in the analysis of experiments with fertilizers." *Biometrics*, **9**, 498–516.

Pritchard, Douglas (1972), *Statistical Design and Analysis Using Experimental Kinetic Data*. Master's Thesis, Queen's University.

Ralston, M. L., and R. I. Jennrich (1978), "DUD, a derivative-free algorithm for nonlinear least squares." *Technometrics*, **20**, 7–14.

Ratkowsky, David A. (1979), "Choosing the 'best' parameterization of the asymptotic regression model." Technical Report, CSIRO Division of Mathematics and Statistics, Tasmania.

Ratkowsky, D. A. (1983), *Nonlinear Regression Modelling: A Unified Practical Approach*. New York: Marcel Dekker.

Ratkowsky, D. A. (1985), "A statistically suitable general formulation for modelling catalytic chemical reactions." *Chemical Engineering Science*, **40**(9), 1623–1628.

Renwick, A. G. (1982), "Pharmacokinetics in toxicology," in A. Wallace Hayes, Ed., *Principles and Methods of Toxicology*. New York: Raven Press, pp. 659–710.

Roller, Duane (1950), *The Early Development of the Concepts of Temperature and Heat: The Rise and Decline of the Caloric Theory*. Cambridge, Mass.: Harvard University Press.

SAS Institute Inc. (1985), *SAS User's Guide: Statistics, Version 5 Edition*. Cary, N.C.: SAS Institute Inc..

SAS Institute Inc. (1985), *SAS/IML™ User's Guide, Version 5 Edition*,. Cary, N.C.: SAS Institute Inc..

Seber, G. A. (1977), *Linear Regression Analysis*. New York: Wiley.

Silvey, S. D., and D. M. Titterington (1973), "A geometric approach to optimal design theory." *Biometrika*, **60**, 21–32.

Smith, B. T., J. M. Boyle, J. J. Dongarra, B. S. Garbow, Y. Ikebe, V. C. Klema, and C. B. Moler (1976), *Matrix Eigensystem Routines—EISPACK Guide*. Springer Verlag.

Sredni, J. (1970), *Problems of Design, Estimation, and Lack of Fit in Model Building*. Ph.D. Thesis, University of Wisconsin—Madison.

St. John, R. C., and N. R. Draper (1975), "D-optimality for regression designs: a review." *Technometrics*, **17**, 15–23.

Steinberg, David M., and William G. Hunter (1984), "Experimental design: review and comment (with discussion)." *Technometrics*, **26**(2), 71–130.

Stewart, G. W. (1973), *Introduction to Matrix Computations*. New York: Academic Press.

Stewart, G. W. (1976), "HQR3 and EXCHNG: Fortran subroutines for calculating the eigenvalues of a real upper Hessenberg matrix." *ACM Transactions on Mathematical Software*, **2**(3), 275–280. (Algorithm 506.)

Stewart, W. E., and J. P. Sorensen (1981), "Bayesian estimation of common parameters from multiresponse data with missing observations." *Technometrics*, **23**, 131–141.

Tierney, Luke, and Joseph B. Kadane (1986), "Accurate approximations for posterior moments and densities." *Journal of the American Statistical Association*, **81**(393), 82–86.

Treloar, M. A. (1974), *Effects of Puromycin on Galactosyltransferase of Golgi Membranes*. Master's Thesis, University of Toronto.

Tufte, Edward R. (1983), *The Visual Display of Quantitative Information*. Cheshire, Conn.: Graphics Press.

Varah, J. M. (1982), "A spline least squares method for numerical parameter estimation in differential equations." *SIAM Journal of Scientific and Statistical Computing*, **3**(1), 28–46.

Wagner, J. G. (1967), "Use of computers in pharmacokinetics." *Clinical Pharmacology and Therapeutics*, **8**, 201.

Wagner, John G. (1975), *Fundamentals of Clincal Pharmacokinetics*. Hamilton, Illinois: Drug Intelligence Publications.

Wald, A. (1943), "On the efficient design of statistical investigations." *Annals of Mathematical Statistics*, **14**, 134–140.

Watts, Donald G. (1981), "A task-analysis approach to designing a regression analysis course." *American Statistician*, **35**(2), 77–84.

Watts, D. G., and D. W. Bacon (1974), "Using a hyperbola as a transition model to fit two-regimen straight-line data." *Technometrics*, **16**, 369–373.

Watts, Donald G., Donald deBethizy, and Robert G. Stiratelli (1986), "Toxicity of Ethyl Acrylate." Technical Report, Rohm and Haas Co., Spring House, Pa.

Williams, E. J. (1962), "Exact fiducial limits in nonlinear estimation." *Journal of the Royal Statistical Society, Ser. B*, **24**, 125–139.

Ziegel, E. R., and J. W. Gorman (1980), "Kinetic modelling with multiresponse data." *Technometrics*, **22**(2), 139–151.

Ziegel, Eric R. (1985), "Discussion of the paper by Bates and Watts." *Technometrics*, **27**(4), 352–357.

Bibliography

BOOKS

Bard, Y. (1974), *Nonlinear Parameter Estimation*. New York: Academic Press.

Beck, J. V., and K. J. Arnold (1977), *Parameter Estimation in Engineering and Science*. New York: Wiley.

Box, George E. P., and Norman R. Draper (1987), *Empirical Model-Building and Response Surfaces*. New York: Wiley.

Box, G. E. P., W. G. Hunter, and J. S. Hunter (1978), *Statistics for Experimenters*. New York: Wiley.

Box, G. E. P., and G. C. Tiao (1973), *Bayesian Inference in Statistical Analysis*. Reading, Mass.: Addison-Wesley.

Chambers, J. M. (1977), *Computational Methods for Data Analysis*. New York: Wiley.

Daniel, C., and F. S. Wood (1980), *Fitting Equations to Data* (second edition). New York: Wiley.

Dennis, Jr., J. E., and Robert B. Schnabel (1983), *Numerical Methods for Unconstrained Optimization and Nonlinear Equations*. Englewood Cliffs, N. J.: Prentice-Hall.

Dixon, W. J., M. B. Brown, L. Engleman, J. W. Frane, M. A. Hill, R. I. Jennrich, and J. D. Toporek (1983), *BMDP Statistical Software*. Berkeley, Calif.: University of California Press.

Draper, N. R., and H. Smith (1981), *Applied Regression Analysis* (second edition). New York: Wiley.

Gallant, A. Ronald (1987), *Nonlinear Statistical Models*. New York: Wiley.

Kennedy, Jr., W. J., and J. E. Gentle (1980), *Statistical Computing*. New York: Marcel Dekker.

Myers, R. H. (1986), *Classical and Modern Regression with Applications*. Boston: Duxbury.

Nash, John C., and Mary Walker-Smith (1987), *Nonlinear Parameter Estimation: An Integrated System in Basic*. New York: Marcel Dekker.

Neter, J., W. Wasserman, and M. H. Kutner (1983), *Applied Linear Regression Models*. Homewood, Ill.: Irwin.

Ratkowsky, D. A. (1983), *Nonlinear Regression Modelling: A Unified Practical Approach*. New York: Marcel Dekker.

SAS Institute Inc. (1985), *SAS User's Guide: Statistics, Version 5 Edition*. Cary, N. C.: SAS Institute Inc..

Snedecor, George W., and William G. Cochran (1980), *Statistical Methods* (seventh edition). Ames, Iowa: Iowa State University Press.

GENERAL ARTICLES

Box, G. E. P. (1960), "Fitting empirical data." *Annals of the New York Academy of Sciences*, **86**, 792–816.

Box, G. E. P., and W. G. Hunter (1962), "A useful method of model building." *Technometrics*, **4**, 301–318.

Box, G. E. P., and W. G. Hunter (1965), "The experimental study of physical mechanisms." *Technometrics*, **7**, 23–42.

Gallant, A. R. (1975), "Nonlinear regression." *American Statistician*, **29**(2), 73–81.

Motulsky, H. J., and L. A. Ransanas (1987), "Fitting curves to data using nonlinear regression: a practical and nonmathematical review." *FASEB Journal*, **1**, 365–374.

Watts, D. G. (1981), "An Introduction to Nonlinear Least Squares," in L. Endrenyi, Ed., *Kinetic Data Analysis—Design and Analysis of Enzyme and Pharmacokinetic Experiments*. New York: Plenum, pp. 1–24.

NONLINEAR LEAST SQUARES—THEORY

Allen, D. M. (1983), "Parameter estimation for nonlinear models with emphasis on compartmental models." *Biometrics*, **39**(3), 629–637.

Bates, D. M., and D. G. Watts (1980), "Relative curvature measures of nonlinearity (with discussion)." *Journal of the Royal Statistical Society, Ser. B*, **42**(1), 1–25.

Bates, D. M., and D. G. Watts (1981), "Parameter transformations for improved approximate confidence regions in nonlinear least squares." *Annals of Statistics*, **9**(6), 1152–1167.

Beal, S. L. (1982), "Reader response: Bayesian analysis of nonlinear models." *Biometrics*, **38**(4), 1089–1092.

Beale, E. M. L. (1960), "Confidence regions in nonlinear estimation (with discussion)." *Journal of the Royal Statistical Society, Ser. B*, **22**, 41–88.

Berkey, C. S. (1982), "Bayesian approach for a nonlinear growth model." *Biometrics*, **38**(4), 953–961.

Clarke, G. P. Y. (1980), "Moments of the least squares estimators in a nonlinear regression model." *Journal of the Royal Statistical Society, Ser. B*, **42**(2), 227–237.

Clarke, G. P. Y. (1987), "Approximate confidence limits for a parameter function in nonlinear regression." *Journal of the American Statistical Association*, **82**(397), 221–230.

Cook, R. D., and C. L. Tsai (1985), "Residuals in nonlinear regression." *Biometrika*, **72**(1), 23–29.

Cook, R. Dennis, and Jeffrey A. Witmer (1985), "A note on parameter-effects curvature." *Journal of the American Statistical Association*, **80**(392), 872–878.

Currie, D. (1982), "Estimating Michaelis–Menten parameters: Bias, variance, and experimental design." *Biometrics*, **38**(4), 907–919.

DiCiccio, T. J. (1984), "On parameter transformations and interval estimation." *Biometrika*, **71**(3), 477–485.

Donaldson, Janet R., and Robert B. Schnabel (1987), "Computational experiences with confidence regions and confidence intervals for nonlinear least squares." *Technometrics*, **29**(1), 67–82.

Gallant, A. R. (1975), "The power of the likelihood ratio test of location in nonlinear regression models." *Journal of the American Statistical Association*, **70**(349), 198–203.

Gallant, A. R. (1975), "Testing a subset of the parameters of a nonlinear regression model." *Journal of the American Statistical Association*, **70**(352), 927–932.

Gallant, A. R. (1977), "Testing a nonlinear regression specification; a nonregular case."

Journal of the American Statistical Association, **72**(359), 523–529.

Guttman, I., and D. A. Meeter (1965), "On Beale's measure of nonlinearity." *Technometrics*, **7**, 623–637.

Halperin, M. (1963), "Confidence interval estimation in nonlinear regression." *Journal of the Royal Statistical Society, Ser. B*, **25**, 330–333.

Hamilton, D. (1986), "Confidence regions for parameter subsets in nonlinear regression." *Biometrika*, **73**(1), 57–64.

Hamilton, D. C., D. G. Watts, and D. M. Bates (1982), "Accounting for intrinsic nonlinearity in nonlinear regression parameter inference regions." *Annals of Statistics*, **10**(2), 386–393.

Hartley, H. O. (1964), "Exact confidence regions for the parameters in nonlinear regression laws." *Biometrika*, **51**, 347–353.

Hougaard, P. (1982), "Parameterizations of non-linear models." *Journal of the Royal Statistical Society, Ser. B*, **44**(2), 244–252.

Hougaard, P. (1985), "The appropriateness of the asymptotic distribution in a nonlinear regression model in relation to curvature." *Journal of the Royal Statistical Society, Ser. B*, **47**(1), 103–114.

Jennrich, R. I. (1969), "Asymptotic properties of nonlinear least squares estimation." *Annals of Mathematical Statistics*, **40**, 633–643.

Kass, Robert E. (1984), "Canonical parameterizations and zero parameter-effects curvature." *Journal of the Royal Statistical Society, Ser. B*, **46**, 86–92.

Katz, D., S. P. Azen, and A. Schumitzky (1981), "Bayesian approach to the analysis of nonlinear models: Implementation and evaluation." *Biometrics*, **37**, 137–142.

Linssen, H. N. (1975), "Nonlinearity measures: A case study." *Statistica Neerlandica*, **29**, 93–99.

Moolgavkar, Suresh H., Edward D. Lustbader, and David J. Venzon (1984), "A geometric approach to nonlinear regression diagnostics with application to matched case-control studies." *Annals of Statistics*, **12**(3), 816–826.

Peduzzi, P. N., R. J. Hardy, and T. R. Holford (1980), "A stepwise variable selection procedure for nonlinear regression models." *Biometrics*, **36**, 511–516. (See also **37**, 595–596.)

Racine-Poon, A. (1985), "A Bayesian approach to nonlinear random effects models." *Biometrics*, **41**(4), 1015–1023.

Ross, G. J. S. (1970), "The efficient use of function minimization in non-linear maximum-likelihood estimation." *Applied Statistics*, **19**, 205–221.

Ross, G. J. S. (1978), "Exact and approximate confidence regions for functions of parameters in non-linear models," in L. Corstein, and J. Hermans, Eds., *COMPSTAT 78, Third Symposium on Computation*. Vienna: Physica-Verlag.

Schwetlick, Hubert, and Volker Tiller (1985), "Numerical methods for estimating parameters in nonlinear models with errors in the variables." *Technometrics*, **27**(1), 17–24.

Wilks, S. S., and J. F. Daly (1939), "An optimum property of confidence regions associated with the likelihood function." *Annals of Mathematical Statistics*, **10**, 225–239.

Williams, E. J. (1962), "Exact fiducial limits in nonlinear estimation." *Journal of the Royal Statistical Society, Ser. B*, **24**, 125–139.

Wolter, K. M., and W. A. Fuller (1982), "Estimation of nonlinear errors-in-variables models." *Annals of Statistics*, **10**(2), 539–548.

Wu, C. F. (1981), "Asymptotic theory of nonlinear least squares estimation." *Annals of Statistics*, **9**, 501–513.

NONLINEAR LEAST SQUARES—COMPUTING

Barham, R. H., and W. Drane (1972), "An algorithm for least squares estimation of nonlinear parameters when some of the parameters are linear." *Technometrics*, **14**, 757–766.

Bates, Douglas M., and Mary J. Lindstrom (1986), "Nonlinear least squares with conditionally linear parameters," in *Proceedings of the Statistical Computing Section*. New York: American Statistical Association.

Bates, D. M., and D. G. Watts (1981), "A relative offset orthogonality convergence criterion for nonlinear least squares." *Technometrics*, **23**(2), 179–183.

Chambers, J. M. (1973), "Fitting nonlinear models: Numerical techniques." *Biometrika*, **60**, 1–13.

Dennis Jr., J. E., D. M. Gay, and R. E. Welsch (1981), "An adaptive nonlinear least-squares algorithm." *ACM Transactions on Mathematical Software*, **7**, 348–368.

Golub, G. H., and V. Pereyra (1973), "The differentiation of pseudo-inverses and nonlinear least squares problems whose variables separate." *J. SIAM*, **10**, 413–432.

Guttman, I., V. Pereyra, and H. D. Scolnik (1973), "Least squares estimation for a class of non-linear models." *Technometrics*, **15**(2), 209–218.

Hartley, H. O. (1961), "The modified Gauss–Newton method for the fitting of non-linear regression functions by least squares." *Technometrics*, **3**, 269–280.

Harville, D. A. (1973), "Fitting partially linear models by weighted least squares." *Technometrics*, **15**(3), 509–515.

Hiebert, K. L. (1981), "An evaluation of mathematical software that solves the nonlinear least squares problem." *ACM Transactions on Mathematical Software*, **7**(1), 1–16.

Jennrich, R. I., and P. B. Bright (1976), "Fitting systems of linear differential equations using computer generated exact derivatives (with discussion)." *Technometrics*, **18**(4), 385–399.

Jennrich, R. I., and P. F. Sampson (1968), "An application of stepwise regression to nonlinear estimation." *Technometrics*, **10**(1), 63–72.

Lawton, W. H., and E. A. Sylvestre (1971), "Elimination of linear parameters in nonlinear regression." *Technometrics*, **13**, 461–467.

Levenberg, K. (1944), "A method for the solution of certain nonlinear problems in least squares." *Quarterly of Applied Mathematics*, **2**, 164–168.

Marquardt, D. W. (1963), "An algorithm for the estimation of non-linear parameters." *J. SIAM*, **11**, 431–441.

Marquardt, D. W. (1970), "Generalized inverses, ridge regression, biased linear estimation, and nonlinear estimation." *Technometrics*, **12**, 591.

Meyer, R. R., and P. M. Roth (1972), "Modified damped least squares." *Journal of the Institute of Mathematics and Its Applications*, **9**, 218.

Pedersen, P. V. (1977), "Curve fitting and modeling in pharmacokinetics and some practical experiences with NONLIN and a new program FUNFIT." *Journal of Pharmacokinetics and Biopharmaceutics*, **5**, 513.

Pedersen, P. V. (1978), "Curve fitting and modeling in pharmacokinetics: A reply from the author." *Journal of Pharmacokinetics and Biopharmaceutics*, **6**, 447.

Peduzzi, P. N., R. J. Hardy, and T. R. Holford (1980), "A stepwise variable selection procedure for nonlinear regression models." *Biometrics*, **36**, 511–516. (See also **37**, 595–596.)

Ralston, M. L., and R. I. Jennrich (1978), "DUD, a derivative-free algorithm for nonlinear least squares." *Technometrics*, **20**, 7–14.

SELF-MODELING

Armstrong, P. W., D. G. Watts, D. C. Hamilton, M. A. Chiong, and J. O. Parker (1979), "Quantification of myocardial infarction: Template model for serial creatine kinase analysis." *Circulation*, **60**(4), 856–865.

Graham, B. V. (1976), "Wavelength discrimination derived from color naming." *Vision Research*, **16**, 559–562.

Guardabasso, V., P. J. Munson, and D. Rodbard (1988), "A versatile method for simultaneous analysis of families of curves." *FASEB Journal*, **2**, 209–215.

Guardabasso, V., D. Rodbard, and P. J. Munson (1987), "A model-free approach to estimation of relative potency in dose-response curve analysis." *American Journal of Physiology*, **252**, E357–E364.

Lawton, W. H., E. A. Sylvestre, and M. S. Maggio (1972), "Self modeling nonlinear regression." *Technometrics*, **14**(3), 513–532.

Levine, H. D., A. L. Rosen, R. DeWoskin, and G. S. Moss (1977), "Application of self-modeling nonlinear regression to ventricular pressure data." *Computers in Biomedical Research*, **10**, 363–372.

Reeves, R. L., R. S. Kain, M. S. Maggio, E. A. Sylvestre, and W. H. Lawton (1973), "Analysis of the visual spectrum of methyl orange in solvents and in hydrophobic binding sites." *Canadian Journal of Chemistry*, **96**, 628–635.

Reeves, R. L., M. S. Maggio, and L. F. Costa (1974), "Importance of solvent cohesion and structure in solvent effects on binding site probes." *Journal of the American Chemical Society*, **96**, 5971–5925.

SPECIAL MODEL FORMS

Allen, D. M. (1983), "Parameter estimation for nonlinear models with emphasis on compartmental models." *Biometrics*, **39**(3), 629–637.

Bates, Douglas M., Dennis A. Wolf, and Donald G. Watts (1985), "Nonlinear least squares and first-order kinetics," in David Allen, Ed., *Proceedings of Computer Science and Statistics: Seventeenth Symposium on the Interface*. New York: North-Holland.

Bliss, C. I., and A. T. James (1966), "Fitting the rectangular hyperbola." *Biometrics*, **22**, 573–602.

Currie, D. (1982), "Estimating Michaelis–Menten parameters: Bias, variance, and experimental design." *Biometrics*, **38**(4), 907–919.

Jennrich, R. I., and P. B. Bright (1976), "Fitting systems of linear differential equations using computer generated exact derivatives (with discussion)." *Technometrics*, **18**(4), 385–399.

Kittrell, J. R. (1970), "Mathematical modelling of chemical reactions." *Advances in Chemical Engineering*, **8**, 97–183.

Kittrell, J. R., W. G. Hunter, and C. C. Watson (1965), "Nonlinear least squares analysis of catalytic rate models." *American Institute of Chemical Engineers Journal*, **11**, 1051–1057.

Mezaki, R., N. R. Draper, and R. A. Johnson (1973), "On the violation of assumptions in nonlinear least squares by interchange of response and predictor variables." *Industrial and Engineering Chemistry Fundamentals*, **12**, 251–254.

Mezaki, R., and J. R. Kittrell (1968), "Nonlinear least squares for model screening." *American Institute of Chemical Engineers Journal*, **14**, 513.

Peterson, T. I., and L. Lapidus (1966), "Nonlinear estimation analysis of the kinetics of

catalytic ethanol dehydrogenation." *Chemical Engineering Science*, **21**, 655–664.

Reilly, P. M., and H. Patino-Leal (1981), "A Bayesian study of the errors-in-variables model." *Technometrics*, **23**, 221–231.

MULTIRESPONSE MODELS

Bates, D. M., and D. G. Watts (1984), "A multi-response Gauss–Newton algorithm." *Communications in Statistics—Simulation and Computation*, **13**(5), 705–715.

Bates, Douglas M., and Donald G. Watts (1985), "Multiresponse estimation with special application to systems of linear differential equations (with discussion)." *Technometrics*, **27**(4), 329–360.

Bates, Douglas M., and Donald G. Watts (1987), "A generalized Gauss–Newton procedure for multi-response parameter estimation." *SIAM Journal of Scientific and Statistical Computing*, **7**(1), 49–55.

Box, G. E. P., and N. R. Draper (1965), "The Bayesian estimation of common parameters from several responses." *Biometrika*, **52**, 355–365.

Box, G. E. P., W. G. Hunter, J. F. MacGregor, and J. Erjavec (1973), "Some problems associated with the analysis of multiresponse models." *Technometrics*, **15**(1), 33–51.

Box, M. J., and N. R. Draper (1972), "Estimation and design criteria for multiresponse nonlinear models with non-homogeneous variance." *Applied Statistics*, **21**, 13–24.

Box, M. J., N. R. Draper, and W. G. Hunter (1970), "Missing values in multi-response nonlinear data fitting." *Technometrics*, **12**, 613–620.

Draper, N. R., H. Kanemasu, and R. Mezaki (1969), "Estimating rate constants." *Industrial and Engineering Chemistry Fundamentals*, **8**, 423–427.

Hunter, W. G. (1967), "Estimation of unknown constants from multi-response data." *Industrial and Engineering Chemistry Fundamentals*, **8**, 423–427.

McLean, D. D., D. J. Pritchard, D. W. Bacon, and J. Downie (1979), "Singularities in multiresponse modelling." *Technometrics*, **21**(3), 291–298.

Mezaki, R., and J. B. Butt (1968), "Estimation of rate constants from multiresponse kinetic data." *Industrial and Engineering Chemistry Fundamentals*, **7**, 120–125.

Stewart, W. E., and J. P. Sorensen (1981), "Bayesian estimation of common parameters from multiresponse data with missing observations." *Technometrics*, **23**, 131–141.

Ziegel, E. R., and J. W. Gorman (1980), "Kinetic modelling with multiresponse data." *Technometrics*, **22**(2), 139–151.

EXPERIMENTAL DESIGN—PRECISE PARAMETER ESTIMATION

Atkinson, A. C., and W. G. Hunter (1968), "The design of experiments for parameter estimation." *Technometrics*, **10**(2), 271–289.

Bates, Douglas M. (1983), "The derivative of $|X'X|$ and its uses." *Technometrics*, **25**(4), 373–376.

Box, George E. P. (1984), "The importance of practice in the development of statistics." *Technometrics*, **26**(1), 1–8.

Box, G. E. P., and H. L. Lucas (1959), "Design of experiments in non-linear situations." *Biometrika*, **46**, 77–90.

Box, M. J. (1968), "The occurrence of replications in optimal designs of experiments to estimate parameters in nonlinear models." *Journal of the Royal Statistical Society, Ser. B*, **30**, 290–302.

Box, M. J. (1968), "The use of designed experiments in nonlinear model building," in Donald G. Watts, Ed., *The Future of Statistics*. New York: Academic Press, pp. 241–257.

Box, M. J. (1970), "Some experiences with a nonlinear experimental design criterion." *Technometrics*, **12**(3), 569–589.

Box, M.J. (1971), "An experimental design criterion for precise parameter estimation of a subset of the parameters in a nonlinear model." *Biometrika*, **58**, 149–153.

Box, M. J. (1971), "Simplified experimental design." *Technometrics*, **13**(1), 19–31.

Box, M. J., and N. R. Draper (1971), "Factorial designs, the $|X'X|$ criterion, and some related matters." *Technometrics*, **13**, 731–742.

Chernoff, H. (1953), "Locally optimal designs in estimating parameters." *Annals of Mathematical Statistics*, **24**, 586–602.

Cochran, W. G. (1973), "Experiments for nonlinear functions." *Journal of the American Statistical Association*, **68**, 771–778.

Cox, D. R. (1984), "Design of experiments and regression." *Journal of the Royal Statistical Society, Ser. A*, **147**(2), 306–315.

Currie, D. (1982), "Estimating Michaelis–Menten parameters: Bias, variance, and experimental design." *Biometrics*, **38**(4), 907–919.

Draper, N. R., and W. G. Hunter (1967), "The use of prior distributions in the design of experiments for parameter estimation in nonlinear estimation." *Biometrika*, **54**, 147–153.

Evans, J. W. (1979), "Computer augmentation of experimental designs to maximize $|X'X|$." *Technometrics*, **21**(3), 321–330.

Graham, R. J., and F. D. Stevenson (1972), "Kinetics of chlorination of niobium oxychloride by phosgene in a tube flow reactor. Application of sequential experimental design." *Industrial and Engineering Chemistry Process Design and Development*, **11**, 160–164.

Hahn, Gerald J. (1984), "Experimental design in the complex world." *Technometrics*, **26**(1), 19–31.

Hamilton, David C., and Donald G. Watts (1985), "A quadratic design criterion for precise estimation in nonlinear regression models." *Technometrics*, **27**(3), 241–250.

Herzberg, A. M., and D. R. Cox (1969), "Recent work on the design of experiments: A bibliography and a review." *Journal of the Royal Statistical Society, Ser. B*, **31**, 29–67.

Hill, P. D. H. (1980), "D-optimal designs for partially nonlinear regression models." *Technometrics*, **22**(2), 275–276.

Hill, W. J., and W. G. Hunter (1974), "Design of experiments for subsets of the parameters." *Technometrics*, **16**, 425–434.

Hill, W. J., W. G. Hunter, and D. W. Wichern (1968), "A joint design criterion for the dual problem of model discrimination and parameter estimation." *Technometrics*, **10**, 145–160.

Hunter, W. G., and A. C. Atkinson (1966), "Statistical designs for pilot plant and laboratory experiments." *Chemical Engineering*, **73**, 159–164.

Hunter, W. G., W. J. Hill, and T. L. Henson (1969), "Designing experiments for precise estimation of all or some of the constants in a mechanistic model." *Canadian Journal of Chemical Engineering*, **47**, 76–80.

Hunter, W. G., J. R. Kittrell, and R. Mezaki (1967), "Experimental strategies for mechanistic models." *Transactions of the Institute of Chemical Engineers*, **45**, T146-T152.

Juusola, J. A., D. W. Bacon, and J. Downie (1972), "Sequential statistical design stategy in an experimental kinetic study." *Canadian Journal of Chemical Engineering*, **50**,

796–801.

Katz, D., and D. Z. D'Argenio (1983), "Experimental design for estimating integrals by numerical quadrature." *Biometrics*, **39**(3), 621–628.

Khuri, A. I. (1984), "A note on D-optimal designs for partially nonlinear regression models." *Technometrics*, **26**(1), 59–61.

Kittrell, J. R., W. G. Hunter, and C. C. Watson (1966), "Obtaining precise parameter estimates for nonlinear catalytic rates." *American Institute of Chemical Engineers Journal*, **12**, 5–10.

Pritchard, D. J., and D. W. Bacon (1977), "Accounting for heteroscedasticity in experimental design." *Technometrics*, **19**(2), 109–115.

Reilly, P. M., R. Bajramovic, G. E. Blau, D. R. Branson, and M. W. Sauerhoff (1977), "Guidelines for the optimal design of experiments to estimate parameters in first order kinetic models." *Canadian Journal of Chemical Engineering*, **55**, 614–622.

St. John, R. C., and N. R. Draper (1975), "D-optimality for regression designs: a review." *Technometrics*, **17**, 15–23.

Steinberg, David M., and William G. Hunter (1984), "Experimental design: Review and comment (with discussion)." *Technometrics*, **26**(2), 71–130.

EXPERIMENTAL DESIGN—MODEL DISCRIMINATION

Atkinson, A. C. (1981), "A comparison of two criteria for the design of experiments for discriminating between models." *Technometrics*, **23**, 301–305.

Atkinson, A. C., and D. R. Cox (1974), "Planning experiments for discriminating between models (with discussion)." *Journal of the Royal Statistical Society, Ser. B*, **36**, 321–348.

Atkinson, A. C., and V. V. Fedorov (1975), "The design of experiments for discriminating between two rival models." *Biometrika*, **62**(1), 57–70.

Atkinson, A. C., and V. V. Fedorov (1975), "Optimal design: Experiments for discriminating between several models." *Biometrika*, **62**(2), 289–304.

Box, G. E. P., and W. J. Hill (1967), "Discrimination among mechanistic models." *Technometrics*, **9**(1), 57–71.

Froment, G. F., and R. Mezaki (1970), "Sequential discrimination and estimation procedures for rate modeling in heterogeneous catalysis." *Chemical Engineering Science*, **25**, 293–301.

Hill, P. D. H. (1978), "A review of experimental design procedures for regression model discrimination." *Technometrics*, **20**(1), 15–21.

Hill, W. J., and W. G. Hunter (1969), "A note on designs for model discrimination: Variance unknown case." *Technometrics*, **11**, 396–400.

Hill, W. J., W. G. Hunter, and D. W. Wichern (1968), "A joint design criterion for the dual problem of model discrimination and parameter estimation." *Technometrics*, **10**, 145–160.

Hunter, W. G., and A. M. Reiner (1965), "Designs for discriminating between two rival models." *Technometrics*, **7**, 307–323.

Kittrell, J. R., and R. Mezaki (1967), "Discrimination among rival Hougen–Watson models through intrinsic parameters." *American Institute of Chemical Engineers Journal*, **13**(2), 389–392.

Moeter, D., W. Pirie, and W. Blot (1970), "A comparison of two model discrimination criteria." *Technometrics*, **12**, 457–470.

Pritchard, D. J., and D. W. Bacon (1974), "Potential pitfalls in model discrimination." *Canadian Journal of Chemical Engineering*, **52**, 103–109.

Reilly, P. M. (1970), "Statistical methods in model discrimination." *Canadian Journal of Chemical Engineering*, **48**, 168–173.

EXPERIMENTAL DESIGN — MULTIRESPONSE MODELS

Box, M. J., and N. R. Draper (1972), "Estimation and design criteria for multiresponse nonlinear models with non-homogeneous variance." *Applied Statistics*, **21**, 13–24.

Draper, N. R., and W. G. Hunter (1966), "Design of experiments for parameter estimation in multiresponse situations." *Biometrika*, **53**, 525–553.

Draper, N. R., and W. G. Hunter (1967), "The use of prior distributions in the design of experiments for parameter estimation in nonlinear situations: Multi-response case." *Biometrika*, **54**, 662–665.

HETEROSCEDASTICITY

Box, G. E. P., and W. J. Hill (1974), "Correcting inhomogeneity of variance with power transformation weighting." *Technometrics*, **16**, 385–389.

Box, M. J., and N. R. Draper (1972), "Estimation and design criteria for multiresponse nonlinear models with non-homogeneous variance." *Applied Statistics*, **21**, 13–24.

Carroll, Raymond J., and David Ruppert (1984), "Power transformation when fitting theoretical models to data." *Journal of the American Statistical Association*, **79**(386), 321–328.

Pritchard, D. J., and D. W. Bacon (1977), "Accounting for heteroscedasticity in experimental design." *Technometrics*, **19**(2), 109–115.

Pritchard, D. J., J. Downie, and D. W. Bacon (1977), "Further considerations of heteroscedasticity in fitting kinetic models." *Technometrics*, **19**(3), 227–236.

DIAGNOSTIC PARAMETERS

Box, G. E. P., and W. G. Hunter (1962), "A useful method of model building." *Technometrics*, **4**, 301–318.

Hunter, W. G., and R. Mezaki (1964), "A model building technique for chemical engineering kinetics." *American Institute of Chemical Engineers Journal*, **10**, 315–322.

Kittrell, J. R., W. G. Hunter, and R. Mezaki (1966), "The use of diagnostic parameters for kinetic model building." *American Institute of Chemical Engineers Journal*, **12**(5), 1014–1017.

APPLICATIONS

Bacon, D. W. (1970), "Making the most of a one-shot experiment." *Industrial and Engineering Chemistry*, **62**(7), 27–34.

Behnken, D. W. (1964), "Estimation of copolymer reactivity ratios: an example of nonlinear estimation." *Journal of Polymer Science Part A*, **2**, 645–668.

Bliss, C. I., and A. T. James (1966), "Fitting the rectangular hyperbola." *Biometrics*, **22**, 573–602.

Boag, I. F., D. W. Bacon, and J. Downie (1975), "Analysis of the reaction network for the vanadium-catalyzed oxidation of ortho-xylene." *Journal of Catalysis*, **38**, 375–384.

Currie, D. (1982), "Estimating Michaelis–Menten parameters: Bias, variance, and experimental design." *Biometrics*, **38**(4), 907–919.

Draper, N. R., H. Kanemasu, and R. Mezaki (1969), "Estimating rate constants." *Industrial and Engineering Chemistry Fundamentals*, **8**, 423–427.

Fisher, R. A. (1939), "The sampling distribution of some statistics obtained from nonlinear equations." *Annals of Eugenics*, **9**, 238–249.

Froment, G. F., and R. Mezaki (1970), "Sequential discrimination and estimation procedures for rate modeling in heterogeneous catalysis." *Chemical Engineering Science*, **25**, 293–301.

Gallant, A. R., and A. Holly (1980), "Statistical inference in an implicit, nonlinear, simultaneous equation model in the context of maximum likelihood estimation." *Econometrica*, **48**, 697–720.

Graham, R. J., and F. D. Stevenson (1972), "Kinetics of chlorination of niobium oxychloride by phosgene in a tube flow reactor. Application of sequential experimental design." *Industrial and Engineering Chemistry Process Design and Development*, **11**, 160–164.

Hoffman, T., and P. M. Reilly (1979), "Transferring information from one experiment to another." *Canadian Journal of Chemical Engineering*, **57**, 367–374.

Hsiang, T., and P. M. Reilly (1971), "A practical method of discriminating among mechanistic models." *Canadian Journal of Chemical Engineering*, **49**, 865–871.

Hunter, W. G. (1967), "Estimation of unknown constants from multi-response data." *Industrial and Engineering Chemistry Fundamentals*, **8**, 423–427.

Hunter, W. G., and A. C. Atkinson (1966), "Statistical designs for pilot plant and laboratory experiments." *Chemical Engineering*, **73**, 159–164.

Hunter, W. G., W. J. Hill, and T. L. Henson (1969), "Designing experiments for precise estimation of all or some of the constants in a mechanistic model." *Canadian Journal of Chemical Engineering*, **47**, 76–80.

Hunter, W. G., J. R. Kittrell, and R. Mezaki (1967), "Experimental strategies for mechanistic models." *Transactions of the Institute of Chemical Engineers*, **45**, T146-T152.

Hunter, W. G., and R. Mezaki (1964), "A model building technique for chemical engineering kinetics." *American Institute of Chemical Engineers Journal*, **10**, 315–322.

Johnson, R. A., N. A. Standal, and R. Mezaki (1968), "Weighted linear plots for discrimination of nonlinear rate models." *Industrial and Engineering Chemistry Fundamentals*, **7**, 181.

Juusola, J. A., D. W. Bacon, and J. Downie (1972), "Sequential statistical design stategy in an experimental kinetic study." *Canadian Journal of Chemical Engineering*, **50**, 796–801.

Kittrell, J. R. (1970), "Mathematical modelling of chemical reactions." *Advances in Chemical Engineering*, **8**, 97–183.

Kittrell, J. R., W. G. Hunter, and R. Mezaki (1966), "The use of diagnostic parameters for kinetic model building." *American Institute of Chemical Engineers Journal*, **12**(5), 1014–1017.

Kittrell, J. R., W. G. Hunter, and C. C. Watson (1965), "Nonlinear least squares analysis of catalytic rate models." *American Institute of Chemical Engineers Journal*, **11**, 1051–1057.

Kittrell, J. R., W. G. Hunter, and C. C. Watson (1966), "Obtaining precise parameter estimates for nonlinear catalytic rates." *American Institute of Chemical Engineers Journal*, **12**, 5–10.

Kittrell, J. R., and R. Mezaki (1967), "Discrimination among rival Hougen-Watson models through intrinsic parameters." *American Institute of Chemical Engineers*

Journal, **13**(2), 389–392.

Kittrell, J. R., R. Mezaki, and C. C. Watson (1965), "Estimation of parameters for nonlinear least squares analysis." *Industrial and Engineering Chemistry*, **57**(12), 18–27.

Kittrell, J. R., R. Mezaki, and C. C. Watson (1966), "Precise determination of reaction orders." *Industrial and Engineering Chemistry*, **58**(5), 50–59.

Kittrell, J. R., R. Mezaki, and C. C. Watson (1966), "Model-building techniques for heterogeneous kinetics." *British Chemical Engineering*, **11**(1), 15–19.

McLean, D. D., D. W. Bacon, and J. Downie (1980), "Statistical identification of a reaction network using an integral plug flow reactor." *Canadian Journal of Chemical Engineering*, **58**, 608–619.

Mezaki, R., and J. B. Butt (1968), "Estimation of rate constants from multiresponse kinetic data." *Industrial and Engineering Chemistry Fundamentals*, **7**, 120–125.

Mezaki, R., N. R. Draper, and R. A. Johnson (1973), "On the violation of assumptions in nonlinear least squares by interchange of response and predictor variables." *Industrial and Engineering Chemistry Fundamentals*, **12**, 251–254.

Mezaki, R., and J. R. Kittrell (1966), "Discrimination between rival models through nonintrinsic parameters." *Canadian Journal of Chemical Engineering*, **44**, 285.

Mezaki, R., and J. R. Kittrell (1967), "Parametric sensitivity in fitting nonlinear kinetic models." *Industrial and Engineering Chemistry*, **59**(5), 63–69.

Mezaki, R., and J. R. Kittrell (1968), "Nonlinear least squares for model screening." *American Institute of Chemical Engineers Journal*, **14**, 513.

Mezaki, R., J. R. Kittrell, and W. J. Hill (1967), "An analysis of kinetic power function models." *Industrial and Engineering Chemistry*, **59**(1), 93–95.

Peterson, T. I., and L. Lapidus (1966), "Nonlinear estimation analysis of the kinetics of catalytic ethanol dehydrogenation." *Chemical Engineering Science*, **21**, 655–664.

Podolski, W. F., and Y. G. Kim (1974), "Modelling the water-gas shift reaction." *Industrial and Engineering Chemistry Process Design and Development*, **13**, 415–421.

Pritchard, D. J., and D. W. Bacon (1974), "Potential pitfalls in model discrimination." *Canadian Journal of Chemical Engineering*, **52**, 103–109.

Pritchard, D. J., and D. W. Bacon (1975), "Statistical assessment of chemical kinetic models." *Chemical Engineering Science*, **30**, 567–574.

Pritchard, D. J., D. D. McLean, D. W. Bacon, and J. Downie (1980), "Testing the assumption of surface homogeneity in modelling catalytic reactions." *Journal of Catalysis*, **61**, 430–434.

Reilly, P. M. (1970), "Statistical methods in model discrimination." *Canadian Journal of Chemical Engineering*, **48**, 168–173.

Reilly, P. M., R. Bajramovic, G. E. Blau, D. R. Branson, and M. W. Sauerhoff (1977), "Guidelines for the optimal design of experiments to estimate parameters in first order kinetic models." *Canadian Journal of Chemical Engineering*, **55**, 614–622.

Reilly, P. M., and G. E. Blau (1974), "The use of statistical methods to build mathematical models of chemical reacting systems." *Canadian Journal of Chemical Engineering*, **52**, 289–299.

Sutton, T. L., and J. F. MacGregor (1977), "The analysis and design of vapour-liquid equilibrium experiments." *Canadian Journal of Chemical Engineering*, **55**, 602–608.

Author Index

Abdollah, S., 306
Abruzzo, C. W., 74, 273
Anderson, D. H., 172, 182, 282
Ansley, C. F., 23
Armstrong, P. W., 69

Bache, C. A., 3, 267
Bacon, D. W., 87, 96, 155, 156
Bard, Y., 49, 74, 77, 79, 138, 141, 164, 168
Bates, D. M., 49, 86, 141, 144, 145, 147, 171, 178, 217, 233, 244, 246, 249, 254, 255, 259, 260, 261, 300
Beale, E. M. L., 225, 232, 233, 261
Becker, R. A., 291
Belsley, D. A., 1, 26
Bischoff, K. B., 168
Bliss, C. I., 205
Box, G. E. P., 1, 3, 7, 24, 27, 28, 42, 70, 81, 93, 94, 122, 123, 124, 125, 127, 131, 134, 135, 137, 138, 139, 140, 147, 148, 155, 156, 157, 161, 213, 218, 220, 261, 272
Box, M. J., 125, 129, 164
Boyle, J. M., 316, 317
Bright, P. B., 172, 178
Brown, R., 310
Bunch, J. R., 13, 81, 145, 156, 244, 289, 295, 302, 316

Caracotsios, M., 68, 69, 168, 179
Carr, N. L., 55, 271
Carroll, R. J., 70, 91
Chambers, J. M., 49, 110, 291
Chiong, M. A., 69
Cleveland, W. S., 110
Cochran, W. G., 123
Cole, K. S., 136
Cole, R. H., 136
Conte, S. D., 69
Cook, R. D., 1, 26, 91
Coutie, G. A., 261
Cox, D. R., 28, 70
Cox, G. M., 123

Daniel, C., 27
Davies, O. L., 123
deBethizy, D., 96, 274
deBoor, C., 69
Dennis, J. E. Jr., 80, 82, 145
Dongarra, J. J., 13, 81, 145, 156, 244, 289, 295, 302, 316, 317
Downie, J., 155, 156
Draper, N. R., vii, 1, 26, 28, 49, 70, 91, 122, 123, 134, 137, 138, 161, 164

Edlefsen, L. E., 291
Ehrenberg, A. S. C., 110
Elliott, J. R., 110, 278
Erjavec, J., 135, 147, 148, 155, 156, 157, 272
Fedorov, V. V., 142
Fisher, R. A., 25
Froment, G. F., 168
Fuguitt, R. E., 68, 135, 157, 165, 272, 310

Garbow, B. S., 316, 317
Gay, D. M., 80
Gentle, J. E., 49
Gill, P. E., 77
Godfrey, K., 168, 180
Golub, G. H., 81, 86, 142
Gorman, J. W., 170, 172, 191, 282

Halperin, M., 229
Hamilton, D. C., 69, 123, 228, 234, 244, 259, 260, 261

Hartley, H. O., 42
Havriliak, S. Jr., 136, 146, 149, 280
Hawkins, J. E., 68, 135, 157, 165, 272, 310
Heyes, J. K., 310
Hill, P. D. H., 129, 131
Hill, W. J., 129, 131, 213
Himmelblau, D. M., 49
Hinkley, D. V., 87
Hocking, R. R., 26
Hougen, O. A., 272
Hubbard, A. B., 170, 188, 282
Huber, P. J., 91
Hunter, J. S., 24, 28, 122
Hunter, W. G., 24, 28, 122, 123, 127, 129, 131, 135, 147, 148, 155, 156, 157, 164, 272

Ikebe, Y., 316, 317

James, A. T., 205
Jenkins, G. M., 93, 94
Jennrich, R. I., 49, 82, 85, 172, 178
Joiner, B. L., 27, 91
Jones, S. D., 291
Jupp, D. L. B., 78, 86
Juusola, J. A., 306

Kadane, J. B., 223
Kanemasu, H., 81
Kaplan, S. A., 74, 273
Kaufman L., 86
Kennedy, W. J. Jr., 49
Khuri, A. I, 129, 131
Kleiner, B., 110
Klema, V. C., 316, 317
Kuh, E., 1, 26

Lawton, W. H., 69
Levenberg, K., 81
Lewis, M., 74, 273
Lindstrom, M. J., 86
Linssen, H. N., 87, 274
Lisk, D. J., 3, 267
Lucas, H. L., 124, 125
Lythgoe, S. C., 311

MacGregor, J. F., 135, 147, 148, 155, 156, 157, 272
Maggio, M. S., 69
Marquardt, D. W., 81
Marske, D., 41, 270, 305
McLean, D. D., 155, 156
Moler, C. B., 13, 81, 145, 156, 244, 289, 295, 302, 316, 317
Montgomery, D. C., vii, 1, 28
Murray, W., 77

Negami, S., 136, 146, 280

Oneill, B., 220

Parker, J. O., 69
Peck, E. A., vii, 1, 28
Peirson, D. R., 110, 278
Pereyra, V., 81, 86, 142
Pritchard, D. J., 155, 156, 306

Ralston, M. L., 49, 82, 85
Ratkowsky, D. A., 72, 213, 215, 249
Renwick, A. G., 97, 101, 277, 306
Robinson, W. E., 170, 188, 282
Roller, D., 268
Ruppert, D., 70, 91

Sampson, P. F., 49
Schnabel, R. B., 80, 82, 145
Seber, G. A., 1, 5, 25
Serum, J. W., 3, 267
Silvey, S. D., 123
Smith, B. T., 316, 317
Smith, H., vii, 1, 26, 28, 49, 70, 91, 123
Sorensen, J. P., 68, 164, 165
Sredni, J., 92, 274
St. John, R. C., 123
Steinberg, D. M., 123, 131
Stewart, G. W., 13, 81, 145, 156, 244, 289, 295, 302, 316
Stewart, W. E., 68, 69, 164, 165, 168, 179
Stiratelli, R. G., 96, 274
Sylvestre, A., 69

Tiao, G. C., 1, 7, 139, 140, 218, 220
Tidwell, P. W., 3
Tierney, L., 223
Titterington, D. M., 123
Treloar, M. A., 33, 126, 269
Tufte, E. R., 110
Tukey, P. W., 110

VanLoan, C., 316
Varah, J. M., 147, 149

Wagner, J. G., 281, 315
Wald, A., 124
Watson, K. M., 272
Watts, D. G., 49, 69, 87, 96, 110, 123, 141, 144, 145, 147, 149, 171, 178, 233, 244, 246, 249, 254, 255, 259, 260, 261, 274, 300
Weinfeld, R. E., 74, 273
Weisberg, S., 1, 26, 91
Welsch, R. E., 1, 26, 80
Wichern, D., 131
Wilks, A. R., 291
Williams, E. J., 229
Wolf, D. A., 171
Wood, F. S., 27
Wright, M. H., 77

Youngs, W. D., 3, 267

Ziegel, E. R., 87, 170, 172, 191, 282

Subject Index

acceleration
  array, 236
  in an arbitrary direction, 239
  normal, 234
  space dimension, 234
  tangential, 234
  vector, 234
accumulated data, 96
  analysis by direct integration, 98
analysis of variance, 29
  nitrite example, 110
arcing, 247
array
  acceleration, 236
  Hessian, 233
  relative curvature, 242
  second derivative, 233
  transformation, 251
Arrhenius relation, 180, 188
assessing fit, 23, 26, 29
  nitrite example, 113, 116
  nonlinear models, 90
assumptions, 23
  additive disturbance, 24, 25
  constant variance, 25, 26
  disturbance, 136
  for least squares, 5
  independence of disturbances, 25
  multiresponse, 136
  normal disturbances, 25, 91
  of correct model, 24
  planar, 43, 229, 232, 245, 256
  uniform coordinate, 43, 229, 232, 256
  zero mean of disturbances, 25
AUC (area under the curve), 180
autocorrelation
  of residuals, 93

Bayes
  HPD region, 7
  inference, 7
  inference for nonlinear models, 216

chi-squared distribution, 16
Cholesky
  decomposition, 145
collinearity, 78, 80
compansion, 247
compartment model, 168
  catenary, 184
  derivative with respect to parameter, 178
  mamillary, 184
  multiresponse estimation, 188
  practical considerations, 179
  sink, 168
  source, 168
  starting values, 182
  unidentifiable, 181
conditional likelihood, 204
conditionally linear
  model, 129
  parameter, 85
confidence
  band for response function, 6, 22
  geometry of interval, 19, 21
  geometry of region, 17
  interval, 6
  interval for expected response, 6, 22
  interval for parameter, 21
  region, 6
  region for nonlinear model, 223
constraint
  in multiresponse estimation, 140
  interval, 77
  on parameter, 77
  order, 78
contour

likelihood, 6, 200
sum of squares, 23, 61
convergence, 40
check, 90
criterion, 49
criterion for multiresponse estimation, 145
geometry, 49
orthogonality criterion, 49
practical considerations, 86
relative offset criterion, 49
to spurious optimum, 154
tolerance level, 49
convolution, 173
correlation
matrix, 22
of residuals, 92
covariance
matrix, 5, 137
curvature
definition, 241
intrinsic, 241
measures of nonlinearity, 232
parameter effects, 241
root mean square (RMS), 254

D-optimal
design criterion, 124
dead time, 175, 191
degrees of freedom, 6, 16
extra parameter, 103
lack of fit, 29
replication, 29
residual, 29
dependencies
in multiresponse data, 154
in multiresponse estimation, 154, 158
derivative matrix, 2, 40, 124, 233
conditioning, 78
derivative
compartment model, 178
numerical, 71
of expectation function, 71
vector, 58
determinant
constraints for multiresponse estimation, 140
criterion for multiresponse estimation, 138
design criterion, 124, 125
evaluation by QR decomposition, 141
gradient of, 142
Hessian of, 142
Jacobian, 12, 38
diagnostics, 24, 26
differential equation
specification of nonlinear model, 68
disturbance
additive assumption, 24
constant variance, 25, 26
independence, 26
independent of expectation function, 25
normal assumption, 25
practical considerations, 69
zero mean, 25
DUD, 82

editing data, 91
eigenvalue, 173
analysis of centered data matrix, 155
eigenvector, 173
ellipse
approximation to sum of squares contour, 63
estimate
least squares, 5
expectation function, 2, 25
correct model, 24
linear approximation to, 40, 232
expectation surface, 36, 38
geometry, 36
linear approximation to, 232
prior density, 217
quadratic approximation, 259
tangent plane, 232
expectation
plane, 10
surface, 9
expected response, 33
confidence interval, 6, 22
vector, 10
experimental design
D-optimal, 124
determinant criterion, 124
for conditionally linear model, 129
for linear expectation functions, 124
for nonlinear expectation functions, 124
general considerations, 122
objectives, 122
sequential, 127

starting, 125
subset, 129
extra determinant
test for nested models, 162
extra sum of squares
analysis for nested models, 103
and nonlinearity, 104
nitrite example, 116

F distribution, 6, 16
fanning, 247

Gauss increment, 40
Gauss–Newton increment, 81
Gauss–Newton
increment for multiresponse estimation, 144
iteration method, 79
method, 40
method for multiresponse estimation, 143
geometry, 36
of confidence region, 17
of convergence, 49
of experimental design determinant criterion, 124
of likelihood approach, 23
of linear least squares, 9
of multiresponse determinant criterion, 139
of nonlinear least squares, 43
of nonlinear models, 36
of sampling theory approach, 15
of the expectation surface, 36
gradient
of determinant, 142
of sum of squares function, 79

half-life, 179
hat matrix, 27
Hessian, 145
approximate, 143
array, 233
of determinant, 139, 142
of sum of squares function, 61, 80
highest posterior density (HPD)
approximate band in multiresponse estimation, 140
approximate interval in multiresponse estimation, 140
approximate region in multiresponse estimation, 139
region, 7
region for nonlinear model, 220
hypothesis, 17

improving convergence
centering and scaling, 78
incremental parameter, 91
nitrite example, 113
incremental
parameter, 104
indicator variable, 104
nitrite example, 110
inference
band, linear approximation, 58
Bayes, 7
in multiresponse estimation, 139
in nonlinear regression, 52
interval, linear approximation, 58
likelihood, 6
linear approximation, 52
linear approximation region, 64
region, 7, 15
sampling theory, 5
intrinsic curvature
geometric interpretation, 245
intrinsic nonlinearity
direct assessment, 256, 262
intrinsic
curvature, 241
nonlinearity, 237
relative curvature array, 242
intrinsically linear
model, 34
iteration, 40

Jacobian, 217
determinant, 12, 38
matrix, 250

lack of fit, 29
analysis, nitrite example, 113
degrees of freedom, 29
mean square, 29
sum of squares, 29
lag, 92
least squares
criterion, 25
estimate, 5
estimates for nonlinear model, 39
geometry, 39

geometry of nonlinear, 43
properties of estimator, 5
Levenberg–Marquardt compromise, 80, 81
likelihood, 60
conditional, 204
contour, 6, 200
function, 4, 23, 25
geometry, 23
inference, 6
interval, 205
profile trace, 207
region, 6, 200, 256
region, scaled, 242
linear approximation, 64
inference band, 58
inference interval, 58
inference region, 64, 200, 232
to expectation function, 40, 229, 232
to expectation surface, 232
to obtain Gauss–Newton increment, 64
to sum of squares function, 61
linear
model, 2
regression, 1
loglikelihood
conditional, 138
function, 60

matrix
centered data, 155
covariance, 137
derivative, 40
effective residual curvature, 260
expected response, 136
exponential, 172, 173
hat, 27
observation, 136
parameter correlation, 54
relative curvature, 244
residual, 136, 155
singular, 155
system transfer, 148, 171
maximum likelihood estimate, 5, 138
missing data
in multiresponse estimation, 164
model assessment, 23, 26
model
linear differential equations, 168
nested, 103, 162
non-nested, 103
selection, nitrite example, 113
specification in nonlinear regression, 67
unidentifiable, 181
multiresponse estimation, 134
advantages and disadvantages, 141
assessing fit, 149
compartment model, 188
convergence criterion, 145
dependencies in data, 154
missing data, 164
model, 134
practical considerations, 146

nested model, 103
extra determinant test, 162
Newton–Raphson
iteration method, 79
nonlinear
regression,, 67
nonlinear
least squares via sums of squares, 60
model, 32
model — intrinsically linear, 34
model — transformably linear, 34
regression, 32
nonlinearity
and profile t plot, 205
and profile traces, 207
intrinsic, 237, 256
of model-data set, 62
parameter effects, 237
relative curvature measures, 232
normal
assumption, 25, 91
distribution, 2, 25
equations, 12
plot, 91
probability plot, 27
spherical distribution, 9, 16, 33

orthogonal
basis, 13
transformation, 16
outlier, 27
overparametrization, 87, 90
nitrite example, 116
overshoot, 64

p-value, 17

parameter effects
curvature, 241
curvature — geometric interpretation, 246
nonlinearity, 237
relative curvature array, 242
parameter transformation
centering and scaling, 78
to improve convergence, 78
parameter
approximate correlation matrix, 90
approximate correlations, 53
approximate covariance matrix, 85
approximate inference region, 52
approximate standard error, 53
arcing, 247
as functions of other variables, 108
compansion, 247
conditionally linear, 36, 76, 85
confidence interval, 6
constraint, 77
correlation matrix, 54
curve, 45
exchangeable, 78, 180
extra degrees of freedom, 103
fanning, 247
incremental, 91, 104
inference region, 15, 52
kinetic, 188
line, 10
line on expectation surface, 39
linear approximation line to curve, 45, 47
nonlinearity, 237
nuisance, 26
plane, 10, 38
process, 108, 188
t ratio, 90
torsion, 247
transformation, 179, 248
partial autocorrelation function, 94
peeling, 74, 97
planar assumption, 43, 45, 229, 256
and intrinsic curvature, 245
planar
assumption, 232
plot
fitted and observed, 91
lag, 92
of residuals, 27
residual vs fitted, 91
time series, 92
posterior density, 7
for nonlinear model, 219
profile trace, 222
practical considerations
accumulated data, 96
assessing fit, 90
check for convergence, 90
collinearity, 78, 80
comparing models, 103
compartment models, 179
conditionally linear parameter, 85
constraint on parameter, 77
correlated residuals, 92
derivative-free methods, 82
disturbance, 69
improving convergence, 78
in multiresponse estimation, 146
in nonlinear regression, 67
Levenberg–Marquardt compromise, 80, 81
model specification, 67
modifying the model, 90
numerical derivatives, 82
obtaining convergence, 86
parameters as functions of other variables, 108
preliminary analysis, 70
presenting the results, 109
QR decomposition, 80
starting values, 72
starting values for compartment models, 182
unidentifiable model, 180
preliminary analysis
nitrite example, 110
prior density
for nonlinear model, 216
noninformative, 7
on expectation surface, 217
probability density function, 2, 24
profile
trace, 207
profile pair sketches, 209
profile *t*, 205
profile trace
posterior, 222

QR decomposition, 13
of residual matrix, 141
of velocity and acceleration matrix, 236

random variable, 1, 24
randomization, 24, 25, 26, 123
rate constant, 168, 179
relative curvature, 241
  algorithm, 244
  array, 242
  matrix, 244
reparametrization, 248
  and parameter effects, 238
replication, 24, 28, 36, 70, 123, 126
  degrees of freedom, 29
  importance of, 26
  mean square, 29
  sum of squares, 29
report
  writing, 109
residual, 4, 24, 40, 90
  autocorrelation function, 94
  correlated, 92
  degrees of freedom, 29
  matrix, 136, 155
  mean square, 6, 30
  normal probability plot, 91
  plot, 91, 149
  studentized, 27
  sum of squares, 4, 29
  vector, 12, 139
  vector, approximate, 260
response
  function confidence band, 6
  space, 10, 36
root mean square (RMS)
  curvature, 254

sampling distribution, 25
second derivative
  array, 233, 250
sigma-minus method
  for accumulated data, 97
singular value decomposition, 156
singular
  data matrix, 155
  residual matrix, 155
stabilizing variance, 28
standard error, 7, 21
  approximate, 53
starting values, 72
  conditionally linear model, 76
  for compartment model, 182
  interpreting derivatives of expectation function, 73
  interpreting expectation function, 72
  multiresponse, 146
  peeling, 74
  reducing dimensions, 76
  systems of differential equations, 147
  transformably linear model, 73
  transforming expectation function, 73
steepest descent, 81
step factor, 42, 64, 84, 85, 145
sum of squares, 4
  contour, 23, 61
  extra, 103
  function, 60
  lack of fit, 29
  replication, 29
  residual, 29
system diagram, 169

T distribution, 6, 7
  multivariate, 7, 139, 220
tail probability, 17
tangent plane, 43
  approximation to expectation surface, 44, 45, 232
tangent
  space dimension, 234
time series, 92
  autoregressive model, 93
  moving average model, 93
torsion, 247
trace
  criterion for multiresponse estimation, 136
transfer matrix, 148, 171
  diagonalizable, 173
transformably linear
  model, 34, 73
transformation
  curvature array, 251
  of parameters, 179, 248
  power, 28
  variance-stabilizing, 28, 26

uniform coordinate
  assumption, 43, 45, 47, 229, 232, 256

variable
  indicator, 104
  lurking, 27
  predictor, 27

variance, 2
  -stabilizing transformation, 26
  constant, 25, 26, 70
  estimate, 6
  nonconstant, 25, 35, 91
  stabilizing transformation, 28
vector
  acceleration, 234
  tangent, 233
volume of distribution, 180